NANOCATALYSTS IN BIOFUEL PROCESS OPTIMIZATION

EDITED BY: Mohammad Rehan, Abdul-Sattar Nizami, Meisam Tabatabaei, Konstantinos Moustakas, Asim Laeeq Khan and Mohammad Zain Khan

frontiers Research Topics

About Frontiers

Frontiers is more than just an open-access publisher of scholarly articles: it is a pioneering approach to the world of academia, radically improving the way scholarly research is managed. The grand vision of Frontiers is a world where all people have an equal opportunity to seek, share and generate knowledge. Frontiers provides immediate and permanent online open access to all its publications, but this alone is not enough to realize our grand goals.

Frontiers Journal Series

The Frontiers Journal Series is a multi-tier and interdisciplinary set of open-access, online journals, promising a paradigm shift from the current review, selection and dissemination processes in academic publishing. All Frontiers journals are driven by researchers for researchers; therefore, they constitute a service to the scholarly community. At the same time, the Frontiers Journal Series operates on a revolutionary invention, the tiered publishing system, initially addressing specific communities of scholars, and gradually climbing up to broader public understanding, thus serving the interests of the lay society, too.

Dedication to Quality

Each Frontiers article is a landmark of the highest quality, thanks to genuinely collaborative interactions between authors and review editors, who include some of the world's best academicians. Research must be certified by peers before entering a stream of knowledge that may eventually reach the public - and shape society; therefore, Frontiers only applies the most rigorous and unbiased reviews.
Frontiers revolutionizes research publishing by freely delivering the most outstanding research, evaluated with no bias from both the academic and social point of view. By applying the most advanced information technologies, Frontiers is catapulting scholarly publishing into a new generation.

What are Frontiers Research Topics?

Frontiers Research Topics are very popular trademarks of the Frontiers Journals Series: they are collections of at least ten articles, all centered on a particular subject. With their unique mix of varied contributions from Original Research to Review Articles, Frontiers Research Topics unify the most influential researchers, the latest key findings and historical advances in a hot research area! Find out more on how to host your own Frontiers Research Topic or contribute to one as an author by contacting the Frontiers Editorial Office: frontiersin.org/about/contact

NANOCATALYSTS IN BIOFUEL PROCESS OPTIMIZATION

Topic Editors:
Mohammad Rehan, King Abdulaziz University, Saudi Arabia
Abdul-Sattar Nizami, Government College University, Lahore, Pakistan
Meisam Tabatabaei, Universiti Malaysia Terengganu, Malaysia
Konstantinos Moustakas, National Technical University of Athens, Greece
Asim Laeeq Khan, COMSATS University Islamabad, Pakistan
Mohammad Zain Khan, Aligarh Muslim University, India

Table of Contents

Editorial: Nanocatalysts in Biofuel Process Optimization

Mohammad Rehan[1]*, Abdul-Sattar Nizami[2], Meisam Tabatabaei[3,4,5,6], Konstantinos Moustakas[7], Asim Laeeq Khan[8], Muhammad Amjad[9] and Mohammad Zain Khan[10]

[1]Center of Excellence in Environmental Studies (CEES), King Abdulaziz University, Jeddah, Saudi Arabia, [2]Sustainable Development Study Center, Government College University, Lahore, Pakistan, [3]Higher Institution Centre of Excellence (HICoE), Institute of Tropical Aquaculture and Fisheries Research (AKUATROP), Universiti Malaysia Terengganu, Terengganu, Malaysia, [4]Henan Province Forest Resources Sustainable Development and High-value Utilization Engineering Research Center, School of Forestry, Henan Agricultural University, Zhengzhou, China, [5]Biofuel Research Team (BRTeam), Terengganu, Malaysia, [6]Microbial Biotechnology Department, Agricultural Biotechnology Research Institute of Iran (ABRII), Agricultural Research, Extension, and Education Organization (AREEO), Karaj, Iran, [7]National Technical University of Athens, School of Chemical Engineering, Unit of Environmental Science & Technology, Athens, Greece, [8]Department of Chemical Engineering, COMSATS University Islamabad, Islamabad, Pakistan, [9]Department of Mechanical, Mechatronics and Manufacturing Engineering, University of Engineering and Technology Lahore (KSK Campus), Lahore, Pakistan, [10]Department of Chemistry, Environmental Research Laboratory, Faculty of Sciences, Aligarh Muslim University, Aligarh, India

Editorial on the Research Topic

Nanocatalysts in Biofuel Process Optimization

INTRODUCTION

The world is facing severe environmental challenges, including increasing consumption of fossil-based energy and its consequent devastative impact, i.e. global warming and climate change. Biofuels are promising alternatives to fossil fuels with tremendous environmental and socio-economic benefits. There has been a considerable deal of research and development carried out on the production of biofuels in the last 2 decades. However, there is still a huge potential for achieving more cost-effective and efficient biofuel production processes through the application of nanotechnology. The exceptional properties of nanomaterials (nanocatalysts) such as high surface area, catalytic performance, crystallinity, durability, energy storage capacity, etc. offer great potential for optimizing biofuel production systems. Nanocatalysts could also serve recovery, reusability, and recycling purposes.

This Research Topic is designed to attract the state-of-the-art recent developments in fabrication, modification, and optimization of advanced nanocatalysts and nanostructured materials for biofuel production processes (**Figure 1**). This Frontiers Research Topic has attracted and compiled 12 top quality research and review articles. The articles have been written by researchers and academics working in institutions at different countries across the world including Australia, China, Egypt, Greece, India, Iran, Malaysia, Netherlands, Pakistan, Saudi Arabia and South Korea. The editorial team of this research topic is very grateful to all the authors for their excellent contributions and making the research topic successful.
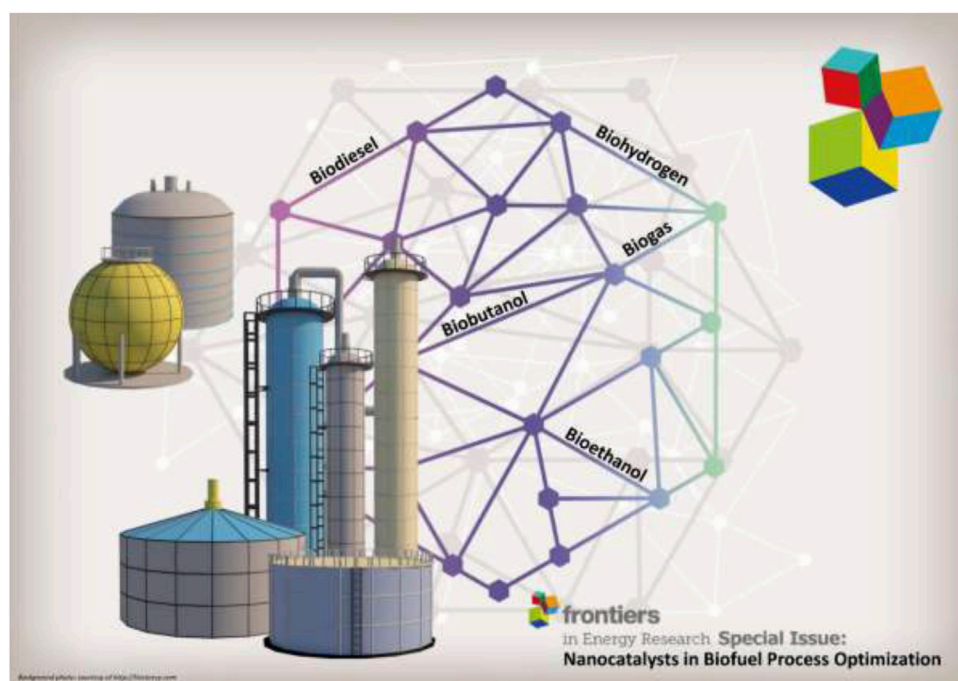
FIGURE 1 | Nanocatalysts in biofuel process optimization

NANOCATALYSTS SYNTHESIS AND CHARACTERIZATION FOR BIOFUEL PRODUCTION

There has been a significant amount of research work conducted in recent years on advanced nanocatalyst fabrication and development for optimization of biofuel processes. Bano et al. presented a comprehensive review on fabrication and optimization of nanocatalyst for biodiesel production. The authors discussed the production of biodiesel produced from various feedstock and using several processes such as pyrolysis, micro-emulsion, direct blending, and *trans*-esterification, with critical discussion focussing on increasing biodiesel production using nanocatalysts. Further, the importance of nanocatalyst in heterogeneous catalysis based *trans*-esterification for large scale biodiesel production was highlighted. Another interesting review on state of the art of catalysts for biodiesel production was published by Rizwanul Fattah et al. The authors reviewed various catalysts used for biodiesel production and compared their suitability and associated challenges in the transesterification process. Homogeneous catalysts are generally efficient in converting biodiesel with low free fatty acid (FFA) and water containing single-origin feedstock. Heterogeneous catalysts, on the other hand, provide superior activity, range of selectivity, good FFA, and water adaptability.

Nayebzadeh et al. studied the influence of fuel to oxidizer ratio on microwave-assisted combustion preparation of nanostructured $KOH/Ca_{12}Al_{14}O_{33}$ catalyst used in efficient biodiesel production. Authors demonstrated a high biodiesel yield of 94.5%, using 450 W, 12:1 methanol to oil ratio,

catalyst loading of 4 wt% for 1 h, through this microwave-enhanced biodiesel production process.

Shaker and Elhamifar synthesised a novel magnetic nanocatalyst, methylene-based organosilica with core-shell structure ($Fe_3O_4@OS–SO_3H$), and used in the production of biodiesel through esterification process. The synthesised catalyst showed good catalytic features and performance in biodiesel production process. Authors also claimed to have recovered and reused the synthesised catalyst several times without significant decrease in its efficiency and stability.

RECENT ADVANCES IN BIOFUEL PRODUCTION

Many studies have been published on advancements in biofuel production as a renewable source of energy. For example, Gholami et al. presented a review study on recent advances of biodiesel production using ionic liquids supported on nanoporous materials as catalysts. The authors discussed the key issues in current catalysts used in biofuel production as well along with the new developments in nanocatalysts. The economic and environmental aspects of different catalysts in biofuel production were also highlighted. Ruhong et al. proposed the utilization of enzymes as catalysts to enhance biofuel production. White-rot fungi is capable of producing extracellular enzymes that degrade lignin structure and facilitate biofuel production from lignocellulosic biomass wastes. The authors claimed to have shown the synergistic effects of the fungal co-culture for biomass treatment and providing a new approach for increasing lignin degradation

along with improving enzymatic catalysis and biofuel production through fungal coculture.

CARBON CAPTURE

Carbon capture and storage is considered as a potential way forward to mitigate environmental pollution caused by fossil fuels. Researchers are trying to optimize the current methods and develop new ones to achieve maximum benefits. Ishaq et al. proposed novel poly deep eutectic solvents (PDESs) based supported liquid membranes for CO_2 capture. The PDESs were synthesized by mixing choline chloride (hydrogen bond acceptor-HBA) and two hydrogen bond donors-HBDs (polyacrylic acid and polyacrylamide) separately in different molar ratios. The PDESs were then impregnated into microporous polyvinylidene fluoride (PVDF) membrane support to synthesise supported liquid membranes (SLMs). Pure and mixed-gases of CO_2, CH_4 and N_2 were tested on these synthesised PDES-SLMs with excellent permeability and selectivity. These cheap and green membranes with promising gas separation performance make them potential alternative to the competing PILs for capturing the greenhouse acid gases.

ENERGY SYSTEMS OPTIMIZATION

Some very interesting and state-of-the-art studies were published on energy systems optimizations in this research topic. For example, He et al. proposed black hole-inspired optimal design of biomethane liquefaction process for small-scale applications. Authors found that the specific energy consumption could be reduced with significant reduction in total exergy destruction by introducing the cryogenic liquid turbine to the single mixed refrigerant-based biomethane liquefaction process. The findings of this research work is a step forward in designing and improving the small-scale biomethane liquefaction process.

Qyyum et al. presented an interesting study on process systems engineering evaluation of prospective working fluids for organic rankine cycles facilitated by biogas combustion flue gases. Authors presented technical and economic analysis along with process system engineering perspective. Authors found i-butanol and n-butanol as promising working fluids, both technically and economically, for high-temperature organic Rankine cycle systems in comparison with toluene. These results will help to develop more energy efficient organic Rankine cycle systems for producing power.

Another interesting study was published on process optimization of nanocatalytic conversion of microalgae to clean bioenergy utilizing the fuzzy multi-criteria decision making processes by Kokkinos et al. Authors assessed technical, economic, environmental and social aspects of the proposed biofuel production system.

Arora et al. presented review study on the valorization of wastewater resources into biofuel and value-added products using microalgal system. Authors reviewed different microalgae cultivation processes including open, closed, and integrated for simultaneous treatment of wastewater and resource recovery. Key

factors affecting the growth of microalgae, such as sunlight, temperature, pH, and nutrients, were also discussed. It was stated that by integrating the wastewater treatment with microalgae biorefinery, it is possible to solve wastewater treatment problems along with generating revenue leading towards a sustainable and circular bio-economy.

A comparative study of techno-economic analysis of two biodiesel production processes was presented by Al-Sakkari et al. One process utilized waste cooking oil as a feedstock with potassium hydroxide homogeneous catalyst and the second process used virgin soybean oil as feedstock with cement kiln dust heterogeneous catalyst. The theoretical purities of biodiesel and glycerol obtained upon conducting the simulation of both processes are high, i.e., 99. 99%. However, the homogeneous process was found economically superior as sensitivity analysis revealed that the profitability of biodiesel production is very sensitive to the feedstock price and recommends shifting toward waste vegetable oils as a cheap feedstock to have a feasible and economic process.

OUTLOOK

Biofuels are promising alternatives to fossil fuels with tremendous environmental and socio-economic benefits. This research topic highlights the emerging technologies and recent developments in nanocatalysts and process optimizations of biofuel production. 12 top quality articles have been published in this research topic on recent developments in nanocatalysts synthesis and biofuel production, carbon capture and energy systems optimization. Key challenges in biofuel and bioenergy are highlighted along with potential of emerging nanocatalysts, biofuel production and process optimization as way forward to shift from fossil fuels towards renewable energy resources.

AUTHOR CONTRIBUTIONS

MR, A-SN, MT, MZ, and KM contributed to conception and design of the study. MR wrote the first draft. AL, MA, and AN reviewed/corrected the first draft of the manuscript with addition of some text in different sections. All authors contributed to manuscript revision, read, and approved the submitted version.

Sulfonic Acid Supported on Magnetic Methylene-Based Organosilica as an Efficient and Recyclable Nanocatalyst for Biodiesel Production via Esterification

Masoumeh Shaker and Dawood Elhamifar *

Department of Chemistry, Yasouj University, Yasouj, Iran

In this paper, a novel sulfonic acid containing magnetic methylene-based organosilica with core-shell structure ($Fe_3O_4@OS - SO_3H$) is synthesized, characterized and its catalytic application is investigated for biodiesel production via esterification of carboxylic acids with alcohols. The $Fe_3O_4@OS - SO_3H$ was synthesized via co-condensation of tetraethyl orthosilicate (TEOS) and 1,2-bis(triethoxysilyl)methane (BTEM) around magnetite nanoparticles. The $Fe_3O_4@OS - SO_3H$ nanocatalyst was characterized by using FT-IR, PXRD, TGA, VSM, TEM and SEM techniques. The catalytic study showed that the $Fe_3O_4@OS - SO_3H$ nanocomposite can be used as an effective, powerful, selective and recyclable catalyst for the esterification of carboxylic acids with alcohols at $70°C$ under solvent-free conditions. This nanocatalyst was recovered and reused several times without significant decrease in efficiency and stability.

Keywords: magnetic nanocatalyst, biodiesel production, esterification, recoverable catalyst, solvent-free conditions

INTRODUCTION

Recently, the use of magnetic nanoparticles has received increasing attention in various industrial and medical applications, such as magnetic resonance imaging (Qiao et al., 2009; Liu et al., 2014; Ni et al., 2017), magnetic recording (Dai et al., 2010), drug delivery (Häfeli et al., 2009; Zhang J. et al., 2013), cancer treatment through magnetic hyperthermia (Lartigue et al., 2011; Kandasamy et al., 2018; Mejías et al., 2018), catalytic industry (Pourjavadi et al., 2012; Wang et al., 2013; Kainz and Reiser, 2014; Iglesias et al., 2015; Ghorbani-Vaghei and Izadkhah, 2018), and spintronic, optoelectronic, and electronic devices (Gandhi et al., 2018; Obeid et al., 2019). In general, the performance and application of these nanoparticles are influenced by their proper design and synthesis. To date, various magnetic nanoparticles have been synthesized, including pure metal nanoparticles (Fe, Co, Ni), metal oxides (Fe_3O_4, γ-Fe_2O_3), ferrites (MFe_2O_4, M = Cu, Ni, Mn, Mg, Co, or Zn), and metal alloys (FePt, CoPt) (Meng et al., 2011; Seinberg et al., 2012; Aissou et al., 2013; Wang et al., 2015; Antonello et al., 2017). Among different magnetic materials, iron oxides are usually the best due to their lower toxicity and good magnetic properties compared with those of other particles. However, these MNPs are highly sensitive to oxidation and aggregation as well as chemically reactive because of their high surface area (Liu et al., 2008; Demirer et al., 2015; Wu et al., 2016; Kolhatkar et al., 2017). These problems limit their widespread applications. Creating a suitable organic or inorganic coating on the surface of magnetic NPs is an efficient way

to overcome these problems. Biopolymers such as dextran, polysorbates, polyaniline, chitosan, and polyethylene glycol; organic surfactants; silica; carbon; and bioactive substances such as liposomes, peptides, and ligands/receptors are important coatings for the protection of magnetic nanoparticles (Colombo et al., 2012; Zhang et al., 2013; Esfahani et al., 2014; Bohara et al., 2016; Kudr et al., 2017; Kalhor and Zarnegar, 2019). Since silica is recognized as "generally safe" in the FDA grouping and because of its poor chemical permeability and high availability of silanol groups on its surface for any modification, it has received much attention among researchers (Chen et al., 2010; Li et al., 2012; Mondal et al., 2012; Maleki et al., 2017; Hajian and Ehsanikhah, 2018; Abaeezadeh et al., 2019; Mirbagheri and Elhamifar, 2019; Nikoorazm and Erfani, 2019; Ramazani et al., 2019; Vahidian et al., 2020). In particular, modification of the surface of magnetite nanoparticles with organosilica precursors, in addition to protecting the magnetic properties of these NPs, increases the surface hydrophobicity due to the presence of organic groups. In fact, this hydrophobicity increases the application of core-shell-structured organosilica-coated magnetite NPs in catalytic and adsorption processes. The modification of magnetic silicas with organic functional groups is achieved *via* the simultaneous co-condensation of mono- or bis(trialkoxysilyl)organic units and tetraalkoxysilanes (TMOS or TEOS) over magnetic Fe_3O_4 NPs (Li et al., 2012; Elhamifar et al., 2018; Mirbagheri and Elhamifar, 2019). Some of recently developed magnetic nanostructures with silica shells are $Fe_3O_4@SiO_2@PMMA$ (Chen et al., 2010), $Fe_3O_4@$mesoporous SBA-15 (Mondal et al., 2012), $Fe_3O_4@MCM$-41@Cu-P2C (Nikoorazm and Erfani, 2019), $Fe_3O_4@MCM$-41-Im@MnPor (Hajian and Ehsanikhah, 2018), $CoFe_2O_4@B_2O_3$-SiO_2 (Maleki et al., 2017), and $Fe_3O_4@nSiO_2@PMO$ (Li et al., 2012).

On the other hand, due to the environmental pollution caused by fossil fuels and the non-renewability of their sources, the need for new energy sources in today's world is increasingly felt. Biodiesels, monoalkyl esters of long-chain fatty acids, have attracted the attention of many researchers as one of the clean renewable fuels. Using biodiesel reduces carbon dioxide emission into the environment (Yang et al., 2008; Kondamudi et al., 2009; Haas et al., 2010; Hu et al., 2012). Biodiesel is produced from vegetable or animal oils. With the growing population and the limitation of water and soil resources for food supply, not only does the use of edible oils as fuel destroy food sources but also it is not economically viable. Therefore, the use of non-edible oils as feedstock for biodiesel fuel production is more attractive. Some of non-edible oils for biodiesel production are Putranjiva oil (*Putranjiva roxburghii*), neem oil (*Azadirachta indica*), Honge oil (*Pongamia pinnata*), and *Jatropha curcas* oil (*Jatropha curcas* L.) (Pan et al., 2018; Zhang et al., 2018a,b; Adeniyi et al., 2019).

The usual method for biodiesel production is the esterification of carboxylic acids and/or alcohols in the presence of homogeneous catalysts (Lien et al., 2010; Socha and Sello, 2010; Lam et al., 2019). However, this strategy suffers from problems such as catalyst and product separation and non-recoverability of the catalyst. Therefore, the recent methods have been developed based on the use of heterogeneous catalysts. Nevertheless, the use of heterogeneous catalysts in industrial applications also

faces limitations such as mass transfer resistance and being time consuming. Nanocatalysts, due to their high surface area and high catalytic activity, can solve the above problems (Chen et al., 2007; Elhamifar et al., 2014; Dimian and Rothenberg, 2016; Laskar et al., 2018; Zhang et al., 2019). Especially, magnetic nanocatalysts are a good option in this regard because their easy magnetic separation avoids catalyst wastage and increases their reuse compared with filtration. Accordingly, a set of different magnetic nanocatalysts has been designed and used in biodiesel production (Hu et al., 2011; Chiang et al., 2015; Dos Santos-Durndell et al., 2018; Xie et al., 2018; Gardy et al., 2019; Sarno and Iuliano, 2019; Touqeer et al., 2019; Xie and Huang, 2019). Some of recently developed nanocatalysts are $Fe_3O_4/Au@CA$-L (Sarno and Iuliano, 2019), Fe_3O_4/MCM-41/ECH/Na_2SiO_3 (Xie et al., 2018), TBD-$Fe_3O_4@$silica (Chiang et al., 2015), KF/CaO–Fe_3O_4 (Hu et al., 2011), $Fe_3O_4@MIL$-100 (Fe) (Xie and Huang, 2019), Fe_3O_4-PDA-Lipase (Touqeer et al., 2019), SO_4/Mg-Al-Fe_3O_4 (Gardy et al., 2019), and Mag/Si (Dos Santos-Durndell et al., 2018).

In continuation of the abovementioned studies, in this study, due to the importance of biodiesel fuels and magnetic organosilica NPs in the catalyst world, we have prepared and developed a novel sulfonic acid containing magnetic organosilica as an effective, powerful, recyclable, and reusable nanocatalyst in the esterification process to produce biodiesel products.

EXPERIMENTAL SECTION

Preparation of $Fe_3O_4@OS$-SH

For this purpose, Fe_3O_4 and $Fe_3O_4@SiO_2$ MNPs were first synthesized according to methods presented by us in previous research studies (Elhamifar et al., 2018; Neysi et al., 2019). Then, $Fe_3O_4@OS$ MNPs were prepared *via* co-condensation of tetraethyl orthosilicate (TEOS) and 1,2-bis(triethoxysilyl)methane (BTEM) around $Fe_3O_4@SiO_2$ NPs. For this, 0.5 g of $Fe_3O_4@SiO_2$ was completely dispersed in a mixture of H_2O (12 mL) and EtOH (50 mL) for 30 min. After that, ammonia (2 mL, 25%) was added in the reaction vessel, and the resulting mixture was stirred at RT for 10 min. Then, tetraethyl orthosilicate (TEOS, 1 mmol) and 1,2-bis(triethoxysilyl)methane (BTEM, 1 mmol) were simultaneously added in the reaction vessel, and this combination was stirred at RT for 16 h. Next, the resulting product was collected using a magnetic field and washed several times with H_2O and EtOH. The obtained material was dried at 70°C and called $Fe_3O_4@OS$. For the preparation of $Fe_3O_4@OS$-SH, 0.5 g of $Fe_3O_4@OS$ was dispersed in dry toluene (25 mL) for 30 min. Then, (3-mercaptopropyl)trimethoxysilane (1 mmol) was added to the reaction flask, and the mixture was refluxed. After 24 h, the resulting material was separated using a magnet and washed with EtOH and H_2O. The final product was dried at 70°C for 6 h and called $Fe_3O_4@OS$-SH (Tai et al., 2017).

Preparation of the $Fe_3O_4@OS$-SO_3H Nanocatalyst

For this, 0.5 g of $Fe_3O_4@OS$-SH was completely dispersed in MeOH (20 mL) under ultrasonic conditions for 20 min. Then,

H_2O_2 (35%, 5 mL) was added to the reaction vessel, for oxidation of SH groups to SO_3H counterparts, and the resulting mixture was stirred at RT for 24 h. After this process, the resulting product was collected by using a magnetic field and washed three times with H_2O and EtOH. To ensure complete protonation, the obtained material was acidified in a H_2SO_4 solution (0.1 M, 25 mL) for 5 h. Then, the solid product was collected using an external magnet, washed completely with deionized water, dried at 70°C for 12 h, and denoted as Fe_3O_4@OS-SO_3H.

Procedure for the Determination of the Acidity of Fe_3O_4@OS-SO_3H

For this, 50 mg of Fe_3O_4@OS-SO_3H was dispersed in an aqueous solution of sodium chloride (1 M, 25 mL) for 20 min, and it was then stirred at room temperature for 72 h. After this, an inverse titration was carried out on the resulting mixture by using NaOH (0.05 M), and the loading of sulfonic acid groups on the Fe_3O_4@OS-SO_3H surface was calculated (2.1 mmol g^{-1}).

General Procedure for the Esterification of Carboxylic Acids in the Presence of the Fe_3O_4-OS-SO_3H Nanocatalyst

For this purpose, carboxylic acid (5 mmol), alcohol (2 mmol), and Fe_3O_4@OS-SO_3H nanocatalyst (0.03 g) were added into a reaction vessel, and this mixture was stirred vigorously at 70°C. The progress of the reaction was monitored by TLC and GC. After finishing the process, ethyl acetate (5 mL) was added, and the catalyst was collected using an external magnet. Then, the residue was decanted with a mixture of ethyl acetate and H_2O to remove unreacted carboxylic acid. The organic phase

was separated and dried over anhydrous Na_2SO_4. A pure ester product resulted after evaporation of the solvent.

Procedure for the Hot Filtration Test

This test was also performed on the esterification of acetic acid by 1-octanol under optimized conditions. For this, after about 50% of the reaction had been completed, it was stopped and the catalyst was separated using an external magnetic field. The catalyst-free residue was allowed to continue to undergo reaction under optimum conditions. After about 20 h, no noticeable conversion was observed, confirming no leaching of active sulfonic acid moieties during reaction conditions.

RESULTS AND DISCUSSION

Firstly, Fe_3O_4 and Fe_3O_4@SiO_2 NPs were first prepared according to our reported methods (Elhamifar et al., 2018; Neysi et al., 2019). Then, Fe_3O_4@OS was synthesized *via* co-condensation of TEOS and BTEM around Fe_3O_4@SiO_2 NPs. Next, the surface of Fe_3O_4@OS NPs was chemically modified with (3-mercaptopropyl)trimethoxysilane groups to give Fe_3O_4@SiO_2-SH nanomaterial. Finally, the SH moieties of the latter material were oxidized in the presence of H_2O_2 to deliver the desired Fe_3O_4@OS-SO_3H nanocatalyst (**Scheme 1**). Fe_3O_4@OS-SO_3H was characterized using various techniques, namely, FT-IR, PXRD, VSM, TEM, SEM, and TGA.

Firstly, the FT-IR spectroscopy technique was used to identify the functional groups of the prepared nanomaterials at each step (**Figure 1**). The observed peak at 576 cm^{-1} for all samples is related to the stretching vibrations of the Fe-O bonds. For Fe_3O_4@SiO_2, Fe_3O_4@OS, and Fe_3O_4@OS-SO_3H, the

SCHEME 1 | Preparation of the Fe_3O_4@OS-SO_3H nanocatalyst.

FIGURE 1 | FT-IR spectra of (A) Fe_3O_4, (B) $Fe_3O_4@SiO_2$, (C) $Fe_3O_4@OS$, and (D) $Fe_3O_4@OS-SO_3H$ nanomaterials.

FIGURE 2 | FT-IR spectra of (A) $Fe_3O_4@OS-SO_3H$ nanocatalyst and (B) $Fe_3O_4@OS-SO_3H$ nanocatalyst after pyridine adsorption.
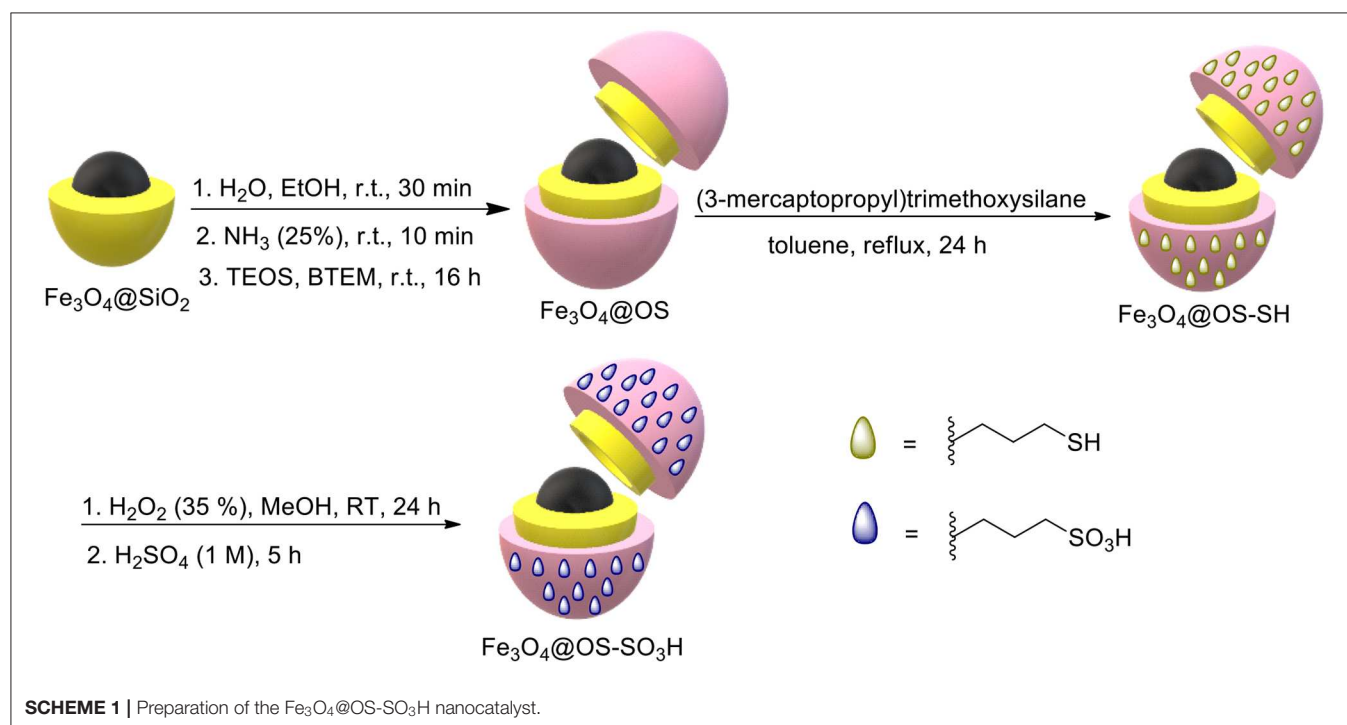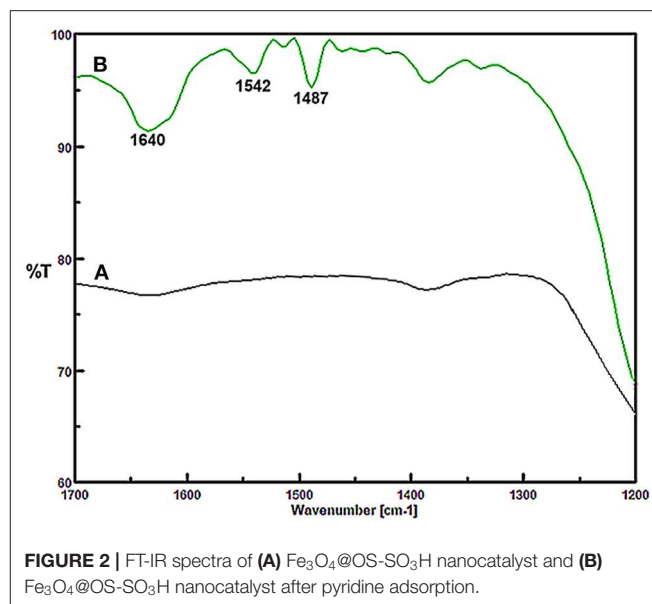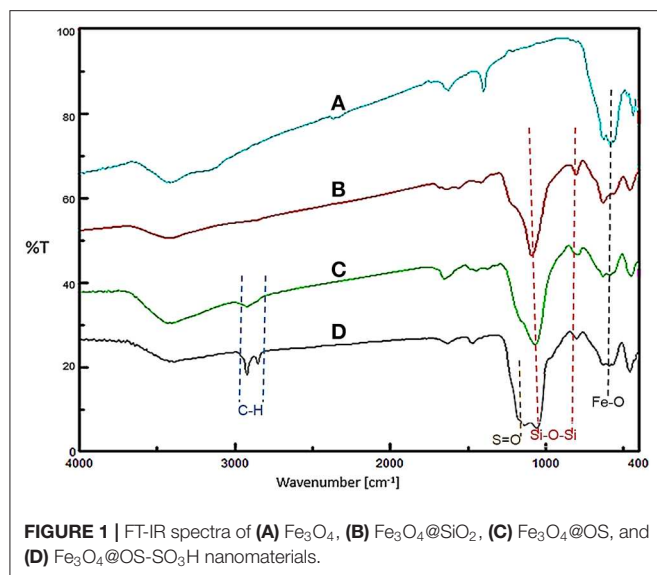
asymmetric and symmetric stretching vibrations of the Si-O-Si bonds appeared at 930 and 1,079 cm^{-1}. The peaks at 2,800–2,930 cm^{-1} can be attributed to the stretching vibration of aliphatic C-H bonds of propyl moieties (**Figures 1C,D**). Importantly, for the $Fe_3O_4@OS-SO_3H$ nanomaterial, the peak observed around 1,105 cm^{-1} is assigned to the S=O stretching vibration of the sulfonic acid groups (**Figure 1D**), indicating successful oxidation of SH to SO_3H moieties.

In the following, the surface acidity of the $Fe_3O_4@OS-SO_3H$ nanocatalyst was evaluated by FT-IR spectroscopy using pyridine as a probe molecule. **Figure 2A** shows the FT-IR spectrum of the nanocatalyst before pyridine adsorption, where no special bands corresponding to pyridine are observed in the region 1,400–1,700 cm^{-1}. In contrast, **Figure 2B** shows that after pyridine adsorption, three peaks clearly appear in regions 1,487, 1,542, and 1,640 cm^{-1}. These emerging bands are due to the interaction of pyridine with Brønsted acid sites to form pyridinium ions, confirming well the immobilization and high stability of sulfonic acid groups on the $Fe_3O_4@OS$ support (Hamoudi and Kaliaguine, 2003; Adam et al., 2012; Upare et al., 2013).

The powder X-ray diffraction (PXRD) analysis of Fe_3O_4, $Fe_3O_4@OS$, and $Fe_3O_4@OS-SO_3H$ nanomaterials showed six sharp peaks at 2θ: 30.15, 35.73, 43.38, 54.09, 57.37, and 62.89 degrees, corresponding to Miller indices of 220, 311, 400, 422, 511, and 440, respectively (**Figure 3**) (Zhang et al., 2014; Liu et al., 2015). The results of this analysis prove that the Fe_3O_4 crystalline structure is preserved during the modification processes (**Figure 3**). Also, the broad peaks appearing at 2θ = 20–25 degrees in **Figures 3B,C** are related to organosilica, confirming the formation of an organosilica shell around the Fe_3O_4 core. It also should be noted that the observation of later peaks at 2θ = 20–25 degrees in **Figure 3C** confirms the chemical stability of the organosilica shell during the surface modification process by the sulfonic acid group (Lee et al., 2008; Wang et al., 2012).

The magnetic properties of Fe_3O_4, $Fe_3O_4@SiO_2$, $Fe_3O_4@OS$, and $Fe_3O_4@OS-SO_3H$ nanomaterials were investigated by vibrating sample magnetometer (VSM) analysis. The results of this analysis showed that all samples have a superparamagnetic behavior with no hysteresis, remanence, and coercivity. The magnetic saturation of Fe_3O_4, $Fe_3O_4@SiO_2$, $Fe_3O_4@OS$, and $Fe_3O_4@OS-SO_3H$ nanomaterials were 75, 55, 47, and 38 emu/g, respectively. The decrease in saturation magnetization, after each step, confirms successful chemical immobilization of silica precursors and sulfonic acid moieties on the surface of the Fe_3O_4 NPs (**Figure 4**). Also, this confirms the high magnetic properties of all prepared materials, which are very important for their easy separation in the chemical processes.

The morphology of the particles at different steps of nanocatalyst preparation was investigated by using SEM (**Figure 5**). This showed a spherical morphology with a uniform size of the particles at different stages. Also, this confirmed that the size of the NPs increased at each step compared with that at the previous step. Especially, the SEM of $Fe_3O_4@OS-SO_3H$ clearly showed the presence of spherical particles with an average size of 70 nm (**Figure 5D**). These types of particles are very good candidates in the catalytic, chromatography, and adsorption processes.

The transmission electron microscopy (TEM) image also showed that the designed nanocatalyst has a core-shell structure with a black core (magnetite particles) and a gray shell (organosilica layer) (**Figure 6**).

Thermogravimetric analysis (TGA) was used for the investigation of the thermal stability of $Fe_3O_4@OS$ and $Fe_3O_4@OS-SO_3H$ nanocomposites (**Figure 7**). As shown, the TGA of both $Fe_3O_4@OS$ and $Fe_3O_4@OS-SO_3H$ samples has approximately the same pattern. This shows three weight losses. The first weight loss (about 3%) below 150°C corresponds to the removal of adsorbed water and alcoholic solvents remaining from the preparation process. The second weight
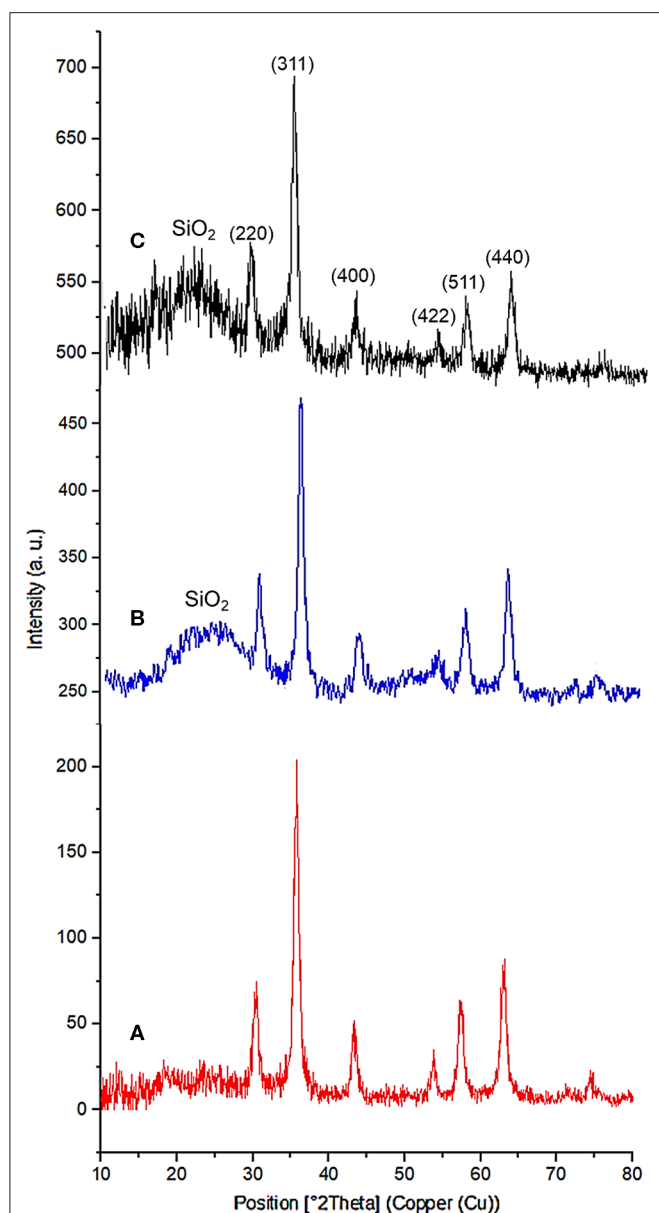
FIGURE 3 | PXRD patterns of the **(A)** Fe$_3$O$_4$, **(B)** Fe$_3$O$_4$@OS, and **(C)** Fe$_3$O$_4$@OS-SO$_3$H nanomaterials.

FIGURE 4 | VSM diagram of the **(A)** Fe$_3$O$_4$, **(B)** Fe$_3$O$_4$@SiO$_2$, **(C)** Fe$_3$O$_4$@OS, and **(D)** Fe$_3$O$_4$@OS-SO$_3$H nanomaterials.

loss (about 8%) between 180 and 250°C is due to the removal of supported propanethiol/propanesulfonic acid moieties. The main weight loss (about 22%) cleared between 251 and 600°C is due to the removal of incorporated methylene groups in the shell framework. These results prove the high thermal stability of the Fe$_3$O$_4$@OS and Fe$_3$O$_4$@OS-SO$_3$H nanocomposites and confirm well immobilization/incorporation of propanethiol/propanesulfonic acid and methylene groups onto/into the material framework.

After successful characterization of Fe$_3$O$_4$@OS-SO$_3$H, its catalytic activity was investigated in esterification of carboxylic acids to produce biodiesel products. In order to achieve the

optimum conditions, the condensation between acetic acid and 1-octanol was selected as the model reaction. The effects of temperature, catalyst loading, and catalyst type were investigated under solvent-free conditions (**Table 1**). The obtained results proved that the catalyst loading is very effective in the progress of the reaction and the best result was delivered in the presence of 0.03 g of the designed catalyst (**Table 1**, entries 1–4). The reaction was also affected by temperature, and the best conversion was obtained at 70°C (**Table 1**, entries 4-6). **Figure 8A** illustrates the influence of temperature on the progress of this process. In the following, to show the exact role of supported sulfonic acids in the catalytic process, the activity of Fe$_3$O$_4$@OS-SH and Fe$_3$O$_4$@OS was studied and the result was compared with that of Fe$_3$O$_4$@OS-SO$_3$H (**Table 1**, entry 4 vs. entries 7 and 8). Interestingly, both sulfonic acid-free nanomaterials delivered no ester product under the same conditions as Fe$_3$O$_4$@OS-SO$_3$H, confirming that the esterification process is completely catalyzed by supported -SO$_3$H moieties. Next, the effect of the molar ratio of 1-octanol to acetic acid was investigated. The results of this study showed that the yield of the desired ester is improved from 35 to 94% as the 1-octanol:acetic acid molar ratio changed from 0.5:5 to 2:5. It is also important to note that when the 1-octanol:acetic acid molar ratio was increased to 3:5, no significant change in the reaction yield was observed (**Table 1**, entry 4 vs. entries 9-11, **Figure 8B**). The effect of time on the progress of the esterification process proved that the conversion of starting materials increases steadily with increasing reaction time (**Table 1**, entry 4 vs. entries 12–15, **Figure 8C**). Accordingly, the use of 0.03 g of Fe$_3$O$_4$@OS-SO$_3$H, 70°C, and solvent-free conditions were chosen as optimum conditions.

After optimization of the reaction conditions, the catalytic activity of Fe$_3$O$_4$@OS-SO$_3$H was investigated in the esterification of different carboxylic acids and alcohols (**Table 2**). The synthesis of ester products with high yields in this process proved that
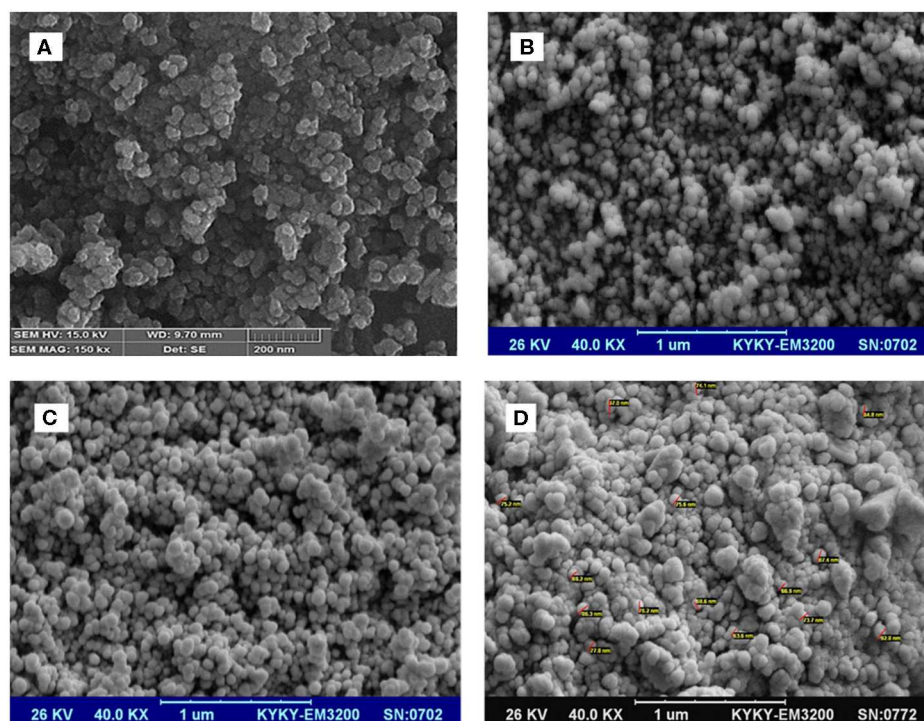
FIGURE 5 | SEM images of the (A) Fe_3O_4, (B) $Fe_3O_4@SiO_2$, (C) $Fe_3O_4@OS$, and (D) $Fe_3O_4@OS-SO_3H$ nanomaterials.
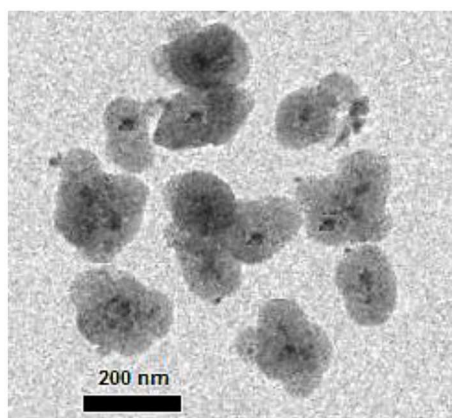
FIGURE 6 | The TEM image of the $Fe_3O_4@OS-SO_3H$ nanocatalyst.

FIGURE 7 | TG analysis of $Fe_3O_4@OS$ (A) and $Fe_3O_4@OS-SO_3H$ (B) materials.

$Fe_3O_4@OS-SO_3H$ is a powerful and efficient nanocatalyst for the preparation of a set of different esters applicable as biodiesel.

One of important properties of nanocatalysts is the recyclability and reusability of these materials without a significant change in their activity and structure. Therefore, next, the recyclability and reusability of $Fe_3O_4@OS-SO_3H$ were studied in the condensation of acetic acid and 1-octanol as a model reaction. The results showed that the $Fe_3O_4@OS-SO_3H$ nanocatalyst can be recycled and reused several times without a significant decrease in efficiency (**Figure 9**).

The IR and PXRD analyses of the recycled nanocatalyst were next performed to study its chemical and structural stability under the applied conditions.

As shown in **Figure 10**, the FT-IR spectrum of the recovered nanocatalyst is approximately the same as the FT-IR spectrum of the fresh nanocatalyst, confirming the high chemical stability of the $Fe_3O_4@OS-SO_3H$ nanocatalyst under the applied conditions.
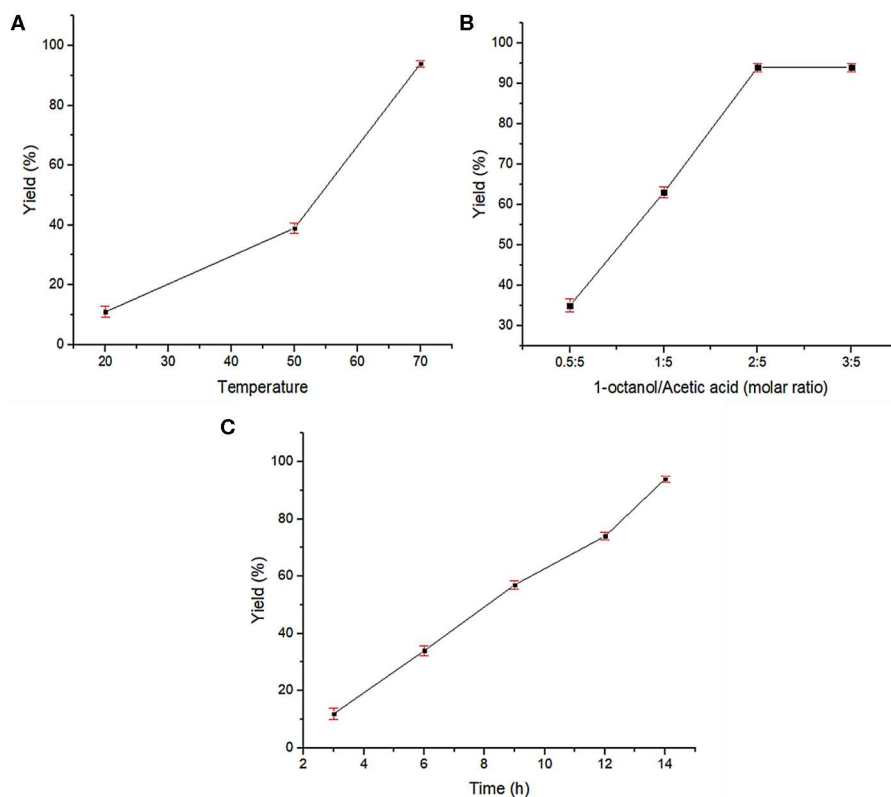
FIGURE 8 | Effects of reaction parameters in the esterification of acetic acid by 1-octanol: **(A)** reaction temperature, **(B)** molar ratio of 1-octanol to acetic acid, and **(C)** reaction time.

TABLE 1 | Effects of catalyst loading, temperature, and catalyst type in the esterification of acetic acid by 1-octanol.

Entry	Catalyst	Catalyst amount	Molar ratio (1-octanol/acetic acid)	T(°C)	Time (h)	Yield (%)[a]
1	—	—	2:5	70	14	—
2	Fe_3O_4@OS-SO_3H	0.01 g	2:5	70	14	34 ± 0.66
3	Fe_3O_4@OS-SO_3H	0.015 g	2:5	70	14	51 ± 0.49
4[b]	**Fe_3O_4@OS-SO_3H**	**0.03 g**	**2:5**	**70**	**14**	**94 ± 0.06**
5	Fe_3O_4@OS-SO_3H	0.03 g	2:5	50	14	39 ± 0.61
6	Fe_3O_4@OS-SO_3H	0.03 g	2:5	RT	14	11 ± 0.89
7	Fe_3O_4@OS-SH	0.03 g	2:5	70	14	—
8	Fe_3O_4@OS	0.03 g	2:5	70	14	—
9	Fe_3O_4@OS-SO_3H	0.03 g	0.5:5	70	14	35 ± 0.65
10	Fe_3O_4@OS-SO_3H	0.03 g	1:5	70	14	63 ± 0.37
11	Fe_3O_4@OS-SO_3H	0.03 g	3:5	70	14	94 ± 0.06
12	Fe_3O_4@OS-SO_3H	0.03 g	2:5	70	3	12 ± 0.88
13	Fe_3O_4@OS-SO_3H	0.03 g	2:5	70	6	34 ± 0.66
14	Fe_3O_4@OS-SO_3H	0.03 g	2:5	70	9	57 ± 0.43
15	Fe_3O_4@OS-SO_3H	0.03 g	2:5	70	12	74 ± 0.26

[a] Isolated yields. [b] Bold values indicate the optimum condition.

TABLE 2 | The esterification of carboxylic acids with alcohols in the presence of the Fe_3O_4@OS-SO_3H nanocatalyst[a].

$$R\text{--}COOH + R'OH \xrightarrow[\text{Solvent free, 70 °C}]{Fe_3O_4@OS\text{-}SO_3H} R\text{--}COOR'$$

Entry	R	R'OH	Time (h)	Yield (%)[b]
1	CH_3	$CH_3(CH_2)_{16}CH_2OH$	17	91 ± 0.09
2	$PhCH_2CH_2$	$CH_3(CH_2)_{16}CH_2OH$	21	90 ± 0.1
3	Ph	$CH_3(CH_2)_{16}CH_2OH$	24	88 ± 0.12
4	$CH_3(CH_2)_7CH{=}CH(CH_2)_7$	$CH_3(CH_2)_{16}CH_2OH$	22	90 ± 0.1
5	CH_3	$CH_3(CH_2)_6CH_2OH$	14	94 ± 0.06
6	$CH_3(CH_2)_7CH{=}CH(CH_2)_7$	$CH_3(CH_2)_6CH_2OH$	19	89 ± 0.11
7	CH_3	$CH_3(CH_2)_5CHOHCH_3$	18	92 ± 0.08
8	Ph	$CH_3(CH_2)_5CHOHCH_3$	24	89 ± 0.11

[a]Reaction conditions: carboxylic acid (5 mmol), alcohol (2 mmol), and catalyst (0.03 g).
[b]Isolated yields.

FIGURE 10 | FT-IR spectrum of the recovered Fe_3O_4@OS-SO_3H nanocatalyst.

FIGURE 9 | Reusability of the Fe_3O_4@OS-SO_3H nanocatalyst.
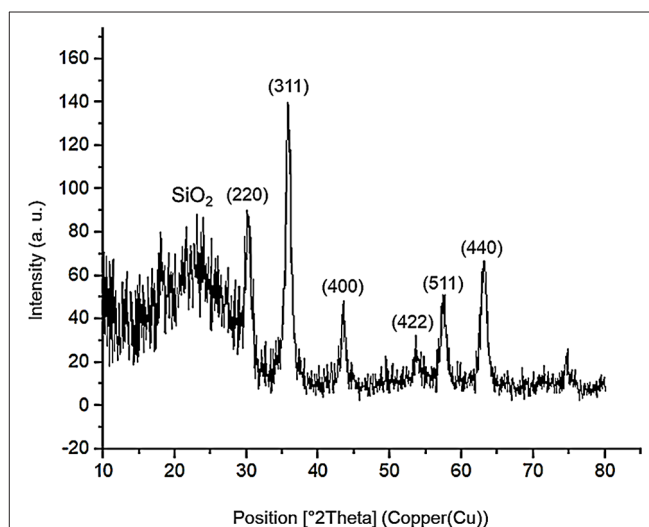
FIGURE 11 | PXRD pattern of the recovered Fe_3O_4@OS-SO_3H nanocatalyst.

TABLE 3 | The comparison study between the efficiency of the present catalyst with that of other catalysts[a].

Entry	Catalyst	Conditions	Recovery times	Reference
1	GO	Cat. 50 wt%, 100°C, 24 h	5	Chen et al., 2017
2	S-MIL-101	Cat. 0.05 g, 70°C, 7 h	3	Hu et al., 2020
3	GO	Cat. 0.1 g, 120°C, 6 h	4	Gao et al., 2015
4	SO_4/Mg-Al-Fe_3O_4	Cat. 4 wt%, 95°C, 5 h	5	Gardy et al., 2019
5	Fe_3O_4@OS-SO_3H	Cat. 0.03 g, 70°C, 14 h	6	This work

[a]GO, graphene oxide; MIL, Material Institute Lavoisier.

The PXRD of the recovered Fe_3O_4@OS-SO_3H also showed six peaks at $2\theta = 30.18, 35.68, 43.30, 54.12, 57.37$, and 62.91 degrees, which are in good agreement with the PXRD pattern of the fresh nanocatalyst. This analysis confirms the high stability of the crystalline structure of Fe_3O_4 nanoparticles during several reuse stages. It also important to mention that the appearance of a broad peak at $2\theta = 20\text{--}25$ degrees, corresponding to the organosilica layer, proves that the organosilica shell remains after several times of recycling and reuse (**Figure 11**).

Next, a hot filtration test was performed to investigate the nature of the catalyst under the applied conditions. For this, after completion of about 50% of the esterification process, the catalyst was removed using a magnetic field and the progress of the residue mixture was monitored. Interestingly, no further conversion was observed in this case. This result confirms no

leaching and the high stability of supported sulfonic acid moieties under reaction conditions.

Finally, the catalytic performance of the Fe$_3$O$_4$@OS-SO$_3$H nanocatalyst was compared with that of a number of previously reported catalysts in the esterification process (**Table 3**). As demonstrated, the efficiency of the present catalyst is much higher than that of most of previously reported systems in terms of recycling times, reaction time, and reaction temperature. These findings may be attributed to the magnetic properties and good lipophilicity of the present catalyst.

CONCLUSION

In summary, in the present study, for the first time a novel sulfonic acid containing magnetic methylene-based organosilica with a core-shell structure (Fe$_3$O$_4$@OS-SO$_3$H) was prepared as an effective nanocatalyst for biodiesel production. The SEM and TEM images of Fe$_3$O$_4$@OS-SO$_3$H demonstrated spherical particles with a core-shell structure for this material. The FT-IR analysis confirmed the successful immobilization of sulfonic acid groups on the Fe$_3$O$_4$@OS nanostructure. The VSM analysis proved the good magnetic properties of Fe$_3$O$_4$@OS-SO$_3$H, and PXRD analysis confirmed the high stability of Fe$_3$O$_4$ NPs during the modification process. TG analysis proved the good immobilization of sulfonic acid and methylene functional groups onto/into the material framework and showed the high thermal stability of the Fe3O4@OS-SO3H nanocatalyst. The Fe$_3$O$_4$@OS-SO$_3$H nanocatalyst was effectively applied in the esterification of carboxylic acids as an effective process for biodiesel synthesis. Also, this catalyst could be recycled and reused several times with its activity kept.

DATA AVAILABILITY STATEMENT

All datasets generated for this study are included in the article/supplementary material.

AUTHOR CONTRIBUTIONS

All authors listed have made a substantial, direct and intellectual contribution to the work, and approved it for publication.

ACKNOWLEDGMENTS

REFERENCES

Abaeezadeh, S., Elhamifar, D., Norouzi, M., and Shaker, M. (2019). Magnetic nanoporous MCM-41 supported ionic liquid/palladium complex: an efficient nanocatalyst with high recoverability. *Appl. Organomet. Chem.* 33:e4862. doi: 10.1002/aoc.4862

Adam, F., Batagarawa, M., Hello, K., and Al-Juaid, S. (2012). One-step synthesis of solid sulfonic acid catalyst and its application in the acetalization of glycerol: crystal structure of cis-5-hydroxy-2-phenyl-1, 3-dioxane trimer. *Chem. Pap.* 66, 1048–1058. doi: 10.2478/s11696-012-0203-x

Adeniyi, A. G., Ighalo, J. O., Adeoye, A. S., and Onifade, D. V. (2019). Modelling and optimisation of biodiesel production from Euphorbia lathyris using ASPEN Hysys. *Appl. Sci.* 1:1452. doi: 10.1007/s42452-019-1522-0

Aissou, K., Alnasser, T., Pecastaings, G., Goglio, G., Toulemonde, O., Mornet, S., et al. (2013). Hierarchical assembly of magnetic L1 0-ordered FePt nanoparticles in block copolymer thin films. *J. Mater. Chem. C* 1, 1317–1321. doi: 10.1039/C2TC00490A

Antonello, A., Jakob, G., Dolcet, P., Momper, R., Kokkinopoulou, M., Landfester, K., et al. (2017). Synergy of miniemulsion and solvothermal conditions for the low-temperature crystallization of magnetic nanostructured transition-metal ferrites. *Chem. Mater.* 29, 985–997. doi: 10.1021/acs.chemmater. 6b03467

Bohara, R. A., Thorat, N. D., and Pawar, S. H. (2016). Role of functionalization: strategies to explore potential nano-bio applications of magnetic nanoparticles. *RSC Adv.* 6, 43989–44012. doi: 10.1039/C6RA02129H

Chen, H., Deng, C., and Zhang, X. (2010). Synthesis of Fe$_3$O$_4$@ SiO$_2$@ PMMA core–shell magnetic microspheres for highly efficient enrichment of peptides and proteins for MALDI-ToF MS analysis. *Angew. Chem. Int. Edn.* 49, 607–611. doi: 10.1002/anie.200904885

Chen, X.-R., Ju, Y.-H., and Mou, C.-Y. (2007). Direct synthesis of mesoporous sulfated silica-zirconia catalysts with high catalytic activity for biodiesel via esterification. *J. Phys. Chem. C* 111, 18731–18737. doi: 10.1021/jp0749221

Chen, Z., Wen, Y., Fu, Y., Chen, H., Ye, M., and Luo, G. (2017). Graphene oxide: an efficient acid catalyst for the construction of esters from acids and alcohols. *Synlett* 28, 981–985. doi: 10.1055/s-0036-1588399

Chiang, Y. D., Dutta, S., Chen, C. T., Huang, Y. T., Lin, K. S., Wu, J. C., et al. (2015). Functionalized Fe$_3$O$_4$@ silica core–shell nanoparticles as microalgae harvester and catalyst for biodiesel production. *ChemSusChem* 8, 789–794. doi: 10.1002/cssc.201402996

Colombo, M., Carregal-Romero, S., Casula, M. F., Gutiérrez, L., Morales, M. P., Böhm, I. B., et al. (2012). Biological applications of magnetic nanoparticles. *Chem. Soc. Rev.* 41, 4306–4334. doi: 10.1039/c2cs15337h

Dai, Q., Berman, D., Virwani, K., Frommer, J., Jubert, P.-O., Lam, M., et al. (2010). Self-assembled ferrimagnet– polymer composites for magnetic recording media. *Nano Lett.* 10, 3216–3221. doi: 10.1021/nl1022749

Demirer, G. S., Okur, A. C., and Kizilel, S. (2015). Synthesis and design of biologically inspired biocompatible iron oxide nanoparticles for biomedical applications. *J. Mater. Chem. B* 3, 7831–7849. doi: 10.1039/C5TB00931F

Dimian, A. C., and Rothenberg, G. (2016). An effective modular process for biodiesel manufacturing using heterogeneous catalysis. *Catal. Sci. Technol.* 6, 6097–6108. doi: 10.1039/C6CY00426A

Dos Santos-Durndell, V. C., Peruzzolo, T. M., Ucoski, G. M., Ramos, L. P., and Nakagaki, S. (2018). Magnetically recyclable nanocatalysts based on magnetite: an environmentally friendly and recyclable catalyst for esterification reactions. *Biofuel Res. J.* 5, 806–812. doi: 10.18331/BRJ2018.5.2.4

Elhamifar, D., Karimi, B., Moradi, A., and Rastegar, J. (2014). Synthesis of sulfonic acid containing ionic-liquid-based periodic mesoporous organosilica and study of its catalytic performance in the esterification of carboxylic acids. *ChemPlusChem* 79, 1147–1152. doi: 10.1002/cplu.201402071

Elhamifar, D., Ramazani, Z., Norouzi, M., and Mirbagheri, R. (2018). Magnetic iron oxide/phenylsulfonic acid: a novel, efficient and recoverable nanocatalyst for green synthesis of tetrahydrobenzo [b] pyrans under ultrasonic conditions. *J. Colloid Interface Sci.* 511, 392–401. doi: 10.1016/j.jcis.2017.10.013

Esfahani, F. K., Zareyee, D., and Yousefi, R. (2014). Sulfonated core-shell magnetic nanoparticle (Fe$_3$O$_4$@ SiO$_2$@ PrSO$_3$H) as a highly active and durable protonic acid catalyst; synthesis of coumarin derivatives through Pechmann reaction. *ChemCatChem* 6, 3333–3337. doi: 10.1002/cctc.201402547

Gandhi, A. C., Pradeep, R., Yeh, Y.-C., Li, T.-Y., Wang, C.-Y., Hayakawa, Y., et al. (2018). Understanding the magnetic memory effect in Fe-doped NiO nanoparticles for the development of spintronic devices. *ACS Appl. Nano Mater.* 2, 278–290. doi: 10.1021/acsanm.8b01898

Gao, X., Zhu, S., and Li, Y. (2015). Graphene oxide as a facile solid acid catalyst for the production of bioadditives from glycerol esterification. *Catal. Commun.* 62, 48–51. doi: 10.1016/j.catcom.2015.01.007

Gardy, J., Nourafkan, E., Osatiashtiani, A., Lee, A. F., Wilson, K., Hassanpour, A., et al. (2019). A core-shell SO$_4$/Mg-Al-Fe$_3$O$_4$ catalyst for biodiesel production. *Appl. Catal. B Environ.* 259:118093. doi: 10.1016/j.apcatb.2019.118093

Ghorbani-Vaghei, R., and Izadkhah, V. (2018). Preparation and characterization of hexamethylenetetramine-functionalized magnetic nanoparticles and their application as novel catalyst for the synthesis of pyranopyrazole derivatives. *Appl. Organomet. Chem.* 32:e4025. doi: 10.1002/aoc.4025

Haas, M. J., Adawi, N., Berry, W. W., Feldman, E., Kasprzyk, S., Ratigan, B., et al. (2010). Butter as a feedstock for biodiesel production. *J. Agric. Food Chem.* 58, 7680–7684. doi: 10.1021/jf1003754

Häfeli, U. O., Riffle, J. S., Harris-Shekhawat, L., Carmichael-Baranauskas, A., Mark, F., Dailey, J. P., et al. (2009). Cell uptake and *in vitro* toxicity of magnetic nanoparticles suitable for drug delivery. *Mol. Pharmaceutics* 6, 1417–1428. doi: 10.1021/mp900083m

Hajian, R., and Ehsanikhah, A. (2018). Manganese porphyrin immobilized on magnetic MCM-41 nanoparticles as an efficient and reusable catalyst for alkene oxidations with sodium periodate. *Chem. Phys. Lett.* 691, 146–154. doi: 10.1016/j.cplett.2017.11.009

Hamoudi, S., and Kaliaguine, S. (2003). Sulfonic acid-functionalized periodic mesoporous organosilica. *Microporous Mesoporous Mater.* 59, 195–204. doi: 10.1016/S1387-1811(03)00311-1

Hu, S., Guan, Y., Wang, Y., and Han, H. (2011). Nano-magnetic catalyst KF/CaO–Fe$_3$O$_4$ for biodiesel production. *Appl. Energy* 88, 2685–2690. doi: 10.1016/j.apenergy.2011.02.012

Hu, S., Luo, X., Wan, C., and Li, Y. (2012). Characterization of crude glycerol from biodiesel plants. *J. Agric. Food Chem.* 60, 5915–5921. doi: 10.1021/jf3008629

Hu, X., Ma, K., Sabbaghi, A., Chen, X., Chatterjee, A., and Lam, F. L. (2020). Mild acid functionalization of metal-organic framework and its catalytic effect on esterification of acetic acid with n-butanol. *Mol. Catal.* 482:110635. doi: 10.1016/j.mcat.2019.110635

Iglesias, D., Sabater, S., Azua, A., and Mata, J. A. (2015). Catalytic applications of magnetic nanoparticles functionalized using iridium N-heterocyclic carbene complexes. *New J. Chem.* 39, 6437–6444. doi: 10.1039/C5NJ00803D

Kainz, Q. M., and Reiser, O. (2014). Polymer and dendrimer-coated magnetic nanoparticles as versatile supports for catalysts, scavengers, and reagents. *Acc. Chem. Res.* 47, 667–677. doi: 10.1021/ar400236y

Kalhor, M., and Zarnegar, Z. (2019). Fe3O4/SO3Hlite-Y as a novel multi-functional and magnetic nanocatalyst for clean and soft synthesis of imidazole and perimidine derivatives. *RSC Adv.* 9, 19333–19346. doi: 10.1039/C9RA02910A

Kandasamy, G., Sudame, A., Luthra, T., Saini, K., and Maity, D. (2018). Functionalized hydrophilic superparamagnetic iron oxide nanoparticles for magnetic fluid hyperthermia application in liver cancer treatment. *ACS Omega* 3, 3991–4005. doi: 10.1021/acsomega.8b00207

Kolhatkar, A. G., Chen, Y.-T., Chinwangso, P., Nekrashevich, I., Dannangoda, G. C., Singh, A., et al. (2017). Magnetic sensing potential of Fe$_3$O$_4$ nanocubes exceeds that of Fe$_3$O$_4$ nanospheres. *ACS Omega* 2, 8010–8019. doi: 10.1021/acsomega.7b01312

Kondamudi, N., Strull, J., Misra, M., and Mohapatra, S. K. (2009). A green process for producing biodiesel from feather meal. *J. Agric. Food Chem.* 57, 6163–6166. doi: 10.1021/jf900140e

Kudr, J., Haddad, Y., Richtera, L., Heger, Z., Cernak, M., Adam, V., et al. (2017). Magnetic nanoparticles: from design and synthesis to real world applications. *Nanomaterials* 7:243. doi: 10.3390/nano7090243

Lam, Y.-P., Wang, X., Tan, F., Ng, W.-H., Tse, Y.-L. S., and Yeung, Y.-Y. (2019). Amide/iminium zwitterionic catalysts for (Trans) esterification: application in biodiesel synthesis. *ACS Catal.* 9, 8083–8092. doi: 10.1021/acscatal.9b01959

Lartigue, L., Innocenti, C., Kalaivani, T., Awwad, A., Sanchez Duque, M. D. M., Guari, Y., et al. (2011). Water-dispersible sugar-coated iron oxide nanoparticles. An evaluation of their relaxometric and magnetic hyperthermia properties. *J. Am. Chem. Soc.* 133, 10459–10472. doi: 10.1021/ja111448t

Laskar, I. B., Rajkumari, K., Gupta, R., Chatterjee, S., Paul, B., and Rokhum, L. (2018). Waste snail shell derived heterogeneous catalyst for biodiesel production by the transesterification of soybean oil. *RSC Adv.* 8, 20131–20142. doi: 10.1039/C8RA02397B

Lee, J., Lee, Y., Youn, J. K., Na, H. B., Yu, T., Kim, H., et al. (2008). Simple synthesis of functionalized superparamagnetic magnetite/silica core/shell nanoparticles and their application as magnetically separable high-performance biocatalysts. *Small* 4, 143–152. doi: 10.1002/smll.200700456

Li, J., Wei, Y., Li, W., Deng, Y., and Zhao, D. (2012). Magnetic spherical cores partly coated with periodic mesoporous organosilica single crystals. *Nanoscale* 4, 1647–1651. doi: 10.1039/c2nr11941b

Lien, Y.-S., Hsieh, L.-S., and Wu, J. C. (2010). Biodiesel synthesis by simultaneous esterification and transesterification using oleophilic acid catalyst. *Ind. Eng. Chem. Res.* 49, 2118–2121. doi: 10.1021/ie901496h

Liu, C. L., Peng, Y. K., Chou, S. W., Tseng, W. H., Tseng, Y. J., Chen, H. C., et al. (2014). One-step, room-temperature synthesis of glutathione-capped iron-oxide nanoparticles and their application in *in vivo* T1-weighted magnetic resonance imaging. *Small* 10, 3962–3969. doi: 10.1002/smll.201303868

Liu, G., Wang, D., Zhou, F., and Liu, W. (2015). Electrostatic self-assembly of Au nanoparticles onto thermosensitive magnetic core-shell microgels for thermally tunable and magnetically recyclable catalysis. *Small* 11, 2807–2816. doi: 10.1002/smll.201403305

Liu, J.-F., Zhao, Z.-S., and Jiang, G.-B. (2008). Coating Fe$_3$O$_4$ magnetic nanoparticles with humic acid for high efficient removal of heavy metals in water. *Environ. Sci. Technol.* 42, 6949–6954. doi: 10.1021/es800924c

Maleki, A., Aghaei, M., Hafizi-Atabak, H. R., and Ferdowsi, M. (2017). Ultrasonic treatment of CoFe$_2$O$_4$@ B$_2$O$_3$-SiO$_2$ as a new hybrid magnetic composite nanostructure and catalytic application in the synthesis of dihydroquinazolinones. *Ultrason. Sonochem.* 37, 260–266. doi: 10.1016/j.ultsonch.2017.01.022

Mejías, R., HernáNdez Flores, P., Talelli, M., Tajada-HerráIz, J. L., Brollo, M. E., Portilla, Y., et al. (2018). Cell-promoted nanoparticle aggregation decreases nanoparticle-induced hyperthermia under an alternating magnetic field independently of nanoparticle coating, core size, and subcellular localization. *ACS Appl. Mater. Interfaces* 11, 340–355. doi: 10.1021/acsami.8b18451

Meng, X., Seton, H. C., Lu, L. T., Prior, I. A., Thanh, N. T., and Song, B. (2011). Magnetic CoPt nanoparticles as MRI contrast agent for transplanted neural stem cells detection. *Nanoscale* 3, 977–984. doi: 10.1039/c0nr00846j

Mirbagheri, R., and Elhamifar, D. (2019). Magnetic ethyl-based organosilica supported schiff-base/indium: a very efficient and highly durable nanocatalyst. *J. Alloys Compd.* 790, 783–791. doi: 10.1016/j.jallcom.2019.03.203

Mondal, J., Sen, T., and Bhaumik, A. (2012). Fe$_3$O$_4$@ mesoporous SBA-15: a robust and magnetically recoverable catalyst for one-pot synthesis of 3, 4-dihydropyrimidin-2 (1 H)-ones via the biginelli reaction. *Dalton Trans.* 41, 6173–6181. doi: 10.1039/c2dt30106g

Neysi, M., Zarnegaryan, A., and Elhamifar, D. (2019). Core–shell structured magnetic silica supported propylamine/molybdate complexes: an efficient and magnetically recoverable nanocatalyst. *N. J. Chem.* 43, 12283–12291. doi: 10.1039/C9NJ01160A

Ni, D., Bu, W., Ehlerding, E. B., Cai, W., and Shi, J. (2017). Engineering of inorganic nanoparticles as magnetic resonance imaging contrast agents. *Chem. Soc. Rev.* 46, 7438–7468. doi: 10.1039/C7CS00316A

Nikoorazm, M., and Erfani, Z. (2019). Core–shell nanostructure (Fe$_3$O$_4$@ MCM-41@ Cu-P2C) as a highly efficient and recoverable nanocatalyst for the synthesis of polyhydroquinoline, 5-substituted 1H-tetrazoles and sulfides. *Chem. Phys. Lett.* 737:136784. doi: 10.1016/j.cplett.2019.136784

Obeid, M. M., Jappor, H. R., Al-Marzoki, K., Al-Hydary, I. A., Edrees, S. J., and Shukur, M. M. (2019). Unraveling the effect of Gd doping on the structural, optical, and magnetic properties of ZnO based diluted magnetic semiconductor nanorods. *RSC Adv.* 9, 33207–33221. doi: 10.1039/C9RA04750F

Pan, H., Li, H., Zhang, H., Wang, A., Jin, D., and Yang, S. (2018). Effective production of biodiesel from non-edible oil using facile synthesis of imidazolium salts-based brønsted-lewis solid acid and co-solvent. *Energy Convers. Manag.* 166, 534–544. doi: 10.1016/j.enconman.2018.04.061

Pourjavadi, A., Hosseini, S. H., Doulabi, M., Fakoorpoor, S. M., and Seidi, F. (2012). Multi-layer functionalized poly (ionic liquid) coated magnetic nanoparticles: highly recoverable and magnetically separable brønsted acid catalyst. *ACS Catal.* 2, 1259–1266. doi: 10.1021/cs300140j

Qiao, R., Yang, C., and Gao, M. (2009). Superparamagnetic iron oxide nanoparticles: from preparations to *in vivo* MRI applications. *J. Mater. Chem.* 19, 6274–6293. doi: 10.1039/b902394a

Ramazani, Z., Elhamifar, D., Norouzi, M., and Mirbagheri, R. (2019). Magnetic mesoporous MCM-41 supported boric acid: a novel, efficient and ecofriendly nanocomposite. *Compos. B. Eng.* 164, 10–17. doi: 10.1016/j.compositesb.2018.11.063

Sarno, M., and Iuliano, M. (2019). Highly active and stable Fe_3O_4/Au nanoparticles supporting lipase catalyst for biodiesel production from waste tomato. *Appl. Surf. Sci.* 474, 135–146. doi: 10.1016/j.apsusc.2018.04.060

Seinberg, L., Yamamoto, S., Gallage, R., Tsujimoto, M., Kobayashi, Y., Isoda, S., et al. (2012). Low temperature solventless synthesis and characterization of Ni and Fe magnetic nanoparticles. *Chem. Commun.* 48, 8237–8239. doi: 10.1039/c2cc33830k

Socha, A. M., and Sello, J. K. (2010). Efficient conversion of triacylglycerols and fatty acids to biodiesel in a microwave reactor using metal triflate catalysts. *Org. Biomol. Chem.* 8, 4753–4756. doi: 10.1039/c0ob00014k

Tai, Z., Isaacs, M. A., Parlett, C. M., Lee, A. F., and Wilson, K. (2017). High activity magnetic core-mesoporous shell sulfonic acid silica nanoparticles for carboxylic acid esterification. *Catal. Commun.* 92, 56–60. doi: 10.1016/j.catcom.2017.01.004

Touqeer, T., Mumtaz, M. W., Mukhtar, H., Irfan, A., Akram, S., Shabbir, A., et al. (2019). Fe_3O_4-PDA-Lipase as surface functionalized nano biocatalyst for the production of biodiesel using waste cooking oil as feedstock: characterization and process optimization. *Energies* 13, 1–19. doi: 10.3390/en13010177

Upare, P. P., Yoon, J.-W., Kim, M. Y., Kang, H.-Y., Hwang, D. W., Hwang, Y. K., et al. (2013). Chemical conversion of biomass-derived hexose sugars to levulinic acid over sulfonic acid-functionalized graphene oxide catalysts. *Green Chem.* 15, 2935–2943. doi: 10.1039/c3gc40353j

Vahidian, M., Elhamifar, D., and Shaker, M. (2020). Core–shell structured magnetic mesoporous silica-titania: a novel, powerful and recoverable nanocatalyst. *Polyhedron* 178:114326. doi: 10.1016/j.poly.2019.114326

Wang, D., Salmon, L., Ruiz, J., and Astruc, D. (2013). A recyclable ruthenium (II) complex supported on magnetic nanoparticles: a regioselective catalyst for alkyne–azide cycloaddition. *Chem. Commun.* 49, 6956–6958. doi: 10.1039/c3cc43048k

Wang, J., Zhou, H., Zhuang, J., and Liu, Q. (2015). Magnetic γ-Fe_2O_3, Fe_3O_4, and Fe nanoparticles confined within ordered mesoporous carbons as efficient microwave absorbers. *Phys. Chem. Chem. Phys.* 17, 3802–3812. doi: 10.1039/C4CP04228J

Wang, Y., Peng, X., Shi, J., Tang, X., Jiang, J., and Liu, W. (2012). Highly selective fluorescent chemosensor for Zn^{2+} derived from inorganic-organic hybrid magnetic core/shell Fe_3O_4@ SiO_2 nanoparticles. *Nanoscale Res. Lett.* 7:86. doi: 10.1186/1556-276X-7-86

Wu, W., Jiang, C. Z., and Roy, V. A. (2016). Designed synthesis and surface engineering strategies of magnetic iron oxide nanoparticles for biomedical applications. *Nanoscale* 8, 19421–19474. doi: 10.1039/C6NR07542H

Xie, W., Han, Y., and Wang, H. (2018). Magnetic Fe_3O_4/MCM-41 composite-supported sodium silicate as heterogeneous catalysts for biodiesel production. *Renew. Energy* 125, 675–681. doi: 10.1016/j.renene.2018.03.010

Xie, W., and Huang, M. (2019). Enzymatic production of biodiesel using immobilized lipase on core-shell structured Fe_3O_4@ MIL-100 (Fe) composites. *Catalysts* 9:850. doi: 10.3390/catal9100850

Yang, F.-X., Su, Y.-Q., Li, X.-H., Zhang, Q., and Sun, R.-C. (2008). Studies on the preparation of biodiesel from zanthoxylum bungeanum maxim seed oil. *J. Agric. Food Chem.* 56, 7891–7896. doi: 10.1021/jf801364f

Zhang, C., Wang, H., Liu, F., Wang, L., and He, H. (2013). Magnetic core–shell Fe_3O_4@ C-SO_3H nanoparticle catalyst for hydrolysis of cellulose. *Cellulose* 20, 127–134. doi: 10.1007/s10570-012-9839-5

Zhang, H., Li, H., Xu, C. C., and Yang, S. (2019). Heterogeneously chemo/enzyme-functionalized porous polymeric catalysts of high-performance for efficient biodiesel production. *ACS Catal.* 9, 10990–11029. doi: 10.1021/acscatal.9b02748

Zhang, J., Shin, M. C., David, A. E., Zhou, J., Lee, K., He, H., et al. (2013). Long-circulating heparin-functionalized magnetic nanoparticles for potential application as a protein drug delivery platform. *Mol. Pharmaceutics* 10, 3892–3902. doi: 10.1021/mp400360q

Zhang, Q., Li, H., and Yang, S. (2018a). Facile and low-cost synthesis of mesoporous Ti–Mo Bi-metal oxide catalysts for biodiesel production from esterification of free fatty acids in jatropha curcas crude oil. *J. Oleo Sci.* 67, 579–588. doi: 10.5650/jos.ess17231

Zhang, Q., Wei, F., Ma, P., Zhang, Y., Wei, F., and Chen, H. (2018b). Mesoporous Al–Mo oxides as an effective and stable catalyst for the synthesis of biodiesel from the esterification of free-fatty acids in non-edible oils. *Waste Biomass Valorization* 9, 911–918. doi: 10.1007/s12649-017-9865-5

Zhang, Y., Ma, W., Li, D., Yu, M., Guo, J., and Wang, C. (2014). Benzoboroxole-functionalized magnetic core/shell microspheres for highly specific enrichment of glycoproteins under physiological conditions. *Small* 10, 1379–1386. doi: 10.1002/smll.201302841

State of the Art of Catalysts for Biodiesel Production

I. M. Rizwanul Fattah[1]*, H. C. Ong[1], T. M. I. Mahlia[1], M. Mofijur[1], A. S. Silitonga[2], S. M. Ashrafur Rahman[3] and Arslan Ahmad[4]

[1] Faculty of Engineering and IT, School of Information, Systems and Modelling, University of Technology, Sydney, NSW, Australia, [2] Department of Mechanical Engineering, Politeknik Negeri Medan, Medan, Indonesia, [3] Biofuel Engine Research Facility, Queensland University of Technology, Brisbane, QLD, Australia, [4] Department of Mechanical Engineering, COMSATS University Islamabad, Sahiwal, Pakistan

Biodiesel is one of the potential alternative energy sources that can be derived from renewable and low-grade origin through different processes. One of the processes is alcoholysis or transesterification in the presence of a suitable catalyst. The catalyst can be either homogeneous or heterogeneous. This article reviews various catalysts used for biodiesel production to date, presents the state of the art of types of catalysts, and compares their suitability and associated challenges in the transesterification process. Biodiesel production using homogeneous and heterogeneous catalysis has been studied extensively, and novel heterogeneous catalysts are being continuously investigated. Homogeneous catalysts are generally efficient in converting biodiesel with low free fatty acid (FFA) and water containing single-origin feedstock. Heterogeneous catalysts, on the other hand, provide superior activity, range of selectivity, good FFA, and water adaptability. The quantity and strengths of active acid or basic sites control these properties. Some of the heterogeneous catalysts such as zirconia and zeolite-based catalysts can be used as both basic and acidic catalyst by suitable alteration. Heterogeneous catalysts from waste and biocatalysts play an essential role in attaining a sustainable alternative to traditional homogeneous catalysts for biodiesel production. Recently, high catalytic efficiency at mild operating conditions has drawn attention to nanocatalysts. This review evaluates state of the art and perspectives for catalytic biodiesel production and assesses the critical operational variables that influence biodiesel production along with the technological solutions for sustainable implementation of the process.

Keywords: biodiesel, transesterification, homogeneous catalyst, heterogeneous catalyst, biocatalyst, nanocatalyst

INTRODUCTION

The exigency of energy, limited reserve, the rapidly rising price of petroleum oil, and the deleterious effect of greenhouse gases have dictated to steer our attention toward alternative sources of energy. The quest for eco-friendly technology is driving the research initiatives to find potential energy sources that are renewable, biodegradable non-toxic, and mostly carbon neutral (Arbab et al., 2015). Historically, fossil fuels have played a vital role in global energy demand (Jayed et al., 2009). The diesel engine, named after its inventor Rudolf Diesel, was patented in 1892 and catered this energy

demand substantially ever since. Being the powerhouse of heavy-duty and commercial transport vehicles has been the most important use of diesel engines, and the importance is increasing consistently. The diesel engine is the most efficient type of internal combustion engine, offering excellent fuel economy and low carbon dioxide (CO_2) emission (Fattah et al., 2018). While diesel engines are arguably superior to any other power-producing device for the transportation sector in terms of efficiency, torque, and overall drivability, they suffer from inferior performance in terms of emissions (Silitonga et al., 2013a).

Biodiesel is a renewable energy source that can replace fossil-based diesel and can reduce the drawbacks of diesel emission (Abedin et al., 2014). Diesel is obtained by fractional distillation from crude petroleum oil that typically contains a mixture of pure hydrocarbon molecules (no oxygen molecule) that range in size from 8 to 21 carbon atoms. Biodiesel, on the other hand, consists of long-chain hydrocarbons with an ester functional group (–COOR). Thus, it is defined as mono-alkyl esters of long-chain fatty acids derived from various feedstocks, namely, plant oils, animal fats, or other lipids, also known as triacylglycerides (TAGs), or more simply, triglycerides (Hoekman and Robbins, 2012). Biodiesel is produced using the transesterification or alcoholysis process, which is usually facilitated by acids, bases, enzymes, and other type and form of catalysts (Ong et al., 2014). The catalysts can be either in a homogeneous or in a heterogeneous phase as of the reactants. If the catalyst remains in the same phase (usually liquid) to the reactants during alcoholysis, then that is the homogeneous catalyst. If the catalyst is in a different phase (usually non-liquid) to the reactants, then that is the heterogeneous catalyst (Ruhul et al., 2015). The appropriate catalyst selection depends on several factors, namely, the amount of free fatty acids (FFAs) in the oil, the water content, etc.

Homogeneous catalysts are generally efficient in converting biodiesel with low FFA and water containing single-origin feedstock (Silitonga et al., 2013a). Oils with higher FFA content lead to the formation of soap, consequently affecting the activity of the catalyst (Fattah et al., 2014a). Besides, the catalyst is partially miscible in biodiesel and miscible in glycerol, which results in problems of product separation from the reactant mixture (Tan et al., 2019). Heterogeneous catalysts, on the other hand, provides high activity, selectivity, and water adaptability due to the presence of a large number of active acid or basic sites. Various reviews have been published before on the topic of catalysts, especially on heterogeneous catalysts. **Table 1** presented below summarizes some of the critical review articles in the last decade, along with their brief introductions. The novelty aspect of this article is to review the works of many researchers on the development of various homogeneous and heterogeneous catalysts used for biodiesel production to date. This article presents different types of catalysts and compares their suitability and associated challenges in the transesterification process with an emphasis on the catalytic activity, selectivity, catalyst loading, and reusability.

BIODIESEL PRODUCTION USING ALCOHOLYSIS

The conventional process for biodiesel production is transesterification or alcoholysis (typically methanolysis), by which the triglycerides are reacted with alcohols (typically methanol), in the presence of a catalyst, either homogeneous or heterogeneous, as a reaction promoter, to produce fatty acid alkyl esters [typically fatty acid methyl esters (FAME)] (Mahlia et al., 2020). Transesterification consists of several consecutive, reversible, and catalyzed reactions where the triglycerides are converted to diglycerides, monoglyceride, and finally glycerin (also known as glycerol) stepwise (Ong et al., 2019). Generally, biodiesel is produced using a single-step transesterification reaction catalyzed by alkali catalysts. However, depending on FFA and water content, a two-step reaction might be required where acid catalyzed alcoholysis, also known as esterification, precedes the transesterification process (Ashraful et al., 2014). The schematic diagram for one- and two-step biodiesel production is shown in **Figure 1**. The property standard of petroleum diesel and biodiesel, according to the American Society for Testing and Materials (ASTM) and European Standard (EN) are shown in **Table 2**.

DIFFERENT CATALYSTS FOR BIODIESEL PRODUCTION

The presence of catalyst increases the rate of the reaction, thereby increasing the yield of the product. Various catalysts are used in the transesterification process for biodiesel production. As discussed previously, the catalysts used for the transesterification reaction are intricate to the group. However, based on previous review articles, these can be divided into four major categories, namely, homogeneous catalysts, heterogeneous catalysts, biocatalysts, and nanocatalysts (Shan et al., 2018; Akubude et al., 2019), which can be further classified into different subgroups. The classification is shown in **Figure 2**.

Transesterification or alcoholysis can be catalyzed both homogeneously and heterogeneously. When catalyzed homogeneously, the reactions are faster typically and require lower loading than that of heterogeneously catalyzed ones. One major drawback of homogeneous catalysts is that the separation of these catalysts from the medium is intricate and often non-economical; as such, reuse of these is often impossible. Apart from that, several washing steps associated with the catalyst removal from the product results in the consumption of water, often deionized, and significant generation of wastewater (De Lima et al., 2016). On the other hand, heterogeneous catalysts are in a different phase than the reaction system, which allows for the removal of catalyst at various stages. These can be reused subsequently without intensive washing steps. Besides, high-purity glycerine can be obtained compared to that of homogeneous catalysis due to considerably fewer dissolved ions, allowing for further use in industrial processes. For the advantages mentioned above, transesterification using

TABLE 1 | Catalytic transesterification review details.

Title of the work	Content	References
"Modern heterogeneous catalysts for biodiesel production: A comprehensive review"	This work focused on different heterogeneous catalysts (acid, base, acid-base) and biocatalyst for biodiesel production	Chouhan and Sarma, 2011
"Inorganic heterogeneous catalysts for biodiesel production from vegetable oils"	This work reviews stable inorganic solid acid catalysts for biodiesel production from vegetable oils	Endalew et al., 2011
"Biodiesel production using enzymatic transesterification—Current state and perspectives"	This work discussed key operational variables that influence lipase activity and stability along with technological solutions for industrial implementation	Gog et al., 2012
"Recent developments on heterogeneous catalysts for biodiesel production by oil esterification and transesterification reactions: A review"	This article discusses the use of heterogeneous catalysts for esterification, transesterification and simultaneous esterification and transesterification	Borges and Díaz, 2012
"Heterogeneous catalysis for sustainable biodiesel production via esterification and transesterification"	This paper discusses the clean synthesis of biodiesel through heterogeneously catalyzed esterification and transesterification process	Lee et al., 2014
"Activity of solid acid catalysts for biodiesel production: A critical review"	This study reviews the activities and advantages of solid acid catalysts, their preparation method and prevailing reaction conditions affecting the catalytic activity	Sani et al., 2014
"State of the art of biodiesel production processes: a review of the heterogeneous catalyst"	This review focuses on various technologies used for biodiesel production, as well as the benefits and limitations of the different types of catalysts	Ruhul et al., 2015
"Heterogeneous basic catalysts for biodiesel production"	This review covers recent achievements in the field of basic heterogeneous catalysts for biodiesel production, focusing on the main systems being employed	De Lima et al., 2016
"Investigation of heterogeneous solid acid catalyst performance on low grade feedstocks for biodiesel production: A review"	This work investigates solid acid heterogeneous catalysts for biodiesel production	Mansir et al., 2017
"A review on latest developments and future prospects of heterogeneous catalyst in biodiesel production from non-edible oils"	This work focusses on heterogeneous catalysts with the highlight on the prospects of commercialization of those catalysts	Mardhiah et al., 2017
"State of the art and prospective of lipase-catalyzed transesterification reaction for biodiesel production"	The work reviews general and novel immobilizing materials, bioreactors for enzymatic transesterification, potential lipase resources, and process modeling for enzymatic transesterification	Amini et al., 2017a
"Application of nanoparticles in biofuels: An overview"	This study explores nanoparticles in biofuel processes such as biodiesel, biohydrogen, biogas, and bioethanol production	Sekoai et al., 2019
"Biodiesel synthesis using natural solid catalyst derived from biomass waste—A review"	This paper assesses the latest breakthroughs involved in the use of catalysts derived from waste biomass	Chua et al., 2020
"Carbon-based catalysts for biodiesel production—A review"	This study focusses on sulfonated carbon-based acid solids originating from either carbohydrate or biomass precursors	Clohessy and Kwapinski, 2020

heterogeneous catalysts has received increased attention over the past decade (Lam et al., 2010; Ling et al., 2019). However, partial leaching of the active sites, destruction of the catalyst microstructure, and organic deposition from the reaction mixture pose a problem for the applicability of these catalysts (Zhang et al., 2020). Therefore, the synthesis of active reusable heterogeneous catalysts is a great challenge in biodiesel production.

Homogeneous Catalysts

Homogeneous catalysis involves a sequence of reactions that is catalyzed by a chemical that is in the same phase as the reaction system. The most preferred catalyst used for the production of biodiesel is the homogeneous catalyst, as they are simple to use and require less time to achieve a complete reaction. Both acidic and basic catalysts come under this category. Homogeneous catalysts are usually dissolved in a solvent that is in the same phase with all reactants.

Base Catalyst

Homogeneous base catalysts are an alkaline liquid such as alkali metal-based hydroxides, namely, sodium or potassium

hydroxide; alkali metal-based oxides such as sodium and potassium methoxides; and carbonates. Base catalysts have high activity in transesterification (Endalew et al., 2011). Metallic hydroxides are frequently used as catalysts due to lower prices but generally possess lower activity than alkoxides. It was reported that the rate of base catalyzed reaction is 4,000 times faster than that of the acid-catalyzed one (De Lima et al., 2016). A known drawback is that the oil containing significant amounts of FFA cannot be converted into biodiesels completely but remains as soap in vast quantities (Helwani et al., 2009). Up to ∼5% FFAs, the reaction can still be catalyzed with an alkali catalyst, but an additional amount of catalyst is required to compensate for the catalyst lost to soap (Gerpen, 2005). Most studies recommend that the FFA content should be <2 wt.% for biodiesel production using the homogeneous catalyst.

Acid Catalyst

The esterification process is catalyzed by Brønsted acids, preferably by sulfonic and sulfuric acids as well as hydrochloric acid (Schuchardt et al., 1998). These catalysts produce very high yields in alkyl esters. However, the reactions are slower

FIGURE 1 | Biodiesel production from feedstock: **(A)** two-step process; **(B)** one-step process (Fattah et al., 2014d; Mofijur et al., 2014).
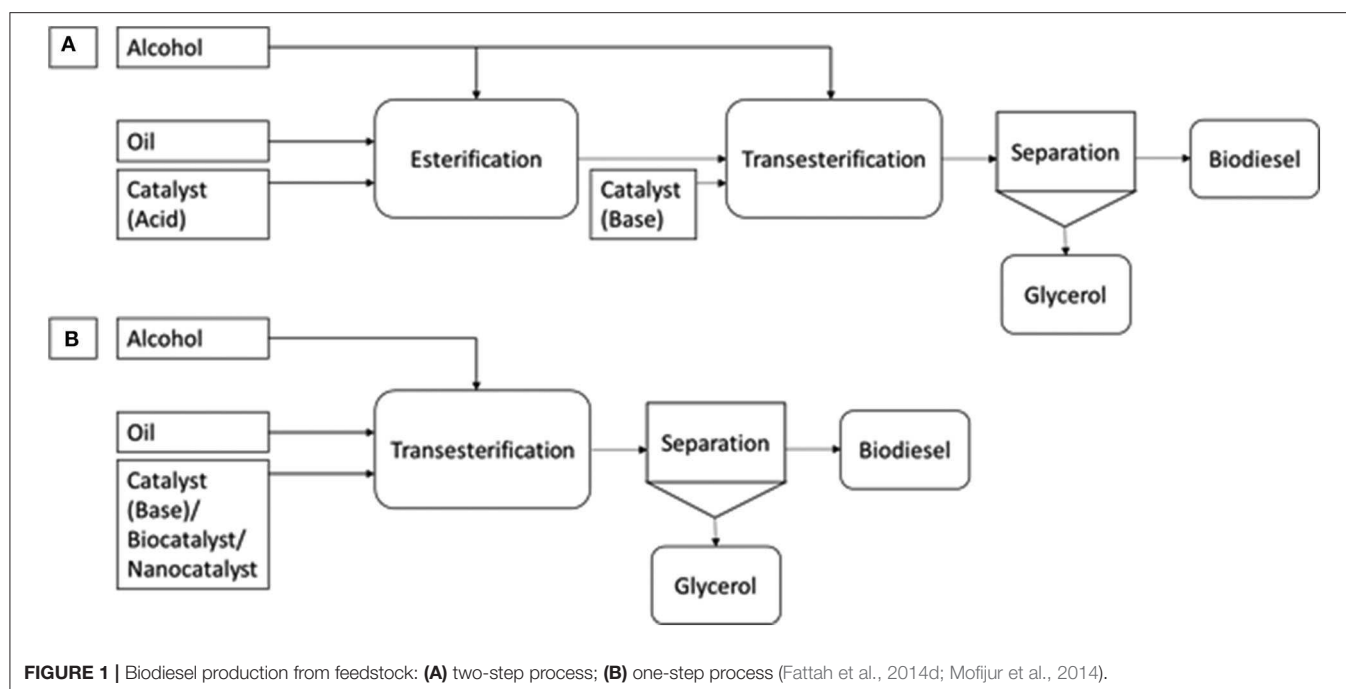
TABLE 2 | Comparison of standards for diesel and biodiesel ASTM and EN standards (Fattah et al., 2013; Knothe and Razon, 2017).

Property	Units	Diesel		Biodiesel (B100)	
		ASTM D975	EN 590	ASTM D6751	EN 14214
Density @ 15°C	kg/m^3		820–845		860–900
Kinematic Viscosity @ 40°C	mm^2/s	1.3–4.1	2–4.5	1.9–6.0	3.5–5.0
Cetane Number, Min.	–	40	51	47	51
Distillation temperature	% vol. recovered	90%: 282°C−338°C	85%: 350°C max	–	–
Ester content		5% vol. max	5% vol. max	–	96.5% min
Ash content, Max.	% wt	0.01	0.01	–	–
Sulfur Content, Max.	% mass	S500: 0.05% S5000: 0.50%	50 mg/kg 10 mg/kg	S15 15 ppm S500 0.05%	10.0 mg/kg
Flash Point	°C	60–80	Min. 55	100–170	Min. 120
Cloud Point	°C	–	Report	Location & season dependent	Location & season dependent
Cold Filter Plugging Point	°C	–	–	Location & season dependent	Location & season dependent
Lubricity, Max.	μm	520	–	460	–
Water and sediment, Max.	vol.%	0.05		0.05	
Water Content, Max.	mg/kg	–	200	-	500
Acid Value, Max.	mgKOH/g	–	–	0.5	0.50
Copper strip corrosion, Max	–	No. 3	Class 1	No. 3	Class 1
Carbon residue on 10% distillation residue, Max.	wt. %	0.15-0.35	0.3	0.05	–
Oxidation stability	–	–	25 g/m^3 max	Min. 3 h	Min 8 h
Iodine Value, Max.	g I$_2$/100 g				120

compared to alkali catalyzed reactions, making the process economically confronting due to the increased energy requirements (Silitonga et al., 2020). Homogeneous acid catalysis is insensitive to FFA content and can catalyze both esterification and transesterification reactions. Despite these added advantages, homogeneous acid catalysis presents the same separation issues as homogeneous base catalysis. Some

investigations using homogeneous catalysts to produce biodiesel from different biodiesel feedstocks are shown in **Table 3**.

Heterogeneous Catalysts

Heterogeneous catalysts are in a phase or state different from those of the reactants. These are the type of catalysts that creates active sites with its reactants regularly during a reaction

FIGURE 2 | Different catalysts used for biodiesel production.
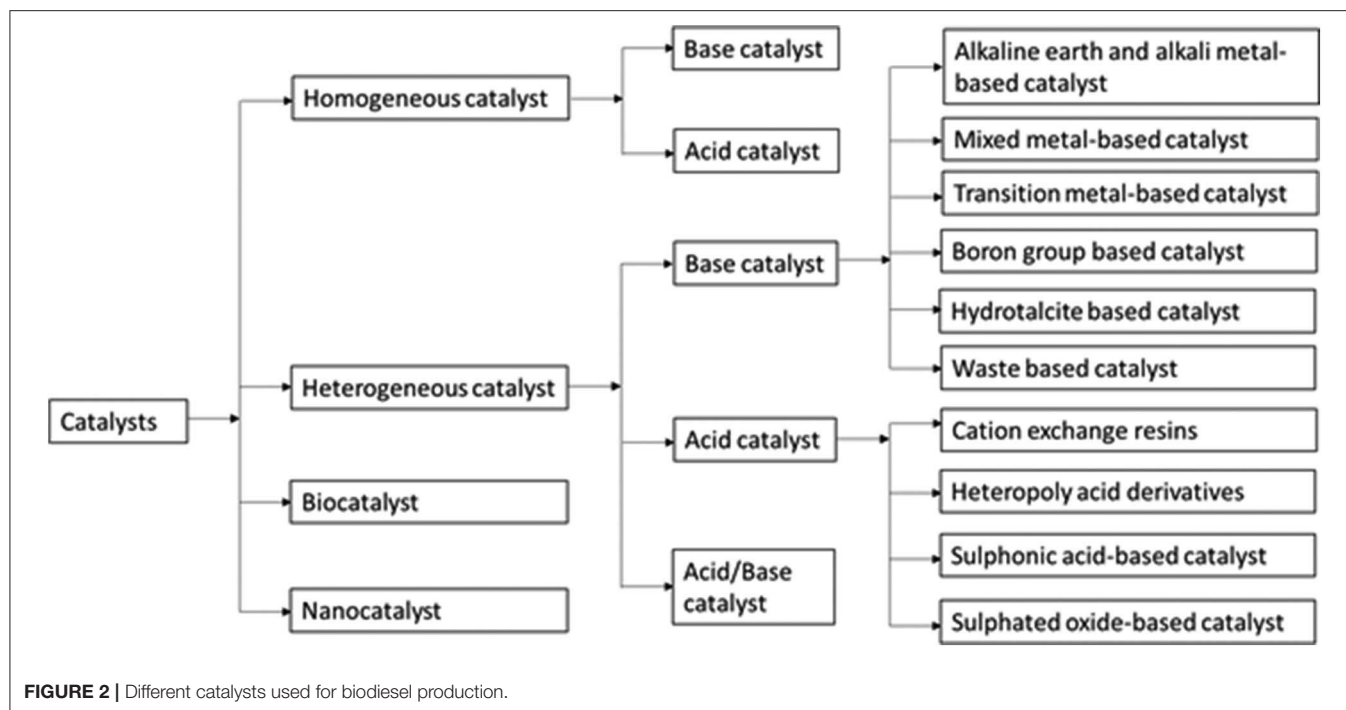
TABLE 3 | Homogeneous catalysts used for biodiesel production from different sources.

Feedstock	Catalyst	Reaction parameters	References
		Oil: alcohol ratio/ Catalyst amount/ Temperature/ Reaction time	
Madhuca longifolia oil	H_2SO_4, KOH	Ester.: 1: 0.35 v/v/ 0.01 v/v/ 60°C/ 30 min Trans.: 1:4 v/v/ 7 g/L/ 60°C/ 30 min	Saravanan et al., 2020
Elaeagnus angustifolia L seed oil	Potassium methoxide	9: 1 M*/ 1 wt.%/ 60 °C/ 1 h	Kamran et al., 2020
Rice bran oil	KOH	10:1 M/ 0.005 v/v/ 50°C/ 2 h	Goga et al., 2019
Sunflower oil	KOH	6:1 M/ 1 wt.%/ 60°C/ 3 h	Dueso et al., 2018
Castor oil	KOH	5.4:1/ 0.73 wt.%/ 64°C/ 2.5 h	Aboelazayem et al., 2018
Millettia pinnata oil	H_2SO_4, CaO	Ester.: 12:1 M/ 1% v/v / 60 °C/ 3 h Trans.: 6:1 M/ 1 wt.%/ 60°C/ 2 h	Ruhul et al., 2017
Jatropha curcas oil	H_2SO_4, NaOH	Ester.: 5:1 v/v/ 0.008 v/v/ 50 °C/ 2 h Trans.: 5:1 v/v/ 8 g/L/ 50°C/ 2 h	Dubey and Gupta, 2017
Rice bran oil	NaOH	6:1 M/ 2 wt.%/ 60°C / 2 h	Wakil et al., 2016
Calophyllum inophyllum oil	H_2SO_4, sodium methoxide	Ester.: 30:1 M/ 10 wt.% / 75°C/ 2 h Trans.: 7.5:1 M/ 1 wt.%/ 55°C/ 1.5 h	Jahirul et al., 2015
Aphanamixis polystachya oil	HCl, KOH	Ester.: 24:1 M/ 1% v/v/ 60°C/ 3 h Trans.: 6:1 M/ 1 wt.%/ 60°C/ 2 h	Palash et al., 2015
Palm oil	KOH	25% v/v/ 1 wt.%/ 60°C / 2 h	Fattah et al., 2014b
Calophyllum inophyllum oil	H_2SO_4, KOH	Ester.: 12:1 M/ 1.5% v/v/ 60°C/ 3 h Trans.: 6:1 M/ 1 wt.%/ 60°C/ 2 h	Fattah et al., 2014c
Ceiba pentandra oil	H_2SO_4, NaOH	Ester.: 8:1 M/ 1% v/v/ 60°C/ 2 h Trans.: 8:1 M/ 1 wt.%/ 50°C/ 1 h	Silitonga et al., 2013b

*M, Molar ratio.

(Melero et al., 2009). Heterogeneously catalyzed methanolysis reaction is very complex because it occurs in a three-phase system consisting of a solid (heterogeneous catalyst) and two immiscible liquid phases (oil and methanol). Some side reactions such as saponification of glycerides and methyl esters and neutralization of FFAs by catalyst also occur concurrently with methanolysis. The main disadvantages of this catalysis include elevated temperatures and higher oil/alcohol ratios than that of
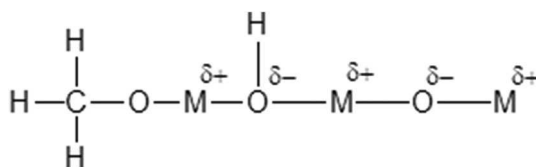
FIGURE 3 | Surface structure of metal oxides (M represents the metal).

the homogeneous catalysis. Other advantages include ease in separation and purification, as well as superior reusability of the catalyst, etc. Heterogeneous catalysts can be divided into acid and base catalysts. These catalysts can be classified as Brønsted or Lewis catalysts (Di Serio et al., 2008). However, in many cases, both types of sites could be present; as such, some of the catalysts can be used as a catalyst to both kind of reactions.

Base Catalyst

A heterogeneous base catalyst aims to overcome constraints such as saponification that hinders the separation of glycerol from the methyl ester layer, associated with the usage of a homogeneous base catalyst. These catalysts also show superior catalytic activity under mild conditions (Calero et al., 2014). These catalysts have many other advantages, namely, non-corrosiveness, environmental friendliness, and less problems in disposal. In addition, they are easily separated from the reaction environment and can be designed to give higher activity, selectivity and longer catalyst lifetime (Liu et al., 2008b). Many metal-based oxides, including alkali metal, alkaline earth metal, and transition metal oxides have been used as catalyst for the transesterification process of oils. The structure of metal oxides consists of positive metal ions (cations) that possess Lewis acid characteristics and negative oxygen ions (anions) that possess Brønsted base characteristics (Di Serio et al., 2008; Zabeti et al., 2009). Sometimes, two or more types of metal oxides are combined to be used as catalysts. Other types of catalysts that predominantly work as base heterogeneous catalysts are boron group-based and waste-based catalysts (Semwal et al., 2011).

Alkaline earth and alkali metal-based catalyst

Metal-based oxides are the most commonly exploited as a heterogeneous catalyst for transesterification. The surface structure of a metal oxide is presented in **Figure 3**. Zhang et al. (1988) demonstrated the basic properties of alkaline earth metal oxides using temperature-programmed desorption (TPD) of adsorbed carbon dioxide analysis. They showed that the amount of basic sites per unit weight approximately corresponds to that of the surface area and follows the sequence: CaO > MgO > SrO > BaO. The oxides of stronger basic sites promote the reaction more effectively.

Among the metal-based catalysts, CaO has been the most studied catalyst material for biodiesel production, as it presents many advantages, namely, long catalyst life, relatively high basic strength, high activity, and low solubility in methanol and requires only moderate reaction conditions (Roschat et al., 2016; Latchubugata et al., 2018). Arun et al. (2017) studied

the biodiesel production from *Terminalia belerica* and *Garcinia gummi-gutta* using calcinated CaO as a heterogeneous catalyst. The calcination process was done in a muffle furnace at 605°C for 5 h, which was preceded by drying in an oven at 125°C for 12 h. The transesterification was carried out at 60°C, 9:1 M methanol/oil ratio, and 2% w/v catalyst for 3 h. Properties of biodiesel produced from these feedstocks were within the range suggested by the American Society for Testing and Materials (ASTM) standard establishing a successful production. Roschat et al. (2016) carried out the transesterification of palm olein oil (FFAs of 0.29 mg KOH/g) using hydrated lime-derived calcium oxide (CaO) as a catalyst. The catalyst was prepared by drying overnight in an oven at 100°C, crushed and sieved, and then calcined in a furnace at different temperatures (700, 800, and 900°C) in the air for 3 h. A biodiesel yield of 97.20% was achieved for 800°C calcined sample. This catalyst could be reused for at least five times without significant yield deterioration (more than 90%).

Du et al. (2019) synthesized three novel carbon-based MgO solid bases using sol–gel and calcination method for biodiesel production from castor oil. These catalysts were identified as MgO-PVA-800, MgO-UREA-800, and MgO-GLY-800, where 800 indicates the calcination temperature, and PVA, UREA, and GLY stands for polyvinyl acetate, urea, and ethylene glycol, respectively. The transesterification was carried out at 12:1 M ethanol/oil ratio, 6 wt.% catalyst concentration at 75°C. The highest conversion rate of 96.5% was obtained with MgO-UREA-800 after 50 min under these conditions. The biodiesel yield for MgO-PVA-800 and MgO-GLY-800 was 93.6 and 91.8%, respectively, for the same reaction time. Manríquez-Ramírez et al. (2013) studied the catalyst activity of impregnated MgO with KOH, NaOH, and cerium nitrate. The basic strength of the samples followed the order: MgO–KOH > MgO–NaOH > MgO–CeO$_2$ as determined by Fourier-transform infrared spectroscopy (FTIR). The reaction was carried out at 60°C with oil/methanol ratio of 4:1, and the biodiesel yields after 1 h of reaction were 44, 56, 78, and <99% for MgO and MgO–CeO$_2$, MgO–NaOH, and MgO–KOH, respectively. It has been reported that MgO has low activity in transesterification of vegetable oils to biodiesel (Liu et al., 2007).

Roschat et al. (2018) studied the biodiesel production process of palm oil using strontium oxide (SrO) via the ethanolysis reaction. The optimum reaction condition for this work was determined experimentally as 80°C reaction temperature, ethanol/oil ratio of 12:1 M, catalyst loading amount of 5 wt.%, and reaction time of 3 h. This resulted in a yield of 98.2% fatty acid ethyl ester. The catalyst can be reused for five times with more than 90% yield. Liu et al. (2007) studied the transesterification of soybean oil to biodiesel using SrO as a solid base catalyst. They proposed the mechanism of the catalytic reaction of SrO, which creates basic intermediate compounds, thereby making it a solid base catalyzed reaction. The results showed that biodiesel yield was <95% at temperatures below 70°C within 30 min. The reusability of SrO was high and could maintain sustained activity even after 10 cycles.

Mootabadi et al. (2010) carried out ultrasonic-assisted transesterification of palm oil using different alkaline earth metal

oxides such as CaO, SrO, BaO, etc. as catalysts. They varied the reaction parameters, namely, reaction time of 10–60 min, alcohol/oil ratio of 3:1–15:1 M, catalyst loading of 0.5–3%, and ultrasonic amplitudes of 25–100%. Their results opposed the previously reported activity ranking of the catalysts as CaO < SrO < BaO. At optimum test conditions, 95% yield was reached in 1 h. When non-optimized conditions were used, the yield of 77.3, 95.2, and 95.2% was reported for CaO, SrO, and BaO catalysts, respectively, for 1 h reaction time. Dai et al. (2018) prepared lithium-based catalyst, lithium–iron oxide ($LiFe_5O_8$-$LiFeO_2$) by homogeneously mixing Fe_2O_3 in an aqueous solution of Li_2CO_3 and then heating this in a muffle furnace at different calcination temperatures and cooling to room temperature afterwards. The catalysts were then used to produce biodiesel from soybean oil where reactions were carried out at 65°C for 2 h utilizing methanol/oil ratio 36:1 M and 8 wt.% catalyst loading. The maximum conversion of 96.5% was achieved when the catalyst calcination temperature of 800°C was used. Moreover, the catalyst can be reused for at least five runs, maintaining the biodiesel yields close to 94%.

Mixed metal-based catalyst

Mixed metal-based oxides are predominantly used as base catalyst depending on the catalyst mixture. Their basicity can be tuned by altering their chemical composition and synthesis procedure (Teo et al., 2017). The type of synthesis method, activation temperature, and structure have a strong influence in the final basicity of the mixed oxides (Mckenzie et al., 1992; Tichit et al., 1995). They were sometimes used as a mixed acid–base catalyst by some researchers. Salinas et al. (2018) studied the catalytic activity of 1–5 wt.% La_2O_3 in ZrO_2 mixed metal oxides produced using sol–gel method and calcined at 600°C in biodiesel production from canola oil through methanolysis reaction. The sol–gel method allows for improving catalytic activity by modifying acid–base properties. It was found that La_2O_3 doped in ZrO_2 forms a monoclinic-ZrO_2 structure and enhances its basicity, which plays a key role in catalysis, and 3 wt.% La_2O_3 was the optimum percentage for the transesterification of canola oil. Limmanee et al. (2013) studied the catalytic activity of nanocrystallite CaMgZn mixed oxides as heterogeneous catalyst prepared using coprecipitation method using Na_2CO_3 as a precipitant in the synthesis of palm kernel oil biodiesel via methanolysis. They reported a maximum yield of 97.5 wt.% over the CaMgZn mixed oxide, prepared with the Ca/Mg/Zn ratio of 3:1:1 under the Na_2CO_3 concentration of 0.75 mol/L and the $CaMg(CO_3)_2$ and $CaZn(CO_3)_2$ metal ions ratio of 1.0 when the reaction conditions were methanol/oil ratio of 20:1 M, 6 wt.% catalyst and 60°C. Santiago-Torres et al. (2014) studied Na_2ZrO_3 as a basic catalyst for the transesterification of soybean oil. They reported a maximum biodiesel conversion efficiency of 98.3% at 3% of catalyst in 3 h of reaction time at 65°C reaction temperature. Lee et al. (2015) synthesized bifunctional acid–base catalyst comprising of mixed metal oxides of Ca and La (CaO–La_2O_3) at various Ca/La atomic ratios via coprecipitation. This integration enhanced the catalytic activity due to the dispersion of CaO on the composite surface, thereby increasing the surface acidic and basic sites compared

to individual oxides. They reported the highest biodiesel yield of 98.76% under conditions of 160°C, 3 h, 25:1 M methanol/oil ratio, and 3 wt.% catalyst.

Transition metal-based catalyst

Titanium oxide (TiO_2) and zinc oxide (ZnO) are among the transition metal oxides that are used as a heterogeneous base catalyst for biodiesel production (Yoo et al., 2010). Kaur et al. (2018) synthesized tungsten (W) supported TiO_2/SiO_2 catalyst using the sol–gel method to study transesterification of waste cottonseed oil to produce biodiesel. The complete transesterification reaction was achieved in 4 h with 1:30 M oil/methanol ratio, 5 wt.% catalyst at 65°C. They also reported good reusability with the catalyst being active in four catalytic runs without significant reduction in activity. Madhuvilakku and Piraman (2013) studied the catalytic activity of mixed oxides of Ti and Zn (TiO_2-ZnO) and ZnO by employing these in palm oil transesterification process. Biodiesel yield of 92% was attained with 200 mg catalyst loading of TiO_2-ZnO, 6:1 M methanol/oil ratio, and 60°C reaction temperature in 5 h. They also reported a better yield compared to ZnO catalyst (83%).

Boron group-based catalyst

Boron group-based compounds, especially alumina (Al_2O_3), are widely utilized for supporting different metal oxides, halides, nitrates, and alloys (Chouhan and Sarma, 2011). Kesserwan et al. (2020) reported on novel hybrid CaO/Al_2O_3 aerogel to catalyze the methanolysis of waste cooking oil. The catalyst was prepared by the rapid epoxide-initiated sol–gel process followed by calcination at 700°C under supercritical carbon dioxide conditions. They reported that, at optimized reaction condition of 11:1 M methanol/oil ratio, 1 wt.% of 3:1 CaO/Al_2O_3 calcined aerogel, 65°C reaction temperature, and 4 h reaction time results in a maximum biodiesel yield of 89.9%. Benjapornkulaphong et al. (2009) studied various Al_2O_3-supported alkali and alkali earth metal nitrates, namely, $LiNO_3/Al_2O_3$, $NaNO_3/Al_2O_3$, $Ca(NO_3)_2/Al_2O_3$, KNO_3/Al_2O_3, and $Mg(NO_3)_2/Al_2O_3$ produced by impregnation method followed by calcination at 450–850°C. They employed these to catalyze the methanolysis of palm kernel oil and coconut oil. They found that calcination temperature affects the yield significantly with $Ca(NO_3)_2/Al_2O_3$ and $LiNO_3/Al_2O_3$ yielding <90% biodiesel when calcined at 450°C, and higher calcination temperature dropped the biodiesel yield. They recommended a catalyst amount of 10 wt.% and 15–20 wt.% of $Ca(NO_3)_2/Al_2O_3$ catalyst for transesterification of palm kernel oil and coconut oil, respectively, when methanol/oil ratio of 65:1 M, temperature of 60°C, and reaction time of 3 h were used.

Hydrotalcite-based catalyst

"Hydrotalcites are a class of anionic and basic clays with a general formulas of $M_{1-x}^{2+}M_x^{3+}(OH_2)^{x+}(A_{x/n})^{n-}.yH_2O$ where M^{2+} and M^{3+} are divalent and trivalent metals, respectively, $A^{n-}(CO_3^-, SO_4^{2-}, Cl^-, NO_3^-)$ is an n-valent anion, and x usually has a value between 0.25 and 0.33" (Helwani et al., 2009; Endalew et al., 2011). Hydrotalcites are predominantly used as heterogeneous base catalyst. The advantages of these catalysts are

their tunable high basic strength obtained by changing the ratio of Mg/Al and the inherent better catalyst morphology compared to alkaline earth metal oxides. However, nonhomogeneity and sensitiveness to FFA and water are the major disadvantages for this type of catalysts. Navajas et al. (2018) studied the catalytic activity of Mg–Al hydrotalcite with Mg/Al ratios of 1.5–5 M, synthesized by coprecipitation, in transesterification of sunflower oil. They reported an optimum conversion of 96% under methanol/oil ratio of 48:1 M, 1 atm, 60°C, 2 wt.% of the catalyst after 24 h. They attributed the activity of catalyst to the presence of Brønsted-type basic sites at the edges of the crystal. Nowicki et al. (2016) studied the catalytic performance of Zr-doped Mg–Al hydrotalcite with varying Zr/Mg molar ratios in transesterification of refined rapeseed oil. They found that tetravalent cation of Zr (Zr^{4+}) was effective in significantly increasing the catalytic activity of the catalyst. They reported the optimum oil conversion of 99.9% for hydrotalcite with the ratio of Zr/Mg/Al = 0.45:2.55:1 M and the reaction condition of 373–393 K temperature, 4.8−5.0 atm pressure, and 6 h reaction time. Trakarnpruk and Porntangjitlikit (2008) studied the catalytic activity of K-loaded calcined Mg–Al hydrotalcite (Mg/AL = 4) in transesterification of palm oil with methanol. They found that the catalyst acts as a basic catalyst. They also reported an 86.6% methyl ester yield at reaction parameters of 30:1 M methanol/oil ratio, 100°C, and 7 wt.% catalyst for 6 h. Zeng et al. (2009) reported that immobilization of Saccharomyces cerevisiae lipase (a biocatalyst) on Mg–Al hydrotalcite (Mg/Al molar ratio, 4.0) by physical adsorption markedly improved performance of the enzyme. The transesterification of refined rape oil was carried out with immobilized lipase (1.5 wt.%) and under atmospheric pressure at 45°C with 96% ester conversion in 4.5 h. The biocatalyst maintained high activity with 81.3% ester conversion after 10 reuse cycles.

Waste-based catalyst

Waste derived from industrial processes and surrounding environment can aid in the development of a low-cost solid base catalyst. These catalysts can promote a sustainable and environment-friendly approach toward biodiesel production (Majhi and Ray, 2016; Pandit and Fulekar, 2017). Calcium-enriched waste products, namely, shells of mussel, egg, cockle, snail, and oyster; fish scales; animal bones; and ash derived from plant species, etc. are easily available at low cost (Marwaha et al., 2018). Calcium obtained from these waste materials could be converted to CaO, which is the most versatile heterogeneous base catalyst, as discussed previously. Yaşar (2019) studied the catalytic activity of waste-eggshell-based CaO and compared it to the pure CaO. Transesterification of rapeseed oil was carried out at 9:1 M methanol/oil ratio, 4 wt.% catalyst, and 60°C reaction temperature for 1 h. The maximum yield for these conditions was 96.81 and 95.12% for CaO and waste-eggshell-based CaO, respectively. Sirisomboonchai et al. (2015) studied the catalytic activity of calcined scallop shell in the transesterification of waste cooking oil using methanol. A yield of 86% was observed in the presence of small amount of water with 5 wt.% catalyst loading, 6:1 M methanol/oil ratio, and 65°C reaction temperature for 2 h. The same catalyst was used for four cycles with 20% reduction

of FAME yield owing to the formation of Ca-glyceroxide on its surface. Hu et al. (2011) studied the catalyst derived from waste freshwater mussel shell in transesterification of Chinese tallow oil. The catalyst was synthesized using the calcination–impregnation–activation method. The mussel shell was first calcined at 900°C followed by impregnation in deionized water and activated by calcination at 600°C for 3 h. Over 90% yields was obtainable with 12:1 M methanol/oil ratio, 5 wt.% catalyst, and reaction temperature of 70°C in 1.5 h. The catalyst also exhibited excellent reusability with only 10–15% decrease in yield after 12 runs.

Acid Catalysts

Heterogeneous acid catalysts have a less corrosive and toxic effect and give rise to fewer environmental problems compared to homogeneous acid catalysts (Aransiola et al., 2014). These catalysts contain a variety of acidic sites with different strengths of Brønsted or Lewis acidity. While these catalysts provide encouraging results under moderate reaction conditions, they react very slowly compared to solid base catalysts. In addition, high catalyst loading, high temperature, and long reaction time are required to employ this type of catalysts (Mansir et al., 2017).

Cation-exchange resins

Many researchers have used cation-exchange resin for biodiesel production at laboratory scale. Cation exchange resins are macroporous and contain numerous acidic sites to catalyze FFAs to biodiesel through heterogeneous esterification reactions and prevent saponification. Fu et al. (2015) studied the catalyst activity of sulfonated polystyrene-divinyl benzene (ST-DVB-SO_3H) macroporous resin in the esterification of high FFA (acid value, 64.9 mg KOH/g) oil. Maximum FFA conversion of 97.8% was achieved when the reaction was carried out under the following conditions: 10 wt.% catalyst loading, methanol/oil ratio of 15:1 M, and 100°C for 3 h. Feng et al. (2011) studied continuous esterification of waste fried oil with an acid value of 36.0 mg KOH/g in a fixed bed reactor using commercial cation-exchange resin (NKC-9). They reported a 98% conversion rate during 500 h run under 2.8:1 methanol/oleic acid mass ratio, 44.0 cm catalyst bed height, 0.62 ml/min feed flowrate, and 65°C reaction temperature.

Heteropoly acid derivatives

Heteropoly acids (HPAs) and their salts as solid (heterogeneous) acid catalysts are also used frequently for the production of biodiesel (Hanif et al., 2017; Alcañiz-Monge et al., 2018). HPAs having a Keggin structure are preferably used because they have high thermal stability and can be synthesized easily compared to other types of HPAs. However, Keggin-type HPA has a low specific surface area, which can be overcome using appropriate supportive material. HPAs supported on the carriers are used in biodiesel production because of their structural mobility and superacidity. Kurhade and Dalai (2018) studied 12-tungstophosphoric acid (TPA) ($H_3PW_{12}O_{40}.nH_2O$) impregnated on the γ-Al_2O_3 catalyst for the biodiesel production. An optimized conversion of 94.9 ± 2.3% can be achieved with 10 wt.% of the catalyst loading, 17.5:1 M

methanol/oil ratio, 200°C, and 4 MPa in 10 h. A conversion of 90.3 ± 4.3% was achieved after the second run. Siddiquee et al. (2011) studied the catalytic activity of mesoporous ordered silica, SBA-15 impregnated with the HPA in the production of biodiesel from the lipid of wastewater sludge. The experiment was carried out in a microreactor setup under varying operating conditions. A biodiesel yield of 30.14 wt.% was obtained with 15% HPA at a temperature of 135°C and a pressure of 135 psi in 3 h reaction time.

Sulfonic acid-based catalysts

Sulfonic acid group catalysts are characterized by sulfonated cross-linked polystyrene and are generally less corrosive and environmentally benign (Mansir et al., 2017). These type of catalysts have enhanced activity due to the attraction of fatty acids and tails of alcohol by the polymer support. In addition, the strong sulfonic acid group attached to the polymer chains increases the acidity of the sites (Vaccari, 1999). The typical examples of these catalysts are nonporous Nafion resins and porous Amberlysts. Liu et al. (2008a) studied the synthesis of mesoporous solid acid catalysts based on sulfonic acid functionalized ordered mesoporous carbons (OMC-SO$_3$H) to use as a heterogeneous acid catalyst for esterification of oleic acid with ethanol. The esterification was performed under an N$_2$ atmosphere in a closed flask at 80°C. The results showed that this catalyst is highly efficient due to its high acid density and hydrophobic surface property. Andrijanto et al. (2012) studied sulfonic acid catalysts supported on hypercrosslinked polystyrene (D5082) for the esterification of oleic acid with methanol. The results showed that D5082 had high catalytic activity despite showing low concentrations of acid sites and acid site strengths, which they attributed to the high accessibility of acid sites throughout the catalyst particles.

Sulfated oxide-based catalyst

Sulfated metal oxides generally work as an acid heterogeneous catalyst in esterification reaction (Chen et al., 2007; Shi et al., 2016). Kaur and Ali (2015) studied the efficacy and reusability of Ce/ZrO$_2$-TiO$_2$/SO$_4^{2-}$, a catalyst in the esterification of oleic acid with methanol or ethanol. The catalyst activity of this catalyst is a function of its Brønsted acidic sites, which depends on the cerium concentration. A 2 wt.% cerium in the catalyst, when calcined at 600°C, showed the highest catalytic activity. With 5 wt.% catalyst, 6:1 M methanol/oil ratio at 65°C and 1 h reaction time achieved <98% conversion for the esterification of vegetable oil. They also reported no significant loss in the catalyst activity until the fifth cycle. Ropero-Vega et al. (2010) studied the catalytic activity of titania sulfated with ammonium sulfate [TiO$_2$/SO$_4^{2-}$-(NH$_4$)$_2$SO$_4$] as well as sulfuric acid (TiO$_2$/SO$_4^{2-}$-H$_2$SO$_4$). They found that sulfated samples showed strong acidity as determined using Hammet indicators. The FTIR analysis of TiO$_2$/SO$_4^{2-}$-(NH$_4$)$_2$SO$_4$ and TiO$_2$/SO$_4^{2-}$-H$_2$SO$_4$ showed the presence of both Lewis and Brønsted acid sites and only Lewis-type sites, respectively. Further analysis showed very high activity for the esterification of fatty acids with ethanol in a mixture of oleic acid (79%). Up to 82.2% conversion of oleic acid was achieved after 3 h of reaction at 80°C.

Acid/Base Catalyst

As discussed previously, oil with high FFA content requires an acid catalyst to esterify the FFA content before transesterification can take place. For biodiesel production from these type of oils, a heterogeneous catalytic system with both acidic and basic sites is capable of esterification and transesterification with minimal soap formation is highly sought after (Semwal et al., 2011). This type of catalysts possesses "Lewis acid" sites, which take part in the esterification reaction of the carboxylic acid with methanol as well as conjugated basic sites that influence the transesterification of triglyceride with methanol. Depending on the type of reactant and reaction parameters, this type of catalysts can work as an acid catalyst, base catalyst, or bifunctional one.

Zirconia and its derivatives

Zirconium dioxide (ZrO$_2$), also known as zirconia, is used as both acid and the base heterogeneous catalyst. The primary nature of this catalyst is acidic, as it has strong surface acidity (Lam et al., 2010). Other derivatives of zirconia include sulfated ZrO$_2$ (Shi et al., 2016), metal oxides with ZrO$_2$ (Guldhe et al., 2017), metal-supported zirconia (Wan Omar and Amin, 2011), zirconia supported metal oxides (Kim et al., 2012), etc. Ibrahim et al. (2019) studied the catalytic activity of ZrO$_2$ loaded into different supports, namely, Al$_2$O$_3$, Fe$_2$O$_3$, TiO$_2$, and SiO$_2$ using hybrid sol–gel autocombustion method. Highest conversion of biodiesel of 48.6% was achieved using alcohol/acid ratio of 120:1 M, 0.1 mass% catalyst, and 120°C reaction temperature for 3 h when ZrO$_2$/SiO$_2$ was used. In addition, the catalyst could be reused five times without significant loss of catalytic activity. Guldhe et al. (2017) studied tungstated zirconia (WO$_3$/ZrO$_2$) as a heterogeneous acid catalyst for the synthesis of biodiesel for S. obliquus lipids. FTIR characterization of catalyst showed the presence of both Brønsted and Lewis acid sites. Optimized biodiesel conversion of 94.58% was achieved at 100°C temperature, 12:1 M methanol/oil ratio, and 15 wt.% of catalyst amount in 3 h. Sun et al. (2010) studied ZrO$_2$ supported La$_2$O$_3$ as a catalyst for the transesterification reaction of sunflower oil with methanol to produce biodiesel. The catalyst was prepared by an incipient wetness impregnation method, followed by drying at 110°C overnight and calcination at 600°C for 4 h in air. They reported that biodiesel conversion was possible due to the basic nature of the catalyst, which was determined using TPD of adsorbed CO$_2$ and 21 wt.% La$_2$O$_3$ loaded on ZrO$_2$ showed the highest basicity. The optimized test conditions were 30:1 M methanol/oil ratio, 200°C reaction temperature, and 5 h of reaction time that resulted in 84.9% biodiesel yield for each case.

Zeolite-based catalyst

Zeolites occur naturally in the form of microporous crystalline aluminosilicates interlinked by oxygen atoms. The chemical composition, pore size structure, and ion exchange properties of zeolites are responsible for their versatile catalytic behavior (De Lima et al., 2016). Zeolite framework structure contains molecular pores and channels of equal sizes, which can absorb molecules that fit into these and exclude the larger ones. This property of zeolite helps to exchange ions that in turn produce negative ion within the structure of the catalyst, thereby

emerging as a base catalyst (Hattori, 1995; Mansir et al., 2017). The base strength of the alkali ion-exchanged zeolite increases with increasing electropositivity of the exchange cation. Both synthetic and natural zeolites are being pursued as promising catalysts. Zeolites have unique properties as catalysts, namely, shape selectivity, ability to maintain electro-neutrality through cation–polar molecules reversible interactions, etc. The weak basic strength and small catalytic pore diameter are the main problems reported for basic zeolite catalysts (Endalew et al., 2011). These can also be used as an acid heterogeneous catalyst.

Li et al. (2019) studied alkaline Li/NaY zeolite catalysts with different molar ratios of Li_2CO_3 to NaY zeolite in the transesterification of castor oil with ethanol. The ideal catalyst was synthesized from fly ash using coprecipitation method with ratio of Li_2CO_3 to NaY zeolite of 1:1 M calcined at 750°C for 4 h. The fatty acid ethyl ester yield of 98.6% was obtained for the reaction conditions of ethanol/oil ratio of 18:1 M, 3 wt.% catalyst, and reaction temperature of 75°C for 2 h. Du et al. (2018) studied the catalytic activity of NaY zeolite-supported La_2O_3 catalysts in the production of castor oil biodiesel. They produced the optimized catalyst, S-La_2O_3/NaY-800, by physically mixing the zeolite NaY, sodium carboxymethyl cellulose (CMC), lanthanum oxide and kaolin (mass ratio of NaY/kaolin/La_2O_3/CMC = 70:20:10:2.5). A surfactant (4 wt.%) was added to this mixture and then calcined at 800°C. Under the optimized reaction conditions: ratio of ethanol to oil of 15:1 M, 10 wt.% catalyst, and reaction temperature of 70°C for 50 min; 84.6% fatty acid ethyl ester was obtained. Doyle et al. (2016) studied the acidic catalytic activity of zeolite Y with Si/Al ratio of 3.1, in the esterification of oleic acid. The optimum oleic acid conversion using the zeolite catalyst was 85% with 6:1 M ethanol/oleic acid ratio, 5 wt.% catalyst loading, and 70°C for 1 h reaction time.

Biocatalysts

The pathway of biodiesel production through chemical catalysis is energy consuming and produces undesired by-products, namely, soaps and polymeric pigments, which hinder the separation of product from glycerol and di- and monoacylglycerols (Gog et al., 2012). Using biocatalysts, these impediments can be eliminated. Biocatalysts, also known as enzymes, are acquired from living organisms that promote chemical reactions without affecting themselves chemically (Amini et al., 2017a,b). Two types of enzymatic biocatalyst are usually used in biodiesel production, namely, extracellular lipases and intracellular lipases. Extracellular lipases are the enzymes that have been recovered from the microorganism broth and then purified. Intracellular lipase, on the other hand, remains either in the cell-producing walls or inside the cell. The major producer microorganisms for extracellular lipases are *Rhizopus oryzae*, *Mucor miehei*, *Candida antarctica*, and *Pseudomonas cepacia*. The commercial immobilized lipases that has been studied thoroughly are Novozym 435, Lipozyme TL IM, Lipozyme RM IM, and Lipase PS-C (Gog et al., 2012). The drawback of using extracellular enzymes as catalyst is the complexity of separation and purification procedures and its associated cost. This can be lowered using microbial cells as whole-cell biocatalysts with acceptable biodiesel yield. Filamentous fungi have been discerned

as whole-cell biocatalysts. However, lipase used in whole-cell form cannot be reused at the end of the reaction.

Unlike the chemical catalysts, biocatalysts apply to a wide range of triglyceride sources, with FFA ranging from 0.5 to 80% (Aransiola et al., 2014). Other advantages of enzymatic biodiesel production include easy product removal, moderate process temperature (35–45°C), zero by-product, and reusability of catalysts (Christopher et al., 2014; Mardhiah et al., 2017). The key parameters affecting the biodiesel yield for enzymatic synthesis are presented in **Figure 4**. As seen in the figure, various factors such as choice of lipase, choice of substrate, substrate concentration, pH of the microenvironment, temperature, spacing between the enzyme molecules and the substrate, etc. affect the biodiesel yield for enzyme-catalyzed transesterification. Some investigations using enzyme-catalyzed transesterification of different biodiesel feedstocks are presented in **Table 4**. As seen from the table, the efficiency of biocatalyzed transesterification process is dependent on enzyme source and operational conditions.

Nanocatalysts

Recently, nanocatalysts have gained significant attention for biodiesel production owing to their high catalytic efficiency (Qiu et al., 2011). These catalysts have a high surface area that results in increased activity compared to conventional catalysts. In addition, these catalysts possess high stability, superior resistance to saponification, efficient surface/volume ratio, and high reusability (Rahmani Vahid et al., 2017). Nanocatalysts can be synthesized using various methods. Some of the methods include self-propagating high-temperature synthesis, microwave combustion, conventional hydrothermal, microwave hydrothermal, microwave solvothermal, sol–gel technique, coprecipitation, impregnation, gas condensation, chemical vapor deposition, electrochemical deposition, vacuum deposition and evaporation, etc. (Quirino et al., 2016; Ambat et al., 2018). Characterization of these catalysts is critical before it can be used for biodiesel production. Different methods have been used to achieve this so far. The most commonly used method for characterization of composition and crystallinity of these catalysts is X-ray diffraction (XRD). The morphology of prepared nanocatalysts and their precursors are determined using scanning electron microscopy (SEM). To analyze the particle diameter and morphology of the catalysts, transmission electron microscopy (TEM) is used. Other characterization methods include Fourier transform infrared (FTIR) spectroscopy that is used for determining assimilation of phases, Barrett–Joyner–Hlenda (BJH) and Brunauer–Emmett–Teller (BET) methods for specific surface area calculation, and thermogravimetric analysis (TGA) for examining the decomposition nature of catalyst samples, etc. (Nayebzadeh et al., 2017; Baskar et al., 2018). Some of the latest works on nanocatalysts for the transesterification reaction are summarized in **Table 5**. As seen from the table, nanocatalyst can achieve high FAME yield with very mild reaction conditions and short reaction times. The reusability of these catalysts is also excellent, as these retain good activity even after 11 cycles depending on the catalyst.

FIGURE 4 | Crucial parameters affecting the biodiesel yield in enzymatic synthesis (Szczesna Antczak et al., 2009).
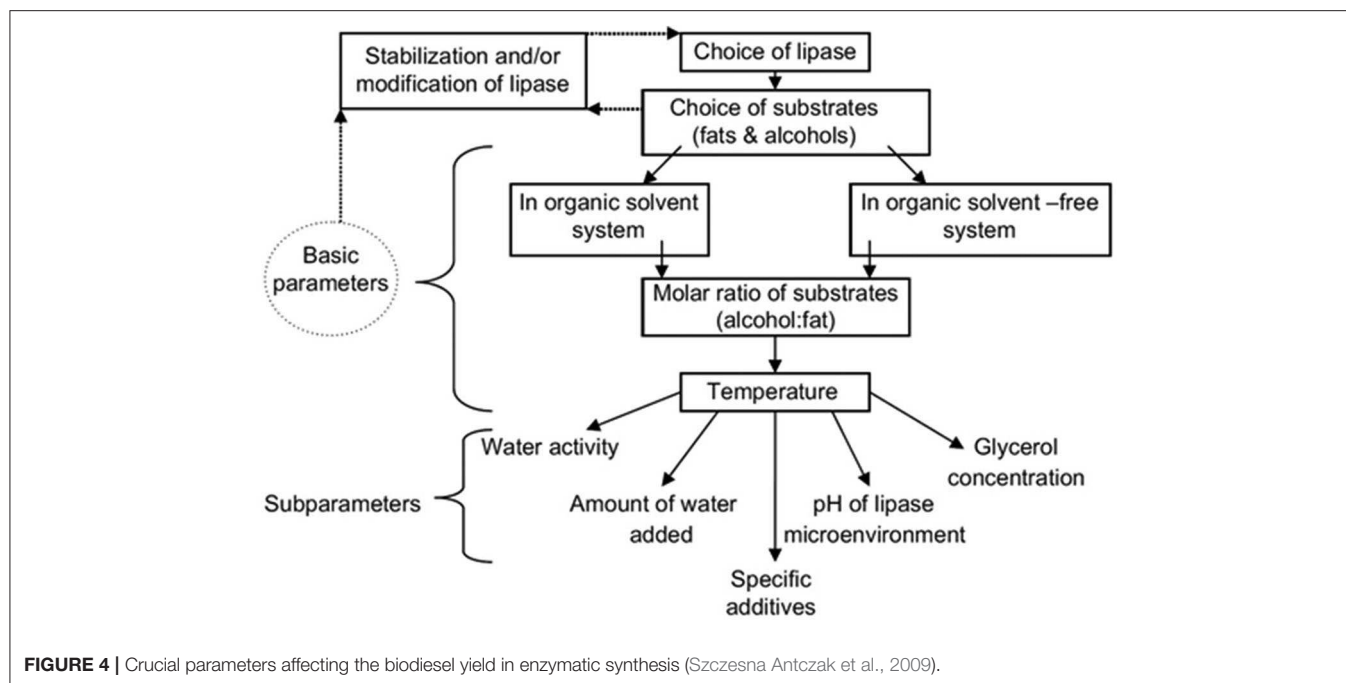
TABLE 4 | Various biocatalysts used for biodiesel production from different sources.

Feedstock	Catalyst	Reaction parameters	Yield (%/wt.%)	References
		Alcohol/Oil to alcohol ratio/Catalyst amount (wt.%)/Temperature (°C)/Reaction time		
Waste cooking oil	Pancreatic lipase	Methanol/3:1/1.5/60/4 h	88%	Jayaraman et al., 2020
Residual fish oil	Novozym 435 lipase	Ethano/35.45:1/35/8 h	82.91 wt.%	Marín-Suárez et al., 2019
Rice bran oil	Rice bran lipase	Methanol/6:1/N.A./40/12 day	83.4 wt.%	Choi et al., 2018
Ocimum basilicum seed oil	Novozym 435 lipase	Methanol/11:1/6/47/68 h	89%	Amini et al., 2017b
Waste vegetable oil	Epobond *Pseudomonas cepacia*	Ethanol/3:1/3/37/1.5 h	46.32%	Lopresto et al., 2015
Calophyllum inophyllum	*Rhizopus oryzae* lipase	Methanol/12:1/20/35/25 h	92%	Arumugam and Ponnusami, 2014
Jatropha curcas	Immobilised *Burkholderia cepacia*	Ethanol/10:1/5.2mg/24 h	78%	Abdulla and Ravindra, 2013
Castor oil	Lipozyme *Thermomyces lanuginosa* IM.	Methanol/3:1/15/45/24 h	67.58 wt.%	Maleki et al., 2013
Corn oil	Lipozyme *Thermomyces lanuginosa* IM.	Ethanol/6:1/2.8/35/12 h	69.2 wt.%	Mata et al., 2012
Pistacia chinensis bge seed oil	*Rhizopus oryzae* lipase	Methanol/5:1/25 IU$_{AI-ROL}$/g/37/60 h (anion exchange resin)	92%	Li et al., 2012
Pistacia chinensis bge seed oil	*Rhizopus oryzae* lipase	Methanol/5:1/7 IU$_{MI-ROL}$/g/37/60 h (macroporous resin)	94%	Li et al., 2012
Jatropha curcas	*Pseudomonas cepacia*	Ethanol/4:1/5–8/40/24 h	98%	Shah and Gupta, 2007

PERSPECTIVES, CHALLENGES, AND FURTHER WORK

Table 6 summarizes the advantages and disadvantages of different types of catalyst based on the above discussion.

Homogeneous catalyst has been exhaustively studied, and challenges have been addressed in the literature. On the other hand, heterogeneous catalysts is a relatively new research area on which significant research is ongoing at present. Several challenges have been reported in the literature for these catalysts:

TABLE 5 | Various nanocatalysts used for biodiesel production from different sources.

Catalyst	Feedstock	Reaction parameters	No of cycle	FAME yield/Conversion (%)	References
		Methanol to oil molar ratio/Temperature (°C)/Catalyst (wt.%)/Time (h)			
$NaAlO_2/\gamma\text{-}Al_2O_3$	Palm oil	20.79:1/64.72/10.89/3	1	97.65	Zhang et al., 2020
			6	93.29	
$25\%MoO_3/B\text{-}ZSM\text{-}5$	Oleic acid	20:1/160/3/6	1	98	Mohebbi et al., 2020
			6	93	
$CaO/CuFe_2O_4$	Chicken fat	15:1/70/3/4 h	1	94.52	Seffati et al., 2019
			–	–	
$KOH/Fe_3O_4@Al_2O_3$	Canola oil	12:1/65 /4/6	1	98.8	Kazemifard et al., 2018
			6	88.4	
$MgO/MgFe_2O_4$	Sunflower oil	12:1/110/4/4	1	91.2	Alaei et al., 2018
			6	82.4	
$Cr/Ca/\gamma\text{-}Al_2O_3$	Cooking oil	18:1/65/6/3	1	92.79	Sulaiman et al., 2017
			6	78.29	
$MgO/MgAl_2O_4$ (untreated and treated with plasma)	Sunflower oil	12:1/110/3/3	1	95.7/96.5	Rahmani Vahid et al., 2017
			5	79.3/91.1	
$\gamma\text{-}Al_2O_3/KI$	Palm oil	14:1/60/4/4	1	98	Islam et al., 2015
			11	79	
$Ca/\gamma\text{-}Al_2O_3$	Corn oil	12:1/65/6/5	1	87.89	Moradi et al., 2015
			5	34.64	
$Cs/Al/Fe_3O_4$	Sunflower oil	14:1/58/6/2	1	95	Feyzi et al., 2013
			4	88	

TABLE 6 | Advantages and disadvantages of different types of catalysts.

Catalyst type	Advantages	Disadvantages	Examples
Homogeneous base catalyst	Strong catalytic activity Inexpensive and widely available No corrosive Ideal for TGAs with low FFA	Possible formation of soap Not suitable for feedstock with high FFA No reusability Requires extensive washing	Sodium or potassium hydroxide; Sodium and potassium methoxides, and carbonates
Homogeneous acid catalyst	Strong catalytic activity Suitable for feedstock with high FFA Do not form soap	The reaction rate is slower compared to the base catalyst Separation and reuse unusual Corrosion problem	Sulfonic acid, sulfuric acid, hydrochloric acid
Heterogeneous base catalyst	Ease of purification of the product Effluent generation minimized Catalyst can be reused	High cost to synthesise catalyst Leaching of active sites may occur	Alkaline earth and alkali metal oxides, transition metal oxides, mixed metal oxides, hydrotalcite
Heterogeneous acid catalyst	Ease of separation Catalyst can be reused	High cost to synthesise catalyst Higher alcohol-to-oil molar ratios High catalyst concentrations Longer reaction time May undergo deactivation	Cation exchanges reins, heteropoly acid derivatives, sulphated oxides, sulphonic acids
Biocatalyst	Ease of separation Mild reaction condition Produces high purity product Insensitive to FFA and water content in the oil Preferred method for low-grade oil	High cost for catalyst synthesis Sensitive to methanol, causing deactivation of the enzyme Very slow reaction rate	Extracellular lipases (Mucor miehei, Rhizopus oryzae, Candida antarctica, Pseudomonas cepacia) and intracellular lipases (Filamentous fungi)
Nanocatalyst	High activity and stability High reusability Mild reaction condition	High cost for catalyst synthesis	Zn, Ca, Mg, Zr based nanocatalysts

1. Short catalyst life, lower reaction rate, and instability have been reported as the main problems for heterogeneous catalysts.
2. Solid base catalysts were reported to be sensitive to CO_2, water, and FFA. These consume and deactivate the catalyst via saponification.
3. Solid acid catalysts were reported to induce leaching and product contamination due to the ionic group being hydrolyzed by water.
4. Lipase inhibition has been reported in the presence of methanol during enzymatic transesterification.
5. In the case of nanocatalysts, at relatively mild operating conditions, it is necessary to increase the reaction time to achieve high performances. However, it is essential to apply severe operating conditions to achieve ordinary reaction times, thereby increasing the energy requirement.

The following aspects need to be addressed in future works:

1. Further investigation into waste-derived catalysts are necessary to develop new catalysts with improved catalytic performance.
2. Development of highly active and selective heterogeneous catalysts that are economically feasible for use in the industrial scale.
3. Exploring new catalyst supports with selective surface area and interconnected system of appropriate pore sizes.
4. Exploring biomass or waste as the source of catalyst to reduce the associated cost and improve sustainability for commercially available solid catalysts.
5. Improving preparation routes and treatment steps for hydrotalcite-based catalysts to transform their application from laboratory to industrial scale.
6. Improving the sensitiveness to FFA and water and the morphology by keeping high basic strength of zeolite-based catalyst.
7. Further investigation into industrial enzymatic biodiesel production for an ensuring viable future option.
8. Energy-efficient and low-cost methods for effective recovery and reuse of nanocatalysts.

CONCLUSION

Laboratory-scale biodiesel production using heterogeneous catalysts have been reported at length in the literature. Among the catalysts, base homogeneous catalysts possess rapid reaction rate and high yield and require mild operating conditions.

However, those are sensitive to FFA content of the oil that causes undesired by-products, namely, soaps and polymeric pigments, making the purification process difficult and impossible to reuse the catalysts. Homogeneous acid catalysts are suitable for those high FFA content oil. However, they suffer some drawbacks, including relatively slow reaction rate, corrosive nature, difficulty in catalyst separation from product, etc. Heterogeneous base catalysts overcome some of the disadvantages of homogeneous base catalysts, namely, ease of separation, simple catalyst recovery techniques, and reusability of catalyst from the product. Heterogeneous acid catalysts show very less sensitivity to high FFA and water content in the feedstock and can easily be recovered, recycled, and reused after the biodiesel production process. Due to current interest in "green" alternatives to chemical catalysts, biocatalysts, i.e., enzymes, have drawn attention. The catalysts work under relatively lower reaction temperature conditions compared to other catalysts and can catalyze low-grade oils with extremely high FFA content. The results obtained have proved that high productivity, involving yield and numbers of reuse, as well as low reaction time, can be achieved when using enzymes. The major limitation is the reaction rate, which is the slowest among all the catalysts. Furthermore, the synthesis of catalysts is more expensive than those of both homogeneous acid and base catalysts. High catalytic efficiency at mild operating conditions has drawn attention to nanocatalysts recently. The development of highly active and selective heterogeneous catalysts, along with their economic feasibility for use in the industrial scale, is a subject that needs to be addressed.

AUTHOR CONTRIBUTIONS

IR formulated the article, written heterogeneous base, and other sections, compiled the whole article. HO contributed heterogeneous acid catalyst section. TM oversaw the work and provided review. MM contributed the homogeneous catalyst section. AS contributed the biocatalyst section. SR contributed the nanocatalyst section. AA reviewed and improved the article. All authors contributed to the article and approved the submitted version.

FUNDING

REFERENCES

Abdulla, R., and Ravindra, P. (2013). Immobilized Burkholderia cepacia lipase for biodiesel production from crude Jatropha curcas L. oil. *Biomass Bioenergy* 56, 8–13. doi: 10.1016/j.biombioe.2013.04.010

Abedin, M. J., Masjuki, H. H., Kalam, M. A., Sanjid, A., Rahman, S. M. A., and Rizwanul Fattah, I. M. (2014). Performance, emissions, and heat losses of palm and jatropha biodiesel blends in a diesel engine. *Ind. Crops Prod.* 59, 96–104. doi: 10.1016/j.indcrop.2014.05.001

Aboelazayem, O., El-Gendy, N. S., Abdel-Rehim, A. A., Ashour, F., and Sadek, M. A. (2018). Biodiesel production from castor oil in Egypt: process optimisation, kinetic study, diesel engine performance and exhaust emissions analysis. *Energy* 157, 843–852. doi: 10.1016/j.energy.2018.05.202

Akubude, V. C., Nwaigwe, K. N., and Dintwa, E. (2019). Production of biodiesel from microalgae via nanocatalyzed transesterification process: a review. *Mater. Sci. Energy Tech.* 2, 216–225. doi: 10.1016/j.mset.2018.12.006

Alaei, S., Haghighi, M., Toghiani, J., and Rahmani Vahid, B. (2018). Magnetic and reusable MgO/MgFe2O4 nanocatalyst for biodiesel production

from sunflower oil: Influence of fuel ratio in combustion synthesis on catalytic properties and performance. *Ind. Crops Prod.* 117, 322–332. doi: 10.1016/j.indcrop.2018.03.015

Alcañiz-Monge, J., Bakkali, B. E., Trautwein, G., and Reinoso, S. (2018). Zirconia-supported tungstophosphoric heteropolyacid as heterogeneous acid catalyst for biodiesel production. *Appl. Cataly. B Environ.* 224, 194–203. doi: 10.1016/j.apcatb.2017.10.066

Ambat, I., Srivastava, V., and Sillanpää, M. (2018). Recent advancement in biodiesel production methodologies using various feedstock: a review. *Renew. Sust. Energy Rev.* 90, 356–369. doi: 10.1016/j.rser.2018.03.069

Amini, Z., Ilham, Z., Ong, H. C., Mazaheri, H., and Chen, W.-H. (2017a). State of the art and prospective of lipase-catalyzed transesterification reaction for biodiesel production. *Energy Convers. Manage.* 141, 339–353. doi: 10.1016/j.enconman.2016.09.049

Amini, Z., Ong, H. C., Harrison, M. D., Kusumo, F., Mazaheri, H., and Ilham, Z. (2017b). Biodiesel production by lipase-catalyzed transesterification of Ocimum basilicum L. (sweet basil) seed oil. *Energy Convers. Manage.* 132, 82–90. doi: 10.1016/j.enconman.2016.11.017

Andrijanto, E., Dawson, E. A., and Brown, D. R. (2012). Hypercrosslinked polystyrene sulphonic acid catalysts for the esterification of free fatty acids in biodiesel synthesis. *Appl. Cataly. B Environ.* 115–116, 261–268. doi: 10.1016/j.apcatb.2011.12.040

Aransiola, E. F., Ojumu, T. V., Oyekola, O. O., Madzimbamuto, T. F., and Ikhu-Omoregbe, D. I. O. (2014). A review of current technology for biodiesel production: State of the art. *Biomass Bioenerg.* 61, 276–297. doi: 10.1016/j.biombioe.2013.11.014

Arbab, M. I., Varman, M., Masjuki, H. H., Kalam, M. A., Imtenan, S., Sajjad, H., et al. (2015). Evaluation of combustion, performance, and emissions of optimum palm–coconut blend in turbocharged and non-turbocharged conditions of a diesel engine. *Energ. Convers. Manage.* 90, 111–120. doi: 10.1016/j.enconman.2014.11.017

Arumugam, A., and Ponnusami, V. (2014). Biodiesel production from Calophyllum inophyllum oil using lipase producing Rhizopus oryzae cells immobilized within reticulated foams. *Renew. Energ.* 64, 276–282. doi: 10.1016/j.renene.2013.11.016

Arun, S. B., Suresh, R., Yatish, K. V., Omkaresh, B. R., and Channa Keshava Naik, N. (2017). Use of CaO and Na_3PO_4 catalysts in the synthesis of biodiesel and investigation of fuel properties. *Mater. Today Proc.* 4, 11111–11117. doi: 10.1016/j.matpr.2017.08.074

Ashraful, A. M., Masjuki, H. H., Kalam, M. A., Rizwanul Fattah, I. M., Imtenan, S., Shahir, S. A., et al. (2014). Production and comparison of fuel properties, engine performance, and emission characteristics of biodiesel from various non-edible vegetable oils: a review. *Energy Convers. Manage.* 80, 202–228. doi: 10.1016/j.enconman.2014.01.037

Baskar, G., Aberna Ebenezer Selvakumari, I., and Aiswarya, R. (2018). Biodiesel production from castor oil using heterogeneous Ni doped ZnO nanocatalyst. *Bioresour. Technol.* 250, 793–798. doi: 10.1016/j.biortech.2017.12.010

Benjapornkulaphong, S., Ngamcharussrivichai, C., and Bunyakiat, K. (2009). Al_2O_3-supported alkali and alkali earth metal oxides for transesterification of palm kernel oil and coconut oil. *Chem. Eng. J.* 145, 468–474. doi: 10.1016/j.cej.2008.04.036

Borges, M. E., and Díaz, L. (2012). Recent developments on heterogeneous catalysts for biodiesel production by oil esterification and transesterification reactions: a review. *Renew. Sust. Energ. Rev.* 16, 2839–2849. doi: 10.1016/j.rser.2012.01.071

Calero, J., Luna, D., Sancho, E. D., Luna, C., Bautista, F. M., Romero, A. A., et al. (2014). Development of a new biodiesel that integrates glycerol, by using CaO as heterogeneous catalyst, in the partial methanolysis of sunflower oil. *Fuel* 122, 94–102. doi: 10.1016/j.fuel.2014.01.033

Chen, X.-R., Ju, Y.-H., and Mou, C.-Y. (2007). Direct synthesis of mesoporous sulfated silica-zirconia catalysts with high catalytic activity for biodiesel via esterification. *J. Phys. Chem. C* 111, 18731–18737. doi: 10.1021/jp0749221

Choi, N., No, D. S., Kim, H., Kim, B. H., Kwak, J., Lee, J.-S., et al. (2018). *In situ* lipase-catalyzed transesterification in rice bran for synthesis of fatty acid methyl ester. *Ind. Crops Prod.* 120, 140–146. doi: 10.1016/j.indcrop.2018.04.049

Chouhan, A. P. S., and Sarma, A. K. (2011). Modern heterogeneous catalysts for biodiesel production: A comprehensive review. *Renew. Sust. Energ. Rev.* 15, 4378–4399. doi: 10.1016/j.rser.2011.07.112

Christopher, L. P., Hemanathan, K., and Zambare, V. P. (2014). Enzymatic biodiesel: challenges and opportunities. *Appl. Energy* 119, 497–520. doi: 10.1016/j.apenergy.2014.01.017

Chua, S. Y., Periasamy, L. A. P., Goh, C. M. H., Tan, Y. H., Mubarak, N. M., et al. (2020). Biodiesel synthesis using natural solid catalyst derived from biomass waste — a review. *J. Industr. Eng. Chem.* 81, 41–60. doi: 10.1016/j.jiec.2019.09.022

Clohessy, J., and Kwapinski, W. (2020). Carbon-based catalysts for biodiesel production—a review. *Appl. Sci.* 10:918. doi: 10.3390/app10030918

Dai, Y.-M., Wang, Y.-F., and Chen, C.-C. (2018). Synthesis and characterization of magnetic $LiFe_5O_8$-$LiFeO_2$ as a solid basic catalyst for biodiesel production. *Catal. Commun.* 106, 20–24. doi: 10.1016/j.catcom.2017.12.002

De Lima, A. L., Ronconi, C. M., and Mota, C. J. A. (2016). Heterogeneous basic catalysts for biodiesel production. *Catal. Sci. Technol.* 6, 2877–2891. doi: 10.1039/C5CY01989C

Di Serio, M., Tesser, R., Pengmei, L., and Santacesaria, E. (2008). Heterogeneous catalysts for biodiesel production. *Energy Fuels* 22, 207–217. doi: 10.1021/ef700250g

Doyle, A. M., Albayati, T. M., Abbas, A. S., and Alismaeel, Z. T. (2016). Biodiesel production by esterification of oleic acid over zeolite Y prepared from kaolin. *Renew. Energy* 97, 19–23. doi: 10.1016/j.renene.2016.05.067

Du, L., Ding, S., Li, Z., Lv, E., Lu, J., and Ding, J. (2018). Transesterification of castor oil to biodiesel using NaY zeolite-supported La_2O_3 catalysts. *Energy Convers. Manag.* 173, 728–734. doi: 10.1016/j.enconman.2018.07.053

Du, L., Li, Z., Ding, S., Chen, C., Qu, S., Yi, W., et al. (2019). Synthesis and characterization of carbon-based MgO catalysts for biodiesel production from castor oil. *Fuel* 258:116122. doi: 10.1016/j.fuel.2019.116122

Dubey, P., and Gupta, R. (2017). Effects of dual bio-fuel (Jatropha biodiesel and turpentine oil) on a single cylinder naturally aspirated diesel engine without EGR. *Appl. Therm. Eng.* 115, 1137–1147. doi: 10.1016/j.applthermaleng.2016.12.125

Dueso, C., Muñoz, M., Moreno, F., Arroyo, J., Gil-Lalaguna, N., Bautista, A., et al. (2018). Performance and emissions of a diesel engine using sunflower biodiesel with a renewable antioxidant additive from bio-oil. *Fuel* 234, 276–285. doi: 10.1016/j.fuel.2018.07.013

Endalew, A. K., Kiros, Y., and Zanzi, R. (2011). Inorganic heterogeneous catalysts for biodiesel production from vegetable oils. *Biomass Bioenergy* 35, 3787–3809. doi: 10.1016/j.biombioe.2011.06.011

Fattah, I. M. R., Kalam, M. A., Masjuki, H. H., and Wakil, M. A. (2014a). Biodiesel production, characterization, engine performance, and emission characteristics of Malaysian Alexandrian laurel oil. *RSC Advanc.* 4, 17787–17796. doi: 10.1039/C3RA47954D

Fattah, I. M. R., Masjuki, H. H., Kalam, M. A., Mofijur, M., and Abedin, M. J. (2014b). Effect of antioxidant on the performance and emission characteristics of a diesel engine fueled with palm biodiesel blends. *Energy Convers. Manag.* 79, 265–272. doi: 10.1016/j.enconman.2013.12.024

Fattah, I. M. R., Masjuki, H. H., Kalam, M. A., Wakil, M. A., Ashraful, A. M., and Shahir, S. A. (2014c). Experimental investigation of performance and regulated emissions of a diesel engine with Calophyllum inophyllum biodiesel blends accompanied by oxidation inhibitors. *Energy Convers. Manag.* 83, 232–240. doi: 10.1016/j.enconman.2014.03.069

Fattah, I. M. R., Masjuki, H. H., Kalam, M. A., Wakil, M. A., Rashedul, H. K., and Abedin, M. J. (2014d). Performance and emission characteristics of a CI engine fueled with Cocos nucifera and Jatropha curcas B20 blends accompanying antioxidants. *Ind. Crops Prod.* 57, 132–140. doi: 10.1016/j.indcrop.2014.03.022

Fattah, I. M. R., Masjuki, H. H., Liaquat, A. M., Ramli, R., Kalam, M. A., and Riazuddin, V. N. (2013). Impact of various biodiesel fuels obtained from edible and non-edible oils on engine exhaust gas and noise emissions. *Renew. Sust. Energ. Rev.* 18, 552–567. doi: 10.1016/j.rser.2012.10.036

Fattah, I. M. R., Ming, C., Chan, Q. N., Wehrfritz, A., Pham, P. X., Yang, W., et al. (2018). Spray and combustion investigation of post injections under low-temperature combustion conditions with biodiesel. *Energy Fuels* 32, 8727–8742. doi: 10.1021/acs.energyfuels.8b00284

Feng, Y., Zhang, A., Li, J., and He, B. (2011). A continuous process for biodiesel production in a fixed bed reactor packed with cation-exchange resin as heterogeneous catalyst. *Bioresour. Technol.* 102, 3607–3609. doi: 10.1016/j.biortech.2010.10.115

Feyzi, M., Hassankhani, A., and Rafiee, H. R. (2013). Preparation and characterization of Cs/Al/Fe3O4 nanocatalysts for biodiesel production. *Energ. Convers. Manage.* 71, 62–68. doi: 10.1016/j.enconman.2013.03.022

Fu, J., Chen, L., Lv, P., Yang, L., and Yuan, Z. (2015). Free fatty acids esterification for biodiesel production using self-synthesized macroporous cation exchange resin as solid acid catalyst. *Fuel* 154, 1–8. doi: 10.1016/j.fuel.2015.03.048

Gerpen, J. V. (2005). Biodiesel processing and production. *Fuel Process. Technol.* 86, 1097–1107. doi: 10.1016/j.fuproc.2004.11.005

Gog, A., Roman, M., Toşa, M., Paizs, C., and Irimie, F. D. (2012). Biodiesel production using enzymatic transesterification – Current state and perspectives. *Renew. Energ.* 39, 10–16. doi: 10.1016/j.renene.2011.08.007

Goga, G., Chauhan, B. S., Mahla, S. K., and Cho, H. M. (2019). Performance and emission characteristics of diesel engine fueled with rice bran biodiesel and n-butanol. *Energy Rep.* 5, 78–83. doi: 10.1016/j.egyr.2018.12.002

Guldhe, A., Singh, P., Ansari, F. A., Singh, B., and Bux, F. (2017). Biodiesel synthesis from microalgal lipids using tungstated zirconia as a heterogeneous acid catalyst and its comparison with homogeneous acid and enzyme catalysts. *Fuel* 187, 180–188. doi: 10.1016/j.fuel.2016.09.053

Hanif, M. A., Nisar, S., and Rashid, U. (2017). Supported solid and heteropoly acid catalysts for production of biodiesel. *Catal. Rev.* 59, 165–188. doi: 10.1080/01614940.2017.1321452

Hattori, H. (1995). Heterogeneous basic catalysis. *Chem. Rev.* 95, 537–558. doi: 10.1021/cr00035a005

Helwani, Z., Othman, M. R., Aziz, N., Kim, J., and Fernando, W. J. N. (2009). Solid heterogeneous catalysts for transesterification of triglycerides with methanol: a review. *Appl. Catal. A Gen.* 363, 1–10. doi: 10.1016/j.apcata.2009.05.021

Hoekman, S. K., and Robbins, C. (2012). Review of the effects of biodiesel on NOx emissions. *Fuel Process. Technol.* 96, 237–249. doi: 10.1016/j.fuproc.2011.12.036

Hu, S., Wang, Y., and Han, H. (2011). Utilization of waste freshwater mussel shell as an economic catalyst for biodiesel production. *Biomass Bioenergy* 35, 3627–3635. doi: 10.1016/j.biombioe.2011.05.009

Ibrahim, M. M., Mahmoud, H. R., and El-Molla, S. A. (2019). Influence of support on physicochemical properties of ZrO2 based solid acid heterogeneous catalysts for biodiesel production. *Catal. Commun.* 122, 10–15. doi: 10.1016/j.catcom.2019.01.008

Islam, A., Taufiq-Yap, Y. H., Ravindra, P., Teo, S. H., Sivasangar, S., and Chan, E.-S. (2015). Biodiesel synthesis over millimetric γ-Al2O3/KI catalyst. *Energy* 89, 965–973. doi: 10.1016/j.energy.2015.06.036

Jahirul, M. I., Brown, R. J., Senadeera, W., Ashwath, N., Rasul, M. G., Rahman, M. M., et al. (2015). Physio-chemical assessment of beauty leaf (Calophyllum inophyllum) as second-generation biodiesel feedstock. *Energy Rep.* 1, 204–215. doi: 10.1016/j.egyr.2015.10.003

Jayaraman, J., Alagu, K., Appavu, P., Joy, N., Jayaram, P., and Mariadoss, A. (2020). Enzymatic production of biodiesel using lipase catalyst and testing of an unmodified compression ignition engine using its blends with diesel. *Renew. Energy* 145, 399–407. doi: 10.1016/j.renene.2019.06.061

Jayed, M. H., Masjuki, H. H., Saidur, R., Kalam, M. A., and Jahirul, M. I. (2009). Environmental aspects and challenges of oilseed produced biodiesel in Southeast Asia. *Renew. Sust. Energ. Rev.* 13, 2452–2462. doi: 10.1016/j.rser.2009.06.023

Kamran, E., Mashhadi, H., Mohammadi, A., and Ghobadian, B. (2020). Biodiesel production from Elaeagnus angustifolia.L seed as a novel waste feedstock using potassium hydroxide catalyst. *Biocatal. Agric. Biotechnol.* 25:101578. doi: 10.1016/j.bcab.2020.101578

Kaur, M., Malhotra, R., and Ali, A. (2018). Tungsten supported Ti/SiO2 nanoflowers as reusable heterogeneous catalyst for biodiesel production. *Renew. Energy* 116, 109–119. doi: 10.1016/j.renene.2017.09.065

Kaur, N., and Ali, A. (2015). Preparation and application of Ce/ZrO2-TiO2/SO42- as solid catalyst for the esterification of fatty acids. *Renew. Energy* 81, 421–431. doi: 10.1016/j.renene.2015.03.051

Kazemifard, S., Nayebzadeh, H., Saghatoleslami, N., and Safakish, E. (2018). Assessment the activity of magnetic KOH/Fe3O4@Al2O3 core–shell nanocatalyst in transesterification reaction: effect of Fe/Al ratio on structural and performance. *Environ. Sci. Pollut. Res.* 25, 32811–32821. doi: 10.1007/s11356-018-3249-7

Kesserwan, F., Ahmad, M. N., Khalil, M., and El-Rassy, H. (2020). Hybrid CaO/Al2O3 aerogel as heterogeneous catalyst for biodiesel production. *Chem. Eng. J.* 385:123834. doi: 10.1016/j.cej.2019.123834

Kim, M., Dimaggio, C., Salley, S. O., and Simon Ng, K. Y. (2012). A new generation of zirconia supported metal oxide catalysts for converting low grade renewable feedstocks to biodiesel. *Bioresour. Technol.* 118, 37–42. doi: 10.1016/j.biortech.2012.04.035

Knothe, G., and Razon, L. F. (2017). Biodiesel fuels. *Prog. Energ. Combust.* 58, 36–59. doi: 10.1016/j.pecs.2016.08.001

Kurhade, A., and Dalai, A. K. (2018). Physiochemical characterization and support interaction of alumina-supported heteropolyacid catalyst for biodiesel production. *Asia-Pac. J. Chem. Eng.* 13:e2249. doi: 10.1002/apj.2249

Lam, M. K., Lee, K. T., and Mohamed, A. R. (2010). Homogeneous, heterogeneous and enzymatic catalysis for transesterification of high free fatty acid oil (waste cooking oil) to biodiesel: a review. *Biotechnol. Advanc.* 28, 500–518. doi: 10.1016/j.biotechadv.2010.03.002

Latchubugata, C. S., Kondapaneni, R. V., Patluri, K. K., Virendra, U., and Vedantam, S. (2018). Kinetics and optimization studies using response surface methodology in biodiesel production using heterogeneous catalyst. *Chem. Eng. Res. Des.* 135, 129–139. doi: 10.1016/j.cherd.2018.05.022

Lee, A. F., Bennett, J. A., Manayil, J. C., and Wilson, K. (2014). Heterogeneous catalysis for sustainable biodiesel production via esterification and transesterification. *Chem. Soc. Rev.* 43, 7887–7916. doi: 10.1039/C4CS00189C

Lee, H. V., Juan, J. C., and Taufiq-Yap, Y. H. (2015). Preparation and application of binary acid–base CaO–La2O3 catalyst for biodiesel production. *Renew. Energy* 74, 124–132. doi: 10.1016/j.renene.2014.07.017

Li, X., He, X.-Y., Li, Z.-L., Wang, Y.-D., Wang, C.-Y., Shi, H., et al. (2012). Enzymatic production of biodiesel from Pistacia chinensis bge seed oil using immobilized lipase. *Fuel* 92, 89–93. doi: 10.1016/j.fuel.2011.06.048

Li, Z., Ding, S., Chen, C., Qu, S., Du, L., Lu, J., et al. (2019). Recyclable Li/NaY zeolite as a heterogeneous alkaline catalyst for biodiesel production: Process optimization and kinetics study. *Energy Convers. Manag.* 192, 335–345. doi: 10.1016/j.enconman.2019.04.053

Limmanee, S., Naree, T., Bunyakiat, K., and Ngamcharussrivichai, C. (2013). Mixed oxides of Ca, Mg and Zn as heterogeneous base catalysts for the synthesis of palm kernel oil methyl esters. *Chem. Eng. J.* 225, 616–624. doi: 10.1016/j.cej.2013.03.093

Ling, J. S. J., Tan, Y. H., Mubarak, N. M., Kansedo, J., Saptoro, A., and Nolasco-Hipolito, C. (2019). A review of heterogeneous calcium oxide based catalyst from waste for biodiesel synthesis. *SN Appl. Sci.* 1:810. doi: 10.1007/s42452-019-0843-3

Liu, R., Wang, X., Zhao, X., and Feng, P. (2008a). Sulfonated ordered mesoporous carbon for catalytic preparation of biodiesel. *Carbon* 46, 1664–1669. doi: 10.1016/j.carbon.2008.07.016

Liu, X., He, H., Wang, Y., and Zhu, S. (2007). Transesterification of soybean oil to biodiesel using SrO as a solid base catalyst. *Catal. Commun.* 8, 1107–1111. doi: 10.1016/j.catcom.2006.10.026

Liu, X., He, H., Wang, Y., Zhu, S., and Piao, X. (2008b). Transesterification of soybean oil to biodiesel using CaO as a solid base catalyst. *Fuel* 87, 216–221. doi: 10.1016/j.fuel.2007.04.013

Lopresto, C. G., Naccarato, S., Albo, L., De Paola, M. G., Chakraborty, S., Curcio, S., et al. (2015). Enzymatic transesterification of waste vegetable oil to produce biodiesel. *Ecotoxicol. Environ. Safe.* 121, 229–235. doi: 10.1016/j.ecoenv.2015.03.028

Madhuvilakku, R., and Piraman, S. (2013). Biodiesel synthesis by TiO2-ZnO mixed oxide nanocatalyst catalyzed palm oil transesterification process. *Bioresour. Technol.* 150, 55–59. doi: 10.1016/j.biortech.2013.09.087

Mahlia, T. M. I., Syazmi, Z. A. H. S., Mofijur, M., Abas, A. E. P., Bilad, M. R., et al. (2020). Patent landscape review on biodiesel production: technology updates. *Renew. Sust. Energ. Rev.* 118:109526. doi: 10.1016/j.rser.2019.109526

Majhi, S., and Ray, S. (2016). A study on production of biodiesel using a novel solid oxide catalyst derived from waste. *Environ. Sci. Pollut. Res.* 23, 9251–9259. doi: 10.1007/s11356-015-4824-9

Maleki, E., Aroua, M. K., and Sulaiman, N. M. N. (2013). Castor oil — a more suitable feedstock for enzymatic production of methyl esters. *Fuel Process. Technol.* 112, 129–132. doi: 10.1016/j.fuproc.2013.03.003

Manríquez-Ramírez, M., Gómez, R., Hernández-Cortez, J. G., Zúñiga-Moreno, A., Reza-San Germán, C. M., et al. (2013). Advances in the transesterification of triglycerides to biodiesel using MgO–NaOH, MgO–KOH and MgO–CeO2 as solid basic catalysts. *Catal. Today* 212, 23–30. doi: 10.1016/j.cattod.2012.11.005

Mansir, N., Taufiq-Yap, Y. H., Rashid, U., and Lokman, I. M. (2017). Investigation of heterogeneous solid acid catalyst performance on low grade feedstocks for biodiesel production: a review. *Energy Convers. Manag.* 141, 171–182. doi: 10.1016/j.enconman.2016.07.037

Mardhiah, H. H., Ong, H. C., Masjuki, H. H., Lim, S., and Lee, H. V. (2017). A review on latest developments and future prospects of heterogeneous catalyst in biodiesel production from non-edible oils. *Renew. Sust. Energ. Rev.* 67, 1225–1236. doi: 10.1016/j.rser.2016.09.036

Marín-Suárez, M., Méndez-Mateos, D., Guadix, A., and Guadix, E. M. (2019). Reuse of immobilized lipases in the transesterification of waste fish oil for the production of biodiesel. *Renew. Energ.* 140, 1–8. doi: 10.1016/j.renene.2019.03.035

Marwaha, A., Rosha, P., Mohapatra, S. K., Mahla, S. K., and Dhir, A. (2018). Waste materials as potential catalysts for biodiesel production: current state and future scope. *Fuel Process. Technol.* 181, 175–186. doi: 10.1016/j.fuproc.2018.09.011

Mata, T. M., Sousa, I. R. B. G., Vieira, S. S., and Caetano, N. S. (2012). Biodiesel production from corn oil via enzymatic catalysis with ethanol. *Energy Fuels* 26, 3034−3041. doi: 10.1021/ef300319f

Mckenzie, A. L., Fishel, C. T., and Davis, R. J. (1992). Investigation of the surface structure and basic properties of calcined hydrotalcites. *J. Catal.* 138, 547–561. doi: 10.1016/0021-9517(92)90306-3

Melero, J. A., Iglesias, J., and Morales, G. (2009). Heterogeneous acid catalysts for biodiesel production: current status and future challenges. *Green Chem.* 11, 1285–1308. doi: 10.1039/b902086a

Mofijur, M., Masjuki, H. H., Kalam, M. A., Atabani, A. E., Rizwanul Fattah, I. M., and Mobarak, H. M. (2014). Comparative evaluation of performance and emission characteristics of Moringa oleifera and Palm oil based biodiesel in a diesel engine. *Ind. Crops Prod.* 53, 78–84. doi: 10.1016/j.indcrop.2013.12.011

Mohebbi, S., Rostamizadeh, M., and Kahforoushan, D. (2020). Effect of molybdenum promoter on performance of high silica MoO_3/B-ZSM-5 nanocatalyst in biodiesel production. *Fuel* 266:117063. doi: 10.1016/j.fuel.2020.117063

Mootabadi, H., Salamatinia, B., Bhatia, S., and Abdullah, A. Z. (2010). Ultrasonic-assisted biodiesel production process from palm oil using alkaline earth metal oxides as the heterogeneous catalysts. *Fuel* 89, 1818–1825. doi: 10.1016/j.fuel.2009.12.023

Moradi, G., Mohadesi, M., Rezaei, R., and Moradi, R. (2015). Biodiesel production using CaO/γ-Al2O3 catalyst synthesized by sol-gel method. *Canad. J. Chem. Eng.* 93, 1531–1538. doi: 10.1002/cjce.22258

Navajas, A., Campo, I., Moral, A., Echave, J., Sanz, O., Montes, M., et al. (2018). Outstanding performance of rehydrated Mg-Al hydrotalcites as heterogeneous methanolysis catalysts for the synthesis of biodiesel. *Fuel* 211, 173–181. doi: 10.1016/j.fuel.2017.09.061

Nayebzadeh, H., Saghatoleslami, N., Haghighi, M., and Tabasizadeh, M. (2017). Influence of fuel type on microwave-enhanced fabrication of $KOH/Ca_{12}Al_{14}O_{33}$ nanocatalyst for biodiesel production via microwave heating. *J. Taiwan Inst. Chem. Eng.* 75, 148–155. doi: 10.1016/j.jtice.2017.03.018

Nowicki, J., Lach, J., Organek, M., and Sabura, E. (2016). Transesterification of rapeseed oil to biodiesel over Zr-dopped MgAl hydrotalcites. *Appl. Catal. A Genrl.* 524, 17–24. doi: 10.1016/j.apcata.2016.05.015

Ong, H. C., Masjuki, H. H., Mahlia, T. M. I., Silitonga, A. S., Chong, W. T., and Yusaf, T. (2014). Engine performance and emissions using *Jatropha curcas*, Ceiba pentandra and Calophyllum inophyllum biodiesel in a CI diesel engine. *Energy* 69, 427–445. doi: 10.1016/j.energy.2014.03.035

Ong, H. C., Milano, J., Silitonga, A. S., Hassan, M. H., Shamsuddin, A. H., Wang, C.-T., et al. (2019). Biodiesel production from Calophyllum inophyllum-Ceiba pentandra oil mixture: Optimization and characterization. *J. Clean. Prod.* 219, 183–198. doi: 10.1016/j.jclepro.2019.02.048

Palash, S. M., Masjuki, H. H., Kalam, M. A., Atabani, A. E., Rizwanul Fattah, I. M., and Sanjid, A. (2015). Biodiesel production, characterization, diesel engine performance, and emission characteristics of methyl esters from *Aphanamixis* polystachya oil of Bangladesh. *Energy Convers. Manag.* 91, 149–157. doi: 10.1016/j.enconman.2014.12.009

Pandit, P. R., and Fulekar, M. H. (2017). Egg shell waste as heterogeneous nanocatalyst for biodiesel production: optimized by response surface methodology. *J. Environ. Manage.* 198, 319–329. doi: 10.1016/j.jenvman.2017.04.100

Qiu, F., Li, Y., Yang, D., Li, X., and Sun, P. (2011). Heterogeneous solid base nanocatalyst: Preparation, characterization and application in biodiesel production. *Bioresour. Technol.* 102, 4150–4156. doi: 10.1016/j.biortech.2010.12.071

Quirino, M. R., Oliveira, M. J. C., Keyson, D., Lucena, G. L., Oliveira, J. B. L., and Gama, L. (2016). Synthesis of zinc aluminate with high surface area by microwave hydrothermal method applied in the transesterification of soybean oil (biodiesel). *Mater. Res. Bull.* 74, 124–128. doi: 10.1016/j.materresbull.2015.10.027

Rahmani Vahid, B., Haghighi, M., Alaei, S., and Toghiani, J. (2017). Reusability enhancement of combustion synthesized $MgO/MgAl_2O_4$ nanocatalyst in biodiesel production by glow discharge plasma treatment. *Energy Convers. Manag.* 143, 23–32. doi: 10.1016/j.enconman.2017.03.075

Ropero-Vega, J. L., Aldana-Pérez, A., Gómez, R., and Niño-Gómez, M. E. (2010). Sulfated titania $[TiO_2/SO_4{}^2-]$: a very active solid acid catalyst for the esterification of free fatty acids with ethanol. *Appl. Catal. A-Gen.* 379, 24–29. doi: 10.1016/j.apcata.2010.02.020

Roschat, W., Phewphong, S., Khunchalee, J., and Moonsin, P. (2018). Biodiesel production by ethanolysis of palm oil using SrO as a basic heterogeneous catalyst. *Mater. Today Proc.* 5, 13916–13921. doi: 10.1016/j.matpr.2018.02.040

Roschat, W., Siritanon, T., Yoosuk, B., and Promarak, V. (2016). Biodiesel production from palm oil using hydrated lime-derived CaO as a low-cost basic heterogeneous catalyst. *Energy Convers. Manag.* 108, 459–467. doi: 10.1016/j.enconman.2015.11.036

Ruhul, A. M., Kalam, M. A., Masjuki, H. H., Fattah, I. M. R., Reham, S. S., and Rashed, M. M. (2015). State of the art of biodiesel production processes: a review of the heterogeneous catalyst. *RSC Advanc.* 5, 101023–101044. doi: 10.1039/C5RA09862A

Ruhul, A. M., Kalam, M. A., Masjuki, H. H., Shahir, S. A., Alabdulkarem, A., Teoh, Y. H., et al. (2017). Evaluating combustion, performance and emission characteristics of Millettia pinnata and Croton megalocarpus biodiesel blends in a diesel engine. *Energy* 141, 2362–2376. doi: 10.1016/j.energy.2017.11.096

Salinas, D., Sepúlveda, C., Escalona, N., Gfierro, J. L., and Pecchi, G. (2018). Sol–gel La_2O_3-ZrO_2 mixed oxide catalysts for biodiesel production. *J. Energ. Chem.* 27, 565–572. doi: 10.1016/j.jechem.2017.11.003

Sani, Y. M., Daud, W. M. A. W., and Abdul Aziz, A. R. (2014). Activity of solid acid catalysts for biodiesel production: a critical review. *Appl. Catal. A Gen.* 470, 140–161. doi: 10.1016/j.apcata.2013.10.052

Santiago-Torres, N., Romero-Ibarra, I. C., and Pfeiffer, H. (2014). Sodium zirconate (Na_2ZrO_3) as a catalyst in a soybean oil transesterification reaction for biodiesel production. *Fuel Process. Technol.* 120, 34–39. doi: 10.1016/j.fuproc.2013.11.018

Saravanan, A., Murugan, M., Sreenivasa Reddy, M., and Parida, S. (2020). Performance and emission characteristics of variable compression ratio CI engine fueled with dual biodiesel blends of Rapeseed and Mahua. *Fuel* 263:116751. doi: 10.1016/j.fuel.2019.116751

Schuchardt, U., Sercheli, R., and Vargas, R. M. (1998). Transesterification of vegetable oils: a review. *J. Braz. Chem. Soc.* 9, 199–210. doi: 10.1590/S0103-50531998000300002

Seffati, K., Honarvar, B., Esmaeili, H., and Esfandiari, N. (2019). Enhanced biodiesel production from chicken fat using CaO/CuFe2O4 nanocatalyst and its combination with diesel to improve fuel properties. *Fuel* 235, 1238–1244. doi: 10.1016/j.fuel.2018.08.118

Sekoai, P. T., Ouma, C. N. M., Du Preez, S. P., Modisha, P., Engelbrecht, N., Bessarabov, D. G., et al. (2019). Application of nanoparticles in biofuels: an overview. *Fuel* 237, 380–397. doi: 10.1016/j.fuel.2018.10.030

Semwal, S., Arora, A. K., Badoni, R. P., and Tuli, D. K. (2011). Biodiesel production using heterogeneous catalysts. *Bioresour. Technol.* 102, 2151–2161. doi: 10.1016/j.biortech.2010.10.080

Shah, S., and Gupta, M. N. (2007). Lipase catalyzed preparation of biodiesel from Jatropha oil in a solvent free system. *Process Biochemi.* 42, 409–414. doi: 10.1016/j.procbio.2006.09.024

Shan, R., Lu, L., Shi, Y., Yuan, H., and Shi, J. (2018). Catalysts from renewable resources for biodiesel production. *Energ. Convers. Manage.* 178, 277–289. doi: 10.1016/j.enconman.2018.10.032

Shi, G., Yu, F., Wang, Y., Pan, D., Wang, H., and Li, R. (2016). A novel one-pot synthesis of tetragonal sulfated zirconia catalyst with high activity for biodiesel

production from the transesterification of soybean oil. *Renew. Energy* 92, 22–29. doi: 10.1016/j.renene.2016.01.094

Siddiquee, M. N., Kazemian, H., and Rohani, S. (2011). Biodiesel production from the lipid of wastewater sludge using an acidic heterogeneous catalyst. *Chem. Eng. Technol.* 34, 1983–1988. doi: 10.1002/ceat.201100119

Silitonga, A. S., Masjuki, H. H., Mahlia, T. M. I., Ong, H. C., Chong, W. T., and Boosroh, M. H. (2013a). Overview properties of biodiesel diesel blends from edible and non-edible feedstock. *Renew. Sust. Energ. Rev.* 22, 346–360. doi: 10.1016/j.rser.2013.01.055

Silitonga, A. S., Ong, H. C., Mahlia, T. M. I., Masjuki, H. H., and Chong, W. T. (2013b). Characterization and production of Ceiba pentandra biodiesel and its blends. *Fuel* 108, 855–858. doi: 10.1016/j.fuel.2013.02.014

Silitonga, A. S., Shamsuddin, A. H., Mahlia, T. M. I., Milano, J., Kusumo, F., Siswantoro, J., et al. (2020). Biodiesel synthesis from Ceiba pentandra oil by microwave irradiation-assisted transesterification: ELM modeling and optimization. *Renew. Energy* 146, 1278–1291. doi: 10.1016/j.renene.2019.07.065

Sirisomboonchai, S., Abuduwayiti, M., Guan, G., Samart, C., Abliz, S., Hao, X., et al. (2015). Biodiesel production from waste cooking oil using calcined scallop shell as catalyst. *Energy Convers. Manage.* 95, 242–247. doi: 10.1016/j.enconman.2015.02.044

Sulaiman, N. F., Wan Abu Bakar, W. A., and Ali, R. (2017). Response surface methodology for the optimum production of biodiesel over Cr/Ca/γ-Al$_2$O$_3$ catalyst: Catalytic performance and physicochemical studies. *Renew. Energy* 113, 697–705. doi: 10.1016/j.renene.2017.06.007

Sun, H., Ding, Y., Duan, J., Zhang, Q., Wang, Z., Lou, H., et al. (2010). Transesterification of sunflower oil to biodiesel on ZrO2 supported La2O3 catalyst. *Bioresour. Technol.* 101, 953–958. doi: 10.1016/j.biortech.2009.08.089

Szczesna Antczak, M., Kubiak, A., Antczak, T., and Bielecki, S. (2009). Enzymatic biodiesel synthesis – Key factors affecting efficiency of the process. *Renew. Energ.* 34, 1185–1194. doi: 10.1016/j.renene.2008.11.013

Tan, Y. H., Abdullah, M. O., Kansedo, J., Mubarak, N. M., Chan, Y. S., and Nolasco-Hipolito, C. (2019). Biodiesel production from used cooking oil using green solid catalyst derived from calcined fusion waste chicken and fish bones. *Renew. Energ.* 139, 696–706. doi: 10.1016/j.renene.2019.02.110

Teo, S. H., Rashid, U., Thomas Choong, S. Y., and Taufiq-Yap, Y. H. (2017). Heterogeneous calcium-based bimetallic oxide catalyzed transesterification of Elaeis guineensis derived triglycerides for biodiesel production. *Energy Convers. Manage.* 141, 20–27. doi: 10.1016/j.enconman.2016.03.042

Tichit, D., Lhouty, M. H., Guida, A., Chiche, B. H., Figueras, F., Auroux, A., et al. (1995). Textural properties and catalytic activity of hydrotalcites. *J. Catal.* 151, 50–59. doi: 10.1006/jcat.1995.1007

Trakarnpruk, W., and Porntangjitlikit, S. (2008). Palm oil biodiesel synthesized with potassium loaded calcined hydrotalcite and effect of biodiesel blend on elastomer properties. *Renew. Energ.* 33, 1558–1563. doi: 10.1016/j.renene.2007.08.003

Vaccari, A. (1999). Clays and catalysis: a promising future. *Appl. Clay Sci.* 14, 161–198. doi: 10.1016/S0169-1317(98)00058-1

Wakil, M. A., Kalam, M. A., Masjuki, H. H., and Rizwanul Fattah, I. M. (2016). Rice bran: a prospective resource for biodiesel production in Bangladesh. *Int. J. Green Energy* 13, 497–504. doi: 10.1080/15435075.2014.966374

Wan Omar, W. N. N., and Amin, N. A. S. (2011). Biodiesel production from waste cooking oil over alkaline modified zirconia catalyst. *Fuel Process. Technol.* 92, 2397–2405. doi: 10.1016/j.fuproc.2011.08.009

Yaşar, F. (2019). Biodiesel production via waste eggshell as a low-cost heterogeneous catalyst: Its effects on some critical fuel properties and comparison with CaO. *Fuel* 255:115828. doi: 10.1016/j.fuel.2019.115828

Yoo, S. J., Lee, H.-S., Veriansyah, B., Kim, J., Kim, J.-D., and Lee, Y.-W. (2010). Synthesis of biodiesel from rapeseed oil using supercritical methanol with metal oxide catalysts. *Bioresour. Technol.* 101, 8686–8689. doi: 10.1016/j.biortech.2010.06.073

Zabeti, M., Wan Daud, W. M. A., and Aroua, M. K. (2009). Activity of solid catalysts for biodiesel production: a review. *Fuel Process. Technol.* 90, 770–777. doi: 10.1016/j.fuproc.2009.03.010

Zeng, H.-Y., Liao, K.-B., Deng, X., Jiang, H., and Zhang, F. (2009). Characterization of the lipase immobilized on Mg–Al hydrotalcite for biodiesel. *Process Biochem.* 44, 791–798. doi: 10.1016/j.procbio.2009.04.005

Zhang, G., Hattori, H., and Tanabe, K. (1988). Aldol addition of acetone, catalyzed by solid base catalysts: magnesium oxide, calcium oxide, strontium oxide, barium oxide, lanthanum (III) oxide and zirconium oxide. *Appl. Catal.* 36, 189–197. doi: 10.1016/S0166-9834(00)80114-1

Zhang, Y., Niu, S., Lu, C., Gong, Z., and Hu, X. (2020). Catalytic performance of NaAlO2/γ-Al2O3 as heterogeneous nanocatalyst for biodiesel production: optimization using response surface methodology. *Energy Convers. Manage.* 203:112263. doi: 10.1016/j.enconman.2019.112263

Influence of Fuel to Oxidizer Ratio on Microwave-Assisted Combustion Preparation of Nanostructured KOH/Ca$_{12}$Al$_{14}$O$_{33}$ Catalyst Used in Efficient Biodiesel Production

Hamed Nayebzadeh[1]*, Mohammad Haghighi[2,3]*, Naser Saghatoleslami[4] and Mohammad Tabasizadeh[5]

[1] Faculty of Material and Chemical Engineering, Esfarayen University of Technology, Esfarayen, Iran, [2] Chemical Engineering Faculty, Sahand University of Technology, Tabriz, Iran, [3] Reactor and Catalysis Research Center (RCRC), Sahand University of Technology, Tabriz, Iran, [4] Department of Chemical Engineering, Faculty of Engineering, Ferdowsi University of Mashhad, Mashhad, Iran, [5] Department of Biosystems Engineering, Faculty of Agriculture, Ferdowsi University of Mashhad, Mashhad, Iran

In this study, the microwave-assisted solution combustion method was utilized for the fabrication of Ca$_{12}$Al$_{14}$O$_{33}$ as support and the amount of urea was assessed as an important parameter during synthesis of the sample. Synthesized Ca$_{12}$Al$_{14}$O$_{33}$ with different fuel amounts was impregnated by KOH and used in the biodiesel production process with canola oil under microwave irradiation. The results presented that the crystallinity, crystalline size, specific surface area, and elemental composition of the final nanocatalysts are affected by the fuel amount. Moreover, during impregnation of potassium components, the structure of support was interestingly transformed from CaAl$_2$O$_4$ to Ca$_{12}$Al$_{14}$O$_{33}$ structure due to the incorporation of potassium in an alumina lattice and more diffusion of calcium cations into a support lattice. On the other hand, when the amount of fuel passed the optimum amount (2 times the stoichiometric amount), the crystallinity was reduced due to the formation of high amounts of smoke during combustion and prevention of the entry of air (oxygen) into the system. The results of the microwave-enhanced transesterification reaction confirmed the results of the analyses that the conversion of 94.5% was obtained using an optimum sample at 450 W, 12 molar ratios of methanol/oil, 4 wt.% catalyst, and 60 min reaction time. According to the stability of the optimum sample [at least three times (>75%)], along with its unique mesoporous structure, uniform dispersion of potassium components, and high basicity sites, it can be considered as a comparable solid base nanocatalyst for biodiesel production.

Keywords: KOH/Ca$_{12}$Al$_{14}$O$_{33}$, nanostructured catalyst, microwave combustion, biodiesel, canola oil

INTRODUCTION

Nowadays, the production of renewable, non-toxic, eco-friendly, and environmentally friendly fuels has been of great concern to scientists and governments. Extensive research has been performed on alternative fuels, among which biodiesel has shown its high potential due to its biodegradability, similar properties to petroleum fuel, low emission profiles, excellent lubrication of the engine system, and suitability for industrial production (Mardhiah et al., 2017). Biodiesel, otherwise called fatty acid methyl ester (FAME), is commonly produced via the transesterification of vegetable oil or animal fats with methanol (Dehghani and Haghigh, 2017; Veillette et al., 2017). In fact, the viscosity of feedstocks, which has some drawbacks for engine and injection systems, is reduced by the reaction. The catalyst has an important role in the transesterification reaction, where homogeneous catalysts such as NaOH and KOH are usually utilized (Avhad and Marchetti, 2015). This reaction is carried out in a short time (about 1.5 h), while the separation process for producing the final biodiesel with an appropriate quality takes a long time (Tangy et al., 2016).

Microwave irradiation as a novel technology has been widely considered in chemical reactions (Ajamein and Haghighi, 2016; Rezaee and Haghighi, 2016) and it has been extensively studied in the field of biodiesel production in order to reduce production and separation times. Refaat et al. reported that, in addition to the reduction of the transesterification reaction time (from 75 to 4 min), the separation time was also reduced (from 60 to 3 min) (Refaat and El Sheltawy, 2008). Although microwave irradiation eases the production and separation processes, the major drawback of homogeneous catalysts is that they produce soap, and thus several separation and purification steps are required to obtain pure biodiesel. These processes could cause significant environmental problems, since wastewater is produced by the washing of biodiesel with water several times for the elimination of the soap. Therefore, heterogeneous catalysts have been suggested for biodiesel production, although they have not been meaningfully studied in the microwave system as compared to the conventional heating system (Li et al., 2013; Allami et al., 2019).

Heterogeneous base catalysts have extensively been proposed for biodiesel production; KOH and CaO are often used as an active phase for increasing the basicity of catalysts. Liao and Chung (2013) studied the performance of KOH/CaO in microwave-assisted biodiesel production. However, the low specific surface area and lower stability of CaO as support or during the active phase, due to a simple reaction with H_2O and CO_2 in the air, are among the issues challenging scientists (de Sousa et al., 2016; Ye et al., 2016). The application of stable basic support was suggested to overcome this problem. Alkali earth aluminates with a general formula $M_xAl_{2y}O_{x+3y}$ (M = Mg, Ba, Sr, and Ca) have some unique properties, such as high stability and thermal resistance (Quirino et al., 2016; Naderi and Nayebzadeh, 2019). It seems that calcium sources such as carbonate, nitrate, etc., due to their low prices, are a sufficient component for the preparation of alkali earth aluminate (Gupta and Agarwal, 2016; Roschat et al., 2016).

In previous studies, conventional catalyst preparation methods such as co-precipitation (Meng et al., 2013; Lu et al., 2015) and sol-gel (Selyunina et al., 2013; Mandić and Kurajica, 2015) were utilized for the fabrication of calcium aluminate. Against these long time catalyst preparation processes, the combustion method as a self-propagating high-temperature synthesis (SHS) method shows itself to be a suitable procedure for the preparation of refractory materials with high purity and significantly lower energy and time consumption (González-Cortés and Imbert, 2013; Chang et al., 2014). This method, unlike other catalyst preparation methods, does not require the annealing of final powder at high temperatures (sometimes over 1,000°C) for extended periods of time (Varma et al., 2016; Nayebzadeh et al., 2019). A primary heat is required to initiate the oxidation/reduction reactions, where microwave irradiation has shown to have efficient external heating due to its uniform heating, fast heating rates, and hot spots, as well as selective absorption of radiation by polar substances. This is why it is called microwave combustion synthesis (MCS) (Specchia et al., 2017; Deganello and Tyagi, 2018).

Although the effect of fuel type and other variables on the structure and properties of calcium aluminate fabricated by the MCS method has been studied with our previous work (Nayebzadeh et al., 2016, 2017a,b), further studies can be performed to obtain a sample with the highest activity and stability. Other parameters such as fuel-to-oxidizer, or fuel ratio (FR), microwave irradiation output power, water content in precursor, and pH of the solution have influence on the properties of the final product synthesized by the MCS method (Rosa et al., 2013; Hashemzehi et al., 2020a). Hashemzehi et al. reported that, for preparation of a nanocatalyst with good crystallinity and high activity for biodiesel production, high microwave power must be used (Hashemzehi et al., 2016). Furthermore, it was reported that FR has the greatest influence on the properties and performance of the final powder due to its effect on the temperature of the exothermic combustion reaction during catalyst preparation (Nasiri et al., 2012; Khoshbin et al., 2016) that has not been studied previously. Therefore, in this study, the effect of FR was assessed on the properties of calcium aluminate as support prepared by the MCS method. After impregnation of the potassium component on the surface of supports, their activity was examined in the microwave-enhanced transesterification of canola oil. The samples were characterized using X-ray Diffraction (XRD), Fourier-transform infrared spectroscopy (FTIR), Brunauer–Emmett–Teller (BET), Thermogravimetric (TG), Energy-dispersive X-ray spectroscopy (EDX), Field Emission Scanning Electron Microscopy (FESEM) analyses, and basicity using Hammett indicator. The level of reusability as an optimum aim for industrial use using a catalyst was evaluated for $KOH/Ca_{12}Al_{14}O_{33}$ nanocatalyst fabricated at optimum FR in the biodiesel production process.

MATERIALS AND METHODS

Materials

Chemical grades of aluminum nitrate ($Al(NO_3)_3.9H_2O$), calcium nitrate ($Ca(NO_3)_2.4H_2O$), potassium hydroxide (KOH), urea

(CH_4N_2O), and methanol (CH_3OH) were purchased from Merck. All the materials were used as received without any further purification. The canola oil was supplied from a local store.

Nanocatalyst Synthesis Procedure

In the MCS method, metal salts such as nitrates are mixed with water and soluble carbohydrates as fuel. In our study, $Al(NO_3)_3.9H_2O$ (20 mmole) and $Ca(NO_3)_2.6H_2O$ (10 mmole) were mixed with 30 mL of deionized water in a beaker and then a desirable amount of urea with 1, 1.5, 2, or 2.5 times of stoichiometric compositions was added. According to propellant chemistry, stoichiometric compositions of the fuel-to-oxidizer ratio were calculated using the total oxidizing and reducing valences of the components (Nayebzadeh et al., 2016). The corresponding chemical reaction for preparation of calcium aluminate with different FRs is shown as follows:

$$Ca(NO_3)_2.4H_2O + 2Al(NO_3)_3.9H_2O + 6.67XCH_4N_2O \rightarrow$$
$$CaAl_2O_4 + (22 + 13.34X)H_2O + 6.67XCO_2 + (4 + 6.67X)N_2,$$
$$X = (1.0, 1.5, 2.0, 2.5) \qquad (1)$$
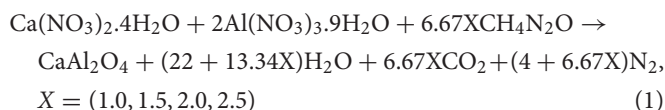
After gelling the mixture by heating at 80°C, the beaker was transformed in the domestic microwave oven (Daewoo, Model No. KOC9N2TB, 900 watts, 2.45 GHz) and irradiated for 10 min. After exhausting the huge amount of gases, the combustion reaction started and the foamy catalyst was produced. The samples were labeled as CA(FR = 1), CA(FR = 1.5), CA(FR = 2), and CA(FR = 2.5).

Potassium components as active phases were impregnated by mixing the supports with the KOH aqueous solution (35 wt.%) and refluxing at 80°C for 2 h. After aging the mixture for 12 h, it was placed in an oven at 110°C overnight to dry. Finally, the powders were calcined at 700°C for 4 h to obtain KCA(FR = 1), KCA(FR = 1.5), KCA(FR = 2), and KCA(FR = 2.5) (Nayebzadeh et al., 2017a). The nanocatalysts synthesis method is shown in **Figure 1**.

Nanocatalysts Characterization Techniques

XRD analysis was performed to determine the crystalline phase of the samples, where a UNISANTIS/XMD 300 apparatus operating at 45 kV and 80 mA with scanning range of 10–60° by means of Cu Kα radiation was utilized. The textural properties of the sample containing a specific surface area, mean pore size, and pore volume were determined using a PHS-1020 (PHSCHINA, China) apparatus by N_2 adsorption/desorption method. TG analysis was utilized for assessing the decomposition of raw materials during catalyst preparation. The phenomenon of microwave combustion reaction was evaluated by TG analysis under air flow in the range of 50–800°C at a heating rate of 20°C/min performed by on an Evolution STA (SETARAm, France) instrument. Using FESEM analysis performed by MIRA3 FEG-SEM (TESCAN, Czech Republic), the morphology and surface structure of the nanocatalysts were assessed. The surface elemental distribution of the samples was depicted by the EDX technique using VEGA II Detector (Czech Republic,

TESCAN). The surface functional groups of the nanocatalysts were assayed by FTIR spectra in the range of 400–4,000 cm^{-1} using a SHIMADZU 4300 (Japan) spectrometer. The Hammett indicators method was used to determine the basic strength (H_) of the samples where bromothymol blue (H_ = 7.2), phenolphthalein (H_ = 9.8), and 2,4-dinitroaniline (H_ = 15.0) were utilized as indicators. By titration of each color changed mixture containing 0.2 g catalyst, 10 mL methanol, and 1 mL Hammett indicator solution via 0.02 mole benzene carboxylic acid/L anhydrous ethanol solution, the basicity of the nanocatalysts was measured (Ye et al., 2014).

Experimental Setup for Catalytic Performance Test

The microwave-enhanced transesterification reaction of canola oil was carried out in a 100 mL glass reactor equipped with a water-cooled condenser for assessment of the catalytic activity of the samples. A modified domestic microwave with a hole of 20 mm at its top was utilized to carry out the reaction at microwave output power of 450 W for 1 h. For each reaction, the glass reactor was loaded by 20 g canola oil, 12 mL methanol (12 methanol/oil molar ratios), and 0.8 g catalyst (4 wt.%). Although the reaction was not performed at the optimum conditions, it can provide a suitable conversion for comparing the catalysts. At the end of the reaction, the biodiesel layer mixture was separated from glycerol and used as a catalyst by centrifuging the mixture at 2,500 rpm for 25 min. Its layer was heated to remove excess methanol and obtain pure biodiesel. The conversion of the reaction was determined based on the FAME content of the produced biodiesel. The FAME content of biodiesel was calculated by the following equation:

$$\text{Conversion (\%) =}$$
$$[(\text{area of all FAME} \times \text{weight of reference})/(\text{area of reference}$$
$$\times \text{weight of biodiesel sample})] \times 100 \qquad (2)$$

where reference is assigned to methyl non-adecanoate as an internal standard. Area of FAME and reference were mentioned to the area of gas chromatographic (GC; Teif Gostar Faraz co., Iran) peaks of produced biodiesel equipped with FID detector and SUPRAWAX-280 capillary column (30 m × 0.25 mm × 0.25 μm).

RESULTS AND DISCUSSION

Nanostructured Catalysts Characterization
XRD Analysis

The effect of FR on the crystalline structure of calcium aluminate is illustrated in **Figure 2**. All the samples show the monoclinic phase of the monocalcium aluminate structure ($CaAl_2O_4$ as called CA) in accordance with the Joint Committee on Powder Diffraction Standards (JCPDS No. 70-0134) database with different peak intensities. In the CaO and Al_2O_3 system, mayenite ($Ca_{12}Al_{14}O_{33}$ as called $C_{12}A_7$) forms as the first structure of calcium aluminate, which quickly reacts with Al_2O_3 to form CA when sintering temperature and time increase (Nayebzadeh et al., 2017b). Janakova et al. reported that CA is formed at reaction
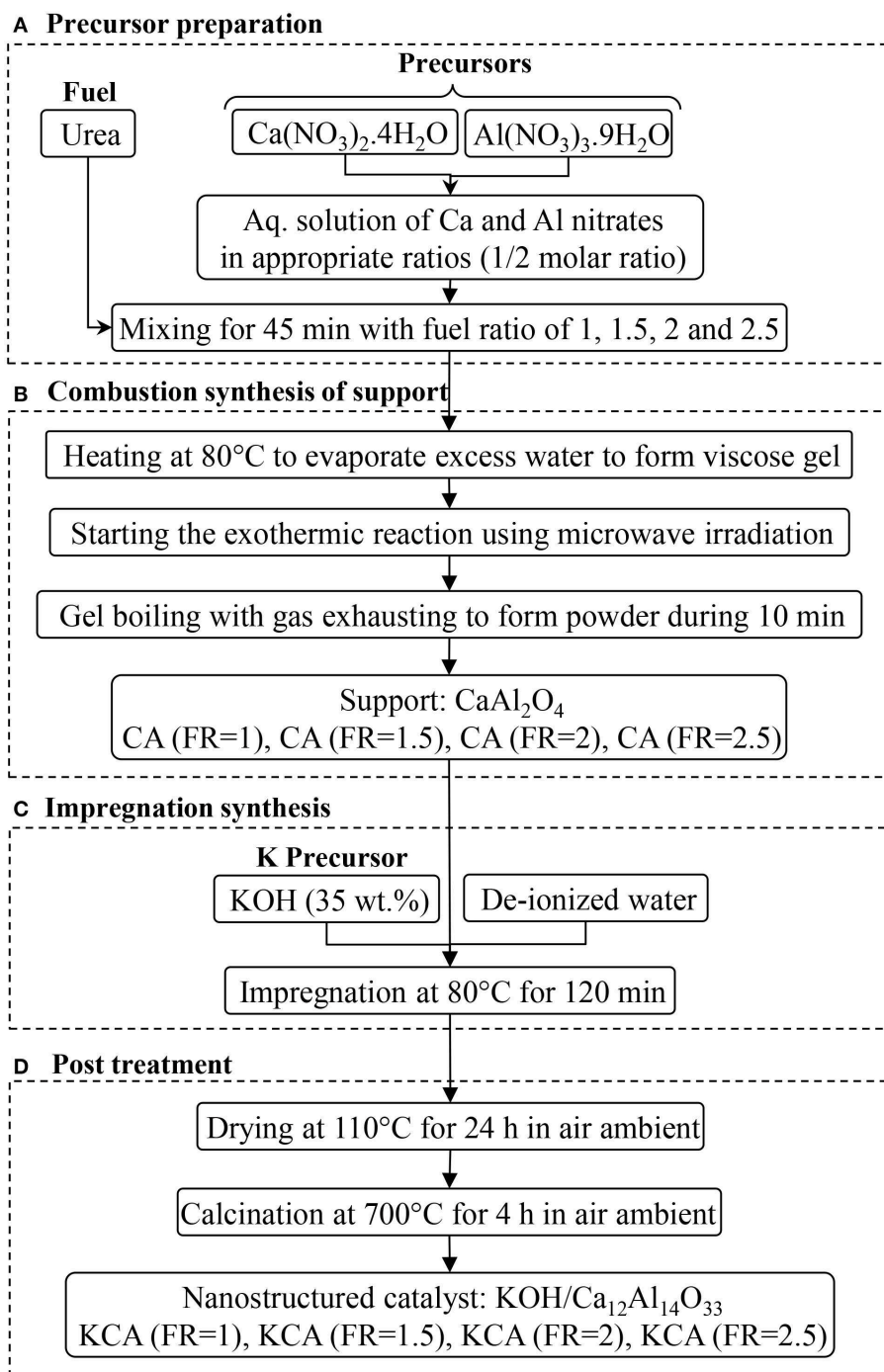
FIGURE 1 | Microwave assisted combustion synthesis of KOH/Ca$_{12}$Al$_{14}$O$_{33}$ nanostructured catalysts with various fuel ratios. **(A)** Precursor preparation. **(B)** Combustion synthesis of support. **(C)** Impregnation synthesis. **(D)** Post treatment.

temperatures up to 1,050°C and higher temperatures are required to have a full crystallinity (Janáková et al., 2007).

The theoretical combustion temperature can be obtained using enthalpy of the reaction and a specific heat capacity of the product when the combustion process assumes adiabatic (Hashemzehi et al., 2020b). If it is assumed that only CaAl$_2$O$_4$

was formed, the adiabatic combustion temperature obtains 923, 1,263, 1,444, and 1,557°C for a fuel ratio of 1–2.5 (see **Supplementary Material**). It shows that the combustion temperature increased sharply by loading higher amounts of fuel while the rate of temperature increasing reduced at a higher fuel ratio. Moreover, less crystallinity of the sample fabricated at a fuel

FIGURE 2 | XRD patterns of synthesized $CaAl_2O_4$ supports with various fuel ratios: **(A)** CA (FR = 1), **(B)** CA (FR = 1.5), **(C)** CA (FR = 2), and **(D)** CA (FR = 2.5).
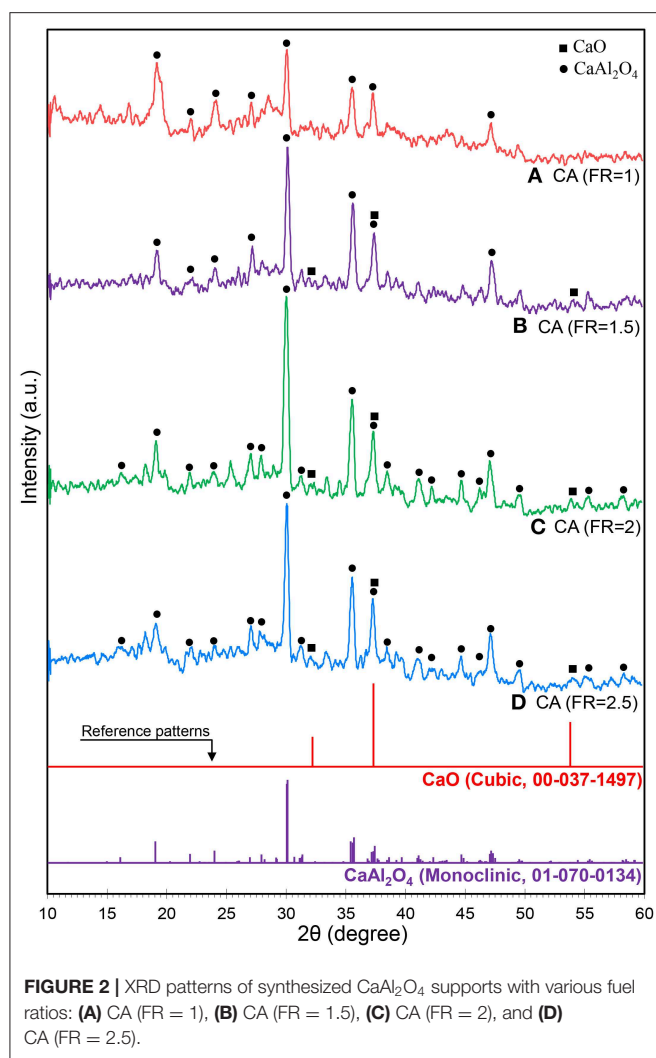
ratio of 1 can be proven by the calculated temperature which was under the minimum temperature needed to obtain well crystalline structure of $CaAl_2O_4$ (1,050°C). Thus, it is proven that the temperature of combustion reaction medium is extremely high (Rodríguez et al., 2012). Therefore, the nanocatalysts at the FR above 1.5 contain CaO, $C_{12}A_7$, CA, and Al_2O_3, with CA being the dominant phase (Rivas Mercury et al., 2005; Ruszak et al., 2011). The diffraction peaks of Al_2O_3 (JCPDS No. 76-0144) and $C_{12}A_7$ (JCPDS No. 78-0910) can be, respectively, observed at 2θ = 25.4° and 18.1°, especially at CA(FR = 2) nanocatalyst.

When the amount of urea increased in the mixture, the burning flame continued from seconds to minutes. An increase of combustion duration caused the formation of the well-defined crystalline structure of CA. The relative crystallinity of the as-prepared CA nanocatalyst, calculated based on the peak at 2θ = 30.1°, clearly proves the effect of fuel increase on the formation of CA (shown in **Table 1**). However, the relative crystallinity decreased at a FR of 2.5. Rapid oxygen transport from air to reaction medium is significantly necessary for complete combustion, as in fuel-rich conditions. However,

oxygen diffusion limitations result in incomplete combustion for the CA(FR = 2.5) nanocatalyst (Ghosh et al., 2010). The effect of reaction temperature can be significantly observed in the crystalline size of CA, as the CA(FR = 2) shows the lowest crystalline size (**Table 1**).

The XRD patterns of the $KOH/Ca_{12}Al_{14}O_{33}$ nanocatalyst are shown in **Figure 3**. It can be clearly observed that the samples were transformed from CA structure to $C_{12}A_7$ phases due to the additional heat treatment and dopant concentration (Avci et al., 2012). The phase transformation is related to the diffusion of Ca^{2+} ions through the CA layer to react with Al_2O_3 in order to form $Ca_3Al_2O_6$ (C_3A) and $C_{12}A_7$, as the stable phase is finally formed at the expense of CA and C_3A (Tao et al., 2012). In addition, the K_2O (JCPDS No. 22-0493) and K_2CO_3 (JCPDS No. 73-0470) phases can be recognized in the XRD patterns of the samples, especially at the KCA(FR = 2) and KCA(FR = 2.5) nanocatalysts. Less amorphous structures in the samples with high crystallinity may allow the potassium component to make individual phases. This phase has a significant effect on the activity of the catalyst in the transesterification reaction (Nayebzadeh et al., 2016).

The relative crystallinity and crystalline size of the samples are also listed in **Table 1**. The KCA(FR = 2) and KCA(FR = 2.5) nanocatalysts show the highest relative crystallinity and the largest crystalline size, respectively, which might be due to the greater formation of large crystals of $C_{12}A_7$.

FTIR Analysis

The FTIR spectra of the $KOH/Ca_{12}Al_{14}O_{33}$ nanocatalysts are illustrated in **Figure 4**. The spectra of all the samples exhibit a bond between 3,200 and 3,400 cm^{-1}, which is related to O-H stretching vibration of absorbed water molecules on the surface of the nanocatalysts. Moreover, a peak at 1670 cm^{-1} is also assigned to the bending vibration of water molecules (Khoshbin and Haghighi, 2014; Kazemifard et al., 2019). The characteristic bond in the range of 3,400–3,600 cm^{-1} can be assigned to Ca/Al-OH groups (Chang et al., 2014). In addition, stretching vibration of Al-O-K groups, due to the attachment of K^+ ions to alumina, is also observed around 3,600 and 1,100 cm^{-1}. The bonds at 1,470, 1,395, 1,020, and 935 cm^{-1} may be associated with the characteristic vibrations of the Al-OH or Al-O-K bonding (Hashemzehi et al., 2016). The characteristic absorption regions of Al-O stretching vibrations for tetrahedral (AlO_4) and octahedral (AlO_6) are, respectively, observed in the 700–850 cm^{-1} and 500–700 cm^{-1} (Kazemifard et al., 2018). The tetrahedral bonds of Al-O confirm the formation of $C_{12}A_7$ structure (Lu et al., 2012). The Ca-O bond is observed around 470 cm^{-1} (Alba-Rubio et al., 2010; Hojjat et al., 2016).

BET and Basicity Analysis

The BET properties of the samples are listed in **Table 1**. The specific surface area of the samples sequentially increased from 58.14 to 95.40 m^2/g by increasing the FR. This could be due to an increase of the amounts of exhausted gas and combustion time during catalyst preparation. A similar phenomenon was also detected for pore volume and mean pore size of the samples, whereas these decreased by increasing the FR from 2 to 2.5.

TABLE 1 | Physicochemical properties of synthesized $CaAl_2O_4$ supports and $KOH/Ca_{12}Al_{14}O_{33}$ nanostructured catalysts.

Nanocatalyst	BET (m²/g)	P_V (cm³)	P_d (nm)	Basicity		Relative Crystallinity[a]		Crystallite size[b] (nm)	
				H_	Strength (mmol/g)	$CaAl_2O_4$	$Ca_{12}Al_{14}O_{33}$	$CaAl_2O_4^c$	$Ca_{12}Al_{14}O_{33}^d$
CA(FR = 1)	–	–	–	<7.2	–	42.4	–	25.9	–
CA(FR = 1.5)	–	–	–	<7.2	–	71.2	–	24.9	–
CA(FR = 2)	–	–	–	<7.2	–	100	–	18.5	–
CA(FR = 2.5)	–	–	–	<7.2	–	80.8	–	22.1	–
KCA(FR = 1)	58.14	0.142	5.43	9.8–15	0.392	–	67.4	–	23.3
KCA(FR = 1.5)	62.52	0.304	6.03	9.8–15	0.400	–	92.7	–	25.8
KCA(FR = 2)	64.20	0.441	7.40	9.8–15	0.404	–	100	–	27.5
KCA(FR = 2.5)	95.43	0.314	5.99	9.8–15	0.404	–	100	–	26.9

[a] Relative crystallinity: XRD relative peak intensity at $2\theta = 30.1°$ for $CaAl_2O_4$ and $18.1°$ for $Ca_{12}Al_{14}O_{33}$.
[b] Crystallite size estimated by Scherre's equation at $2\theta = 30.1°$ for $CaAl_2O_4$ and $18.1°$ for $Ca_{12}Al_{14}O_{33}$.
[c] Crystallite phase: Monoclinic (JCPDS: 01-070-0134, $2\theta = 19.0, 22.0, 23.9, 27.9, 30.1, 35.7, 37.4, 47.2$).
[d] Crystallite phase: Cubic (JCPDS: 01-078-910, $2\theta = 18.1, 27.8, 29.8, 33.4, 36.7, 41.2, 46.7, 55.2, 57.5$).
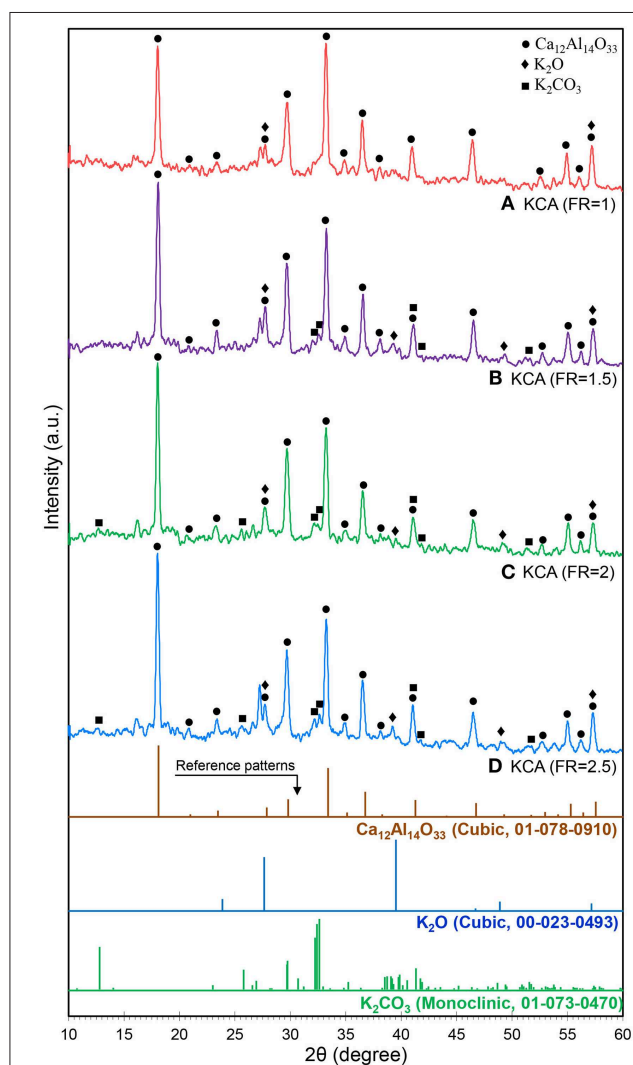
FIGURE 3 | XRD patterns of synthesized $KOH/Ca_{12}Al_{14}O_{33}$ nanostructured catalysts with various fuel ratios: **(A)** KCA(FR = 1), **(B)** KCA(FR = 1.5), **(C)** KCA(FR = 2), and **(D)** KCA(FR = 2.5).

In the biodiesel production process, porosity of the catalyst can even play a larger role than the surface area. The diffusion of triglycerides molecules into catalyst pores contains seven stages, including: (1) passing through the external film of the catalyst, (2) diffusing into the pores, (3) adsorbing on the active surface, (4) reacting the reactants, (5) disposing the products (biodiesel and glycerol) from the catalyst surface, (6) diffusing toward the outside through the pores, and (7) passing through the external film (Ebadinezhad and Haghighi, 2020). Therefore, the pore size must be insufficient in order to perform the stages 3–7. It was mentioned that the pores must be at least 6 nm in diameter for easy permeation of triglycerides macromolecules (Jacobson et al., 2008). A number of studies have emphasized that restricted diffusion transpires when reactant molecules and pores have comparable dimensions (Lukić et al., 2010). Therefore, triglycerides molecules can easily diffuse through the pores of the major part of the KCA(FR = 2) nanocatalyst, leading to an efficient contact to be established between the reactant and active site. In addition, the KCA(FR = 2) nanocatalyst also shows the largest pores volume.

As shown in **Table 1**, the basicity of the as-prepared catalysts was not meaningfully changed by an increased FR. The basicity is defined as a basic site for a catalyst where KOH plays the most important role in increasing the basic strength. Here, the support (CA) showed insignificant basicity strength in the studied region. Since the amount of impregnated potassium compounds on the catalysts is constant, the samples showed a similar basicity strength.

TG Analysis

The TG plots of the monocalcium aluminate prepared by different FRs, which explain the level of completing the combustion reaction, are illustrated in **Figure 5**. The weight loss below 150°C is assigned to the elimination of water from the surface of supports and/or in raw material structure where the CA(FR = 1) showed the highest weight loss (5.5%) (Nayebzadeh et al., 2016). The second reduction in weight in the range of 150–500°C is owed to pyrolysis of organic groups

FIGURE 4 | FTIR spectra of synthesized KOH/Ca$_{12}$Al$_{14}$O$_{33}$ nanostructured catalysts with various fuel ratios: **(A)** KCA(FR = 1), **(B)** KCA(FR = 1.5), **(C)** KCA(FR = 2), and **(D)** KCA(FR = 2.5).
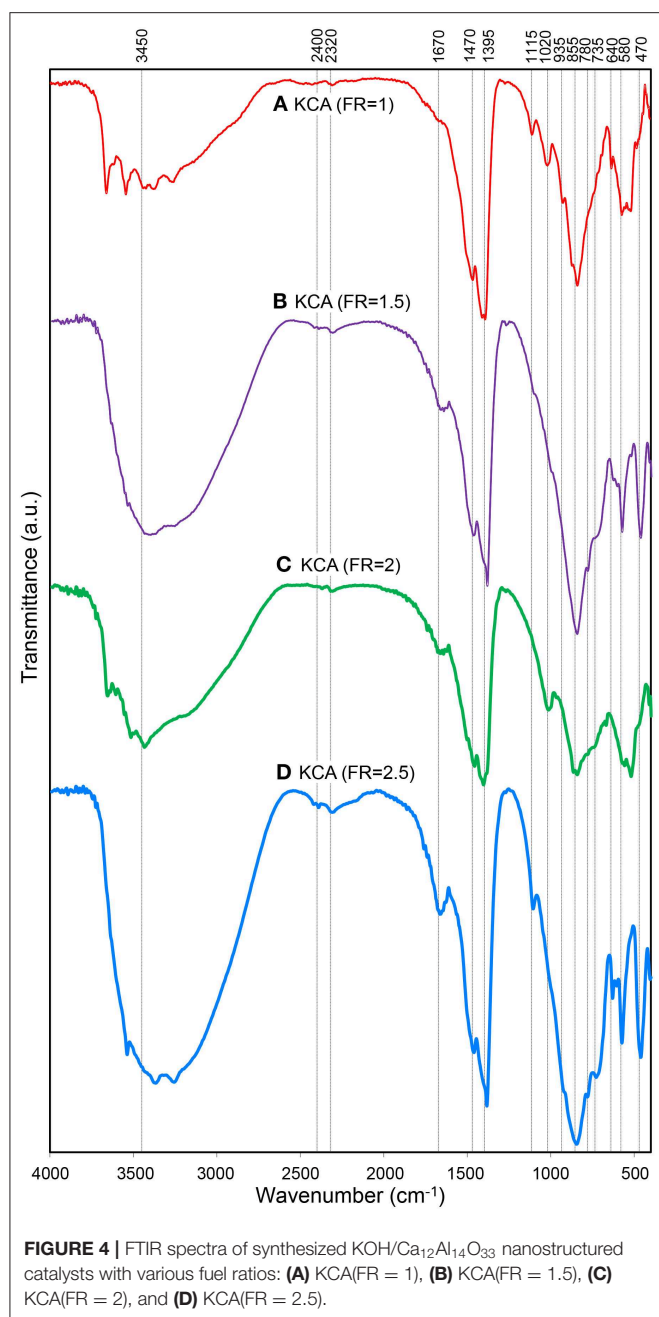
and/or nitrate precursors, which exhibit incomplete combustion reaction (Chen et al., 2014). CA(FR = 1) and CA(FR = 2.5) have high weight loss (around 15%), which is in good agreement with the results of relative crystallinity obtained from the XRD patterns. It confirms that the optimization of the FR in the combustion method is important for obtaining the highest combustion temperature to synthesize the catalyst with a good structure and high crystallinity (Rahmani Vahid and Haghighi, 2016). The last reduction in weight occurred in the range of 500–600°C, which could correspond to the incorporation of calcium components in the alumina lattice to

form CaAl$_2$O$_4$. Moreover, such a reduction could be attributed to the transition of alumina from the amorphous to crystalline phase, where the CA(FR = 1) illustrates the highest amount of amorphous phases followed by the CA(FR = 1.5) and CA(FR = 2.5) samples with 3.7 and 5.2% weight loss, respectively (Yousefi et al., 2019). The CA(FR = 2) nanocatalyst with 2.5% weight loss confirms that the fuel-to-oxidizer ratio of 2 is an appropriate amount for the preparation of monocalcium aluminate (CaAl$_2$O$_4$) as support.

EDX Analysis

The EDX analysis results of the KOH/Ca$_{12}$Al$_{14}$O$_{33}$ nanocatalysts (KCAs) are depicted in **Figure 6**. It can be seen that all the samples contain Al, Ca, K, and O elements and no impurity was observed. The KCAs nanocatalysts show similar element distribution percentages of Al, Ca, and K to the parent solution (35.1, 31.8, and 33.1% for Al, Ca, and K, respectively). Due to the increased combustion reaction and increased alumina in the structure with an increasing fuel ratio, the amount of Al element subsequently increased from 29.4% for the KCA(FR = 1) to 40.3% for the KCA(FR = 2.5). Moreover, the potassium component increased with an increase of the FR from 1 to 2 and then was decreased by more fuel loading. This can be related to the extreme increase of the KCA(FR = 2.5) specific surface area that caused the potassium components' distribution to decrease (as seen in **Figure 6D**). The dot-mapping of the samples clearly exhibited that the potassium components were homogeneously dispersed on the surface of support, especially in the KCA(FR = 2) nanocatalyst (**Figure 6C**), which can result in an appropriate activity of the sample.

FESEM Analysis

The FESEM images of the CA(FR = 2) and KCA(FR = 2) nanocatalysts are illustrated in **Figure 7**. The combustion cavities as external gates provided during the CA(FR = 2) preparation show large diameters in the range of 300–600 nm, and cause the penetration resistance to be reduced for permeation of the reactant (especially large molecules of triglycerides) (Rahmani Vahid and Haghighi, 2016). Moreover, the morphology of the sample shows that the temperature of the combustion reaction was appropriate, such that the particle size with good distribution sizes can be observed. According to a surface particle size distribution histogram, the CA(FR = 2) nanocatalyst shows the size of the particles to be in the range of 5–17 nm with an average size of 11 nm, where the particles with 10–12 nm have the highest frequency.

The KCA(FR = 2) nanocatalyst is shown in the right side of **Figure 7**, in which the morphology of the CA(FR = 2) was not clearly changed by potassium loading. However, the surface particles size distribution was changed; accordingly, the average particle size increased from 11 nm to 12 nm by potassium loading. The results can be proved by the XRD analysis, where the crystalline size increased due to phase transformation from CA to C$_{12}$A$_7$. The phase transformation effect on the particle size is due to the increased bond length between Ca, Al, and O in the mayenite structure as compared to monocalcium aluminate.
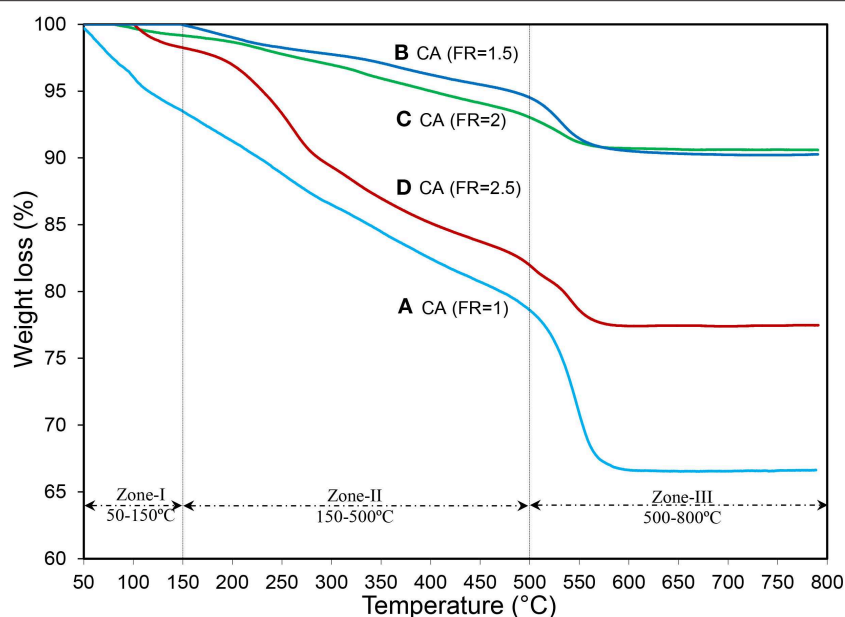
FIGURE 5 | TG analysis of synthesized $CaAl_2O_4$ supports with various fuel ratios: **(A)** CA(FR = 1), **(B)** CA(FR = 1.5), **(C)** CA(FR = 2), and **(D)** CA(FR = 2.5).

Minimum and maximum particle sizes of the KCA(FR = 2) nanocatalyst are, respectively, 7.4 and 18.9 nm.

Catalytic Performance Study Toward Biodiesel Production

The activity of the $KOH/Ca_{12}Al_{14}O_{33}$ nanocatalysts is illustrated in **Figure 8**. As expected, the KCA(FR = 2) and KCA(FR = 2.5) nanocatalysts showed higher activity in the conversion of canola oil to biodiesel. The samples showed a high specific surface area and mean pore size, which led to unimpeded permeation of reactants through the porosity of the catalysts, making more contact with their active phases. Moreover, the crystallinity and basicity of these samples were much more than those of the other samples, proving their higher activity. Therefore, the KCA(FR = 2) nanocatalyst was selected as the optimum catalyst and the FR of 2 seemed to be the best ratio for the preparation of calcium aluminate supported by the potassium components.

Dall'Oglio et al. (2014) have conducted a study on the aluminum, calcium, manganese, titanium, and magnesium oxides as support for biodiesel production under microwave irradiation. The results exhibited that alumina was the best support where K_2CO_3/Al_2O_3 showed the highest activity (98%) at the reaction conditions of methanol/oil molar ratio of 16 and 10 wt.% of the catalyst and reaction time of 30 min. The other potassium precursor showed an intermediate biodiesel conversion. The yield of 60 and 40% was, respectively, obtained using the KOH/Al_2O_3 and KI/Al_2O_3 catalyst in the microwave-assisted biodiesel production. At these conditions, the CaO/Al_2O_3, CaO/TiO_2, and CaO/MnO_2 catalysts converted 46.2, 36.6, and 49.2% of soybean oil to biodiesel, respectively. This means that the $Ca_{12}Al_{14}O_{33}$ might be one of the best supports for the loading of active phases for biodiesel production.

Reusability of KCA(FR = 2) Nanocatalyst in the Biodiesel Production

The reusability of catalysts is an important element in the industrial application of catalysts (Nayebzadeh et al., 2014). To assess the stability of KCA(FR = 2) as an optimum nanocatalyst, it was separated from the reaction mixture after each run by centrifuging the mixture at 6,000 rpm for 20 min and washed with methanol twice time to eliminate the reactants and products from porosities. Then it was dried and calcined at 700°C for 1 h and reused. The results are presented in **Figure 9**. It can be seen that the catalytic activity of KCA(FR = 2) nanocatalyst decreased from 94.5 to 80.7%, which can be related to leaching and/or poisoning of active phases (potassium components), that can be proven by the brown color of glycerol. However, in the third use, the activity of the catalyst did not meaningfully change and a yield of 76.4% was obtained. The yield slightly decreased with further uses, as a yield of 70.6% was obtained in the fifth run. The results signify that some potassium components have weak bonds with the surface of calcium aluminate as support. The results confirm that the calcium aluminate as support protects its stability during the reaction and could be an appropriate support among those reported so far for loading species for industrial application in the biodiesel production process.

Comparing the Results With Other Studies

The activity of the samples was compared with other studies as illustrated in **Table 2**. KOH/calcium aluminate presents good activity in the transesterification reaction as high as CaO [used in conventional (Ye et al., 2016) or microwave (Hsiao et al., 2011) heating systems]. However, CaO can react to methanol to form calcium methoxide in reaction mediums, reduce the
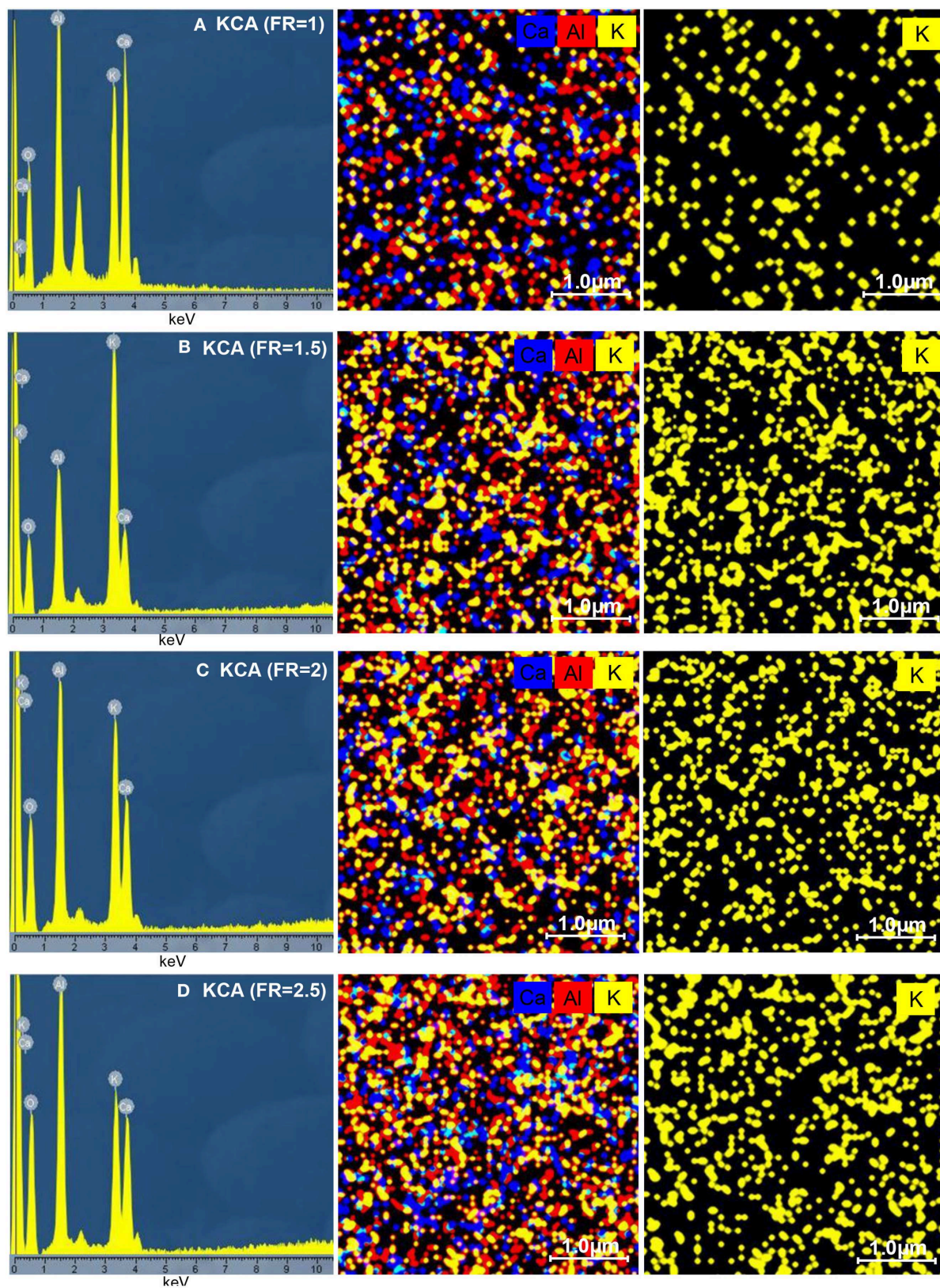
FIGURE 6 | EDX analysis of synthesized $KOH/Ca_{12}Al_{14}O_{33}$ nanostructured catalysts with various fuel ratios: **(A)** KCA(FR = 1), **(B)** KCA(FR = 1.5), **(C)** KCA(FR = 2), and **(D)** KCA(FR = 2.5).
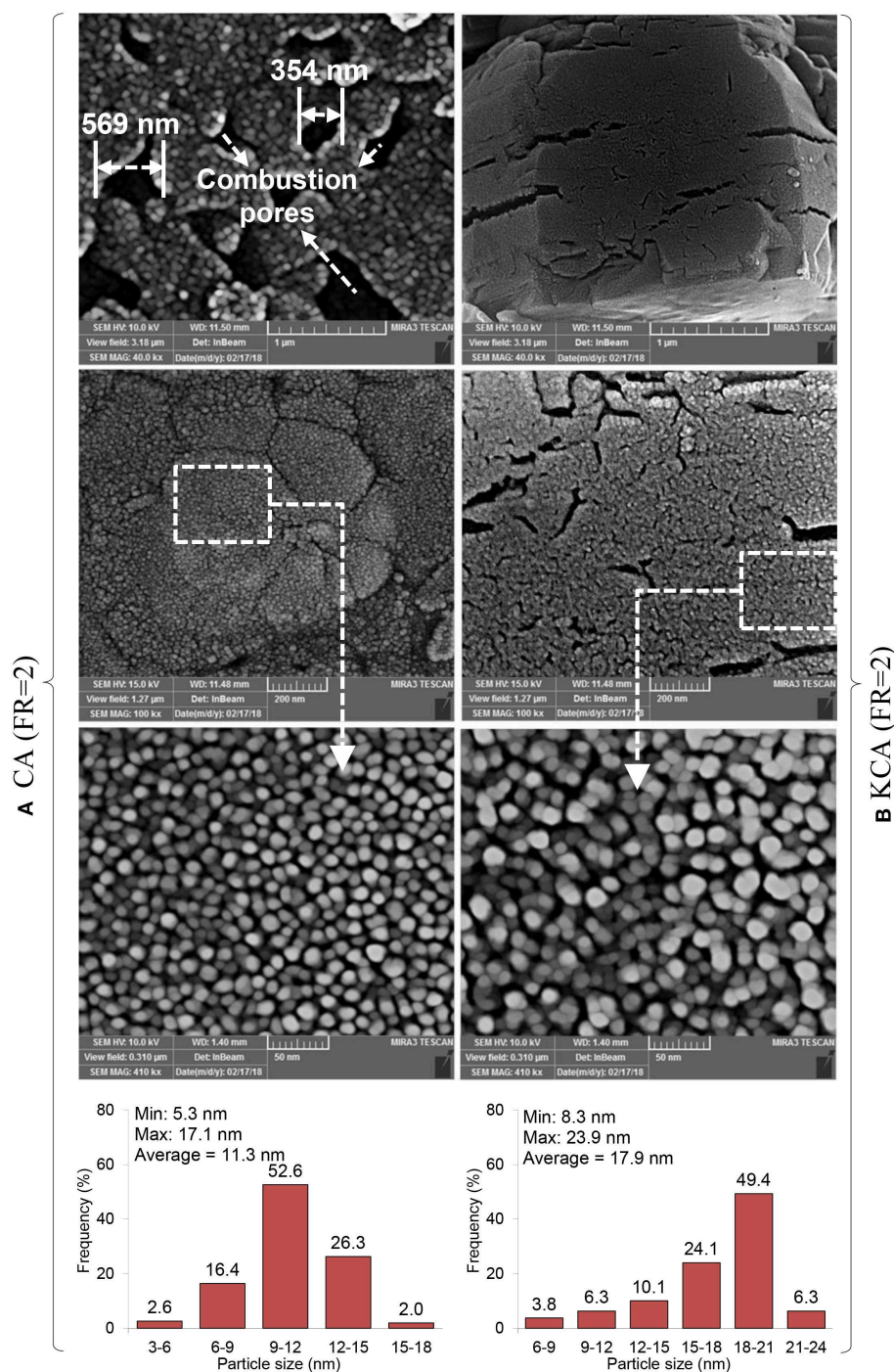
FIGURE 7 | FESEM images of synthesized $CaAl_2O_4$ support and $KOH/Ca_{12}Al_{14}O_{33}$ nanostructured catalyst: **(A)** CA(FR = 2) and **(B)** KCA(FR = 2).

reaction conversion, and cause high leaching due to the solubility of methanol in a biodiesel layer (de Sousa et al., 2016). Although eggshell as a catalyst, which contains CaO as major material, shows high activity, it was obtained at a high microwave power and duration, or at a high methanol and catalyst concentration (Khemthong et al., 2012; Peng et al., 2018).

The prepared nanocatalyst also presented good activity when the reaction conditions were milder than in other studies. Doping the calcium into an alumina structure can enhance the basicity of the support along with improving the leaching problem of Ca ions reported in previous studies. In addition, the calcium aluminate has different structures that can be studied
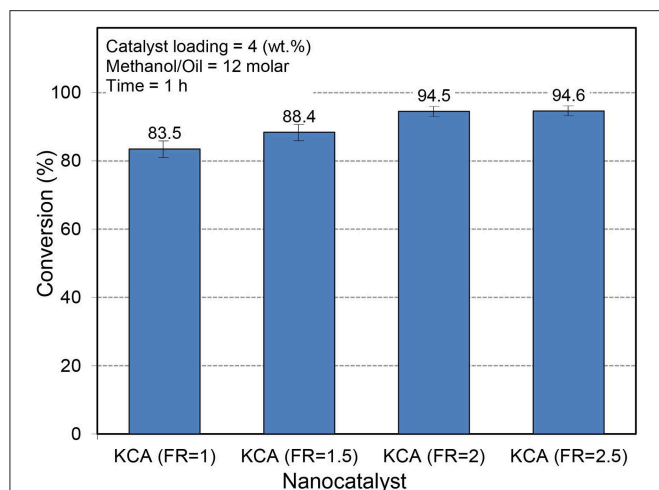
FIGURE 8 | Influence of fuel ratio on the catalytic performance of synthesized KOH/Ca$_{12}$Al$_{14}$O$_{33}$ nanostructured catalysts with various fuel ratios.
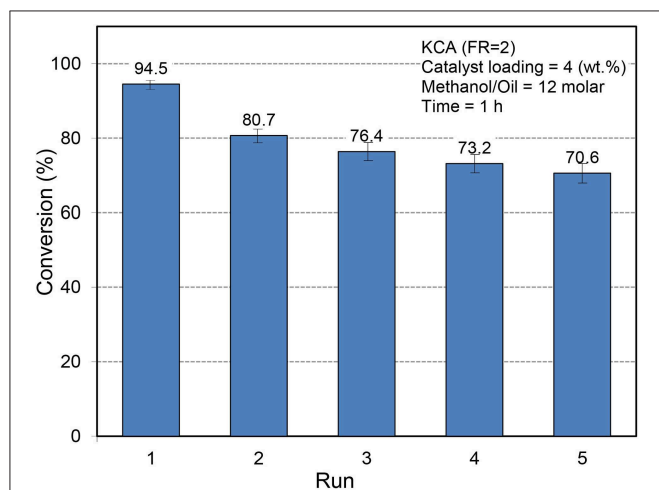
FIGURE 9 | Reusability of KOH/Ca$_{12}$Al$_{14}$O$_{33}$ nanostructured catalysts toward biodiesel production from canola oil.

to obtain the most active and stable structure for the biodiesel production process.

Moreover, the production procedure is so simple to set up on an industrial scale to reduce the catalyst preparation cost. However, bonding the potassium ions with the surface of the calcium aluminate can be a challenge for enhancing its reusability. It seems that utilizing other types of potassium precursors and the optimization of impregnation conditions may facilitate bonding of K ions with Ca and Al ions, which will be studied in our future work. Therefore, it seems that KOH/calcium aluminate can be further studied to assess its ability to be used for industrial application.

CONCLUSIONS

CaAl$_2$O$_4$ as alkali calcium aluminate was successfully synthesized by the MCS method, and the effect of fuel amount during the catalyst preparation was assessed. Furthermore, the samples were impregnated by the potassium components to improve their catalytic activity for the transesterification of canola oil to biodiesel through microwave irradiation. The characterization results revealed that the monocalcium aluminate prepared by urea as fuel with twice the stoichiometric amount has a high crystallinity and good precursor decomposition during combustion. This structure was transformed to Ca$_{12}$Al$_{14}$O$_{33}$ structure during potassium loading and calcination due to the diffusion of Ca^{2+} ions in a monocalcium aluminate lattice and/or reaction of the potassium component with alumina to form potassium aluminate. KOH/Ca$_{12}$Al$_{14}$O$_{33}$ showed nanoscale particles where the potassium components were uniformly dispersed on the surface of support. The nanocatalyst, due to its high specific surface area, mean pore size, crystallinity, and basicity, converted high amounts of canola oil to biodiesel through microwave irradiation. The microwave-enhanced biodiesel production was performed under conditions of 450 watts, 12 molar ratio of methanol/oil, 4 wt.% of catalyst, and 1 h reaction time, where a yield of 94.5% was obtained. The nanocatalyst presented a suitable reusability although it required optimizing amounts of the potassium components.

TABLE 2 | Comparison of catalytic performance of various catalysts in biodiesel production process under microwave irradiation.

Catalyst	Feedstock	Transesterification condition				Yield (%)	References
		Mw. P (W)	MORb	Cc (wt.%)	td (min)		
KOH/calcium aluminate	Soybean	450	12	4	60	94.5	This study
CaO	Soybean	300 (60°C)	7	3	60	96.6	Hsiao et al., 2011
Eggshells (CaO)	WCO	900 (65°C)	9	5	165		Peng et al., 2018
Eggshells (CaO)	Palm	900	18	15	4	96.7	Khemthong et al., 2012
NaOH/ZnO	Soybean	180°C	20	2	180	77.82	Quirino et al., 2017
Ca(OH)$_2$/Fe$_3$O$_4$	Jatropha-Castor	900 (65°C)	12	2	35	95	Chang et al., 2017
CaO	Palm	150	9	5	60	89.9	Ye et al., 2016
SO$_3$H–ZnAl$_2$O$_4$	Palm (esterification)	800 (60°C)	9	1.5	20	94.6	Soltani et al., 2017
Sulfonated activated carbon	Soybean	600 (75 °C)	6	20	20	88.7	Rocha et al., 2019
ZrO$_2$/Bamboo ash	Soybean	900 (60°C)	15	12	60	96	Fatimah et al., 2019

DATA AVAILABILITY STATEMENT

The datasets generated for this study are available on request to the corresponding author.

AUTHOR CONTRIBUTIONS

Conceptualization of the work was done by NS. MH and HN performed the experiments. The graphs and tables were prepared by HN and MH. The results were analyzed by HN, MH, and MT. After writing the manuscript HN, MH, NS, and MT checked its writing quality. All authors contributed to the article and approved the submitted version.

FUNDING

SUPPLEMENTARY MATERIAL

The Supplementary Material for this article can be found online at: https://www.frontiersin.org/articles/10.3389/fenrg.2020.00106/full#supplementary-material

REFERENCES

Ajamein, H., and Haghighi, M. (2016). Influence of ambient gas on microwave-assisted combustion synthesis of CuO–ZnO–Al₂O₃ nanocatalyst used in fuel cell grade hydrogen production via methanol steam reforming. *Ceram. Int.* 42, 17978–17989. doi: 10.1016/j.ceramint.2016.07.092

Alba-Rubio, A. C., Santamaría-González, J., Mérida-Robles, J. M., Moreno-Tost, R., Martín-Alonso, D., Jiménez-López, A., et al. (2010). Heterogeneous transesterification processes by using CaO supported on zinc oxide as basic catalysts. *Catal. Today* 149, 281–287. doi: 10.1016/j.cattod.2009.06.024

Allami, H. A., Tabasizadeh, M., Rohani, A., Farzad, A., and Nayebzadeh, H. (2019). Precise evaluation the effect of microwave irradiation on the properties of palm kernel oil biodiesel used in a diesel engine. *J. Clean. Prod.* 241:117777. doi: 10.1016/j.jclepro.2019.117777

Avci, N., Korthout, K., Newton, M. A., Smet, P. F., and Poelman, D. (2012). Valence states of europium in CaAl₂O₄:Eu phosphors. *Opt. Mater. Express* 2, 321–330. doi: 10.1364/OME.2.000321

Avhad, M. R., and Marchetti, J. M. (2015). A review on recent advancement in catalytic materials for biodiesel production. *Renew. Sustain. Energy Rev.* 50, 696–718. doi: 10.1016/j.rser.2015.05.038

Chang, K.-L., Lin, Y.-C., Jhang, S.-R., Cheng, W. L., Chen, S.-C., and Mao, S.-Y. (2017). Rapid Jatropha-Castor biodiesel production with microwave heating and a heterogeneous base catalyst nano-Ca(OH)₂/Fe₃O₄. *Catalysts* 7:203. doi: 10.3390/catal7070203

Chang, Y.-P., Chang, P.-H., Lee, Y.-T., Lee, T.-J., Lai, Y.-H., and Chen, S.-Y. (2014). Morphological and structural evolution of mesoporous calcium aluminate nanocomposites by microwave-assisted synthesis. *Microporous Mesoporous Mater.* 183, 134–142. doi: 10.1016/j.micromeso.2013.09.013

Chen, J., Jia, L., Guo, X., Xiang, L., and Lou, S. (2014). Production of novel biodiesel from transesterification over KF-modified Ca-Al hydrotalcite catalyst. *RSC Adv.* 4, 60025–60033. doi: 10.1039/C4RA09214G

Dall'Oglio, E. L., de Sousa, P. T. Jr., de Oliveira, P. T. J., de Vasconcelos, L. G., Parizotto, C. A., and Kuhnen, C. A. (2014). Use of heterogeneous catalysts in methylic biodiesel production induced by microwave irradiation. *Química Nova* 37, 411–417. doi: 10.5935/0100-4042.20140081

de Sousa, F. P., dos Reis, G. P., Cardoso, C. C., Mussel, W. N., and Pasa, V. M. D. (2016). Performance of CaO from different sources as a catalyst precursor in soybean oil transesterification: Kinetics and leaching evaluation. *J. Environ. Chem. Eng.* 4, 1970–1977. doi: 10.1016/j.jece.2016.03.009

Deganello, F., and Tyagi, A. K. (2018). Solution combustion synthesis, energy and environment: Best parameters for better materials. *Progress Cryst. Growth Character. Mater.* 64, 23–61. doi: 10.1016/j.pcrysgrow.2018.03.001

Dehghani, S., and Haghigh, M. (2017). Sono-sulfated zirconia nanocatalyst supported on MCM-41 for biodiesel production from sunflower oil: influence of ultrasound irradiation power on catalytic properties and performance. *Ultras. Sonochem.* 35, 142–151. doi: 10.1016/j.ultsonch.2016.09.012

Ebadinezhad, B., and Haghighi, M. (2020). Sono-solvothermal decoration of pore size controlled SAPO-34 by nano-ceria for green fuel production via esterification reaction. *Chem. Eng. J.* 125146. doi: 10.1016/j.cej.2020.125146

Fatimah, I., Rubiyanto, D., Taushiyah, A., Najah, F. B., Azmi, U., and Sim, Y.-L. (2019). Use of ZrO₂ supported on bamboo leaf ash as a heterogeneous catalyst in microwave-assisted biodiesel conversion. *Sustain. Chem. Pharm.* 12:100129. doi: 10.1016/j.scp.2019.100129

Ghosh, S. K., Prakash, A., Datta, S., Roy, S. K., and Basu, D. (2010). Effect of fuel characteristics on synthesis of calcium hydroxyapatite by solution combustion route. *Bull. Mater. Sci.* 33, 7–16. doi: 10.1007/s12034-010-0010-3

González-Cortés, S. L., and Imbert, F. E. (2013). Fundamentals, properties and applications of solid catalysts prepared by solution combustion synthesis (SCS). *Appl. Catal. A General* 452, 117–131. doi: 10.1016/j.apcata.2012.11.024

Gupta, J., and Agarwal, M. (2016). Preparation and characterizaton of CaO nanoparticle for biodiesel production. *AIP Confer. Proc.* 1724:020066. doi: 10.1063/1.4945186

Hashemzehi, M., Pirouzfar, V., Nayebzadeh, H., and Alihosseini, A. (2020a). Effect of synthesizing conditions on the activity of zinc-copper aluminate nanocatalyst prepared by microwave combustion method used in the esterification reaction. *Fuel* 263:116422. doi: 10.1016/j.fuel.2019.116422

Hashemzehi, M., Pirouzfar, V., Nayebzadeh, H., and Alihosseini, A. (2020b). Application of response surface methodology to optimize high active Cu-Zn-Al mixed metal oxide fabricated via microwave-assisted solution combustion method. *Adv. Powder Technol.* 31, 1470–1479. doi: 10.1016/j.apt.2020.01.010

Hashemzehi, M., Saghatoleslami, N., and Nayebzadeh, H. (2016). A study on the structure and catalytic performance of ZnₓCu₁₋ₓAl₂O₄ catalysts synthesized by the solution combustion method for the esterification reaction. *Comptes Rendus Chim.* 19, 955–962. doi: 10.1016/j.crci.2016.05.006

Hojjat, M., Nayebzadeh, H., Khadangi-Mahrood, M., and Rahmani-Vahid, B. (2016). Optimization of process conditions for biodiesel production over CaO–Al₂O₃/ZrO₂ catalyst using response surface methodology. *Chem. Papers* 71, 689–698. doi: 10.1007/s11696-016-0096-1

Hsiao, M.-C., Lin, C.-C., and Chang, Y.-H. (2011). Microwave irradiation-assisted transesterification of soybean oil to biodiesel catalyzed by nanopowder calcium oxide. *Fuel* 90, 1963–1967. doi: 10.1016/j.fuel.2011.01.004

Jacobson, K., Gopinath, R., Meher, L. C., and Dalai, A. K. (2008). Solid acid catalyzed biodiesel production from waste cooking oil. *Appl. Catal. B Environ.* 85, 86–91. doi: 10.1016/j.apcatb.2008.07.005

Janáková, S., Salavcová, L., Renaudin, G., Filinchuk, Y., Boyer, D., and Boutinaud, P. (2007). Preparation and structural investigations of sol–gel derived -doped. *J. Phys. Chem. Solids* 68, 1147–1151. doi: 10.1016/j.jpcs.2006.12.034

Kazemifard, S., Nayebzadeh, H., Saghatoleslami, N., and Safakish, E. (2018). Assessment the activity of magnetic KOH/Fe₃O₄@Al₂O₃ core–shell nanocatalyst in transesterification reaction: effect of Fe/Al ratio on structural and performance. *Environ. Sci. Pollut. Res.* 25, 32811–32821. doi: 10.1007/s11356-018-3249-7

Kazemifard, S., Nayebzadeh, H., Saghatoleslami, N., and Safakish, E. (2019). Application of magnetic alumina-ferric oxide nanocatalyst supported by KOH for in-situ transesterification of microalgae cultivated in wastewater medium. *Biomass Bioener.* 129:105338. doi: 10.1016/j.biombioe.2019.105338

Khemthong, P., Luadthong, C., Nualpaeng, W., Changsuwan, P., Tongprem, P., Viriya-empikul, N., et al. (2012). Industrial eggshell wastes as the heterogeneous

catalysts for microwave-assisted biodiesel production. *Catal. Today* 190, 112–116. doi: 10.1016/j.cattod.2011.12.024

Khoshbin, R., and Haghighi, M. (2014). Direct conversion of syngas to dimethyl ether as a green fuel over ultrasound-assisted synthesized CuO-ZnO-Al$_2$O$_3$/HZSM-5 nanocatalyst: effect of active phase ratio on physicochemical and catalytic properties at different process conditions. *Catal. Sci. Technol.* 4, 1779–1792. doi: 10.1039/C3CY01089A

Khoshbin, R., Haghighi, M., and Margan, P. (2016). Combustion dispersion of CuO–ZnO–Al$_2$O$_3$ nanocatalyst over HZSM-5 used in DME production as a green fuel: effect of citric acid to nitrate ratio on catalyst properties and performance. *Energy Convers. Manage.* 120, 1–12. doi: 10.1016/j.enconman.2016.04.076

Li, Y., Ye, B., Shen, J., Tian, Z., Wang, L., Zhu, L., et al. (2013). Optimization of biodiesel production process from soybean oil using the sodium potassium tartrate doped zirconia catalyst under microwave chemical reactor. *Bioresour. Technol.* 137, 220–225. doi: 10.1016/j.biortech.2013.03.126

Liao, C.-C., and Chung, T.-W. (2013). Optimization of process conditions using response surface methodology for the microwave-assisted transesterification of Jatropha oil with KOH impregnated CaO as catalyst. *Chem. Eng. Res. Design* 91, 2457–2464. doi: 10.1016/j.cherd.2013.04.009

Lu, S., Chunfeng, H., Yoshio, S., and Qing, H. (2012). Study of phase transformation behaviour of alumina through precipitation method. *J. Phys. D Appl. Phys.* 45:215302. doi: 10.1088/0022-3727/45/21/215302

Lu, Y., Zhang, Z., Xu, Y., Liu, Q., and Qian, G. (2015). CaFeAl mixed oxide derived heterogeneous catalysts for transesterification of soybean oil to biodiesel. *Bioresour. Technol.* 190, 438–441. doi: 10.1016/j.biortech.2015.02.046

Lukić, I., Krstić, J., Glišić, S., Jovanović, D., and Skala, D. (2010). Biodiesel synthesis using K$_2$CO$_3$/Al–O–Si aerogel catalysts. *J. Serbian Chem. Soc.* 75, 789–801. doi: 10.2298/JSC090707047L

Mandić, V., and Kurajica, S. (2015). The influence of solvents on sol–gel derived calcium aluminate. *Mater. Sci. Semiconductor Process.* 38, 306–313. doi: 10.1016/j.mssp.2015.01.004

Mardhiah, H. H., Ong, H. C., Masjuki, H. H., Lim, S., and Lee, H. V. (2017). A review on latest developments and future prospects of heterogeneous catalyst in biodiesel production from non-edible oils. *Renew. Sustain. Energy Rev.* 67, 1225–1236. doi: 10.1016/j.rser.2016.09.036

Meng, Y.-L., Wang, B.-Y., Li, S.-F., Tian, S.-J., and Zhang, M.-H. (2013). Effect of calcination temperature on the activity of solid Ca/Al composite oxide-based alkaline catalyst for biodiesel production. *Bioresour. Technol.* 128, 305–309. doi: 10.1016/j.biortech.2012.10.152

Naderi, F., and Nayebzadeh, H. (2019). Performance and stability assessment of Mg-Al-Fe nanocatalyst in the transesterification of sunflower oil: effect of Al/Fe molar ratio. *Indus. Crops Prod.* 141:111814. doi: 10.1016/j.indcrop.2019.111814

Nasiri, H., Bahrami Motlagh, E., Vahdati Khaki, J., and Zebarjad, S. M. (2012). Role of fuel/oxidizer ratio on the synthesis conditions of Cu–Al$_2$O$_3$ nanocomposite prepared through solution combustion synthesis. *Mater. Res. Bull.* 47, 3676–3680. doi: 10.1016/j.materresbull.2012.06.041

Nayebzadeh, H., Saghatoleslami, N., Haghighi, M., and Tabasizadeh, M. (2017b). Influence of fuel type on microwave-enhanced fabrication of KOH/Ca$_{12}$Al$_{14}$O$_{33}$ nanocatalyst for biodiesel production via microwave heating. *J. Taiwan Inst. Chem. Eng.* 75, 148–155. doi: 10.1016/j.jtice.2017.03.018

Nayebzadeh, H., Saghatoleslami, N., Haghighi, M., and Tabasizadeh, M. (2019). Catalytic activity of KOH–CaO–Al$_2$O$_3$ nanocomposites in biodiesel production: impact of preparation method. *Int. J. Self Propagat. High Temp. Synth.* 28, 18–27. doi: 10.3103/S1061386219010102

Nayebzadeh, H., Saghatoleslami, N., Maskooki, A., and Vahid, B. R. (2014). Preparation of supported nanosized sulfated zirconia by strontia and assessment of its activities in the esterification of oleic acid. *Chem. Biochem. Eng. Q.* 25, 259–265. doi: 10.15255/CABEQ.2013.1894

Nayebzadeh, H., Saghatoleslami, N., and Tabasizadeh, M. (2016). Optimization of the activity of KOH/calcium aluminate nanocatalyst for biodiesel production using response surface methodology. *J. Taiwan Inst. Chem. Eng.* 68, 379–386. doi: 10.1016/j.jtice.2016.09.041

Nayebzadeh, H., Saghatoleslami, N., and Tabasizadeh, M. (2017a). Application of microwave irradiation for preparation of a KOH/calcium aluminate nanocatalyst and biodiesel. *Chem. Eng. Technol.* 40, 1826–1834. doi: 10.1002/ceat.201600466

Peng, Y.-P., Amesho, K. T. T., Chen, C.-E., Jhang, S.-R., Chou, F.-C., and Lin, Y.-C. (2018). Optimization of biodiesel production from waste cooking oil using waste eggshell as a base catalyst under a microwave heating system. *Catalysts* 8:81. doi: 10.3390/catal8020081

Quirino, M. R., Oliveira, M. J. C., Keyson, D., Lucena, G. L., Oliveira, J., and Gama, L. (2016). Synthesis of zinc aluminate with high surface area by microwave hydrothermal method applied in the transesterification of soybean oil (biodiesel). *Mater. Res. Bull.* 74, 124–128. doi: 10.1016/j.materresbull.2015.10.027

Quirino, M. R., Oliveira, M. J. C., Keyson, D., Lucena, G. L., Oliveira, J., and Gama, L. (2017). Synthesis of zinc oxide by microwave hydrothermal method for application to transesterification of soybean oil (biodiesel). *Mater. Chem. Phys.* 185, 24–30. doi: 10.1016/j.matchemphys.2016.09.062

Rahmani Vahid, B., and Haghighi, M. (2016). Urea-nitrate combustion synthesis of MgO/MgAl$_2$O$_4$ nanocatalyst used in biodiesel production from sunflower oil: Influence of fuel ratio on catalytic properties and performance. *Energy Convers. Manage.* 126, 362–372. doi: 10.1016/j.enconman.2016.07.050

Refaat, A. A., and El Sheltawy, S. T. (2008). Time factor in microwave-enhanced biodiesel production. *WSEAS Trans. Environ. Dev.* 4, 279–288.

Rezaee, L., and Haghighi, M. (2016). Citrate complexation microwave assisted synthesis of Ce$_{0.8}$Zr$_{0.2}$O$_2$ nanocatalyst over Al$_2$O$_3$ used in CO oxidation for hydrogen purification: influence of composite loading and synthesis method. *RSC Adv.* 6, 34055–34065. doi: 10.1039/C6RA02973F

Rivas Mercury, J. M., De Aza, A. H., and Pena, P. (2005). Synthesis of CaAl$_2$O$_4$ from powders: Particle size effect. *J. Eur. Ceram. Soc.* 25, 3269–3279. doi: 10.1016/j.jeurceramsoc.2004.06.021

Rocha, P. D., Oliveira, L. S., and Franca, A. S. (2019). Sulfonated activated carbon from corn cobs as heterogeneous catalysts for biodiesel production using microwave-assisted transesterification. *Renew. Energy* 143, 1710–1716. doi: 10.1016/j.renene.2019.05.070

Rodríguez, M. A., Aguilar, C. L., and Aghayan, M. A. (2012). Solution combustion synthesis and sintering behavior of CaAl$_2$O$_4$. *Ceram. Int.* 38, 395–399. doi: 10.1016/j.ceramint.2011.07.020

Rosa, R., Veronesi, P., and Leonelli, C. (2013). A review on combustion synthesis intensification by means of microwave energy. *Chem. Eng. Process. Process Intensif.* 71, 2–18. doi: 10.1016/j.cep.2013.02.007

Roschat, W., Siritanon, T., Yoosuk, B., and Promarak, V. (2016). Biodiesel production from palm oil using hydrated lime-derived CaO as a low-cost basic heterogeneous catalyst. *Energy Convers. Manage.* 108, 459–467. doi: 10.1016/j.enconman.2015.11.036

Ruszak, M., Witkowski, S., Pietrzyk, P., Kotarba, A., and Sojka, Z. (2011). The role of intermediate calcium aluminate phases in solid state synthesis of mayenite (Ca$_{12}$Al$_{14}$O$_{33}$). *Funct. Mater. Lett.* 4, 183–186. doi: 10.1142/S1793604711001907

Selyunina, L. A., Mishenina, L. N., Slizhov, Y. G., and Kozik, V. V. (2013). Effect of citric acid and ethylene glycol on the formation of calcium aluminate via the sol–gel method. *Russian J. Inorgan. Chem.* 58, 450–455. doi: 10.1134/S0036023613040165

Soltani, S., Rashid, U., Nehdi, I. A., Al-Resayes, S. I., and Al-Muhtaseb, A. A. H. (2017). Sulfonated mesoporous zinc aluminate catalyst for biodiesel production from high free fatty acid feedstock using microwave heating system. *J. Taiwan Inst. Chem. Eng.* 70, 219–228. doi: 10.1016/j.jtice.2016.10.054

Specchia, S., Ercolino, G., Karimi, S., Italiano, C., and Vita, A. (2017). Solution combustion synthesis for preparation of structured catalysts: a mini-review on process intensification for energy applications and pollution control. *Int. J. Self Propagat. High Temp. Synth.* 26, 166–186. doi: 10.3103/S1061386217030062

Tangy, A., Pulidindi, I. N., and Gedanken, A. (2016). SiO$_2$ beads decorated with SrO nanoparticles for biodiesel production from waste cooking oil using microwave irradiation. *Energy Fuels* 30, 3151–3160. doi: 10.1021/acs.energyfuels.6b00256

Tao, G., Hua, Z., Gao, Z., Chen, Y., Wang, L., He, Q., et al. (2012). Synthesis and catalytic activity of mesostructured KF/CaxAl$_2$O$_{(x+3)}$ for the transesterification reaction to produce biodiesel. *RSC Adv.* 2, 12337–12345. doi: 10.1039/c2ra22218c

Varma, A., Mukasyan, A. S., Rogachev, A. S., and Manukyan, K. V. (2016). Solution combustion synthesis of nanoscale materials. *Chem. Rev.* 116, 14493–14586. doi: 10.1021/acs.chemrev.6b00279

Veillette, M., Giroir-Fendler, A., Faucheux, N., and Heitz, M. (2017). Esterification of free fatty acids with methanol to biodiesel using heterogeneous catalysts: from model acid oil to microalgae lipids. *Chem. Eng. J.* 308, 101–109. doi: 10.1016/j.cej.2016.07.061

Ye, B., Qiu, F., Sun, C., Li, Y., and Yang, D. (2014). Biodiesel production from soybean oil using heterogeneous solid base catalyst. *J. Chem. Technol. Biotechnol.* 89, 988–997. doi: 10.1002/jctb.4190

Ye, W., Gao, Y., Ding, H., Liu, M., Liu, S., Han, X., et al. (2016). Kinetics of transesterification of palm oil under conventional heating and microwave irradiation, using CaO as heterogeneous catalyst. *Fuel* 180, 574–579. doi: 10.1016/j.fuel.2016.04.084

Yousefi, S., Haghighi, M., and Rahmani Vahid, B. (2019). Role of glycine/nitrates ratio on structural and texture evolution of MgO-based nanocatalyst fabricated by hybrid microwave-impregnation method for biofuel production. *Energy Convers. Manage.* 182, 251–261. doi: 10.1016/j.enconman.2018.12.067

Check for
updates

Recent Advances of Biodiesel Production Using Ionic Liquids Supported on Nanoporous Materials as Catalysts: A Review

Ali Gholami[1,2], Fathollah Pourfayaz[1,2]* and Akbar Maleki[3]

[1] Department of Renewable Energies and Environment, Faculty of New Sciences & Technologies, University of Tehran, Tehran, Iran, [2] Nanoenergy Laboratory, Faculty of New Sciences and Technologies, University of Tehran, Tehran, Iran, [3] Faculty of Mechanical Engineering, Shahrood University of Technology, Shahrood, Iran

For the last two decades, the biodiesel attracted increasing attention as a promising biofuel to replace fossil diesel. However, the non-recyclability of homogeneous alkali catalysts and waste generation due to subsequent water washing remained as one of the major drawbacks of the biodiesel production process in the industry. Ionic liquids are one of the best alternatives to replace alkali catalysts owing to their unique properties such as non-volatility, excellent solubility for various organic and inorganic materials, structure tunability, environment-friendliness, and wide liquid temperature. However, high viscosity and difficult recovery have limited their application. Recently, heterogenization of ionic liquids on solid supports has been proposed to circumvent these issues. Among these solids, nanoporous materials have shown great potential in providing stable supports with high porosity and specific surface area. This paper reviews the recent developments in designing ionic liquids deposited on nanoporous materials as catalysts for biodiesel production. The emphasis was on the application of this type of catalysts for the optimization of reaction conditions. Moreover, challenges and opportunities for improving the overall production process in the presence of these catalysts were discussed. Despite that high biodiesel yields were obtained over many of nanoporous material-supported ionic liquids, their significantly higher cost compared to the conventional catalysts remained a major challenge. This issue can be overcome by employing less expensive cations and anions, increasing the loading amount of ionic liquids, and improving catalyst reusability in future studies.

Keywords: biodiesel, nanoporous materials, ionic liquids, catalyst, transesterification

INTRODUCTION

Nowadays, due to the non-renewability of fossil fuels and their negative environmental impacts, the necessity of finding alternative energy sources is well-established. With this respect, renewable energy sources have been considered as one of the most promising options for the last few decades, as they are cleaner and more environment-friendly and can contribute to the sustainable development of societies (Dincer, 2000; Panwar et al., 2011).

As the most common renewable energy resource, biomass has a significant contribution to the world economy and provides a range of biofuels and chemicals (Chum and Overend, 2001; McKendry, 2002; Dodds and Gross, 2007). In 2017, nearly 11% of the world's energy demand was supplied by biomass. However, contributing to 65% of the world's total final consumption, oil has remained as the main energy source in the transportation sector (International Energy Agency, 2019). This necessitates more production and incorporation of biofuels, especially in the transportation fleet, to reduce dependence on petroleum and its negative impacts on the environment.

Biodiesel is one of the popular forms of biofuel which is obtained from vegetable oils and animal fats and is considered as an attractive alternative to fossil diesel (Van Gerpen, 2005). It is renewable, non-toxic, biodegradable, sulfur, and benzene-free, can be used in common diesel engines with no modification, and its blending with fossil diesel at any given ratio is possible (Demirbas, 2006; Nabi et al., 2006; Khan et al., 2009; Kumar et al., 2010; Mekhilef et al., 2011). Owing to these benefits, 36 billion liters of biodiesel were produced around the globe in 2017. This figure is expected to rise by 9% through 2027 (OECD/FA, 2018).

Despite paramount advantages, biodiesel has some technical, economic, and environmental drawbacks. Compared to fossil diesel, biodiesel presents weaker oxidative stability and cold flow properties, higher viscosity and density, and higher NO_x emissions (Monyem and Van Gerpen, 2001; Agarwal et al., 2006; Canakci, 2007; Tesfa et al., 2010). However, the most challenging disadvantage of biodiesel is its higher production cost in comparison with fossil diesel, which is mainly due to the high cost of feedstock and inefficient production processes (Hasheminejad et al., 2011; Yaakob et al., 2014; Ullah et al., 2015).

The most common and economically feasible method of biodiesel production at an industrial scale is the alkali-catalyzed transesterification of fresh vegetable oils (Gebremariam and Marchetti, 2018). However, over 80% of biodiesel production cost stems from employing fresh edible oils as feedstock (Mansir et al., 2018). Therefore, the best way to reduce the production cost of biodiesel is the use of alternative, cheaper sources of lipids such as waste cooking oil, non-edible Jatropha, algae, municipal sewage sludge, and recycled grease trap waste (Nagarajan et al., 2013; Yusuf and Kamarudin, 2013; Olkiewicz et al., 2016; Abdurakhman et al., 2018; Tran et al., 2018). Nevertheless, the high free fatty acid (FFA) content of these feedstocks results in saponification and emulsification in the presence of homogeneous base catalysts, which reduces biodiesel yield and hinders its separation from glycerol (Ghiaci et al., 2011; Alegria et al., 2014). Moreover, these catalysts are corrosive, difficult to be recovered and reused and are removed from the reaction mixture by water washing, which produces considerable amounts of wastewater (Takase et al., 2014; Lee et al., 2015; Sirisomboonchai et al., 2015).

One way to avoid the saponification problem is the use of homogeneous acids such as sulfuric acid and hydrochloric acid. These acids are tolerant of FFAs and esterify them into biodiesel, but they require higher temperature and pressure, a higher amount of alcohol, and longer reaction time to yield high biodiesel conversion (Su, 2013). Furthermore,

corrosiveness, undesired byproducts, negative environmental impacts, the requirement of additional neutralization and separation processes, and difficult recovery have restrained the application of homogeneous acid catalysts at industrial scale (Han et al., 2013).

Ionic liquids (ILs) have recently emerged as one of the most promising options to replace conventional homogeneous catalysts. ILs are organic salts composed of cations and anions with melting points below 100°C (Liu C. Z. et al., 2012; Fang et al., 2014). They are nearly non-volatile, soluble in organic and inorganic materials, remarkably less toxic compared to the traditional organic solvents, possess wide liquids temperature and significant thermal and chemical stability (Fauzi and Amin, 2012; Muhammad et al., 2015). These unique materials are also recyclable and environmentally-friendly (Fan et al., 2013; Montalban et al., 2018; Gholami et al., 2019). More importantly, the properties of ILs can be altered and designed for a specific application by changing the type of cation or anion in their structure (Pandey, 2006; Luo et al., 2013). Owing to these interesting properties, ILs have been employed not only in catalysis but also as base materials and solvents in electrochemistry (Osada et al., 2016; Watanabe et al., 2017), extraction, and separation (Ventura et al., 2017; Berthod et al., 2018), biology and biotechnology (Egorova et al., 2017; Claus et al., 2018) and tribology (Amiril et al., 2017).

With regards to biodiesel production, ILs have been used as catalysts for the transesterification reaction, as cosolvents for stabilizing enzymes in biocatalyzed transesterification, and as solvents for extracting lipids from biomass, FFAs from oily feedstocks, and unsaturated esters and triacylglycerols from biodiesel (Troter et al., 2016). Employing ILs as novel catalysts for transesterification of triglycerides into biodiesel could lead to high yields with the less complex production process and reduces equipment corrosion, saponification, and waste generation (Ullah et al., 2018). Nevertheless, several drawbacks have hindered the widespread application of ionic liquids in the biodiesel industry. These include high cost, high viscosity, tedious recovery demanding expensive and energy-consuming processes, and large concentration in catalysis (Vallette et al., 2006; Bourbigou et al., 2010; Troter et al., 2016). The high cost of ILs can be outweighed by their overall benefits in many cases (Troter et al., 2016), but their high viscosity and inconvenient separation procedure remain a serious challenge for employing ILs in industrial plants.

To overcome the aforementioned problems, ILs can be heterogenized using solid materials. These supported ILs (SILs) provide the reaction catalysis with new opportunities, as they inherit the characteristics of both homogeneous and heterogeneous catalysts. Using SILs combines the possibility of facile separation and recovery of heterogeneous catalysts with the homogeneous media for reactants, the latter is provided by the IL layer on the solid surface. Moreover, fixed-bed reactors can be used for continuous production (Riisager et al., 2006a,b). Hence, many studies have investigated the utilization of SILs as catalysts for transesterification, in which a variety of solid carriers such as silica (Zhen et al., 2014), resin (Abreu et al., 2005), and polymers (Liang, 2013a,b) have been employed.

However, these catalysts exhibit weak catalytic activities due to high mass-transfer resistance and low amount of ILs grafted on the surface of the carrier. The main reason for these drawbacks is attributed to the small specific surface area, low pore volume, wide-range pore distribution, and irregular pore shape of the conventional solid supports (Zhen et al., 2012; Zhang et al., 2013). Therefore, the search for more suitable solid supports for immobilization of ILs continues.

Nanoporous materials are of great potential in tackling the aforesaid issues associated with ILs heterogenization. They possess high surface area, uniform pore distribution, and a large number of active sites per unit surface area. In virtue of these characteristics, these solids have been used not only as novel supports for ILs (Selvam et al., 2012), but also as green catalysts for biofuel production (Fu et al., 2018; Sharma et al., 2018).

Regarding to the role of ILs, nanoporous materials or their combination in various processes, many valuable reviews can be found in the literature. However, no review has solely focused on the function of nanoporous materials as supports for ILs in biodiesel production. Consequently, there is a lack of information on the present status of this research area, such as different nanoporous supports, synthesis routes, and optimum reaction conditions. In this paper, we comprehensively discussed the recent developments in synthesizing ILs-nanoporous materials hybrid catalysts for biodiesel production. We mainly focused on the application of different types of these catalysts for the optimization of transesterification reaction conditions. The results from each category were compared together to highlight the most promising classes for future studies. Moreover, to put further light on the future pathways, challenges, and opportunities for improving the overall production process in terms of technical and economic aspects were discussed.

NANOPOROUS MATERIALS-SUPPORTED ILS IN BIODIESEL PRODUCTION

Nanoporous materials are a class of substances that contain nanoscale pores (Fu et al., 2018). According to the International Union of Pure and Applied Chemistry, these materials are divided into three groups based on their pore diameter: microporous (pore diameter under 2 nm), mesoporous (pore diameter between 2 and 50 nm) and macroporous (pore diameter above 50 nm) (Rouquerol et al., 1994). They have been widely used in industrial areas such as petroleum refining, detergents, medicinal applications, and separation since the dimensions of the pores are controllable (Valtchev et al., 2009).

To date a variety of nanoporous materials have been used to heterogenize ILs for transesterification catalysis. **Figure 1** depicts the classification of these materials. In the majority of the researches that have been performed to date, silicon-based supports and polymers have been studies, followed by metal-organic frameworks (MOFs) and nanoporous carbon. Furthermore, in terms of pore size, mesoporous materials have attracted the most attention. On the other hand, only a few studies investigated the effect of micro and macroporous materials-supported ILs as catalysts for biodiesel production.

This might be related to the interesting properties of mesoporous solids which will be discussed in the following sections.

ILs Supported on Silicon-Containing Materials
ILs on Microporous Silica-Gel
Zeolites are the most common type of microporous silica-based materials. However, they are not very good candidates for being used as supports for ILs in biodiesel production. This can be ascribed to their small pore sizes which restrict the diffusion of large molecules like triglyceride to the active sites (Valtchev et al., 2009). As a result, instead of zeolites, Cao et al. (2016) focused on the immobilization of IL on microporous silica-gel. They prepared an acidic IL with 1-allyl-1H-imidazole, 1,3-propyl sulfonic acid lactone and H_2SO_4. This IL was then immobilized on thiol-group functionalized microporous silica-gel to fabricate a solid catalyst for biodiesel production from waste cooking oil (3-Mercaptopropyl) trimethoxysilane was employed to functionalize silica-gel with thiol groups. The resultant catalyst showed a high specific surface area (278.6 m^2/g) and was not decomposed below 250°C. By using the catalyst dosage of 5 wt.% and methanol to waste cooking oil molar ratio of 25–1, the maximum yield of 87.58% was obtained over the catalyst at 60°C and reflux of methanol for 20 h. The reaction yield decreased to around 70% after the catalyst was reused for 5 times. This resulted from the leaching of IL from the surface of the silica-gel support.

ILs on Mesoporous SBA-15
The limited pore size of zeolites and other microporous silica materials led to the invention of mesoporous silica materials, which have unique properties such as well-defined and uniform pore size, significantly high surface area, large pore volume, and facile surface functionalization (Al Othman, 2012; Da'na, 2017). Owing to these properties, mesoporous silica-based materials have had the most contribution to the heterogenization of ILs for biodiesel production.

SBA-15 is a type of mesoporous silica-based material containing uniform hexagonal pores which have a tunable diameter of 5–15 nm. In addition to the general benefits of mesoporous solids, it is cheap, chemically inert, and thermodynamically stable. Moreover, it possesses narrow pore size distribution and various functional chemical groups could be grafted on its surface due to the presence of abundant active sites (Yuan et al., 2020).

Mesoporous materials based on silicon have one weakness in common: They possess a limited number of functional groups. This reduces the loading rate of IL as well as catalytic activity (Cheng et al., 2013; Liang, 2014). The functionalization of these materials by acidic groups turns them into an attractive heterogeneous catalyst for the esterification of carboxylic acids. However, one problem associated with the utilization of mesoporous silica in this reaction is its hydrophilic nature. This results in the deactivation of active sites in the presence of water, which is a by-product of the esterification reaction. To address this issue, Karimi and Vafaeezadeh (2012) confined the IL 1-methyl-3-octylimidazolium hydrogen

FIGURE 1 | Classification of nanoporous materials used as supports for ILs in (trans)esterification reaction (SBA, Santa Barbara Amorphous; PILs, Polymeric ionic liquids; MIL, Materiaux de l′ Institute Lavoisier; HKUST, Hong Kong University of Science and Technology; UiO, Universitetet i Oslo).
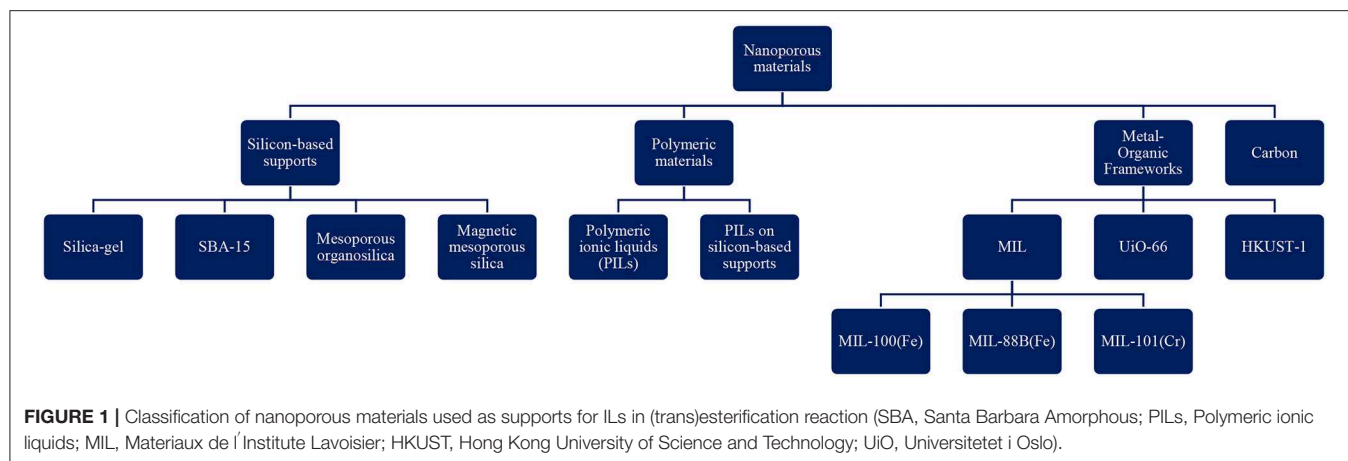
sulfate ([MOIm]HSO$_4$) inside the mesochannels of SBA-15-functionalized propylsulfonic acid by impregnation method. To this end, the solid support was impregnated with [MOIm]HSO$_4$ in an acetone solution. The supported IL was obtained after stirring at room temperature for 3 h and evaporation of acetone under vacuum. The resultant catalyst was able to effectively catalyze the esterification of different carboxylic acids with ethanol at room temperature, in which at least 87% yield was obtained within 40 h. The high yield was attributed to the synergetic effect between the grafted sulfonic acid groups and the anions of IL. The incorporation of the hydrophobic IL bearing N-octyl group also improved the mass transfer rate and expelled the produced water out of the catalyst surface during the reaction.

Incorporation of metals into SBA-15 is another way to adjust its catalytic performance (Sasidharan et al., 2009). Zhang et al. (2012) synthesized an iron incorporated SBA-15 (Fe-SBA-15) and used it as a support for Bronsted acidic IL 1-(propyl-3-sulfonate)-3-(3-trimethoxysilylpropyl) imidazolium hydrogen sulfate ([SO$_3$H-PIm-CPMS] [HSO$_4$]). The IL was immobilized on the support by the impregnation method. First, Fe-SBA-15 was activated at 150°C for 10 h. Then both support and IL were added to toluene and the mixture was heated to reflux for 20 h under the N$_2$ atmosphere. The final product was washed with diethyl ether and dried under vacuum. This catalyst was employed in esterification of oleic acid with methanol, where under the conditions of 5 wt.% catalyst dosage, methanol to oleic acid molar ratio of 6–1, a reaction time of 3 h and temperature of 90°C, the conversion of oleic acid reached to 87.7%. Compared to the case when IL was supported on SBA-15, the IL/Fe-SBA-15 showed a higher catalytic activity despite having less Bronsted acidic sites. This was attributed to the cooperative effect of Lewis and Bronsted acidic sites.

In another study conducted by Wang et al. (2018), three acidic ILs 1-(3-sulfonate)-propyl-3-allylimidazolium hydrogen sulfate, trifluoromethanesulfonate, and dihydrogen phosphotungstate were covalently immobilized on SBA-15 through thiol-ene reaction. To this end, SBA-15 was modified with KH-590 to obtain a thiol-group functionalized SBA-15 (SBA-15-SH). In

the next step, IL was dissolved in methanol at around 40°C, and then SBA-15-SH was dispersed in the solution. To initiate the thiol-ene reaction, azobisisobutyronitrile was added and the mixture was heated at 60°C for 12 h. The produced solid was separated by filtration, washed with methanol and dried at 60°C under vacuum for 3 h. The supported 1-(3-sulfonate)-propyl-3-allylimidazolium dihydrogen phosphotungstate showed the best catalytic performance in the esterification of palmitic acid with methanol due to high acidity of phosphotungstic acid and higher loading rate compared to the other two catalysts. Another factor responsible for the higher yield for phosphotungstate based catalyst was its larger molecule, which resulted in remarkable stearic hinderance and more exposure of active sites to the reactants. The catalyst could be reused 5 times without a considerable decrease in ester yield, which demonstrates the high potential of thiol-ene reaction to produce supported ILs with high stability.

Generally, the conversion of triglycerides to methyl/ethyl esters can be achieved under milder reaction conditions when basic ILs are used (Gholami et al., 2019). Accordingly, the potential of SBA-15-supported basic IL 4-butyl-1,2,4-triazolium hydroxide in transesterification of soybean oil with methanol was investigated by Xie et al. (2015a). The catalyst was synthesized by grafting of 4-butyl-1-triethoxysilylpropyl-triazolium chloride onto the surface of SBA-15 through the formation of Si-O bonds. To this end, after dissolving the IL in anhydrous toluene and adding the SBA-15, the mixture was refluxed in the N$_2$ atmosphere for 24 h. The mixture was allowed to cool down to room temperature, and then a solid was obtained by filtration, washing with acetone and drying under vacuum at 40°C for 3 h. The obtained solid was then extracted with diethyl ether and dichloromethane mixture for 6 h and was dissolved in a tetramethylammonium hydroxide solution in methanol. The solution was stirred at room temperature for 4 h, through which the chloride anions were exchanged to hydroxides. Finally, the catalyst was obtained after filtration, washing with ethanol and drying at 60°C under vacuum for 12 h. Employing this heterogeneous catalyst resulted in the conversion of 95.4% at optimum reaction conditions of 8 h, 65°C, methanol to oil molar

ratio of 20–1 and catalyst concentration of 7 wt.%. After 4 catalytic cycles, the conversion remained over 84%.

The catalytic activity of basic ILs strongly depends on basicity. However, it should be noted that excessive loading of IL on the support results in decreased catalytic activity, as it reduces the specific surface area. Therefore, the amount of grafted IL on the support should be optimized. As an example, in another work by Xie et al. (2015b), the basic IL 1,3-dicyclohexyl-2-octylguanidine (DCOG) was anchored onto the SBA-15 by grafting method. In the first step, DCOG and 1,3-glycidyloxypropyl-trimethoxysilane were added to dry N,N-dimethylformamide and the mixture was stirred at room temperature for 48 h under N_2 atmosphere to yield DCOG-organosilane. Afterwards, SBA-15 was dispersed in dry toluene and refluxed for 2 h with stirring under N_2 atmosphere. The DCOG-organosilane containing solution was then added to SBA-15 and toluene solution at room temperature. The resultant mixture was refluxed with stirring in the N_2 atmosphere for 24 h. The mixture was cooled down to room temperature and the solid product was filtered, washed with toluene and methanol, extracted with a diethyl ether and dichloromethane mixture at 70°C and dried under vacuum at 60°C for 12 h. By using 8 wt.% of this catalyst, the conversion of soybean oil reached 92.6% after 15 h. The catalytic activity increased when the loading amount of IL was lower than 2.5 g/g SBA-15, while a further increase of this figure did not show a significant effect on the catalytic performance.

ILs on Mesoporous Organosilica

The inclusion of organic functional into the structure of inorganic mesoporous silica materials leads to the formation of mesoporous organosilicas. These organic-inorganic hybrid mesoporous materials compensate the drawbacks of both siliceous mesoporous supports, i.e., limited number of functional groups, and organic carriers, i.e., low mechanical strength, weak thermal stability, and poor structure of the pore.

One problem associated with the use of SBA-15-supported ILs in the esterification reaction is the leaching of ILs from the surface of the support, which limits catalyst recoverability and reusability. Elhamifar et al. (2014) demonstrated that this issue can be overcome by covalent bonding of IL on mesoporous silica. Using this method, they supported 1-methyl-3-octylimidazolium hydrogen sulfate ([OMIm]HSO_4) IL on sulfonic acid functionalized periodic mesoporous organosilica (PMO-IL-SO_3H). After the preparation of PMO-IL, it was modified through grafting of (3-mercaptopropyl) trimethoxysilane. To this end, PMO-IL was added to dry toluene at room temperature under stirring for 5 min (3-mercaptopropyl) trimethoxysilane was then added to the solution and the mixture was refluxed under the argon atmosphere for 24 h. The resultant solid, PMO-IL-SH, was separated by filtration, washed with dry toluene and dried at 70°C for one night. In the second step, SH groups were oxidized to SO_3H using H_2O_2. In this process, PMO-IL-SH was added to hydrogen peroxide and stirred at room temperature for 24 h. Afterwards, a dilute solution of sulfuric acid was added to the mixture under stirring for 30 min. PMO-IL-SO_3H was obtained after filtering, washing with deionized water and ethanol and drying at 60°C for 12 h. The obtained catalyst

was used in the esterification of various carboxylic acids with different alcohols, where the yield remained over 82%. The high efficiency was ascribed to the presence of imidazolium anion and sulfonic acid groups in the mesochannels of the carrier and their synergetic cooperation. They also stated that the nanostructure of PMO-IL with the imidazolium framework was responsible for the good stability of sulfonic acid sites.

Fan et al. (2018) prepared the acidic organosilica material SO_4^{2-}/ZrO_2-SiO_2(Et) by a one-step co-condensation method and the subsequent hydrothermal treatment. Acidic IL sulfonic acid functionalized imidazolium hydrogen sulfate ([Ps-im] HSO_4) was then immobilized on the acidic organosilica carrier by the chemical grafting. **Figure 2** illustrates the four steps involved in the production process of the catalyst. First (3-chloropropy) triethoxysilane and SO_4^{2-}/ZrO_2-SiO_2(Et) were dispersed in dry toluene. After stirring at 90°C for 24 h, the mixture was cooled, and SO_4^{2-}/ZrO_2-SiO_2(Et)-$(CH_2)_3$-Cl was obtained by filtering, washing with toluene, dichloromethane and diethyl ether and drying at 100°C for 12 h. In the second step, this product along with imidazole was added to dry toluene, and SO_4^{2-}/ZrO_2-SiO_2(Et)-im was produced using the same process as the previous step. In the next step, this product was dispersed in dry toluene and 1,3-propane sultone was added to the mixture. After undergoing the same process as the previous steps, SO_4^{2-}/ZrO_2-SiO_2(Et)-Ps-im was obtained. Finally, this solid was suspended in dry dichloromethane and concentrated sulfuric acid (98%) was added dropwise at 0°C under vigorous stirring. The mixture was then stirred at room temperature for 24 h. After washing the resultant material with dichloromethane and diethyl ether and drying it at 100°C for 12 h, the catalyst [SO_4^{2-}/ZrO_2-SiO_2(Et)-Ps-im]HSO_4 was obtained. This catalyst was used to produce biodiesel from soybean oil, where under optimum reaction conditions of 5 wt.% catalyst concentration, the temperature of 150°C, methanol to oil molar ratio of 18–1, a 99% yield was obtained after 3 h. The hybrid support possessed stronger Bronsted and Lewis acid sites compared to SO_4^{2-}/ZrO_2, which was attributed to the improved hydrophobicity and porosity of the surface resulted from the incorporation of ethane-bridge organosilica moieties. Despite having lower acidity, the catalyst gave a higher yield as compared with the pure ([Ps-im] HSO_4) owing to the synergetic impact of Bronsted and Lewis acid sites. The catalyst maintained its activity after 5 consecutive runs and exhibited excellent resistance to oleic acid and water.

ILs on Magnetic Mesoporous Silica

Magnetic mesoporous silica is one of the most important classes of mesoporous materials that have been used as carriers for ILs. Magnetic mesoporous materials can combine the benefits of mesoporous and magnetic materials, and facilitate the separation of the catalyst from reaction mixture through a magnetic field. By immobilizing the acidic IL 1-Allyl-3-(butyl-4-sulfonyl) imidazolium trifluoromethanesulfonate ([BsAIm][OTf]) on magnetic mesoporous silica, Zhen et al. (2012) prepared a magnetic mesoporous silica-supported IL for esterification of oleic acid with methanol. **Figure 3** illustrates the process for the synthesis of this catalyst. The magnetic carrier was synthesized by embedding the cobalt ferrite nanoparticles in silica using

FIGURE 2 | The synthesis process of [SO_4^{2-}/ZrO$_2$-SiO$_2$(Et)-Ps-im]HSO$_4$ [Redrawn from Fan et al. (2018)].
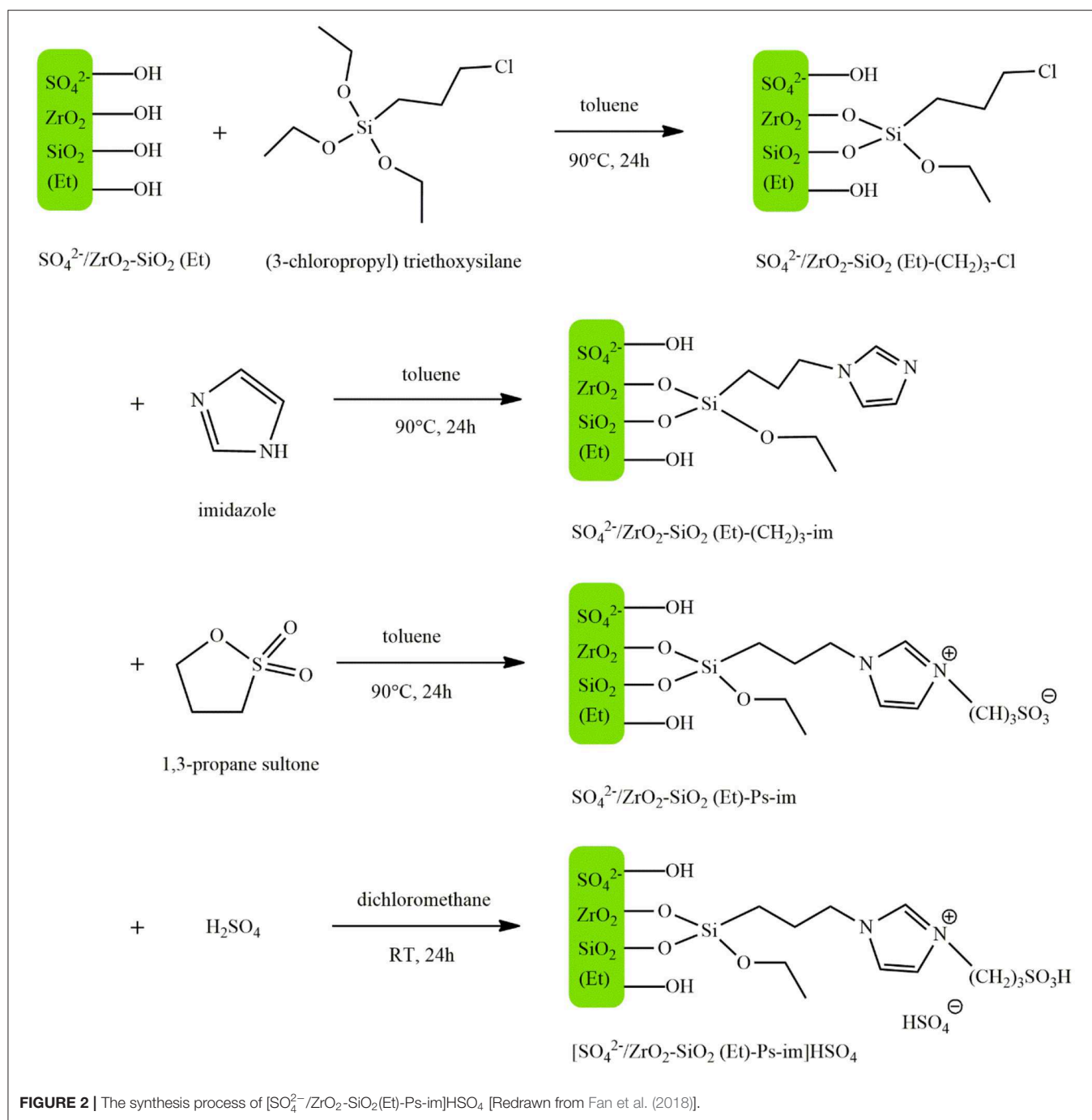
the sol-gel method and then modified with (3-mercaptopropyl) trimethoxysilane to add sulfhydryl groups to its structure. The IL was then supported on the modified magnetic mesoporous silica through a radical reaction between the allyl and sulfhydryl groups. After 12 h, the conversion of oleic acid reached 87% using a 10 wt.% catalyst dosage. They found that an increase in sulfhydryl loading of modified mesoporous silica resulted in a decrease in pore diameter, the amount of IL supported on the carrier, and conversion. Moreover, the catalyst did not

show high stability and reusability due to the hydrolysis or alcoholysis of the Si-O bonds on the support under harsh reaction conditions 110°C.

The catalytic performance of mesoporous silica-based ILs could be even better than that of the ILs supported on nanoparticles. Zhang et al. (2013) prepared 1-Allyl-dodecyl imidazolium hydroxide ([ADIm][OH]) basic IL immobilized on magnetic mesoporous SiO$_2$/CoFe$_2$O$_4$ nanoparticles (SCF) and magnetic CoFe$_2$O$_4$ nanoparticles (CF) and compared

FIGURE 3 | Schematic of the synthesis process of [BsAlm][OTf]@SiO$_2$/CoFe$_2$O$_4$ [Redrawn with modification from Zhen et al. (2012)].
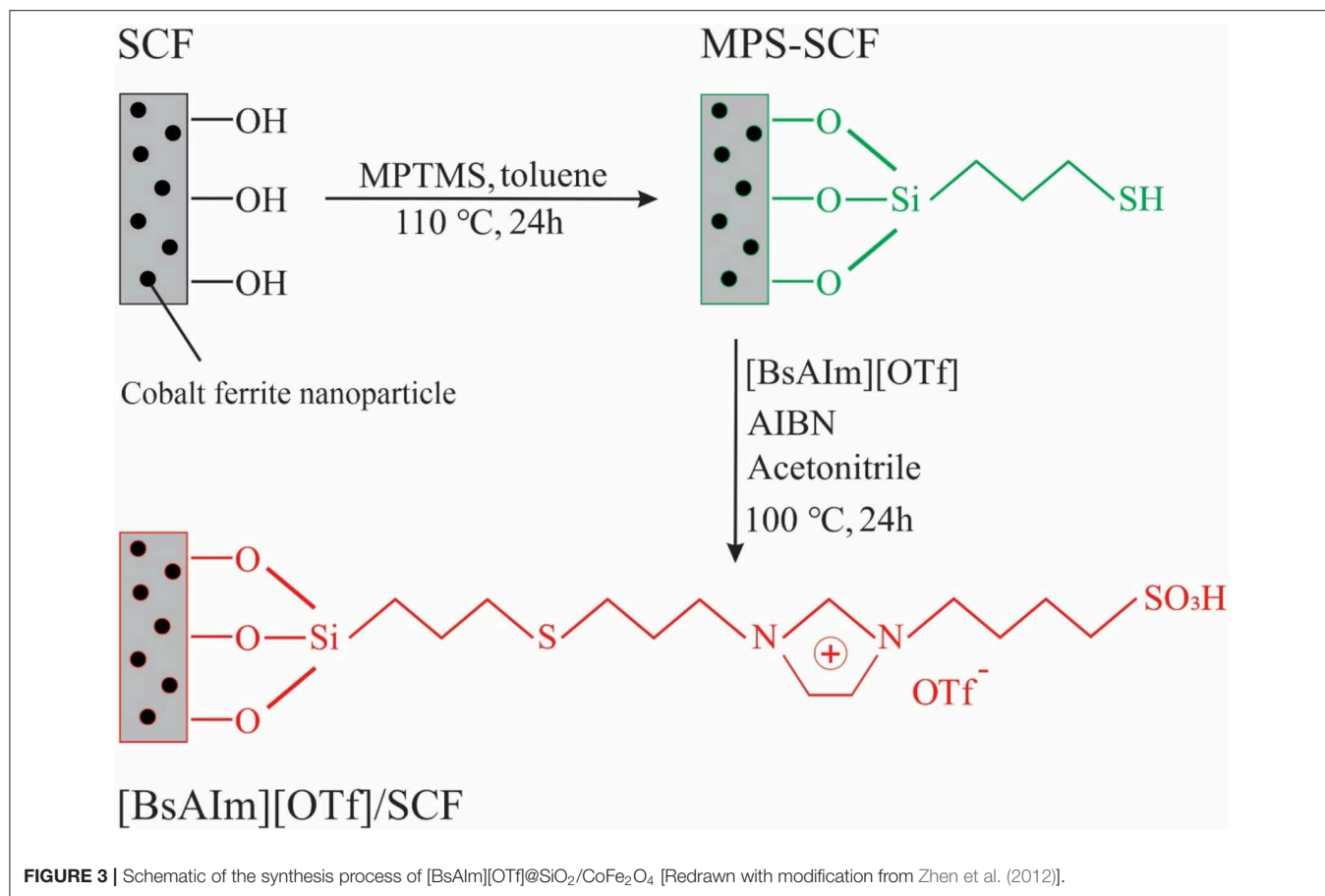
their catalytic activity in the transesterification of glycerol trioleate. For the synthesis of [ADIM][OH]/SCF, the carrier was first modified with 3-mercaptopropyltrimethoxysilane through thermal treatment at 110°C for 24 h. The modified SCF particles were washed with acetone and dried. In the next step, IL was supported on the carrier through the free radical reaction between allyl groups of IL and sulfhydryl groups of the carrier. To this end, [ADIm][Br] was first produced from the reaction between 1-allylimidazole and n-dodecyl bromide at 60°C for 24 h. After washing with diethyl ether and drying in vacuum, [ADIm][Br] and modified SCF were added to acetonitrile and the reaction was initiated by azobisisobutyronitrile at 100°C for 24 h. The produced solid [ADIm][Br]/SCF was washed with methanol and then was added into a flask along with NaOH and dichloromethane. The mixture was reacted at room temperature for 24 h and [ADIm][OH]/SCF was obtained after washing with water and ethanol and drying at 60°C. Both catalysts showed better catalytic performances than NaOH, with IL/SCF led to a slightly higher yield than CF. The mesoporous structure of SCF made it difficult for the large molecule of triglyceride to diffuse into the pores and reach the active sites of IL, so the reaction rate and yield were low at the beginning of the reaction. However, the long and narrow pores also prevented the triglyceride and intermediate diglyceride to escape from the surface of the carrier, thus providing longer contact opportunities for reactants and

intermediate with catalytic sites. On the other hand, there were no pores on the surface of CF, and as a result, all the catalytic active sites in the bulk of IL/CF were easily accessible for reactants, increasing the reaction rate compared to IL/SCF at initial stages of transesterification. Nevertheless, because of the absence of pores and pore diffusion effects, triglyceride molecules were able to leave the catalytic sites freely, reducing the reaction yield at longer reaction times compared to the IL/SCF. The existence of mesopores and pore diffusion effect also provided the active sites with more protection and reduced their loss to some extent, due to which IL/SCF exhibited a higher yield in comparison to IL/CF after three cycles.

Wan et al. (2015a) employed Fe$_3$O$_4$ nanoparticles to fabricate a magnetic mesoporous silica material and used it as support for acidic IL 3-sulfopropyl-1-(3-propyltrimethoxysilane) imidazolium hydrogen sulfate ([SO$_3$H-PIM-TMSP] HSO$_4$). The Fe$_3$O$_4$ nanoparticles were produced by the solvothermal method. Then, they were coated with silica layer through hydrolysis and condensation of tetraethyl orthosilicate in the mixture of water, ethanol and ammonia, producing Fe$_3$O$_4$@SiO$_2$ particles. Afterwards, these particles were coated with a composite layer consist of cetyltrimethylammonium bromide (CTAB) and silica by using tetraethyl orthosilicate and CTAB. After removing CTAB, magnetic mesoporous Fe$_3$O$_4$@SiO$_2$@mSiO$_2$ particles were obtained. In the next step, the IL was supported

on the mesoporous silica by covalent immobilization, with Fe_3O_4 and mesoporous silica-based IL as core and shell, respectively. Typically, a mixture of IL and mesoporous carrier in dry toluene was prepared. The mixture was refluxed for 24 h under N_2 atmosphere. Then, the produced material was washed with diethyl ether and dried under vacuum at 323 K for 8 h, yielding $IL/Fe_3O_4@SiO_2@mSiO_2$. In this catalyst, the function of non-porous inner silica layer was to protect the Fe_3O_4 nanoparticles, while the outer mesoporous layer acted as support. At optimum reaction conditions of 10.6 wt.% catalyst dosage, oleic acid to ethanol molar ratio of 6–1, a reaction time of 4 h and a temperature of 110°C, the catalyst yielded 93.5% conversion in the esterification of oleic acid with ethanol.

Based on the above discussion, there are two main methods for supporting ILs on silicon-based materials: Impregnation and grafting. Impregnation consists of physical adsorption of the IL, whereas in grafting the IL is immobilized on the surface through a chemical bond. Impregnation is simpler and less expensive than chemical grafting, but the resultant catalyst does not usually show good stability because the active sites are fallen off the surface of the support. In contrast, chemical grafting results in catalysts with higher stabilities, but it is more complicated and time-consuming, as well as consumes extra chemicals and reagents which increases the fabrication cost.

In chemical grafting, the IL is immobilized on the carrier surface through Si-O-Si covalent bonds. These bonds are formed by a chemical reaction between the silane groups and silanol groups on the carrier surface. There are two ways to incorporate silane groups in the structure of final catalyst. In the first method, which we call carrier modification, the as-synthesized carrier is functionalized with silane groups. Then, IL is connected to the silanol group through another group such as propyl or thiol. In the second method, called direct immobilization, the silane groups are first incorporated in IL structure, and then the IL is directly immobilized on the support.

Table 1 summarizes the optimized reaction conditions over ILs/silicon materials hybrid catalysts. As can be seen, all studies synthesized catalysts with large specific surface areas and obtained high biodiesel yields. Except for researches conducted by Karimi and Vafaeezadeh (2012) and Zhang et al. (2012), chemical grafting was used in all other studies for catalyst synthesis. Although Karimi and Vafaeezadeh (2012) did not report the biodiesel yield after several catalytic cycles, the results reported by Zhang et al. (2012) show that impregnation may also result in a catalyst with good stability. As impregnation is simpler and less-expensive than grafting, further studies on using this synthesis method with critical attention on recyclability are worth conducting in the future.

The high specific surface area of microporous silica-gel led to a comparable biodiesel yield with mesoporous silica supports. However, a higher amount of alcohol and longer reaction time was required which can be attributed to the smaller pore diameter of silica-gel and limited diffusion of the reactants as a result. These problems may be overcome by employing basic ILs which accompany lower alcohol consumption and shorter reaction time compared to acidic ILs. The effect of direct immobilization of IL

on the recyclability of the final catalyst can also be investigated in future research.

Most studies in this category have been focused on SBA-15. By comparing the results, one could conclude that the modification of carrier with thiol groups (Wang et al., 2018) has the same effect on reaction yield and catalyst stability as the impregnation method (Zhang et al., 2012). On the other hand, by supporting basic ILs on SBA-15 using direct immobilization, Xie et al. (2015a,b) synthesized heterogeneous catalysts with higher stabilities. When the carrier is modified through thiol-ene reaction, the silane group on the surface is first attached to one atom of S through a propyl group. Then, this atom is connected to the cation of IL via another propyl group. In direct immobilization, on the other hand, the IL is directly attached to the silane group through a propyl group.

Among all the research on IL/silicon-based supports, Fan et al. (2018) obtained the best results. They reported almost 99% efficiency in transesterification of soybean oil with relatively low catalyst concentration and more importantly, the reaction yield remained over 95% after 5 catalytic cycles. Moreover, when the water and oleic acid contents of the feedstock were 5 wt.% and 9 wt.%, respectively, the yield of biodiesel was higher than 98%. These results indicate that mesoporous organosilica materials have great potential in (trans)esterification. Despite that Fan et al. (2018) first modified the organosilica by silane groups, they used a step-by-step procedure to immobilize the IL on the carrier so that the cation of IL was finally attached to the organosilica support by propyl-Si-O-Si bonds, the same method employed by Xie et al. (2015a,b).

Finally, in all three studies on magnetic mesoporous silica supports, high yields were reported. However, the catalysts fabricated by Zhen et al. (2012) and Zhang et al. (2013) did not show good recyclability due to the leaching of active sites, which was resulted from the breaking of Si-O bonds under harsh reaction conditions. In both studies, the support was first functionalized with thiol groups and then IL was attached to the support via free radical addition reaction between allyl groups of the IL and thiol groups on the surface of the carrier. On the contrary, Wan et al. (2015a) first functionalized the IL with silane groups, and then directly immobilized it on the magnetic silica support. The reaction yield remained over 87% after the catalyst was reused for 6 times.

In summary, direct immobilization of IL on the surface of mesoporous silica carrier through silane groups seems to reduce the leaching of IL and improve the catalyst recyclability compared to the case where thiol groups are used.

ILs Supported on Nanoporous Polymers

Organic polymers containing nanopores possess controlled wettability, flexible chemical tenability, and remarkable chemical stability in addition to the high surface area. Generally, these materials can be easily fabricated through hard-templating, soft-templating and template-free methods, and are functionalized by several strategies such as post-modification, co-polymerization of skeleton molecules with functional groups and self-polymerization of functional organic groups (Sun et al., 2015).

TABLE 1 | Supported ILs on silica-based materials.

Feedstock	Catalyst	Surface area (m^2/g)	Pore volume (cm^3/g)	Average pore diameter (nm)	Catalyst dosage (wt.%)	Temperature (°C)	Alcohol/oil molar ratio	Reaction time (h)	Yield (%)	Yield after reuse (%)	Reuse times	References
Oleic acid	[BsAIm][OTf]@ SiO$_2$/CoFe$_2$O$_4$	267.15	–	–	10	100	–	12	87	–	–	Zhen et al., 2012)
Waste cooking oil	IL/silica-gel	278.6	–	1.382	5	60	25	20	87.58	70	5	Cao et al., 2016
Different carboxylic acids	[MOIm]HSO$_4$/SBA-15-Pr-SO$_3$H	–	–	–	–	25–30	–	40	87–96%	–	–	Karimi and Vafaeezadeh, 2012
Oleic acid	[SO$_3$H-PIm-CPMS][HSO$_4$]/Fe-SBA-15	305	0.87	6.2	5	90	6	3	87.7	80.8	6	Zhang et al., 2012
Palmitic acid	SBA-15@IL	162.5	0.269	6.57	15	65	9	8	88.1	80	5	Wang et al., 2018
Soybean oil	SBA-15-pr-ILOH	341	0.78	5.58	7	65	20	8	95.4	84.7	4	Xie et al., 2015a
Soybean oil	SBA-15-pr-DCOG	267	0.48	4.25	8	65	15	15	92.6	86.2	5	Xie et al., 2015b
Different carboxylic acids	PMO-[OMIm]HSO$_4$-SO$_3$H	504	0.93	9.3	–	60–75	–	12–24	82–95%	–	–	Elhamifar et al., 2014
Soybean oil	SO$_4^{2-}$/ZrO$_2$-SiO$_2$(Et)-[Ps-im]HSO$_4$	200.6	0.459	8.8	5	150	18	3	98.99	95.22	5	Fan et al., 2018
Glycerol trioleate	[ADIm][OH]@ SiO$_2$/CoFe$_2$O$_4$	–	–	–	–	170	–	6	86.54	<40	3	Zhang et al., 2013
Oleic acid	[SO$_3$H-PIM-TMSP]HSO$_4$/Fe$_3$O$_4$@ SiO$_2$@mSiO$_2$	175	–	–	10.6	110	6	4	93.5	87.4	6	Wan et al., 2015a

58

Polymeric Ionic Liquids

The functionalization of nanoporous polymers with ILs leads to the fabrication of so-called polymeric or polymerized ionic liquids or poly(ionic liquids)s (PILs). These polyelectrolytes consist of a polymeric backbone and an IL species in each monomer repeating units. PILs have been widely used as catalyst, catalyst support and pre-catalyst as they are mechanically stable and their catalytic influence can be controlled by the possibility of choosing a variety of cations and anions and tuning the macromolecular structure (Qian et al., 2017). There are two principal strategies to fabricate PILs, i.e. direct polymerization of IL monomers and post-modification of an already existing polymer. The structure, merits, and shortcomings of a PIL strongly depend on the synthesis technique and polymerization methodology (Yuan and Antonietti, 2011).

In the post-modification route, an existing precursor polymer is functionalized via chemical reactions. PILs obtained from this strategy possess the same number of monomeric units, architecture, and monomer composition as the primary polymer chains. Consequently, the desirable architecture and composition of PILs can be achieved by choosing a precursor with suitable structure, mass, and architecture (Yuan and Antonietti, 2011). The modification of nanoporous polymers for the preparation of PIL catalysts and their use in the biodiesel production process was first reported by Liu F. et al. (2012). They synthesized several mesoporous superhydrophobic polydivinylbenzenes by solvothermal co-polymerization of divinylbenzene with a series of vinyl-based monomers, followed by quaternary ammonization with CH_3I and ion exchange with HSO_3CF_3. Compared to the same homogeneous ILs and ILs supported on SBA-15 and Amberlyst 15, the obtained IL-functionalized mesoporous polymers gave higher palmitate yield in transesterification of tripalmitin. This was attributed to the excellent adsorption of the reactants on the catalyst as a result of its significant wettability for the reactants. The catalyst was also well-recyclable because of the stable polymer structure. However, very high alcohol to tripalmitin molar ratio (90–1) and long reaction time (16 h) were required to achieve high yields.

Templating is an effective method for the synthesis of nanoporous polymers. Noshadi et al. (2014) successfully synthesized acidic PILs with an average pore size of 11.1 nm using resol and Pluronic F127, as precursor and template, respectively. The crosslinker hexamethylenetetramine (HMTA) was used to link the precursor to the template. After template removal through calcination, an ordered mesoporous resin (OMR-[HMTA]) was obtained using the crosslinker HMTA. Following modification of the mesoporous polymer through quaternary ammonization with 1,4-butanesultone and anion exchange with H_2SO_4, the polymeric ionic liquid OMR-[C_4HMTA][SO_4H] was obtained. Due to high acidity, high specific surface area, and a stable hydrophobic polymeric structure, this catalyst outperformed HCl and Amberlyst 15 in the esterification of a brown grease feed with high FFA content. The conversion of FFA to biodiesel reached 99.5% only with a methanol-to-grease molar ratio of 9:1 at 65°C within 1.5 h. The yield of esterification decreased from 99.5 to 96% after 5 times of the PIL catalyst

recovery indicating its reasonable chemical stability. The brown grease with a FFA content of 90% was transesterified with a yield of 75% in the presence of this catalyst. The corresponding value for Amberlyst 15 was 65%. However, due to the need for high volumes of alcohol (the methanol-to-feed molar ratio of 40–1) and moderate yield, this catalyst is not suitable for the transesterification reaction presumably due to its small pores that do not provide adequate space for the diffusion of larger triglyceride molecules.

Adding sulfonic groups to a polymer functionalized with an acidic ionic liquid (IL) may significantly improve both acidity and catalytic activity. After synthesizing a mesoporous polymer through copolymerization of divinylbenzene with 1-vinylimidazole, Pan et al. (2016) functionalized the resulting polymer with an IL through quaternary ammonization with 1, 3-propanesultone and anion exchange with H_2SO_4. The resulting acidic PIL was sulfonated with chlorosulfonic acid to add a sulfonic acid group to the monomer. Within 4 h, the conversion of oleic acid reached 98% in the presence of a 5 wt.% catalyst with a methanol-to-oil molar ratio of 30–1 at 100°C. Moreover, simultaneous esterification and transesterification of Jatropha oil with a high acid value of 15 mg KOH/g were carried out in the presence of the catalyst. A conversion of 94% was obtained within 8 h at 160°C with a methanol-to-oil ratio of 50:1 (mol/mol) and 6 wt.% catalyst. Despite the lower acidity of this catalyst than Amberlyst 15, its BET surface area was 5 times higher leading to a significant increase in the conversion.

One limitation of some PILs used in biodiesel production is their nano-scale particles causing loss of catalyst during separation from reaction products. Increasing the particle size to micro-scale facilitates catalyst separation and reduces relevant costs. Using the procedure shown in **Figure 4**, Feng et al. (2017) synthesized acidic PIL microspheres with an approximate diameter of 500 μm through copolymerization of 1-vinylimidazole, divinylbenzene and styrene and then quaternary ammonization with 1,3-propanesultone and anion exchange with H_2SO_4. The resulting catalyst, P(VB-VS)HSO$_4$, had an oleophilic mesoporous polymer network with a high specific surface area and abundant mesopores leading to the increased contact area of reactants with active sites and thereby enhanced mass transfer. Due to the good chemical and thermal stability of the catalyst, the conversion of transesterification of soapberry oil remained over 90% after 6 times of catalyst recovery. Interestingly, catalyst loss was nearly zero during recovery and reuse due to micron-sized catalyst particles. Moreover, the resulting PIL led to a high biodiesel production yield from various feeds with high acid values.

It has been reported that post-modification of the mesoporous melamine-formaldehyde as a class of covalent organic polymers (COPs) with ILs creates an ideal PIL for catalyzing esterification reactions. The repeating units in the mesoporous melamine-formaldehyde are connected through irreversible covalent bonds leading to high chemical and hydrothermal stability. Since this polymer is synthesized from low-cost available monomers, i.e., melamine and para-formaldehyde, its production cost is lower than divinylbenzene-based polymers. As another advantage,

FIGURE 4 | Fabrication procedure of P(VB-VS)HSO$_4$ [Redrawn with modification from Feng et al. (2017)].
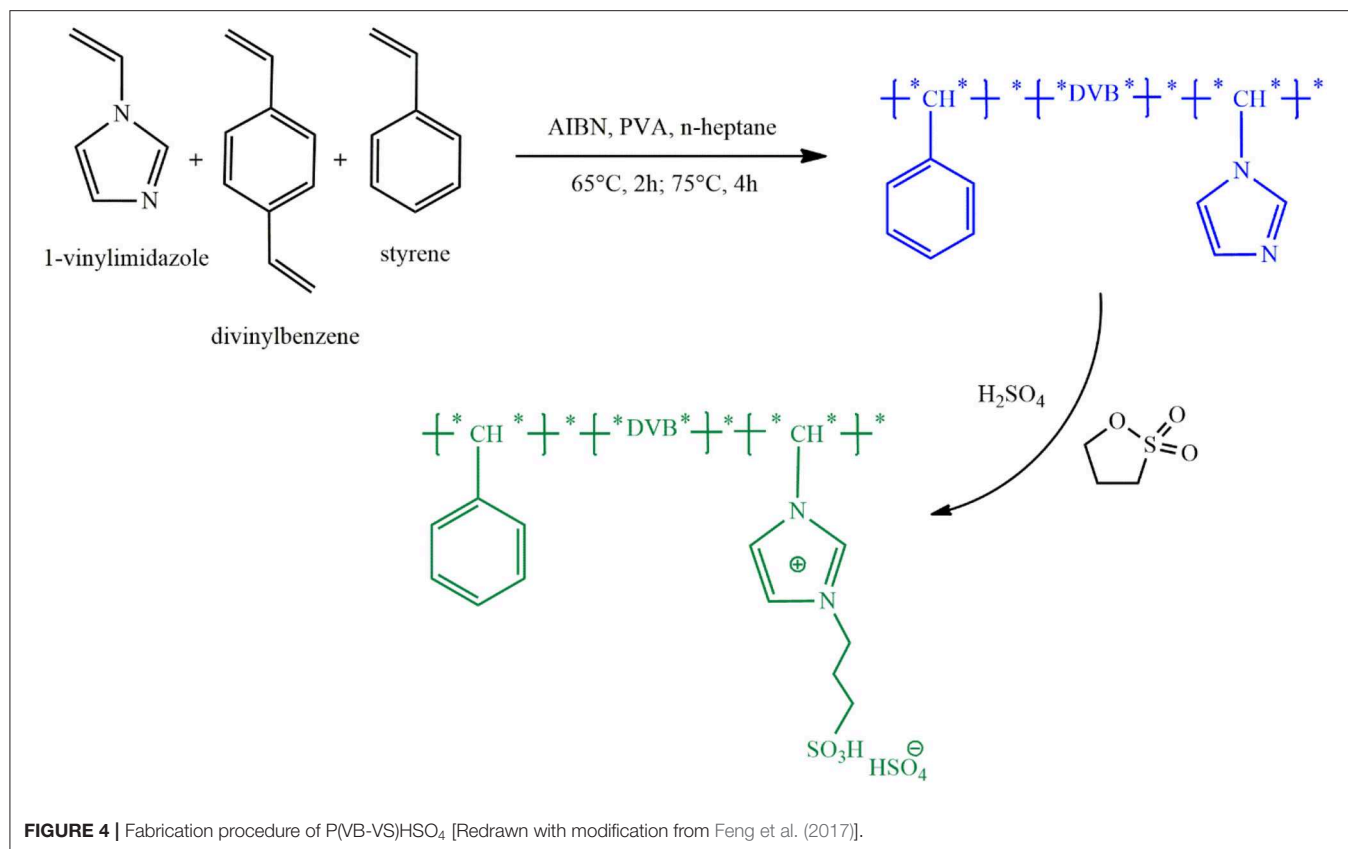
many aminal groups and triazine rings in the polymer network provide abundant sites for functionalization. Pan et al. (2019) synthesized this polymer by templating using Pluronic F127 and sodium dodecyl sulfate as templates. The polymer was then modified with 1,3- propanesultone and anion exchange with H$_3$PW$_{12}$O$_{40}$ to obtain the MMFP-IL PIL. High acidity and surface area of this catalyst led to a yield of 95% in converting oleic acid to biodiesel. Strong covalent bonds between the polymer and IL as well as the stable structure of the catalyst led to its acceptable activity after 4 times of reuse.

There has been recently a great interest in the use of cheap monomers to reduce PIL production costs. For instance, Pei et al. (2019) used petroleum pitch as a monomer to produce a mesoporous polymer through hypercrosslinking. The resulting polymer was first functionalized by allyl chloride and then imidazole and ultimately modified through reaction with 1,3-propanesultone and anion exchange with 1,3-p-toluenesulfonic acid to achieve the PIL [HCPpitch–Im–Pros][Tos]. Oleic acid was esterified on this catalyst up to a yield of 93%, and the catalyst was used 5 times with an insignificant catalyst loss. Since the chlorine ions are replaced with imidazole groups in this method, the number of functional groups in the polymer increases with further chlorine grafting on the polymer leading to an increase in catalytic activity.

Direct copolymerization of divinylbenzene with IL monomers is a less expensive process for the synthesis of PILs which eliminates the use of expensive coupling reagents.

Polydivinylbenzene can enhance the mass transfer rate and prevent the acid sites from falling off the surface owing to its high hydrophobic BET surface area. Liang (Liang, 2013a) fabricated an acidic PIL using the procedure illustrated in **Figure 5**. The Bronsted acidic IL monomer [SO$_3$H(CH$_2$)$_3$ VIm]HSO$_4$ was synthesized via the reaction between 4-vinylpyridine and 1,3-propane sulfonate, followed by acid treatment with H$_2$SO$_4$. The obtained monomer then was successfully copolymerized with divinylbenzene and was used in transesterification of waste cooking oil with methanol. After 12 h, a 99.1% biodiesel yield was achieved with 50 mg catalyst amount at 70°C and methanol to oil molar ratio of 15–1. After being used for 6 times, the reaction yield was still 99%, demonstrating its high stability.

Some PILs have a small specific surface area leading to inadequate access of reactants to catalytic sites. Hard templating of nanoparticles can be used to overcome this problem, which is a facile and effective method for producing porous materials with a suitable pore structure. However, a suitable template is required for this purpose to generate a uniform pore structure and its facile removal from the polymer at the end of the process. Wu et al. (2016a) used Fe$_3$O$_4$ nanoparticles as a template for the synthesis of a PIL catalyst. To this end, Fe$_3$O$_4$ nanoparticles were first modified with 3-methacryloxypropyltrimethoxy-silane and then polymerized with the IL monomer 1-vinyl-3-(3-sulfopropyl)imidazolium hydrogen sulfate. An acidic macroporous catalyst was obtained

FIGURE 5 | The synthesis procedure of mesoporous acidic PIL [Redrawn with modification from Liang (2013a)].
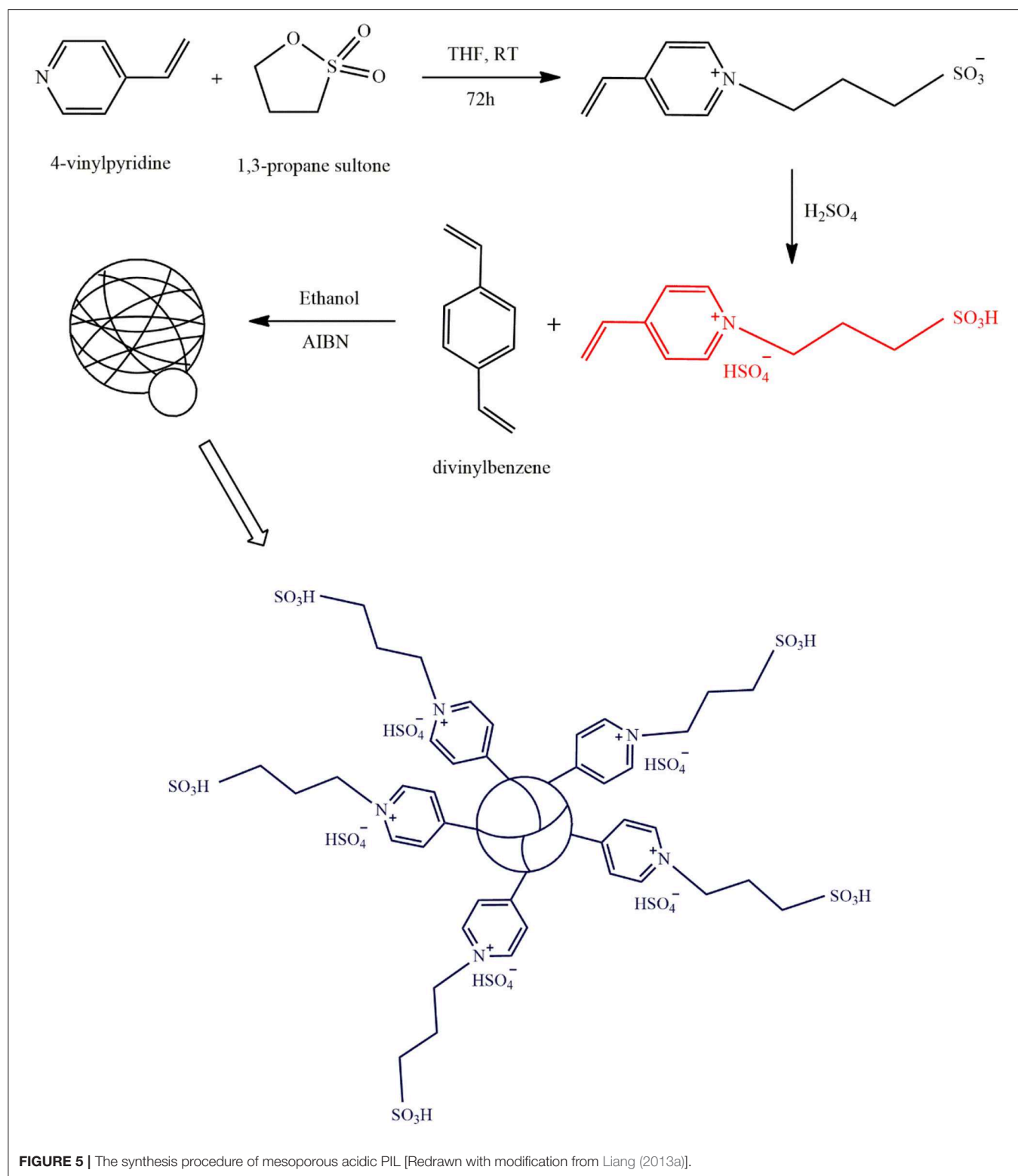
by removing Fe_3O_4 nanoparticles by water/ethanol/hydrochloric acid solution and ultrasonication. Conversion of over 90% was obtained with this PIL to convert oleic acid to methyl oleate. The resulting PIL contained a large number of sulfonic acid

and hydrogen sulfate groups. The PIL was reused up to 6 times without leaching its acidic sites.

In another study, Wu et al. (2016c) synthesized a magnetic PIL functionalized with phosphotungstic acid using Fe_3O_4

nanoparticles and copolymerization of the acidic IL monomer 1-vinyl-3-(3-sulfopropyl) imidazolium hydrogen sulfate with the crosslinker divinylbenzene. To functionalize Fe_3O_4 nanoparticles with vinyl groups, 3-(trimethoxysilyl)propyl methacrylate was used. The highly acidic catalyst used for esterification of oleic acid at a methanol-to-oil molar ratio of 12:1 at 90°C led to a conversion of 93.4% after 5 h in the presence of 13 wt.% catalyst. Due to good magnetic properties, the catalyst was easily separated from products and reused for 6 times.

In addition to hydrophobicity, tunable wetting of catalyst for both reactants and products is of great importance, as it improves the performance and recoverability of the catalyst. A basic PIL was synthesized through radical polymerization of 1-octyl-3-vinylimidazolium bromide with the crosslinker 1,4-butanediyl-3-bis-1-vinylimidazole and then anion exchange with KOH (Jiang et al., 2017). The resulting polymer contained mesopores with an average diameter of 35 nm and basicity of 3.67 mmol/g. The rough surface of this polymer with a unique porous structure, an organic hydrophobic framework, and long chains of IL monomers led to a superhydrophobic polymer. Moreover, the high affinity of this catalyst for methanol and soybean oil led to the high yield of transesterification reaction. On the other hand, the basic PIL was incompatible with glycerol leading to desorption of the byproduct, glycerol, from the catalyst surface. The catalyst resisted against a water content of up to 1.5 wt.% (relative to oil) and the triglyceride conversion reduced from 96.3 to 85% after 5 times of catalyst reuse. The conversion was lower than the heterogeneous CaO catalyst due to the lower basicity of the PIL. However, due to the lack of metal ions in the PIL structure, it does not cause environmental pollution unlike CaO.

The free radical polymerization between an IL monomer and divinylbenzene in the presence of the radical initiator azobisisobutyronitrile (AIBN) is a common method for the synthesis of PILs. Bian et al. (2019) synthesized an acidic PIL by this method and used it for esterification of oleic acid. The IL monomer was synthesized through the reaction of methyldiallylamine with 1,3-propanesulton and then ion exchange with trifluoromethanesulfonic acid. Despite the lower acidity of the resulting catalyst than Amberlyst 15, it led to a higher yield for methyl oleate production due to the higher surface area of the PIL (301.1 m^2/g) than Amberlyst 15 (47.2 m^2/g). The resulting PIL also had a reasonable recovery and reuse capacity.

The results of research on biodiesel production over PILs are summarized in **Table 2**. As can be seen, except for the conversion of brown grease (trans)esterification was successfully catalyzed by all the synthesized PILs with yields higher than 90%, and the minimum yield after several catalytic cycles was 74%.

The post-modification method was used in the first six studies (Liu F. et al., 2012; Noshadi et al., 2014; Pan et al., 2016, 2019; Feng et al., 2017; Pei et al., 2019), in which the IL is supported on an as-synthesized polymer. This method is based on three consecutive steps including polymer synthesis, modification through quaternary ammonization, and ion exchange. Among the aforementioned studies, Liu F. et al. (2012) reported the highest reaction yield and best recyclability, which can be ascribed to the use of super acid SO_3CF_3 anion. However, this

result was accompanied by the highest alcohol consumption and the longest reaction time in this category, which is probably due to the lack of catalytic sites on the imidazolium cation. This speculation is confirmed by investigating the results of the next studies, in which more moderate reaction conditions were obtained by attaching a sulfonic acid group to the cations of PILs. When more acid sites are available for reactants, the reaction rate is increased and less alcohol is consumed.

In the next five studies (Liang, 2013a; Wu et al., 2016a,b,c; Jiang et al., 2017; Bian et al., 2019), direct polymerization was employed in which the IL monomer is first prepared and then the resultant PIL is obtained from copolymerization of IL monomer and divinylbenzene. Among this group, Liang (2013a) reported the best results in the transesterification of waste cooking oil. A yield of higher than 99% with only 1 wt.% catalyst dosage was obtained and the yield remained at 99% after 6 catalytic cycles. This significant activity and reusability of the catalyst can be due to the very high specific surface area (>500 m^2/g) and the simultaneous presence of SO_3H and HSO_4 groups in the cation and anion, respectively.

The only basic PIL in this group was fabricated by Jiang et al. (2017) and showed high yield and good stability in the transesterification of soybean oil. However, given to its basic nature, lower alcohol consumption and shorter reaction time are expected compared to the acidic PILs, which is not observed. This may be due to the presence of octyl groups on the imidazolium cation of PIL and its complex cross-linker. Although incorporating these groups enhances hydrophobicity and expels glycerol from the surface of the catalyst, it limits the diffusion of reactants toward the active sites.

Among all studies focused on PILs, Bian et al. (2019) synthesized the only PIL with a non-cyclic diallylamine cation and obtained good results both in terms of yield and mild reaction conditions in the esterification of oleic acid.

From what mentioned earlier, it can be concluded that both post-modification and direct polymerization could result in highly active PIL catalysts for (trans)esterification. Nevertheless, given the low price of divinylbenzene, using a template-free method could reduce the fabrication cost of final polymer compared to the templating technique. Furthermore, direct polymerization is less complicated than the post-modification method, so the synthesis cost of PILs could be reduced by direct polymerization of IL monomer with the cheap divinylbenzene as co-polymer.

Polymeric Ionic Liquids Supported on Silicon-Based Materials

In addition to the direct use of PILs as esterification and transesterification catalysts, the immobilization of these materials on nanoporous supports has also been studied. For example, palygorskite is a mineral with a nanofiber-like structure containing aluminum and hydrated magnesium. These nanofibers have a diameter of 100–500 nm with a length of 1–2 μm. High specific surface area, high thermal and mechanical stability, and abundant silanol units on the surface have turned this substance good support. Moreover, this substance is abundant in nature and sufficient hydroxyl groups can be created

TABLE 2 | Polymeric ionic liquid catalysts for (trans) esterification.

Feedstock	Catalyst	Surface area (m^2/g)	Pore volume (cm^3/g)	Average pore diameter (nm)	Catalyst dosage (wt.%)	Temperature (°C)	Alcohol/oil molar ratio	Reaction time (h)	Yield (%)	Yield after reuse (%)	Reuse times	References
Tripalmitin	PDVB-[C$_3$vim][SO$_3$CF$_3$]	–	–	–	6	65	90	16	>99.9	98.1	5	Liu F. et al., 2012
FFA	OMR-[C$_4$HMTA][SO$_4$H]	406	0.5	11.1	5	65	9	1.5	99.5	96	5	Noshadi et al., 2014
Brown grease					5	65	40	5	75	–	–	
Oleic acid	MPD-SO$_3$H-IL	281	0.94	27	5	100	30	4	98	93	4	Pan et al., 2016
Jatropha oil					6	160	50	8	94	74	4	
Soapberry oil	P(VB-VS)HSO$_4$	100.1	0.33	18.9	8.7	150	29.1	8	95.2	90.9	6	Feng et al., 2017
Oleic acid					5	90	8.7	4	97.5	–	–	
Oleic acid	MMFP-IL	283	–	–	4	90	12	3	95	88	4	Pan et al., 2019
Oleic acid	[HCPpitch–Im–Pros][Tos]	380	0.21	2.56	8	70	7	3	93	92	5	Pei et al., 2019
Waste cooking oil	Acidic PIL	523	–	–	1	70	15	12	99.1	99	6	Liang, 2013a
Oleic acid	Fe$_3$O$_4$@(poly[VSIM][HSO$_4$])	43.6	–	–	8.5	80	12	4.5	92.6	89.3	6	Wu et al., 2016a
Oleic acid	Fe$_3$O$_4$@PILPW	–	–	–	13	90	12	5	93.4	89.6	6	Wu et al., 2016a,b
Soybean oil	BPIL	103	0.32	35	9.15	65	21.9	9.33	96.3	85	5	Jiang et al., 2017
Oleic acid	PIL-M	301.1	2.249	–	6	80	9	3	95.9	>90	4	Bian et al., 2019

by acid activation to increase its grafting density. Zhang W. et al. (2017) synthesized a mesoporous acidic PIL with an average pore diameter of 19 nm. The vinyl groups were grafted on the surface of palygorskite through reaction with γ-methacryloxypropyl trimethoxy silane and then grafting polymerization of the acidic IL monomers 1-butysulfonate-3-vinylimidazole hydrogensulfate in the presence of AIBN was performed. In the synthesis of this PIL, the weight ratio of the IL to palygorskite, temperature, reaction time and AIBN level affect the amount of ionic liquid immobilized on the support and thus should be optimized. A yield of 69% was reported for methyl ester in the presence of the immobilized PIL, which reduced to 22% after 6 times of catalyst recovery. This significant reduction in reaction yield was attributed to the dissolution of IL in methanol and its reduced loading on the support, adhesion of esters on the support and reduced specific surface area and active sites and catalyst loss in the recovery process.

Later, the palygorskite-supported PIL was used for the preparation of a hybrid organic-inorganic pervaporation catalytic membrane. In addition to the catalytic effect, these membranes increase the efficiency of equilibrium reactions by removing one of the products from the reaction medium. The membrane was prepared by mixing poly(vinyl alcohol) with the PIL supported on palygorskite and succinic acid was used to link Poly(vinyl alcohol) through crosslink reaction. Adding a solid catalyst to poly(vinyl alcohol) improved thermal and mechanical stability and hydrophobicity of the PIL. Although the membrane successfully removed water produced from esterification of oleic acid, the maximum yield was about 5% due to very low PIL levels supported on palygorskite in the membrane structure and its very low effective contact area (24.6 cm^2) (Li et al., 2020).

Another class of supports used for immobilizing PILs is nanoporous magnetic silica that facilitates PIL separation from the reaction mixture by an external magnetic field. Zhang H. et al. (2017) immobilized a basic PIL on the magnetic mesoporous support, Fe$_3$O$_4$@SiO$_2$@SBA-15 (FnmS), by radical polymerization. **Figure 6** shows the fabrication route to this catalyst. To prepare the support, Fe$_3$O$_4$ nanoparticles were first prepared by the solvothermal method and then coated with SiO$_2$ by the sol-gel method to obtain Fe$_3$O$_4$@SiO$_2$ microspheres. Thereafter, the external layer of the mesoporous silica was formed on the support by adding tetraethyl orthosilicate, P123, and HCl. The resulting magnetic mesoporous support was functionalized with sulfhydryl groups after reaction with (3-mercaptopropyl)trimethoxysilane. The IL monomer was produced from the reaction of 1-vinylimidazole with ethyl bromide and then participated in precipitation polymerization with a crosslinker and 2,2′-azobis(2-methylpropionitrile). Eventually, the hydroxide ions replaced bromide ions through ion exchange with tetramethylammonium hydroxide to obtain the basic Fnms-PIL catalyst. In addition to a high surface area, the density of basic sites was high and grafting of organic functional groups did not negatively affect the mesoporous structure. The yield of transesterification reaction of the non-edible vegetable oil in the presence of this catalyst under mild reaction conditions including a methanol-to-oil molar ratio of

9:1, a catalyst concentration of 4 wt.% and the reaction time of 5 h at 85°C was 92.8%, which remained about 90% after 5 times of catalyst reuse.

As mentioned above, water as an esterification product negatively affects the catalytic activity and causes leaching of active sites. In another study, Zhang et al. (2018) synthesized several acidic FnmS-PIL catalysts and found an increase in the catalytic activity and resistance to water with increasing the length of alkyl groups attached to FnmS and anion acidity. An increase in the length of alkyl groups used for functionalizing the support improved its hydrophobicity. Among various catalysts containing the anions $CF_3SO_3^-$, HSO_4^-, Cl^-, $1/3\ PW_{12}O_{40}^{3-}$, the catalyst containing $CF_3SO_3^-$ showed the highest yield due to the higher acidity of this anion. The catalyst showed a good performance in converting oleic acid and Euphorbia lathyris L with a high acid number. A yield of over 90% was obtained when the water content in the feed increased up to 6 wt.%.

Fe$_3$O$_4$ nanoparticles are coated by a silica layer primarily for two reasons. First, magnetic nanoparticles are aggregated and form large clusters due to the bipolar-bipolar magnetic property. This in turn causes the non-uniform distribution of the catalyst in the reaction mixture and thereby reduced catalytic activity. Second, the silica layer prevents corrosion of iron oxide nanoparticles under harsh conditions. Recently, an acidic catalyst has been synthesized through radical copolymerization of the IL monomer 1-vinyl-3-(3-sulfopropyl)imidazolium hydrogen sulfate and Fe$_3$O$_4$/SiO$_2$ nanocomposites functionalized with vinyl groups (Xie and Wang, 2020). The vinyl groups were grafted on the Fe$_3$O$_4$/SiO$_2$ support through reaction with 1-vinyltriethoxysilane. The resulting hybrid organic-inorganic catalyst successfully converted 93.3% of oil to biodiesel through esterification and transesterification of oil with high FFA content, whereas FFA was completely converted into biodiesel. The conversion of the oil to biodiesel was lower in the presence of the unsupported homopolymer. Given the same number of acidic sits, this was related to the lower surface area in this case. Moreover, due to strong covalent bonds between the grafted IL and the support, the active acidic sites were preserved on the support surface so that conversion of over 80% was obtained after 5 times of catalyst reuse.

To summarize the above discussion, the supported PILs are synthesized by copolymerization of the IL monomer and carrier, and Si-O-Si bonds are used to attach the cation of IL to the surface of mesoporous silica. To connect the cations to Si atoms, various chemical groups such as vinyl, propyl, and thiol have been employed.

Table 3 compiles the results of previous research on biodiesel production over mesoporous silica-supported PILs. Overall, excluding the results found by Zhang W. et al. (2017) and Li et al. (2020), the other studies reported satisfactory findings.

In both studies conducted by Zhang W. et al. (2017) and Li et al. (2020), the catalyst was fabricated by copolymerization reaction between the IL monomer 1-butysulfonate-3-vinylimidazole hydrogensulfate and palygorskite as the support. In each unit of the resultant catalyst, the imidazolium cation is attached to one Si atom through a long chain containing propyl

FIGURE 6 | The synthesis process of $Fe_3O_4@SiO_2@SBA-15-BPIL$ [Redrawn from Zhang H. et al. (2017)].
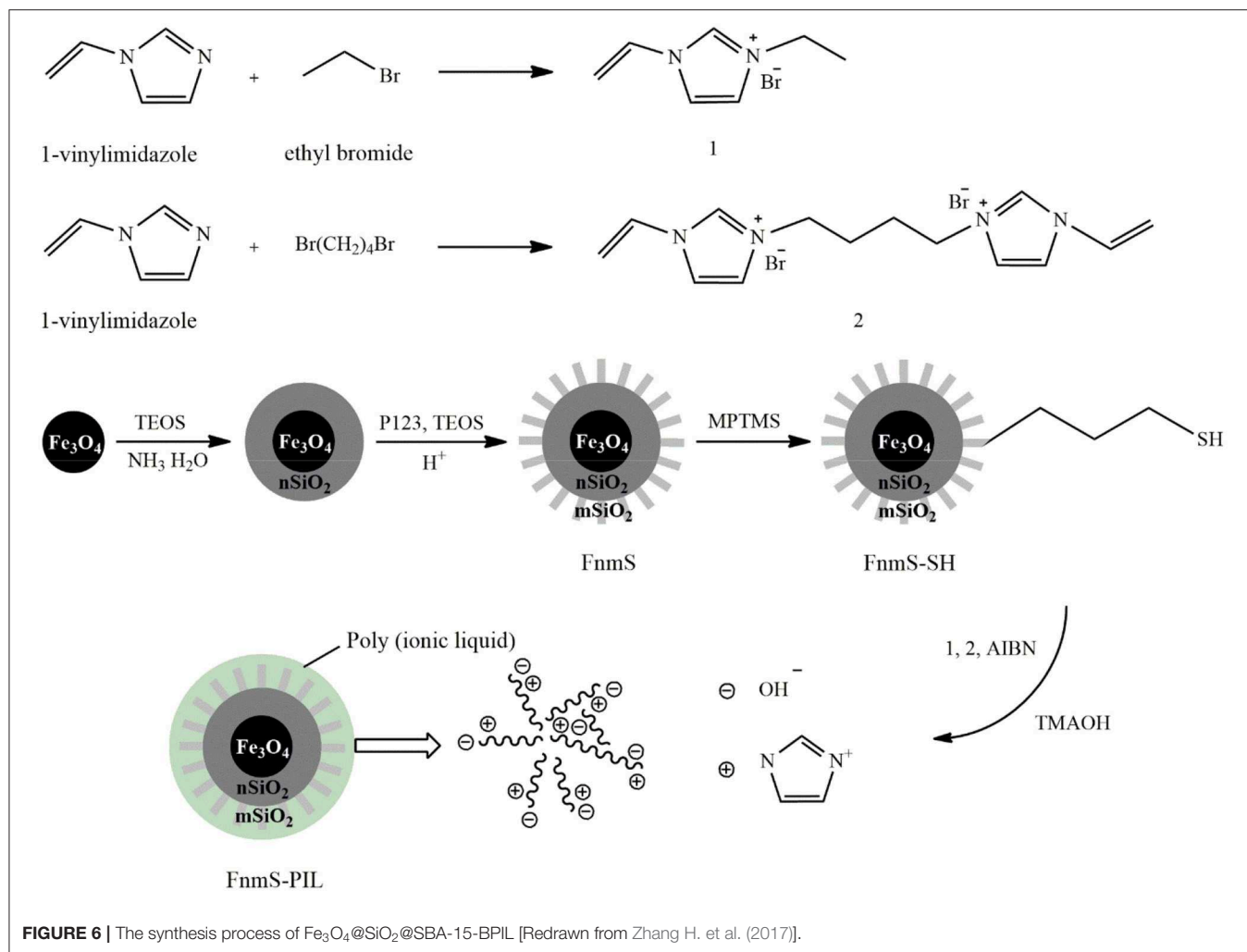
and vinyl groups. In the presence of PAL-PILs catalyst, the reaction yield fell dramatically after 6 cycles, which was due to the leaching of the PILs and active sites and significant reduction in specific surface area (from 43 to 11 m^2/g) as a result of the adhesion of esters on the palygorskite. Therefore, the stability of active sites should be improved, for which the IL can be attached to palygorskite through silane or thiol groups.

On the other hand, the very low yield was obtained by Li et al. (2020) when CPVA/PAL-PILs were employed. This resulted from the limited number of active sites and negligible specific surface area of the catalyst. In PAL-PILs, the amount of PIL loaded on the support was 41%. But the main issue is associated with the loading amount of PAL-PILs on the CPVA which was very low (around 2%), which dramatically reduces the number of accessible active sites. Moreover, polyvinyl alcohol may cover these active sites and limit the diffusion of the reactants. Therefore, increasing the specific surface area and PIL loading will be the main challenge in future studies.

The sole basic PIL in this group was synthesized and supported on magnetic mesoporous silica by Zhang H. et al. (2017). They used thiol groups to attach the imidazolium cation

of PIL to the carrier which led to a high biodiesel yield and good stability. The same method was employed for immobilizing an imidazolium-based acidic PIL on magnetic mesoporous silica and satisfactory results were obtained (Zhang et al., 2018). These results demonstrate the good performance of the thiol-ene reaction for supporting PILs on silica materials.

Finally, vinyl groups were employed by Xie and Wang (2020) for the immobilization of an acidic PIL on a magnetic mesoporous silica carrier. The strong covalent bonds were responsible for the reasonable recyclability and high biodiesel yield in the transesterification of soybean oil. Therefore, incorporation of vinyl groups can result in high stability catalysts.

ILs Supported on MOFs

Metal-organic frameworks (MOFs) are crystalline nanoporous materials that are obtained by combining inorganic nodes (including metal ions or clusters of metal ions) and organic ligands. MOFs have numerous advantages such as high thermal stability, ordered structures, very low density, a large internal surface area up to over 6,000 m^2/g, and facile preparation through self-assembly (Gangu et al., 2016). Depending on the type of

TABLE 3 | Polymeric ionic liquids on mesoporous silica.

Feedstock	Catalyst	Surface area (m²/g)	Pore volume (cm³/g)	Average pore diameter (nm)	Catalyst dosage (wt.%)	Temperature (°C)	Alcohol/oil molar ratio	Reaction time (h)	Yield (%)	Yield after reuse (%)	Reuse times	References
Oleic acid	PAL–PILs	43	–	19	7	75	12	5	>69	22	6	Zhang W. et al., 2017
Oleic acid	CPVA/PAL-PILs		0.00246	–	–	75	10	20	5	–	–	Li et al., 2020
Firmiana platanifolia L.f. oil	Fe_3O_4@SiO_2@SBA-15-BPIL	153.2	–	4.1	4	85	9	5	92.8	90	5	Zhang H. et al., 2017
Oleic acid	Fe_3O_4@SiO_2@SBA-15-APIL	128.1	–	4.2	4	75	17	3.1	95.3	87.5	5	Zhang et al., 2018
Euphobia lathyrism L. oil					5	120	18	6	91.7	–	–	
FFA	Fe_3O_4/SiO_2-PIL	58.99	0.14	9.1	9	120	35	6	100	–	–	Xie and Wang, 2020
Soybean oil					9	120	35	6	93.3	84.5	5	

metal ions and organic linkers and direction of linkages between ions, many MOFs with a variety of framework geometries can be designed. These structures contain voids or pores that their size, shape, and functionalization can be well-controlled unlike zeolites. Therefore, these pores can be used to confine the desired molecules (Safaei et al., 2019).

MOFs have recently played a key role in heterogenizing ILs to be used in various areas including gas adsorption, catalysis, and fabrication of nanoporous carbon. In addition to a large number of nanopores in their crystalline structure, their properties such as pore size, surface area, framework topology, and polarity of the inner surface are tunable (Fujie and Kitagawa, 2016). MOFs are very similar to ILs in this regard. As properties of ILs are determined by cations and anions used in their structures, properties of MOFs can be designed by using various metal ions and organic ligands.

In general, there are two methods for incorporation of ILs in the structure of MOFs: ionothermal synthesis and post-synthetic modification. As a solvothermal method, an IL is used as a solvent in the ionothermal method, and IL cations are attached to negatively charged MOF frameworks. Given the strong interaction of cations and the MOF framework, the useful properties are limited in comparison with the bulk IL. Furthermore, functional groups used in this method should be compatible with the host MOF, thus a limited number of ILs and MOFs can be used. In contrast, ILs are used in the as-synthesized MOFs in the post-synthesis method. As a result, the need for compatibility of ILs and MOFs is eliminated to a large extent and a wide range of both materials can be used (Cota and Martinez, 2017). Accordingly, the post-synthesis method has been used in all studies on the application of hybrid IL-MOF catalysts for biodiesel production.

MIL Supported ILs

For the first time, Wan et al. (2015b) confined ILs in the polyoxometalate-based MIL-100(Fe) (POM-MIL-100) to be used as a heterogeneous catalyst for biodiesel production. The MOF was synthesized by the hydrothermal method by combining $FeCl_3.6H_2O$, phosphotunhstic acid ($H_3PW_{12}O_{40}$), and benzene-1,3,5-tricarboxylic acid (H_3BTC) leading to confining of $H_3PW_{12}O_{40}$ in the MIL-100(Fe) framework. The IL 1-(propyl-3-sulfonate) imidazolium hydrogen sulfate $[SO_3H\text{-}(CH_2)_3\text{-}HIM][HSO_4]$ was converted into the IL $[SO_3H\text{-}(CH_2)_3\text{-}HIM]_3PW_{12}O_{40}$ through anion exchange with $H_3PW_{12}O_{40}$ and encapsulated in the MOF framework. To this end, POM-MIL-100 was added to the IL-methanol solution and the resulting mixture was vigorously stirred for 10 min and then treated with ultrasound waves for 30 min. The mixture was stirred for another 12 h at room temperature. Eventually, the resulting solid was centrifuged and washed with diethyl ether and dried in a vacuum oven at 60°C. The catalyst (POM-IL@MIL-100) led to a conversion of 94.6% in converting oleic acid with ethanol under optimal conditions. It was more active than MIL-100 and POM-MIL-100, which can be related to the high acidity (1.74 mmol/g) of the catalyst caused by the synergistic effect of Brønsted acid sites of the IL and Lewis acid sites provided by Fe^{III} ions. The

catalyst was recovered 6 times and reused without any significant reduction in the conversion.

In 2016, Han et al. (2016) developed a novel method for confining the dicationic IL $[SO_3H-(CH_2)_3-IM]_2C_4[HSO_4]_2$ in the MIL-100(Fe) framework. In this method known as the impregnation-reaction-encapsulation process, small molecules of the IL diffused into nanopores of the MOF and began to grow in the nanopores up to a point that was no longer able to escape from the MOF cages due to their large size. To this end, $[SO_3H-(CH_2)_3-HIM][HSO_4]$ was added to a solution of methanol and MIL-100(Fe). After stirring for 30 min, 1,4-dibromobutane was dropwise added to the mixture at $0°C$ and stirred for 12 h at $25°C$ and for another 12 h at $60°C$. The resulting solid was centrifuged and after washing with methanol, was performed with methanol at $40°C$ for another 12 h. Eventually, the product was dried under vacuum at $80°C$ for 12 h. 15 wt.% of the catalyst (MIL-100(Fe)@DAILs) converted 93.5% of oleic acid into methyl oleate. After 5 times of reuse, the conversion reduced to 86%. The results of FTIR spectra revealed that the size of dicationic IL molecules (length: 1.93 nm, width: 0.9) caused their confinement in the mesocages of the MOF (diameter: 2.9) so that they were not able to escape through 0.86 nm apertures. In contrast, the catalyst obtained from direct impregnation of the IL $[SO_3H-(CH_2)_3-HIM][HSO_4]$ (length: 1.05 nm, width: 0.6 nm) led to a conversion of 22.3% after 5 times of reuse indicating leaching of large amounts of the IL from the MOF mesocages.

In recent years, magnetic MOFs have been used as the support of ILs in biodiesel production. Wu et al. (2016b) prepared an acidic heterogeneous catalyst for ethyl oleate production through confining the Brønsted acidic IL 1,4-butanediyl-3,3'-bis-(3-sulfopropyl) imidazolium dihydrogensulfate in the magnetic MOF $Fe_3O_4@NH_2$-MIL-88B(Fe). The magnetic support functionalized with amino groups was obtained through thermal treatment of 2-aminoterephthalic acid, $FeCl_3.6H_2O$, N,N-dimethyl formamide, and Fe_3O_4 nanoparticles. The support was then dispersed with the IL in ethanol and mixed for 24 h at $110°C$ to obtain the catalyst DAIL-$Fe_3O_4@NH_2$-MIL-88B(Fe) through the interaction of amino and sulfonic acid groups. A conversion of 93.2% was obtained for the reaction of oleic acid with ethanol, which was higher than the unsupported ionic liquid catalyst. A lower conversion was obtained when the monocationic IL $[SO_3H-(CH_2)_3-IM][HSO_4]$ was immobilized on the support due to the lower number of SO_3H and HSO_4 groups and thereby a lower acidity.

Besides direct use of ILs, tandem post-synthetic modification can be also used for the incorporation of ILs in the MOF structure. One approach is to place functional groups on the IL and then immobilization of the functionalized IL on MOFs. Using this method, Han et al. (2018) first functionalized the ILs 2-mercaptobenzimidazole (MBI) with electron-enriched thiol groups. The resulting IL was then immobilized on the surface of MIL-101(Cr) through S-Cr coordination bonds. To synthesize the catalyst, MBI was first dissolved in ethanol and then MIL-101(Cr) was added. After 24 h mixing at room temperature, centrifugation, washing the solid with ethanol, and drying under vacuum at $60°C$, MIL-101(Cr)@MBI was obtained. Thereafter, MIL-101(Cr)@SO_3-$(CH_2)_3$-HMBI was obtained by dispersing

MIL-101(Cr)@MBI in ethyl acetate and reacting with 1,3-propanesulfonate for 12 h at $60°C$. Eventually, the product was dissolved in ethanol and reacted with H_2SO_4 for 24 h at $60°C$ to obtain MIL-101(Cr)@$[SO_3H-(CH_2)_3-HMBI][HSO_4]$. **Figure 7** shows the procedure for the synthesis of this catalyst. The results showed that immobilization of the acidic IL on MIL-101(Cr) through S-Cr coordination bonds not only increased the oleic acid conversion but also improved catalyst reusability as compared with the neat MOF.

UiO Supported ILs

In a recent study by Xie and Wan (2019), the IL $[SO_3H-(CH_2)_3-HIM][HSO_4]$ was encapsulated in the POM-UiO-66-2COOH framework. The MOF was synthesized through the *in-situ* reaction of $ZrCl_4$, $H_3PW_{12}O_{40}$, and 1,2,4,5-benzene-tetracarboxylic acid. Subsequent anion exchange between the acidic IL and the heteropoly anion led to the synthesis of ILs/POM/UiO-66-2COOH. A conversion of 95.8% was obtained for transesterification of soybean oil with methanol using this catalyst under optimal conditions. Strong interactions between sulfonic acid groups and heteropoly tungstate molecules effectively prevented the loss of active species from the MOF support and led to reasonable stability of the catalyst during multiple recoveries and reuse cycles. The catalyst showed higher activity in FFA esterification than the transesterification of soybean oil.

Ye et al. (2019) proposed a new method for confining the acidic IL 1,3-biscarboxymethyl-imidazolium hydrosulfate in the UiO-66 framework. In the so-called approximate ligand substitution method, parts of ligands were eliminated through MOF etching by propionic acid to produce the hierarchical porous UiO-66 with a large number of defects and Lewis acid sites. Then, the IL precursor was supported on H-UiO-66 through bidentate coordination bonds between a COO^- group and two unsaturated Zr ions. The final catalyst was obtained by the addition reaction of the modified MOF with H_2SO_4. This catalyst showed higher activity in the esterification of oleic acid (93.8%) than the bulk IL (89.2%), UiO-66 (25.6%), and H-UiO-66 (78.6%). UiO-66 also showed a catalytic activity due to defects and unsaturated Zr atoms in its natural structure leading to the opening of Lewis acid sites. However, these Lewis acids are not well accessible due to the lower diameter of pore aperture than the oleic acid molecule. By opening this MOF structure and with an increase in the size of pores, the catalytic activity of H-UiO-66 becomes much greater than MOF. By immobilizing the IL in the MOF structure, Brønsted acid sites are added to the Lewis acid sites leading to an increase in the acidity and thereby reaction yield.

HKUST Supported ILs

Using the tandem post-synthetic modification method, ILs with ions larger than the aperture diameter of the pores can be incorporated into MOF pores (Fujie and Kitagawa, 2016). In another approach of this method, MOFs can be functionalized through unsaturated metal centers (UMCs). In this method, active species are grafted through coordination covalent bonds with UMCs. Chen et al. (2016) used this method for the
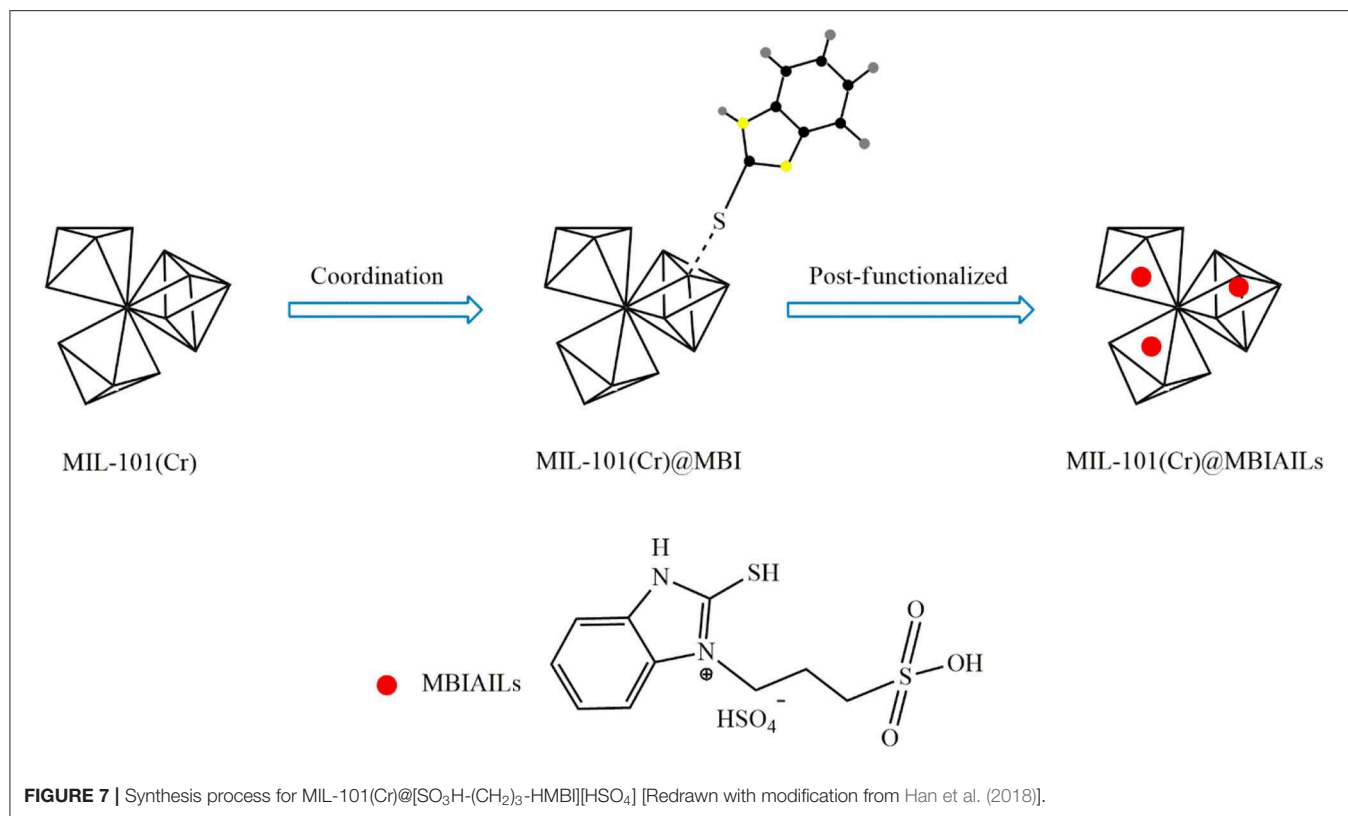
FIGURE 7 | Synthesis process for MIL-101(Cr)@[SO$_3$H-(CH$_2$)$_3$-HMBI][HSO$_4$] [Redrawn with modification from Han et al. (2018)].

functionalization of HKUST-1 through coordination bonding of Cu^{2+} metal centers with thiol functional groups (S-Cu coordination bonds). For the synthesis of thiol-functionalized HKUST-1, ethanedithiol was dissolved in anhydrous toluene and HKUST-1 was gradually added to the resulting solution. The mixture was stirred for 24 h at room temperature and the resulting suspension was centrifuged. The resulting solid was washed with ethanol and then dried under vacuum at room temperature. Thereafter, this substance was dispersed in the IL [HVIm-(CH$_2$)$_3$SO$_3$H]HSO$_4$ in anhydrous ethanol. After rising the temperature to 80°C, AIBN was added under nitrogen and the reaction continued for 30 h. The product was separated by filtration and then was washed several times with ethanol to remove excess IL. Finally, the catalyst IL@HKUST-1 was obtained by drying under vacuum at 60°C for 12 h. The catalyst was synthesized through covalent bonding of the vinyl groups of the IL with thiol groups in the HKUST-1 structure to achieve a conversion of 92.1% in the esterification of oleic acid to methanol. The conversion reduced to 86.3% after 5 catalytic cycles due to the decomposition of the HKUST-1 structure and thereby loss of active IL.

In another study, Xie and Wan (2018) immobilized amino-functionalized ILs on the magnetic HKUST-1. The layer-by-layer assembly was used to prepare Fe$_3$O$_4$@HKUST-1 composites. The Fe$_3$O$_4$ nanoparticles were first modified with mercaptoacetic acid and then added to the Cu(CH$_3$COO)$_2$.H$_2$O solution in ethanol. The resulting mixture was stirred for 30 min at 70°C and the obtained solid was dispersed in H$_3$BTC solution in ethanol. After

1 h stirring of the mixture at 70°C and separation of the solid with a magnet and washing with ethanol, the production cycle was terminated. After 20 same cycles, Fe$_3$O$_4$@HKUST-1 with a core-shell structure was obtained. The composite was then added to the amino-functionalized IL solution in ethanol and the mixture was stirred for 24 h at 60°C. Eventually, the basic magnetic catalyst Fe$_3$O$_4$@HKUST-1-ABILs was obtained after magnetic separation, washing with ethanol, and drying. In this process, the IL was added to the MOF structure through N-Cu coordination bonds. The basic catalyst led to a conversion of 92.3% in transesterification of soybean oil at an ethanol-to-oil molar ratio of 30:1 and a catalyst dosage of 1.2% within 3 h. The catalyst was used 5 times without a significant reduction in the conversion.

Table 4 presents the results of previous studies on (trans)esterification of various feedstock over MOF-supported ILs. As can be seen, yields of higher than 90% were obtained in all studies.

Regarding the research on MIL supports, ILs were either encapsulated inside the MIL framework (Wan et al., 2015b; Han et al., 2016) or immobilized on the surface of the framework (Wu et al., 2016a,b; Han et al., 2018). The results suggest that encapsulation leads to catalysts with better recyclability (higher yield after multiple reuses) compared to surface immobilization. On the other hand, a higher amount of catalyst is required for high biodiesel yields when encapsulation is employed. This can be attributed to the fact that when IL is confined inside the framework, the leaching of active species is reduced but the active

TABLE 4 | ILs immobilized on metal organic frameworks.

Feedstock	Catalyst	Surface area (m²/g)	Pore volume (cm³/g)	Catalyst dosage (wt.%)	Temperature (°C)	Alcohol/oil molar ratio	Reaction time (h)	Yield (%)	Yield after reuse (%)	Reuse times	References
Oleic acid	POM-IL@MIL-100	167	38	15	111	11	5	94.6	89.5	6	Wan et al., 2015b
Oleic acid	MIL-100(Fe)@DAILs	170.2	0.2	15	67	8	5	93.5	86	5	Han et al., 2016
Oleic acid	DAIL–Fe$_3$O$_4$@NH$_2$-MIL-88B(Fe)	103.6	–	8.5	90	10.5	4.5	93.2	83	6	Wu et al., 2016a,b
Oleic acid	MIL-101(Cr)@[SO$_3$H-(CH$_2$)$_3$-HMBIj][HSO$_4$]	472.9	0.24	11	67	10	4	91	82.1	6	Han et al., 2018
FFA	AILs/HPW/UiO-66-2COOH	8.63	0.04	10	110	35	1.3	99.3	–	–	Xie and Wan, 2019
Soybean oil	[(CH$_2$COOH)$_2$IM]HSO$_4$@H-UiO-66	748	–	6.28	80	10.39	5	93.82	90.95	5	Ye et al., 2019
Oleic acid	IL@HKUST-1	386.9	0.23	15	90	12	4	92.1	86.3	5	Chen et al., 2016
Soybean oil	Fe$_3$O$_4$@HKUST-1-ABILs	23.7	0.15	1.2	65	30	3	92.3	>80	5	Xie and Wan, 2018

sites are less exposed to the reactants. On the contrary, in surface immobilization, the catalytic sites have more exposure to the reactants and lower catalyst dosage is required for a certain yield. However, as the IL is attached to the surface of the framework, its leaching will rise. Immobilization of IL on the surface of the MIL framework through SO$_3$H-NH$_2$ bonds (Wu et al., 2016a,b) has shown the same effect on recyclability as the direct attachment of the IL via S-Cr bonds (Han et al., 2018).

Ye et al. (2019), which employed the etching method for confining IL (CH$_2$COOH)$_2$IM][HSO$_4$] inside UiO-66 framework, obtained a higher yield and better performance after several catalytic cycles by using a lower catalyst dosage. The MOF framework is partly broken by etching and more catalytic sites present in the IL are exposed to the reactants. This reduces the required catalyst concentration. On the other hand, leaching is decreased because the IL is attached to the framework through strong double Zr-O coordination bonds, which improves the reaction yield after multiple reuses.

In both works connected with HKUST-1, the ILs were immobilized on the surface of frameworks. Chen et al. (2016) first functionalized the framework by thiol groups and then the IL was attached to the framework through vinyl-thiol interactions. Therefore, the IL was immobilized on the framework via S-Cu coordination bonds. On the other hand, Xie and Wan (Xie and Wan, 2018) first functionalized the IL with amino groups and then attached it to the surface of the framework through N-Cu coordination bonds. Both resultant catalysts showed good activities, especially Fe$_3$O$_4$@HKUST-1-ABILs which with only 1.2 wt.% dosage led to over 90% biodiesel yield in transesterification of soybean oil.

Given to what mentioned earlier, all three methods have resulted in catalysts with high activity and reasonable reusability. However, the etching method combines the advantages of encapsulation and surface immobilization in fabricating a MOF-based IL catalyst. Thus, further research on the synthesis of new catalysts using this approach with an emphasis on the transesterification of non-edible and high FFA content oils is recommended.

ILs Supported on Nanoporous Carbon

Graphene-based nanomaterials as novel carbon materials with a nanosheet structure have a high surface area and good mechanical flexibility and thermal stability (Novoselov et al., 2004; Wang et al., 2012; Zhou et al., 2014; Hu et al., 2015, 2017). This causes reduced mass transfer resistance, good exposure of active sites, and improved recyclability of these nanomaterials and turns them ideal supports for active species such as ILs (Liu et al., 2015).

Despite these advantages, the synthesis of graphene-based nanomaterials with high surface area and abundant nanopores through a facile low-cost method is a great challenge. Moreover, these nanomaterials are chemically neutral making their functionalization by acidic functional groups difficult (Tang et al., 2015). Doping can be used to overcome this drawback and to modify other properties of nanoporous carbon materials (Albero and Garcia, 2015). Liu et al. (2015) produced a graphene-like nanoporous carbon by carbonizing melamine and glucose and

subsequent doping with N_2. Melamine and glucose were first mixed and crushed and then carbonized in a tube furnace under N_2 gas flow at 800°C. After cooling down the furnace, N-doped graphene-like nanoporous carbon (GNC) was obtained. Thereafter, GNC was added to a mixture of toluene and 1,3-propanesultone and the resulting mixture was refluxed at 110°C for 24 h to complete the quaternary ammonization reaction. After cooling down to the room temperature, the mixture was stirred for 24 h at room temperature for anion exchange with toluene and HSO_3CF_3. Finally, the solid was separated by filtration and washed with CH_2Cl_2 and dried for 12 h at 60°C to obtain the heterogeneous acidic catalyst GNC-[C_3N][SO_3CF_3]. This catalyst was used for the transesterification of tripalmitin with methanol. After 14 h, a conversion of 88.5% was obtained at 65°C, which was higher than that in the presence of Amberlyst 15, SBA-15-SO_3H and $H_3PW_{12}O_{40}$. The catalyst also showed good activity in the transesterification of sunflower oil, which was comparable with sulfuric acid. In addition to high acidity, 2D nanosheets provide the very good accessibility of reactants to active catalyst sites. Moreover, the good stability of the catalyst provides the possibility for 5 times of reuse in the transesterification reaction.

Despite good results, the use of nanoporous carbon materials functionalized with ILs as a catalyst for biodiesel synthesis is limited to this study. Thus, there is an obvious need for further research in this area.

LIMITATIONS AND PROSPECTS

In general, a suitable heterogeneous catalyst for (trans)esterification of oil should have a porous structure with abundant pores, high BET surface area, high basicity or acidity, high density of active species, and good dispersion of active sites. These properties increase the contact area of active sites with reactants leading to enhanced diffusion and mass transfer and thereby catalytic activity (Pirez et al., 2012; Wang et al., 2015). According to the above discussions, by combining unique properties of ILs and nanoporous materials, a catalyst with high activity and reasonable stability can be synthesized. Since these properties can be tailored, hydrophobicity, adsorption of reactants, and desorption of products from the catalyst surface can be well-designed.

In most of the studies, a BET surface area of higher than 100 m^2/g was reported. However, according to the results of Wu et al. (2016a), Xie and Wang (2020), and Xie and Wan (2018, 2019) high yields can be obtained with smaller surface areas. Xie and Wan (2019) reported a 95.8% biodiesel yield in transesterification of soybean oil over AILs/HPW/UiO-66-2COOH with a specific surface area of 8.63 m^2/g. On the other hand, the very low yield was obtained with a BET surface area of 0.00246 m^2/g (Li et al., 2020). Therefore, a minimum BET surface area of 8 m^2/g is recommended to achieve high conversions.

The catalyst acidity or basicity plays a key role in the catalyst activity so that acidity or basicity of the surface is directly related to the catalytic activity. Acidic or basic sites are required for the activation of carbonyl groups in the triglyceride molecules and

initiation of the transesterification reaction (Xie and Wan, 2019). The acid content of acidic ILs/nanoporous materials varied from 1.13 to 4.3 mmol/g in the literature. The corresponding range for basicity was 2.03–3.67 mmol/g. Based on these results, one can conclude that the minimum acidity and basicity to achieve high biodiesel yields are around 1 and 2 mmol/g, respectively. Furthermore, the resistance of acidic catalysts against heat as well as water and FFA content of the feedstock prevent loss of active sites and improve recoverability and reusability of the catalyst.

The average pore diameter is another important factor that specifically affects reaction time. According to Granados et al. (2007) and Coenen (1986), a minimum pore diameter of 3.5 nm is preferable for producing biodiesel. However, high conversion and yield after multiple reuses was reported by Pei et al. (2019), using an average pore diameter of 2.56 nm. Therefore, a pore diameter of >2.5 nm should be considered to achieve high yields under mild reaction conditions.

The most serious obstacle for employing IL/nanoporous material hybrids is the high synthesis cost. To compare the cost of supported ILs with traditional catalysts, a cost estimation based on the synthesis routes proposed by previous studies was performed. The cost for all chemicals and reagents were obtained from Sigma-Aldrich. For NaOH and H_2SO_4, the prices presented by industrial manufacturers on Alibaba website were used. **Table 5** gives information on the estimated fabrication cost of some supported ILs. As can be seen from the table, with a synthesis cost of $1/g, the acidic PIL Poly[$SO_3H(CH_2)_3VIm$]HSO_4 is the cheapest of all, following by IL/silica-gel and SBA-15-pr-ILOH. On the other hand, magnetic mesoporous ILs Fe_3O_4@HKUST-1-ABILs and Fe_3O_4@SiO_2@SBA-15-BPIL are the most expensive which is obviously due to the more reagents required and longer and more complicated fabrication process of these catalysts.

It should be noted that the final cost of catalyst in the biodiesel production process is mostly affected by catalyst dosage and the number of reuse times. Lower catalyst dosages and more catalytic cycles reduce the final cost of catalyst. For example, among other catalysts, synthesis of 1 g of Fe_3O_4@HKUST-1-ABILs costs the most. However, taking into account the catalyst's low consumption and good reusability, it is the second least consumed catalyst and costs lower than some of the other supported-ILs in the production of 1,000 g biodiesel. Even by considering these two key factors, the costs of heterogeneous IL catalysts per 1,000 g biodiesel is far higher than the conventional NaOH and H_2SO_4. The acidic PIL Poly[$SO_3H(CH_2)_3VIm$]HSO_4 costs the least among all other heterogeneous ILs with only $1.67/1,000 g biodiesel. This is roughly 44 times higher than the cost for H_2SO_4 which is a common homogeneous acid catalyst for (trans)esterification of high FFA oils. On the other hand, Fe_3O_4@HKUST-1-ABILs is the most cost-effective basic supported IL, which costs ∼5,040 times higher than NaOH.

One should consider that these estimations are based on the synthesis processes in laboratories. These figures would significantly reduce if heterogeneous ILs were produced at the industrial scale. DeSantis et al. (2017) estimated a total production cost of $53.75/kg ($0.054/g) for HKUST-1 at a plant capacity of 50,000 ton/yr, which is 108 times as high as the cost for

TABLE 5 | Estimation of synthesis cost for various types of heterogeneous ILs.

Catalyst	Catalyst cost ($/g)	Catalyst dosage (wt.%)	Reuse time	Catalyst used for production of 1,000 g biodiesel (g)	Catalyst cost for production of 1,000 g biodiesel ($)
IL/silica-gel	1.32	5	5	10	13.2
SBA-15-pr-ILOH	3	7	4	17.5	52.5
SO_4^{2-}/ZrO_2-SiO_2(Et)-[Ps-im]HSO_4	4.4	5	5	10	44
P(VB-VS)HSO_4	4.3	8.7	6	14.5	62.4
Poly[SO_3H(CH_2)$_3$VIm]HSO_4	1	1	6	1.67	1.67
Fe_3O_4@SiO_2@SBA-15-BPIL	6.9	4	5	8	55.2
Fe_3O_4@HKUST-1-ABILs	10.5	1.2	5	2.4	25.2
NaOH	0.0005	1	0	10	0.005
H_2SO_4	0.00025	15	0	150	0.0375

NaOH. Also, the supported IL costs could be further reduced by increasing the loading amount of IL and improving the catalyst reusability. In the case of Poly[SO_3H(CH_2)$_3$VIm]HSO_4, as an example, decreasing the catalyst dosage by half and increasing the number of reuse times to 100 would result in an approximately same cost/1,000 g biodiesel as H_2SO_4. Another option is the use of cheaper anions and cations for IL synthesis. For instance, choline-based ILs are less expensive compared to many ILs because choline chloride as the main raw material is relatively cheap and commercially available for purchase (Andreani and Rocha, 2012).

FUTURE PERSPECTIVES OF BIODIESEL PRODUCTION PROCESS OVER IL-NANOPOROUS MATERIAL HYBRIDS

According to the results in the above, almost in all studies, the reaction conversion, number of catalytic cycles, and yield after multiple recovery and reuse are reasonable indicating the accurate design of the catalyst by selecting suitable ILs and nanoporous materials. These results also indicate the high potential of IL-nanoporous material (NPM) hybrids as good alternatives for traditional catalysts for biodiesel production. Nonetheless, by focusing on some limitations in future studies a big step can be taken toward the use of these catalysts in the biodiesel industry.

Oleic acid has been used in most studies as the feedstock. It should be noted that esterification of oleic acid is only a model reaction for biodiesel production, and esterification and transesterification of diverse feedstocks such as algae (Nagarajan et al., 2013), municipal sewage sludge (Olkiewicz et al., 2016), and recycled grease trap waste (Tran et al., 2018) may provide more realistic results on the catalytic activity of IL-NPM hybrid materials. This becomes more significant considering that optimal conditions reported for transesterification are harsher than esterification.

The other challenge is harsh reaction conditions, especially high alcohol-to-oil molar ratios (up to 90:1) and long reaction times (up to 40 h). This is originated from the heterogeneous nature of the catalyst leading to the formation of three phases in the reaction medium and reduced mass transfer due to the immiscibility of oil and alcohol. To achieve mild reaction conditions, intensification processes such as microwave, microchannel, hydrodynamic cavitation, and ultrasonic reactors can be used (Tabatabaei et al., 2019). Using various technologies, these reactors increase the mass transfer rate while reducing the reaction time. For example, hydrodynamic cavitation significantly increases the contact area of cavitation-induced alcohol and oil phases and facilitates transesterification reaction with a high yield at room temperature with lower energy consumption and also alcohol-to-oil molar ratio (Gholami et al., 2018).

In most studies, optimal conditions for biodiesel production have been obtained through the one variable at a time method. Since this methodology does not consider the effect of interactions of effective variables on the reaction yield, the resulting conditions and yield do not necessarily reflect optimal conditions (Montgomery, 2013). On the other hand, the pore size of nanoporous materials, especially MOFs, can be tailored. However, this advantage has not been still used for the optimization of transesterification conditions. The synthesis of catalysts with different pore sizes and investigation of the effect of this parameter on the yield and reusability may help to develop an optimal stable catalyst. Moreover, optimal conditions and more realistic maximum yields can be obtained by combining this innovation with the design of experiments (DOE) and response surface methodology (RSM).

Further studies on the kinetics of transesterification in the presence of IL-NPM catalysts, especially in intensification reactors, may lead to design a suitable alternative process for conventional industrial units. Since ILs and nanoporous materials can be produced from a wide range of eco-friendly materials, the above process may play a key role in the sustainable development and reduction of adverse environmental effects.

CONCLUSION

The literature on biodiesel production using nanoporous materials functionalized with ILs as catalyst was reviewed. A

variety of hybrids of ILs and nanoporous materials including nanoporous silica, polymers, MOFs, and carbon materials have been used for catalyzing the (trans) esterification reaction. All these materials have led to satisfactory results in biodiesel production. Moreover, these hybrids were considered attractive alternatives for conventional homogenous catalysts due to ease of separation, good stability, and activity after multiple catalytic cycles. Nonetheless, high synthesis cost, harsh reaction conditions, especially high alcohol-to-oil molar ratios, and long reaction times due to the heterogeneous nature of the catalyst were considered great challenges. The use of intensification processes may be a suitable solution to this problem. Moreover, tunable properties of IL-nanoporous material hybrids such as pore size and

surface area reflected the need for further studies on the effect of catalyst structure on the yield and optimal reaction conditions and structure optimization. In particular, it was recommended to investigate the use of MOFs for facilitating catalyst separation from products given the ease of synthesis, flexible design, and the possibility to combine their properties with magnetic nanoparticles.

AUTHOR CONTRIBUTIONS

AG: conceptualization, methodology, data curation, writing, and original draft preparation. FP: conceptualization, methodology, supervision, writing-reviewing, and editing. AM: writing-reviewing and editing.

REFERENCES

Abdurakhman, Y. B., Putra, Z. A., Bilad, M. R., Nordin, N. A. H. M., and Wirzal, M. D. H. (2018). Techno-economic analysis of biodiesel production process from waste cooking oil using catalytic membrane reactor and realistic feed composition. *Chem. Eng. Res. Des.* 134, 564–574. doi: 10.1016/j.cherd.2018.04.044

Abreu, F. R., Alves, M. B., Macedo, C. C. S., Zara, L. F., and Suarez, P. A. Z. (2005). New multi-phase catalytic systems based on tin compounds active for vegetable oil transesterificaton reaction. *J. Mol. Catal. A Chem.* 227, 263–267. doi: 10.1016/j.molcata.2004.11.001

Agarwal, D., Sinha, S., and Agarwal, A. K. (2006). Experimental investigation of control of NOx emissions in biodiesel –fueled compression ignition engine. *Renew. Energy* 31, 2356–2369. doi: 10.1016/j.renene.2005.12.003

Al Othman, Z. A. (2012). A review: fundamental aspects of silicate mesoporous materials. *Materials* 5, 2874–2902. doi: 10.3390/ma5122874

Albero, J., and Garcia, H. (2015). Doped graphenes in catalysis. *J. Mol. Catal. A Chem.* 408, 296–309. doi: 10.1016/j.molcata.2015.06.011

Alegria, A., de Arriba, A. L. F., Moran, J. R., and Cuellar, J. (2014). Biodiesel production using 4-dodecylbenzenesulfonic acid as catalyst. *Appl. Catal. B Environ.* 160–161, 743–756. doi: 10.1016/j.apcatb.2014.06.033

Amiril, S. A. S., Rahim, E. A., and Syahrullail, S. (2017). A review on ionic liquids as sustainable lubricants in manufacturing and engineering: recent research, performance, and applications. *J. Clean. Prod.* 168, 1571–1589. doi: 10.1016/j.jclepro.2017.03.197

Andreani, L., and Rocha, J. D. (2012). Use of ionic liquids in biodiesel production: a review. *Brazil. J. Chem. Eng.* 29, 1–13. doi: 10.1590/S0104-66322012000100001

Berthod, A., Ruiz-Angel, M. J., and Carda-Broch, S. (2018). Recent advances on ionic liquid uses in separation techniques. *J. Chromatogr. A.* 1559, 2–16. doi: 10.1016/j.chroma.2017.09.044

Bian, Y., Zhang, J., Liu, C., and Zhao, D. (2019). Synthesis of cross-linked poly acidic ionic liquids and its application in biodiesel production. *Catal. Lett.* 150, 969–978. doi: 10.1007/s10562-019-02988-0

Bourbigou, H. O., Magna, L., and Morvan, D. (2010). Ionic liquids and catalysis: recent progress from knowledge to applications. *Appl. Catal. A General* 373, 1–56. doi: 10.1016/j.apcata.2009.10.008

Canakci, M. (2007). The potential of restaurant waste lipids as biodiesel feedstocks. *Bioresour. Technol.* 98, 183–190. doi: 10.1016/j.biortech.2005.11.022

Cao, Y., Zhou, H., and Li, J. (2016). Preparation of a supported acidic ionic liquid on silica-gel and its application to the synthesis of biodiesel from waste cooking oil. *Renew. Sustain. Energy Rev.* 58, 871–875. doi: 10.1016/j.rser.2015.12.237

Chen, C., Wu, Z., Que, Y., Li, B., Guo, Q., Li, Z., et al. (2016). Immobilization of a thiol-functionalized ionic liquid onto HKUST-1 through thiol compounds as the chemical bridge. *RSC Adv.* 6, 54119–54128. doi: 10.1039/C6RA03317B

Cheng, W., Chen, X., Sun, J., Wang, J., and Zhang, S. (2013). SBA-15 supported triazolium-based ionic liquids as highly efficient and recyclable catalysts for fixation of CO₂ with epoxides. *Catal. Today* 200, 117–124. doi: 10.1016/j.cattod.2012.10.001

Chum, H. L., and Overend, R. P. (2001). Biomass and renewable fuels. *Fuel Process. Technol.* 71, 187–195. doi: 10.1016/S0378-3820(01)00146-1

Claus, J., Sommer, F. O., and Kragl, U. (2018). Ionic liquids in biotechnology and beyond. *Solid State Ionics* 314, 119–128. doi: 10.1016/j.ssi.2017.11.012

Coenen, J. W. E. (1986). Catalytic hydrogenation of fatty oils. *Indus. Eng. Chem. Fundamentals* 25, 43–52. doi: 10.1021/i100021a006

Cota, I., and Martinez, F. F. (2017). Recent advances in the synthesis and applications of metal organic frameworks doped with ionic liquids for CO₂ adsorption. *Coordinat. Chem. Rev.* 351, 189–204. doi: 10.1016/j.ccr.2017.04.008

Da'na, E. (2017). Adsorption of heavy metals on functionalized-mesoporous silica: a review. *Microporous Mesoporous Mater.* 247, 145–157. doi: 10.1016/j.micromeso.2017.03.050

Demirbas, A. (2006). Biodiesel production via non-catalytic SCF method and biodiesel fuel characteristics. *Energy Convers. Manage.* 47, 2271–2282. doi: 10.1016/j.enconman.2005.11.019

DeSantis, D., Mason, J. A., James, B. D., Houchins, C., Long, J. R., and Veenstra, M. (2017). Techno-economic analysis of metal-organic frameworks for hydro-gen and natural gas storage. *Energy Fuels* 31, 2024–2032. doi: 10.1021/acs.energyfuels.6b02510

Dincer, I. (2000). Renewable energy and sustainable development: a crucial review. *Renew. Sustain. Energy Rev.* 4, 157–175. doi: 10.1016/S1364-0321(99)00011-8

Dodds, D. R., and Gross, R. A. (2007). Chemicals from biomass. *Science* 318, 1250–1251. doi: 10.1126/science.1146356

Egorova, K. S., Gordeev, E. G., and Ananikov, V. P. (2017). Biological activity of ionic liquids and their application in pharmaceutics and medicine. *Chem. Rev.* 117, 7132–7189. doi: 10.1021/acs.chemrev.6b00562

Elhamifar, D., Karimi, B., Moradi, A., and Rastegar, J. (2014). Synthesis of a novel sulfonic acid containing ionic-liquid-based periodic mesoporous organosilica and study of its catalytic performance in the esterification of carboxylic acids. *ChemPlusChem* 79, 1147–1152. doi: 10.1002/cplu.201402071

Fan, M., Huang, J., Yang, J., and Zhang, P. (2013). Biodiesel production by transesterification catalyzed by an efficient choline ionic liquid catalyst. *Appl. Energy* 108, 333–339. doi: 10.1016/j.apenergy.2013.03.063

Fan, M., Liu, H., and Zhang, P. (2018). Ionic liquid on the acidic organic-inorganic hybrid mesoporous material with good acid-water resistance for biodiesel production. *Fuel* 215, 541–550. doi: 10.1016/j.fuel.2017.11.085

Fang, Z., Smith, R. L., and Qi, X. (2014). *Production of Biofuels and Chemicals With Ionic Liquids*. Dordrecht: Springer.

Fauzi, A. H. M., and Amin, N. A. S. (2012). An overview of ionic liquids as solvents in biodiesel synthesis. *Renew. Sustain. Energy Rev.* 16, 5770–5786. doi: 10.1016/j.rser.2012.06.022

Feng, Y., Li, L., Wang, X., Yang, J., and Qiu, T. (2017). Stable poly (ionic liquid) with unique crosslinked microsphere structure as efficient catalyst for transesterification of soapberry oil to biodiesel. *Energy Convers. Manage.* 153, 649–658. doi: 10.1016/j.enconman.2017.10.018

Fu, J., Detsi, E., and De Hosson, J. T. M. (2018). Recent advances in nanoporous materials for renewable energy resources conversion into fuels. *Surf. Coat. Technol.* 347, 320–336. doi: 10.1016/j.surfcoat.2018.05.001

Fujie, K., and Kitagawa, H. (2016). Ionic liquid transported into metal–organic frameworks. *Coordinat. Chem. Rev.* 307, 382–390. doi: 10.1016/j.ccr.2015.09.003

Gangu, K. K., Maddila, S., Makkamala, S. B., and Jonnalagadda, S. B. (2016). A review on contemporary Metal–Organic Framework materials. *Inorgan. Chim. Acta* 446, 61–74. doi: 10.1016/j.ica.2016.02.062

Gebremariam, S. N., and Marchetti, J. M. (2018). Economics of biodiesel production: review. *Energy Convers. Manage.* 168, 74–84. doi: 10.1016/j.enconman.2018.05.002

Ghiaci, M., Aghabarari, B., Habibollahi, S., and Gil, A. (2011). Highly efficient Bronsted acidic ionic liquid-based catalysts for biodiesel synthesis from vegetable oils. *Bioresource Technol.* 102, 1200–1204. doi: 10.1016/j.biortech.2010.09.095

Gholami, A., Hajinezhad, A., Pourfayaz, F., and Ahmadi, M. H. (2018). The effect of hydrodynamic and ultrasonic cavitation on biodiesel production: an exergy analysis approach. *Energy* 160, 478–489. doi: 10.1016/j.energy.2018.07.008

Gholami, A., Pourfayaz, F., Hajinezhad, A., and Mohadesi, M. (2019). Biodiesel production from Norouzak (*Salvia leriifolia*) oil using choline hydroxide catalyst in a microchannel reactor. *Renew. Energy* 136, 993–1001. doi: 10.1016/j.renene.2019.01.057

Granados, M. L., Poves, M. D. Z., Alonso, D. M., Mariscal, R., Galisteo, F. C., Moreno-Tost, R., et al. (2007). Biodiesel from sunflower oil by using activated calcium oxide. *Appl. Catal. B Environ.* 73, 317–326. doi: 10.1016/j.apcatb.2006.12.017

Han, M., Gu, Z., Chen, C., Wu, Z., Que, Y., Wang, Q., et al. (2016). Efficient confinement of ionic liquids in MIL-100(Fe) frameworks by the "impregnation-reaction-encapsulation" strategy for biodiesel production. *RSC Adv.* 6, 37110–37117. doi: 10.1039/C6RA00579A

Han, M., Li, Y., Gu, Z., Shi, H., Chen, C., Wang, Q., et al. (2018). Immobilization of thiol-functionalized ionic liquids onto the surface of MIL-101(Cr) frameworks by SCr coordination bond for biodiesel production. *Colloids Surf. A Physicochem. Eng. Aspects* 553, 593–600. doi: 10.1016/j.colsurfa.2018.05.085

Han, X. X., He, Y. F., Hung, C. T., Liu, L. L., Huang, S. J., and Liu, S. B. (2013). Efficient and reusable polyoxometalate-based sulfonated ionic liquid catalysts for palmitic acid esterification to biodiesel. *Chem. Eng. Sci.* 104, 64–72. doi: 10.1016/j.ces.2013.08.059

Hasheminejad, M., Tabatabaei, M., Mansourpanah, Y., Khatami far, M., and Javani, A. (2011). Upstream and downstream strategies to economize biodiesel production. *Bioresource Technol.* 102, 461–468. doi: 10.1016/j.biortech.2010.09.094

Hu, H., Xin, J. H., Hu, H., Wang, X., and Kong, Y. (2015). Metal-free graphene-based catalyst—Insight into the catalytic activity: a short review. *Appl. Catal. A General* 492, 1–9. doi: 10.1016/j.apcata.2014.11.041

Hu, M., Yao, Z., and Wang, X. (2017). Graphene-based nanomaterials for catalysis. *Indus. Eng. Chem. Res.* 56, 3477–3502. doi: 10.1021/acs.iecr.6b05048

International Energy Agency (2019). *Key World Energy Statistics*. Paris.

Jiang, B., Wang, Y., Zhang, L., Sun, Y., Yang, H., Wang, B., et al. (2017). Biodiesel production via transesterification of soybean oil catalyzed by superhydrophobic porous poly(ionic liquid) solid base. *Energy Fuels* 31, 5203–5214. doi: 10.1021/acs.energyfuels.7b00443

Karimi, B., and Vafaeezadeh, M. (2012). SBA-15-functionalized sulfonic acid confined acidic ionic liquid: a powerful and water-tolerant catalyst for solvent-free esterifications. *Chem. Commun.* 48, 3327–3329. doi: 10.1039/c2cc17702a

Khan, S. A., Rashmi, Hussain, M. Z., Prasad, S., and Banerjee, U. C. (2009). Prospects of biodiesel production from microalgae in India. *Renew. Sustain. Energy Rev.* 13, 2361–2372. doi: 10.1016/j.rser.2009.04.005

Kumar, D., Kumar, G., and Singh, P. C. P. (2010). Fast, easy ethanolysis of coconut oil for biodiesel production assisted by ultrasonication. *Ultrasonics Sonochem.* 17, 555–559. doi: 10.1016/j.ultsonch.2009.10.018

Lee, S. L., Wong, Y. C., Tan, Y. P., and Yew, S. Y. (2015). Transesterification of palm oil to biodiesel by using waste obtuse horn shell-derived CaO catalyst. *Energy Convers. Manage.* 93, 282–288. doi: 10.1016/j.enconman.2014.12.067

Li, M., Zhang, W., Zhou, S., and Zhao, Y. (2020). Preparation of poly(vinylalcohol)/palygorskite-poly(ionic liquids) hybrid catalytic

membranes to facilitate esterification. *Separat. Purif. Technol.* 230:115746. doi: 10.1016/j.seppur.2019.115746

Liang, X. (2013a). Novel acidic ionic liquid polymer for biodiesel synthesis from waste oils. *Appl. Catal. A General* 455, 206–210. doi: 10.1016/j.apcata.2013.01.036

Liang, X. (2013b). Novel efficient procedure for biodiesel synthesis from waste oils using solid acidic ionic liquid polymer as the catalyst. *Indus. Eng. Chem. Res.* 52, 6894–6900. doi: 10.1021/ie303564b

Liang, X. (2014). Novel ionic liquid supported on a magnetic core and its catalytic activities. *Indus. Eng. Chem. Res.* 53, 17325–17332. doi: 10.1021/ie502681w

Liu, C. Z., Wang, F., Stiles, A. R., and Guo, C. (2012). Ionic liquids for biofuel production: opportunities and challenges. *Appl. Energy* 92, 406–414. doi: 10.1016/j.apenergy.2011.11.031

Liu, F., Kong, W., Wang, L., Yi, X., Noshadi, I., Zheng, A., et al. (2015). Efficient biomass transformations catalyzed by graphene-like nanoporous carbons functionalized with strong acid ionic liquids and sulfonic groups. *Green Chem.* 17, 480–489. doi: 10.1039/C4GC01052C

Liu, F., Wang, L., Sun, Q., Zhu, L., Meng, X., and Xiao, F. S. (2012). Transesterification catalyzed by ionic liquids on superhydrophobic mesoporous polymers: heterogeneous catalysts that are faster than homogeneous catalysts. *J. Am. Chem. Soc.* 134, 16948–16950. doi: 10.1021/ja307455w

Luo, H., Fan, W., Li, Y., and Nan, G. (2013). Biodiesel production using alkaline ionic liquid and adopted as lubricity additive for low-sulfur diesel fuel. *Bioresource Technol.* 140, 337–341. doi: 10.1016/j.biortech.2012.11.112

Mansir, N., Teo, S. H., Rashid, U., Saiman, M. I., Tan, Y. P., Alsultan, G. A., et al. (2018). Modified waste egg shell derived bifunctional catalyst for biodiesel production from high FFA waste cooking oil. A review. *Renew. Sustain. Energy Rev.* 82, 3645–3655. doi: 10.1016/j.rser.2017.10.098

McKendry, P. (2002). Energy production from biomass (part 1): overview of biomass. *Bioresour. Technol.* 83, 37–46. doi: 10.1016/S0960-8524(01)00118-3

Mekhilef, S., Siga, S., and Saidur, R. (2011). A review on palm oil biodiesel as a source of renewable fuels. *Renew. Sustain. Energy Rev.* 15, 1937–1949. doi: 10.1016/j.rser.2010.12.012

Montalban, M. G., Villora, G., and Licence, P. (2018). Ecotoxicity assessment of dicationic versus monocationic ionic liquids as a more environmentally friendly alternative. *Ecotoxicol. Environ. Safety* 150, 129–135. doi: 10.1016/j.ecoenv.2017.11.073

Montgomery, D. C. (2013). *Design and Analysis of Experiments, 8th Edn*. Hoboken, NJ: John Wiley & Sons, Inc.

Monyem, A., and Van Gerpen, J. H. (2001). The effect of biodiesel oxidation on engine performance and emissions. *Biomass Bioenergy* 20, 317–325. doi: 10.1016/S0961-9534(00)00095-7

Muhammad, N., Elsheikh, Y. A., Abdul Mutalib, M. I., Bazmi, A. A., Khan, R. A., Khan, H., et al. (2015). An overview of the role of ionic liquids in biodiesel reactions. *J. Indus. Eng. Chem.* 21, 1–10. doi: 10.1016/j.jiec.2014.01.046

Nabi, M. N., Akhter, M. S., and Shahadat, M. M. Z. (2006). Improvement of engine emissions with conventional diesel fuel and diesel-biodiesel blends. *Bioresour. Technol.* 97, 372–378. doi: 10.1016/j.biortech.2005.03.013

Nagarajan, S., Chou, S. K., Cao, S., Wu, C., and Zhou, Z. (2013). An updated comprehensive techno-economic analysis of algae biodiesel. *Bioresource Technol.* 145, 150–156. doi: 10.1016/j.biortech.2012.11.108

Noshadi, I., Kanjilal, B., Du, S., Bollas, G. M., Suib, S. L., Provatas, A., et al. (2014). Catalyzed production of biodiesel and bio-chemicals from brown grease using ionic liquid functionalized ordered mesoporous polymer. *Appl. Energy* 129, 112–122. doi: 10.1016/j.apenergy.2014.04.090

Novoselov, K. S., Geim, A. K., Morozov, S. V., Jiang, D., Zhang, Y., Dubonos, S. V., et al. (2004). Electric field effect in atomically thin carbon films. *Science* 306, 666–669. doi: 10.1126/science.1102896

OECD/FA (2018). *OECD-FAO Agricultural Outlook 2018-2027*. Paris; Rome: OECD Publishing; FAO.

Olkiewicz, M., Torres, C. M., Jimenez, L., Font, J., and Bengoa, C. (2016). Scale-up and economic analysis of biodiesel production from municipal primary sewage sludge. *Bioresource Technol.* 214, 122–131. doi: 10.1016/j.biortech.2016.04.098

Osada, I., de Vries, H., Scrosati, B., and Passerini, S. (2016). Ionic-liquid-based polymer electrolytes for battery applications. *Angew. Chem.* 55, 500–513. doi: 10.1002/anie.201504971

Pan, H., Li, H., Liu, X. F., Zhang, H., Yang, K. L., Huang, S., et al. (2016). Mesoporous polymeric solid acid as efficient catalyst for (trans)esterification of crude Jatropha curcas oil. *Fuel Process. Technol.* 150, 50–57. doi: 10.1016/j.fuproc.2016.04.035

Pan, H., Li, H., Zhang, H., Wang, A., and Yang, S. (2019). Acidic ionic liquid-functionalized mesoporous melamine-formaldehyde polymer as heterogeneous catalyst for biodiesel production. *Fuel* 239, 886–895. doi: 10.1016/j.fuel.2018.11.093

Pandey, S. (2006). Analytical applications of room-temperature ionic liquids: a review of recent efforts. *Anal. Chim. Acta* 556, 38–45. doi: 10.1016/j.aca.2005.06.038

Panwar, N. L., Kaushik, S. C., and Kothari, S. (2011). Role of renewable energy sources in environmental protection: a review. *Renew. Sustain. Energy Rev.* 15, 1513–1524. doi: 10.1016/j.rser.2010.11.037

Pei, B., Xiang, X., Liu, T., Li, D., Zhao, C., Qiu, R., et al. (2019). Preparation of chloromethylated pitch–based hyper–crosslinked polymers and an immobilized acidic ionic liquid as a catalyst for the synthesis of biodiesel. *Catalysts* 9:963. doi: 10.3390/catal9110963

Pirez, C., Caderon, J. M., Dacquin, J. P., Lee, A. F., and Wilson, K. (2012). Tunable KIT-6 mesoporous sulfonic acid catalysts for fatty acid esterification. *ACS Catal.* 2, 1607–1614. doi: 10.1021/cs300161a

Qian, W., Texter, J., and Yan, F. (2017). Frontiers in poly(ionic liquid)s: syntheses and applications. *Chem. Soc. Rev.* 46, 1124–1159. doi: 10.1039/C6CS00620E

Riisager, A., Fehrmann, R., Haumann, M., and Wasserscheid, P. (2006a). Supported ionic liquid phase (SILP) catalysis: an innovative concept for homogeneous catalysis in continuous fixed-bed reactors. *Eur. J. Inorganic Chem.* 4, 695–706. doi: 10.1002/ejic.200500872

Riisager, A., Fehrmann, R., Haumann, M., and Wasserscheid, P. (2006b). Supported ionic liquids: versatile reaction and separation media. *Topics Catal.* 40, 91–102. doi: 10.1007/s11244-006-0111-9

Rouquerol, J., Avnir, D., Fairbridge, C. W., Everett, D. H., Haynes, J. M., Pernicone, N., et al. (1994). Recommendations for the characterization of porous solids. *Pure Appl. Chem.* 66, 1739–1758. doi: 10.1351/pac199466081739

Safaei, M., Foroughi, M. M., Ebrahimpour, J., Jahani, S., Omidi, A., and Khatami, M. (2019). A review on metal-organic frameworks: synthesis and applications. *TrAC Trends Anal. Chem.* 118, 401–425. doi: 10.1016/j.trac.2019.06.007

Sasidharan, M., Kiyozumi, Y., Mal, N. K., Paul, M., Rajamohanan, P. R., and Bhaumik, A. (2009). Incorporation of tin in different types of pores in SBA-15: Synthesis, characterization and catalytic activity. *Microporous Mesoporous Mater.* 126, 234–244. doi: 10.1016/j.micromeso.2009.05.038

Selvam, T., Machoke, A., and Schwieger, W. (2012). Supported ionic liquids on non-porous and porous inorganic materials-a topical review. *Appl. Catal. A General* 445–446, 92–101. doi: 10.1016/j.apcata.2012.08.007

Sharma, S., Saxena, V., Baranwal, A., Chandra, P., and Pandey, L. M. (2018). Engineered nanoporous materials mediated heterogeneous catalysts and their implications in biodiesel production. *Mater. Sci. Energy Technol.* 1, 11–21. doi: 10.1016/j.mset.2018.05.002

Sirisomboonchai, S., Abuduwayiti, M., Guan, G., Samart, C., Abliz, S., Hao, X., et al. (2015). Biodiesel production from waste cooking oil using calcined scallop shell as catalyst. *Energy Convers. Manage.* 95, 242–247. doi: 10.1016/j.enconman.2015.02.044

Su, C. H. (2013). Recoverable and reusable hydrochloric acid used as a homogeneous catalyst for biodiesel production. *Appl. Energy* 104, 503–509. doi: 10.1016/j.apenergy.2012.11.026

Sun, Q., Dai, Z., Meng, X., and Xiao, F. S. (2015). Porous polymer catalysts with hierarchical structures. *Chem. Soc. Rev.* 44, 6018–6034. doi: 10.1039/C5CS00198F

Tabatabaei, M., Aghbashlo, M., Dehghani, M., Panahi, H. K. S., Mollahosseini, A., Hosseini, M., et al. (2019). Reactor technologies for biodiesel production and processing: a review. *Progress Energy Combust. Sci.* 74, 239–303. doi: 10.1016/j.pecs.2019.06.001

Takase, M., Zhang, M., Feng, W., Chen, Y., Zhao, T., Cobbina, S. J., et al. (2014). Application of zirconia modified with KOH as heterogeneous solid base catalyst to new non-edible oil for biodiesel. *Energy Convers. Manage.* 80, 117–125. doi: 10.1016/j.enconman.2014.01.034

Tang, J., Liu, J., Li, C., Li, Y., Tade, M. O., Dai, S., et al. (2015). Synthesis of nitrogen-doped mesoporous carbon spheres with extra-large pores through

assembly of diblock copolymer micelles. *Angew. Chem. Int. Edn.* 54, 588–593. doi: 10.1002/anie.201407629

Tesfa, B., Mishra, R., Gu, F., and Powles, N. (2010). Prediction models for density and viscosity of biodiesel and their effects on fuel supply system in CI engines. *Renew. Energy* 35, 2752–2760. doi: 10.1016/j.renene.2010.04.026

Tran, N. N., Tisma, M., Budzaki, S., McMurchie, E. J., Gonzalez, O. M. M., Hessel, V., et al. (2018). Scale-up and economic analysis of biodiesel production from recycled grease trap waste, Applied *Energy*, 229, 142–150. doi: 10.1016/j.apenergy.2018.07.106

Troter, D. Z., Todorovic, Z. B., Dokic-Stojanovic, D. R., Stamenkovic, O. S., and Veljkovic, V. B. (2016). Application of ionic liquids and deep eutectic solvents in biodiesel production: a review. *Renew. Sustain. Energy Rev.* 61, 473–500. doi: 10.1016/j.rser.2016.04.011

Ullah, Z., Bustam, M. A., and Man, Z. (2015). Biodiesel production from waste cooking oil by acidic ionic liquid as a catalyst. *Renew. Energy* 77, 521–526. doi: 10.1016/j.renene.2014.12.040

Ullah, Z., Khan, A. S., Muhammad, N., Ullah, R., Alqahtani, A. S., Shah, S. N., et al. (2018). A review on ionic liquids as perspective catalysts in transesterification of different feedstock oil into biodiesel. *J. Mol. Liquids* 266, 673–686. doi: 10.1016/j.molliq.2018.06.024

Vallette, H., Pican, S., Boudou, C., Levillain, J., Plaquevent, J. C., and Gaumont, A. C. (2006). Palladium catalyzed C-P cross-coupling reactions in ionic liquids. *Tetrahedron Lett.* 47, 5191–5193. doi: 10.1016/j.tetlet.2006.05.100

Valtchev, V., Mintova, S., and Tsapatsis, M. (2009). *Ordered Porous Solids: Recent Advances and Prospects, 1st Edn*. Oxford: Elsevier.

Van Gerpen, J. (2005). Biodiesel processing and production. *Fuel Process. Technol.* 86, 1097–1107. doi: 10.1016/j.fuproc.2004.11.005

Ventura, S. P. M., e Silva, F. A., Quental, M. V., Mondal, D., Freire, M. G., and Coutinho, J. A. P. (2017). Ionic-liquid-mediated extraction and separation processes for bioactive compounds: past, present, and future trends. *Chem. Rev.* 117, 6984–7052. doi: 10.1021/acs.chemrev.6b00550

Wan, H., Chen, C., Wu, Z., Que, Y., Feng, Y., Wang, W., et al. (2015b). Encapsulation of heteropolyanion-based ionic liquid within the metal–organic framework MIL-100(Fe) for biodiesel production. *ChemCatChem* 7, 441–449. doi: 10.1002/cctc.201402800

Wan, H., Wu, Z., Chen, W., Guan, G., Cai, Y., Chen, C., et al. (2015a). Heterogenization of ionic liquid based on mesoporous material as magnetically recyclable catalyst for biodiesel production. *J. Mol. Catal. A Chem.* 398, 127–132. doi: 10.1016/j.molcata.2014.12.002

Wang, H., Maiyalagan, T., and Wang, X. (2012). Review on recent Progress in nitrogen-doped graphene: synthesis, characterization, and its potential applications. *ACS Catal.* 2, 781–794. doi: 10.1021/cs200652y

Wang, Y., Wang, D., Tan, M., Jiang, B., Zheng, J., Tsubaki, N., et al. (2015). Monodispersed hollow SO₃H-functionalized carbon/silica as efficient solid acid catalyst for esterification of oleic acid. *ACS Appl. Mater. Interfaces* 7, 26767–26775. doi: 10.1021/acsami.5b08797

Wang, Y., Zhao, D., Wang, L., Wang, X., Li, L., Xing, Z., et al. (2018). Immobilized phosphotungstic acid based ionic liquid: application for heterogeneous esterification of palmitic acid. *Fuel* 216, 364–370. doi: 10.1016/j.fuel.2017.11.153

Watanabe, M., Thomas, M. L., Zhang, S., Ueno, K., Yasuda, T., and Dokko, K. (2017). Application of ionic liquids to energy storage and conversion materials and devices. *Chem. Rev.* 117, 7190–7239. doi: 10.1021/acs.chemrev.6b00504

Wu, Z., Chen, C., Guo, Q., Li, B., Que, Y., Wang, L., et al. (2016a). Novel approach for preparation of poly (ionic liquid) catalyst with macroporous structure for biodiesel production. *Fuel* 184, 128–135. doi: 10.1016/j.fuel.2016.07.004

Wu, Z., Chen, C., Wan, H., Wang, L., Li, Z., Li, B., et al. (2016b). Fabrication of magnetic NH2-MIL-88B (Fe) confined Brønsted ionic liquid as an efficient catalyst in biodiesel synthesis. *Energy Fuels* 30, 10739–10746. doi: 10.1021/acs.energyfuels.6b01212

Wu, Z., Chen, C., Wang, L., Wan, H., and Guan, G. (2016c). Magnetic material grafted poly(phosphotungstate-based acidic ionic liquid) as efficient and recyclable catalyst for esterification of oleic acid. *Indus. Eng. Chem. Res.* 55, 1833–1842. doi: 10.1021/acs.iecr.5b02906

Xie, W., Hu, L., and Yang, X. (2015a). Basic ionic liquid supported on mesoporous SBA-15 silica as an efficient heterogeneous catalyst for biodiesel production. *Indus. Eng. Chem. Res.* 54, 1505–1512. doi: 10.1021/ie5045007

Xie, W., and Wan, F. (2018). Basic ionic liquid functionalized magnetically responsive Fe$_3$O$_4$@HKUST-1 composites used for biodiesel production. *Fuel* 220, 248–256. doi: 10.1016/j.fuel.2018.02.014

Xie, W., and Wan, F. (2019). Immobilization of polyoxometalate-based sulfonated ionic liquids on UiO-66-2COOH metal-organic frameworks for biodiesel production via one-pot transesterification-esterification of acidic vegetable oils. *Chem. Eng. J.* 365, 40–50. doi: 10.1016/j.cej.2019.02.016

Xie, W., and Wang, H. (2020). Immobilized polymeric sulfonated ionic liquid on core-shell structure Fe$_3$O$_4$/SiO$_2$ composites: a magnetically recyclable catalyst for simultaneous transesterification and esterifications of low-cost oils to biodiesel. *Renew. Energy* 145, 1709–1719. doi: 10.1016/j.renene.2019.07.092

Xie, W., Yang, X., and Fan, M. (2015b). Novel solid base catalyst for biodiesel production: mesoporous SBA-15 silica immobilized with 1,3-dicyclohexyl-2-octylguanidine. *Renew. Energy* 80, 230–237. doi: 10.1016/j.renene.2015.02.014

Yaakob, Z., Narayanan, B. N., Padikkaparambil, S., Unni, K. S., and Akbar, P. M. (2014). A review on the oxidation stability of biodiesel. *Renew. Sustain. Energy Rev.* 35, 136–153. doi: 10.1016/j.rser.2014.03.055

Ye, C., Qi, Z., Cai, D., and Qiu, T. (2019). Design and synthesis of ionic liquid supported hierarchically porous Zr metal–organic framework as a novel Brønsted–Lewis acidic catalyst in biodiesel synthesis. *Indus. Eng. Chem. Res.* 58, 1123–1132. doi: 10.1021/acs.iecr.8b04107

Yuan, J., and Antonietti, M. (2011). Poly(ionic liquid)s: Polymers expanding classical property profiles. *Polymer* 52, 1469–1482. doi: 10.1016/j.polymer.2011.01.043

Yuan, S., Wang, M., Liu, J., and Guo, B. (2020). Recent advances of SBA-15-based composites as the heterogeneous catalysts in water decontamination: a mini-review. *J. Environ. Manage.* 254:109787. doi: 10.1016/j.jenvman.2019.109787

Yusuf, N. N. A. N., and Kamarudin, S. K. (2013). Techno-economic analysis of biodiesel production from Jatropha curcas via a supercritical methanol process. *Energy Convers. Manage.* 75, 710–717. doi: 10.1016/j.enconman.2013.08.017

Zhang, H., Li, H., Pan, H., Wang, A., Souzanchi, S., Xu, C., et al. (2018). Magnetically recyclable acidic polymeric ionic liquids decorated with hydrophobic regulators as highly efficient and stable catalysts for biodiesel production. *Appl. Energy* 223, 416–429. doi: 10.1016/j.apenergy.2018.04.061

Zhang, H., Li, H., Pan, H., Wang, A., Xu, C., and Yang, S. (2017). Magnetically recyclable basic polymeric ionic liquids for efficient transesterification of *Firmiana platanifolia*, L.f. oil into biodiesel. *Energy Convers. Manage.* 153, 462–472. doi: 10.1016/j.enconman.2017.10.023

Zhang, L., Cui, Y., Zhang, C., Wang, L., Wan, H., and Guan, G. (2012). Biodiesel production by esterification of oleic acid over Bronsted acidic ionic liquid supported onto Fe-incorporated SBA-15. *Indus. Eng. Chem. Res.* 51, 16590–16596. doi: 10.1021/ie302419y

Zhang, W., Li, M., Wang, J., Zhao, Y., Zhou, S., and Xing, W. (2017). Heterogeneous poly(ionic liquids) catalyst on nanofiber-like palygorskite supports for biodiesel production. *Appl. Clay Sci.* 146, 167–175. doi: 10.1016/j.clay.2017.05.031

Zhang, Y., Jiao, Q., Zhen, B., Wu, Q., and Li, H. (2013). Transesterification of glycerol trioleate catalyzed by basic ionic liquids immobilized on magnetic nanoparticles. *Appl. Catal. A General* 453, 327–333. doi: 10.1016/j.apcata.2012.12.029

Zhen, B., Jiao, Q., Wu, Q., and Li, H. (2014). Catalytic performance of acidic ionic liquid-functionalized silica in biodiesel production. *J. Energy Chem.* 23, 97–104. doi: 10.1016/S2095-4956(14)60122-4

Zhen, B., Jiao, Q., Zhang, Y., Wu, Q., and Li, H. (2012). Acidic ionic liquid immobilized on magnetic mesoporous silica: preparation and catalytic performance in esterification. *Appl. Catal. A General* 445–446, 239–245. doi: 10.1016/j.apcata.2012.08.023

Zhou, X., Qiao, J., Yang, L., and Zhang, J. (2014). A review of graphene-based nanostructural materials for both catalyst supports and metal-free catalysts in PEM fuel cell oxygen reduction reactions. *Adv. Energy Mater.* 4:1301523. doi: 10.1002/aenm.201301523

Synergistic Treatment of Alkali Lignin via Fungal Coculture for Biofuel Production: Comparison of Physicochemical Properties and Adsorption of Enzymes Used As Catalysts

Ruhong Luo[1,2], Qiang Liao[1,2]*, Ao Xia[1,2]*, Zhichao Deng[1,2], Yun Huang[1,2], Xianqing Zhu[1,2] and Xun Zhu[1,2]

[1] Key Laboratory of Low-grade Energy Utilization Technologies and Systems, Chongqing University, Ministry of Education, Chongqing, China, [2] Institute of Engineering Thermophysics, Chongqing University, Chongqing, China

White-rot fungi is capable of producing extracellular enzymes that degrade lignin structure and facilitate biofuel production from lignocellulosic biomass wastes. However, fungal monocultures are constrained by low activities of the lignin-degrading enzyme system, leading to poor treatment efficiency and a long duration, which are not advantageous for large-scale applications. To improve enzyme production and enhance lignin degradation, a novel coculture system was proposed using the white-rot fungi *Phanerochaete chrysosporium* and *Irpex lacteus* CD2. The degradation efficiency of the alkali lignin by the fungal coculture was 26.4%, which was higher than that of the fungal monocultures. It was due to the production of lignin degrading enzymes was promoted in the liquid medium. Scanning electron microscopy, Fourier transform infrared, thermogravimetric and mercury porosimeter analyses results revealed that the alkali lignin treated with the fungal coculture had the largest porosity, and the degree of destruction of the alkali lignin structure by the fungal coculture was higher than that of the fungal monocultures. Meanwhile, the nonproductive adsorption of enzymes on alkali lignin was significantly reduced by 61.0% when the biomass was treated with the fungal coculture. As a result, the nonproductive adsorption was remarkably reduced, while it significantly improved the cellulase catalysis efficiency. These results demonstrated the synergistic effects of the fungal coculture for biomass treatment and provided a new approach for increasing lignin degradation while improving enzymatic catalysis and biofuel production through fungal coculture.

Keywords: biomass hydrolysis, white-rot fungi, coculture, lignin, enzyme absorption

---

INTRODUCTION

Lignocellulosic biomass from agricultural residues is an abundant resource in China, with an annual productivity of 980 million tons, which is equal to approximately 490 million tons of coal (Isroi et al., 2011). However, a mass of lignocellulosic biomass is incinerated in the field, it not only pollutes the environment but also wastes many resources. Converting lignocellulosic biomass to biofuels, such as bioethanol, biohydrogen and biomethane, has significant energy savings and emission reduction benefits (Xia et al., 2016).

Lignocellulose is mainly composed of three components: lignin, cellulose and hemicellulose. Cellulose and hemicellulose are polysaccharide structures that can be directly hydrolyzed by enzymes into available reducing sugars. However, lignin is a complex cross-linked phenolic polymer, which is composed of guaiacyl propane units (G), syringyl propane units (S) and p-hydroxyphenyl propane units (H) at different ratios (Christopher et al., 2014). The presence of lignin makes it difficult to directly utilize the polysaccharides in lignocellulosic biomass. The removal of lignin improves the accessibility of the polysaccharides, resulting in high biomass conversion efficiency and an economically feasible production process. Without an appropriate pretreatment method, only 20% of the theoretical maximum yield can be obtained by enzymatic hydrolysis (Suksong et al., 2020).

Biological pretreatment methods have attracted interest because of their potential advantages over other pretreatment methods, such as lower energy consumption, no chemical reagents and greater substrate and reaction specificity (Sindhu et al., 2016). The most promising microorganisms are white-rot fungi (WRF), which is the only group known to be able to completely degrade lignin into CO_2 and H_2O at a normal temperature and pressure (Zhang et al., 2019). Several WRF, such as *Phanerochaete chrysosporium*, *Pleurotus ostreatus*, and *Irpex lacteus*, have been identified for their efficient degradation of lignin in a variety of lignocellulosic biomass materials (Isroi et al., 2011). The high lignin degradation ability of WRF is due to their unique extracellular lignin degrading enzymes (LDEs) system, such as lignin peroxidases (LiP), laccase (Lac), and manganese peroxidases (MnP) (Sharma et al., 2019). When reactive oxygen is used as an intermediary condition for lignin degradation, LDEs degrade lignin into a pool of heterogeneous aromatics, which are ultimately metabolized by the secreting organism or other microbes (Ren et al., 2016).

At present, most studies have improved the selective degradation efficiency of lignin by optimizing monoculture conditions or by screening natural strains. For example, Dong et al. (2013) introduced the characteristics and process of using three WRF to degrade sugarcane bagasse, and found that *P. chrysosporium* was the most effective lignin-degrading strain. Salvachúa et al. (2013) proved that *I. lacteus* has the ability to selectively and efficiently degrade lignin in wheat straw. By comparing the extracellular secretases of *I. lacteus* and *P. chrysosporium*, it was found while both have the ability to efficiently degrade lignin, the LDEs secreted by the two WRF are different. Zeng et al. (2013) detected the activity of Lac and MnP in stationary cultures of *I. lacteus*. In contrast, stationary cultures of a highly degradative strain of *P. chrysosporium* only exhibited activities

of LiP and MnP. However, the fungal monocultures produce few types of LDEs, resulting in poor effects and low efficiency in the lignin treatment process. As a result, the duration of the biological pretreatment is too long to be applied at a large scale.

In wood and many other microenvironments, fungi typically live and grow in close proximity to each other, and these fungi may display synergistic interactions (Yadav and Chandra, 2015). The fungal coculture could lead to higher enzyme production through synergistic interactions, and this result depends on the particular species in combination or the mode of interaction between species (Chen et al., 2019). In a coculture system, the evaluation of antagonistic effects of the selected fungal cocultures is important for producing LDEs (Tesfaw and Assefa, 2014). Experimental evidence have suggested that the competition for space and nutrients may result in the enhanced degradation of lignin and in elevated production of LDEs such as MnP and Lac (Dong et al., 2014; Wang et al., 2014; Li et al., 2019). Additionally, in the different WRF coculture systems, the LDEs that play a major role in the lignin degradation process are also different. Lac might play the central role in the lignin degradation process in one coculture system, while in others, MnP or LiP or even Lac-MnP or Lac-LiP-MnP might be responsible for such a process (Sun et al., 2011). In recent years, some researchers have obtained fungal cocultures that efficiently degrade lignin by screening WRF in natural environments (Mishra et al., 2017; Chen et al., 2019). *P. chrysosporium* and *I. lacteus* are two types of WRF with strong abilities to degrade lignin in nature. However, under standard culture conditions, the LDEs system secreted by *P. chrysosporium* and *I. lacteus* are different. The complementarity nature of the LDEs produced by different WRF and their impacts on the subsequent enzymatic hydrolysis process during fungal coculture have not yet been reported in the literatures.

The innovation of this study is to propose a new coculture system of *P. chrysosporium* and *I. lacteus* CD2, based on their complementarity LDEs, to treat alkali lignin as a model compound derived from lignocellulose biomass. The objectives of this study are to study the degradation efficiency of fungal coculture on alkali lignin, and to assess the effects of alkali lignin modification from fungi treatment on enzymatic hydrolysis and adsorption.

MATERIALS AND METHODS

Strains, Enzymes, and Chemicals

The fungus *P. chrysosporium* was obtained from the Guangdong Culture Collection Center (Guangdong, China). The fungus *I. lacteus* CD2 was obtained from the China General Microbiological Culture Collection Center (Beijing, China). The strains stored at 4°C were inoculated in fresh Potato dextrose agar (PDA) slant culture medium. The PDA slant culture medium was prepared as follows: peeled potato blocks were boiled for 20 min and filtered, then 2% (w/v) of glucose and 2% (w/v) of agar was added to the filtrate and its pH was regulated to 7.6. The culture medium was then steam-

sterilized at 121°C for 20 min using a high-pressure steam sterilizer. The inoculations were cultured for 7 days at 28°C. The spores of the two fungi were removed from the PDA slant culture medium and stored at 4°C until use.

The alkali lignin and all of the chemicals used in this work were purchased from Sigma-Aldrich and were of analytical reagent grade. The enzyme used in the experiment was a commercial complex enzyme called Cellic CTec2 (Novozymes, China) with an activity of 70 filter paper unit (FPU)/ml. The FPU was measured by following the National Renewable Energy Laboratory standard biomass analytical procedures (Lindedam et al., 2014).

Antagonistic Experiment

The inoculation ring was dipped into the spores, and the two fungi were inoculated on the PDA solid plate medium. The inverted plates were cultured at 28°C in a constant temperature incubator, and the growth of fungi was observed every day (Schoneberg et al., 2015).

Degradation of Alkali Lignin by Fungal Monoculture and Coculture

In Erlenmeyer flasks, 0.2 g of alkali lignin and 40 ml of the liquid medium were steam-sterilized at 121°C for 20 min. The substrates were inoculated with spores to achieve an initial content of 10^6 spores/ml. The treatment experiment was conducted at 180 rpm and 28°C for 21 days in a shaker bath. Samples were taken by different time intervals (samples were taken every day in the first week, and every other day from the second week to the third week) and were diluted five times, centrifuged at 8,000 rpm for 10 min, and filtered, then the absorbance of the alkali lignin was measured at optical density 280 nm (Hao et al., 2015). The degradation rate was calculated by weight. All of the experiments and analyses were conducted in triplicate.

The fungi degradation medium components were glucose (2 g/L), MgSO$_4$·7H$_2$O (0.1 g/L), KH$_2$PO$_4$ (1 g/L), ammonium tartrate (0.4 g/L), Tween 80 (0.5 ml/L), CaCl$_2$ (0.1 g/L), veratryl alcohol (0.57 ml/L), and 1 ml of trace element solution per liter of medium solution. The trace element solution contained MnSO$_4$ (0.5 g/L), Al(K(SO$_4$)$_2$)·12H$_2$O (0.02 g/L), FeSO$_4$·7H$_2$O (0.1 g/L), H$_3$BO$_3$ (0.01 g/L), CoCl$_2$·6H$_2$O (0.1 g/L), ZnSO$_4$·7H$_2$O (0.1 g/L), and CuSO$_4$·5H$_2$O (0.01 g/L) (Asina et al., 2016).

Lignin Degrading Enzymes Activity Assays

Lignin-degrading enzyme activities were assayed from the liquid cultures. The enzyme assays were conducted in a 3 ml reaction mixture at 25°C by using the extracellular medium of the fungal culture. The Lac activity was measured spectrophotometrically by the oxidation of ABTS [2,2′-azinobis-(3-ethylbenzthiazoline-6-sulphonate)] (Sigma Aldrich) (More et al., 2011). The reaction mixture contained 0.5 mM ABTS, 2.8 ml of 0.1 M sodium acetate (pH = 4.5), and 0.1 ml of the culture supernatant and was incubated for 5 min. The absorbance was read at 420 nm in a spectrophotometer with deionized water as the blank. One unit was defined as the amount of Lac that oxidized 1 μmol of ABTS substrate per min. The MnP activity was determined by the method of Wiberth (Wiberth et al., 2018). The 3 ml reaction mixture contained 50 mM sodium malonate (pH = 4.5), 2 mM

MnSO$_4$, 0.1 mM H$_2$O$_2$, and 0.5 ml of the enzyme solution. The reaction was initiated at 37°C, and the initial rate of Mn(III) malonate formation was determined using a spectrophotometer by following the initial increase in absorbance at 270 nm (ε = 11,590 M/cm). One unit of MnP activity was defined as the amount of MnP that catalyzed the formation of 1 μmol of Mn(III) per min. The activity of LiP was measured at 310 nm using veratryl alcohol as the substrate (Yang et al., 2013). The standard reaction mixture (3 ml) contained 0.2 mM veratryl alcohol, 0.15 mM H$_2$O$_2$ and the enzyme solution in 100 mM sodium tartrate buffer (pH = 3.0). One unit of LiP was defined as the amount of enzyme necessary to oxidize 1.0 mmol veratryl alcohol per min. One-way ANOVA analysis was performed to assess significant differences among groups.

Chemical Structure Analysis of Alkali Lignin

The Fourier transform infrared (FTIR) spectra was used to demonstrated the chemical group changes before and after fungi treatment. FTIR scans were conducted at 400–4,000 cm^{-1}. Background scanning was performed for correction before data collection. Scanning electron microscope (SEM) was used to evaluate the microstructural changes in the alkali lignin before and after treatment. The porosity test was carried out by the mercury intrusion porosimetry method, and. The tests were performed at a pressure of up to 33,000 psia. The thermogravimetric (TG) properties of all the samples were obtained to thermal stability changes before and after treatment, and the element analysis was used to determine the content of C, H, N, O, and S in the samples. The alkali lignin samples were placed in the oven to dry at 105°C for 2–3 h to remove moisture from the samples before the TG analysis.

Enzymes Hydrolysis and Adsorption

To evaluate the effect of the alkali lignin treated by fungi on cellulose hydrolysis, the enzymatic hydrolysis of Avicel was conducted in a flask containing sodium citrate buffer (0.1 M, pH = 4.8) for 72 h at 50°C. Specifically, the solid substrate loading rate was 1% (w/w), and the mixture was stirred in a shaker bath at 160 rpm. The dose of the hydrolysis enzyme (SAE0020) was 50 FPU/g substrate. The hydrolysis efficiency of Avicel was evaluated by the yield of reducing sugar. The yield of reducing sugar was determined by the 3,5-dinitrosalicylic acid method (Lee et al., 2020).

Studying the isothermal adsorption line of enzymes on alkali lignin before and after fungi treatment, the concentration of the different enzyme proteins was 0.1–2.0 mg/ml. Alkali lignin and the enzyme were incubated in a flask that contained 0.1 M sodium citrate buffer (pH = 4.8) at 50°C with shaking (160 rpm) for 3 h to reach equilibrium (Deng et al., 2019). The amount of protein adsorbed on the alkali lignin was calculated by weight. The free protein concentration was determined using the Bio-Rad protein assay, which is a Bradford-based colorimetric method, and bovine serum albumin (Sigma-Aldrich) was used as a standard (Ku et al., 2013).

According to published literature (Yang and Fang, 2015), the adsorption of enzymes on the alkali lignin can be described by the following Langmuir equation (Eq. 1):
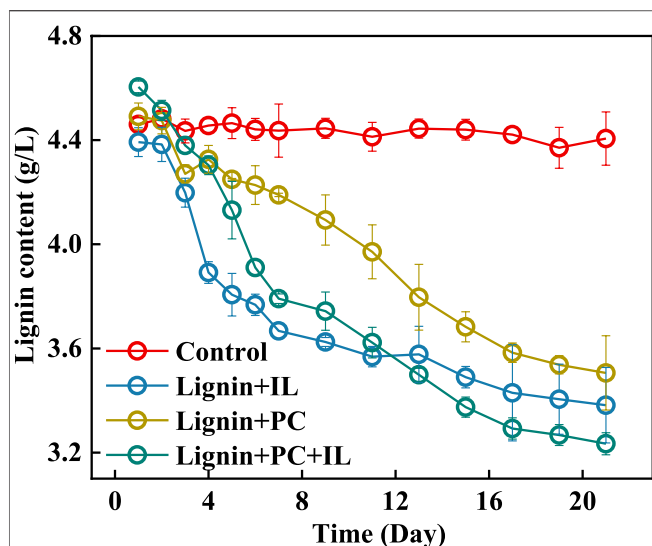
FIGURE 1 | Degradation of alkali lignin by fungal monocultures and coculture.

$$E_{ads} = \frac{[E_{max}] \cdot K \cdot [E_{free}]}{1 + K \cdot [E_{free}]} \tag{1}$$

where E_{ads} is the amount of enzyme adsorbed on the lignin (mg/g lignin), E_{free} is the free enzyme concentration (mg/ml) in the suspension, E_{max} is the maximum enzyme adsorption capacity of lignin (mg/g lignin), and K is the Langmuir adsorption constant (ml/mg enzyme).

Machine and Equipment

The culture medium was sterilized by using a high-pressure steam sterilizer (YXQ-LS, BOXUN, China). All the treatments were conducted in shaker bath (ZWYR-2102, ZHICHENG, China). The FTIR spectra were obtained using an FTIR Microscope (Nicolet iN10, Thermo Scientific, United States) equipped with a deuterated triglycine sulfate detector. A SEM (VEGA 3 LMH, TESCAN, Czech Republic) was used to obtain the surface morphology of the alkali lignin at a voltage of 10 kV. The porosity was performed using the Micromertics Instruments Corporation AutoPore IV 9500. The thermal stability properties were analyzed via a TG analyzer (STA409PC, NETZSCH, Germany) at a constant heating rate of 10°C/min. The atmosphere was N$_2$, and the flow rate was 100 ml/min. The contents of C, H, N, O and S were determined by an element analyzer (FLASH 2000, Thermo Scientific, America).

RESULTS AND DISCUSSION

Antagonistic Experiment

To analyze whether *P. chrysosporium* and *I. lacteus* are suited to simultaneous culture, the antagonistic characteristics between the fungi was tested. **Supplementary Figure 1** displays the coculture of the two fungi in a PDA solid plate medium on the seventh day.
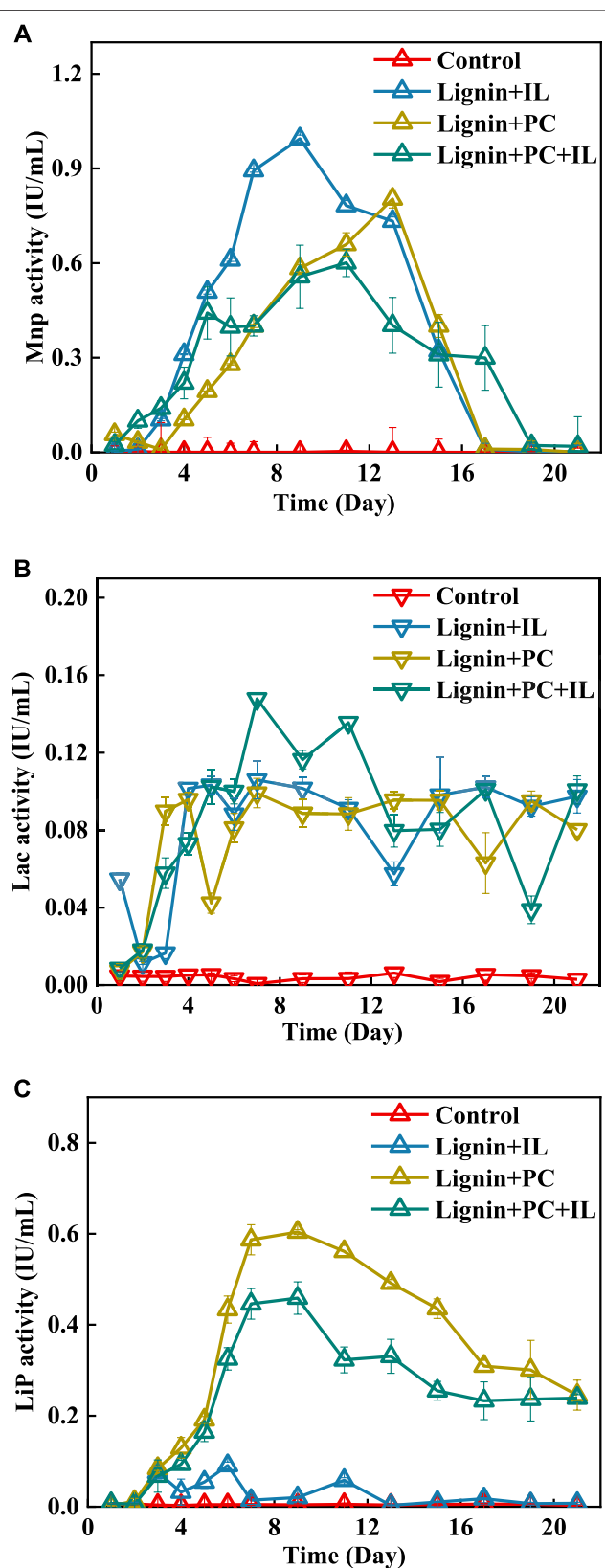
FIGURE 2 | LDEs during alkali lignin degradation for **(A)** MnP, **(B)** Lac, and **(C)** LiP.

P. chrysosporium were the white spherical particles on the PDA solid plate medium, and *I. lacteus* were the white hyphae. The two types of WRF grew evenly on the surface of the PDA solid plate medium, and there was no blank in the middle of the plate (Yao et al., 2016). The results implied the two fungi are suited to synchronous coculture, and it is predicted that this coculture of fungi could synergistically degrade alkali lignin.

Fungal Degradation Characteristics of Alkali Lignin

Figure 1 shows the degradation of alkali lignin by fungi cultivated under different methods. The degradation effects of different fungi on lignin showed significant differences compared with control ($p < 0.01$). During the first 3 days, the fungi initially used the glucose in the medium as the main source of carbon for growth, so the concentration of alkali lignin changed only slightly. After that, the fungal growth reached the logarithmic phase, and the fungi began to use the alkali lignin in the medium as the main carbon source, resulting in a gradual decrease in the concentration of alkali lignin.

The extracellular lignolytic enzymes from the fungi synergistically cleave the C_α–C_β bonds and oxidize C_α, and the major route of lignin degradation is the cleavage of the C_α–C_β bonds by LiP, MnP, and Lac (Harmanpreet et al., 2017). **Figure 2** shows the LDEs activity during the fungal degradation of alkali lignin. The activity of Lac and Lip showed significant differences compared with control ($p < 0.05$). Because *P. chrysosporium* and *I. lacteus* could not fully secrete these three lignin-degrading enzymes (Arora and Sharma, 2010), the Lac activity during alkali lignin degradation was lower than the LiP and MnP activities. In the initial stage of alkali lignin degradation, the MnP activity produced by the monoculture of *I. lacteus* was much higher than that produced by the other two fungal culture methods, but *I. lacteus* produced almost no LiP enzyme. It was speculated that the degradation of alkali lignin was dominated by MnP. MnP was considered to be the main enzyme involved in the partial mineralization of a broad spectrum of aromatic substances (Parikh et al., 2014).

The MnP production over time for the fungal coculture and monocultures is summarized in **Figure 2A**. Because the control group did not have LDEs, the degradation efficiency of the alkali lignin was unchanged. For the monoculture of *I. lacteus*, the time for the biomass to reach the logarithmic phase was shorter than that of the fungal coculture. The rapid increase in the demand for a carbon source for *I. lacteus* has resulted in the production of more LDEs. The MnP activity produced by *I. lacteus* was the highest and showed a stable increased in expression during the first week. The MnP activity for *I. lacteus* reached 0.99 IU/ml on the seventh day, which was 41.3 and 44% higher than that of *P. chrysosporium* and the fungal coculture, respectively. Therefore, the degradation efficiency of alkali lignin treated by *I. lacteus* was the highest, reaching 16.6% in the first week, compared with *P. chrysosporium* (6.7%) and the fungal coculture (15.6%). *P. chrysosporium* produced MnP and very little Lac during the treatment, and the MnP activity was lower than that of *I. lacteus* and the fungal coculture, so *P. chrysosporium* had the lowest alkali lignin degradation efficiency.
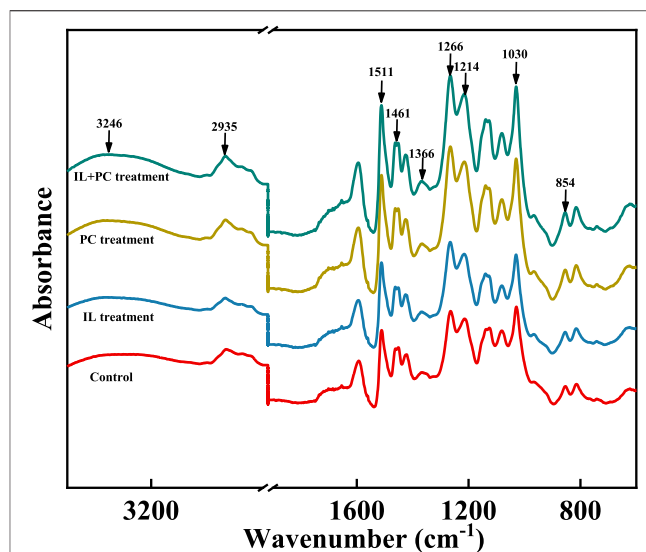
FIGURE 3 | FTIR spectra of alkali lignin samples before and after fungi treatment.

Limited by fungal biomass, the highest activity of MnP produced in the fungal coculture occurred later than that of *I. lacteus*. After the first week, the MnP activity produced by *I. lacteus* and *P. chrysosporium* decreased significantly, but that produced by the fungal coculture still increased. On the 17th day, the activity of MnP was almost absent in the fungal monocultures, whereas in the fungal coculture, the activity of MnP was still 0.3 IU/ml. In addition, the enzymes produced by the fungal coculture included not only MnP and Lac but also LiP produced by *P. chrysosporium*. Thus, a high MnP activity and the synergistic effects of three major LDEs resulted a higher degradation rate for the fungal coculture compared to the fungal monocultures during the last week. At the end of the experiment, the degradation efficiency of alkali lignin by the fungal coculture was the highest at 29.8%, compared with *P. chrysosporium* (21.9%) and *I. lacteus* (23.0%). As evaluated above, the coculture of *P. chrysosporium* and *I. lacteus* could effectively accelerate the degradation of alkali lignin and promoted the production of LDEs.

Chemical Structure of Alkali Lignin in Fungi Treatment
Fourier Transform Infrared Analysis

The FTIR spectra of the alkali lignin before and after the fungi treatments are shown in **Figure 3**, and the major bands are assigned in **Table 1** (Kobayashi et al., 2009). The alkali lignin treated by fungi has changed significantly in the fingerprint region (1,300–600 cm^{-1}), corresponding to the stretching vibrations of different groups in the lignin (Ying et al., 2018). This suggested that the overall structure of the alkali lignin had been destroyed after fungi treatment.

In the range of 3,200–3,400 cm^{-1}, the peaks of the autoclave-sterilized lignin appeared at 3,246 cm^{-1}, and the peaks of lignin after fungi treatment appeared at 3,362 cm^{-1} (*P. chrysosporium*),

TABLE 1 | Fourier transform infrared peak assignments in alkali lignin samples.

Wavenumber (cm^{-1})	Assignment
3,246	Stretching vibration of hydroxyl group in hydrogen bonds
2,935	C–H stretching vibration of CH$_2$, CH$_3$, and CH$_3$O groups
1,511	C=C stretching vibration peak in benzene ring
1,461	Asymmetric vibration of C–H in CH$_3$ and CH$_2$
1,365	In-plane deformation vibration of phenolic hydroxyl group and CH$_3$
1266,1241	C–O stretching in G-type lignin
1,030	C–O stretching in cellulose and hemicellulose
854	C–H out-of-plane deformation vibration of guaiacyl propane

3,370 cm^{-1} (*I. lacteus*), and 3,354 cm^{-1} (fungal coculture). This indicated that the degree of O–H association between the alkali lignin molecules was reduced and the molecular structure of the alkali lignin was ruptured during the treatment (Sun et al., 2016). The signal intensity of the alkali lignin at 2,935 cm^{-1} decreased, indicating that some of the guaiacyl and syringyl methoxy groups in the alkali lignin were broken during the fungi treatment. After fungi treatment, there was a decrease in the intensity of the stretching vibration peak (1,461 cm^{-1}) of the alkali lignin, which was derived from methylene, indicating that some macromolecular lignin was degraded (Sun et al., 2018). After fungi treatment, the peaks at 1,600 and 1,511 cm^{-1} increased, which represent the vibration of C=C on the benzene ring, indicating the depolymerization of macromolecular lignin (Liu et al., 2014). The fingerprint characteristic absorption peak of syringyl increased after fungi treatment, suggesting that syringyl lignin was further degraded and more syringyl units were released (Singh et al., 2015).

Scanning Electron Microscope and Porosity Analysis

Figure 4 shows the microstructure of the alkali lignin treated by the fungal monocultures and coculture. It can be observed that the shape of the autoclaved alkali lignin (**Figure 5A**) was irregular
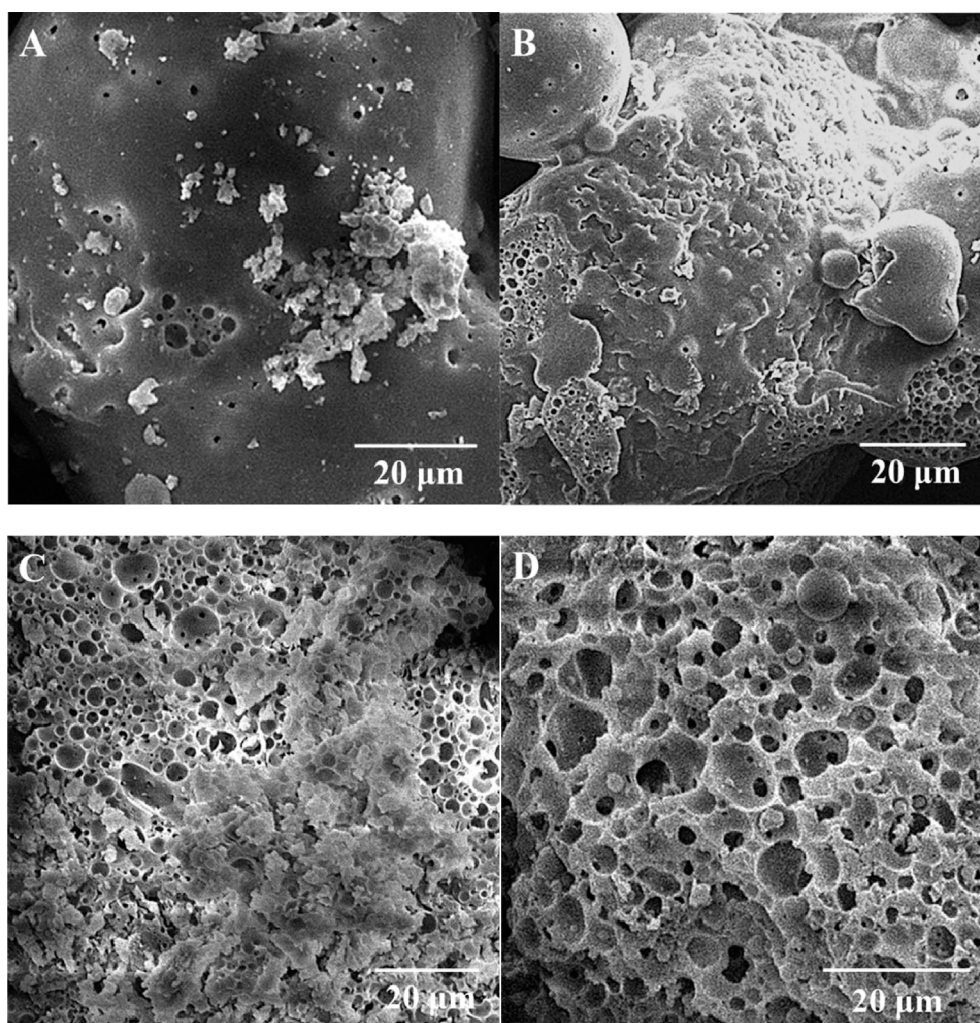
FIGURE 4 | Scanning electron microscopy images of **(A)** autoclaved alkali lignin, **(B)** *I. lacteus* treatment, **(C)** *P. chrysosporium* treatment, and **(D)** fungal coculture treatment.

FIGURE 5 | DTG and TG analyses of alkali lignin before and after fungi treatment.
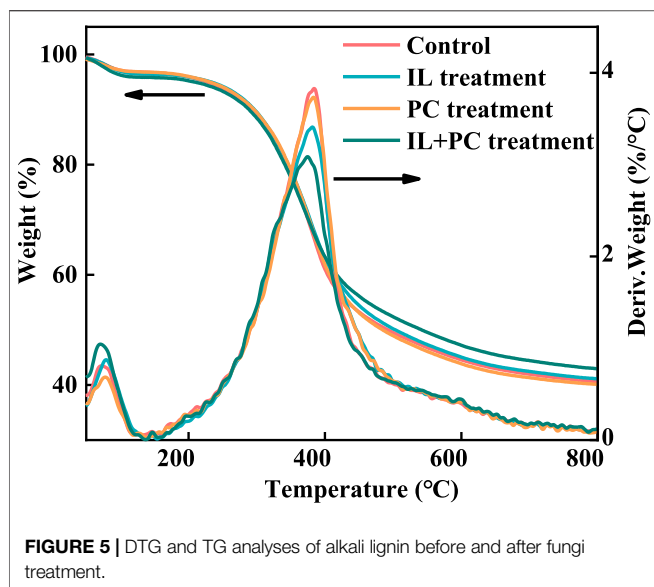
polygons and was composed of many irregular spherical particles. After fungi treatment, the surface gradually became rough and many pores were formed due to fungi degradation (**Figure 4B,C**). In addition, for the alkali lignin treated by the fungal coculture (**Figure 4D**), many micropores adhering to the surfaces of large pores could be found compared to alkali lignin treated by the fungal monocultures. The destruction of alkali lignin treated by the fungal coculture was greater than that by the fungal monocultures.

The porosity and pore diameter distribution of the alkali lignin are shown in **Table 2**. Megapores (>10,000 nm) increased 3.0% after the alkali lignin treated by the fungal coculture, but the macropores (2,500–10,000 nm) of the alkali lignin treated by the fungal monocultures increased 4.36 (*I. lacteus*) and 6.72% (*P. chrysosporium*). These results indicated that the damage to the alkali lignin by the fungal coculture was greater than that by the monocultures, which was confirmed by the SEM results. The porosity of the alkali lignin increased after being treated with *I. lacteus* and the fungal coculture. The total pore area was greatly increased after the fungi treatment, which proved that the alkali lignin formed more porous structures after fungi treatment and that the macromolecular lignin was depolymerized.

Thermogravimetric/Differential Thermogravimetric Analysis

Figure 5 shows the TG and differential TG curves of the autoclaved and fungi-treated alkali lignin samples. The pyrolysis process of the alkali lignin samples could be divided into dehydration and lignin degradation stages. According to the TG curves, the residue char contents of the alkali lignin were 39.9% (Control), 40.5% (*I. lacteus*), 39.6% (*P. chrysosporium*), and 42.1% (fungal coculture) (Park et al., 2017). The residual char content is related to the ratio of G and S in alkali lignin (Yang et al., 2010). G has better thermal stability than the other two lignin monomers; therefore, the larger the proportion of G, the more char that remains (Shen et al., 2011). It could be speculated that some of the G-lignin was consumed during the fungal coculture treatment, which was confirmed by previous FTIR results. From the differential TG curve, the maximum decomposition rate of the autoclave-sterilized alkali lignin appeared at 385°C, but the temperature peak of the alkali lignin after fungi treatment was shifted left. This suggested that the alkali lignin was converted to small molecule aromatic compounds with poor thermal stability during the fungi treatment process (Cao and Aita, 2013). It is worth mentioning that the temperature peak of the alkali lignin treated with the fungal coculture was advanced by 11°C (374°C), indicating that the alkali lignin had the poorest thermal stability after the fungal coculture treatment.

Element Analysis

The element analysis and degree of unsaturation of the autoclaved and fungi-treated alkali lignins are shown in **Table 3**. The degree of unsaturation of the alkali lignin was further reduced by fungi treatment. This indicated that the dense structure of the alkali lignin was depolymerized during fungi treatment, and some of the macromolecular lignin was degraded. The degree of unsaturation of alkali lignin decreased 3.5% after the fungal coculture treatment compared to the autoclaved alkali lignin. After fungi treatment, the mass percentage of elemental sulfur decreased in alkali lignin, suggesting that the elemental sulfur in alkali lignin was dissolved during the treatment (Xu et al., 2013).

Effects of Alkali Lignin Modification on Enzymatic Hydrolysis and Adsorption
Nonproductive Adsorption of Enzymes

Figure 6 shows the isothermal adsorption of cellulase by alkali lignin at different free enzyme concentrations. The Langmuir adsorption isotherm equation could accurately describe the adsorption of cellulase on alkali lignin. It could be seen that as the free enzyme concentration increased, the adsorption capacity becomes saturated, and the autoclaved alkali lignin had the largest adsorption capacity. After the fungi treatment of alkali lignin, the

TABLE 2 | Mercury intrusion porosimetry results of alkali lignin samples.

Sample	Porosity (%)	Total pore area (m²/g)	Average pore area (nm)	Pore diameter distribution (%) (nm)		
				500–2,500	2,500–10,000	>10,000
Autoclaved	64.3	4.0	1,498.6	7.6	22.9	67.2
IL	64.7	36.0	164.0	8.4	27.3	62.1
PC	60.9	53.1	111.8	9.0	29.7	58.9
Coculture	66.7	53.5	115.3	6.3	21.8	70.2

TABLE 3 | Element content of alkali lignin.

Sample	C (wt%)	O (wt%)	H (wt%)	N (wt%)	S (wt%)	Formula of C_{900}	Degree of unsaturation
Control	58.9	33.2	5.8	0.4	1.5	$C_{900}H_{1063}O_{380}N_5S_9$	372
IL	60.3	30.4	6.0	0.3	1.4	$C_{900}H_{1074}O_{340}N_4S_8$	366
PC	62.0	29.9	5.9	0.2	1.3	$C_{900}H_{1057}O_{326}N_2S_7$	374
Coculture	60.6	30.1	6.1	0.5	1.2	$C_{900}H_{1087}O_{335}N_6S_7$	359

adsorption capacity decreased by 36.4% (*I. lacteus* treatment), 43.2% (*P. chrysosporium* treatment), and 52.3% (fungal coculture treatment) compared with the autoclaved alkali lignin.

Table 4 shows the adsorption parameters, which were estimated by fitting the enzymatic adsorption data to the Langmuir model. The maximum adsorption capacities (E_{max}) of lignin were 0.44 (Control), 0.28 (*I. lacteus* treatment), 0.25 (*P. chrysosporium* treatment), and 0.21 (fungal coculture treatment) mg/g lignin. The autoclaved alkali lignin had the strongest adsorption capacity, and could adsorb approximately 40–50% more protein than the alkali lignin treated with the fungal coculture. The autoclaved alkali lignin had the highest affinity (K) for the enzyme (8.7 ml/mg protein), while the affinities for the enzyme were 25.3, 32.2, and 20.0% lower than that of the autoclaved alkali lignin for the alkali lignin treated with *I. lacteus*, *P. chrysosporium*, and the fungal coculture, respectively. The strength of the absorption between the alkali lignin and the enzyme was characterized by the coefficient K, which was calculated using the maximum adsorption capacity multiplied by the Langmuir adsorption constant (Deng et al., 2019). This is consistent with the results of previous hydrolysis experiments. It was speculated that the fungi treatment of alkali lignin degraded the macromolecular alkali lignin, which generated more exposed carboxylic groups. This could make the lignin more hydrophilic, which would decrease the

hydrophobic interaction between the alkali lignin and enzymes and reduce the nonproductive adsorption of cellulase (Yuan et al., 2018).

Enzymatic Hydrolysis of Avicel

The decreased nonproductive adsorption of cellulase on alkali lignin would lead to an increase in the yield of reducing sugar during the hydrolysis of Avicel. **Figure 7** presents the enzymatic hydrolysis of Avicel with or without the addition of alkali lignin. All alkali lignins had an inhibitory effect on the reducing sugar yield. The 72 h glucan conversion efficiencies with the addition of differently treated alkali lignin were 50.6% (*I. lacteus* treatment), 50.3% (*P. chrysosporium* treatment), and 54.1% (fungal coculture treatment). The Avicel without the addition of alkali lignin had the maximum reducing sugar yield at 72 h of 56.5%.

Although the addition of alkali lignin had an inhibitory effect on the hydrolysis saccharification process of Avicel, the fungi-treated lignin had less of a negative effect than the autoclaved alkali lignin. After adding alkali lignin that was treated with the fungal coculture, the reducing sugar yield could reach 95.8% of that without alkali lignin, which was the highest yield among all of the fungi treatments. This result was due to the decrease in absorption capacity of the alkali lignin for the hydrolysis enzyme after fungi treatment.

Practical Implications

The results obtained in this study may provide an efficient approach for the biological pretreatment of lignocellulosic biomass for biofuel production. To further improve the feasibility of fungal coculture system for a large-scale application in the future, more research should be devoted to revealing the complex interaction between mixed enzymes generated by fungal coculture system during the biodegradation of lignocellulosic biomass, and developing advanced bioreactors for the efficient fungal treatment process for biomass conversion. Also, technical-economic assessment and life cycle assessment should be carried out to demonstrate the feasibility of such a pretreatment system based on the long-term operation performance.

FIGURE 6 | Cellulase enzyme adsorption on alkali lignin before and after fungi treatment.
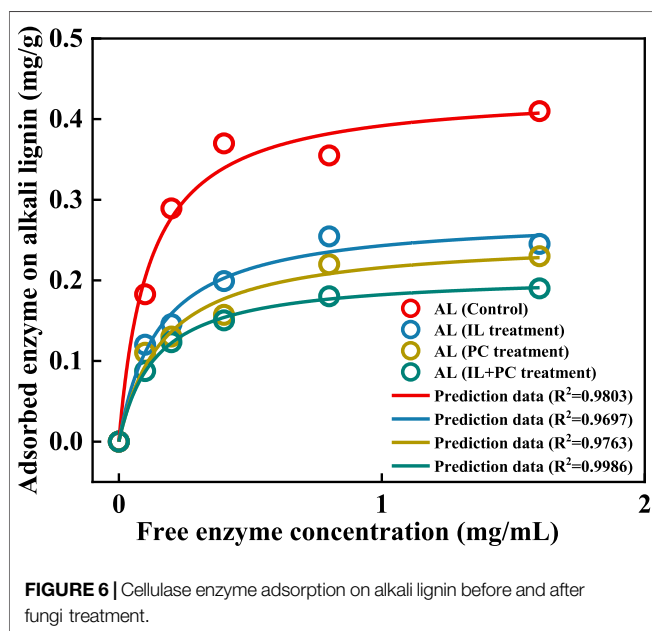
TABLE 4 | Langmuir adsorption isotherm parameters.

Sample	E_{max} (mg/g)	K (ml/mg)
Control	0.44	8.7
IL	0.28	6.5
PC	0.25	5.9
Coculture	0.21	7.0
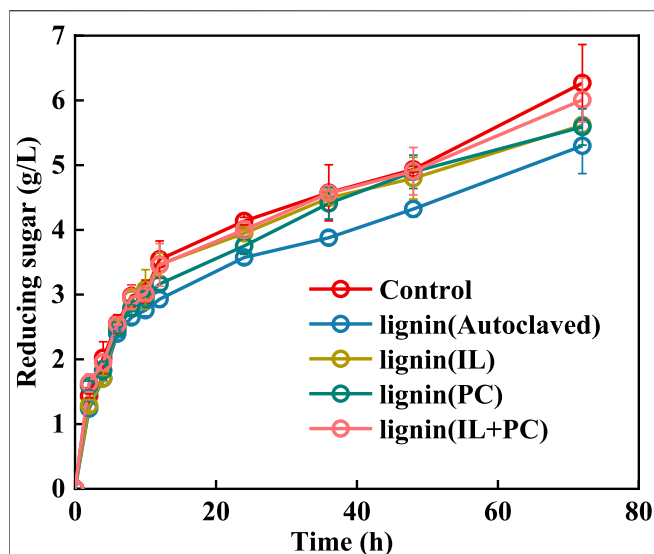
FIGURE 7 | Effects of fungi-treated lignin on reducing sugar yield in the enzymatic saccharification of Avicel.

CONCLUSION

The limitations of fossil fuels have led to an increase production of biofuels from renewable lignocellulosic biomass sources. Therefore, improving the efficiency of biological pretreatment of lignocellulosic biomass has become the most important point for the development of biofuels. This study opens a new opportunity to improve the efficiency of biological pretreatment and biomass conversion. The degradation efficiency of alkali lignin treated by the fungal coculture reached 26.4%, which is 3.4 and 5.2% higher than the monocultures of *I. lacteus* and *P. chrysosporium*, respectively. Physicochemical analyses showed that the chemical groups of the alkali lignin were changed significantly after fungal treatment.

The alkali lignin generated more carboxylic groups, which increased its hydrophilicity and reduced the absorption of alkali lignin to cellulase. The nonproductive adsorption of cellulase on alkali lignin decreased by 40–50% compared with the control group.

DATA AVAILABILITY STATEMENT

All datasets presented in this study are included in the article/**Supplementary Material**.

AUTHOR CONTRIBUTIONS

RL: Methodology, investigation, writing—original draft preparation. QL and AX: Conceptualization, supervision. YH, ZD, and XiZ: Writing—review and editing. XuZ: Project administration.

FUNDING

SUPPLEMENTARY MATERIAL

The Supplementary Material for this article can be found online at: https://www.frontiersin.org/articles/10.3389/fenrg.2020.575371/full#supplementary-material

REFERENCES

Arora, D. S., and Sharma, R. K. (2010). Ligninolytic fungal laccases and their biotechnological applications. *Biotechnol. Appl. Biochem.* 160 (6), 1760–1788. doi:10.1007/s12010-009-8676-y

Asina, F., Brzonova, I., Voeller, K., Kozliak, E., Kubátová, A., Yao, B., et al. (2016). Biodegradation of lignin by fungi, bacteria and laccases. *Bioresour. Technol.* 220, 414–424. doi:10.1016/j.biortech.2016.08.016

Cao, S., and Aita, G. M. (2013). Enzymatic hydrolysis and ethanol yields of combined surfactant and dilute ammonia treated sugarcane bagasse. *Bioresour. Technol.* 131, 357–364. doi:10.1016/j.biortech.2012.12.170

Chen, K.-J., Tang, J.-C., Xu, B.-H., Lan, S.-L., and Cao, Y. (2019). Degradation enhancement of rice straw by co-culture of *Phanerochaete chrysosporium* and *Trichoderma viride*. *Sci. Rep.* 9 (1), 1–7. doi:10.1038/s41598-019-56123-5

Christopher, L. P., Yao, B., and Ji, Y. (2014). Lignin biodegradation with laccase-mediator systems. *Front. Energy Res.* 2, 12. doi:10.3389/fenrg.2014.00012

Deng, Z., Xia, A., Liao, Q., Zhu, X., Huang, Y., and Fu, Q. (2019). Laccase pretreatment of wheat straw: effects of the physicochemical characteristics and the kinetics of enzymatic hydrolysis. *Biotechnol. Biofuels* 12 (1), 159. doi:10.1186/s13068-019-1499-3

Dong, X. Q., Yang, J. S., Zhu, N., Wang, E. T., and Yuan, H. L. (2013). Sugarcane bagasse degradation and characterization of three white-rot fungi. *Bioresour. Technol.* 131, 443–451. doi:10.1016/j.biortech.2012.12.182

Dong, Y.-C., Dai, Y.-N., Xu, T.-Y., Cai, J., and Chen, Q.-H. (2014). Biodegradation of chestnut shell and lignin-modifying enzymes production by the white-rot fungi *Dichomitus squalens, Phlebia radiata*. *Bioproc. Biosyst. Eng.* 37 (5), 755–764. doi:10.1007/s00449-013-1045-9

Hao, X., Quansheng, Y., Dan, S., Honghui, Y., Jidong, L., Jiangtao, F., et al. (2015). Fabrication and characterization of PbO$_2$ electrode modified with [Fe(CN)$_6$]$^{3-}$ and its application on electrochemical degradation of alkali lignin. *J. Hazard Mater.* 286, 509–516. doi:10.1016/j.jhazmat.2014.12.065

Isroi, I., Millati, R., Niklasson, C., Taherzadeh, M. J., and Lundquist, K. (2011). Biological treatment of Lignocelluloses with white-rot funghi and its applications: review. *BioResources* 6 (4), 5224–5259. doi:10.2172/1830

Kobayashi, N., Okada, N., Hirakawa, A., Sato, T., Kobayashi, J., Hatano, S., et al. (2009). Characteristics of solid residues obtained from hot-compressed-water treatment of woody biomass. *J. Ind. Eng. Chem. Res.* 48 (1), 373–379. doi:10.1021/ie800870k

Ku, H.-K., Lim, H.-M., Oh, K.-H., Yang, H.-J., Jeong, J.-S., and Kim, S.-K. (2013). Interpretation of protein quantitation using the Bradford assay: comparison with two calculation models. *Anal. Biochem.* 434 (1), 178–180. doi:10.1016/j.ab.2012.10.045

Lee, D.-S., Lee, Y.-G., Song, Y., Cho, E.-J., and Bae, H.-J. (2020). Hydrolysis Patterns of xylem tissues of hardwood pretreated with acetic acid and hydrogen peroxide. *Front. Energy Res.* 8, 34. doi:10.3389/fenrg.2020.00034

Li, X., He, Y., Zhang, L., Xu, Z., Ben, H., Gaffrey, M. J., et al. (2019). Discovery of potential pathways for biological conversion of poplar wood into lipids by co-fermentation of *Rhodococci* strains. *Biotechnol. Biofuels* 12 (1), 60. doi:10.1186/s13068-019-1395-x

Lindedam, J., Bruun, S., Jørgensen, H., Decker, S. R., Turner, G. B., DeMartini, J. D., et al. (2014). Evaluation of high throughput screening methods in picking up differences between cultivars of lignocellulosic biomass for ethanol production. *Biomass Bioenergy* 66, 261–267. doi:10.1016/j.biombioe.2014.03.006

Liu, Y., Hu, T., Wu, Z., Zeng, G., Huang, D., Shen, Y., et al. (2014). Study on biodegradation process of lignin by FTIR and DSC. *Environ. Sci. Pollut. Res.* 21 (24), 14004–14013. doi:10.1007/s11356-014-3342-5

Meehnian, H., Jana, A. K., and Jana, M. M. (2017). Pretreatment of cotton stalks by synergistic interaction of *Daedalea flavida* and *Phlebia radiata* in co-culture for improvement in delignification and saccharification. *Int. Biodeterior. Biodegrad.* 117, 68–77. doi:10.1016/j.ibiod.2016.11.022

Mishra, V., Jana, A. K., Jana, M. M., and Gupta, A. (2017). Enhancement in multiple lignolytic enzymes production for optimized lignin degradation and selectivity in fungal pretreatment of sweet sorghum bagasse. *Bioresour. Technol.* 236, 49–59. doi:10.1016/j.biortech.2017.03.148

More, S. S., Renuka, P. S., Pruthvi, K., Swetha, M., Malini, S., and Veena, S. M. (2011). Isolation, purification, and characterization of fungal laccase from *Pleurotus* sp. *Enzym. Res.* 2011, 248735. doi:10.4061/2011/248735

Parikh, J., Nadagouda, V., and Shukla, M. D. (2014). Production of lignin degrading enzymes namely Laccase, Manganese Peroxidase (MnP) and Lignin Peroxidase (LiP) of selected white-rot fungus in solid state fermentation (solid media). *Res. J. Biotechnol.* 9 (10), 80–82. doi:10.5897/ajb2014.14331

Park, S. Y., Kim, J.-Y., Youn, H. J., and Choi, J. W. (2018). Fractionation of lignin macromolecules by sequential organic solvents systems and their characterization for further valuable applications. *Int. J. Biol. Macromol.* 106, 793–802. doi:10.1016/j.ijbiomac.2017.08.069

Ren, N.-Q., Zhao, L., Chen, C., Guo, W.-Q., and Cao, G.-L. (2016). A review on bioconversion of lignocellulosic biomass to H₂: key challenges and new insights. *Bioresour. Technol.* 215, 92–99. doi:10.1016/j.biortech.2016.03.124

Salvachúa, D., Martínez, A. T., Tien, M., López-Lucendo, M. F., García, F., de los Ríos, V., et al. (2013). Differential proteomic analysis of the secretome of *Irpex lacteus* and other white-rot fungi during wheat straw pretreatment. *Biotechnol. Biofuels* 6 (1), 115. doi:10.1186/1754-6834-6-115

Schöneberg, A., Musa, T., Voegele, R. T., and Vogelgsang, S. (2015). The potential of antagonistic fungi for control of fusarium graminearumandFusarium crookwellensevaries depending on the experimental approach. *J. Appl. Microbiol.* 118 (5), 1165–1179. doi:10.1111/jam.12775

Sharma, H. K., Xu, C., and Qin, W. (2019). Biological pretreatment of lignocellulosic biomass for biofuels and bioproducts: an overview. *Waste Biomass Valoriz.* 10 (2), 235–251. doi:10.1007/s12649-017-0059-y

Shen, Q., Zhang, T., Zhang, W.-X., Chen, S., and Mezgebe, M. (2011). Lignin-based activated carbon fibers and controllable pore size and properties. *J. Appl. Polym. Sci.* 121 (2), 989–994. doi:10.1002/app.33701

Sindhu, R., Binod, P., and Pandey, A. (2016). Biological pretreatment of lignocellulosic biomass – an overview. *Bioresour. Technol.* 199, 76–82. doi:10.1016/j.biortech.2015.08.030

Singh, S., Cheng, G., Sathitsuksanoh, N., Wu, D., Varanasi, P., George, A., et al. (2015). Comparison of different biomass pretreatment techniques and their impact on chemistry and structure. *Front. Energy Res.* 2, 62. doi:10.3389/fenrg.2014.00062

Suksong, W., Wongfaed, N., Sangsri, B., Kongjan, P., Prasertsan, P., Podmirseg, S. M., et al. (2020). Enhanced solid-state biomethanisation of oil palm empty fruit bunches following fungal pretreatment. *Ind. Crop. Prod.* 145, 112099. doi:10.1016/j.indcrop.2020.112099

Sun, C., Xia, A., Liao, Q., Fu, Q., Huang, Y., Zhu, X., et al. (2018). Improving production of volatile fatty acids and hydrogen from microalgae and rice residue: effects of physicochemical characteristics and mix ratios. *Appl. Energy* 230, 1082–1092. doi:10.1016/j.apenergy.2018.09.066

Sun, F.-h., Li, J., Yuan, Y.-x., Yan, Z.-y., and Liu, X.-f. (2011). Effect of biological pretreatment with *Trametes hirsuta* yj9 on enzymatic hydrolysis of corn stover. *Int. Biodeterior. Biodegrad.* 65 (7), 931–938. doi:10.1016/j.ibiod.2011.07.001

Sun, S., Huang, Y., Sun, R., and Tu, M. (2016). The strong association of condensed phenolic moieties in isolated lignins with their inhibition of enzymatic hydrolysis. *Green Chem.* 18 (15), 4276–4286. doi:10.1039/c6gc00685j

Tesfaw, A., and Assefa, F. (2014). Co-culture: a great promising method in single cell protein production. *Biotechnol. Mol. Biol. Rev.* 9 (2), 12–20. doi:10.5897/bmbr2014.0223

Wang, W., Yuan, T., and Cui, B. (2014). Biological pretreatment with white rot fungi and their co-culture to overcome lignocellulosic recalcitrance for improved enzymatic digestion. *Bioresources* 9 (3), 3968–3976. doi:10.15376/biores.9.3.3968-3976

Wiberth, C.-C., Casandra, A.-Z. C., Zhiliang, F., and Gabriela, H. (2018). Oxidative enzymes activity and hydrogen peroxide production in white-rot fungi and soil-borne micromycetes co-cultures. *Ann. Microbiol.* 69 (2), 171–181. doi:10.1007/s13213-018-1413-4

Xia, A., Jacob, A., Tabassum, M. R., Herrmann, C., and Murphy, J. D. (2016). Production of hydrogen, ethanol and volatile fatty acids through co-fermentation of macro- and micro-algae. *Bioresour. Technol.* 205, 118–125. doi:10.1016/j.biortech.2016.01.025

Xu, G., Wang, L., Liu, J., and Wu, J. (2013). FTIR and XPS analysis of the changes in bamboo chemical structure decayed by white-rot and brown-rot fungi. *Appl. Surf. Sci.* 280, 799–805. doi:10.1016/j.apsusc.2013.05.065

Yadav, S., and Chandra, R. (2015). Syntrophic co-culture of *Bacillus subtilis* and *Klebsiella pneumonia* for degradation of kraft lignin discharged from rayon grade pulp industry. *J. Environ. Sci.* 33, 229–238. doi:10.1016/j.jes.2015.01.018

Yang, C.-Y., and Fang, T. J. (2015). Kinetics of enzymatic hydrolysis of rice straw by the pretreatment with a bio-based basic ionic liquid under ultrasound. *Process Biochem.* 50 (4), 623–629. doi:10.1016/j.procbio.2015.01.013

Yang, Q., Zhang, H., Li, X., Wang, Z., Xu, Y., Ren, S., et al. (2013). Extracellular enzyme production and phylogenetic distribution of yeasts in wastewater treatment systems. *Bioresour. Technol.* 129, 264–273. doi:10.1016/j.biortech.2012.11.101

Yang, X., Ma, F., Zeng, Y., Yu, H., Xu, C., and Zhang, X. (2010). Structure alteration of lignin in corn stover degraded by white-rot fungus *Irpex lacteus* CD2. *Int. Biodeterior. Biodegrad.* 64 (2), 119–123. doi:10.1016/j.ibiod.2009.12.001

Yao, L., Zhu, L.-P., Xu, X.-Y., Tan, L.-L., Sadilek, M., Fan, H., et al. (2016). Discovery of novel xylosides in co-culture of basidiomycetes *Trametes versicolor* and *Ganoderma applanatum* by integrated metabolomics and bioinformatics. *Sci. Rep.* 6 (1), 33237. doi:10.1038/srep33237

Ying, W., Shi, Z., Yang, H., Xu, G., Zheng, Z., and Yang, J. (2018). Effect of alkaline lignin modification on cellulase-lignin interactions and enzymatic saccharification yield. *Biotechnol. Biofuels* 11 (1), 214. doi:10.1186/s13068-018-1217-6

Yuan, Y., Zhai, R., Li, Y., Chen, X., and Jin, M. (2018). Developing fast enzyme recycling strategy through elucidating enzyme adsorption kinetics on alkali and acid pretreated corn stover. *Biotechnol. Biofuels* 11 (1), 316. doi:10.1186/s13068-018-1315-5

Zeng, G.-M., Zhao, M.-H., Huang, D.-L., Lai, C., Huang, C., Wei, Z., et al. (2013). Purification and biochemical characterization of two extracellular peroxidases from *Phanerochaete chrysosporium* responsible for lignin biodegradation. *Int. Biodeterior. Biodegrad.* 85, 166–172. doi:10.1016/j.ibiod.2013.07.005

Zhang, K., Xu, R., Abomohra, A. E.-F., Xie, S., Yu, Z., Guo, Q., et al. (2019). A sustainable approach for efficient conversion of lignin into biodiesel accompanied by biological pretreatment of corn straw. *Energy Convers. Manag.* 199, 111928. doi:10.1016/j.enconman.2019.111928

Novel Poly Deep Eutectic Solvents Based Supported Liquid Membranes for CO$_2$ Capture

Manzar Ishaq[1], Mazhar Amjad Gilani[2], Zobila Muhammad Afzal[2], Muhammad Roil Bilad[3], Abdul-Sattar Nizami[4], Mohammad Rehan[5], Eza Tahir[4] and Asim Laeeq Khan[1]*

[1]Department of Chemical Engineering, COMSATS University Islamabad, Islamabad, Pakistan, [2]Department of Chemistry, COMSATS University Islamabad, Islamabad, Pakistan, [3]Chemical Engineering Department, Universiti Teknologi PETRONAS, Perak, Malaysia, [4]Sustainable Development Study Centre, Government College University, Lahore, Pakistan, [5]Center of Excellence in Environmental Studies (CEES), King Abdulaziz University, Jeddah, Kingdom of Saudi Arabia

The poly deep eutectic solvents (PDESs), a potential substituent to ionic liquids, have emerged as relatively new material and have been successfully applied in catalysis, nanotechnology, and, more importantly, in gas separation. Herein, the PDESs were incorporated for the first time in the CO$_2$ capturing membranes to exploit their inherent advantages in the acid gas capture. The PDESs were synthesized by mixing choline chloride (hydrogen bond acceptor-HBA) and two hydrogen bond donors-HBDs (polyacrylic acid and polyacrylamide) separately in different molar ratios. The physical changes of the resulting homogeneous mixture along with the Fourier Transform Infrared confirmed the successful synthesis of the PDESs. Afterward, these PDESs were impregnated into microporous polyvinylidene fluoride (PVDF) membrane support to fabricate supported liquid membranes (SLMs). The gas performance of the prepared PDES-SLMs was tested under pure and mixed-gas conditions for CO$_2$, CH$_4$, and N$_2$. The PDES-SLMs showed a significantly high CO$_2$/CH$_4$ and CO$_2$/N$_2$ selectivities of the order of 55.5 and 60, respectively. To evaluate their practical implication, the SLMs were investigated systematically under different operating conditions such as choline content, temperature, volume fraction of the CO$_2$ in the feed, and the activation energy required for CO$_2$ capture. The synthesized SLMs showed exceptional results in both permeability and selectivity viewpoint. The remarkable SLMs gas performance can be ascribed to the basicity, molar free volume, and the H-bonding strength of the synthesized PDESs. The green potential, low cost, and the promising gas separation performance make theses PDESs a favorable alternative to the competing PILs in capturing the greenhouse acid gases.

Keywords: carbon dioxide capture, poly deep eutectic solvents, supported liquid membrane, permeability, selectivity

---

INTRODUCTION

The carbon dioxide (CO_2), primarily released to the environment by the consumption of fossil fuels and other major industrial processes, contributes to 60% of the greenhouse gases and, posing the threat of global warming (Coninck et al., 2005). As a result, there is an urgent requirement of effective CO_2 capturing technologies to control the emissions of greenhouse gases. Primarily there are three methods of CO_2 capturing, i.e., Pre-combustion, Post-combustion, and oxy-fuel method. The conventional technologies for CO_2 suppression include cryogenic distillation, adsorption, and absorption. In the cryogenic distillation, CO_2 is captured at low temperature, and the process involves compression and expansion of the CO_2, and at the end, liquefied CO_2 is obtained. This technology has limitations of high energy consumption, special equipment requirement, and small concentration of CO_2, which make the process uneconomical as it cannot be used at a large scale. The absorption method usually employs the amine-based porous adsorbents for CO_2 capturing. This process involves both physisorption and chemisorption of the acid gas. The main disadvantage of the adsorption method is difficult regeneration and scarcity of suitable adsorbents (Shen et al., 2020). In the absorption technique, CO_2 is separated based on solubility in the solvent. CO_2 is absorbed in a solvent, then separated from the solvent at high temperature, and solvent is regenerated. The absorption could be physical or chemical. The main issue with absorption technology is high energy requirement and the need for particular green solvents with high CO_2 solubility values (de Almeida Quintino, 2014; Songolzadeh et al., 2014). These techniques are energy intensive because of the solvent regeneration and elevated operating conditions (Tuinier et al., 2010; Wang et al., 2011). The membrane technology provides numerous advantages over other conventional techniques such as eco-friendliness, low energy demand, ease of operation, and one-step separation (Bernardo et al., 2009; Peng et al., 2014; Pan et al., 2020). In particular, the supported liquid membranes (SLMs), especially supported ionic liquid membranes (SILMs) have been investigated broadly, which combine the highly processable and flexible polymeric support impregnated with ionic liquids (ILs) for CO_2 capture (Malik et al., 2011; Uchytil et al., 2011).

The inherent advantages of ILs such as high thermal stability, extremely low vapor pressure, and non-flammability, make them suitable options for CO_2 capture (Meine et al., 2010; Emel'yanenko et al., 2014). Additionally, the relatively new idea of combining polymer and IL as polymerized ionic liquid (PIL) membranes was put forward by Bara et al. for the first time in 2007 (Bara et al., 2007). The PIL membranes share the advantageous properties of ILs along with high mechanical stability of the membranes under high pressure. However, the CO_2 permeabilities of these PIL dense membranes were found to be significantly lower because of low diffusion rate of the acid gas through them (Bara et al., 2007; Bara et al., 2008a). The PIL based SLMs have also been fabricated and investigated for their potential in increasing CO_2 permeability and CO_2/light gas selectivity by relying on the solubility selectivity (Bara et al., 2008b; Bara et al., 2009b; McDanel et al., 2014). Despite these
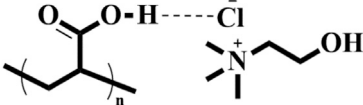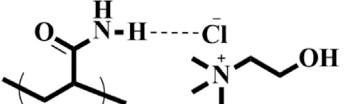
many advantages discussed above, several drawbacks of ILs have also been articulated, such as extremely high viscosity, toxicity, synthesis cost, and non-biodegradability (Pham et al., 2010; Biczak et al., 2014). Therefore, there is a need for green substituent of ILs in the field of SLM that can selectively separate the acid gas from the mixture of gases.

In this context, deep eutectic solvents (DESs), obtained because of hydrogen bonding formed between the hydrogen bond acceptor (HBA) and hydrogen bond donor (HBD), are a promising alternative (Francisco et al., 2013; García et al., 2015). The melting point of the DESs lies far below the melting points of the individual precursors, which is a characteristic feature of the eutectic solvents. The characteristic properties of the DESs can also be tuned according to the application requirement by altering the choice of HBA and HBD and their molar ratios (García et al., 2015). The DESs have many advantages compared to ILs, such as cost-effectiveness, biodegradability, ease of synthesis, and biocompatibility (Smith et al., 2014). The very first DES reported by Abbott et al. was formed between choline chloride-HBA (a vitamin B component) and urea-HBD (Abbott et al., 2003). Afterward, most of the DESs reported were primarily obtained from the choline chloride because it is a biodegradable and low cost, as the price of choline based DESs is merely 4–9% of the conventional ILs (Ma et al., 2018).

In the past decade, a plethora of review articles on CO_2 absorption by the DESs have been published so far, showing high DESs affinity for CO_2 (García et al., 2015; Aissaoui et al., 2017; Sarmad et al., 2017; Zhang et al., 2018). The polymerized deep eutectic solvents (PDESs), are a new class of DESs in which the HBD part is polymerizable (Zhang et al., 2012; Mota-Morales et al., 2013; Ren'ai et al., 2018). PDESs have also been investigated like PILs, for CO_2 capture in the absorption process by Isik et al. (Isik et al., 2016a; Isik et al., 2016b), showed significantly high CO_2 uptakes. The polymerizable HBD was employed to synthesize PDESs for CO_2 absorption process, while the HBD was polymerized using photo polymerization. The results of the investigations revealed that the PDESs are excellent CO_2 sorbents (Isik et al., 2016a; Isik et al., 2016b). However, the risk of a complete conversion of the HBD to polymerized HBD and the maintenance of HBA-HBD interactions cannot be neglected.

To the best of our knowledge, PDESs have never been investigated in membrane-based CO_2 capturing. The ambition behind this study is the findings of molecular dynamics simulation work investigated by Shen and Hung (2017), which revealed that the DESs family could efficiently be incorporated in the porous support of SLMs for CO_2 capture. Therefore, this study, for the first time, used polymerized HBD to make DES with the HBA to avoid the risk of incomplete polymerization; plus the energy requirements reduced significantly for such chemistry. Polyacrylic acid (PAA) and polyacrylamide (PAM) were chosen as polymerized HBDs, and four types of PDESs were synthesized using choline chloride as HBA. These novel PDESs were impregnated as membrane liquids in the SLMs. The performance of the synthesized SLMs was evaluated with the CO_2 permeability and CO_2/CH_4 selectivity to estimate the practical implication of these SLMs. The effect of operating conditions on membrane separation performance was also analyzed.

TABLE 1 | Composition and nomenclature of the synthesized PDESs.

Composition	Molar ratio (HBD:HBA)	Code	Chemical structure
ChCl/PAA	15:1	PDES-1	
ChCl/PAA	20:1	PDES-2	
ChCl/PAM	15:1	PDES-3	
ChCl/PAM	20:1	PDES-4	

MATERIALS AND METHODS

Choline chloride (≥99%), polyacrylic acid (Mn 1,500 g mol^{-1}), poly acrylamide (Mn 1,000 g mol^{-1}) were used in the synthesis of PDES. Polyvinylidene difluoride (PVDF) and N-Methyl-2-Pyrrolidone (NMP) were used to prepare membrane support. Sigma Aldrich supplied all materials. Chemicals were used as provided by the company.

Synthesis of PDESs

PDESs were prepared using the choline chloride (ChCl) as HBA and the polymers-HBDs (PAA and PAM) in two different molar ratios of 15:1 and 20:1, respectively. In a typical procedure, HBD and HBA were mixed in a suitable amount in a sample bottle using a magnetic stirrer. The mixture was heated to 80°C with continued stirring. A homogeneous viscous liquid (PDES) was obtained at the end of 30 min of simultaneous heating and stirring. The mixture was kept under the same reaction conditions for 2 h to ensure complete conversion. By repeating the similar procedure, four different PDESs were synthesized. The composition and nomenclature of the PDESs are presented in **Table 1**.

SLM Fabrication

PDES-SLMs were prepared by using a PVDF ultrafiltration membrane as a support material. The phase inversion method was used to prepare PVDF membrane support. 15 wt% solution of PVDF was mixed with NMP and stirred for 24 h. Subsequently, a clear homogenous solution was formed that was then casted using Elcometer. 250 μm thickness was maintained during the casting process, and a cast film was formed. The phase transformation was accomplished by dipping the cast membrane in a nonsolvent (water) coagulation bath for 10 min to ensure the complete phase inversion. The synthesized membrane support was placed in a desiccator for 24 h to remove any volatile or water content present. The PVDF membrane sheet was placed in the desiccator overnight to ensure the complete drying to facilitate the incorporation of the PDES liquid on to the surface of the porous membrane. Subsequently, the SLM-1 based on PDES-1 was prepared using the impregnation method. In this typical method, 3 ml of the PDES-1 liquid was evenly spread on the surface of the PVDF support. Afterward, the membrane was placed in the circular permeation cell at 2 bar nitrogen pressure for 1 h to ensure the impregnation of the PDES-1 into the pores of the PVDF support. As evidence of complete impregnation, a thin layer of the PDES-1 was obtained at the bottom of the PVDF support. The same method was adopted for preparing SLM-2 SLM-3, and SLM-4 based on the corresponding PDES-2-4. The schematic image of synthesized SLMs is presented in **Figure 1**.

Characterization Techniques

The interaction between HBD and HBA has been confirmed through Fourier Transform Infrared (FTIR) spectroscopy. The FTIR spectra of the HBD and HBA and the PDESs were obtained in a scan range of 4000–800 cm^{-1} at room temperature with a resolution of 8 cm^{-1}. The FTIR spectra were taken using Thermo-Nicolet (6700P) FTIR Spectrometer (USA). Viscosities of the PDESs are very crucial in deciding their practical applications, particularly as membrane liquid in SLMs. The viscosities of the PDESs were determined at room temperature using Ubbelohde viscometer. The vibrating tube densitometer Krüss DS7800 model was used to measure the density of the PDESs at atmospheric pressure.

Membrane Performance Testing

Gas separation performance of the prepared membranes was tested in a custom-built permeation setup by calculating pure

FIGURE 1 | Schematic representation of SLM.

FIGURE 2 | Set-up for pure and mixed-gas evaluation of membranes.
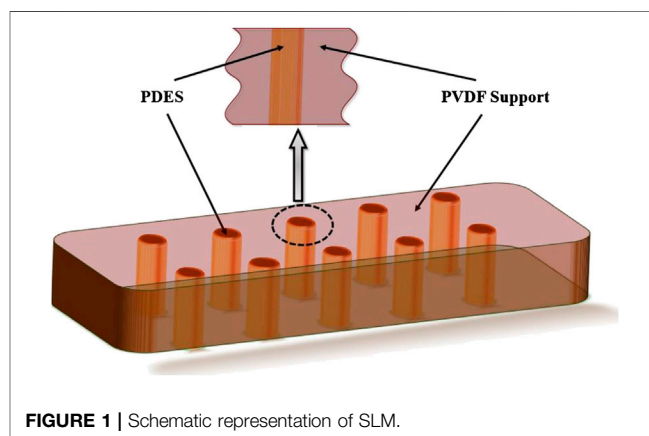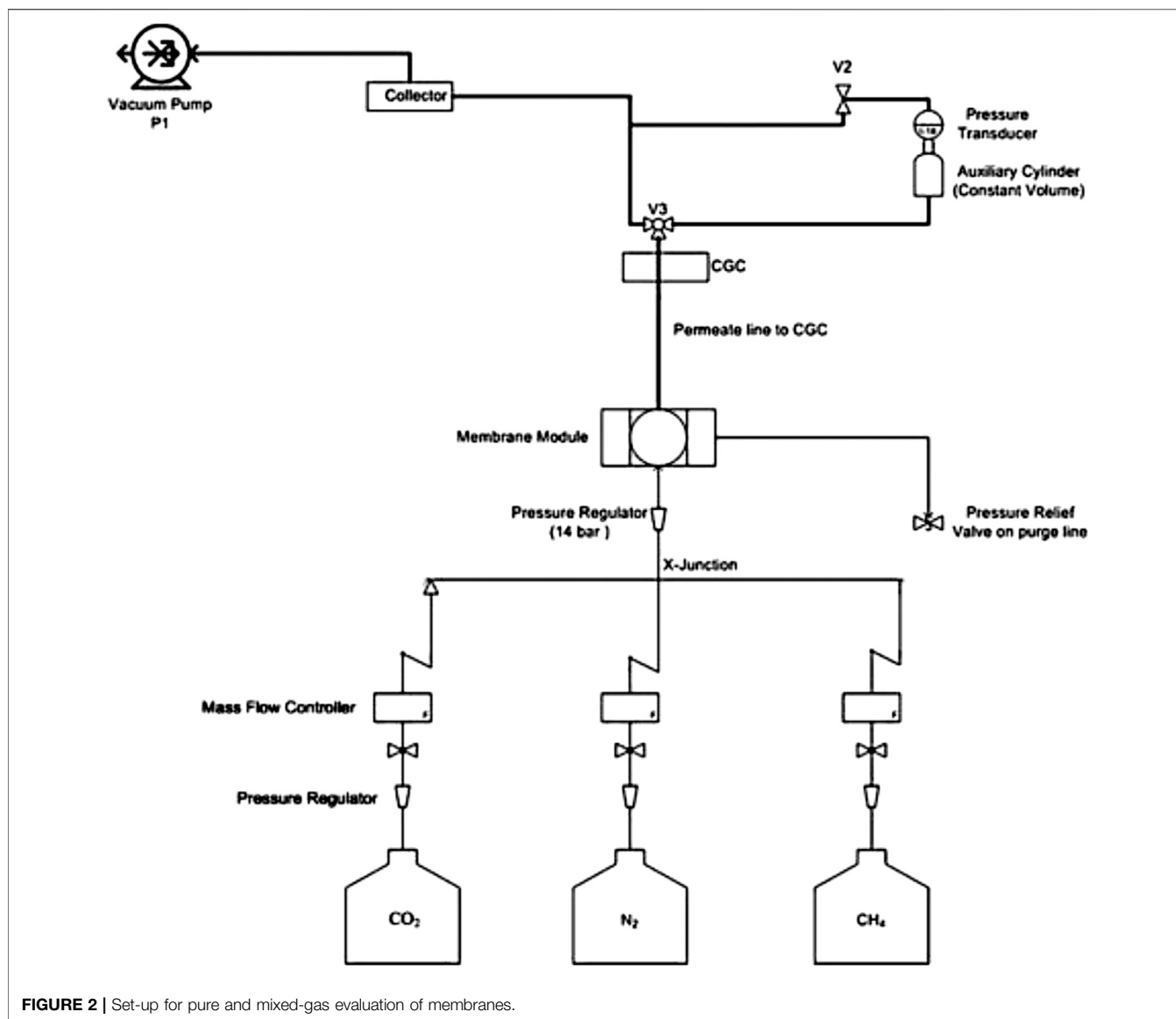
and mixed gas permeabilities and selectivities. Gas permeation was tested at isochoric conditions (constant volume and variable pressure). The pressure of the setup is increased with time. A gas chromatograph equipped with two thermal conductivity detectors, at the front and back of gas chromatograph, was used to analyze the compositions of retentate and permeate. The schematic gas separation setup is shown in **Figure 2**. This setup is constructed of stainless steel. The composition and flow rate of the feed gas is controlled by Mass flow controller. The flow rate could vary from 0 to 1 L/ min. The functional area of membrane in single cell permeation setup is 3.8 cm². The working principle and specifications of the setup are defined elsewhere (Khan et al., 2010). The prepared membranes were positioned on the metallic porous support and airtight. The gas feed was introduced at 1 L/min into the

membrane system. The prepared membranes were analyzed within the feed temperature range of 298–338 K to investigate the temperature effect on the gas separation performance. All the experiments were repeated at least three times to eliminate any ambiguity. The SILMs follow the solution diffusion mechanism for the transport of the gasses through them, according to this model

$$J = DS, \tag{1}$$

where J Permeability, D Diffusion Coefficient, S Solubility Coefficient.

The time lag method was adopted to calculate "D" and "S" (Crank, 1975; Ash and Barrie, 1986). In this method, a high vacuum is applied at one side of the test gas, and D is calculated by calculating the lag time before the steady-state is achieved.

FIGURE 3 | (A) FTIR spectra of PAA based PDESs. **(B)** FTIR spectra of PAM based PDESs.

RESULTS AND DISCUSSION

Characterization of the PDESs

The FTIR spectra of the DESs and their individual precursors, presented in **Figures 3A,B**, have confirmed the interaction between individual precursors resulting in the formation of DES. The characteristic peak analysis of the PDESs presented **Figure 3** revealed that it is an approximately an overlap of its constituting components. The characteristic peaks of all the individual components did not disappear in the PDESs spectra showing that the structural integrity of these components has been maintained. The characteristic peaks of ChCl obtained at 3,200 cm^{-1} correspond to hydroxyl (OH bending) group. While the peak obtained at 1,480 cm^{-1} corresponds to alkyl group present in the structure of ChCl (Ullah et al., 2015). In case of pure PAA, the broad vibrational band observed between 3,200 and 3,600 cm^{-1} exhibits the OH stretching in all the PAA containing samples. The other important band that appeared at 1,682 cm^{-1} represents the carbonyl group present in the PAA (Mota-Morales et al., 2013). In case of pure PAM, the band obtained between 3,450 and 3,300 cm^{-1} represent the amine group (NH$_2$ stretching). The bands at 1,702 and 1,640 cm^{-1} attributed to the carbonyl group (C=O) present. (Kumar et al., 2012). The peaks that appeared between 1,300–1,180 cm^{-1} are ascribed to the–C–N–linkage and CH$_2$ groups (Dumitrescu et al., 2015).

The carboxylic group present in PAA was found to be in its acid form that is reflected in the peaks obtained at 1,736 and 1,711 cm^{-1}, in PDES-1 and PDES-2, respectively (Mota-Morales et al., 2013). This feature revealed that the interaction between the PAA and ChCl was through hydrogen bonding, a characteristic property of the DESs. The band at 1,480 cm^{-1} in case of pure ChCl is shifted toward shorter wave number as the percentage of ChCl is increased. Interestingly, the NH$_2$ bands are shifted toward lower wave number, which confirms the formation of the hydrogen bond between the HBA and HBD moieties (Yue et al., 2012). Additionally, it may be observed in case of all the PDESs spectra that the characteristic peaks undergo redshift as the concentration of the choline content is increased in the PDESs. This can be attributed to the strength of H-bond formed between the polymer and the ChCl, i.e., lower the wave number stronger the H-bond (Jiang et al., 2017).

The molar volume (V) of CO_2 sorbent is a critical factor in determining the maximum amount of the gas sorbed per unit volume of the sorbent (Camper et al., 2006). Therefore, the molar volume of the PDESs was measured by the experimental values of density using the following equation.

$$V = \frac{M_{\text{PDES}}}{\rho}.$$ (4)

In the above equation, M_{PDES} and ρ are the molar mass and density of the PDESs, respectively. Where the M_{PDES} for the prepared PDESs was determined by using the following equation established for the DESs (Abbott et al., 2011; Peng et al., 2014),

$$M_{\text{PDES}} = \frac{X_{\text{HBA}}M_{\text{HBA}} + X_{\text{HBD}}M_{\text{HBD}}}{X_{\text{HBA}} + X_{\text{HBD}}},$$ (5)

An auxiliary cylinder of 50 cm^3 equipped with a pressure transducer that records the rate of increase in pressure is joined to a vacuum pump by valve V. The test gas was fed from one side of the cylinder while keeping the other side at vacuum until the steady-state achieved. The time lag intercept θ was calculated from the plotted graph of increasing gas pressure on the vacuum side. The following equation was used to calculate "D"

$$D = \frac{l^2}{6\theta},$$ (2)

where l is membrane thickness. After calculating the D, the S was calculated using **Eq. 1**. The selectivity of the gas A over gas component B was calculated using the following equation.

$$\alpha_{A/B} = \frac{P_A}{P_B}.$$ (3)

TABLE 2 | Physical properties of the PDESs.

PDESs code	M_{PDES} (g mol^{-1})	Viscosity (cP)	Density (g cm^{-3})	Molar volume (cm^3 mol^{-1})
PDES-1	224.64	439.01	1.21	185.65
PDES-2	204.4	418.24	1.19	171.76
PDES-3	193.39	387.40	1.14	169.64
PDES-4	180.59	353.66	1.11	162.69

where X and M represent the mole ratio and molar mass (g mol^{-1}) of the HBAs and HBDs, respectively. The physical properties of the prepared PDESs are presented in **Table 2**. The viscosity and density, being the critical parameters for SLM fabrication, were measured three times with great care, and the average of the values are displayed. It can be observed from **Table 2** that the prepared PDESs are moderately viscous. However, these values are lower and comparable to most of the ILs and DESs (García et al., 2015).

Performance of Synthesized PDES-SLMs

The gas performance of the synthesized PDES-SLMs was analyzed by using pure gases CO$_2$, N$_2$, and CH$_4$, and the results are presented in **Table 3**. The solution-diffusion mechanism is responsible for the transport of CO$_2$ through the SLMs. It is a three-step mechanism in which the CO$_2$ is first dissolved in the impregnated liquid, diffuses through it, and then for the concentration gradient, is desorbed to the permeate side of the SLMs. The CO$_2$/CH$_4$ and CO$_2$/N$_2$ selectivities for both types of SLMs were found to be significantly higher between 45.37–50.71 and 56.05–60, respectively. In the case of CO$_2$/CH$_4$, the SLM-2 membrane showed the highest selectivity, and for CO$_2$/N$_2$, the SLM-4 was the membrane with the highest selectivity. These significantly high selectivities can be attributed to the high solubility of the CO$_2$ in the DESs (Abbott et al., 2004; García et al., 2015; Aissaoui et al., 2017). The selectivity results can also be justified on the ground of kinetic diameter of the analyzed gases (de Almeida Quintino, 2014). The PDES-SLMs prefer the permeation of small molecules and renders large molecules to pass through the membrane. The kinetic diameter of CO$_2$ (3.30 Å) is small as compared to the N$_2$ (3.64 Å) and CH$_4$ (3.80 Å) that favors the improved selectivity of CO$_2$/CH$_4$ and CO$_2$/N$_2$. Moreover, the higher values of selectivity may also be ascribed to the lower molar volume of the prepared PDESs. This can be satisfactorily explained by using Camper model (Scovazzo, 2009), according to which the solubility of CO$_2$ is higher in low molar volume liquids. The molar volume of the prepared PDESs presented in **Table 2** has lower values than most of the commercially used ILs (Scovazzo, 2009). Interestingly, it

can be observed from **Table 3** that the CO$_2$/CH$_4$ and CO$_2$/N$_2$ selectivities were found to be increased by increasing the ChCl molar ratio. The increase in selectivity can be explained based on molar free volume and the basicity of the DESs (Trivedi et al., 2016; Ghaedi et al., 2017b). It is well established that the molar free volume and basicity of the DESs increase on par with the ChCl content in the DESs (Abbott et al., 2017). The increase in the molar free volume and basicity of the DES give rise to the permeability of the CO$_2$, which resulted in high values of selectivities.

The acid gas permeability through the prepared SLMs can be illustrated using the hole theory explained by Abbott and coworkers (Abbott et al., 2007). According to this theory, free spaces between the individual ionic moieties of the PDES permit the ions to move through it. Ion-HBD interactions control the size of these holes (Abbott et al., 2007). The PAA based SLMS (SLM-1 and SLM-2) showed notable CO$_2$ permeability of the order 19.45 and 19.9 Barrer, respectively. The permeability of these novel PDES-SLMs is comparable to the first-ever reported PIL membranes, which were in the range of 9–32 Barrer (Bara et al., 2007). Although the viscous membrane liquids are generally assumed to have lower CO$_2$ permeability values (Scovazzo, 2009), the prepared PDESs have shown significant CO$_2$ permeability values. This can be ascribed to the high solubility of the acid gas in the membrane liquid, as the molecular interaction is mainly assumed to govern the permeability rather than the bulk properties (Iarikov et al., 2011). This can also be supported by the reduced permeability values of CH$_4$ and N$_2$, as witnessed in the case of permeability results presented in **Table 3**. Moreover, the PAM based SLMs coded as SLM-3 and SLM-4 exhibited higher permeabilities than the SLM-1 and SLM-2. These SLMs showed significantly higher CO$_2$ permeability values than most of the functionalized imidazolium-based PIL membranes (Bara et al., 2008a; Horne et al., 2015). The SLM-4 showed the maximum CO$_2$ permeability of the order of 25 Barrer. The reason for this high permeation is the higher solubility, lower molar volumes, and moderate viscosities than the PAA based PDESs (SLM-1,2), as enlisted in **Table 2**.

TABLE 3 | CO$_2$/CH$_4$ and CO$_2$/N$_2$ ideal gas permeability and selectivity.

SLMs code	Permeability (Barrer)			Selectivity	
	CO$_2$	CH$_4$	N$_2$	P_{CO2}/P_{CH4}	P_{CO2}/P_{N2}
SLM-1	20.56	0.42	0.37	48.95	55.57
SLM-2	21.3	0.42	0.38	50.71	56.05
SLM-3	24.5	0.54	0.43	45.37	56.98
SLM-4	27	0.58	0.45	46.55	60.00

TABLE 4 | CO$_2$/CH$_4$ and CO$_2$/N$_2$ mixed gas permeability and selectivity.

SLMs code	Permeability (Barrer)			Selectivity	
	CO$_2$ (Barrer)	CH$_4$ (Barrer)	N$_2$ (Barrer)	P_{CO2}/P_{CH4}	P_{CO2}/P_{N2}
SLM-1	19.45	0.40	0.37	47.50	52.57
SLM-2	19.9	0.40	0.38	49.25	52.37
SLM-3	23.4	0.54	0.42	43.22	55.71
SLM-4	25	0.58	0.45	44.03	55.56
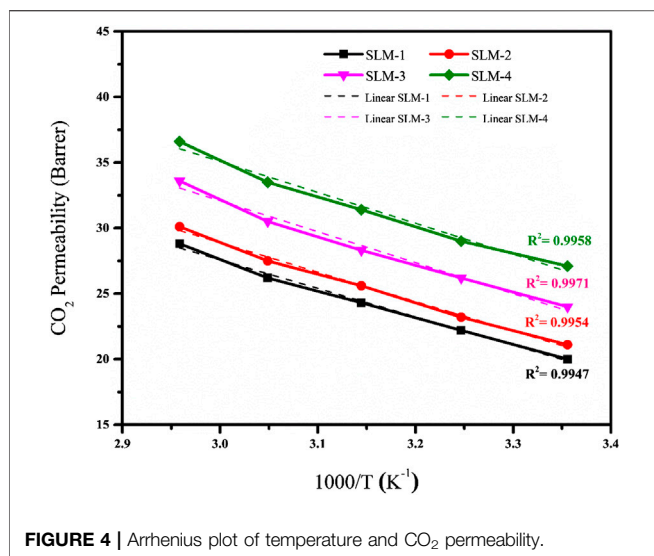
FIGURE 4 | Arrhenius plot of temperature and CO$_2$ permeability.

The increase in ChCl concentration increases the intermolecular interactions (H-bonding) between the ChCl and HBD polymers, as anticipated in the FTIR spectra presented in **Figures 3A,B**. Therefore, the CO$_2$ permeability of the PDESs is expected to decrease at higher ChCl concentrations because of stronger intermolecular interactions between the PDES moieties, which in turn reduced the attraction for third moiety CO$_2$. On the contrary, the CO$_2$ permeability was found to be increased, instead of decreasing, on a par with ChCl concentration in both types of HBDs, i.e., 20.5 to 21.3 in PAA-SLMs and 24.5 to 27 Barrer for PAM-SLMs when ChCl mole ratio was increased from 15 to 20. This peculiar behavior of CO$_2$ permeability of the PDES-SLMs could be explained better through Lewis acid-base relation of the acid gas and the PDESs. It is well established that the basicity of the DESs increased to a significant level by increasing the ChCl concentration in the DESs, thereby making the DESs more attractive media for the acid gas capture (Abbott et al., 2017).

The mixed gas (50/50 wt%) permeability and the selectivity results were also evaluated, and the results are presented in **Table 4** to prove the application of the DESs on a commercial scale. The permeability of the CO$_2$ for polymeric membranes is generally reduced under mixed-gas conditions because of the competitive sorption through the membranes. This competitive phenomenon also lowers the selectivity because of the hindrance created by the CH$_4$ and N$_2$ molecules. Interestingly, the mixed gas results for SLMs were not significantly different from the pure gas measurements. This could be attributed to the fact that solubility selectivity governs the membrane selectivity while the gas diffusivity selectivity remains constant for a given gas pair, which is the main difference between supported liquid and polymeric membranes (Condemarin and Scovazzo, 2009). Contrarily, with polymeric membranes, the solubility selectivity remains the same, and diffusivity selectivity governs the overall selectivity of the membrane (Camper et al., 2006). This can be explained by considering the polymer matrix swelling, which alters the diffusivity in polymeric membranes while the diffusivity selectivity performs an insignificant role in case of SLMs.

TABLE 5 | Activation energies of the PDES-SLMs.

Membrane code	Activation energy—E_a (KJ/mol)
SLM-1	4.34
SLM-2	4.3
SLM-3	4.1
SLM-4	4.04

Effect of Temperature on CO$_2$ Permeability

The CO$_2$ permeability through all SLMs is significantly affected by changing the operating temperature, as reflected in **Figure 4**. The CO$_2$ permeability exhibits Arrhenius behavior with a coefficient of determination (R^2) higher than 0.99 for all of the PDES-SLMs. It is well reported that the solubility of the CO$_2$ in the DESs decrease with the increment in temperature (Li et al., 2008). Moreover, the solubility selectivity is governing the overall performance on the SLMs. Thus, the permeability is expected to decrease with the rise in the operating temperature. However, the CO$_2$ permeability, instead of decreasing, increased on par with the temperature for all the synthesized PDESs-SLMs. On average, every SLM exhibited a rise in the CO$_2$ permeability of the order of 12 Barrer by increasing the temperature in the range of 298–338 K. The maximum increment in the CO$_2$ permeability was witnessed in the case of SLM-2 of the order of 13.2 Barrer. However, this increment in the permeability can be explained by the viscosity and molar free volume parameters. This increase in permeability can be attributed to the lowering of the viscosities of the PDESs at elevated temperatures (D'Agostino et al., 2011). Moreover, the increase in temperature increases the ionic motions in the PDESs, which in turn increases the chain mobility and the hole size of the PDESs, thereby increasing the permeability of the acid gas through the SLMs. It is a valid argument that the molar free volume of the DESs also increased at the elevated temperatures resulting in the more permeability of the penetrant gas through the SLMs (Ghaedi et al., 2017a). The increment of CO$_2$ permeability with temperature was also found to be in good agreement with the ILs literature
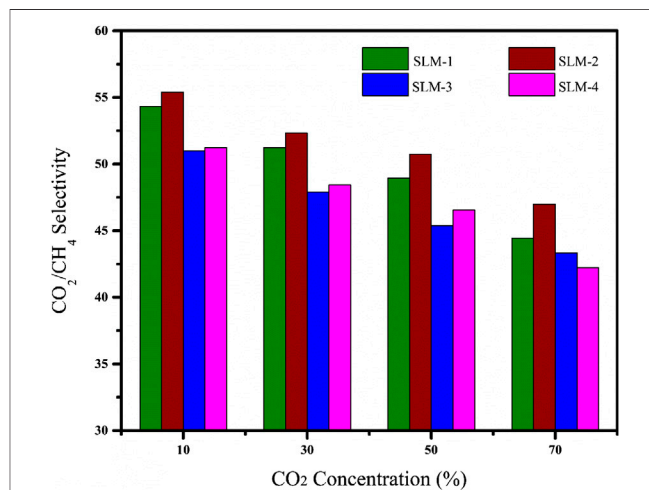
FIGURE 5 | Effect of CO$_2$ concentration in feed on CO$_2$/CH$_4$ selectivity.

FIGURE 6 | CO$_2$/CH$_4$ separation performance comparison on upper bound [61]. The chart is plotted on a log-log scale and PIL and PIL/IL membrane data taken from references (Bara et al., 2007; Bara et al., 2008a; Bara et al., 2008b; Bara et al., 2009a; Bara et al., 2009b; Tomé et al., 2013a; Tomé et al., 2013b; Carlisle et al., 2013; McDanel et al., 2014; Horne et al., 2015).
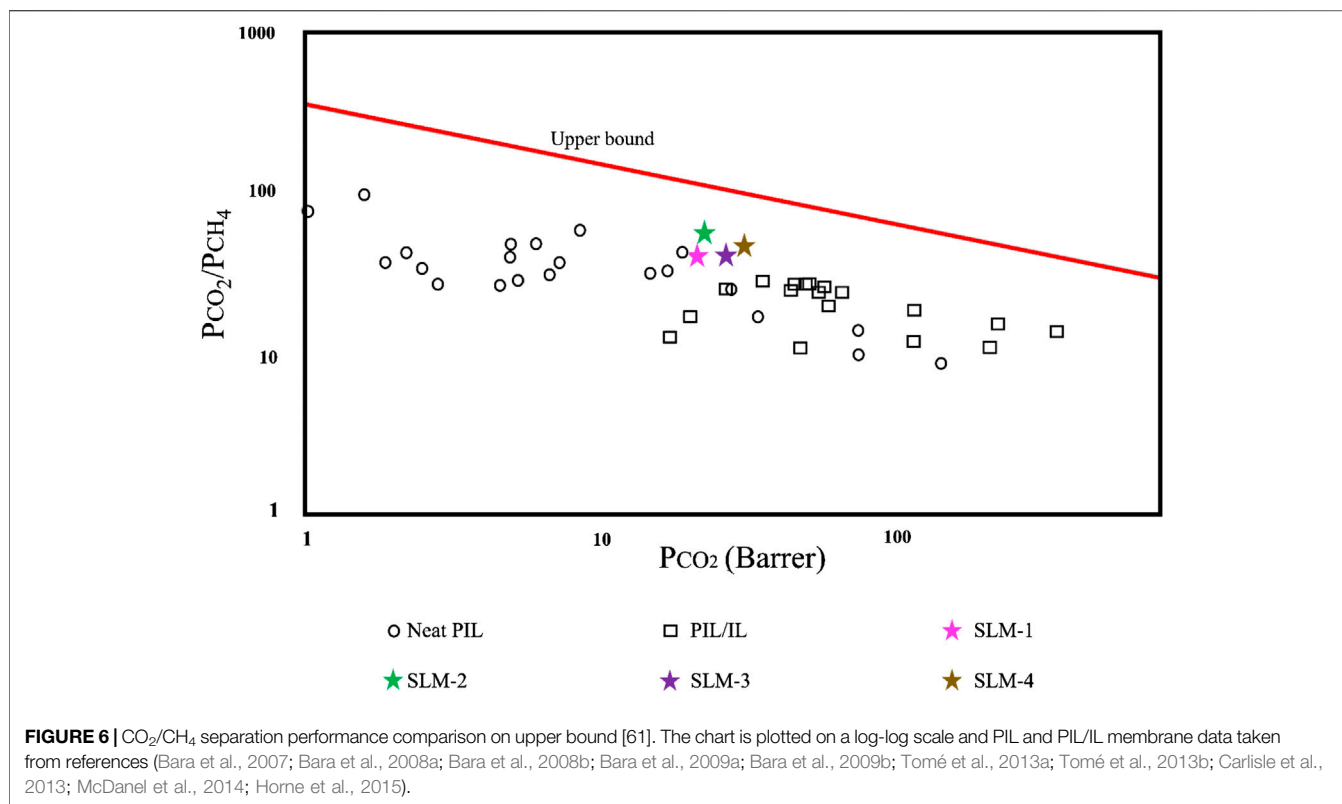
(Jindaratsamee et al., 2011; Santos et al., 2014). Therefore, the increase in temperature resulted in an increase in the CO$_2$ permeability for all PDES-SLMs.

The acid gas permeability was correlated to the feed temperature via activation energy (E_a) in the Arrhenius equation as under

$$P = P_0 \exp\left(-E_a/RT\right), \qquad (6)$$

where P CO$_2$ permeability, P_0 pre-exponential factor, R gas constant, T feed temperature.

The activation energies (E_a) of CO$_2$ permeation for all the PDESs-SLMs are listed in **Table 5**. The PDES-SLMs showed remarkably lower E_a values in the range of 4.04–4.34 kJ/mol. Interestingly, the SLMs E_a values found in this study were significantly lower than most of the reported SILMs using the same PVDF support, which exhibited the E_a values in a range of 16.55–19.37 kJ/mol (Jindaratsamee et al., 2011; Santos et al., 2014). The practical implication of this study and prolific addition to membrane literature is evident from the lower experimental E_a values of the SLMs. It can be observed from **Table 5** that the SLM-4 presented the lowest E_a value of 4.04 kJ/mol, thereby making the CO$_2$ easier to permeate through the membrane. This can be ascribed to the molar free volume and the lower viscosity of the polyacrylamide.

Effect of CO$_2$ Concentration on CO$_2$/CH$_4$ Selectivity

The CO$_2$ concentration in the feed has a significant effect on the CO$_2$/CH$_4$ selectivity, as shown in **Figure 5**. In CO$_2$/CH$_4$ pair, the

selectivity decreased by increasing the CO$_2$ concentration in the feed from 10 to 70%. The higher values of selectivity at low feed concentration is due to the relative ease of the CO$_2$ solubility and lesser possibility of matrix swelling by CO$_2$ plasticization through the PDESs. On increasing the CO$_2$ concentration from 10 to 70%, the decrease in the selectivity was not significant that supports the argument of the absence of facilitated transport. In facilitated transport, the carriers become saturated at high CO$_2$ concentration, which enormously lowers the selectivity of the given gas pairs (Bao and Trachtenberg, 2006; Iarikov and Oyama, 2011).

Comparison With PIL Based SLMs With Reported Literature

The gas performance of the synthesized PDES-SLMs and previously reported PIL membrane literature is plotted on the Robeson plot (Robeson, 2008) in **Figure 6**, which is considered as a benchmark in gauging the performance of the membranes. The Robeson plot is an illustration of ideal selectivity for a given gas pair against permeability of the permeate gas. At the same time, the upper bound line can be viewed as a target for the membrane developers to design new materials (Robeson, 2008). It can be witnessed from **Figure 6** that the prepared PDES-SLMs lie very close to the upper bound, characterized by higher selectivities and significantly high CO$_2$ permeabilities as compared to the neat PIL and PIL/IL composite membranes. Most of the reported neat PIL membranes lie on the top left side, exhibiting significant CO$_2$/CH$_4$ selectivities. The very first neat PIL membranes incorporating imidazolium cations on polystyrene and polyacrylate backbone

showed CO_2 permeability as low as nine Barrer and moderate CO_2/CH_4 selectivities from 17 to 39 (Bara et al., 2007). The second generation of the functionalized PIL membranes improved the CO_2 permeability from 8 to 14 Barrers, while reduced CO_2/CH_4 selectivity (29–37) (Horne et al., 2015). The cross-linked PIL membranes showed extremely low CO_2 permeabilities (3.8–4.4 Barrer) for low diffusivity and moderate CO_2/CH_4 selectivities (22–28) (Bara et al., 2008a). The highly permeable PIL membranes were also developed with a permeability of 130 Barrer, although CO_2/CH_4 selectivity was significantly reduced (8.7), which rendered their practical implications where high throughput is required (Carlisle et al., 2013). Conclusively, the functionalization or the variation of cation of neat PIL membranes was not sufficient to endorse the large improvement in gas permeability along with the permselectivity.

These PIL/IL composite membranes were thought to overcome the permeability drawbacks of neat PIL membranes. Incorporating the free IL in PIL matrix increased permeability by approximately 400% as compared to neat PIL membranes (Bara et al., 2008b). However, the CO_2/CH_4 selectivity was reduced to 27, with the difference of minus 25% as compared to the neat PIL membranes (Bara et al., 2008b). The functionalization of free IL with ether, fluoroalkyl, siloxane, alkyl, and nitrile exhibited increased CO_2 permeabilities (47–53 Barrer). However, the CO_2/CH_4 selectivity remained almost unaffected (Bara et al., 2009b). The PIL/IL composite having nitrile group exhibited the highest CO_2/CH_4 selectivity of 28 (Bara et al., 2009b). Besides the functionalization, the amount of free IL was also increased to 50, 60, and 75% to investigate the effect of the concentration of the PIL/IL composite on the gas performance of the membranes (McDanel et al., 2014). The highest CO_2 permeability achieved was 100 Barrer, but the CO_2/CH_4 selectivity was only up to 20. It was concluded that the increase of free IL above a certain level makes the PIL membranes similar to SILMs (McDanel et al., 2014). It is evident from **Figure 6** that the PIL/IL composite membranes also have a severe drawback of reduced selectivity, which makes them impractical in the applications where high purity streams are required.

The PDES-SLMs represents an improvement over the PIL and PIL/IL composite membranes reported in the literature. The synthesized membranes are approaching the upper bound, and systematic research can be targeted to improve the CO_2 permeability while retaining the CO_2/CH_4 selectivity. Besides, the seemingly large combinations of HBAs and HBDs and the tunable nature of the PDESs opens a wide research window in this area. The initial proof of concept for PDES-SLMs is very promising, and novel aspects of this work in synthesizing a green and low-cost substituent of PIL membranes can successfully be achieved with improved acid gas performance as compared to the competitive PIL membrane literature.

Practical Implications of This Study

The membrane technology provides an energy efficient and robust solution for environmental problems. This study focuses on resolving the low permeability and selectivity plus the environmental concerns posed by commonly used CO_2

capturers. The comparison with the previously reported neat PIL and PIL/IL membranes revealed that the novel synthesized PDES-SLM has shown significant improvement in CO_2 permeability and CO_2/CH_4 selectivity. Moreover, another limitation of the membrane based separation systems is the demand of the large surface area. This problem was successfully resolved by the use of yet another membrane module called hollow fiber membrane. The hollow fiber membrane provides a significantly high surface area to volume ratio, and using PDESs in this type of membrane is an interesting idea. This idea has been tested using IL in the hollow fiber module and conceded prolific separation results (Wickramanayake et al., 2013). However, the mechanical stability of the membrane and the drawbacks of IL and rendered the application of these membranes on a commercial scale. The biocompatibility and low cost PDES-SLM should find practical applications in CO_2 sequestering and sweetening of natural gas. The mechanical stability of the suggested membrane system could also be enhanced by applying different membrane fabrication methods and investigating the separation performance under a wide range of pressure (Kim et al., 2011). This study has investigated the novel PDES-SLMs and provided promising results. The practical application of this work would certainly be found by the encouraging idea of using the PDES based hollow fiber membranes.

CONCLUSIONS

A novel study on synthesis, characterization, and the gas separation performance of SLMs using PDESs obtained from already polymerize HBDs is presented. The homogeneous clear solution and FTIR analysis confirmed the formation of the PDESs because of strong hydrogen bonding between the HBAs and HBDs. The PDES prepared herein provided an easy and energy-efficient approach of CO_2 capture by eliminating the complex synthetic steps. The CO_2 permeability of the prepared PDES-SLMs was increased with increasing ChCl content in the PDESs. The SLMs exhibited significantly high values of CO_2 permeability and CO_2/CH_4 selectivity in gas separation experiments. The CO_2 permeability in the PDES-SLMs increased with operating temperature for a decrease in the viscosity of the PDESs at elevated temperatures. The effect of increasing CO_2 concentration in the feed gas mixture proved the absence of facilitated transport in the SLMs. The comparison of the results obtained in this work with the competing literature indicated that PDESs are promising alternatives to the PILs in the membrane-based separations. The present work is one of the very first milestones in this field of PDES based SLM for CO_2 capture. It will open a window of opportunity to design PDESs with task-specific HBD and HBA that might reduce the permeability-selectivity trade-off and surpass the upper-bound.

DATA AVAILABILITY STATEMENT

All datasets presented in this study are included in the article.

AUTHOR CONTRIBUTIONS

All authors listed have made a substantial, direct, and intellectual contribution to the work and approved it for publication.

REFERENCES

Abbott, A. P., Alabdullah, S. S., Al-Murshedi, A. Y., and Ryder, K. (2017). Brønsted acidity in deep eutectic solvents and ionic liquids. *Faraday Discuss.* 206, 365–377. doi:10.1039/C7FD00153C

Abbott, A. P., Boothby, D., Capper, G., Davies, D. L., and Rasheed, R. K. (2004). Deep eutectic solvents formed between choline chloride and carboxylic acids: versatile alternatives to ionic liquids. *J. Am. Chem. Soc.* 126 (29), 9142–9147. doi:10.1021/ja048266j

Abbott, A. P., Capper, G., Davies, D. L., Rasheed, R. K., and Tambyrajah, V. (2003). Novel solvent properties of choline chloride/urea mixtures. *Chem. Commun.* 1, 70–71. doi:10.1039/B210714G

Abbott, A. P., Harris, R. C., and Ryder, K. (2007). Application of hole theory to define ionic liquids by their transport properties. *J. Phys. Chem.* 111 (18), 4910–4913. doi:10.1021/jp0671998

Abbott, A. P., Harris, R. C., Ryder, K. S., D'Agostino, C., Gladden, L. F., and Mantle, M. D. (2011). Glycerol eutectics as sustainable solvent systems. *Green Chem.* 13 (1), 82–90. doi:10.1039/C0GC00395F

Aissaoui, T., AlNashef, I. M., Qureshi, U. A., and Benguerba, Y. (2017). Potential applications of deep eutectic solvents in natural gas sweetening for CO$_2$ capture. *Rev. Chem. Eng.* 33 (6), 523–550. doi:10.1515/revce-2016-0013

Ash, R., and Barrie, J. (1986). Time lag in diffusion. *J. Phys. Chem.* 31 (5), 1209–1218. doi:10.1021/j150547a018

Bao, L., and Trachtenberg, M. (2006). Facilitated transport of CO$_2$ across a liquid membrane: comparing enzyme, Amine, and Alkaline. *J. Membr. Sci.* 280 (1–2), 330–334. doi:10.1016/j.memsci.2006.01.036

Bara, J. E., Carlisle, T. K., Gabriel, C. J., Camper, D., Finotello, A., Gin, D. L., et al. (2009a). Guide to CO$_2$ separations in imidazolium-based room-temperature ionic liquids. *Ind. Eng. Chem. Res.* 48 (6), 2739–2751. doi:10.1021/ie8016237

Bara, J. E., Hatakeyama, E. S., Gabriel, C. J., Zeng, X., Lessmann, S., Gin, D. L., et al. (2008a). Synthesis and light gas separations in cross-linked gemini room temperature ionic liquid polymer membranes. *J. Membr. Sci.* 316 (1–2), 186–191. doi:10.1016/j.memsci.2007.08.052

Bara, J. E., Hatakeyama, E. S., Gin, D. L., and Noble, R. (2008b). Improving CO$_2$ permeability in polymerized room-temperature ionic liquid gas separation membranes through the formation of a solid composite with a room-temperature ionic liquid. *Polym. Adv. Technol.* 19 (10), 1415–1420. doi:10.1002/pat.1209

Bara, J. E., Lessmann, S., Gabriel, C. J., Hatakeyama, E. S., Noble, R. D., Gin, D. L., et al. (2007). Synthesis and performance of polymerizable room-temperature ionic liquids as gas separation membranes. *Ind. Eng. Chem. Res.* 46 (16), 5397–5404. doi:10.1021/ie0704492

Bara, J. E., Noble, R. D., and Gin, D. L. (2009b). Effect of "Free" cation substituent on gas separation performance of polymer– room-temperature ionic liquid composite membranes. *Ind. Eng. Chem. Res.* 48 (9), 4607–4610. doi:10.1021/ie801897r

Bernardo, P., Drioli, E., and Golemme, G. J. (2009). Membrane gas separation: a review/state of the art. *Ind. Eng. Chem. Res.* 48 (10), 4638–4663. doi:10.1021/ie8019032

Biczak, R., Pawłowska, B., Bałczewski, P., and Rychter, P. (2014). The role of the anion in the toxicity of imidazolium ionic liquids. *J. Hazard. Mater.* 274, 181–190. doi:10.1016/j.jhazmat.2014.03.021

Camper, D., Bara, J., Koval, C., and Noble, R. J. (2006). Bulk-fluid solubility and membrane feasibility of Rmim-based room-temperature ionic liquids. *Ind. Eng. Chem. Res.* 45 (18), 6279–6283. doi:10.1021/ie060177n

Carlisle, T. K., Wiesenauer, E. F., Nicodemus, G. D., Gin, D. L., and Noble, R. D (2013). Ideal CO$_2$/light gas separation performance of poly (vinylimidazolium) membranes and poly (vinylimidazolium)-ionic liquid composite films. *Ind. Eng. Chem. Res.* 52 (3), 1023–1032. doi:10.1021/ie202305m

Condemarin, R., and Scovazzo, P. J. C. E. J. (2009). Gas permeabilities, solubilities, diffusivities, and diffusivity correlations for ammonium-based room

temperature ionic liquids with comparison to imidazolium and phosphonium RTIL data. *Chem. Eng. J.* 147 (1), 51–57. doi:10.1016/j.cej.2008.11.015

Coninck, H., Loos, M., Metz, B., Davidson, O., and Meyer, L. (2005). IPCC special report on carbon dioxide capture and storage. New york: Cambridge University Press

Crank, J. (1975). *Mathematics of diffusion.* 2nd ed., Chap. iv. Oxford: Clarendon Press.

D'Agostino, C., Harris, R. C., Abbott, A. P., Gladden, L. F., and Mantle, M. (2011). Molecular motion and ion diffusion in choline chloride based deep eutectic solvents studied by 1 H pulsed field gradient NMR spectroscopy. *Phys. Chem. Chem. Phys.* 13 (48), 21383–21391. doi:10.1039/C1CP22554E

de Almeida Quintino, E. F. (2014). *A study about CO$_2$/CH$_4$ separation using polymeric membranes.* Rio de Janeiro: Universidade Federal do Rio de Janeiro.

Dumitrescu, A., Lisa, G., Iordan, A., Tudorache, F., Petrila, I., Borhan, A., et al. (2015). Ni ferrite highly organized as humidity sensors. *Mater. Chem. Phys.* 156, 170–179. doi:10.1016/j.matchemphys.2015.02.044

Emel'yanenko, V. N., Boeck, G., Verevkin, S. P., and Ludwig, R. (2015). Volatile times for the very first ionic liquid: understanding the vapor pressures and enthalpies of vaporization of ethylammonium nitrate. *Chem. Eur. J.* 20 (37), 11640–11645. doi:10.1002/chem.201403508

Francisco, M., van den Bruinhorst, A., and Kroon, M. (2013). Low-transition-temperature mixtures (LTTMs): a new generation of designer solvents. *Angewandte Chemie Int. Ed.* 52 (11), 3074–3085. doi:10.1002/anie.201207548

García, G., Aparicio, S., Ullah, R., and Atilhan, M. (2015). Deep eutectic solvents: physicochemical properties and gas separation applications. *Energy Fuels.* 29 (4), 2616–2644. doi:10.1021/ef5028873

Ghaedi, H., Ayoub, M., Sufian, S., Lal, B., and Shariff, A. (2017a). Measurement and correlation of physicochemical properties of phosphonium-based deep eutectic solvents at several temperatures (293.15–343.15 K) for CO$_2$ capture. *J. Chem. Thermodyn.* 113, 41–51. doi:10.1016/j.jct.2017.05.020

Ghaedi, H., Ayoub, M., Sufian, S., Shariff, A. M., Hailegiorgis, S. M., and Khan, S. N. (2017b). CO$_2$ capture with the help of Phosphonium-based deep eutectic solvents. *J. Mol. Liq.* 243, 564–571. doi:10.1016/j.molliq.2017.08.046

Horne, W. J., Andrews, M. A., Shannon, M. S., Terrill, K. L., Moon, J. D., Hayward, S. S., et al. (2015). Effect of branched and cycloalkyl functionalities on CO2 separation performance of poly (IL) membranes. *Sep. Purif. Technol.* 155, 89–95. doi:10.1016/j.seppur.2015.02.009

Iarikov, D. D., and Oyama, S. T. (2011). "Review of CO$_2$/CH$_4$ separation membranes," in *Membrane science and technology.* (New York, NY: Elsevier), 91–115.

Iarikov, D., Hacarlioglu, P., and Oyama, S. (2011). Supported room temperature ionic liquid membranes for CO$_2$/CH$_4$ separation. *Chem. Eng. J.* 166 (1), 401–406. doi:10.1016/j.cej.2010.10.060

Isik, M., Ruiperez, F., Sardon, H., Gonzalez, A., Zulfiqar, S., and Mecerreyes, D. (2016a). Innovative poly (ionic liquid) s by the polymerization of deep eutectic monomers. *Macromol. Rapid Commun.* 37 (14), 1135–1142. doi:10.1002/marc.201600026

Isik, M., Zulfiqar, S., Edhaim, F., Ruiperez, F., Rothenberger, A., Mecerreyes, D., et al. (2016b). Sustainable poly (ionic liquids) for CO$_2$ capture based on deep eutectic monomers. *ACS Sust. Chem. Eng.* 4 (12), 7200–7208. doi:10.1021/acssuschemeng.6b02137

Jiang, B., Dou, H., Zhang, L., Wang, B., Sun, Y., Yang, H., et al. (2017). Novel supported liquid membranes based on deep eutectic solvents for olefin-paraffin separation via facilitated transport. *J. Membr. Sci.* 536, 123–132. doi:10.1016/j.memsci.2017.05.004

Jindaratsamee, P., Shimoyama, Y., Morizaki, H., and Ito, A. (2011). Effects of temperature and anion species on CO$_2$ permeability and CO$_2$/N$_2$ separation coefficient through ionic liquid membranes. *J. Chem. Thermodyn.* 43 (3), 311–314. doi:10.1016/j.jct.2010.09.015

Khan, A. L., Basu, S., Cano-Odena, A., and Vankelecom, I. (2010). Novel high throughput equipment for membrane-based gas separations. *J. Membr. Sci.* 354 (1–2), 32–39. doi:10.1016/j.memsci.2010.02.069

Kim, D.-H., Baek, I.-H., Hong, S.-U., and Lee, H.-K. (2011). Study on immobilized liquid membrane using ionic liquid and PVDF hollow fiber as a support for CO_2/N_2 separation. *J. Membr. Sci.* 372 (1–2), 346–354. doi:10.1016/j.memsci.2011.02.025

Kumar, P., Choonara, Y. E., Toit, L. C. d., Modi, G., Naidoo, D., and Pillay, V. (2012). Novel high-viscosity polyacrylamidated chitosan for neural tissue engineering: fabrication of anisotropic neurodurable scaffold via molecular disposition of persulfate-mediated polymer slicing and complexation. *Int. J. Mol. Sci.* 13 (11), 13966–13984. doi:10.3390/ijms131113966

Li, X., Hou, M., Han, B., Wang, X., and Zou, L. (2008). Solubility of CO_2 in a choline chloride+ urea eutectic mixture. *J. Chem. Eng. Data.* 53 (2), 548–550. doi:10.1021/je700638u

Ma, C., Xie, Y., Ji, X., Liu, C., and Lu, X. (2018). Modeling, simulation and evaluation of biogas upgrading using aqueous choline chloride/urea. *Appl. Energy.* 229, 1269–1283. doi:10.1016/j.apenergy.2017.03.059

Malik, M. A., Hashim, M. A., and Nabi, F. (2011). Ionic liquids in supported liquid membrane technology. *Chem. Eng. J.* 171 (1), 242–254. doi:10.1016/j.cej.2011.03.041

McDanel, W. M., Cowan, M. G., Carlisle, T. K., Swanson, A. K., Noble, R. D., and Gin, D. (2014). Cross-linked ionic resins and gels from epoxide-functionalized imidazolium ionic liquid monomers. *Polymer* 55 (16), 3305–3313. doi:10.1016/j.polymer.2014.04.039

Meine, N., Benedito, F., and Rinaldi, R. (2010). Thermal stability of ionic liquids assessed by potentiometric titration. *Green Chem.* 12 (10), 1711–1714. doi:10.1039/C0GC00091D

Mota-Morales, J. D., Gutiérrez, M. C., Ferrer, M. L., Sanchez, I. C., Elizalde-Peña, E. A., Pojman, J. A., et al. (2013). Deep eutectic solvents as both active fillers and monomers for frontal polymerization. *J. Polym. Sci. Part A: Polym. Chem.* 51 (8), 1767–1773. doi:10.1002/pola.26555

Pan, H., Liu, Y., Xia, Q., Zhang, H., Guo, L., Li, H., et al. (2020). Synergetic combination of a mesoporous polymeric acid and a base enables highly efficient heterogeneous catalytic one-pot conversion of crude Jatropha oil into biodiesel. *Green Chem.* 22 (5), 1698–1709. doi:10.1039/C9GC04135D

Peng, Y., Li, Y., Ban, Y., Jin, H., Jiao, W., Liu, X., et al. (2014). Metal-organic framework nanosheets as building blocks for molecular sieving membranes. *Science* 346 (6215), 1356–1359. doi:10.1126/science.1254227

Pham, T. P. T., Cho, C.-W., and Yun, Y.-S. (2010). Environmental fate and toxicity of ionic liquids: a review. *Water Res.* 44 (2), 352–372. doi:10.1016/j.watres.2009.09.030

Ren'ai, L., Zhang, K., Chen, G., Su, B., Tian, J., He, M., et al. (2018). Green polymerizable deep eutectic solvent (PDES) type conductive paper for origami 3D circuits. *Chem. Commun.* 54 (18), 2304–2307. doi:10.1039/C7CC09209A

Robeson, L. M. (2008). The upper bound revisited. *J. Membr. Sci.* 320 (1–2), 390–400. doi:10.1016/j.memsci.2008.04.030

Santos, E., Albo, J., and Irabien, A. (2014). Acetate based supported ionic liquid membranes (SILMs) for CO_2 separation: influence of the temperature. *J. Membr. Sci.* 452, 277–283. doi:10.1002/cssc.201600987

Sarmad, S., Mikkola, J. P., and Ji, X. (2017). Carbon dioxide capture with ionic liquids and deep eutectic solvents: a new generation of sorbents. *Chem. Sust. Chem.* 10 (2), 324–352. doi:10.1002/cssc.201600987

Scovazzo, P. (2009). Determination of the upper limits, benchmarks, and critical properties for gas separations using stabilized room temperature ionic liquid membranes (SILMs) for the purpose of guiding future research. *J. Membr. Sci.* 343 (1–2), 199–211. doi:10.1016/j.memsci.2009.07.028

Shen, Y., and Hung, F. (2017). A molecular simulation study of carbon dioxide uptake by a deep eutectic solvent confined in slit nanopores. *J. Phys. Chem. C* 121 (44), 24562–24575. doi:10.1021/acs.jpcc.7b07315

Shen, Z., Cai, Q., Yin, C., Xia, Q., Cheng, J., Li, X., et al. (2020). Facile synthesis of silica nanosheets with hierarchical pore structure and their amine-functionalized composite for enhanced CO_2 capture. *Chem. Eng. Sci.* 217, 115528. doi:10.1016/j.ces.2020.115528

Smith, E. L., Abbott, A. P., and Ryder, K. S. (2014). Deep eutectic solvents (DESs) and their applications. *Chem. Rev.* 114 (21), 11060–11082. doi:10.1021/cr300162p

Songolzadeh, M., Soleimani, M., Takht Ravanchi, M., and Songolzadeh, R. J. (2014). Carbon dioxide separation from flue gases: a technological review emphasizing reduction in greenhouse gas emissions. *Sci. World J.* 2014, 1–14. doi:10.1155/2014/828131

Tomé, L. C., Aboudzadeh, M. A., Rebelo, L. P. N., Freire, C. S., Mecerreyes, D., and Marrucho, I. (2013a). Polymeric ionic liquids with mixtures of counter-anions: a new straightforward strategy for designing pyrrolidinium-based CO_2 separation membranes. *J. Mater. Chem.* 1 (35), 10403–10411. doi:10.1039/C3TA12174G

Tomé, L. C., Mecerreyes, D., Freire, C. S., Rebelo, L. P. N., and Marrucho, I. (2013b). Pyrrolidinium-based polymeric ionic liquid materials: new perspectives for CO_2 separation membranes. *J. Membr. Sci.* 428, 260–266. doi:10.1016/j.memsci.2012.10.044

Trivedi, T. J., Lee, J. H., Lee, H. J., Jeong, Y. K., and Choi, J. W. (2016). Deep eutectic solvents as attractive media for CO_2 capture. *Green Chem.* 18 (9), 2834–2842. doi:10.1039/C5GC02319J

Tuinier, M., van Sint Annaland, M., Kramer, G. J., and Kuipers, J. (2010). Cryogenic CO_2 capture using dynamically operated packed beds. *Chemical Engineering Science* 65 (1), 114–119. doi:10.1016/j.ces.2009.01.055

Uchytil, P., Schauer, J., Petrychkovych, R., Setnickova, K., and Suen, S. (2011). Ionic liquid membranes for carbon dioxide–methane separation. *J. Membr. Sci.* 383 (1–2), 262–271. doi:10.1016/j.memsci.2011.08.061

Ullah, R., Atilhan, M., Anaya, B., Khraisheh, M., García, G., ElKhattat, A., et al. (2015). A detailed study of cholinium chloride and levulinic acid deep eutectic solvent system for CO_2 capture via experimental and molecular simulation approaches. *Phys. Chem. Chem. Phys.* 17 (32), 20941–20960. doi:10.1039/C5CP03364K

Wang, M., Lawal, A., Stephenson, P., Sidders, J., and Ramshaw, C. J. (2011). Post-combustion CO_2 capture with chemical absorption: a state-of-the-art review. *Chem. Eng. Res. Des.* 89 (9), 1609–1624. doi:10.1016/j.cherd.2010.11.005

Wickramanayake, S., Hopkinson, D., Myers, C., Sui, L., and Luebke, D. (2013). Investigation of transport and mechanical properties of hollow fiber membranes containing ionic liquids for pre-combustion carbon dioxide capture. *J. Membr. Sci.* 439, 58–67. doi:10.1016/j.memsci.2013.03.039

Yue, D., Jia, Y., Yao, Y., Sun, J., and Jing, Y. (2012). Structure and electrochemical behavior of ionic liquid analogue based on choline chloride and urea. *Electrochim. Acta.* 65, 30–36. doi:10.1016/j.electacta.2012.01.003

Zhang, Q., Vigier, K. D. O., Royer, S., and Jerome, F. (2012). Deep eutectic solvents: syntheses, properties and applications. *Chem. Soc. Rev.* 41 (21), 7108–7146. doi:10.1039/C2CS35178A

Zhang, Y., Ji, X., and Lu, X. (2018). Choline-based deep eutectic solvents for CO_2 separation: review and thermodynamic analysis. *Renew. Sust. Energy Rev.* 97, 436–455. doi:10.1016/j.rser.2018.08.007

Check for updates

Comparative Technoeconomic Analysis of Using Waste and Virgin Cooking Oils for Biodiesel Production

Eslam G. Al-Sakkari [1]*, Mohammed G. Mohammed [1,2], Alaaeldin A. Elozeiri [1], Omar M. Abdeldayem [1,3], Mahmoud M. Habashy [1,3], Ee Shen Ong [3], Eldon R. Rene [3], Ibrahim Ismail [1†] and Ibrahim Ashour [1,4]

[1] Environmental Engineering Program, Zewail City of Science and Technology, Giza, Egypt, [2] Chemical Engineering Department, Faculty of Engineering, Cairo University, Giza, Egypt, [3] Department of Environmental Engineering and Water Technology, UNESCO-IHE Institute for Water Education, Delft, Netherlands, [4] Chemical Engineering Department, Faculty of Engineering, Minia University, El-Minia, Egypt

This study aims to provide the technoeconomic aspects of two clean processes for biodiesel production. The first process utilizes waste cooking oil as a feedstock and potassium hydroxide as a homogeneous catalyst. The second process uses cement kiln dust heterogeneous catalyst and virgin soybean oil. A comparison was performed between the results of the technical and economic assessments to determine the more feasible process. Theoretical purities of biodiesel and glycerol obtained upon conducting the simulation of both processes are high, i.e., 99.99%. However, the homogeneous process is economically superior as its payback period is slightly more than 1 year while the return on investment is higher than 74%, and the unit production cost is USD 1.067/kg biodiesel. Sensitivity analysis revealed that the profitability of biodiesel production is very sensitive to the feedstock price and recommends shifting toward waste vegetable oils as a cheap feedstock to have a feasible and economic process.

Keywords: biodiesel, waste cooking oil, cement kiln dust, technoeconomic study, sensitivity analysis

HIGHLIGHTS

- Waste cooking oil (WCO) and cement kiln dust (CKD) were used for biodiesel production
- Comparative technoeconomic analysis was done for two biodiesel production processes
- Homogeneous technology using WCO was a more feasible path for biodiesel production
- Biodiesel production profitability is very sensitive to the price of the feedstock

INTRODUCTION

The transportation sector is considered to be a key contributor to climate change threats, with 24% of global carbon dioxide (CO_2) emissions in 2016 (International Energy Association, 2018, CO_2 Emissions from Fuel Combustion 2018 Highlights). Between 1990 and 2016, the carbon footprint of this sector increased by 71% (Hosking et al., 2011). The land transport is estimated to consume around 80% of the whole transportation energy, where the light-duty vehicles are the highest consumers followed by the freight trucks (WHO, 2012; health cobenefits of climate change mitigation-transport sector). Long-lived CO_2 emission and short-lived black carbon (BC) are the main contributors to climate change from the transportation sector (Brewer, 2019). It is estimated

that 19% of the global BC emissions are released from the transportation sector, specifically diesel vehicles (Helmers et al., 2019). Although the BC persists in the atmosphere for a few weeks only, its greenhouse effect is more impactful than CO_2. Besides climate change, air pollutants emitted by diesel vehicles represent a threat to human health and the environment (Reche et al., 2015; Yang et al., 2019).

The replacement and/or adaptation of biodiesel over conventional diesel are in alignment with several sustainable development goals such as climate action and sustainable cities and communities (United Nations, 2015. Sustainable Development Knowledge Platform). Hence, several governments and organizations adapted several green policies to use a considerable percentage of biofuels along with conventional fossil fuels to decrease their environmental impacts (Baena-Moreno et al., 2020). Biodiesel has been recognized recently as an environmental replacement for conventional petroleum diesel as it is associated with less environmental impacts (Živković and Veljković, 2018). For instance, it was found that biodiesel blend (B20: a mixture of 20% biodiesel and 80% petroleum diesel) is less opaque and produces less hydrocarbon and carbon monoxide emissions than petroleum diesel (Abed et al., 2019; Raman et al., 2019). Biodiesel is a monoalkyl ester of long-chain fatty acids that can be produced from renewable biological feedstock: vegetable oils, nonedible oils, animal fats, or waste oils (Al-Sakkari et al., 2017b; Dhawane et al., 2019). Different edible oils were used for biodiesel production such as soybean oil, rapeseed oil, and palm oil (Lam and Lee, 2011; Colombo et al., 2019; Essamlali et al., 2019; Raman et al., 2019). However, waste vegetable cooking oil and nonedible oils are more promising as a feedstock due to their low cost compared to edible ones (Mardhiah et al., 2017). Interestingly, many nonedible seed oils were found to be suitable for biodiesel synthesis such as *Jatropha curcas*, *Ricinus communis*, *Madhuca indica*, and *Pongamia pinnata* oils (Arumugam and Ponnusami, 2019; Elango et al., 2019; Awais et al., 2020; Kaur and Bhaskar, 2020).

Biodiesel is commonly produced from oils through transesterification reaction (also called alcoholysis reaction) (Moazeni et al., 2019). In the transesterification reaction, triglycerides in oils and fats react with alcohol to form biodiesel and glycerol (GLC) (Tapanwong and Punsuvon, 2019) as shown in **Figure 1**. Methanol (MeOH) is usually used due to its availability and low price. The produced biodiesel from the reaction of oils and MeOH is fatty acid methyl ester. Ethanol is used for biodiesel production in countries where its price is lower than that of MeOH such as Brazil (Mączyńska et al., 2019). Transesterification reaction is reversible; therefore, excess alcohol is added (usually 1.6 times the stoichiometric amount) to enhance the forward reaction and increase the conversion (Zaharudin et al., 2018; Banerjee et al., 2019).

In commercial processes, the reaction is performed in the presence of a catalyst to speed up the reaction (El-Sheltawy and Al-Sakkari, 2016). Commonly used catalysts are acidic, alkaline (which can be homogeneous or heterogeneous), or enzyme catalysts (Gollakota et al., 2019; Li et al., 2019; Moazeni et al., 2019). Alkaline homogeneous catalysts such as sodium and potassium hydroxide are used for the commercial production of biodiesel from feedstocks having concentrations of free fatty acids (FFA) below 2%. Those alkaline catalysts cannot be used

for higher FFA concentration because saponification reaction takes place as a side reaction as shown in **Eq. 1** (El Sheltawy et al., 2019). Saponification reaction does not consume the catalyst only but also produces a soap that acts as an emulsifier and makes separating biodiesel from GLC very difficult (Chanakaewsomboon et al., 2020).

Low-cost feedstocks are usually rich in FFA (Al-Sakkari et al., 2020); therefore, acid pretreatment is necessary to promote the esterification of FFA in the presence of acid or enzyme catalyst according to **Eq. 2** (Hosney et al., 2020). Enzyme catalysts lead to higher reaction rates than acid catalysts; however, they are unpractical to use in industrial scale due to their high price (Tabatabaei et al., 2019; Urbain et al., 2019). Transesterification reaction can be performed without a catalyst in supercritical conditions however, it is not economically feasible since these conditions require high utility costs (Kumar et al., 2020).

$$FFA + NaOH \rightarrow soap + water \qquad (1)$$

$$FFA + MeOH \overset{H_2SO_4}{\Rightarrow} FAME + water \qquad (2)$$
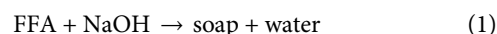
Biodiesel production is a rewarding process that is expected to be profitable at a large scale (Gebremariam and Marchetti, 2018b). Hence, detailed technoeconomic studies are essential to prove its feasibility and sensitivity to changes in market prices. Previous technoeconomic studies have been performed to compare the feasibility of biodiesel production processes from various feedstocks such as single-cell oils and acidic oils using different catalysts at different production capacities (Gebremariam and Marchetti, 2018a; Gebremariam and Marchetti, 2019; Parsons et al., 2019). The comparison is based on economic factors such as return on investment (ROI), net present value (NPV), and payback time. Additionally, sensitivity analysis of these factors as a function of expected changes in raw materials and products' price is also taken into considerations.

This study aims to present a technoeconomic study on two processes for biodiesel production. The first process uses waste cooking oil in the presence of KOH as a homogeneous catalyst which is the conventional biodiesel production method. The second process uses virgin soybean oil in the presence of a newly developed cement kiln dust (CKD) heterogeneous catalyst (Al-Sakkari et al., 2017a). It should be mentioned that the price of waste cooking oil in this study is related to the Egyptian market, yet the study is still applicable and valid to be applied globally.

METHODOLOGY

Summary of Process Designs
The present homogeneous process was first presented by Al-Sakkari et al. (2018a). In contrast, the heterogeneous process was presented in the study of El-Sheltawy et al. (2016). **Figures 2** and **3** show the process flow diagrams of the homogeneously and heterogeneously catalyzed processes, respectively. **Table 1** summarizes the equipment used in each PFD. The detailed process flow diagrams are mentioned in **Supplementary Materials**.
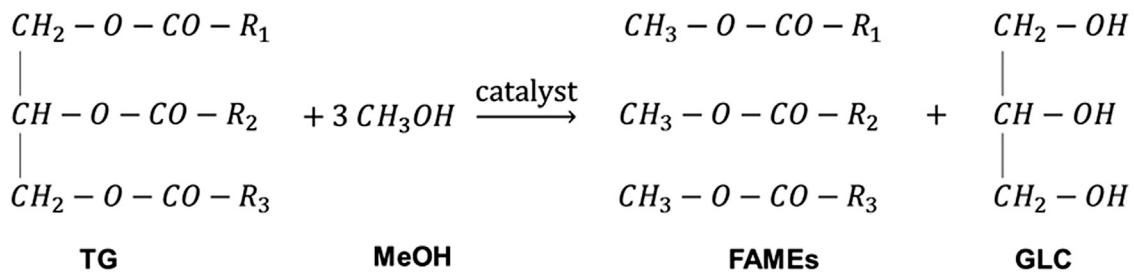
FIGURE 1 | Transesterification reaction for biodiesel production. R_1, R_2, and R_3 are long-chain hydrocarbon/fatty acids.
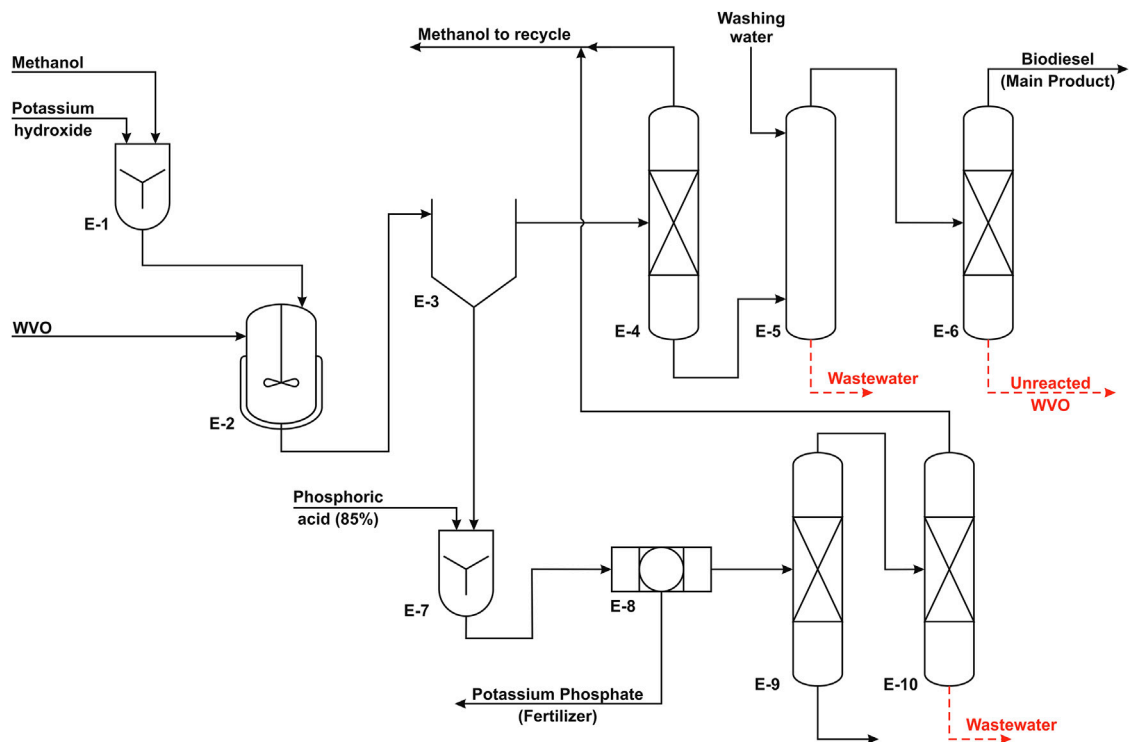
FIGURE 2 | Process flow diagram of the homogeneous process (adapted from Al-Sakkari et al., 2018a).

In the homogeneous process, the feedstock is waste vegetable oil (WVO) with low FFA content, and the catalyst is potassium hydroxide. On the other side, the catalyst in the heterogeneous process is calcined cement kiln dust (CCKD) particles in micron scale, and the feedstock is virgin soybean oil. MeOH is used for the alcoholysis purpose in both cases.

Summary Design of the Homogenous Process
Process Description
The suggested process for biodiesel production includes three major units. The first is the production unit where methyl ester (biodiesel) is produced from the reaction of waste vegetable oil with MeOH in the presence of KOH catalyst. In the second unit,

the reactor effluent is fed to a gravity separator (decanter) to separate biodiesel (light layer) from GLC (heavy layer). This separation is followed by the biodiesel purification unit where crude biodiesel is distilled and water washed until its purity matches the ASTM D6751 standards. The last unit is the GLC purification unit, where crude GLC is treated with phosphoric acid to remove the catalyst and produce potassium phosphate as a by-product and then distilled in two columns to separate GLC from MeOH that is recycled to the reaction unit.

Biodiesel Production Unit
In this production unit, biodiesel is being produced according to the optimal conditions that have been investigated earlier in an

FIGURE 3 | Process flow diagram of the heterogeneous process (adapted from El-Sheltawy et al., 2016).
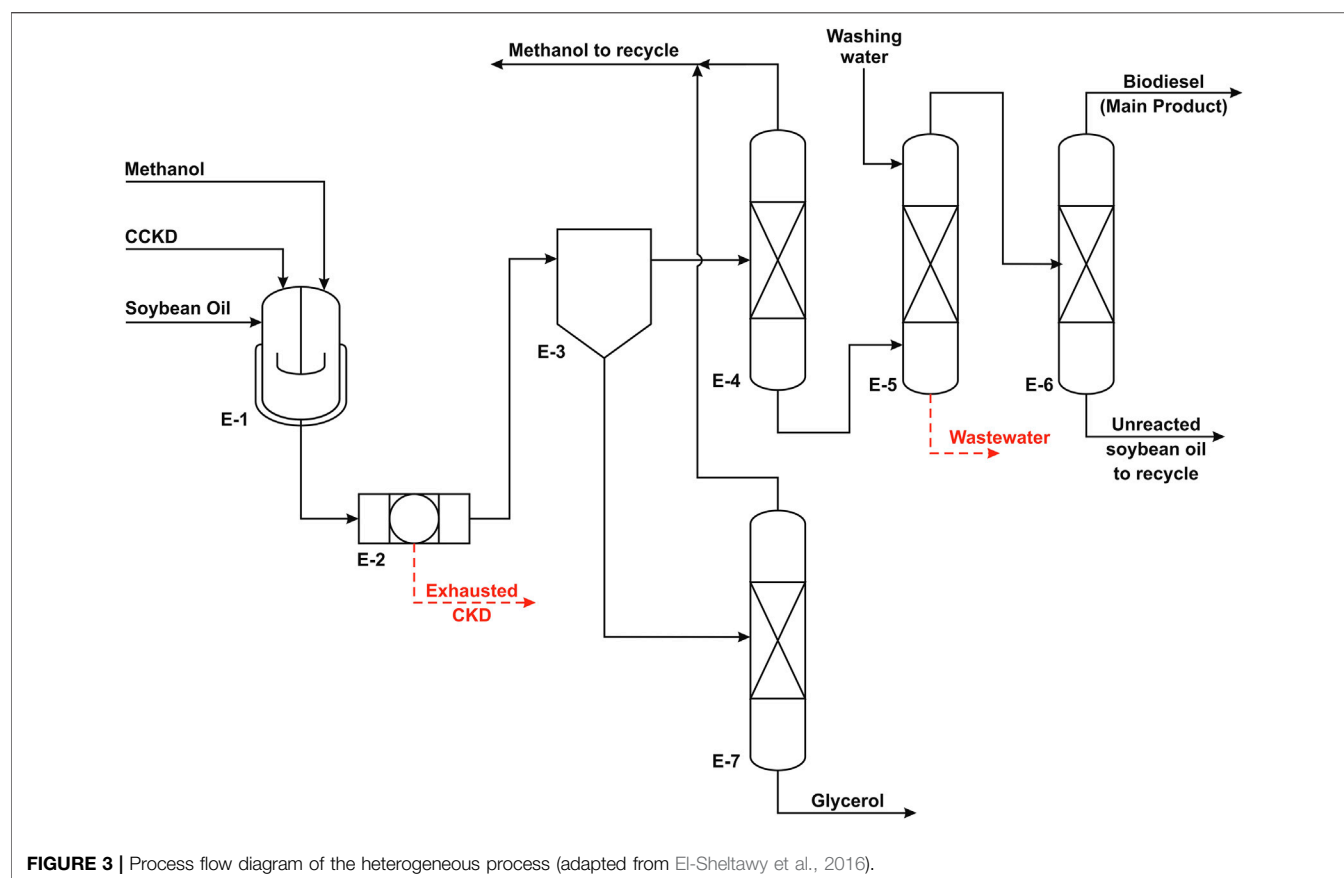
TABLE 1 | Summary of process equipment used in the homogenous and heterogeneous processes.

Homogeneous process		Heterogeneous process	
Code	Equipment	Code	Equipment
E-1	Mixer	E-1	Reactor
E-2	Reactor	E-2	Filter
E-3	Settler	E-3	Settler
E-4	Methanol distillation column 1	E-4	Methanol distillation column
E-5	Washing vessel	E-5	Washing vessel
E-6	Biodiesel distillation column	E-6	Biodiesel distillation column
E-7	Neutralizer	E-7	Glycerol distillation column
E-8	Filter	—	—
E-9	Glycerol distillation column	—	—
E-10	Methanol distillation column 2	—	—

experimental study (Al-Sakkari et al., 2018b). The suggested process is carried out in an isothermal batch reactor at 65°C while using MeOH to oil molar ratio of 6 : 1 and KOH as a catalyst with the loading of 1 weight % of WVO with a reaction time of 1 h. The optimum agitation speed that was reached during the experimental study was ~400 rpm; however, this value should be adjusted on scaling up to confirm the constant mass transfer rate. The reaction conversion is 95% under the mentioned conditions. It is possible to make the process more energy efficient by using the reactor

effluent stream to heat the feed to the reactor. This will reduce the temperature of the effluent stream, which enhances the separation efficiency of GLC and biodiesel layers in the decanter. The decanter is designed to have a residence time of 12 h to ensure efficient separation.

Biodiesel Purification Unit

The aim of this unit is the removal of MeOH and unreacted WVO from biodiesel to meet ASTM D6751 standards. The residual MeOH associated with the biodiesel layer is removed by distillation where MeOH is produced as a top product. The removed MeOH is recycled to the MeOH tank to reduce any potential process losses. It was found that the MeOH content in this biodiesel layer is ~2–3 wt%. The bottom products are directed to a washing vessel to wash out any traces of MeOH, GLC, soaps, and catalyst residues using warm demineralized washing water. A coalescer is attached to that vessel to produce a top product clear from water contaminations. GLC washing should be performed under laminar flow conditions at relatively high temperature, e.g., 80°C. After that, a vacuum distillation column is used to remove any unreacted oil. Vacuum conditions are used to avoid any thermal cracking of biodiesel and the unreacted oil. Finally, the purified biodiesel is pumped and injected using some additives such as TBHQ in a well-insulated storage tank to increase biodiesel stability and

reduce/eliminate oxidation during storage. The additives are commonly added at 1 wt% of biodiesel as recommended by Chakraborty and Baruah (2012) and Dwivedi et al. (2018).

Glycerol Purification Unit

This unit produces high purity GLC from the crude GLC layer that is composed of GLC (around 50%), potassium hydroxide, and FFA. This is achieved first by neutralizing potassium hydroxide using commercial phosphoric acid to produce potassium phosphate that is a by-product (e.g. fertilizer). During potassium hydroxide neutralization, FFA are separated spontaneously as a separate phase on the surface of GLC that is skimmed and removed later. After neutralization, the purity of the produced GLC increases to around 80%. Afterward, crude GLC is pumped to an atmospheric distillation column to wash out any excess MeOH as well as contaminated water to produce high-grade GLC that is cooled and stored at ambient temperature. The aqueous phase from atmospheric distillation is fed to another distillation column to recover the excess MeOH used in the reaction and reuse it in the reaction.

Summary Design of Heterogeneous Process

The heterogeneous process consists of three main units: the biodiesel production unit, the biodiesel purification unit, and the GLC purification unit. Each process is described briefly in the following sections.

Biodiesel Production

The biodiesel production reaction is carried out at 65°C in an isothermal batch reactor. MeOH is loaded into the reactor at a rate of 12 mol MeOH/mol oil followed by the addition of the catalyst, CKD. The CKD loading is 3.5% of the weight of oil to ensure high reaction conversion. The reaction takes place in two sequential cycles with 6 h of total reaction time. Under such operating condition, the conversion is estimated to be approximately 51%. The reactor effluent is filtered in a filter press to remove all the solid catalyst from the mixture. The separation results in two separate layers that will be purified to produce high purity biodiesel and GLC.

Biodiesel Purification

Biodiesel layer purification involves three steps. First, the extra MeOH which accounts for around 3% of the mixture is recovered using distillation and reused in the reaction. The MeOH-free mixture is washed using the same volume of freshwater in a washing vessel to remove any MeOH traces and GLC content as well as suspended catalyst resides or leached oxide if present. The washing vessel is equipped with a coalescer to remove any water droplets. The flow in the washing vessel is ensured to be laminar to prevent emulsification and facilitate the separation of used washing water. Finally, the ester stream is transferred to a vacuum distillation column to separate the purified fraction from the unreacted oil. The biodiesel is produced as a top product that is cooled and pumped to storage tanks.

Glycerol Purification

The GLC layer stream is fed to a distillation unit to extract the excess MeOH that is recycled to the reaction. The bottom product from the GLC purification column is nearly pure and clear of any dissolved solids and suspended catalyst residues. It is cooled and pumped to storage tanks.

Cost Estimation

The economic study starts with an estimation of the fixed cost, production cost, and the profit achieved for both processes. The two processes are then compared according to their economic feasibility based on a biodiesel production rate of 24,000 kg/day. Moreover, it includes a study of the economic sensitivity of both processes to the factors that have the most significant impact on their profitability.

Cost estimation was studied based on the cost for capital, equipment, raw materials, operation, utilities, and labor according to literature (Gebremariam and Marchetti, 2018a) and the current market price in Egypt. For estimating the purchased cost of equipment (PCE), we used the method developed by Peters and Timmerhaus (Peters et al., 2003) with the chemical engineering plant cost index 591.34 for the year 2018 (Jenkins, 2019). **Table 2** summarizes all the estimated costs included in the physical plant cost (PPC) for both processes; the estimation of these prices was performed as suggested by the reference mentioned earlier. **Table 2** also includes indirect plant costs and fixed and working capital investments for both processes. The total capital investment shows that the homogeneous process requires capital investment 39% less than that of the heterogeneous process.

The total production cost includes variable and fixed charges. Variable charges represent the expenses associated with the manufacturing process such as the costs of required raw materials, utilities, shipping, and labor. The raw materials' market price demand of each raw material for the homogeneous and heterogeneous processes and the total expected raw materials' costs are summarized in **Table 3**. Required utilities such as cooling water, steam, and their costs for each process were calculated separately. The total labor cost is calculated for 330 annual working days using the average hourly labor cost in Egypt, for the year 2018 (Egypt Minimum Monthly Wages). Fixed charges represent the charges that do not change considerably from year to year and are not associated with the manufacturing process such as depreciation, taxes, and insurance. Fixed charges were calculated according to the procedure suggested by Peters and Timmerhaus (Peters et al., 2003).

Breakeven Point

The basic idea of breakeven point analysis is to plot the production expenses, sales, and revenues against the percentage of full production capacity in order to determine the point at which both production expenses and sales are equal, and hence the revenues are zero. This point is called the breakeven point. Expenses, sales, and revenues are first calculated at different percentages of full production capacity, i.e., 0 and 10% till reaching 100%, and are plotted against the corresponding percentages to determine the zero-revenue point, i.e., breakeven point. It should be noticed that the lower the point is, the more profitable and feasible the process is.

TABLE 2 | Detailed calculations of the physical plant costs, indirect plant costs, and the total capital investments of the homogeneous and heterogeneous processes.

Expense category	Estimation basis	Cost in $	
		Homogeneous process	Heterogeneous process
Purchase cost of equipment (PCE)	—	$829,819	$1,365,208
Installation	40% of PCE	$331,928	$546,083
Piping	70% of PCE	$580,874	$955,645
Instrumentation	20% of PCE	$165,964	$273,042
Electrical	10% of PCE	$82,982	$136,521
Buildings	15% of PCE	$124,473	$204,781
Utilities	5% of PCE	$414,910	$682,604
Storage	15% of PCE	$124,473	$204,781
Site development	10% of PCE	$82,982	$136,521
Auxiliary building	15% of PCE	$124,473	$204,781
Physical plant cost (PPC)	—	$2,862,877	$4,709,967
Engineering and design	30% of PPC	$858,863	$1,412,990
Contractor's fee	5% of PPC	$143,144	$235,498
Contingency	10% of PPC	$286,288	$470,997
Indirect plant cost (IPC)	—	$1,288,295	$2,119,485
Fixed capital investment (FCI)	PPC + IPC	$4,151,172	$6,829,452
Working capital investment (WCI)	5% of TCI	$218,483	$359,445
Total capital investment (TCI)	FCI + WCI	$4,369,655	$7,188,897

TABLE 3 | Market costs, annual consumptions, and total cost of raw materials for the homogeneous and heterogeneous processes.

Raw material	Cost ($/kg)	Homogeneous process		Heterogeneous process	
		Consumption (106 kg/year)	Cost (10^5 $/year)	Consumption (106 kg/year)	Cost (10^5 $/year)
Methanol	0.45	0.922	4.15	0.845	3.8
Used oil	0.50	8.64	43.2	0	0
Potassium hydroxide	1.00	0.0864	0.864	0	0
Phosphoric acid	1.90	0.0586	1.11	0	0
Water	0.0011	15.8	0.174	15.8	0.174
Fresh oil	1.00	0	0	7.92	79.2

Sensitivity Analysis

In this study, the focus was profitability to the change (increase and decrease) in raw materials and products' prices. The effect of changing the prices on the interest rate of return (IRR) at which the NPV of the project equals zero was studied. The calculated values of IRR are plotted against the percentage change of prices of both the products and the raw materials. Furthermore, they are compared to the interest rate (IR) value of 10% to check on the profitability of the process. The process is considered feasible and profitable if the IRR is greater than IR.

RESULTS AND DISCUSSION

Process Designs
Material and Energy Balance of the Homogeneous Process

The material and energy balance calculations were performed using Aspen Plus software (Thermodynamic model was NRTL General). **Supplementary Appendix S1** summarizes the material and energy balance calculation results of the proposed process. It

can be observed that the highest flow rates were for the inlet and outlet streams of the batch reactor compared to other streams. These high flow rates result from the short time taken for charging and discharging the batch reaction processes. Also, water traces in the recycled MeOH that come from the GLC purification unit are eliminated to avoid any water accumulation in the system, which is harmful to the transesterification reaction. Water removal can be achieved by adsorption instead of distillation for small flow rates.

Summary of Material and Energy Balances of the Heterogeneous Process

From the experimental results, the oil conversion at the assigned conditions is 51%; hence the daily amount of oil required for a biodiesel production rate of 24 ton/day is 47 tons. Catalyst loading is 1.65 tons which correspond to 3.5 wt% of the total oil introduced, and the MeOH loading rate into the reactor is 19 ton/day to match the specifications mentioned earlier. The summary of operating conditions and composition of each stream of the processes is available in **Supplementary Appendix S2**.

The flow rates of streams S-1 to S-5 may appear to be larger than other streams as they serve as the point of charging and

discharging the biodiesel batch reactors. After cooling, the excess MeOH and unreacted oil are recycled to enhance the process profitability. Besides, the cost of heating and cooling is minimized by heat integration, such as using wastewater from the biodiesel washing step for heating the batch reactor.

Cost Estimation

Total production cost was calculated based on the fixed and variable production costs for both processes and was found to be 8.45 million dollars for the homogenous process and 14.81 million dollars for the heterogeneous process. **Table 4** shows the total annual production and sales of the main and side products of the homogeneous and heterogeneous processes; the results indicate that both processes seem to achieve the same annual profit. However, for profitability, indicators were calculated to compare the economic feasibility of both processes: annual gross profit, annual net profit, payback period, and ROI. The values and the method of calculation of the indicators are shown in **Table 5**; these indicators show that the heterogeneous process is economically infeasible in contrary to the homogeneous process. Based on **Tables 2** and **3**, the heterogeneous process is unprofitable due to the high cost of fresh oil used and the high costs of large equipment used to separate the solid catalyst after the reaction.

The profitability study recommends the homogeneous process over the heterogeneous process. Further analysis of the economic feasibility is done and presented in the sensitivity analysis section.

Breakeven Point Analysis

Breakeven point analysis was performed for both processes. The heterogeneous process was found to be unprofitable due to high fixed charges as well as using expensive feedstock; therefore, it has no breakeven point as indicated from **Figure 4B**. These results are in alignment with the previously mentioned results (*Cost Estimation*). However, in the case of a homogeneous process, **Figure 4A** depicts a breakeven point at about 30% of the full capacity. This finding indicates a highly profitable process for biodiesel production.

Sensitivity Analysis

In this section, the sensitivity of the process profitability to the change of raw materials and products' prices are presented. It was found that the processes are very sensitive to the prices of feedstock oil and the main product "biodiesel." The process profitability is not sensitive to changes in prices of other materials and utilities when compared to the prices of oil and biodiesel. In this study, it was assumed that the plant would work at full capacity for 10 years after installation and startup periods which would take 6 months each. Discount cumulative cash flow diagrams (**Figures 5A,B**) are used as preliminary indicators to compare the profitability of both processes over the project lifetime.

From **Figures 4** and **5**, it can be concluded that the homogeneous process is profitable since the payback period is about 1.07 years. This can be attributed to the utilization of relatively cheap feedstock besides operating at mild reaction conditions, i.e., MeOH to oil molar ratio of 6 : 1, reaction temperature of 65°C, and 1% catalyst loading. Moreover, the obtained conversion is high, i.e., 95%, in a shorter reaction time

of about 1 h compared to the heterogeneous process. These conditions also affect the whole profitability positively by decreasing the load on the following separation equipment. In contrast, the heterogeneous process is unprofitable at its current state. The process profitability can be enhanced by using WVO as a feedstock instead of the expensive virgin oil feedstock. The following sensitivity analysis results support this recommendation.

As mentioned previously, the goal of the sensitivity analysis is to study the effect of changing the prices on the IRR at which the NPV of the project equals zero. **Figures 5A,B** show the calculated values of IRR as a function of the percentage change of prices of both products and raw materials. Furthermore, they are compared to the IR value of 10% (highlighted in green in **Figures 6A,B**) to check the profitability of the process. The process is considered feasible and profitable if the IRR is greater than IR.

As shown in **Figure 5**, the homogeneous process at its current state (0% change in prices) has high profitability as the IRR equals about 83.57%, which is significantly higher than IR. The figure also shows that IRR increases to approximately 130% due to a decreased in the oil price by 50%. Similarly, IRR will have a value of about 182% if the biodiesel price increases by 50%. On the other hand, for the heterogeneous process to be profitable, the feedstock cost should be lower by 27.5% or the biodiesel selling price should be higher by 25%. These observations confirm the previous recommendation of using waste oils instead of virgin oils, besides the need to conduct a new investigation about the ability and efficiency of using CCKD as a heterogeneous catalyst to produce biodiesel from WVO. Obviously, the processes in both cases are more sensitive to the change of biodiesel price than to the change of oil price. However, it is more economical to find a cheaper oil feedstock than increasing the selling price of biodiesel which is constrained by the market.

Comparison With Literature Reports on the Technoeconomic Feasibility of Biodiesel Production

Many researchers are concerned about the feasibility of biodiesel production through different techniques (Fazal et al., 2011; Marchetti, 2011; Basili and Rossi, 2018; Kookos, 2018). Accordingly, they assessed the economic aspects and parameters of various manufacturing processes such as the fixed, operating, and production cost (Skarlis et al., 2012; Gülşen et al., 2014; Gebremariam and Marchetti, 2018b). For instance, Santana et al. (2010) conducted a technoeconomic analysis on biodiesel synthesis from virgin castor oil through homogeneously catalyzed transesterification, where sodium hydroxide (NaOH) was used as a catalyst and ethanol was utilized as a reactant in excess (12 : 1 ethanol to oil molar ratio). According to the authors, the cost of virgin oil was found to have the greatest attribution to the biodiesel production cost which ranged from 0.92 to USD 1.56/L according to the cost and quality of feedstock in addition to the process size. One of the most important recommendations of this study is to use WCO as a feedstock in order to raise process profitability.

TABLE 4 | Market prices, annual production, and total sales of products for the homogeneous and heterogeneous processes.

	Selling price ($/L)	Homogeneous process		Heterogeneous process	
		Production (10⁶ L/year)	Sales (10⁶ $/year)	Production (10⁶ L/year)	Sales (10⁶ $/year)
Biodiesel	$1.25	9	11.25	9.03	11.3
Glycerol	$1.62	0.63	1.02	0.64	1.03
K₃PO₄	$2.20	0.11	0.24	0	0
Total annual sales (TAS)	—	—	12.51	—	12.33

TABLE 5 | Profitability indicators for homogeneous and heterogeneous processes.

Profitability indicator	Formula	Homogeneous process	Heterogeneous process
Gross profit (GP) (10⁶ $/year)	$TAS - TPC$	4.05	−2.5 (not profitable)
Net profit (NP) (10⁶ $/year)	$80\%\ of\ GP$	3.24	—
Payback period (years)	$\frac{FCI}{NP + Depreciation}$	1.07	—
ROI (%)	$\frac{NP}{TCI}$	74.2	—

FIGURE 4 | Breakeven point analysis of the **(A)** homogeneous process and **(B)** heterogeneous process.
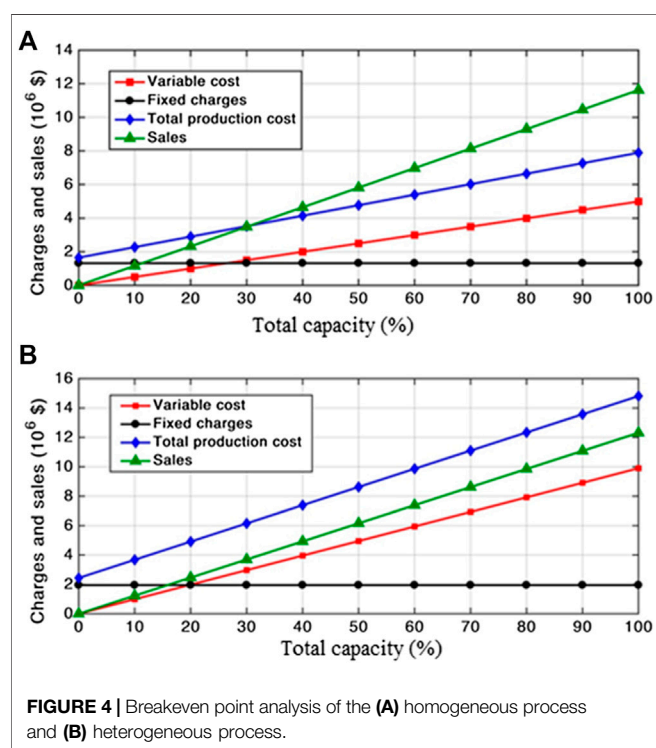
In a more recent study, a two-step biodiesel production process was evaluated technically and economically (Gebremariam and Marchetti, 2018c). Sulfuric acid (H_2SO_4) was used as a catalyst for the pretreatment step, whereas calcium oxide (CaO) was utilized as a heterogeneous base catalyst for the transesterification step. This two-step technique was proposed as a result of using acidic oil as a low-cost feedstock. Two other processes were also investigated; one of them used sulfuric acid only as of the catalyst and the other one utilized calcium oxide (CaO) only for the conversion of acidic

waste oil to methyl esters. This study concluded that using calcium oxide alone was the best economically.

On the other hand, the least feasible process was the one converting acidic oil using sulfuric acid as a catalyst without the aid of CaO. This is logically correct as this process needs severe conditions and high alcohol amount in addition to the long reaction time. It should be mentioned that the economic parameters considered in this study included the payback period, production cost, and ROI%. The payback period of the CaO process was calculated as 1.33 years, and the ROI% was observed to be 75.09%, whereas the unit production cost of biodiesel had the value of USD 0.7791/kg. The flow rate of biodiesel exiting from the optimum process was 5,132 kg/h at a conversion of 97.58% which was attained at the conditions of 9 : 1 ethanol to oil molar ratio, 7 wt% CaO loading, and 75°C where the residence time was 2 h.

Another study performed by the same research group suggested four alternative processes for biodiesel synthesis from high FFA content waste oil as a cheap feedstock (Gebremariam and Marchetti, 2018a). In all alternatives, sulfuric acid was utilized as the catalyst for acidic oil conversion into fatty acid methyl esters and calcium oxide was used only for catalyst neutralization after the reaction. The difference between all these proposed schemes was the arrangement of the downstream processes in order to purify produced biodiesel. The second scenario or alternative in this study was found to be superior economically over the others. It suggested that neutralization should be done directly after reaction followed by centrifugation for solids removal, ethanol recovery, GLC separation, and finally biodiesel purification from heavy wastes. The payback period of this process was 4.51 years. Besides, the unit production cost was USD 1.058/kg biodiesel, and the ROI% was only 22.19%. When compared with the previous study, this process is much less feasible and cannot be recommended for commercial production of biodiesel, although the feedstock is a cheap one. This also confirms the superiority of base-catalyzed biodiesel production over the acidic techniques. It should
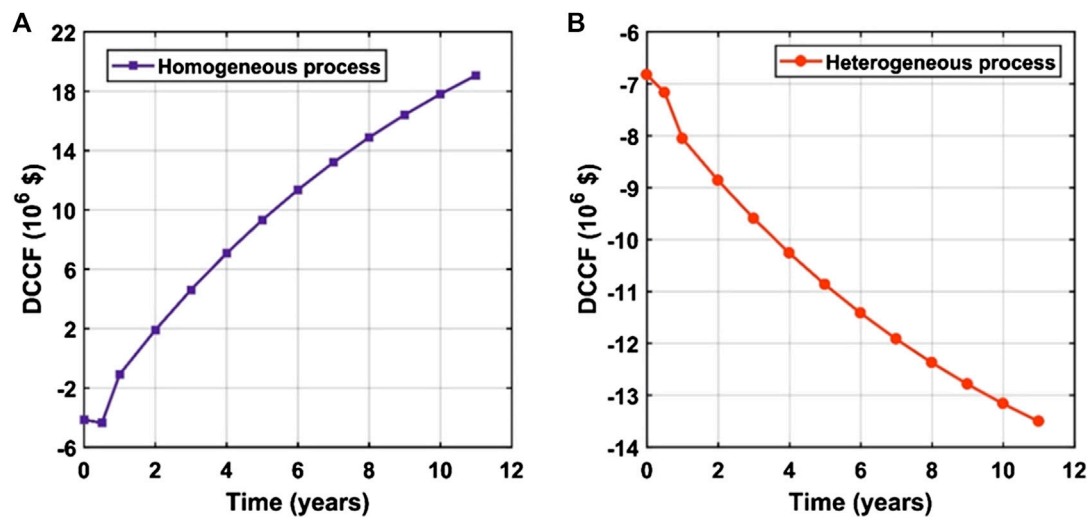
FIGURE 5 | Discount cumulative cash flow as a function of the operating time (years) for the **(A)** homogeneous process and **(B)** heterogeneous process.
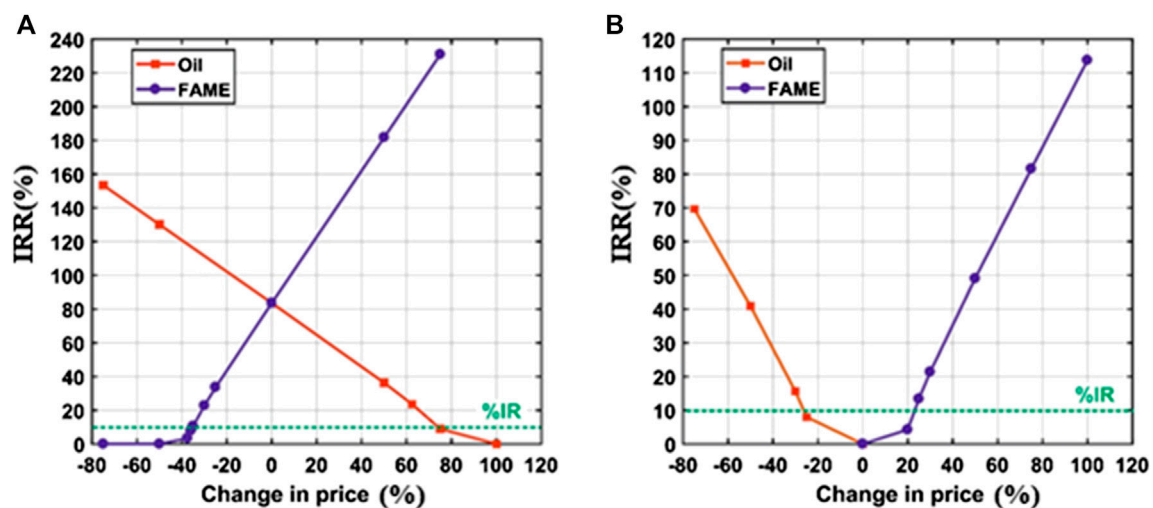
Figure 6 | IRR (%) sensitivity to the change of market prices of oil and FAME for the **(A)** homogeneous process and **(B)** heterogeneous process. The dotted green lines represent the IR.

be stated that the flow rate of biodiesel production related to this scenario is 5,282 kg/h, and the factory operates 7,920 h per year.

Moreover, the utilization of KOH as the homogeneous catalyst for biodiesel production from WCO was analyzed economically (Karmee et al., 2015). The production capacity of this plant was 8,000 ton per year. The unit production cost was estimated as USD 0.8686/kg biodiesel. For the same capacity, H_2SO_4 and Novozyme 435 were used as catalysts as well. Surprisingly, the unit production cost in the case of sulfuric acid was equal to almost USD 0.75/kg biodiesel. Novozyme 435 catalyzed process was the most expensive one among those three proposed processes as the production cost equivalent to 1 kg of biodiesel was USD 1.048.

Upon utilizing basic CaO heterogeneous catalyst, Gebremariam and Marchetti (2019) suggested four different scenarios to accomplish acidic oil conversion into biodiesel. Three scenarios considered the direct transesterification without any preesterification steps; nonetheless, only one alternative, i.e., scenario II, included preesterification using sulfuric acid as a catalyst followed by transesterification by ethanol in the presence of CaO. It is worthy mentioning that the processes without preesterification step resulted in the production of the considerable amount of calcium soaps which is usually considered as an undesired side product. However, in that study, the authors considered it a valuable by-product that can add to process feasibility; However, they were removed using a centrifuge. Unfortunately, despite avoiding the production of any

TABLE 6 | Summary of economic performance indicators of the suggested process and other published processes.

Reference	Feedstock	Catalyst	Reaction conversion (%)	Plant capacity (1,000 ton/year)	Unit production cost (USD/kg biodiesel)	Payback period, years	ROI (%)
Santana et al. (2010)	Castor oil	Sodium hydroxide	100	–	1.05–1.77	–	–
Gebremariam and Marchetti, (2018c)	Acidic oil with 10% FFA content	Calcium oxide	97.58	41	0.7791	1.33	75.09
Gebremariam and Marchetti, (2018a)	Acidic oil	Sulfuric acid	97.57	41	1.058	4.51	22.19
Gebremariam and Marchetti, 2019	Acidic oil	Sulfuric acid	96	37.8	0.777	1.82	55.04
Karmee et al., 2015	Waste cooking oil	Sulfuric acid	–	8	0.75	–	–
		Potassium hydroxide	–	8	0.869	–	–
Proposed homogenous process	Waste vegetable oil	Potassium hydroxide	95	7.9	1.67	1.07	74.2

soap, scenario II was the worst concerning GLC purity and the economics. For example, ROI% of this process was only 36.81% compared to the highest one, i.e., 56.26%, related to scenario III. In addition, it had the highest unit production cost of USD 0.8617/kg biodiesel in comparison with the lowest one of scenario IV, which was the only USD 0.777/kg biodiesel. Regarding the payback period, it was estimated to have the values of 2.72, 1.78, and 1.82 for scenarios II, III, and IV, respectively. The authors concluded that alternative IV is superior over the other scenarios because it yielded highly pure biodiesel, i.e., 99.9% purity, and GLC 99% pure with a performance factor of 1.02. It was also an excellent and feasible option for biodiesel production from the acidic oil which is a cheap raw material. The production rate of this scenario was 5,256.6 kg/h, and the reaction took place in two reactors in series.

In comparison with the aforementioned processes for biodiesel production, the proposed homogeneous process in the current study represents a competitive one as it can be observed from **Table 6**. The payback period is relatively low as it takes the value of 1.07 years while the ROI% is as high as 74.18% and the unit production cost is USD 1.067/kg biodiesel. Furthermore, the purities of both biodiesel and GLC are high, i.e., 99.999%. This study is also in good agreement with literature and matches the previous technoeconomic studies as it confirmed that the high production process has economic sensitivity towards the type, origin and price of feedstock used.

CONCLUSIONS AND RECOMMENDATIONS FOR FUTURE WORK

This comparative technoeconomic study illustrated that the homogeneous process has a relatively high profitable profile as its payback period is only 1.07 years besides having an IRR of 83.57%. Moreover, its breakeven point is 30% of the full capacity. On the contrary, the heterogeneous process is infeasible; therefore, the homogeneous process is preferable. Sensitivity analysis revealed the high sensitivity of biodiesel production toward feedstock price. For instance, the oil price should be reduced by 27.5% to gain profit from the heterogeneous process.

It is highly recommended to use waste vegetable oil as a feedstock for the heterogeneous process to enhance process profitability. Accordingly, a detailed study of the optimization of the factors affecting biodiesel production from waste vegetable oil using cement kiln dust as a heterogeneous catalyst should be performed to meet the sustainable development goals. This study will give the optimum conditions needed to conduct a detailed process simulation and test the process from an economic viewpoint. For a more accurate comparison, life cycle assessment should be performed on the different production processes to not only select the most feasible option, but also find the greenest path for biodiesel production.

DATA AVAILABILITY STATEMENT

The raw data supporting the conclusions of this article will be made available by the authors, without undue reservation.

AUTHOR CONTRIBUTIONS

EA: investigation, validation, data analysis, writing—Original draft, visualization, conceptualization, methodology, project administration. MM: investigation, validation, data analysis, writing—original draft, visualization, conceptualization, methodology, supervision. AE: investigation, writing—original draft and visualization. OA: writing—original draft. MH: writing—original draft. EO: writing—original draft. ER: revision and supervision. II: revision and supervision. IA: revision and supervision.

ACKNOWLEDGMENTS

SUPPLEMENTARY MATERIAL

The Supplementary Material for this article can be found online at: https://www.frontiersin.org/articles/10.3389/fenrg.2020.583357/full#supplementary-material.

REFERENCES

Abed, K. A., Gad, M. S., El Morsi, A. K., Sayed, M. M., and Elyazeed, S. A. (2019). Effect of biodiesel fuels on diesel engine emissions. *Egypt. J. Pet.* 28, 183–188. doi:10.1016/j.ejpe.2019.03.001

Al-Sakkari, E. G., Abdeldayem, O. M., El-Sheltawy, S. T., Abadir, M. F., Soliman, A., Rene, E. R., et al. (2020). Esterification of high FFA content waste cooking oil through different techniques including the utilization of cement kiln dust as a heterogeneous catalyst: a comparative study. *Fuel* 279, 118519. doi:10.1016/j. fuel.2020.118519

Al-Sakkari, E. g., El-Sheltawy, S. t., Abadir, M. f., Attia, N. k., and El-Diwani, G. (2017a). Investigation of cement kiln dust utilization for catalyzing biodiesel production via response surface methodology. *Int. J. Energy Res.* 41, 593–603. doi:10.1002/er.3635

Al-Sakkari, E. G., El-Sheltawy, S. T., Attia, N. K., and Mostafa, S. R. (2017b). Kinetic study of soybean oil methanolysis using cement kiln dust as a heterogeneous catalyst for biodiesel production. *Appl. Catal. B Environ.* 206, 146–157. doi:10.1016/j.apcatb.2017.01.008

Al-Sakkari, E. G., El-Sheltawy, S. T., Soliman, A., and Ismail, I. (2018a). Methanolysis of low FFA waste vegetable oil using homogeneous base catalyst for biodiesel production: new process design. *J. Adv. Chem. Sci.* 4, 593–597. doi:10.30799/jacs.196.18040401

Al-Sakkari, E. G., El-Sheltawy, S. T., Soliman, A., and Ismail, I. (2018b). Transesterification of low FFA waste vegetable oil using homogeneous base catalyst for biodiesel production: optimization, kinetics and product stability. *J. Adv. Chem. Sci.* 4, 586–592. doi:10.30799/jacs.195.18040305

Arumugam, A., and Ponnusami, V. (2019). Biodiesel production from *Calophyllum inophyllum* oil a potential non-edible feedstock: an overview. *Renew. Energy.* 131, 459–471. doi:10.1016/j.renene.2018.07.059

Awais, M., Musmar, S. e. A., Kabir, F., Batool, I., Rasheed, M. A., Jamil, F., et al. (2020). Biodiesel production from melia azedarach and *Ricinus communis* oil by transesterification process. *Catalysts* 10, 427. doi:10.3390/catal10040427

Baena-Moreno, F. M., Sebastia-Saez, D., Wang, Q., and Reina, T. R. (2020). Is the production of biofuels and bio-chemicals always profitable? Co-production of biomethane and urea from biogas as case study. *Energy Convers. Manag.* 220, 113058. doi:10.1016/j.enconman.2020.113058

Banerjee, S., Sahani, S., and Chandra Sharma, Y. (2019). Process dynamic investigations and emission analyses of biodiesel produced using Sr-Ce mixed metal oxide heterogeneous catalyst. *J. Environ. Manag.* 248, 109218. doi:10.1016/j.jenvman.2019.06.119

Basili, M., and Rossi, M. A. (2018). *Brassica carinata*-derived biodiesel production: economics, sustainability and policies. The Italian case. *J. Clean. Prod.* 191, 40–47. doi:10.1016/j.jclepro.2018.03.306

Brewer, T. L. (2019). Black carbon emissions and regulatory policies in transportation. *Energy Pol.* 129, 1047–1055. doi:10.1016/j.enpol.2019.02.073

Chakraborty, M., and Baruah, D. C. (2012). Investigation of oxidation stability of *Terminalia belerica* biodiesel and its blends with petrodiesel. *Fuel Process. Technol.* 98, 51–58. doi:10.1016/j.fuproc.2012.01.029

Chanakaewsomboon, I., Tongurai, C., Photaworn, S., Kungsanant, S., and Nikhom, R. (2020). Investigation of saponification mechanisms in biodiesel production: microscopic visualization of the effects of FFA, water and the amount of alkaline catalyst. *J. Environ. Chem. Eng.* 8, 103538. doi:10.1016/j.jece.2019.103538

Colombo, K., Ender, L., Santos, M. M., and Chivanga Barros, A. A. (2019). Production of biodiesel from Soybean oil and methanol catalyzed by calcium oxide in a recycle reactor. *S. Afr. J. Chem. Eng.* 28, 19–25. doi:10.1016/j.sajce.2019.02.001

Dhawane, S. H., Al-Sakkari, E. G., and Halder, G. (2019). Kinetic modelling of heterogeneous methanolysis catalysed by iron induced on microporous carbon supported catalyst. *Catal. Lett.* 149, 3508–3524. doi:10.1007/s10562-019-02905-5

Dwivedi, G., Verma, P., and Sharma, M. P. (2018). Optimization of storage stability for karanja biodiesel using box-behnken design. *Waste Biomass Valor.* 9, 645–655. doi:10.1007/s12649-016-9739-2

Egypt minimum monthly wages. Available at: https://tradingeconomics.com/egypt/minimum-wages (Accessed September 18, 2020).

El-Sheltawy, S. T., and Al-Sakkari, E. G. (2016). Recent trends in solid waste utilisation for biodiesel production. *J. Solid Waste Technol. Manag.* 42, 302–312.

El-Sheltawy, S. T., Al-Sakkari, E. G., and Fouad, M. (2016). Modeling and process simulation of biodiesel production from soybean oil using cement kiln dust as a heterogeneous catalyst. *J. Solid Waste Technol. Manag.* 42, 313–324.

El Sheltawy, S. T., Al-Sakkari, E. G., and Fouad, M. M. K. (2019). "Waste-to-energy trends and prospects: a review," in *Waste management and resource efficiency*. Editor S. K. Ghosh (Singapore: Springer), 673–684. doi:10.1007/978-981-10-7290-1_56

Elango, R. K., Sathiasivan, K., Muthukumaran, C., Thangavelu, V., Rajesh, M., and Tamilarasan, K. (2019). Transesterification of castor oil for biodiesel production: process optimization and characterization. *Microchem. J.* 145, 1162–1168. doi:10.1016/j.microc.2018.12.039

Essamlali, Y., Amadine, O., Fihri, A., and Zahouily, M. (2019). Sodium modified fluorapatite as a sustainable solid bi-functional catalyst for biodiesel production from rapeseed oil. *Renew. Energy.* 133, 1295–1307. doi:10.1016/j.renene.2018.08.103

Fazal, M. A., Haseeb, A. S. M. A., and Masjuki, H. H. (2011). Biodiesel feasibility study: an evaluation of material compatibility; performance; emission and engine durability. *Renew. Sustain. Energy Rev.* 15, 1314–1324. doi:10.1016/j.rser.2010.10.004

Gebremariam, S. N., and Marchetti, J. M. (2018a). Biodiesel production through sulfuric acid catalyzed transesterification of acidic oil: techno economic feasibility of different process alternatives. *Energy Convers. Manag.* 174, 639–648. doi:10.1016/j.enconman.2018.08.078

Gebremariam, S. N., and Marchetti, J. M. (2018b). Economics of biodiesel production: Review. *Energy Convers. Manag.* 168, 74–84. doi:10.1016/j.enconman.2018.05.002

Gebremariam, S. N., and Marchetti, J. M. (2018c). Techno-economic feasibility of producing biodiesel from acidic oil using sulfuric acid and calcium oxide as catalysts. *Energy Convers. Manag.* 171, 1712–1720. doi:10.1016/j.enconman.2018.06.105

Gebremariam, S. N., and Marchetti, J. M. (2019). Techno-economic performance of a bio-refinery for the production of fuel-grade biofuel using a green catalyst. *Biofuels Bioprod. Bioref.* 13, 936–949. doi:10.1002/bbb.1985

Gollakota, A. R. K., Volli, V., and Shu, C.-M. (2019). Transesterification of waste cooking oil using pyrolysis residue supported eggshell catalyst. *Sci. Total Environ.* 661, 316–325. doi:10.1016/j.scitotenv.2019.01.165

Gülşen, E., Olivetti, E., Freire, F., Dias, L., and Kirchain, R. (2014). Impact of feedstock diversification on the cost-effectiveness of biodiesel. *Appl. Energy.* 126, 281–296. doi:10.1016/j.apenergy.2014.03.063

Helmers, E., Leitão, J., Tietge, U., and Butler, T. (2019). CO₂-equivalent emissions from European passenger vehicles in the years 1995-2015 based on real-world use: assessing the climate benefit of the European "diesel boom." *Atmos. Environ.* 198, 122–132. doi:10.1016/j.atmosenv.2018.10.039

Hosking, J., Mudu, P., and Fletcher, E. (2011). *Health co-benefits of climate change mitigation: transport sector.* Geneva, Switzerland: World Health Organization.

Hosney, H., Al-Sakkari, E. G., Mustafa, A., Ashour, I., Mustafa, I., and El-Shibiny, A. (2020). A cleaner enzymatic approach for producing non-phthalate plasticiser to replace toxic-based phthalates. *Clean Technol. Environ. Policy.* 22, 73–89. doi:10.1007/s10098-019-01770-5

International Energy Association (2018). *CO₂ emissions from fuel combustion 2018 highlights.* Paris, France: International Energy Association. Available at: https://webstore.iea.org/co2-emissions-from-fuel-combustion-2018-highlights (Accessed September 18, 2020).

Jenkins, S. (2019). Chemical engineering plant cost index: 2018 annual value. *Chem. Eng.* Available at: https://www.chemengonline.com/2019-cepci-updates-january-prelim-and-december-2018-final/?printmode=1 (Accessed September 18, 2020).

Karmee, S., Patria, R., and Lin, C. (2015). Techno-economic evaluation of biodiesel production from waste cooking oil-A case study of Hong Kong. *Int. J. Mol. Sci.* 16, 4362–4371. doi:10.3390/ijms16034362

Kaur, R., and Bhaskar, T. (2020). "Potential of castor plant (*Ricinus communis*) for production of biofuels, chemicals, and value-added products," in *Waste biorefinery.* Editors T. Bhaskar, A. Pandey, E. R. Rene, and D. C. W. Tsang (Amsterdam, Netherlands: Elsevier), 269–310. doi:10.1016/B978-0-12-818228-4.00011-3

Kookos, I. K. (2018). Technoeconomic and environmental assessment of a process for biodiesel production from spent coffee grounds (SCGs). *Resour. Conserv. Recycl.* 134, 156–164. doi:10.1016/j.resconrec.2018.02.002

Kumar, L. R., Yellapu, S. K., Tyagi, R. D., and Drogui, P. (2020). Cost, energy and GHG emission assessment for microbial biodiesel production through valorization of municipal sludge and crude glycerol. *Bioresour. Technol.* 297, 122404. doi:10.1016/j.biortech.2019.122404

Lam, M. K., and Lee, K. T. (2011). "Production of biodiesel using palm oil," in *Biofuels.* Editors A. Pandey, C. Larroche, S. C. Ricke, C.-G. Dussap, and E. Gnansounou (Amsterdam, Netherlands: Academic Press), 353–374. doi:10.1016/B978-0-12-385099-7.00016-4

Li, H., Liu, F., Ma, X., Wu, Z., Li, Y., Zhang, L., et al. (2019). Catalytic performance of strontium oxide supported by MIL-100(Fe) derivate as transesterification catalyst for biodiesel production. *Energy Convers. Manag.* 180, 401–410. doi:10.1016/j.enconman.2018.11.012

Mączyńska, J., Krzywonos, M., Kupczyk, A., Tucki, K., Sikora, M., Pińkowska, H., et al. (2019). Production and use of biofuels for transport in Poland and Brazil – the case of bioethanol. *Fuel*, 241, 989–996. doi:10.1016/j.fuel.2018.12.116

Marchetti, J. M. (2011). The effect of economic variables over a biodiesel production plant. *Energy Convers. Manag.* 52, 3227–3233. doi:10.1016/j.enconman.2011.05.008

Mardhiah, H. H., Ong, H. C., Masjuki, H. H., Lim, S., and Lee, H. V. (2017). A review on latest developments and future prospects of heterogeneous catalyst in biodiesel production from non-edible oils. *Renew. Sustain. Energy Rev.* 67, 1225–1236. doi:10.1016/j.rser.2016.09.036

Moazeni, F., Chen, Y.-C., and Zhang, G. (2019). Enzymatic transesterification for biodiesel production from used cooking oil, a review. *J. Clean. Prod.* 216, 117–128. doi:10.1016/j.jclepro.2019.01.181

Parsons, S., Abeln, F., McManus, M. C., and Chuck, C. J. (2019). Techno-economic analysis (TEA) of microbial oil production from waste resources as part of a biorefinery concept: assessment at multiple scales under uncertainty. *J. Chem. Technol. Biotechnol.* 94, 701–711. doi:10.1002/jctb.5811

Peters, M., Timmerhaus, K., and West, R. (2003). *Plant design and economics for chemical engineers.* 5th ed. New York, NY: McGraw-Hill. Available at: https://catalog.lib.ncsu.edu/catalog/NCSU1640313 (Accessed February 10, 2019)

Raman, L. A., Deepanraj, B., Rajakumar, S., and Sivasubramanian, V. (2019). Experimental investigation on performance, combustion and emission analysis of a direct injection diesel engine fuelled with rapeseed oil biodiesel. *Fuel* 246, 69–74. doi:10.1016/j.fuel.2019.02.106

Reche, C., Rivas, I., Pandolfi, M., Viana, M., Bouso, L., Àlvarez-Pedrerol, M., et al. (2015). Real-time indoor and outdoor measurements of black carbon at primary schools. *Atmos. Environ.* 120, 417–426. doi:10.1016/j.atmosenv.2015.08.044

Santana, G. C. S., Martins, P. F., de Lima da Silva, N., Batistella, C. B., Maciel Filho, R., and Wolf Maciel, M. R. (2010). Simulation and cost estimate for biodiesel production using castor oil. *Chem. Eng. Res. Des.* 88, 626–632. doi:10.1016/j.cherd.2009.09.015

Skarlis, S., Kondili, E., and Kaldellis, J. K. (2012). Small-scale biodiesel production economics: a case study focus on Crete Island. *J. Clean. Prod.* 20, 20–26. doi:10.1016/j.jclepro.2011.08.011

Tabatabaei, M., Aghbashlo, M., Dehhaghi, M., Panahi, H. K. S., Mollahosseini, A., Hosseini, M., et al. (2019). Reactor technologies for biodiesel production and processing: a review. *Prog. Energy Combust. Sci.* 74, 239–303. doi:10.1016/j.pecs.2019.06.001

Tapanwong, M., and Punsuvon, V. (2019). Production of ethyl ester biodiesel from used cooking oil with ethanol and its quick glycerol-biodiesel layer separation using pure glycerol. *Int. J. Geomate.* 17, 109–114. doi:10.21660/2019.61.4808

United Nations (2015). Sustainable development Knowledge Platform. Available at: https://sustainabledevelopment.un.org/topics/sustainabledevelopmentgoals (Accessed September 18, 2020)

Urbain, F., Du, R., Tang, P., Smirnov, V., Andreu, T., Finger, F. et al. (2019). Upscaling high activity oxygen evolution catalysts based on CoFe₂O₄ nanoparticles supported on nickel foam for power-to-gas electrochemical conversion with energy efficiencies above 80%. *Appl. Catal. B Environ.* 259, 118055. doi:10.1016/j.apcatb.2019.118055

WHO (2012). Health co-benefits of climate change mitigation - transport sector. Available at: https://www.who.int/hia/green_economy/transport_sector_health_co-benefits_climate_change_mitigation/en/ (Accessed January 26, 2019)

Yang, H.-H., Dhital, N. B., Wang, L.-C., Hsieh, Y.-S., Lee, K.-T., Hsu, Y.-T., et al. (2019). Chemical characterization of fine particulate matter in gasoline and diesel vehicle exhaust. *Aerosol Air Qual. Res.* 19, 1439–1449. doi:10.4209/aaqr.2019.04.0191

Zaharudin, N. A., Rashid, R., Azman, L., Esivan, S. M. M., Idris, A., and Othman, N. (2018). "Enzymatic hydrolysis of used cooking oil using immobilized lipase," in *Sustainable technologies for the management of agricultural wastes applied environmental science and engineering for a sustainable future.* Editor Z. A. Zakaria (Singapore: Springer), 119–130. doi:10.1007/978-981-10-5062-6_9

Živković, S., and Veljković, M. (2018). Environmental impacts the of production and use of biodiesel. *Environ. Sci. Pollut. Res.* 25, 191–199. doi:10.1007/s11356-017-0649-z

GLOSSARY

BC: Black carbon

CCKD: Calcined cement kiln dust

CKD: Cement kiln dust

FAME: Fatty acid methyl ester

FFA: Free fatty acids

FCI: Fixed capital investment

GLC: Glycerol

IR: Interest rate

IRR: Interest rate of return

NPV: Net present value

PCE: Purchase cost of equipment

PPC: Physical plant cost

ROI: Return on investment

SDGs: Sustainable development goals

TBHQ: Tertiary butylhydroquinone

TCI: Total capital investment

TG: Triglycerides

TPC: Total production cost

WCI: Working capital investment

WVO: Waste vegetable oil.

Fabrication and Optimization of Nanocatalyst for Biodiesel Production: An Overview

Sayfa Bano, Adil Shafi Ganie, Saima Sultana, Suhail Sabir and Mohammad Zain Khan*

Environmental Research Laboratory, Department of Chemistry, Aligarh Muslim University, Uttar Pradesh, India

Necessity and exploitation of fossil fuel products are implacable in serving the needs of humanity despite being a finite and limited resource. To meet the thrust of energy, biofuels derived from varieties of renewable resources are imperative in fulfilling the demand of renewable fuels on a large scale without creating environmental concerns. Biofuels are inevitably the result of the carbon fixation process which stores chemical energy, ultimately reducing the total amount of carbon dioxide. Different kinds of biofuels like bioethanol, biomethanol, biogas, and biodiesel are derived depending on varieties of feedstock materials. Among these, production of biodiesel augments the progression of clean and renewable fuel. In this review, we have discussed the production of biodiesel derived from various feedstock and using several processes like pyrolysis, direct blending, micro-emulsion, and trans-esterification, with critical discussion focussing on increasing biodiesel production using nanocatalysts. Biodiesel production mainly proceeds through homogenous and heterogeneous catalysis via trans-esterification method. The review further discusses the significance of nanocatalyst in heterogeneous catalysis based trans-esterification for large scale biodiesel production. With the advent of nanotechnology, designing and modification of nanocatalyst gives rise to attractive properties such as increased surface area, high thermal stability, and enhanced catalytic activity. The role of nanocatalysts have been extensively studied and investigated in regard to the increased biodiesel production. Along with the modification of nanocatalysts, we have briefly discussed the physico-chemical properties and the role of the optimization parameters as it plays a pivotal role in enhancing the biodiesel production commercially.

Keywords: biofuels, biodiesel, nanocatalyst, response surface methodology (RSM), trans-esterification reaction

INTRODUCTION

Since early human history, wood has been a major source of energy. With increasing time, there has been an ultimate shift to fossil fuels, which accounts for the majority of energy production (Le Quynh et al., 2017; Youse et al., 2019). Incessant globalization and industrialization has led to spike in the utilization of fossil fuel products like petroleum and coal (Touqeer et al., 2020). As global energy consumption is mainly dependent on the endangered and depleting fossil fuel reservoirs, the need for renewable energy or fuel sources is growing due to the ever-increasing demand. The demand for global energy by 2020 was estimated to be around 15 million tons of oil equivalent. Increasing energy consumption substantially demands higher energy, but the finite supply end will eventually delimit

the depleting fossil fuel reservoirs. With the significant increase in global energy demand, developing renewable energy sources on a large scale plays an extensive role in overcoming the continuously growing need and demand (Martchamadol and Kumar, 2012).

To overcome this serious issue, there is an urgent need to develop or alleviate an alternate renewable energy source which poses as a clean fuel. Renewable sources contribute only around 20% to the global energy demand, while the remaining 80% is fulfilled by fossil fuels (Veronica Winoto, 2019). With the advancement in technology, various innovative ideas can uplift renewable energy technologies to new heights and provide sustainable ways to fulfil the increasing demand along with a clean environment (Azyan et al., 2018). The majority of the renewable sources like wind, solar, hydel and biofuels do not correspond to the estimated energy requirements. Among these, biofuel production currently serves as a new contributor in order to meet the growing energy demand. It mainly emphasizes biomass conversion to liquid fuels like bioethanol, biodiesel and biogases.

Among these, biodiesel as a potential fuel is developing at a faster rate, thereby controlling and plummeting the use of fossil fuels and other non-renewable resources (Prokopowicz et al., 2015). It is mainly focussed on biomass conversion to liquid fuels. To date, biomass has not been extensively used as reliable energy source in comparison to fossil fuels (Le et al., 2017). Identifying biomass feedstock as a raw material is an important task, as it is easily affected by factors such as moisture content and pre-treatment processes. Due to the low energy density of biomass, it is also inconvenient in handling, transportation and storage conditions, setting a major drawback in large scale biodiesel production (Nizami and Rehan, 2018). Currently, enormous amounts of research on increasing biodiesel production have attained large public interest corresponding to huge hikes in oil prices, the necessity of increased energy security and concern regarding emissions of harmful greenhouse gas from fossil fuels (Balat, 2011).

Biodiesel production will eventually present the best solution over other conventional fuels. Biodiesel, a liquid fuel comprising of long chain fatty acid esters derived from vegetable oils, animal fats, micro and macro algal oil. Biodiesel production using nanocatalysts is one of the promising and advanced approaches for carrying out the process on a large scale (Talebian-kiakalaieh et al., 2013). Its physico-chemical properties can be easily varied by using a nanocatalyst, which produces different compositions of fatty acids methyl esters (FAME). Fatty acids methyl esters FAME composition includes saturated and unsaturated fatty acids, palmitic acid, myristic acid, and oleic acid. These methyl esters composition primarily govern the parameters like density, viscosity, cetane number and acid value which eventually affect the quality and quantity of biodiesel (Chozhavendhan et al., 2020).

Conventionally, biodiesel is produced by using homogenous and heterogeneous catalysis. As heterogeneous catalysts have various advantages of recyclability and reusability, basic catalyst is predominantly used in *trans*-esterification process of biodiesel production. However, these solid catalysts require more quantity and provide less surface area, thus reducing the overall

activity of the catalyst (Borah et al., 2019). With the advent of nanotechnology, nanocatalysts play a prominent role in improving the yield and production quality of biodiesel along with the reduction in reaction time. Involvement of a nanocatalyst also leads to reduction in reaction temperatures, catalyst weight and alcohol to oil ratio. Ibrahim et al. (2020) have reported the role and amount of the nanocatalyst in biodiesel production. It was found that nanocatalysts play a prominent role in increasing the rate of reaction without being self-deteriorated. It also significantly lowers the activation energy of the reaction profiles. Additionally, the amount of nanocatalyst is also a critical parameter in determining the yield of biodiesel production (Ibrahim et al., 2020). Another researcher has also investigated the role of nanocatalysts especially in biodiesel production. It was observed that with zero catalyst loading under given reaction conditions, no biodiesel production was found, hence the presence and amount of nanocatalysts are vital for production of biodiesel (Anbessie et al.,2019).

Vast development in designing and fabrication of nanocatalyst contributes to many areas ranging from different kind of metal oxides (mixed metal oxides, alloys), hydrocalcite based catalyst, zeolite and other carbonaceous material based nanocatalysts (Talebian-kiakalaieh et al., 2013). These highly developed catalysts mainly possess excellent properties in withstanding the reaction conditions and also provide a large surface area to volume ratio. Assembling of different types of nanocatalysts also plays an important role depending on the nature and conditions of catalytic reactions, which in turn vary to a greater extent under different operating environments. It also evidently acts as an interface between homogenous and heterogeneous catalysis while monitoring its size at atomic level which eventually increases surface area as compared to solid acid/base based catalyst (Zuliani et al., 2018; Pan et al., 2019). By modulating the nanomaterial's surface, properties like catalyst active site, acidity or basicity and porosity can be greatly enhanced. Apart from this, morphology of the nanocatalyst can be extensively studied by varying reaction conditions of the synthesis. Various morphology such as nanocrystals, nanosponges, and nanocubes, expose different active sites with rough and mesoporous structure, thus overall increasing the surface area and reactivity (Fawaz et al., 2019). These highly developed nanocatalysts will eventually increase the production of biodiesel. Surface functionalization is prominent in increasing the overall acidity of nanocatalysts, eventually enhancing the catalytic activity, and introducing magnetic nanomaterials will help in easy separation recoverability and reusability (Gardy et al., 2017; Gardy et al., 2018).

Besides development in nanocatalyst areas, physico-chemical properties of biodiesel are also essential in estimating the quality and quantity of production for biodiesel. It is mainly dependent on the type of feedstock and pre-treatment process it undergoes (Hassan and Hossein, 2019). The pre-treatment process is quite a significant figure in controlling moisture content, estimation of free fatty acids, and final biodiesel products, etc. It will also improve the storage and transportation of the biodiesel keeping its stability intact (Amirthavalli and Warrier 2019). Biodiesel production is also dependent on the optimization parameters of the reaction conditions like methanol to oil molar ratio, catalyst

amount, reaction temperature, and reaction time based on a few newly developed types of software like MINITAB and Response Surface Methodology (RSM). The optimized parameters are largely responsible for an increase in biodiesel production and can be easily operated on a large scale (Alaei et al., 2018).

This review presents a brief discussion on different types of biofuels with special focus on biodiesel production and its methodology. Herein, critical discussion emphasizes recent developments in the field of nanocatalysts in the production of biodiesel using heterogeneous catalysis via *trans*-esterification reaction. Different types of nanocatalyst and their effect on production have also been mentioned. Along with this, various physico-chemical properties and optimization parameters involved in biodiesel production have been significantly elaborated for increasing its production on industrial scale.

BIOFUELS: A SUSTAINABLE ENERGY SOURCE

Biofuels are the end products of a biological fixation process, mainly derived from renewable resources like wood, cellulosic and lignocellulosic material, edible and non-edible products, producing different kinds of biofuels like biohydrogen, bioethanol, biomethanol and biodiesel (Kushwaha et al., 2018 Khan et al., 2018;). Preceding through generation and covering the basic need in the energy sector via fossil fuels, biofuels on a large scale can minimize pollution and also reduce the depletion of ozone layer.

Biofuel production encompasses three categories based on its source of production. First and second generation fuels were produced from edible and starch based feedstock which is inefficient in terms of large production and price hike, as it poses certain disadvantages of being an energy intensive source, a time consuming task, and causing the release of harmful gases. However, third generation biofuels are mainly derived from effective feedstock sources and developed catalytic conversion processes. It mainly relies on the utilization of non-edible, lignocellulosic, and microalgae-based feedstock (Rai et al., 2016; Thangaraj et al., 2019). **Figure 1** briefly illustrates the stages in the production of biofuels.

Biofuels are mainly categorized into biogas, bioethanol, and biodiesel. Biogas production is aided with the help of anaerobic digestion (AD) using sewage sludge, agricultural waste, and other products. Increased biogas production can be attained under optimized conditions with the help of a nanocatalyst (Kovács et al., 2013; Deepanraj and Senthilkumar, 2020). It mainly includes biomethane, biohydrogen and carbon dioxide. They are produced either from pyrolysis or gasification process involving renewable resources followed by its conversion to gases like methane, ammonia, and hydrogen sulphide etc. under anaerobic conditions (Kana et al., 2012). Various other gases are also produced which can be further used in different synthesis processes (Li et al., 2020; Senés-Guerrero et al., 2019). In comparison to their bulk counterparts, nanomaterials with excellent structural and morphological properties significantly enhance the methane production. Large quantities of biomethane can be used as a fuel directly as it resembles properties of natural gas, or it can also be converted to electricity via fuel cell technology (Deepanraj et al., 2016; Deepanraj and Senthilkumar, 2020). However, it cannot be commercially used

FIGURE 1 | Different stages of biofuel production.
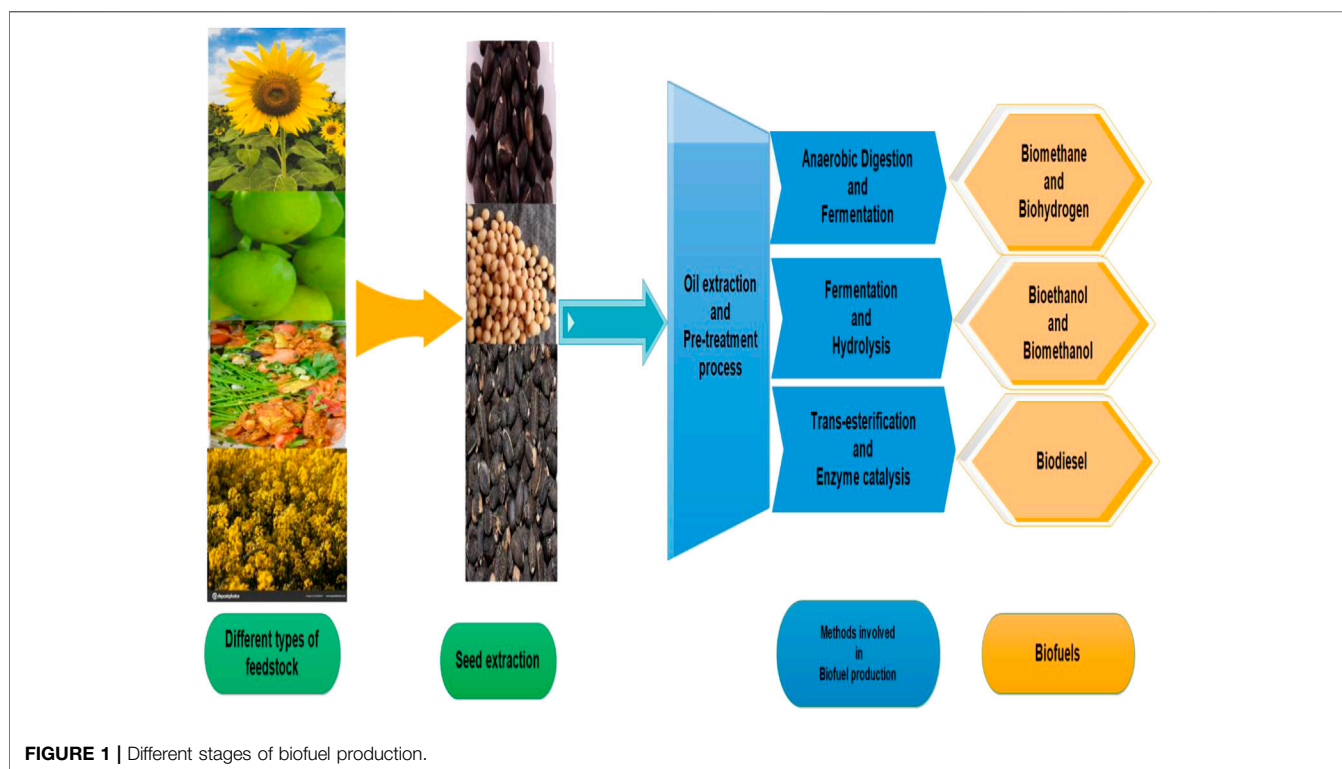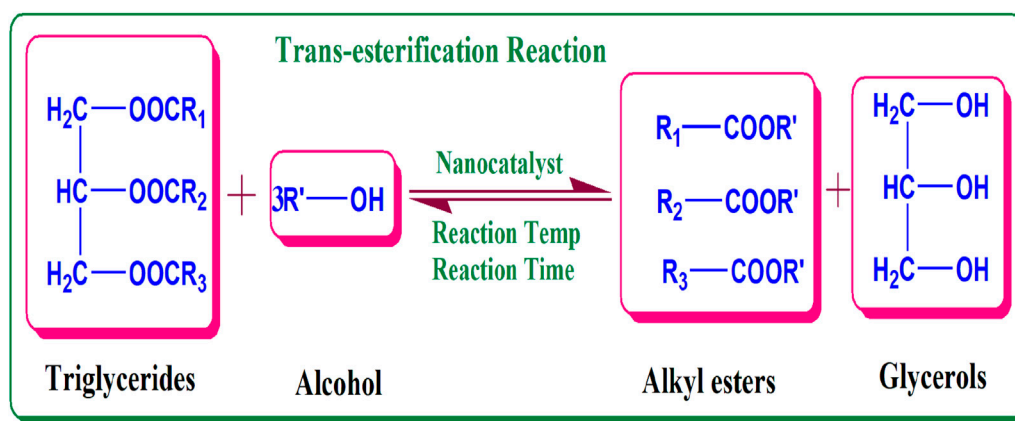
FIGURE 2 | Reaction involved in biodiesel production via *trans*-esterification method (Anbessie et al., 2019).

as a fuel because of certain limitations regarding storage and transportation.

Biomethanol and bioethanol are alcoholic products derived from either enzymatic conversion of starch and sugar as feedstock materials or chemical conversion of lignocellulosic material as feedstock, which undergoes various pre-treatment processes followed by hydrolysis of 5/6 carbon sugars, and further distilled to produce fuel grade ethanol (Shalaby, 2013; Chen and Fu, 2016; Kushwaha et al., 2018). Bioethanol is used on a large scale as compared to biomethanol because of various advantages like its non-corrosive nature, cost efficientness and lower energy requirements (Khan et al., 2019). It was also reported that USA and Brazil are the largest consumers of bioethanol as an energy source over conventional fuel because of its low emissions of harmful gases, low production cost, and feasible availability of feedstock materials (Shalaby, 2013). It can easily replace gasoline so as to avoid CO_2, NO, CO, and other harmful gas emissions.

Biodiesel, as a potential clean fuel, is mainly produced by *trans*-esterification of vegetable oils using methanol and a nanocatalyst. Chemically, it is fatty acid alkyl esters produced from *trans*-esterification of triglycerides with methanol as an alcohol source producing esters of fatty acids and glycerol (Anbessie et al., 2019). **Figure 2** encodes the reaction involved in the production of biodiesel.

The produced biodiesel mainly consists of different types of fatty acids depending on its composition. It is highly renewable, non-toxic and biodegradable with low sulphur content and reduced harmful gas emissions. It is an environmentally benign fuel mitigating the detrimental effects of fossil fuels. They can also be used as a blend with diesel fuel, thereby reducing the amount of pollutants and harmful gases released from conventional fuels as biodiesel is mainly derived from *trans*-esterification of oils at a given operating condition.

Feedstock and Technique for Biomass Conversion to Biodiesel

Feedstock mainly consists of oils and fats majorly derived from plants and animals. These feedstock materials are mainly

biodegradable and non-toxic materials for their utilization in *trans*-esterification process. Choosing a good raw material is a first and basic criterion in biodiesel production. Plant derived feedstock is mainly categorised into edible and non-edible oil. The production and cultivation of feedstock is mainly dependent on geographical conditions of the given area. For biogas and bioethanol production, animal and plant waste products, organic waste materials, starch, cellulosic, and lignocellulosic are widely investigated, as biodiesel production was largely derived from edible oils like safflower, palm oil, sunflower, and coconut oil etc. However, it posed serious issues of food security and increasing consumption leading to high cost thus, reducing its utilization on a large scale.

However, non-edible feedstock has become a great rescue in this regard, as it can be cultivated on a large scale. It mainly includes jatropa, jojoba, neem, rubber seed tree, and tobacco seed, etc. The most studied feedstock materials are Jojoba (El-seesy et al., 2016) and Jatropa (Chavan et al., 2015). Jojoba is a shrub belonging to the *Simmondsiaceace* family, producing 45–55% of fatty acids while Jatropa majorly contributes due to rapid growth and high seed productivity. It is profoundly grown in tropical and sub-tropical regions of the world, and is also an easily cultivated plant with a maximum amount of fatty acid content. Besides plants, animal fats and waste cooking oil can also be a promising and economical feedstock in biodiesel production (Behzadi and Farid, 2007). These waste cooking oils containing free fatty acids are ultimately reduced by using pre-treatment processes and alkali based *trans*-esterification process as high fatty acid content leads to soap formation. However, the pre-treatment process is mainly affected by various reaction parameters (Faisal et al., 2018). Biodiesel production mainly occurs by esterification and *trans*-esterification of free fatty acids and triglycerides, as the amount of free fatty acid corresponds to its yield.

An important class of bacteria, algae, fungi (Azhar et al., 2017) and microbes can also be used in biodiesel production. They consist of both photosynthetic and non-photosynthetic micro-organisms, mainly derived from stagnant ponds (Zhang et al., 2013). They create a new platform for the generation of oils used in biodiesel production with various advantages of easy production, highly rich

TABLE 1 | Different types of feedstock used in biodiesel production.

Edible feedstock	Non-edible feedstock	Algae based feedstock
Safflower	Jatropa	Cyanobacteria
Sunflower`	Babassu	Microalgae oil
Coconut	Tallow	Microbes
Palm oil	Jojoba	Red algae
Rice bran	Rapeseed	Diatoms
Canola	Karanja oil	Brown algae
Corn	Tobacco	
Wheat	Neem	
Barley	Rubber seed	
Soybean	Waste cooking oil	
	Animal fats	
	Mahua	
	Salmon oil	
Shalaby (2013); Zahan and Kano (2018); Singh and Gaurav (2018); Thangaraj et al. (2019)	Shuit et al. (2015); Anbessie et al. (2019)	Hossain et al. (2019a)

in oil content, no release of CO_2, self-generating, highly feasible, and cheap. They mostly include cyanobacteria, microalgae, and microbes (Hossain et al., 2019a). **Table 1** presents various types of feedstock, and an evaluation of these wide feedstock will eventually increase biodiesel production on a large scale, mitigating the use of previous materials.

Biomass conversion of the feedstock is mainly based on techniques such as thermal treatment, pyrolysis, and gasification, etc. Conversion of biomass to biodiesel generally proceeds via many processes like thermochemical and biological processes. The thermochemical process is the most significant route in biomass conversion as it further extends to various categories depending on the type of feedstock used. It is mainly divided into different routes like pyrolysis, liquefaction, and gasification. They mainly produce syn gas, tar, and oil which can be utilised for further application regarding various fuel production. In biodiesel production, oil extraction is a major step, which can also be extracted from enzyme extraction, mechanical extractor, and solvent extraction method depending on the nature of feedstock (Achten et al., 2008; Akia et al., 2014; Mishra and Goswami, 2017). Oil extraction is very important in quantifying the production of biodiesel, as it mainly contributes to the nature of fatty acids methyl esters content which majorly affects the physico-chemical properties of the final products.

Recent technological advances may correspond to production of biofuels such as biohydrogen biomethane and by carbon dioxide reduction via chemical and electrochemical techniques. They mainly produce methane and hydrogen under anaerobic conditions by using bacteria as feedstock material. Different species of bacteria can be cultured depending on its growth conditions certainly increasing the quantity of biogas production which ultimately can be converted into either electricity or in C1 derived fuel which can be used as biodiesel fuel (Anwer et al., 2019).

Types of Catalysis Involved in Biodiesel Production

Since the production of biodiesel, various methods like direct blending, pyrolysis, micro-emulsification and *trans*-esterification

have been implemented. All the methods are feasible to a certain extent along with some advantages and disadvantages as elaborated in **Table 3**. Biodiesel synthesis proceeding through direct blending, pyrolysis, and micro-emulsification methods are insufficient for large scale production. Among these techniques *trans*-esterification is the best technique which proceeds via catalytic reaction involving fatty acids and methanol in the presence of a catalyst, has evolved with various advantages like increased production, easy separation, and limitation of mass transfer resistance.

It is further divided into homogenous and heterogeneous catalysis. Homogenous catalysis proceeds through acid and base catalyzed reaction. Base catalyzed reaction is much faster than acid catalyzed reaction giving maximum yield. The most commonly used catalysts are NaOH, KOH, $NaOCH_3$, and $KOCH_3$ (Gardy et al., 2017; Silveira et al., 2019), operating under mild temperatures giving maximum yields (Gardy et al., 2019b). It also requires high-grade feedstock oil to minimize the saponification reaction making the process more cost consumptive. While acid catalyzed reactions require high temperature and longer reaction times. It is also proven that triglycerides conversion was maximally achieved by homogenous catalysis owing to good catalytic activity and high reaction rate (Ibrahim et al., 2020). However, it shows serious issues related to separation and purification of catalyst and product. The more often catalysts are consumed, they generate heavy amounts of wastewater and cause equipment corrosion (Gardy et al., 2019). To overcome the significant shortcomings of homogenous catalysis, heterogeneous catalysis is widely investigated in trans-esterification reaction. It is much more efficient and can be easily recycled depending on the nature catalyst. Heterogeneous catalysis is further sub-divided on the basis of type of catalyst used like alkali-, acid-, and enzyme-based *trans*-esterification process (Marwaha et al., 2018). It mainly depends on the type of metal, metal oxides, acids, bases, hydrocalcites and zeolites supported by the nanocatalyst being used. **Table 4** summarizes the research findings in context of the role of catalysis involved in biodiesel production.

Unlike homogenous catalysis, heterogenous catalysis can significantly convert low grade feedstock oil and fats using a

TABLE 2 | Advantages and disadvantages of biodiesel preparation methods.

Biodiesel preparation methods	Methodology	Advantages	Disadvantages
Direct blending	Pre-heated oils are mixed with commercial diesel in appropriate ratio and the final mixture is used as fuel	No requirement of chemical and additional processing	Insufficient for long term use, high viscosity in comparison to standard fuel, low volatility and eventually cause engine blockage
Pyrolysis or thermal cracking	Biodiesel conversion proceeds through thermal treatment of vegetable oil or animal fat etc. below its boiling point	Effective and pollution free, no need of further separation or purification	High cost equipment, expensive and low biodiesel purity due to contamination of residues
Micro-emulsification	Thermodynamically stable process, require extraneous mixing of vegetable oil or fat, surfactant and solvent like methanol, butanol etc.	Simple process and used for highly viscous oil	Incomplete combustion and release of excessive carbon deposits
Trans-esterification	In this method, triglycerides react with methanol in presence of catalyst producing fatty acid methyl esters and glycerol followed by separation and purification	Mild reaction conditions, high conversion rate and easily processed on large scale production	Waste-water generation, formation of side products and treatment of low fatty acid content
	Mishra and Goswami (2017); Srivastava et al. (2018); Zahan and Kano (2018)	Mishra and Goswami (2017); Srivastava et al. (2018); Zahan and Kano (2018)	Mishra and Goswami (2017); Srivastava et al. (2018); Zahan and Kano (2018)

solid acid catalyst. Solid acid and base catalyzed reactions eventually increase the catalytic efficiency and undergo both esterification and *trans*-esterification reactions simultaneously under extreme reaction conditions. It has shown much tolerance over high free fatty acids content and water. Recent development on synthesizing solid acid and base catalysts with mono-functionality or bi-functionality will eventually enhance the catalytic activity and the reaction conditions will be improved. Extensive research has been developed on synthesizing the novel solid acid catalyst by using organic polymer and imidazole salt based bi-functional catalysts which worked significantly under milder reaction conditions as compared to previous reported literature (Pan et al., 2020). Pan et al. have reported the synthesis of an imidazole salt-based catalyst, namely 1,3-disulfonic acid imidazolium tetrachloroferrate ([DSI] [$FeCl_4$]) bi-functional catalyst possessing Lewis (L)acid and Brønsted (B) acidic properties. The developed catalyst has shown excellent catalytic activity in the conversion of FPLF oil to biodiesel with a conversion efficiency of 97%. Owing to its bifunctionality the number of acidic active sites were increased significantly with mesoporous morphology which in turn helps in increasing the overall production of biodiesel from FPLF oil. The catalyst has high acidic properties with a B/L molar ratio of 2.12 revealing that the active sites are mainly the representation of cation and anion respectively in comparison to commercially available resins which overall increases the catalytic activity. The role of the catalyst was briefly analyzed in the presence and absence of the catalyst. In the absence of the catalyst the reaction barely proceeds, while taking $FeCl_3$ as a homogenous catalyst, biodiesel production of 63.2% was obtained, and using [DSI] [Cl] as catalyst, 86.0% of biodiesel was reported. As these catalysts serve as homogenous catalysts, this mainly brings the problematic issues of catalyst separation and reusability. However, when the reaction was done using [DSI] [$FeCl_4$] as a solid acid heterogeneous catalyst, the corresponding biodiesel production of 97.0% was achieved under mild reaction conditions which is due to the presence of BA and LA character. The catalyst heterogeneity was also confirmed from FT-IR spectra representing the intact acidic and basic active sites. The catalyst was also reused for four runs with the yields of 95% (Pan et al., 2018).

Another study reported on synthesizing heterogeneous solid acid catalysts using ionic liquids functionalized with melamine-formaldehyde polymer. The catalyst has been used for biodiesel production from oleic acid under mild reaction conditions. These catalysts showed a mesoporous and coral-like structure with a rough surface, indicating the combination of amorphous covalent-organic polymers basically imparting excellent structural and thermal stability. The catalyst possessed a surface area of 283.0 m^2/g with a corresponding porosity of 0.65–0.99 obtained from the hysteresis loop, confirming its structural integrity with thermal stability up to 300°C. This study also depicted the role of the catalyst in biodiesel production, as mentioned, the absence of catalyst produces low yield, while varying catalyst amount from 1 to 4 wt%, the biodiesel yield increases from 57 to 95%. The increase in production is mainly because of the presence of large acidic

TABLE 3 | Summary of research findings on homogenous and heterogeneous catalysis.

Title of published work	Main content	References
Carbon-based catalysts for biodiesel production—A review	This work highlights the production of biodiesel from either carbohydrate or biomass precursors using carbon-based catalyst	Clohessy and Kwapinski (2020)
Recent advances of biodiesel production using ionic liquids supported on nanoporous materials as catalysts: A review	This study focuses on the utilisation of tunable properties of IL-nanoporous materials for biodiesel production	Ali et al. (2020)
State of the art of biodiesel production processes: a review of the heterogeneous catalyst	This study focuses on various technologies used for biodiesel production	Ruhul et al. (2015)
A review on latest developments and future prospects of heterogeneous catalyst in biodiesel production from non-edible oils	This review highlights the importance of heterogeneous catalysts with special emphasis on the prospects of commercialization of those catalysts	Mardhiah et al. (2017)
Biodiesel production using enzymatic transesterification—Current state and perspectives	This work discussed key operational variables that influence lipase activity and stability along with technological solutions for industrial implementation	Gog et al. (2012)
Modern heterogeneous catalysts for biodiesel production: A comprehensive review	This work focused on different heterogeneous catalysts (acid, base, acid-base) and biocatalyst for biodiesel production	Chouhan and Sarma (2011)
Characterization of MgO nanocatalysts to produce biodiesel from goat fat using trans-eserification process	This study highlights the biodiesel production from goat fat	Hassan and Hossein (2019)

active sites and the large surface area of the catalyst which increases the overall catalytic activity. The catalyst has also been evaluated for reusability tests with a production efficiency of 88% for four runs (Pan et al., 2019). The newly developed catalyst can be efficiently and robustly used in biodiesel production.

Solid base catalysts are also deemed to have high conversion efficiency along with easy separation and recyclability. Synthesizing solid base catalysts from natural resources will be efficient in cheap biodiesel production. Dai et al. reported the synthesis of Si and Al doped lithium carbonate compound derived from clay materials using one-pot blending and grinding followed by heating at a high temperature. The optimum doping and calcination temperature significantly increase the number of active basic sites thus increasing the catalytic activity. Beyond optimum calcination temperature, the surface morphology reveals high agglomeration, further decreasing the pore size and diameter. The catalyst was utilized for biodiesel production using soybean oil at optimum reaction parameters (reaction temp.–65°C, reaction time-4 h, methanol to oil molar ratio-36:1 and catalyst weight-8 wt%) producing a yield of 98–99%. The catalyst was however recycled for a seventh run with an insignificant loss of activity (Dai et al., 2020). Roy et al. discussed another solid base catalyst $BaSnO_3$ as single-phase perovskite. The base catalyst of different Ba:Sn ratios at varying calcination temperatures was synthesized by the impregnation method. The Ba:Sn ratio of 1:1 and calcination temperature of 850°C was used for trans-esterification of waste cooking oil for biodiesel production. The optimized $BaSnO_3$ was found to be highly active with a large surface area and pore diameter of 144.09 m^2/g and 28.34 nm respectively. The average pore size distribution mainly corresponds to a mesoporous range. The optimum reaction conditions like catalyst weight –2.5 wt%, reaction temperature and time, –65°C and 25 min respectively, and a methanol to oil molar ratio of –16:1 produces a biodiesel yield of 98% and the recyclability of the catalyst for up to 5 cycles with total production of 81.6% (Roy et al, 2020; Sulaiman et al., 2019). However, it was observed that this solid base catalyst also uses extreme reaction conditions and a high alcohol to oil ratio. The extreme reaction conditions will delimit its large scale production and commercialization.

Furthermore, the presence of nanocatalysts in heterogeneous catalysis present a new pathway for synthesizing different nanocatalytic materials, which significantly enhanced the biodiesel production corresponding to its high catalytic activity, large surface area and high porosity. As a bulk metal oxide-based catalyst shows instability at high temperatures, which leads to catalyst deactivation along with the metal leaching and surface deformation creating major hindrance in increased biodiesel production. To overcome these serious drawbacks, recent extensive studies have been focused pertinently on developing a wide variety of nanocatalysts based on supported materials like zeolites, zirconia, polymers, and heteropolyacids catalysts, which significantly impart chemical and structural stability to sustain high reaction temperatures and longevity with increased catalytic activity (Zuliani et al., 2018).

The enzyme catalyzed reactions are quite expensive and process under milder reaction conditions corresponding to less energy consumption with a simplified purification process. Low grade feedstock with high free fatty acid content can also be converted easily. Nanocatalysts immobilized over enzymes present a new perspective in the production of biodiesel. However, it still cannot be used on large scale due to factors like long reaction time, type of enzyme immobilized, operating conditions like pH, and temperature (Mishra and Goswami, 2017; Sarno and Iuliano, 2019).

APPLICATION OF NANOCATALYST FOR BIODIESEL PRODUCTION

Nanocatalyst properties like catalytic activity, specificity and overall stability affect the cost of biodiesel production. Catalytic activity is affected by physical, mechanical, and thermal degradation. Numerous modifications of nanocatalysts are being designed, and it has been concluded that powdered acidic and basic catalysts are unsuitable for production on an industrial scale, owing to its small particle size of catalyst as it substantially affects catalytic activity and methyl ester yield (Azyan et al., 2018; Silveira et al., 2019). The structural and morphological nature of a catalyst plays a huge role in heterogeneous catalysis. Spherical catalysts have a good stability and are easy to separate from the reaction mixture. Designing nanocatalysts in order to have better stability over high temperatures is also a main parameter affecting the reaction conditions, as it also increases the chances of recyclability and reusability of the nanocatalyst (Rasouli and Esmaeili, 2019). Fabrication of nanocatalysts in the production of biodiesel has gained enormous interest in recent years. Various types of catalysts consisting of inorganic components such as oxides, sulphides, and metal salts as well as organic, including ion exchange resin and enzyme are being developed and the comparative study of different types of catalysts are mentioned in **Figure 3**. In light of nanotechnology, synthesizing the catalyst on a large scale would need to surpass many hurdles posed by the utilization of conventional catalysts (Deepalakshmi et al., 2015). The solid based catalyst also has serious problems of mass transfer resistance, time consumption, fast deactivation, and inefficiency of catalysts in long term use (Fattah et al., 2020). To overcome the limitations of solid based catalyst, nanocatalysts can be exploited to introduce lewis acidic or basic characters, increased acidity and active sites to the composites in order to improve its efficiency in catalysing the *trans*-esterification reaction. Nanocatalyst modification using different materials are of current interest as it significantly increases the surface area and porosity, reduces the leaching of metal ions, and increases the withstanding ability to acidic and environment thermal stability.

Many researchers have now focused on the development of nanocatalysts consisting of polymer, zeolite, and carbon-based nanomaterials, which mainly present attractive properties of high catalytic activity, reducing the reaction time and temperature. Thus, modification and synthesis of nanocatalysts will provide a significant increase in biofuel production (Marwaha et al., 2018).

The newly developed nanocatalyst can be synthesized by many possible methods like precipitation, impregnation, chemical vapour deposition (CVD), and electrochemical deposition techniques. However, precipitation and impregnation methods are cheap and cost effective, but they restrict a limitation on the regular size control and the overall morphology of the nanocatalyst. As CVD and electrochemical techniques produce a well-controlled morphology and size of the nanoparticles, they are rather expensive and require high temperatures. To overcome these challenges, we have discussed various kinds of nanocatalysts and their role in increasing biofuel production (Saoud, 2018).

Metal Oxides-Based Nanocatalysts

Metal oxide based solid catalysts are being conventionally used in biodiesel production. These catalysts play a very important role in homogenous catalysis and are largely responsible for the conversion of processed feedstock on a large scale. These correspond to major production of biodiesel. These catalysts pose certain limitations in the reduction of its activity as it cannot be separated after its use with increasing reaction time. Developing newly modified nanocatalysts based on oxides of various metals like Ca, Zn, Mg etc. plays a pivotal role in catalyzing the reaction along with an increase in production (Rengasamy et al., 2014; Thangaraj et al., 2019). **Table 4** summarises the utilization of metal oxide based nanocatalysts for increasing biodiesel production.

As Bharti and Singh (2019) reported the synthesis of a calcium oxide nanocatalyst via the sol-gel method, and utilized it in the synthesis of biodiesel using soybean oil as feedstock material. The nanocatalyst has proven to be efficient and effective in terms of possessing increased active sites, high surface to volume ratio, with a small particle size of 8 nm in correspondance to nanoscale level/nanometric scale. The BET surface area and pore diameter were found to be 67.78 m^2/g and 3.302 nm which is also high as compared to commercially available CaO catalysts. The increasing surface area is mainly due to small particle size, which correspondingly increases the reaction rate. After considering various optimization parameters like catalyst amount, methanol to oil ratio, and reaction temperature, a biodiesel production of 97.61% was obtained (Bharti and Singh, 2019). The CaO nanocatalyst can easily convert a maximum amount of fatty acids and oils, but it is unsuitable for long term use due to leaching and blockage of active sites. However, doping of metal and metal oxides can significantly reduce its inefficiency to a large extent.

Borah et al. (2019) also studied Zn doped egg-shell CaO nanocatalyst for *trans*-esterification of waste cooking oil used as feedstock. The nanocatalyst was synthesized using a wet impregnation method by varying Zn^{2+} concentration (0.5–2 wt %) doped with CaO. The nanocatalyst with 1 wt% Zn/CaO showed a spherical shaped morphology with non-uniform size having an average particle size of 30–42 nm thus creating more active sites and increased activity. However, with increasing Zn^{2+} concentration beyond, the catalytic activity of the nanocatalyst decreases while the spherical shape morphology also becomes distorted, thereby reducing the number of active sites as confirmed from SEM images. Besides this, the catalyst amount

was concomitantly varied up to 5 wt% giving maximum biodiesel production. The nanocatalyst at the given operating conditions of 5 wt% catalyst amount, 20:1 molar ratio of methanol to oil at 65°C reaction temperature and 4-h reaction time has provided maximum biodiesel production of 96.74%. It was further reused for five runs, but the yield decreased gradually which may be because of catalyst poisoning and leaching of metal ions. The comparison of XRD spectra of fresh and reused catalysts also revealed the loss of crystallinity contributing to the decrease in overall catalytic activity (Borah et al., 2019).

Todorović et al. (2019) also reported the optimization of various reaction variables like methanol to oil ratio (7.1:1), catalyst concentration (0.7 M), and reaction temperature of 52°C in biodiesel production using a CaO nanocatalyst and crude biodiesel as co-solvent with corresponding biodiesel yield of 99.8%. The catalyst was reportedly used four times with varying reaction conditions giving a biodiesel conversion of 97.7% in 5 h at the second cycle (Todorović et al., 2019). Various researchers have also reported the synthesis and utilization of CaO and doped CaO nanoparticles as nanocatalysts because of large surface area to volume ratios, and high basicity which results in an increase in conversion of fatty acids to fatty acid methyl esters.

Rahman et al. demonstrated the synthesis of calcium oxide nanoparticles using waste chicken eggshells by a calcination method, further using a wet impregnation method, it was doped with Zn and Cu metal respectively. Biodiesel production using doped CaO nanocatalyst shows increased production under the given optimized reaction parameter of methanol to oil molar ratio (6:1), catalyst amount (5 wt%) and reaction temperature and time of 65°C and 2.5 h respectively. Among these three nanocatalysts, Zn/CaO have shown maximum efficiency in biodiesel production along with its reusability of up to seven consecutive cycles with an approximate corresponding yield of 85% (Rahman et al., 2018). As CaO nanocatalyst is a highly investigated basic catalyst in *trans*-esterification reaction, it also contributes negatively to the conversion efficiency because of leaching. Leaching is mainly caused by hydrolyzation of the catalyst and it ultimately results in saponification, thus reducing the overall catalytic activity and selectivity of the catalyst. Wen et al. has reported the development of Li doped MgO nanocatalyst at its dosage of 9%, yielding 93.9% at a reaction temperature of 60°C using a molar ratio of methanol to oil of 12:1 (Wen et al., 2010). These catalysts provide more basic site formation due to the incorporation of Li, thereby increasing the biofuel production. Xie et al. (2007b) has developed other nanocatalysts like Na doped ZnO and Li doped ZnO, and utilized it in *trans*-esterification reaction showing good catalytic activity mainly corresponding to the amount of lithium loading (Xie et al., 2007b).

Regarding binary metal oxides, Mguni et al. (2012) reported sunflower oil being used as a feedstock material and nanocatalyst MgO deposited on TiO_2 used as supporting material. The developed nanocatalyst has been used for the production of biodiesel by varying the catalyst concentration and reaction temperature. The MgO concentration of 10, 20, 30% weight

have been loaded over TiO_2 nanoparticles which has been utilized further for biodiesel production of 84, 91, 95% at temperature 250°C, while 15, 35, and 42% at corresponding temperature of 150°C respectively indicating the effect of temperature. The effect of MgO loading increases the catalytic activity with limited loss of leaching and catalytic activity (Mguni et al., 2012).

Vahid and Haghighi (2016) reported the nanocatalyst MgO/$MgAl_2O_4$ based on spinel structure of magnesium, mainly synthesized from the combustion method followed by the impregnation method. The prepared catalyst possessed high surface area with excellent morphological properties and has been utilized for biodiesel production using sunflower oil as the feedstock. In this study, the effect of the fuel ratio was analyzed while synthesizing the catalyst. It was evident that the fuel ratio has a significant impact on morphology, pore size, pore diameter and specific surface area. The optimum fuel ratio of 1.5 has shown the specific surface area and average pore diameter of 60.6 m^2/g and 6.3 nm respectively. With increasing fuel ratio, the crystallinity and surface area of the catalyst increases, indicating the complete conversion of the precursors into final products. The optimized catalyst was further tested for biodiesel production at operating reaction parameters (reaction temperature-110°C, reaction time-3 h, catalyst amount-3 wt% and M:O ratio-12:1) with a conversion efficiency of 95.7%. The catalyst has been further analyzed for reusability tests with loss in catalytic efficiency of 5–9% after the third run, which is due to leaching of active species MgO, however after the third run there is insignificant loss in the activity of the catalyst (Vahid and Haghighi, 2016). As observed from the study, MgO doping also has a substantial impact on improving the biodiesel yield.

Apart from this, a TiO_2 based nanocatalyst has also been extensively investigated with several modifications. Gardy et al. (2017) significantly discussed the modification of TiO_2 based nanocatalysts in biodiesl production. A mesoporous TiO_2/$PrSO_3H$ solid acid nanocatalyst was developed by the grafting method. In this study propyl sulfonic acid was loaded for TiO_2 support and was simultaneously used for the esterification and *trans*-esterification process for biodiesel production using used cooking oil as feedstock. FAME conversion of 98.3% was achieved. Increased conversion mainly corresponds to post functionalization over nanostructured material due to the hydrophilic sulphonic group which increases the acidic strength and active site of the nanocatalyst, providing more accessibility between feedstock oil and methanol. The nanocatalysts were recycled and reused for four runs without appreciable loss in catalytic activity (Gardy et al. (2017)).

Further novel modification of TiO_2 nanoparticles (NPs) based on solid acid magnetic catalysts have been synthesized using the functionalization of TiO_2 NPs. The SO_4/Fe-Al-TiO_2 catalyst uses alumina as buffer layer, while hematite was employed to impart the magnetic character. The buffer layer is used to prevent the setback, as magnetic material loses its activity under acidic conditions. Sandwiching the metal oxides with polymer and stable materials will improve the overall stability of the catalyst. Then sulfation was done using chlorosulphonic acid in order to impart Brønsted acidity. The novel catalyst was

utilized in the *trans*-esterification of waste cooking oil with a conversion efficiency of 96%. The catalytic activity was attributed to the incorporation of sulphate which provides significant acidity to the overall catalyst, while magnetic material will ease in the separation procedure with small amounts of loss during the recovery procedure. The catalysts were efficiently used for ten cycles without any loss in their activity. The catalyst was quite effective for simultaneous esterification and *trans*-esterification reaction and feedstock containing high (20 wt. %) free fatty acids content. (Gardy et al., 2018). Ambat et al. reported the synthesis of TiO$_2$ nanoparticle doped with potassium tartarate by the impregnation method and further utilized linseed oil for biodiesel production. The potassium tartarate doping significantly increases the basicity of the nanocatalyst, giving a maximum production of 98.9%. The catalyst showed promising results up to five cycles without loss in its activity (Ambat et al., 2018b)

Various magnetite based nanocatalysts have been prepared and further utilized for *trans*-esterification of triglycerides for biodiesel production (Shi et al., 2017). Feyzi et al. (2013) studied the *trans*-esterification reaction of sunflower oil using the nanocatalyst Cs/Al/Fe$_3$O$_4$ under optimized reaction conditions, leading to 94.8% production of biodiesel while showing excellent catalytic activity. The present nanocatalyst reports the effect of different molar ratios of Cs-Al and Cs-Fe on the nanocatalyst, while calcination temperature and time have also been analyzed in order to maximize the overall performance of synthesized nanocatalyst. The magnetic nanocatalysts have shown excellent catalytic activity at an optimum calcination temperature and time of 500°C and 7 h. From the given study it was confirmed that beyond optimum conditions the nanocatalyst shows morphological and textural differences owing to an agglomeration caused by sintering, the surface area has also been reduced as confirmed from BET surface area analysis. The nanocatalyst optimization followed by reaction parameters optimization presents a significant increase in biodiesel production (Feyzi et al., 2013).

Mixed metal oxides nanoparticles also impart a good interaction between free fatty acids and methanol, besides excellent tolerance at high temperatures giving enhanced production.

Future studies can be focused on analyzing the phase structure of TiO$_2$ nanoparticles and other metal oxides while doping with polymeric and carbon based nanomaterials, to significantly improve the stability and catalytic activity of the nanocatalyst which correspondingly increases biodiesel yield.

Carbon Based Nanocatalysts

Nanocatalysts derived from carbon materials like graphene, carbon nanotubes (Gardy et al., 2019b), and reduced graphene oxides have shown good physical and chemical properties corresponding to different morphologies and sizes of the derived nanocomposite materials (Shu et al., 2019; Nizami and Rehan, 2018). Poonjarernsilp et al. has reported the use of multiwall porous nanohorn carbon nanotubes (CNT) dispersed in Fe/Fe$_2$O$_3$ mixed nanoparticles for simultaneous determination of *trans*-esterification reaction (Poonjarernsilp

et al., 2014). Guan et al. (2017) reported the *trans*-esterification of triglycerides using sulphonated multiwalled CNT as a nanocatalyst. Biodiesel production of 97.8% was obtained in 1 h, at 150°C, and with 3.7 wt% catalysts. It was revealed that nanocatalysts with acidic character, and high porosity and surface area leads to better catalytic activity of the nanocatalyst (Guan et al., 2017). **Table 5** represents the use of carbon based nanocatalysts in enhanced biodiesel production.

As carbon nanotubes possess both chemical and structural stability, Zhang et al. (2014) described the synthesis of carbon based nanostructured materials using stainless steel as substrate materials, as it can be easily involved in heterogeneous catalysis due to easy separation and recycling. The CNT was multi functionalized using various procedures. Biodiesel conversion of 85% was obtained with the simultaneous use of the nanocatalyst for 95 h without losing its structural integrity and morphology (Zhang et al., 2014). Another group (Asri et al., 2020) reported the synthesis of multiwalled CNT loaded with varying ZnO nanoparticles. The developed heterogeneous solid acid nanocatalysts have been utilized for *trans*-esterification of Kesambi oil giving methyl esters production of 13.82% while using only 20 wt% of ZnO loaded MWCNT. Carbon nanotubes mainly possess high specific surface area, but its surface area has been reduced greatly upon ZnO loading. The active sites predominantly increase, ultimately increasing the reaction rate and overall activity of the nanocatalyst, also the mass transfer is greatly reduced (Asri et al., 2020).

Shuit et al. (2015) also reported the use of sulphonated multiwalled carbon nanotubes (s-MWCNT) for esterification of palm fatty acid distillate. The s-MWCNT have shown better catalytic activity in comparison to metal oxide doped CNT with minimum loading of 3 wt%, reaction time and temperature of 2 h and 170°C respectively, yielding methyl esters of 93.5%. The nanocatalysts have been utilized for 5 consecutive runs giving 75% yield. It can also be easily regenerated with sulphuric acid and further utilized producing a yield of 86.2%. The regeneration process is important in retaining the lost sulphonic group during the leaching process (Shuit and Tan, 2015). Ibrahim et al. (2020) reported the impregnation of sodium oxide over carbon nanotubes for *trans*-esterification of waste cocking oil. The nanocatalysts have shown excellent catalytic activity due to the presence of sodium ions and oxide ions. The cation imparts lewis acidity while the anion acts as a Brønsted base, thus overall enhancing the catalytic activity with biodiesel production of 97%. It is found to be unstable after 3 cycles because of leaching, which causes deactivation of active sites (Ibrahim et al., 2020).

Carbon nanotubes were also utilized as catalysts, using a homogenous alkali catalyst as reported by Shankar et al. (2017). Biodiesel production from cottonseed oil was evaluated using *trans*-esterification reaction using homogenous alkali-based carbon nanotubes as a nanocatalyst, giving an optimum yield of 95% within a time range of 60–120 min (Shankar et al., 2017). Various groups have also used immobilized lipase enzymes over multiwalled carbon nanotubes for biodiesel production as it exhibits enhanced thermal stability and recyclability (Fan et al.,

2017). Fan et al. (2017) reported the synthesis of multiwalled CNT filled with iron oxide further linking with polyamidoamine dendrimers and finally immobilised it over *Burkholderia Cepacia Lipase* (BCL). The developed catalyst has shown higher catalytic activity due to the presence of large dendrimers linked over to the surface of the nanotubes, giving an ultimate yield of 92.8%, with excellent recyclability up to 20 successive runs along with retaining the activity of catalyst to around 90%. The nanocatalyst can be easily separated due to presence of magnetic iron oxide (Fan et al., 2017). This biotechnological application can be used on a large scale if processed properly, minimizing the large utilization of the nanocatalyst.

Graphene oxide also showed better conversion of fatty acids because of greater surface area and different functional group. Borah et al. (2018) synthesized *in situ* TiO$_2$/reduced graphene oxide nanocomposites involving heterogeneous catalysis of waste cooking oil via *trans*-esterification reaction. The optimized conditions were found to be a methanol to oil molar ratio of 12:1 at 65°C for 3h at a catalyst loading of 1.5 wt% and corresponds to a conversion efficiency of 98%. The catalyst was dried at 100°C for 2 h and was reused for three cycles with an efficiency of 78.86% (Borah et al., 2018).

Biochar based nanocatalysts are important in catalyzing the biodiesel production. It is mainly derived from pyrolysis and hydrothermal carbonization of various biomass materials, followed by its functionalization using various materials like metal and metal oxides nanoparticles, sulphonated groups, and nitrogen-containing groups in order to increase its active sites, catalytic activity, porosity, and effective surface area. The other carbon based nanocatalyst can be easily derived from fly ash and sugar-based nanomaterials using the carbonization method, and can be further analyzed for *trans*- esterification reaction. It was observed that biodiesel production increases, but the catalyst suffers thermal instability and also requires a long reaction time (Abdullah et al., 2017; Gardy et al., 2019b).

Rashid et al. (2019) utilized palm kernel shell as feedstock material for biodiesel production using biochar-based sulphonated zirconium catalyst yielding a fatty acid methyl ester production of 94.3% using only 3 wt% catalyst amount at a reaction temperature and time of 75°C and 3 h respectively. The catalyst has also shown successful reusability over five successive cycles with a conversion efficiency of 80% (Rahman et al., 2018; Rashid et al., 2019).

Zeolite Based Nanocatalyst

The utilization of zeolite materials has seen upsurge in recent years. They are widely investigated, as they significantly possess specific characteristics like high surface area and thermal stability, presence of active acidic and basic sites (Martínez et al., 2011), high catalytic activity, easily modified structure by using different functionalities, and metal exchange (Zhang et al., 2019). As compared to natural zeolite materials, synthetic-based materials are extensively used on a commercial scale. Their properties can be modified by varying the concentration of silicates and aluminates materials, it can also be predominantly used or modified by using various metal and metal oxide nanoparticles exchange to obtain pure crystalline,

uniform pore and particle size materials. It is used as a carrier or support system when impregnated with different nanoparticles of metal oxides like Fe$_2$O$_3$, CaO, MgO, etc. (Go et al., 2007; Centi et al., 2012). Commercially available synthetic zeolites are ZSM-5, X, Y, and beta zeolites that are mainly used for biodiesel production (Abukhadra et al., 2019). Summary of different zeolites based nanocatalysts involved in biodiesel production are reported in the **Table 6**.

Xie et al. (2007a) shown the *trans*-esterification of soybean oil as feedstock using KOH loaded NaX zeolite. The obtained optimized reaction conditions were 3 wt% catalyst amounts, methanol to oil ratio of 10:1, reaction time and temperature of 8 h and 65°C respectively. The biodiesel production was found to be 85.6% (Xie et al., 2007a). This zeolite was synthesized and analyzed using different compositions of x and y for obtaining the maximum yield of biodiesel production. The acidic property of zeolites is due to imbalance in charge present on alumina and silica units, which mainly contribute to the aluminosilicates framework. Overall the uniform pore size and acidity are a considerably important parameter in enhancing the biodiesel (Fattahi et al., 2019; Mohebbi et al., 2020).

Another group has (Pratap et al., 2015) reported the use of NaY and KOH/NaY zeolites catalyst in trans–esterification of Madhuca indica oil. These zeolites have attained a conversion efficiency of 98.9%. As these catalysts are recycled and reused several times, they can be easily activated by washing with methanol followed by calcination in a muffle furnace for a given period of time. Due to the presence of large basic sites, its catalytic activity has increased to a greater extent (Pratap et al., 2015). However, synthesizing nanocatalysts with zeolite plays an important role in achieving maximum conversion, recyclability, and reusability of the catalyst involved in *trans*-esterification reaction. Trans esterification of soybean oil to biodiesel is carried out using zeolite supported CaO as strong base catalysts (Wu et al., 2013). Zhuang Li reported the synthesis of Li/Na based zeolites, by hydrothermal and micro-emulsion methods and further used for fatty acid methyl production using castor oil as a feedstock material. To obtain the high catalytic activity the synthesized particles were calcined at various calcination temperatures, which is maximally useful for a greater conversion of biodiesel. It was reported that using an optimized catalyst amount of 3 wt% and an alcohol to oil molar ratio of 18:1, biodiesel yield was found to be 98.6% with reaction temperature and time of 75°C and 2 h respectively. The catalyst has also shown excellent recyclability and reusability (Li et al., 2019).

Martinez et al. described the utilization of CaO nanoparticles/ NaX zeolite for *trans*-esterification of sunflower oil under optimized conditions giving 93.5% biodiesel production (Martínez et al., 2011). Wu et al. demonstrated CaO/NaY zeolites with a conversion efficiency of 95%. However, at certain high temperatures, CaO may lose its activity due to leaching and instability. To overcome these shortcomings, Firouzjaee and Taghizadeh, 2017 reported the nanomagnetic based zeolite catalyst CaO/NaY-Fe$_3$O$_4$ which shows excellent stability at high temperatures, along with ease in the separation process. Various parameters are being monitored,

revealing a conversion efficiency of 95.37% using canola oil as feedstock material (Firouzjaee and Taghizadeh, 2017).

Recently, ZSM based materials have been synthetically modified by the desilication method followed by impregnation to increase the yield of biofuel production. Alaba et al. reported the synthesis of a modified form of ZSM-5 (ZBio) to produce mesoporous zeolites named as 0.3 mesoZBio and 0.4 mesoZBio. In this study, a pyrolysis method was employed to examine the kinetics involved in biodiesel production from shea butter using these catalysts. The analysis was monitored by Thermo-gravimetric analysis. ZBio shows the higher activation energy which is because of the presence of acid active sites producing a large biodiesel production. It may also be confirmed that the direct functional group acidity and porosity are directly related the biodiesel yield of 87% that was achieved (Vieira et al., 2013; Alaba et al., 2016a). Furthermore, the modification of zeolites with MoO_3 nanoparticles was synthesized by a hydrothermal method followed by an impregnation method. The molybdenum impregnation mainly decreases the strength of acid sites and increases the concentration of acidic active sites. The optimized 25% MoO3 showed spherical morphology with high crystallinity and mesoporous structure which predominantly increases the conversion process with an efficiency of 98%. The increased catalytic activity is because of high crystallinity and increased acidity. From the given study it can be concluded that functionalization of zeolites with the nanocatalyst will provide a new insight in increasing the production of biodiesel on large scale (Mohebbi et al., 2020).

PHYSICO-CHEMICAL STUDIES OF BIODIESEL PRODUCTION

Physico-chemical properties test methods for free fatty acids (FFA) content and FAME (fatty acid methyl esters) play a very important role in biofuel production. The biodiesel quality is mainly based on standardized conditions specified by ASTM (American Society for testing Materials), European standard (EN) and Czech Republic (CSN). The quality of biodiesel must meet the given specifications. The properties such as density, kinematic viscosity, oxidation stability, flash point, cloud point, and fire point of the biodiesel produced by utilizing different nanocatalysts were reported and compared with the ASTM (D6751) and EN 14214 standards of biodiesel (Lima et al., 2010 Hoang, 2018; Huang et al., 2020; Lima et al., 2010).These properties are specifically affected by high free fatty acid percentage, water content, and impurities. Estimation of acid value and saponification value of feedstock are also significant as they correspondingly determine the yield and purity of biodiesel.

Abukhadra et al. (2019) have significantly discussed the trans-esterification reaction under normal stirring and ultrasonic stirring. Interestingly, it shows that the given physico-chemical properties were affected, also the FAME composition differs verily and maximum production of 98.8% was achieved within a time period of 120 min (Abukhadra et al., 2019). Trans-esterification reaction involving different nanocatalysts will ultimately produce varieties of FAME compositions. Gardy et al. (2017), Gardy et al. (2018) has analyzed the effect of different nanocatalysts over the same feedstock (waste cooking oil) which produce different compositions of fatty acid methyl esters. For nanocatalyst TiO_2/$PrSO_3H$, FAME composition includes palmitic acid methyl ester, stearic acid methyl ester, oleic acid methyl ester, linoleic acid methyl ester, linoleic acid methyl ester, and gadoleic acid methyl ester (Gardy et al., 2017), while SO_4/Fe-Al-TiO_2 nanocatalyst majorly contributes to methyl palmitate, methyl oleate, and methyl linoleate (Gardy et al., 2018). Fatty acid methyl ester compositions produced by using an Na_2O/CNT nanocatalyst were found to be myristic acid methyl ester, palmitic acid methyl ester, linoleic acid methyl ester, and oleic acid methyl ester. Major amounts of palmitic and oleic acid were found as it was confirmed by GC analysis. An amount of saturated and unsaturated fatty acid methyl ester (Dantas et al., 2020; Ibrahim et al., 2020) was also reported. The physicochemical studies for various nanocatalysts used in deriving biodiesel have been discussed in **Table 8**.

Density Measurement

The density is defined as weight per unit volume, its measurement is important for the mass to volume conversion process required in biofuel production. It has significant impact on fuel quality. Blending of biodiesel fuel and correct formulation of blend are estimated by density measurement (Giakoumis and Sarakatsanis, 2018; NguyenThi et al., 2018). Though density of biodiesel mainly depends on the types of oil used and its treatment process (Pham et al., 2018). It is also affected by molecular weight of the components i.e. fatty acids. High molecular weight corresponds to high density which affects the quality of the fuel. It is significantly reported that low density is better for good quality of fuel (Hoang, 2018). Standard test methods for density measurements are done via pycnomter. The formula for density measurement is given in **Eq. 1** (Karmakar et al., 2018).

$$Density = \frac{(Mass\ of\ pycnometer\ with\ biodiesel) - (Mass\ of\ empty\ pycnometer)}{Biodiesel\ volume}$$

(1)

It is determined at temperatures ranging from 15 to 20°C depending on the standard specifications (Lima et al., 2010). It reveals information about homogeneity and atomization of the fuel (Ismail and Ali, 2015). Besides experimental determination, theoretical density measurement using optimization software is suitable in finding the correct composition of methyl esters (Pratas et al., 2011). Density can be significantly reduced by the *trans*-esterification process to achieve the limits of the specified standard.

Study of Kinematic Viscosity

Viscosity is a substantial parameter as an estimation of the quality of biodiesel. Viscosity indicates the fuel flowing ability as it affects the operation of fuel injection equipment especially at low temperatures (Ong et al., 2020). During the atomization process, high viscosity fuel leads to large droplets formation, thus creating operational problems, increased carbonization eventually leads to increased emission and smoke, while fuel with too low viscosity will results in leakage and increased wear, hence it significantly affects engine performance (Bassam et al., 2019; Huang et al., 2020). Influence of high viscosity of biodiesel

as compared to diesel fuel leads to concern in process equipment and design. Experimental viscosity measurement is done at a temperature of 40°C using a viscometer. The kinematic viscosity of biodiesel as per ASTM D6751 and EN 14214 was given to 1.9–6 and 3.5–5.0 mm^2/s respectively (Isioma et al., 2013).

Viscosity of biodiesel is primarily dependent on the type of feedstock and treatment it undergoes. FAME derived from edible oil does require less mild conditions to meet the standard of biodiesel as reported by this. While FAME conversion obtained from waste cooking oil possesses high viscosity and requires much treatment (Bikash et al., 2018; Douvartzides et al., 2019). Thus, it is quite tedious to determine viscosity at an experimental level under different reaction conditions in order to obtain optimized parameters. Therefore, it is imperative to approach theoretically the qualitative and quantitative examination of the quality of biodiesel derived from different sources under different reaction conditions. Scientists have used a number of correlation models based on length of carbon chain of methyl esters and degree of unsaturation. Krisnanykura et al. (2006) reported the methyl esters based on coconut oil based on different sets of parameters with maximum deviation of 9.2%. Pinzi et al. (2013) also reported the theoretical approach based on MLR multiple response optimizations for analyzing the degree of unsaturation and length of carbon chain to the obtained biodiesel viscosity.

In order to study and evaluate more than two properties Huang et al. (2020) group have extensively reported the multiple variables such as the effect of fatty acid methyl esters (FAME) composition and temperature over kinematic viscosity according to the following standard EN14103 and ASTM-D 445-88 for about 16 biodiesel and 55 FAME –FAME binary blends. The analysis was examined by using two correlation models. Firstly, multiple linear regression (MLR) analysis for kinematic viscosity–composites relationship at 40°C while the second correlation was reported between composition-temperature dependent viscosity correlations based on Arrhenius kinetics Chavarria-Hernandez method using viscosity data from Freitas (Hoang, 2018). From the given statistical model, analyzing different kinds of FAME compositions have shown dependency on the viscosity value on temperature which can help in lowering the temperature under optimized conditions.

Determination of Acid Values and Iodine Values

Assessing the acid value is an important parameter as it affects the quality of a particular biodiesel. It is defined as the presence of free acids in the given sample. It can be measured by neutralizing the sample using a specific amount of KOH as an excess of free fatty acid leads to catalyst deactivation and soap formation. Generally, the acid value of feedstock should range in between 1.86–3.31 mg KOH/g oil. However, for waste cooking oil, free fatty acid should be below 4 mg KOH/g in order to avoid the pre-treatment process, below this can directly be used for trans esterification reaction (Ismail and Ali, 2015). The biodiesel derived from flaxseed oil has value of 0.186 ± 0.02 mg KOH/g, thus falling under the value of the standard method (Ahmad et al., 2019). The acid value is dependent on the type of feedstock used. It was also

reported that waste cooking oil shows a high acid value because of thehuge amount of free fatty acid content. High acid value is also responsible for reducing engine performance and causing corrosion. Thus, depending on the content of free fatty acids, reaction conditions needs to be operated in order to maximize the yield.

The iodine value is defined as the measurement of degree of unsaturation. It also depends on the nature and type of feedstock and extremely influences the fuel oxidative ability. The diesel fuel must have an iodine value below 120 g I$_2$/100 g of the given sample. It will determine the unsaturation degree in a given mixture of fatty acids. Higher iodine value corresponds to lower oxidative stability. It will also reveal information about sludge formation in fuel, affect lubricant quality, and also cause corrosion (Bassam et al., 2019).

Cetane Number and Saponification Value

Saponification value is defined as milligrams of KOH used to saponify 1 g of fat or oil under a given condition. It is a measure of length and molecular weight of fatty acids. Crude esters have a higher saponification value than oil, and range from 199 to 207 mg KOH/g oil (Shalaby, 2013). Longer fatty acids chains have low saponification values as the number of free carboxylic acid groups decrease per unit fat or oil mass. It mainly measures the average molecular weight of the oil or fats present in the given sample. However, the saponification value of biodiesel and crude feedstock does not differ significantly as the average molecular weight undergo small changes. The variation in saponification values are almost similar (Gopinath et al., 2009).

Determination of cetane number is a crucial parameter in quantifying the ignition ability of the fuel. It corresponds to the ability of the fuel to auto ignite quickly after being injected into fuel line, and also shows the ignition quality of the fuel. Higher cetane number corresponds to better ignition quality while low cetane number primarily affects engine parameters with increased emission of smoke, combustion instability, also excessive deposition of unburn materials in engine (Ismail and Ali, 2015). Cetane numbers increase with the increasing length of fatty acids chain. Biodiesel possesses higher cetane numbers as compared to diesel fuel (Adebayo and Ameen, 2011).

Cloud and Pour Point

Cloud point (CP) is defined as the temperature at which wax crystals become visible when the fuel is cooled. It causes solidification of fuel at lower temperatures which could cause blockage in fuel lines. Cold point is estimated from ASTM Standards D5771, D5772, D5773, and D2500 (Sierra-cantor and Guerrero-fajardo, 2017). A Differential Scanning Calorimetry (DSC) curve can easily examine the formation of crystallization biodiesel (Gardy et al., 2017). Increase in crystallization will eventually cause agglomeration in the fuel thus deteriorating the engine performance. It can also cause blockages in the fuel filters of the engine due to thickening, which eventually ceases the fuel flowability. Easy crystallization of fuel is mainly due to the presence of a high amount of saturated fatty acids.

Pour point is the lowest temperature at which fuel starts flowing. Biodiesel derived from high saturated fatty acid

content possess a high value of pour point which indicates poor fuel property. The *trans*-esterification process greatly reduces the value of pour point in order to provide better quality fuel. As high fatty acid content after catalysis shows significant viscosity which also hampers fuel property.

Flash Point

Flash point is defined as the temperature at which fuel will ignite when exposed to flame. Biodiesel fuels have higher flash points in comparison to petrochemical derived fuels, and hence lead to safe transportation and storage of fuels (Esmaeili et al., 2019; Rasouli and Esmaeili, 2019). Low value of flash point indicates high volatility, it is also helpful in the classification of fuel in order to reduce the risk involved in handling and transportation. Biodiesel's flash point is greater than diesel fuel. The value of biodiesel based on these specification standards EN 14214 and ASTM 6751 must be a minimum of 120 and 130°C respectively. It is also easily affected by the presence of impurities like moisture content, unreacted alcohol, and oil content. Thus, it indirectly helps in identifying the quality of biodiesel fuels.

OPTIMIZATION PARAMETERS OF RAW MATERIALS FOR INCREASING BIODIESEL PRODUCTION

Another important parameter after selecting raw materials based on their physico-chemical properties, is optimizing the reaction conditions for ultimately carrying out the reaction in order to obtain maximum yield, as shown in **Figure 4**. Earlier optimization was carried out using variation of independent

and dependent variables while recording the single response at a time. This maximizes the time consumption along with increasing the chance of ineffectiveness in results as it does not involve the interaction of multiple variables at a time. However, developing new statistical tools and methods would easily process all the running parameters giving significant results (Borah et al., 2019). The reaction parameters were optimized using various software analysis of non-linear techniques like the Taguchi method using MINITAB software, Artificial Neural Network (ANN), Genetic Algorithm (GN), fuzzy logic, design of experiments, and Response Surface Methodology (RSM). In order to increase the biogas yield, ANN and GN are used in the design of experiment and fuzzy logic. These mathematical models are efficient in optimizing multiple reaction parameters at a time. It is also helpful in investigating the reaction kinetics and microbial culture communities which can increase its yield (Kana et al., 2012).

Among these non-linear techniques, RSM is an important tool for investigating the predominant reaction parameters consisting of molasses concentration, initial pH (Hamouda et al., 2015), reaction time and temperature, molar alcohol to oil ratio, and catalyst amount involved in production of bioethanol and biodiesel. Thus, it majorly improves the productivity, reduces time, material, and cost by optimization (Esmaeili et al., 2019).

RSM is an important tool to investigate the variation of different parameters in anaerobic fermentation and catalytic processes, thus improving the productivity of biodiesel by reducing material cost and reaction time by optimization. However in biodiesel production, evaluating the effect of operational parameters like molar ratio, reaction time, temperature and catalyst loading using different types of oil as
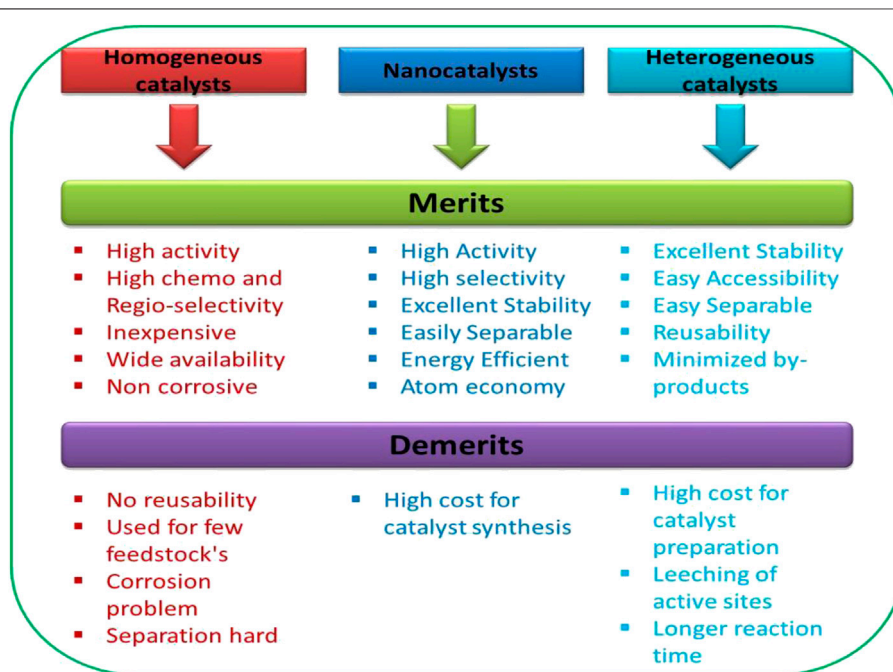
FIGURE 3 | Comparative study of different types of catalysts for biodiesel production.

FIGURE 4 | Illustration of various optimization parameters in biodiesel production.
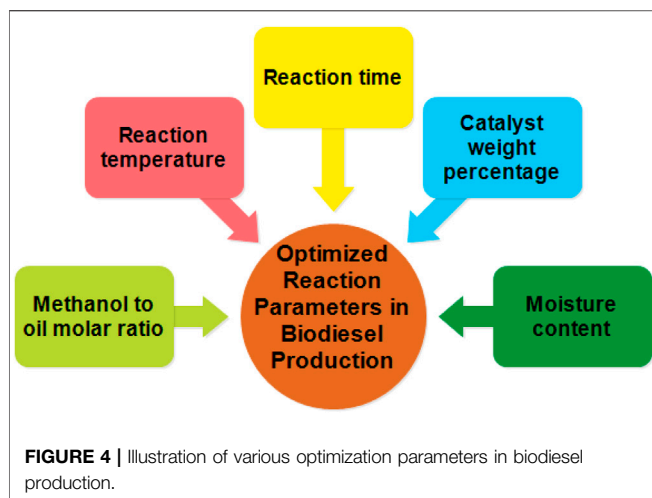
fuel with the help of RSM based experimental design will ultimately increase biofuel production, mainly biodiesel. It is a statistical tool based on mathematical and correlation models accounting for various reaction parameters like molar ratio of alcohol and oil, reaction time and temperature, and catalyst loading concentration. It also requires various other software for analyzing the dependent and independent variables based on regression analysis and analysis of coefficient of variance (ANOVA) in order to optimize and increase the yield of biodiesel. As reported by Ghalandari et al. (2019) *trans*-esterification of canola oil to methyl esters (biodiesel) in the presence of the magnetic core-mesoporous shell $KOH/Fe_3O_4@ɣ$-Al_2O_3 nanocatalyst was investigated using Response Surface Methodology (RSM) based on the Box-Behnken design (BBD) to optimize the influence of important operating variables on the yield of biodiesel. A biodiesel yield of 97.4% was achieved under optimum reaction conditions with excellent agreement between the predicted and experimental results (Ghalandari et al., 2019). Reaction temperature and free fatty acid content was found to be playing the main role in optimizing the reaction conditions, mainly *trans*-esterification. Free fatty acids content is found to be predominant in waste cooking oil, as high fatty acid leads to soap formation.

Reducing the concentration by using pre-treatment processes, followed by alkali-based *trans*-esterification process is an important step in maximizing the yield (Bankovi et al., 2014). It is also imperative that while using methanol as an alcohol source at atmospheric pressure, the temperature should be kept within the boiling point range as reported by many researchers. The esterification process is mainly influenced by the molar ratio of methanol: oil and catalyst concentration due to the impact of the molecular structure on the equilibrium reaction and functional substituents of types of alcohol and acid. However, the conversion rate of oil to methyl ester increases with reaction time, initial mixing and dispersion of methanol makes the reaction slower during 1–5 min, the maximum biodiesel production increases over a 15 min duration and decreases gradually. Reaction time can be effectively reduced by using various new heating techniques like infra-red and microwave

techniques. Important parameters determining the yield of biodiesel production are discussed as follows.

Methanol to Oil Ratio

The most important factor in biofuel production is the alcohol to oil molar ratio, type of alcohol and triglycerides used. The most probable M:O ratio is 3:1, as it is beneficial in increasing the solubility of oil and contact time. High molar ratio results in greater conversion of ester within a short span of time (Nanasaheb and Chandrakant, 2012). Stoichiometrically, 3 mol of alcohol and 1 mol of triglycerides are required for esterification process in order to yield 3 mol of fatty acids and 1 mol of glycerol. High fatty acid content needs a large amount of alcohol in order to proceed with the reaction in the forward direction, as the molar ratio is predominantly dependent on the nature of the oil and catalyst used. Using an optimized amount of alcohol subsequently increases biofuel production. However, using an excess of alcohol will eventually block the active sites of the catalyst and also increase backward reaction more favorably (Gashaw et al., 2015). Various alcohols like methanol, ethanol, propanol, and butanol are mostly used in the *trans*-esterification process. As reported by many researchers, methanol is mostly used due to low cost, but ethanol can also be used because of its environmentally friendly nature and its production from agricultural waste products (Hossain and Boyce, 2009; Deepalakshmi et al., 2015).

Moisture Content

While synthesizing biodiesel, *trans*-esterification is an obvious process as it mainly requires free fatty acid. Moisture content is inevitable with feedstock, and it plays a significant role in deterring the reaction condition due to the formation of soap, ultimately reducing the efficiency of the catalyst, hence reducing the yield of biofuel production. Moisture content also does give different by-products based on the type of catalysis i.e. acid and base catalyzed reaction. Pre-treatment processing of feedstock materials plays an important role in increasing the biofuel production (Gashaw et al., 2015).

Catalyst Weight (Nanocatalyst)

This is another key factor contributing towards the biodiesel production. The nature and amount of catalyst is mainly dependent on the reaction conditions required i.e. acidic or basic. It is also inadvertently dependent on the nature of feedstock used. If the feedstock is pure with normal moisture and free fatty acid contents, the optimized amount of nanocatalyst is enough in order to carry out the desired reaction. However, if the feedstock has a high moisture and free fatty acid content, the occurring *trans*-esterification process is actually insignificant as it mostly leads to soap formation and decreases the yield of biodiesel production. Considering the latter case, an increased amount of nanocatalyst will certainly increase the biodiesel production. Thus, proper pre-treatment process of feedstock is very important in controlled optimization of the nanocatalyst (Gashaw et al., 2015).

Considering all substantial parameters, the average catalyst amount in most of the study was reported in between 1–6 wt% for

optimum amount of the triglycerides content, it also significantly varied depending on the scale of production. However, in some cases it was reported to be high depending on the reaction conditions. Generally high catalyst weight was found to have negative impact on catalytic reaction as it creates mass transfer limitations and reduces the interaction of active sites caused by agglomeration (Kazemifard et al., 2018). Beyond the optimized amount, further addition will decrease production and it is not very effective economically.

Reaction Temperature

In order to increase the yield, reaction temperature also plays a significant role. An increase in temperature increases the reaction rate and kinetics ultimately reducing the reaction time (Gashaw et al., 2015). The *trans*-esterification process is usually done below the boiling temperature of alcohol within an optimum temperature range of 50–60°C depending on the type of oil used. High temperature mostly corresponds to the evaporation of alcohol used. As reported by many groups, at normal temperature, a 78% conversion is easily achieved within a 60–90 min time period (Hossain and Boyce, 2009).

Reaction Time

The temperature and time play a corresponding role in *trans*-esterification of oils or fatty acid esters. With an increase in time, fatty acid conversion increases, as initially the conversion is slow due to the dispersion and mixing of oil to methanol or alcohol. As the reaction proceeds towards the threshold, the conversion is usually faster owing to faster reaction kinetics. The nature of the catalyst has a high impact on reaction time as a mixed nanocatalyst requires much less time i.e. 1–2 h. It was reported that within 90 min, maximum ester conversion was achieved, however further increase in time does not increase the yield owing to the reversible nature of reaction, leading to more production of glycerol (Hossain and Boyce, 2009; Gashaw et al., 2015).

As these reaction parameters are being monitored primarily, various groups have reported maximum yield of biofuel production based on these reaction parameters. Since optimization of these parameters is mainly done via following statistics models like RSM and other models, using techniques like ANOVA and BBD configuration in order to find the significance in between these parameters (Anr et al., 2016).

JeyaKumar and Narayanasamy (2019) has reported the use of quadratic model ANOVA using BBD design for initializing the impact between parameters. After fitting in the given model, the most important parameters were found to be reaction time and catalyst loading. However, the variation of other parameters like molar oil ratio and temperature does not yield any significant changes in biofuel production (Jeyakumar and Narayanasamy, 2019). In order to find the significant optimized parameter, all parameters have to be considered first. However, as reported by Lee et al. (2011) based on findings that optimum biodiesel production was obtained at a lower molar ratio of methanol to oil and reaction temperature, 1:8 and 55°C respectively. It was also observed that increasing methanol concentration increases glycerol solubility, ultimately reducing the yield of final products. Significantly optimized components like a catalyst loading and reaction time of 0.6%, 80 min does contribute greater yields in the biodiesel production while rendering the saponification process. The extremely low and high catalyst loading does not give any significant results. The optimum reaction time of 80 min was found to be extremely influential in attaining the maximum biodiesel production. From the given observation, it can be inferred that at a given molar ratio, reaction temperature (55°C) and reaction time (80 min), the optimized catalyst loading was found to be 0.6%, mainly corroborating that lower catalyst loading gives a maximum yield of 92.43% (Lee et al., 2011).

Varghese et al. has reported the usage of 0.25% catalyst loading with other optimum reaction conditions like a reaction time and temperature of 30 min and 60°C respectively with a molar ratio of methanol to oil 6:1 (Ainun et al., 2017). **Table 8** briefly summarizes the role of nanocatalysts and the importance of optimization of parameters in enhancing the yield of biodiesel. Other parameters like co-solvent, reactor mixing speed, and type of reactor also show considerable effects on commercialization and large scale production of biodiesel (Chozhavendhan et al., 2020).

CHALLENGES AND LIMITATIONS

There are various potential challenges faced during the production of biodiesel. Starting from selection of biomass as raw materials in

TABLE 4 | Summary of the increased biodiesel production via metal oxide based nanocatalyst.

Nanocatalyst	Feedstock	Catalyst weight (%)	Specific surface area (m²/g)	Reaction time (h)/temp (°C)	Biodiesel yield (%)	References
Nano-MgO	Goat fat	1	40.44	3/70	93.12	Hassan and Hossein (2019)
MgO/MgFe₂O₄	Sunflower oil	4	97.8	4/110	91.2	Alaei et al. (2018)
γ-Al₂O₃/KI	Palm oil	4	349	4/60	98	Islam et al. (2015)
Ca/γ-Al₂O₃	Corn oil	6	6.85	5/65	87.89	Moradi et al. (2015)
KOH/Fe₂O₃/Al₂O₃	Canola oil	4	20.46	6/65	98.8	Kazemifard et al. (2018)
CaO@Fe₂O₃	Soyabean oil	2	—	3/70	98.8	Shi et al. (2017)
Na₂SiO₃	Animal fat	0.5	—	0.5/220	95.6	Yin et al. (2010)
CaO/CuFe₂O₄	Chicken fat	3	—	4/70	94.52	Seffati et al. (2019)
[BsAlm][OTf]@ SiO₂/CoFe₂O₄	Oleic acid	10	364.05	12/100	87	Zhen et al. (2012)
Cr/Ca/γ-Al₂O₃	Cooking oil	6	164.32	3/65	92.79	Sulaiman et al. (2017)

TABLE 5 | Summary of the involvement of carbon-based nanocatalysts in increased biodiesel production.

Nanocatalyst	Mode of synthesis	Feedstock	Catalyst amount (wt%)	Methanol to oil ratio	Reaction time (h) and reaction temp. (°C)	Biodiesel yield (%)	Recyclability	References
KOH loaded MWCNTs	Impregnation method	Canola oil	3.02	13.56:1	3.34/60	94.23	3	Omraei et al. (2013)
Silicon carbide/sodium hydroxide-graphene oxide (SiC/NaOH-GO)	*In-situ* impregnation method	Rapeseed oil oleic acid	5	48:1	0.1/65	96	3	Loy et al. (2019)
Na$_2$O/CNT	Impregnation method	Used cooking oil	3	20:1	3/65	97	3	Ibrahim et al. (2020)
s-MWCNT	—	Oleic acid	0.20	5.8:1	1.5/135	95.46	—	Zhang et al. (2009)
Sulfonated biochar and activated carbon (AC)	Pyrolysis method	Vegetable oil	2–8	6:1	6/55–60	97	6	Kastner et al. (2012)

TABLE 6 | The summary of zeolite-based nanocatalysts for increased biodiesel production.

Nanocatalyst	Mode of synthesis	Feedstock	Catalyst amount (wt%)	Methanol: oil ratio	Reaction time (h)	Reaction temperature (°C)	Biodiesel yield (%)	References
Zeolite/chitosan/KOH	—	Waste cooking oil	1	1:7	3	40 V(MI)	93	Fereidooni and Mehrpooya (2017)
Lanthanum-natural zeolite (La/NZA)	Impregnation method	Crude palm oil (CPO)	1	9:1	1	60	85.37	Setianingsih et al. (2018)
ZSM-5 (nanosheets)	Hydrothermal method	Linoleic acid	10	6:1	4	180	95.12	Fawaz et al. (2019)
Mesoporous ZSM-5	Disilication method	Shea butter	1	5:1	3 h	200	74.0	Alaba et al. (2016b)
Li/NaY zeolite	Hydrothermal and microemulsion-assisted co-precipitation method	Castor oil	3	18:1	2	75	98.6	Li et al. (2019)
High silica MoO$_3$/B-ZSM-5 nanocatalyst	Hydrothermal technique followed by wet impregnation method	WCO	3	2.40	6	160	98	Mohebbi et al. (2020)

Microwave irradiation (MI).

TABLE 7 | Comparison of the physico-chemical properties of biodiesel derived from different nanocatalysts with standard methods.

Nanocatalyst	Density (kg/cm^3)	Kinematic viscosity (mm^2/s)	Flash point (°C)	Acid value (mgKOH/g)	Water content	Cetane value	References
MgO	0.866	—	—	0.05	—	—	Amirthavall and (2019)
Zn doped CaO nanocatalyst	0.873	3.7	142	0.15	—	—	Borah et al. (2019)
TiO$_2$/PrSO$_3$H	0.898	4.8	171	0.41	—	—	Gardy et al. (2017)
TiO$_2$–0.5 C$_4$H$_5$KO$_6$ catalyst	0.891	3.5	173	—	—	57	Ambat et al. (2018a)
Synthetic B/ZP catalyst	0.872	3.84	178.5	0.041		53.7	Abukhadra et al. (2019)
ASTM D6751	0.82–0.90 (20°C)	—	>130	<0.8	<0.05	>47	—
EN14214	0.86–0.90 (15°C)	—	>120	<0.5	<0.05	>41	—

TABLE 8 | Summary of nanocatalysts and optimization parameters used in production of biodiesel.

Nanocatalyst	Mode of synthesis	Feedstock	Alcohol to oil molar ratio	Catalyst amount (wt%)	Reaction time	Reaction temp	Biodiesel yield (%)	References
SO$_4$/Mg-Al-Fe$_3$O$_4$ catalyst	Co-precipitation	WCO	9:1	4.0	300 min	95°C	98.5	Gardy et al. (2019a)
MgO nanoparticles	Sol-gel	Waste cooking oil	10:1	2	2 h	60°C	80	Amirthavalli and Warrier (2019)
CuO-CaO catalyst	Sol-gel	Moringa oleifera oil	0.3:1	4	150 min	65°C	95.24	Nomura et al. (2019)
CaO nanoparticles	Thermal decomposition	WCO oil	8:1	1	90 min	50°C	96	Anbessie et al. (2019)
KOH/Ca$_{12}$ Al$_{14}$O$_{33}$ nanocatalyst	Combustion method	Canola oil	12:1	4	60 min	450 WMI	83.5	Nayebzadeh et al. (2017)
KF/CaO–Fe$_3$O$_4$	Impreg nation method	Stillingia oil	12:1	4	3 h	65°C	95	Hu et al. (2011)
(MgO) catalysts	Co-precipitation method	Waste cooking oil using	24:1	2	1 h	65°C	93.3	John et al. (2018)
(KOH)	—	Coconut oil	6:1	1.0	60 min	70°C	97.20	Samuel et al. (2016)
CaO derived from egg shell	Calcination-hydration-dehydration as	*Scenedesmus armatus*	10:1	1.61	4 h	75°C	90.44	Pandit and Fulekar (2019)
MgO-La$_2$O$_3$ nanocatalysts	Co-precipitation method	Sunflower oil	18:1	3	5 h	65°C	97.7	Feyzi et al. (2017)
Sr$_3$Al$_2$O$_6$	Sol-gel	Soybean oil	25:1	1.3	61 min	60°C	95.7	Rashtizadeh et al. (2014)
Au@Ag core-shell NPs	Deposition method	Sunflower oil	5:1	5	2.0 h	65°C	86.9	Banerjee et al. (2014)
K$_2$CO$_3$/Al$_2$O$_3$	Impregnation method	Sunflower oil	12:1	5	4 h	80°C	99.3	Silveira et al. (2019)

Microwave irradiation (MI).

order to obtain free fatty acids that are used as feedstock material. Transforming biomass is a prerequisite task so as to minimize the obstacles caused later in the production of biodiesel. Biomass obtained from edible materials has a limited production as it mainly contributes to derived food. As deforestation and problematic issues of fossil fuel derived products has plagued its zenith, large scale plantation of non-edible plants in order to retrieve oil is an important and main concern. Another stage is the technological development required in extraction of oils from feedstock. Each and every stage in biofuel production is energy intensive and needs to be properly optimized. Furthermore, different types of nanocatalysts can be investigated depending on the morphology and size of nanoparticles which also play a pivotal role in maximizing the yield of biofuel, as structural and catalytic stability of nanocatalysts at high temperatures is also a major issue and concern in augmenting the overall productivity of biofuel. So fabrication and modification of nanocatalysts of high surface to volume ratio, catalytic stability, and high catalytic activity is significant in optimizing the parameters of biodiesel production while maintaining an environmental-friendly approach to minimize chemical based pollution during nanocatalyst synthesis.

CONCLUSION

Biodiesel production plays a prominent role in alleviating the utilization of energy generation from fossil derived products. Despite lower energy production in comparison to fossil fuels, the novel designing of nanocatalysts, producing microbial cultures and developing optimization techniques are succinctly helpful in expanding the large-scale production of biodiesel.

In this review the detailed discussion on biodiesel production via trans-esterification reaction has been presented. The role of nanocatalysts in heterogeneous catalysis has been analyzed on the basis of its type and vastness. The metal oxides based nanocatalysts are attributed with the exceptional properties of large surface area to volume ratio, different morphology and high activity as well as selectivity of the catalyst. Nanomagnetic and mixed metal oxide based nanocatalyst have played a substantial role in enhancing specific surface area, pore size and average pore diameter. Using innumerable functionalized groups, significant modification of nanocatalysts can be achieved which ultimately increase the overall acidity, reduces the leaching of active metals and creates more active acidic and basic sites for the catalytic reaction. Inevitably, advancement in nanotechnology significantly limits the use of fossil fuels and also mitigates the pollution level. However, the biodiesel production still faces some major challenges like identifying feedstock, as a concerning task corresponding to biofuel production, mainly biodiesel. Biodiesel derived from edible oils are posing certain restrictions relating to cost and food related issues. In comparison to this, non-edible oils and classes of microalgae show better prospects in regard to esterification process of free fatty acids. As pre-treatment of

the feedstock is a necessary step in minimizing the formation of side-reactions and the saponification process, it mostly hinders the production of biodiesel by affecting its physico-chemical properties thus reducing the overall quality of biodiesel. Monitoring optimization of reaction parameters and physico-chemical properties are imperatively significant in increasing biodiesel production. Using optimum amounts of nanocatalyst, reaction parameters like methanol to oil ratio, catalyst weight, reaction temperature and time can be significantly improved, thus overall increasing the quality and quantity of biodiesel.

FUTURE OUTLOOK

In light of the review, future studies can be significantly made in the following directions to overcome the existing limitations regarding biodiesel production:

Devising a plan for large-scale usability of non-edible feedstock oils and exploration in increasing the production of algae based biomass which possess major content of oil.

Developing nanocatalysts possessing multi-functionality active sites, which concomitantly minimize the effect of leaching and can also withstand disintegration during the trans-esterification reaction.

Functionalization of carbonaceous and zeolite-based catalysts using nanomaterials and polymeric materials for increasing its catalytic activity, specificity, and stability.

Exploiting structural modification based on morphology and size of the nano-based materials so as to enhance the reaction kinetics involved in biodiesel production.

Evolving statistical tools for effective optimization of reaction conditions on a large scale.

Finally, technological advancement is necessary in establishing the reaction process on a large scale to minimize the mass-transfer resistance, extensive energy usage, and utilization of by-products. Thereby increasing the scope in maintaining the optimized reaction conditions, and hence increasing the biodiesel production.

AUTHOR CONTRIBUTIONS

SB, SaS and AG have contributed to outlining the structure and writing of the manuscript. MK and SuS have reviewed the manuscript thoroughly.

ACKNOWLEDGMENTS

REFERENCES

Abdullah, S. H. Y. S., Hanapi, N. H. M., Azid, A., Umar, R., Juahir, H., Khatoon, H., et al. (2017). A review of biomass-derived heterogeneous catalyst for a sustainable biodiesel production. *Renew. Sustain. Energy Rev.* 70, 1040–1051. doi:10.1016/j.rser.2016.12.008

Abukhadra, M. R., Ibrahim, S. M., Yakout, S. M., El-zaidy, M. E., and Abdeltawab, A. A. (2019). Synthesis of Na⁺ trapped bentonite/zeolite-P composite as a novel catalyst for effective production of biodiesel from palm oil; E ff ect of ultrasonic irradiation and mechanism. *Energy Convers. Manag.* 196, 739–750. doi:10.1016/j.enconman.2019.06.027

Achten, W. M. J., Verchot, L., Franken, Y. J., Mathijs, E., Singh, V. P., Aerts, R., et al. (2008). Jatropha bio-diesel production and use. *Biomass Bioenergy* 32, 1063–1084. doi:10.1016/j.biombioe.2008.03.003

Adebayo, G. B., and Ameen, M. O. (2011). Physico-chemical properties of biodiesel produced from Jatropha Curcas oil. *J. Microbiol. Biotechnol. Res.*, 1 (1), 12–16.

Ahmad, T., Danish, M., Kale, P., Geremew, B., Adeloju, S. B., Nizami, M., et al. (2019). Optimization of process variables for biodiesel production by transesterification of flaxseed oil and produced biodiesel characterizations. *Renew. Energy*, 139, 1272–1280. doi:10.1016/j.renene.2019.03.036

Ainun, H., Bhargavi, G., Rao, P. N., and Lutero, D. S. (2017). "Ultrasonication assisted production of biodiesel from sunflower oil by using CuO: Mg heterogeneous nanocatalyst," in IOP Conference Series: Materials Science and Engineering, 1–7. doi:10.1088/1757-899X/225/1/012213

Akia, M., Yazdani, F., Motaee, E., Han, D., and Arandiyan, H. (2014). A review on conversion of biomass to biofuel by nanocatalysts. *Biofuel Res. J.* 1, 16–25. doi:10.18331/BRJ2015.1.1.5

Alaba, A. P., Sani, Y. M., Mohd, W., and Daud, W. M. W. A. (2016a). A comparative study on thermal decomposition behavior of biodiesel samples produced from shea butter over micro- and mesoporous ZSM-5 zeolites using different kinetic models. *J. Therm. Anal. Calorim.* 126 (2), 943–948. doi:10.1007/s10973-016-5505-8

Alaba, P. A., Sani, M. Y., Mohammad, Y. I., Abakr, A. Y., and Daud, W. M. W. A. (2016b). Synthesis and application of hierarchical mesoporous HZSM-5 for biodiesel production from shea butter. *J. Taiwan Inst. Chem. Eng.* 59, 405–412. doi:10.1016/j.jtice.2015.09.006

Alaei, S., Haghighi, M., Toghiani, J., and Rahmani Vahid, B. (2018). Magnetic and reusable MgO/MgFe₂O₄ nanocatalyst for biodiesel production from sunflower oil: influence of fuel ratio in combustion synthesis on catalytic properties and performance. *Ind. Crops Prod.* 117, 322–332. doi:10.1016/j.indcrop.2018.03.015

Ali, J., Fathollah, P., and Akbar, M. (2020). Recent advances of biodiesel production using ionic liquids supported on nanoporous materials as catalysts: a Review. *Fr. En. Res.* 8, 144. doi:10.3389/fenrg.2020.00144

Ambat, I., Srivastava, V., Haapaniemi, E., and Sillanpää, M. (2018a). Application of potassium ion impregnated titanium dioxide as nanocatalyst for transesterification of linseed oil. *Energy and Fuels* 32 (11), 11645–11655. doi:10.1021/acs.energyfuels.8b03310

Ambat, I., Srivastava, V., and Sillanpää, M. (2018b). Recent advancement in biodiesel production methodologies using various feedstock: a review. *Renew. Sustain. Energy Rev.* 90, 356–369. doi:10.1016/j.rser.2018.03.069

Amirthavalli, V., and Warrier, A. R. (2019). Production of biodiesel from waste cooking oil using MgO nanocatalyst. *AIP Conf. Proc.* 2115, 030609. 10.1063/1.5113448

Anbessie, T., Mamo, T. T., and Mekonnen, Y. S. (2019). Optimized biodiesel production from waste cooking oil (WCO) using calcium oxide (CaO) nano-catalyst. *Sci. Rep.* 9, 18982. doi:10.1038/s41598-019-55403-4

Anr, R., Saleh, A. A., Islam, S., Hamdan, S., and Maleque, A. (2016). Biodiesel production from crude jatropha oil using a highly active heterogeneous nanocatalyst by optimizing transesterification reaction parameters. *Energy Fuels* 30, 334–343. doi:10.1021/acs.energyfuels.5b01899

Anwer, A. H., Khan, M. D., Khan, N., Nizami, A. S., Rehan, M., and Khan, M. Z. (2019). Development of novel MnO₂ coated carbon felt cathode for microbial electroreduction of CO₂ to biofuels. *J. Environ. Manag.* 249, 109376. doi:10.1016/j.jenvman.2019.109376

Asri, N. P., Yuniati, Y., Hindarso, H., Supraptoand Yogaswara, R. R. (2020). "Biodiesel production from Kesambi (*Schleichera oleosa*) oil using multi-walled carbon nanotubes supported zinc oxide as a solid acid catalyst," in IOP Conference Series: Earth and Environmental Science, 1–9. doi:10.1088/1755-1315/456/1/012003

Azhar, S. M. H., Abdulla, R., Jambo, S. A., Marbawi, H., Azlan, J., Azifa, A., et al. (2017). Yeasts in sustainable bioethanol production: a review. *Biochem. Biophys. Rep.* 10, 52–61. doi:10.1016/j.bbrep.2017.03.003

Azyan, N., Adila, F., Sulaiman, S., and Jamal, P. (2018). Thermally produced nano catalyst for biodiesel production: a review. *J. Adv. Res. Fluid Mech. Therm. Sci.* 2 (2), 139–147.

Balat, M. (2011). Potential alternatives to edible oils for biodiesel production–a review of current work. *Energy Convers. Manag.* 52 (2), 1479–1492. doi:10.1016/j.enconman.2010.10.011

Banerjee, M., Dey, B., Talukdar, J., and Chandra, M. (2014). Production of biodiesel from sun flower oil using highly catalytic bimetallic gold - silver core - shell nanoparticle. *Energy* 69, 695–699. doi:10.1016/j.energy.2014.03.065

Bankovi, I. B., Stojkovi, I. J., Stamenkovi, O. S., and Veljkovic, V. B. (2014). Waste animal fats as feedstocks for biodiesel production. *Renew. Sustain. Energy Rev.* 32, 238–254. doi:10.1016/j.rser.2014.01.038

Bassam, A., Abatal, M., Tzuc, O. M., Pedro, L. C. S., and Aguilar-uc, C. (2019). Physical and chemical properties of biodiesel obtained from amazon Sailfin Catfish (*Pterygoplichthys pardalis*) biomass oil. *J. Chem.* 2019, 7829630. doi:10.1155/2019/7829630

Behzadi, S., and Farid, M. M. (2007). Review: examining the use of different feedstock for the production of biodiesel. *Asia-Pac. J. Chem. Eng.* 2, 480–486. doi:10.1002/apj

Bharti, P., and Singh, B. (2019). Process optimization of biodiesel production catalyzed by CaO nanocatalyst using response surface methodology. *J. Nanostruct. Chem.* 9 (4), 269–280. doi:10.1007/s40097-019-00317-w

Bikash, B., Choudhury, N. D., and Bora, D. K. (2018). "Physicochemical assessment of Pumpkin (*Cucurbita pepo* L.) seed oil as a viable feedstock for biodiesel production oil extraction,"in *Conference proceedings of the second international conference on recent advances in bioenergy research* (Newyork, NY, Springer).

Borah, J. M., Das, A., Das, V., Bhuyan, N., and Deka, D. (2019). Transesteri fi cation of waste cooking oil for biodiesel production catalyzed by Zn substituted waste egg shell derived CaO nanocatalyst. *Fuel* 242, 345–354. doi:10.1016/j.fuel.2019.01.060

Borah, J. M., Devi, A., Abha, R., Deka, D., Guan, Q., Li, Y., et al. (2018). Biodiesel production from waste cooking oil catalyzed by in-situ decorated TiO₂ on reduced graphene oxide nanocomposite.*CATCOM* 2012 (3), 7250–7258. doi:10.1155/2012/542426

Centi, G., Perez-pariente, J., and Roth, W. J. (2012). Zeolite-based materials for novel catalytic applications: opportunities , perspectives and open problems. *Catal. Today* 179, 2–15. doi:10.1016/j.cattod.2011.10.006

Chavan, S. B., Kumbhar, R. R., Madhu, D., Singh, B., and Sharma, Y. C. (2015). Synthesis of biodiesel from Jatropha curcas oil using waste eggshell and study of its fuel properties. *RSC Adv.* 5, 63596–63604. doi:10.1039/c5ra06937h

Chen, H., and Fu, X. (2016). Industrial technologies for bioethanol production from lignocellulosic biomass. *Renew. Sustain. Energy Rev.* 57, 468–478. doi:10.1016/j.rser.2015.12.069

Chouhan, A. P. S., and Sarma, A. K. (2011). Modern heterogeneous catalysts for biodiesel production: a comprehensive review. *Renew. Sust. Energ. Rev.* 15, 4378–4399. doi:10.1016/j.rser.2011.07.112

Chozhavendhan, S., Vijay Pradhap Singh, M., Fransila, B., Praveen Kumar, R., and Karthiga Devi, G. (2020). A review on influencing parameters of biodiesel production and purification processes. *Current Res. Green Sust. Chem.* 1–2, 1–6. doi:10.1016/j.crgsc.2020.04.002

Clohessy, J., and Kwapinski, W. (2020). Carbon-based catalysts for biodiesel production—a review. *Appl. Sci.* 10, 918. doi:10.3390/app10030918

Dai, Y. M., Lin, J. H., Huang, S. T., Lee, W. L. W., Hsieh, C. H., Chen, F. H., et al. (2020). Natural soil and lithium carbonate as economical solid-base catalysts for biodiesel production. *Energy Rep.* 6, 2743–2750. doi:10.1016/j.egyr.2020.09.041

Dantas, J., Leal, E., Cornejo, D. R., Kiminami, R. H. G. A., and Costa, A. C. F. M. (2020). Biodiesel production evaluating the use and reuse of synthesized in pilot-scale. *Arabian J. Chem.* 13 (1), 3026–3042. doi:10.1016/j.arabjc.2018.08.012

Deepalakshmi, S., Sivalingam, A., Thirumarimurugan, M., and Sivakumar, P. (2015). Environmental effects optimization of biodiesel synthesis from Calophyllum inophyllum. *Energy Sources, Part A Recovery, Util. Environ. Eff.* 37 (00), 2601–2608. doi:10.1080/15567036.2015.1007403

Deepanraj, B., and Senthilkumar, N. (2020). Biogas from food waste through anaerobic digestion: optimization with response surface methodology. *Biomass Convers. Biorefin.*, 85–96.

Deepanraj, B., Sivasubramanian, V., and Jayaraj, S. (2016). Multi-response optimization of process parameters in biogas production from food waste using Taguchi – Grey relational analysis. *Energy Convers. Manag.* 141, 429–438. doi:10.1016/j.enconman.2016.12.013

Douvartzides, S. L., Charisiou, N. D., Papageridis, K. N., and Goula, M. A. (2019). Green diesel: biomass feedstocks, production technologies, catalytic research, fuel properties and performance in compression ignition internal combustion engines. *Energies* 12, 809. doi:10.3390/en12050809

El-seesy, A. I., Abdel-rahman, A. K., Bady, M., and Ookawara, S. (2016). The influence of multi-walled carbon nanotubes additives into non-edible biodiesel-diesel fuel blend on diesel engine performance and emissions. *Energy Procedia.* 100 166–172. doi:10.1016/j.egypro.2016.10.160

Esmaeili, H., Yeganeh, G., and Esmaeilzadeh, F. (2019). Optimization of biodiesel production from Moringa oleifera seeds oil in the presence of nano - MgO using Taguchi method. *Int. Nano Lett.* 9 (3), 257–263. doi:10.1007/s40089-019-0278-2

Faisal, A., Priji, P., Unni, P., Nair, K., and Kulangara, M. (2018). Optimization of parameters for the production of biodiesel from rubber seed oil using onsite lipase by response surface methodology. *3 Biotech.* 8 (11), 459. doi:10.1007/s13205-018-1477-7

Fan, Y., Su, F., Li, K., Ke, C., and Yan, Y. (2017). Carbon nanotube filled with magnetic iron oxide and modified with polyamidoamine dendrimers for immobilizing lipase toward application in biodiesel production. *Sci. Rep.* 7, 45643. doi:10.1038/srep45643

Fattah, I. M. R., Ong, H. C., Mahlia, T. M. I., Mofijur, M., and Silitonga, A. S. (2020). State of the art of catalysts for biodiesel production. *Front. Energy Res.* 8, 101. doi:10.3389/fenrg.2020.00101

Fattahi, N., Triantafyllidis, K., Luque, R., and Ramazani, A. (2019). Zeolite-based catalysts: a valuable approach toward. *Catalysts* 9, 758. doi:10.3390/catal9090758

Fawaz, E. G., Salam, D. A., Pinard, L., and Daou, T. J. (2019). Catalysis science & technology crystal morphologies of HZSM-5 zeolites for the catalyst effectiveness †. *Catal. Sci. Technol.* 9, 5456–5471. doi:10.1039/c9cy01427f

Fereidooni, L., and Mehrpooya, M. (2017). Experimental assessment of electrolysis method in production of biodiesel from waste cooking oil using zeolite/chitosan catalyst with a focus on waste biorefinery. *Energy Convers. Manag.* 147, 145–154. doi:10.1016/j.enconman.2017.05.051

Feyzi, M., Hassankhani, A., and Rafiee, H. R. (2013). Preparation and characterization of Cs/Al/Fe$_3$O$_4$ nanocatalysts for biodiesel production. *Energy Convers. Manag.* 71, 62–68. doi:10.1016/j.enconman.2013.03.022

Feyzi, M., Hosseini, N., Yaghobi, N., and Ezzati, R. (2017). Preparation, characterization, kinetic and thermodynamic studies of MgO-La$_2$O$_3$ nanocatalysts for biodiesel production from sunflower oil. *Chem. Phys. Lett.* 677, 19–29. doi:10.1016/j.cplett.2017.03.014

Gardy, J., Hassanpour, A., Lai, X., Ahmed, M. H., and Rehan, M. (2017). Applied catalysis B: environmental biodiesel production from used cooking oil using a novel surface functionalised TiO$_2$ nano-catalyst. *Appl. Catal. B Environ.* 207, 297–310. doi:10.1016/j.apcatb.2017.01.080

Gardy, J., Nourafkan, E., Osatiashtiani, A., Lee, A. F., and Wilson, K. (2019a). Applied catalysis B: environmental a core-shell SO$_4$/Mg-Al-Fe$_3$O$_4$ catalyst for biodiesel production. *Appl. Catal. B Environ.* 259, 118093. doi:10.1016/j.apcatb.2019.118093

Gardy, J., Osatiashtiani, A., Céspedes, O., Hassanpour, A., Lai, X., Lee, A. F., et al. (2018). Applied Catalysis B: environmental A magnetically separable SO$_4$/Fe-Al-TiO$_2$ solid acid catalyst for biodiesel production from waste cooking oil. *Appl. Catal. B Environ.* 234, 268–278. doi:10.1016/j.apcatb.2018.04.046

Gardy, J., Rehan, M., Hassanpour, A., Lai, X., and Nizami, A. (2019b). Advances in nano-catalysts based biodiesel production from non-food feedstocks. *J. Environ. Manag.* 249, 109316. doi:10.1016/j.jenvman.2019.109316

Gashaw, A., Getachew, T., and Abile, T. (2015). A review on biodiesel production as alternative fuel. *J. For. Prod. Ind.* 4 (2), 80–85.

Ghalandari, A., Taghizadeh, M., and Rahmani, M. (2019). Statistical optimization of the biodiesel production process using a magnetic core-mesoporous shell KOH/Fe$_3$O$_4$ @ g -Al$_2$O$_3$ nanocatalyst. *Chem. Eng. Technol.* 42 (1), 89–99. doi:10.1002/ceat.201700658

Giakoumis, E. G., and Sarakatsanis, C. K. (2018). Estimation of biodiesel cetane number, density, kinematic viscosity and heating values from its fatty acid weight composition. *Fuel* 222, 574–585. doi:10.1016/j.fuel.2018.02.187

Go, J. M., Romero, M. D., Ovejero, G., Uguina, M. A., and Rodrı, A. (2007). Fast tailoring of the acid – base properties in the NaX zeolite by cesium-exchange under microwave heating. *Microporous Mesoporous Mater.* 98, 317–322. doi:10.1016/j.micromeso.2006.09.024

Gog, A., Roman, M., Tosa, M., Paizs, C., and Irimie, F. D. (2012). Biodiesel production using enzymatic transesterification – current state and perspectives. *Renew. Energy* 39, 10–16. doi:10.1016/j.renene.2011.08.007

Gopinath, A., Puhan, S., and Nagarajan, G. (2009). Theoretical modeling of iodine value and saponification value of biodiesel fuels from their fatty acid composition. *Renew. Energy* 34 (7), 1806–1811. doi:10.1016/j.renene.2008.11.023

Guan, Q., Li, Y., Chen, Y., Shi, Y., Gu, J., Li, B., et al. (2017). Biodiesel production through triglycerides transesterification. *RSC Adv.* 7, 7250–7258. doi:10.1039/c6ra28067f

Firouzjaee, M. H., and Taghizadeh, M. (2017). Optimization of process variables for biodiesel production using the. *Chem. Eng. Technol.* 40 (6), 1140–1148. doi:10.1002/ceat.201600406

Hamouda, H. I., Nassar, H. N., Madian, H. R., Amr, S. S. A., and El-gendy, N. S. (2015). Response surface optimization of bioethanol production from sugarcane molasses by pichia veronae Strain HSC-22. *Biotechnol. Res. Internat.* 2015, 905792. 10.1155/2015/905792

Hassan, R., and Hossein, E. (2019). Characterization of MgO nanocatalysts to produce biodiesel from goat fat using trans-esterification process. *Biotech.* 9, 429. doi:10.1007/s13205-019-1963-6

Hoang, A. T. (2018). Prediction of the density and viscosity of biodiesel and the influence of biodiesel properties on a diesel engine fuel supply system. *J. Mar. Eng. Technol.* 4177, 1–13. doi:10.1080/20464177.2018.1532734

Hossain, A. B. M. S., and Boyce, A. N. (2009). Biodiesel production from waste sunflower cooking oil as an environmental recycling process. *Bulg. J. Agric. Sci.* 15 (4), 312–317.

Hossain, N., Mahlia, T. M. I., and Saidur, R. (2019a). Biotechnology for biofuels latest development in microalgae - biofuel production with nano - additives. *Biotechnol. Biofuels* 12, 125. doi:10.1186/s13068-019-1465-0

Hu, S., Guan, Y., Wang, Y., and Han, H. (2011). Nano-magnetic catalyst KF/CaO – Fe$_3$O$_4$ for biodiesel production. *Appl. Energy* 88 (8), 2685–2690. doi:10.1016/j.apenergy.2011.02.012

Huang, Y., Li, F., Bao, G., Wang, W., and Wang, H. (2020). Estimation of kinematic viscosity of biodiesel fuels from fatty acid methyl ester composition and temperature. *J. Chem. Eng. Data* 65, 2476–2485. doi:10.1021/acs.jced.9b01127

Ibrahim, M. L., Adlina Nik Abdul Khalil, N. N., Islam, A., Rashid, U., Ibrahim, S. F., Mashuri, S. I. S., et al. (2020). Preparation of Na$_2$O supported CNTs nanocatalyst for e ffi cient biodiesel production from waste-oil. *Energy Convers. Manag.* 205, 112445. doi:10.1016/j.enconman.2019.112445

Isioma, N., Muhammad, Y., Sylvester, O. D., Innocent, D., and Linus, O. (2013). Cold flow properties and kinematic viscosity of biodiesel. *Univ. J. Chem.* 1 (4), 135–141. doi:10.13189/ujc.2013.010402

Islam, A., Taufiq-Yap, Y. H., Ravindra, P., Teo, S. H., Sivasangar, S., and Chan, E.-S. (2015). Biodiesel synthesis over γ-Al2O3/KI catalyst. *Energy* 89, 965–973. doi:10.1016/j.energy.2015.06.036

Ismail, S. A. A., and Ali, R. F. M. (2015). Physico-chemical properties of biodiesel manufactured from waste frying oil using domestic adsorbents. *Sci. Technol. Adv. Mater.* 16 (3), 034602. doi:10.1088/1468-6996/16/3/034602

Jeyakumar, N., and Narayanasamy, B. (2019). Environmental effects optimization of used cooking oil methyl ester production using response surface methodology. *Energy Sources, Part A Recov., Util. Environ. Eff.* 41 (19), 2313–2325. doi:10.1080/15567036.2018.1555633

John, A. A. L., Judith, K. J., and Udaya, V. (2018). Optimization of biodiesel production from waste cooking oil by magnesium oxide nanocatalyst synthesized using coprecipitation method. *Clean Technol. Environ. Policy* 20 (6), 1219–1231. doi:10.1007/s10098-018-1547-x

Kana, E. B. G., Oloke, J. K., Lateef, A., and Adesiyan, M. O. (2012). Modeling and optimization of biogas production on saw dust and other co-substrates using artificial neural network and genetic algorithm. *Renew. Energy* 46, 276–281. doi:10.1016/j.renene.2012.03.027

Karmakar, R., Kundu, K., and Rajor, A. (2018). Fuel properties and emission characteristics of biodiesel produced from unused algae grown in India. *Petrol. Sci.* 15 (2), 385–395. doi:10.1007/s12182-017-0209-7

Kastner, J. R., Miller, J., Geller, D. P., Locklin, J., Keith, L. H., and Johnson, T. (2012). Catalytic esterification of fatty acids using solid acid catalysts generated from biochar and activated carbon. *Catal. Today* 190 (1), 122–132. doi:10.1016/j.cattod.2012.02.006

Kazemifard, S., Nayebzadeh, H., Saghatoleslami, N., and Safakish, E. (2018). Assessment the activity of magnetic KOH/Fe$_3$O$_4$ @Al$_2$O$_3$ core–shell nanocatalyst in transesterification reaction: effect of Fe/Al ratio on structural and performance. *Environ. Sci. Pollut. Res.* 25, 32811–32821. doi:10.1007/s11356-018-3249-7

Khan, O., Yadav, A. K., Khan, M. E., and Parvez, M. (2019). Characterization of bioethanol obtained from Eichhornia Crassipes plant; its emission and performance analysis on CI engine. *Energy Sources, Part A: recovery, Util., Environ. Eff.*, 1–11. doi:10.1080/15567036.2019.1648600

Kovács, K. L., Ács, N., Kovács, E., Wirth, R., Rákhely, G., Strang, O., et al. (2013). Improvement of biogas production by bioaugmentation. *BioMed Res. Internat.* 2013, 482653. 10.1155/2013/482653

Krisnangkura, K., Yimsuwan, T., and Pairintra, R. (2006). An empirical approach in predicting biodiesel viscosity at various temperatures. *Fuel* 85, 107–113. doi:10.1016/j.fuel.2005.05.010

Kushwaha, D., Upadhyay, S. N., and Mishra, P. K. (2018). "Nanotechnology in bioethanol/biobutanol production nanotechnology in bioethanol/biobutanol production," in *Nanotechnology for biofuel production. biofuel and biorefinery technologies* (Cham, Switzerland: Springer International Publishing). doi:10.1007/978-3-319-75052-1

Le Quynh, H., Vestergaard, M. C., and Tamiya, E. (2017). Carbon-based nanomaterials in biomass-based fuel-fed fuel cells. *Sensors* 17, 2587. doi:10.3390/s17112587

Lee, H. V., Yunus, R., Juan, J. C., and Tau, Y. H. (2011). Process optimization design for jatropha-based biodiesel production using response surface methodology. *Fuel Process. Technol.* 92, 2420–2428. doi:10.1016/j.fuproc.2011.08.018

Li, P., He, C., Li, G., Ding, P., Lan, M., and Gao, Z. (2020). Biological pretreatment of corn straw for enhancing degradation efficiency and biogas production. *Bioengineered* 11 (1), 251–260. doi:10.1080/21655979.2020.1733733

Li, Z., Ding, S., Chen, C., Qu, S., Du, J., Lu, J., et al. (2019). Recyclable Li/NaY zeolite as a heterogeneous alkaline catalyst for biodiesel production: process optimization and kinetics study. *Energy Convers. Manag.* 192, 335–345. doi:10.1016/j.enconman.2019.04.053

Lima, L. S., Barbosa, T. P., da Silva, L. F. B., Santo Filho, D. M. E., Castro, C. S. C., Dos Santos, J. J. P., Jr., et al. (2010). Biodiesel density characterization using a pycnometer. *Simposio de Metrología*, 1–8.

Loy, A. C. M., Quitain, A. T., Lam, K. M., Yusup, S., Sasaki, M., and Kida, T. (2019). Development of high microwave-absorptive bifunctional graphene oxide-based catalyst for biodiesel production. *Energy Convers. Manag.* 180, 1013–1025. doi:10.1016/j.enconman.2018.11.043

Mardhiah, H. H., Ong, H. C., Masjuki, H. H., Lim, S., and Lee, H. V. (2017). A review on latest developments and future prospects of heterogeneous catalyst in biodiesel production from non-edible oils. *Renew. Sust. Energ. Rev.* 67, 1225–1236. doi:10.1016/j.rser.2016.09.036

Martchamadol, J., and Kumar, S. (2012). Thailand's energy security indicators. *Renew. Sustain. Energy Rev.* 16 (8), 6103–6122. doi:10.1016/j.rser.2012.06.021

Martínez, S. L., Romero, R., Romero, A., Víctor, S., and Natividad, R. (2011). Preparation and characterization of CaO nanoparticles/NaX zeolite catalysts for the transesterification of sunflower oil. *Ind. Eng. Chem. Res.* 50, 2665–2670. doi:10.1021/ie1006867

Marwaha, A., Dhir, A., Mahla, S. K., and Mohapatra, S. K. (2018). An overview of solid base heterogeneous catalysts for biodiesel production. *Catal. Rev.* 60 (4), 594–628. doi:10.1080/01614940.2018.1494782

Mguni, L. L., Meijboom, R., and Jalama, K. (2012). Biodiesel production over nano-MgO supported on titania. *Internat. J. Mat. Metall. Eng.* 6 (4), 380–384.

Mishra, V. K., and Goswami, R. (2017). A review of production , properties and advantages of biodiesel. *Biofuels* 1–17. doi:10.1080/17597269.2017.1336350

Mohebbi, S., Rostamizadeh, M., and Kahforoushan, D. (2020). Effect of molybdenum promoter on performance of high silica MoO$_3$/B-ZSM-5 nanocatalyst in biodiesel production. *Fuel* 266, 1–8. doi:10.1016/j.fuel.2020.117063

Moradi, G., Mohadesi, M., Rezaei, R., and Moradi, R. (2015). Biodiesel production using CaO/γ-Al$_2$O$_3$ catalyst synthesized by sol-gel method. *Canad. J. Chem.Eng.* 93, 1531–1538. doi:10.1002/cjce.22258

Nanasaheb, D. S., and Chandrakant, M. K. (2012). Preparation of methyl esters from thespesia populnea l . oil and its engine exhausts studies *thespesia populnea l* . oil and its engine. *Int. J. Green Energy* 9, 130–138. doi:10.1080/15435075.2011.621495

Nayebzadeh, H., Saghatoleslami, N., Haghighi, M., and Tabasizadeh, M. (2017). KOH/Ca12Al14O33 nanocatalyst for biodiesel production via microwave. *J. Taiwan Inst. Chem. Eng.* 1–8. doi:10.1016/j.jtice.2017.03.018

NguyenThi, T. X., Bazile, J. P., and Bessières, D. (2018). Density measurements of waste cooking oil biodiesel and diesel blends over extended pressure. *Energies* 11, 1212. doi:10.3390/en11051212

Nizami, A., and Rehan, M. (2018). Towards nanotechnology-based biofuel industry. *Biofuel Res. J.*, 18, 798–799. doi:10.18331/BRJ2018.5.2.2

Nomura, K., Terwilliger, P., Niju, S., Raj, F. R., Anushya, C., and Balajii, M. (2019). Optimization of acid catalyzed esterification and mixed metal oxide catalyzed transesterification for biodiesel production from Moringa oleifera oil, *Green Process. Synth.* 8, 756–775. doi:10.1515/gps-2019-0045

Omraei, M., Sheibani, S., Sadrameli, S. M., and Tow, J. (2013). Preparation of biodiesel using KOH-MWCNT catalysts: an optimization study. *Ind. Eng. Chem. Res.* 52, 1829–1835. doi:10.1021/ie301418y

Ong, H. C., Mofiju, M., Silitonga, A. S., Gumilang, D., Kusumo, F., and Mahlia, T. M. I. (2020). Physicochemical properties of biodiesel synthesised from Grape seed, Philippine tung, Kesambi, and palm oils. *Energies* 13, 1319. doi:10.3390/en13061319

Pan, H., Li, H., Zhang, H., Wang, A., Jin, D., and Yang, S. (2018). Effective production of biodiesel from non-edible oil using facile synthesis of imidazolium salts-based BrØnsted-Lewis solid acid and co-solvent. *Energy Convers. Manag.* 166, 534–544. doi:10.1016/j.enconman.2018.04.061

Pan, H., Li, H., Zhang, H., Wang, A., and Yang, S. (2019). Acidic ionic liquid-functionalized mesoporous melamine-formaldehyde polymer as heterogeneous catalyst for biodiesel production. *Fuel* 239, 886–895. doi:10.1016/j.fuel.2018.11.093

Pan, H., Liu, Y., Xia, Q., Zhang, H., Guo, L., Li, H., et al. (2020). Synergetic combination of a mesoporous polymeric acid and a base enables highly efficient heterogeneous catalytic one-pot conversion of crude: jatropha oil into biodiesel. *Green Chem.* 22 (5), 1698–1709. doi:10.1039/c9gc04135d

Pandit, P. R., and Fulekar, M. H. (2019). Biodiesel production from Scenedesmus armatus using egg shell waste as nanocatalyst. *Mater. Today: Proc.* 10, 75–86. doi:10.1016/j.matpr.2019.02.191

Pérez, A., Casas, A., Fernández, C. M., Ramos, M. J., and Rodríguez, L. (2010). Winterization of peanut biodiesel to improve the cold flow properties. *Bioresour. Technol.* 101 (19), 7375–7381. doi:10.1016/j.biortech.2010.04.063

Pham, M. T., Hoang, A. T., Anh, T. L., Rahman, A., Al Tawaha. A. R. M., and Le, V. V. (2018). Measurement and prediction of the density and viscosity of biodiesel blends. *Internat. J. Technol.* 9, 1015. doi:10.14716/ijtech.v9i5.1950

Pinzi, S., Leiva-candia, D., López-garcía, I., Redel-macías, M. D., and Dorado, M. P. (2013). Latest trends in feedstocks for biodiesel production. *Biofuels, Bioprod. Bioref.* 8, 126–143. doi:10.1002/bbb.1435

Poonjarernsilp, C., Sano, N., and Tamon, H. (2014). Applied catalysis B: environmental Hydrothermally sulfonated single-walled carbon nanohorns for use as solid catalysts in biodiesel production by esterification of palmitic acid. *Appl. Catal. B Environ.* 147, 726–732. doi:10.1016/j.apcatb.2013.10.006

Pratap, S. R., Shamshuddin, S. Z. M., Thimmaraju, N., Shyamsundar, M., and Reena, S. S. (2015). Kinetics of transesterification of Madhuca Indica oil over modified zeolites: biodiesel synthesis. *Bangladesh J. Sci. Ind. Res.* 50 (4), 271–278. doi:10.3329/bjsir.v50i4.25836

Pratas, M. J., Freitas, S. V. D., Oliveira, M. B., Monteiro, S. C., and Lima, S. (2011). Biodiesel density: experimental measurements and prediction models. *Energy Fuels* 25, 2333–2340. doi:10.1021/ef2002124

Prokopowicz, A., Zaciera, M., Sobczak, A., Bielaczyc, P., and Woodburn, J. (2015). The effects of neat biodiesel and biodiesel and hvo blends in diesel fuel on exhaust emissions from a light duty vehicle with a diesel engine. *Environ. Sci. Technol.* 49, 7473–7482. doi:10.1021/acs.est.5b00648

Rahman, W. U., Fatima, A., Anwer, A. H., Athar, M., Khan, M. Z., Khan, N. A., et al. (2018). Biodiesel synthesis from eucalyptus oil by utilizing waste egg shell derived calcium based metal oxide catalyst. *Process Saf. Environ. Protect.* 122, 1–35. doi:10.1016/j.psep.2018.12.015

Rai, M., César, J., Soler, M. F., Ricardo, P., Marcelino, F., Brumano, L. P., et al. (2016). Strategic role of nanotechnology for production of bioethanol and biodiesel. *Nanotechnol. Rev.* 5 (2), 231–250. doi:10.1515/ntrev-2015-0069

Rashid, U., Soltani, S., Shean, T., Choong, Y., and Nehdi, I. A. (2019). Palm biochar-based sulphated zirconium (Zr-AC-HSO3) catalyst for methyl ester production from palm fatty acid distillate. *Catalysts* 9, 1029. doi:10.3390/catal9121029

Rashtizadeh, E., Farzaneh, F., and Talebpour, Z. (2014). Bioresource technology synthesis and characterization of $Sr_3Al_2O_6$ nanocomposite as catalyst for biodiesel production. *Bioresour. Technol.* 154, 32–37. doi:10.1016/j.biortech.2013.12.014

Rasouli, H., and Esmaeili, H. (2019). Characterization of MgO nanocatalyst to produce biodiesel from goat fat using transesterification process. *3 Biotech* 9, 429. doi:10.1007/s13205-019-1963-6

Rengasamy, M., Anbalagan, K., Mohanraj, S., and Pugalenthi, V. (2014). Biodiesel production from Pongamia pinnata oil using synthesized iron nanocatalyst. *Internat. J. ChemTech Res.* 6 (10), 4511–4516.

Roy, T., Sahani, S., Madhu, D., and Chandra Sharma, Y. (2020). A clean approach of biodiesel production from waste cooking oil by using single phase $BaSnO_3$ as solid base catalyst: mechanism, kinetics & E-study. *J. Clean. Prod.* 265, 121440. doi:10.1016/j.jclepro.2020.121440

Ruhul, A. M., Kalam, M. A., Masjuki, H. H., Fattah, I. M. R., Reham, S. S., and Rashed, M. M. (2015). State of the art of biodiesel production processes: a review of the heterogeneous catalyst. *RSC Adv.* 5, 101023–101044. doi:10.1039/C5RA09862A

Samuel, O. D., Giwa, S. O., and El-, A. (2016). Optimization of coconut oil ethyl esters reaction variables and prediction model of its blends with diesel fuel for density and kinematic viscosity model. *Biofuels* 7269, 1–11. doi:10.1080/17597269.2016.1192445

Saoud, K. (2018). *Nanocatalyst for biofuel production: a review*. New York, NY: Springer International Publishing. doi:10.1007/978-3-319-75052-1

Sarno, M., and Iuliano, M. (2019). Biodiesel production from waste cooking oil. *Green Process. Synth.* 8, 828–836.

Seffati, K., Honarvar, B., Esmaeili, H., and Esfandiari, N. (2019). Enhanced biodiesel production from chicken fat using $CaO/CuFe_2O_4$ nanocatalyst and its combination with diesel to improve fuel properties. *Fuel* 235, 1238–1244. doi:10.1016/j.fuel.2018.08.118

Senés-Guerrero, C., Contreras, A. C., Lobo, J. F., BenitoTinoco, P., SillerCepeda, J. H., and Pacheco, A. (2019). Biogas - producing microbial composition of an anaerobic digester and associated bovine residues. *MicrobiologyOpen* 8, 854. doi:10.1002/mbo3.854

Setianingsih, A., Wisrayetti, K., and Bahri, S. (2018). "Effect of Lanthanum-Natural Zeolite , La/NZA catalyst on biodiesel production from crude palm oil," in *IOP conference series: materials science and engineering*, 11. doi:10.1088/1757-899X/345/1/012007

Shalaby, E. A. (2013). Biofuel: sources , extraction and determination. doi:10.5772/51943

Shankar, A. A., Pentapati, P. R., and Prasad, R. K. (2017). Biodiesel synthesis from cottonseed oil using homogeneous alkali catalyst and using heterogeneous multi walled carbon nanotubes: characterization and blending studies. *Egyptian J. Petrol.* 26 (1), 125–133. doi:10.1016/j.ejpe.2016.04.001

Shi, M., Zhang, P., Fan, M., and Jiang, P. (2017). Influence of crystal of Fe_2O_3 in magnetism and activity of nanoparticle $CaO@Fe_2O_3$ for biodiesel production. *Fuel* 197, 343–347. doi:10.1016/j.fuel.2017.02.060

Shu, Q., Zhang, Q., Xu, G., and Wang, J. (2009). Preparation of biodiesel using s-MWCNT catalysts and the coupling of reaction and separation. *Food Bioprod. Process.* 87, 164–170. doi:10.1016/j.fbp.2009.01.004

Shuit, S. H., and Tan, S. H. (2015). Biodiesel production via esterification of palm fatty acid distillate using sulphonated multi-walled carbon nanotubes as a solid acid catalyst: process study , catalyst reusability and kinetic study. *Bioenerg. Res.* 8, 605–617. doi:10.1007/s12155-014-9545-2

Shuit, S. H., Ng, E. P., and Tan, H. S. (2015). A facile and acid-free approach towards the preparation of sulphonated multi-walled carbon nanotubes as a strong protonic acid catalyst for biodiesel production. *J. Taiwan Inst. Chem. Eng.* 1–9. doi:10.1016/j.jtice.2015.02.018

Sierra-cantor, J. F., and Guerrero-fajardo, C. A. (2017). Methods for improving the cold fl ow properties of biodiesel with high saturated fatty acids content: a review. *Renew. Sustain. Energy Rev.* 72, 774–790. doi:10.1016/j.rser.2017.01.077

Silveira, E. G., Haber, V., Reyero, I., and Serrano-lotina, A. (2019). Biodiesel production from heterogeneous catalysts based K_2CO_3 supported on extruded γ -Al_2O_3. *Fuel* 241, 311–318. doi:10.1016/j.fuel.2018.12.074

Singh, A., and Gaurav, K. (2018). Advancement in catalysts for transesterification in the production of Biodiesel: a review. *J Biochem Tech* 9 (1), 17–27.

Srivastava, N., Srivastava, M., Gupta, V. K., Manikanta, A., Mishra, K., Singh, S., et al. (2018). Recent development on sustainable biodiesel production using sewage sludge. *3 Biotech.* 8 (5), 1–11. doi:10.1007/s13205-018-1264-5

Sulaiman, N. F., Azelee, W., Abu, W., Toemen, S., Kamal, N. M., and Nadarajan, R. (2019). In depth investigation of bi-functional , Cu/Zn/g -Al_2O_3 catalyst in biodiesel production from low-grade cooking oil: optimization using response surface methodology. *Renew. Energy* 135, 408–416. doi:10.1016/j.renene.2018.11.111

Sulaiman, N. F., Wan Abu Bakar, W. A., and Ali, R. (2017). Response surface methodology for the optimum production of biodiesel over $Cr/Ca/\gamma$-Al_2O_3 catalyst: catalytic performance and physicochemical studies. *Renew. Energy* 113, 697–705. doi:10.1016/j.renene.2017.06.007

Talebian-kiakalaieh, A., Aishah, N., Amin, S., and Mazaheri, H. (2013). A review on novel processes of biodiesel production from waste cooking oil. *Appl. Energy* 104, 683–710. doi:10.1016/j.apenergy.2012.11.061

Thangaraj, B., Solomon, P. R., Muniyandi, B., Ranganathan, S., and Lin, L. (2019). Catalysis in biodiesel production — a review. *Clean Energy* 3 (1), 2–23. doi:10.1093/ce/zky020

Todorović, Z. B., Troter, D. Z., Đokić-stojanović, D. R., and Veličković, A. V. (2019). Optimization of CaO-catalyzed sunflower oil methanolysis with crude biodiesel as a cosolvent. *Fuel*, 23, 903–910. doi:10.1016/j.fuel.2018.10.056

Touqeer, T., Mumtaz, M. W., Mukhtar, H., Irfan, A., Akram, S., Shabbir, A., et al. (2020). Fe3O4-PDA-lipase as surface functionalized nano biocatalyst for the production of biodiesel using waste cooking oil as feedstock: characterization and process optimization. *Energies* 13, 177. doi:10.3390/en13010177

Vahid, B. R., and Haghighi, M. (2016). Urea-nitrate combustion synthesis of MgO/MgAl₂ O_4 nanocatalyst used in biodiesel production from sunflower oil: influence of fuel ratio on catalytic properties and performance. *Energy Convers. Manag.* 126, 362–372. doi:10.1016/j.enconman.2016.07.050

Veronica Winoto, N. Y. (2019). Optimization of biodiesel production using nanomagnetic CaO-based catalysts with subcritical methanol transesterification of rubber seed oil. *Energies* 12, 230. doi:10.3390/en12020230

Vieira, S. S., Magriotis, Z. M., Santos, N. A. V., Saczk, A. A., Hori, C. E., and Arroyo, P. A. (2013). Bioresource Technology Biodiesel production by free fatty acid esterification using lanthanum (La^{3+}) and HZSM-5 based catalysts. *Bioresour. Technol.* 133, 248–255. doi:10.1016/j.biortech.2013.01.107

Wen, Z., Yu, X., Tu, S., Yan, J., and Dahlquist, E. (2010). Synthesis of biodiesel from vegetable oil with methanol catalyzed by Li-doped magnesium oxide catalysts. *Appl. Energy* 87 (3), 743–748. doi:10.1016/j.apenergy.2009.09.013

Wu, H., Zhang, J., Wei, Q., Zheng, J., and Zhang, J. (2013). Transesterification of soybean oil to biodiesel using zeolite supported CaO as strong base catalysts. *Fuel Process. Technol.* 109, 13–18. doi:10.1016/j.fuproc.2012.09.032

Xie, W., Huang, X., and Li, H. (2007a). Soybean oil methyl esters preparation using NaX zeolites loaded with KOH as a heterogeneous catalyst. *Bioresour. Technol.* 98, 936–939. doi:10.1016/j.biortech.2006.04.003

Xie, W., Yang, Z., and Chun, H. (2007b). Catalytic properties of lithium-doped zno catalysts used for biodiesel preparations. *Ind. Eng. Chem. Res.* 46, 7942–7949. doi:10.1021/ie070597s

Yin, J. Z., Ma, Z., Hu, D. P., Xiu, Z. L., and Wang, T. H. (2010). Biodiesel production from subcritical methanol transesterfication of soyabean oil with sodium silicate. *Energy Fuel.* 24, 3179–3182

Youse, S., Haghighi, M., and Vahid, B. R. (2019). Role of glycine/nitrates ratio on structural and texture evolution of MgO-based nanocatalyst fabricated by hybrid microwave-impregnation method for biofuel production. *Energy Convers. Manag.* 182, 251–261. doi:10.1016/j.enconman.2018.12.067

Zahan, K. A., and Kano, M. (2018). Biodiesel production from palm oil, its by-products, and mill effluent: a review. *Energies* 11 (8), 1–25. doi:10.3390/en11082132

Zhang, D., Wei, D., Li, Q., Ge, X., Guo, X., Xie, Z., et al. (2014). High performance catalytic distillation using CNTs-based holistic catalyst for production of high quality biodiesel. *Sci. Rep.* 4, 4021. doi:10.1038/srep04021

Zhang, X. L., Yan, S., Tyagi, R. D., and Surampalli, R. Y. (2013). Biodiesel production from heterotrophic microalgae through transesteri fi cation and nanotechnology application in the production. *Renew. Sustain. Energy Rev.* 26, 216–223. doi:10.1016/j.rser.2013.05.061

Zhang, Z., Yuan, X., Miao, S., Li, H., Shan, W., and Jia, M. (2019). Effect of Fe additives on the catalytic performance of Ion-exchanged CsX zeolites for side-chain Alkylation of Toluene with methanol. *Catalysts* 9, 829. doi:10.3390/catal9100829

Zhen, B., Jiao, Q., Zhang, Y., Wu, Q., and Li, H. (2012). Acidic ionic liquid immobilized on magnetic mesoporous silica: preparation and catalytic performance in esterification. *Appl. Catal. A General* 445–446, 239–245. doi:10.1016/j.apcata.2012.08.023

Zuliani, A., Ivars, F., and Luque, R. (2018). Advances in nanocatalyst design for biofuel production. *ChemCatChem*, 10, 1968–1981. doi:10.1002/cctc.201701712

Optimizing Microalgal Biomass Feedstock Selection for Nanocatalytic Conversion Into Biofuel Clean Energy, Using Fuzzy Multi-Criteria Decision Making Processes

Konstantinos Kokkinos[1], Vayos Karayannis[2] and Konstantinos Moustakas[3]*

[1]Department of Energy Systems, University of Thessaly, Larissa, Greece, [2]Department of Chemical Engineering, University of Western Macedonia, Kozani, Greece, [3]School of Chemical Engineering, National Technical University of Athens, Athens, Greece

Biofuel production from microalgae non-food feedstock is a challenge for strengthening Green energy nowadays. Reviewing the current technology, there is still reluctance in investing towards the production of new algal strains that yield more oil and maximize capital gains. In the current work, the microalgal feedstock selection problem is investigated for increased lipid production and nano-catalytic conversion into clean biofuel. For that purpose, a variety of Fuzzy Multi-Criteria Decision Making processes and a multitude of Optimization criteria spanning to technological, environmental, economic, and social aspects are used. The strains selected for the analysis are *Chlorella* sp., *Schizochytrium* sp., *Spirulina* sp., and *Nannochloropsis* sp. The methods applied are fuzzy analytic hierarchy process, FTOPSIS (fuzzy technique for the order of preference to the ideal solution), and FCM (fuzzy cognitive mapping). Pairwise comparison matrices were calculated using data from extensive literature review. All aforementioned fuzzy logic methodologies are proven superior to their numeric equivalent under uncertain factors that affect the decision making, such as cost, policy implications, and also geographical and seasonal variation. A major finding is that the most dominant factor in the strain selection is the high lipid content. Moreover, the results indicate that the *Chlorella Vulgaris* microalgae is ranked as the best choice by the FTOPSIS method followed by the *Nannochloropsis* strain, and *Spirulina Platensis* was found to be the last in performance. The best and worst case scenario run with FCM experimentally verify this choice indicating that *Chlorella Vulgaris* follows this trend of selection mostly with the technological and the economic criteria for both the sigmoid and the hyperbolic tangent deep-learning functions used.

Keywords: biofuel, clean energy, microalgal biomass, feedstock selection, optimization, fuzzy multi-criteria decision making, nanocatalyst, conversion

INTRODUCTION

Bioenergy and biofuel production in the framework of sustainability has gained significant interest in recent years and represents one of the main priorities in energy research. Biofuel, especially, has proven to be the ultimate alternative for green and renewable energy production, which drastically reduces greenhouse emissions despite the high operating cost and the technological process irregularities in the involved supply chain (Chandel et al., 2018; Gardy et al., 2019). Due to renewable biofuel potential for green recovery, biomass production has recently attracted enormous attention worldwide for contributing to climate change mitigation (Roussos et al., 2019). In this context, biomass production is a non-toxic technology that creates renewable energy utilizing established procedures specific to the desired biofuel production (Sindhu et al., 2017). Lately, special interest has been shown and directed to the microbial fuel cells, among which microalgae in particular presents a promising environmental adaptability in preserving nutrients and storing lipids that can be extracted to provide a sustainable energy source. This can migitate the gap between economic development and environmental preservation (Nizami et al., 2017).

Microalgae is the primary third generation biofuel (non-food) source that has been proved to be superior for biofuel production among other conventional terrestrial crops in terms of cell structure, growth rate, and photosynthetic yield (Viswanath et al., 2010; Dutta, Daverey, and Lin 2014). Specifically, microalgae are individual plant cells that can be cultivated either in photo-bioreactors, or in specially constructed open ponds or even in a hybrid combination of both systems (usually raceway open ponds and closed photo-bioreactors). They utilize CO_2, micronutrients, and solar light to multiply and produce raw microalgal biomass containing carbohydrates, lipids, and proteins (Arora et al., 2019; Papapolymerou et al., 2019; Zhang et al., 2020).

Cultivation of microalgae offers distinct advantages that ensure process viability and sustainability as feedstock for clean biofuel energy production (Chisti 2008; Li et al., 2008; Singh and Gu 2010; Carmichael et al., 2017; Yadav et al., 2020). The most important advantages include: 1) increased biomass production capability, 2) minimal nutrient requirements, fewer water needs and even possibility of using wastewaters containing residual nutrients and also no requirements for herbicides or pesticides, with expected environmental and economic gains, 3) less land demand, thus avoiding competition with other land-based crops also taking into account the potential for cultivation in non-arable areas, and 4) resistance of several species to salinity or even growth in marine environment with obvious benefits for cultivation in coastal areas.

Especially, microalgal biomass is a renewable energy source with its carbon content being totally derived from carbon dioxide (CO_2) and also with the perspective of fixing and recycling CO_2 exhausts from fossil fuel burning, (e.g. from co-located thermal power plants) in algal biomass production towards CO_2 bio-mitigation and global carbon emission reductions. In the context of circular bio-economy, additional advantages include: 1) a more efficient microalgal oil extraction ability, 2)

an increased biofuel biodegradability and non-toxicity, 3) the possibility of co-generation of other products for use in food, cosmetics and medical industry, 4) the potential for exploitation of new by-products as crop fertilizers or food additives, (e.g. the remaining algal biomass being rich-in protein, carbohydrates and small quantities of non-extractable lipids and micronutrients).

According to (Nwokoagbara et al., 2015), the stages in producing biofuels from microalgae are the following:

- microalgae strain selection and cultivation,
- harvesting,
- algal oil extraction via pretreatment (drying) and treatment (fluid extraction) via various physicochemical processes, and finally
- oil transformation to produce the desired type of biofuel.

For the conversion of microalgal biomass-derived oil feedstock into biofuel by the catalytic transesterification reaction, alkalis (KOH or NaOH) have been used as homogeneous catalysts (Campbell 2008), while porous microspheres, (e.g., zirconia, titania and alumina) have been used as heterogeneous ones (Raehtz. 2009). At the boundary between them, nanocatalysts with enhanced stability, catalytic activity, low cost, recyclability, and reusability are increasingly being considered to provide new pathways for efficient and environment-friendly biofuel production. The latest achievements in nanomaterial design for algal lipid transformation include a photochemically synthetized $SrTiO_3$ nanocatalyst (for microalgae *Chlorella vulgaris*), a Fe_2O_3 nanocatalyst, a KOH-supported magnetic alumina-ferric oxide nanocatalyst, and a poly-ethylen-glycol encapsulated $ZnOMn^{2+}$ nanocatalyst (for *Nanochloropsis oculata*) (Banerjee et al., 2019; Kazemifard et al., 2019; Vinoth Arul Raj et al., 2019; Aghilinategh, Barati, and Hamadanian 2020; Safakish et al., 2020).

Generally, the overall process optimization includes very complex research issues and involves diverse limitations in components and system parameters, in order to establish a viable large-scale microalgal oil production for biofuel (Carmichael et al., 2017). In order to maximize the quantities of biofuel generation, an optimization of microalgae cultivation with improved productivity is a prerequisite, taking into consideration the advancements in physicochemical parameters, including temperature light irradiation, CO_2 incoming feed etc., for enhancing microalgal biomass yield (Gouveia 2011; N.; Hossain and Mahila, 2019). Moreover, apart from the harvesting, processing, and fuel extraction methodologies, according to (Viswanath et al., 2010), most critical decisions are especially related to the microalgal strain selection focusing on properties of critical significance such as: 1) the growth rate of the plants, 2) the lipid content, 3) the fatty acid profile, and 4) the ease of harvesting to make the technology one that is worth advancing and which has the corresponding economic impact to decisively contribute to the sustainability of the process. Actually, some microalgae strains favor high biomass production while others favor high lipid concentration, thus it is important to select an appropriate

algae strain with both high biomass and oil productivity, which also can be grown at relatively low cost (Hossain et al., 2008; Yoo et al., 2010). Moreover, genetic and metabolic engineering approaches have lately been investigated for improving the valuable lipid content in microalgae that are increasingly considered as promising "cell factories" (Naghshbandi et al., 2020).

Nevertheless, extended research has shown that already over 50,000 microalgae species have been recorded and around 30,000 of them have been studied. Furthermore, there is not any classification of the already analyzed strains in terms of their properties (both chemical, physical, and biological). Having the aforementioned facts in mind, microalgal strain selection becomes a critical and multi-various decision making problem depending on a repertoire of criteria of diverse methodological categories and uneven weight importance. To deal with the microalgae strain selection problem using conventional MCDM methodologies is not convenient due to the fact that there is a multitude of decision making variables involved that are of non-numeric nature. Furthermore, the participation of experts' opinion in the process automatically initiates the mixing of categorical properties having linguistic values. Additionally, attacking the problem using a participatory modeling methodology naturally inserts a variety of uncertainties related to the strain selection, and again all subjectivities of experts in the field can only be expressed using fuzzy linguistic variables as opposed to regular numeric quantities (Zhao, Xu, and Ren 2019; Lak Kamari et al., 2020). On the other hand, the involvement of fuzzy linguistic variables when applying multi-criteria decision making has shown to reveal the most influential criteria and parameters that are associated with the uncertainties occurring. So far, restricted information is reported in literature about the application of fuzzy MCDM methodologies in the critical task of the optimized selection of microalgae strains as feedstock for biofuel, given their ample differences in physico-chemical and biological properties that can strongly affect the overall production process.

The primary aim/objective of the present novel research is to systematically analyze and evaluate the potential of microalgae strains for clean biofuel production. For that purpose, an innovative holistic approach is proposed, which includes participatory modeling and a robust repertoire of advanced fuzzy logic-based multi-criteria processes/methodologies, namely FAHP, FTOPSIS, and FCM, to address and minimize uncertainties involved towards investing into microalgal potential plants that use selected feedstock. Moreover, the optimization criteria are classified into technological, environmental, social, and economic ones.

With the involvement of experts in the field, the most important parameters of the above four categories were identified. Then, a simple questionnaire was given to local and regional stakeholders of biofuel production industry, competent authorities officials and local residents to provide feedback relatively to the importance of each criterion used in relation to strain type. The set of available answers was scaled using intutionistic and linguistic values, thereby triggering the participation of the fuzzy MCDM methodologies mentioned

above. The interoperability of the above criteria is not generally helpful, as there may exist negative or converse causalities between any two criteria elements. However, this is the reason that, in participatory modeling, regional and local stakeholders contribute on the creation, establishment and refinement of these causalities (Kokkinos and Karayannis 2020). The opinion of stakeholders is obtained using either surveys or focus groups. The answers acquired are treated using the aforementioned procedures to evaluate candidate decisional scenaria and/or to find near optimal solutions to the optimization problem at hand.

The structure and major contents of this study are: i. in section two, the methodologies are thoroughly presented with regard to the fuzzy processes used for finding the best suitable microalgal strain to produce biofuel. The criteria for the evaluation are taken mostly by the literature and experts on the field. A detailed description of the questionnaire used, the classification of criteria and the feedback of the local and regional stakeholders weighing and contemplating these criteria are also included; ii. Section three calculates the criteria priorities in a decision matrix for the case of FAHP, setting initially the hierarchy and the weight fuzzy scale. Similar approach is shown for the case of FTOPSIS, using triangular fuzzy membership functions. For the FCM case, a steady-state analysis is presented separately for each strain case scenario as well as best and worst case scenario of alternating the involved criteria. Furthermore, the results, discussion, and assessment are illustrated along with the overall procedure application in specific locations in Greece; and finally iii. main conclusions and future challenges of the problem under consideration are presented.

METHODOLOGIES

Microalgal Biomass Cultivation for Biofuel Production

Compliance With Ethical Principles

The present research methodology upholds high ethical standards. In that sense, ethics approval was not required in accordance with the local legislation and/or the institutional requirements. Indeed neither animal subjects nor human subjects/patients are involved. Moreover, identifiable personal human data are not included in the social surveys performed for the purpose of the study, which fully complied with the ethical principles. Specifically, all participants were given all the appropriate information regarding the aim and the content of the survey and especially the confidentiality and the anonymity of the participants, and finally they were asked whether they wanted to participate. Thus all participants volunteered to provide their opinions about the concepts of the study. At the same time, participants were informed about any possible shortcomings of the survey and particularly on the effort of the researchers to totally avoid the introduction of any bias either via questioning of certain scope or via the outcome statistics. Furthermore, the social survey was not sponsored by any organization or private sector business but it was solely aiming to record and assess the public opinion and potential acceptance relative to the growth and/or

the worthiness of producing Green energy through the use of microalgal biomass renewable source and its processing into clean biofuel.

Participatory Modeling Process and Proposed Decision-Making Logical Architecture

The participatory modeling approach can be utilized to create the causal loop from all involved stakeholders to integrate: 1) microalgal cultivation methodologies, 2) social and environmental aspects and 3) economic aspects to introduce a comprehensive scheme of promoting specific strains that maximize profit. The goal is to understand the limitations and the extensions of the problem while at the same time, the stakeholders can discover all the drivers and factors that participate on this issue (Suprun et al., 2018). The work of Salim et al. (2019) identified the barriers, the drivers, and the enablers concerning the development and the management of renewable energy production plants. They also identified all criteria to initiate such development. Specifically for the case of microalgal cultivation for biofuel production, the strain selection is a multifaceted and complex problem involving various conflicting criteria. The multitude of interlinked factors affecting the process makes the strain selection a MCDM problem. According to (Wohlfahrt et al., 2019), there is a necessity to focus on criteria that improve the biomass transformation which corresponds to biofuel improvement with regard to sustainability. For that reason, we need to review the factors of critical significance in relation to bio-economy systems and how these systems interact, the level of their heterogeneity, the bending and flexibility of stakeholders' strategies, the panoramic view of all spatiotemporal scales for the microalgal cultivation as well as other exogenous parameters such as the energy price market, the climate and various regional regulations and bylaws. The work of (Köhler. 2019) indicates the most important directions for sustainable innovation in terms of sustainability and biofuel production via evolutionary economics and technological innovation using agent based models that represent the neo-Schumpeterian ideas in terms of sustainable energy transitions. Towards the same lines of research, the work of Wang et al. (2019) assessed mostly the socioeconomic aspects in the production of aviation biofuel for the case of Brazil. This work provides a variety of scenarios illustrating the technological coefficients of the MCDM model. However, the above research works represent only a small sample of the available research directly related to the assessment of the multi-criteria problem of sustainable biofuel production. The survey of Hossard and Chopin. (2019) shows that there at least ~2000 research articles up until 2019 that tackle the problem of sustainable biofuel production involving multi-criteria issues such as change, scale, pollution, biodiversity, practices, and terms on biophysical/regulatory conditions.

According to (Bekirogullari et al., 2020; Juan et al., 2020; Markou. 2020; Sung et al., 2020), the most popular systems for microalgal cultivation are summarized as follows:

- *Outdoor cultivation systems* which are open water repository systems (ponds, lakes etc.) that enable microalgae to treat nitrogen and phosphorus in the wastewater.
- *Indoor cultivation* such as large cultivation bags and tubular photobioreactors suitable for microalgae cultivation

independently from the weather conditions avoiding contamination.
- *Hybrid photobioreactor systems* which use photobioreactors initially and then open systems to increase the biomass production.
- *Microalgal biofilm systems* that mostly deal with microalgal cultivation in wastewater, and
- *Systems of microalgae cultivation in beads of alginate* that trap algal cells in wastewater management plants.

To the best of our knowledge, the most relevant research that relates all categories of criteria to biomass and biofuel production belongs to (Bueyuektahtakin and Cobuloglu. 2014). The combination of the above literature with the surveying of a broad expert body gave us the following **Table 1** of candidate criteria clustered into the four categories. Out of these criteria, according to (Viswanath et al., 2010) the most important technological criteria are the growth rate, the fatty acid profile, the ease of harvesting but above all the lipid content.

The above mentioned criteria are used to determine their fuzzy weights each in their specific category. For that reason four types of simple questionnaires were distributed to experts as well as to the competent authorities' officials and other relevant stakeholders. The scaling on the answer choices was done using seven fuzzy linguistic values spanning from highly unimportant to highly important levels. The set of the methodologies used in the determination of the most important strains is shown in the following **Figure 1** and it works as a logical architecture of the overall participatory modeling approach. More specifically, we first apply FAHP and FTOPSIS to calculate the pairwise comparison matrices of the criteria at hand. Four such matrices were computed, one for each category of criteria. This allowed us to do scenario analysis (steady state, worst and best case) for each one of aforementioned categories of criteria to evaluate their relative significance and importance.

Fuzzy Sets Theory and FAHP Method

Fuzzy sets were introduced by (Zadeh. 1965). Fuzzy sets differentiate from other set types because they contain elements that present a degree of membership i.e., making it possible to represent the imprecision level in non-numeric variables. Fuzzy relations are a generalization of L-Relations (Burgin and Kuznetsov. 1992) and they assign a membership grade in each set entity as a mapped value between 0 and 1. By permiting gradual assessment of the membership of set elements, fuzzy theory suceeds to provide significant results in fuzzy linguistics (Cock et al., 2000), in decision making (Kokkinos et al., 2019; Wang and Peng. 2020) and in clustering (Ullah et al., 2020).

The AHP method was introduced by (Saaty, 1987) to provide ratio scaling and since then, it has become the *de facto* tool to perform MCDM. The method however is applied only for problems of crisp numeric variables. To overcome the problem, FAHP was introduced by (Chang, 1996). FAHP calculates the relative importance between any pair of criteria in a hierarchy setup for a specific problem. The method uses

ID	Technological	ID	Environmental	ID	Economic	ID	Social
T1	Energy content	EN1	Land/waterbody use	EC1	Microalgae (raw material) cost	S1	Competition for food
T2	Energy efficiency	EN2	Water quality requirement	EC2	Investment cost	S2	Technological development
T3	Ease of harvesting	EN3	Biodiversity and aquatic life	EC3	Cost of cultivation or nutrients	S3	Sustainable development
T4	Primary energy ratio	EN4	CO_2 sequestration ability	EC4	Cost of harvesting	S4	Social acceptability
T5	Biomass content	EN5	Cultivation methods	EC5	Co-utilization	S5	Job creation
T6	Oil content	EN6	Pollution	EC6	Robustness	S6	Social benefits
T7	Lipid content	EN7	Chemical usage	EC7	Storage cost		
T8	Fatty acid profile	EN8	Light intensity	EC8	Transportation cost		
T9	Growth rate	EN9	Resistance to contamination	EC9	Payback period		
T10	Reliability	EN10	Particles emission				
T11	Safety	EN11	Impact on ecosystems				
T12	Availability of nutrients	EN12	Visual impact				
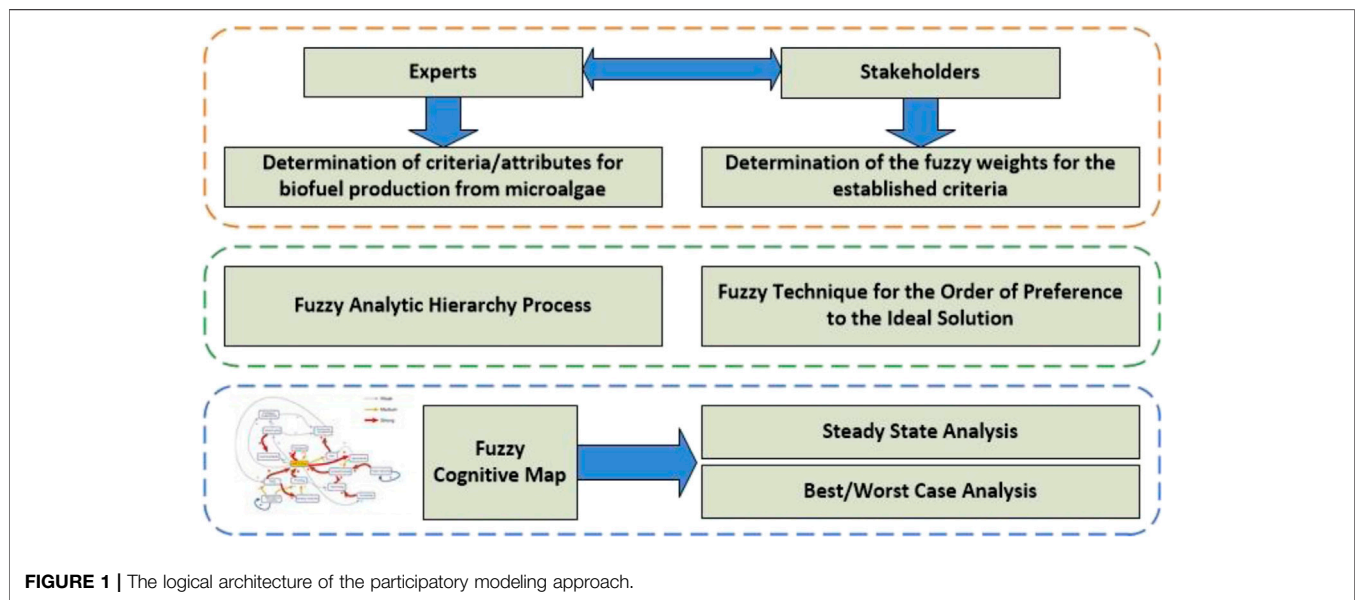
FIGURE 1 | The logical architecture of the participatory modeling approach.
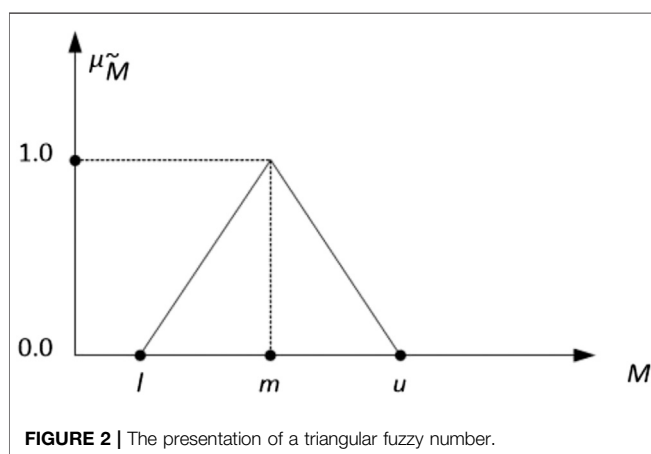
FIGURE 2 | The presentation of a triangular fuzzy number.

triangular fuzzy numbers (TFNs) and a pairwise comparison to compute the fuzzy evaluation matrix. The TFNs are defined by the triplet (l, m, u) where $(l \leq m \leq u)$ and their corresponding

memebrship function is depicted in the following equation whereas the visual representation is shown in **Figure 2**.

$$\mu(x) = \begin{cases} \dfrac{x-l}{m-l}, & l \leq x \leq m, \\ \dfrac{u-x}{u-m}, & m \leq x \leq u, \\ 0, & \text{otherwise.} \end{cases}$$

According to Altintas et al. (2020), the method performs a pairwise comparison between any two criteria translated from linguistic values to TFNs based on a nine-integer scale mapping which is depicted in **Table 2**. Intermediate numbers in the numeric scale get an analogous comproming in the triangular fuzzy scale. Additionally, the following set of algebraic operations is defined by Kahraman et al. (2003); Noorul Haq and Kannan. (2006); Chamodrakasv et al. (2010); and Chan et al. (2008) to calculate the pairwise comparison between criteria. The operations shown (apart from the representation of a TFN) are the following in this order: inverse of a fuzzy number, addition of two numbers,

Definition	Crisp values (intensity of importance)	Fuzzy triangular scale $\tilde{M} = (l, m, u)$.
Equally important	1	(1,1,1)
Weakly important	3	(1,3,5)
Fairly important	5	(3,5,7)
Strongly important	7	(5,7,9)
Absolutely important	9	(7,9,9)

subtraction, multiplication, inner product, and summation of a set of fuzzy numbers respectively.

$$\tilde{M} = (l, m, u),$$

$$\left(\tilde{M}\right)^{-1} = (l, m, u)^{-1} = \left(\frac{1}{u}, \frac{1}{m}, \frac{1}{l}\right),$$

$$\tilde{M}_1 \oplus \tilde{M}_2 = (l_1, m_1, u_1) \oplus (l_2, m_2, u_2) = (l_1 + l_2, m_1 + m_2, u_1 + u_2),$$

$$\tilde{M}_1 - \tilde{M}_2 = (l_1, m_1, u_1) - (l_2, m_2, u_2)$$
$$= (l_1 - l_2, m_1 - m_2, u_1 - u_2),$$

$$\tilde{M}_1 \otimes \tilde{M}_2 = (l_1, m_1, u_1) \otimes (l_2, m_2, u_2) = (l_1 l_2, m_1 m_2, u_1 u_2),$$

$$\prod_{i=1}^{n} \tilde{M}_i = \left(\prod_{i=1}^{n} l, \prod_{i=1}^{n} m, \prod_{i=1}^{n} u\right),$$

$$\sum_{i=1}^{n} \tilde{M}_i = \left(\sum_{i=1}^{n} l, \sum_{i=1}^{n} m, \sum_{i=1}^{n} u\right).$$

Assuming a set of n-criteria then the corresponding comparison matrix is given in the form:

$$\tilde{M}_{ij} = \begin{bmatrix} \tilde{M}_{11} & \tilde{M}_{12} & \cdots & \tilde{M}_{1n} \\ \tilde{M}_{21} & \tilde{M}_{22} & \dots & \tilde{M}_{2n} \\ \vdots & \vdots & \cdots & \vdots \\ \tilde{M}_{n1} & \tilde{M}_{n2} & \dots & \tilde{M}_{nn} \end{bmatrix}$$

$$= \begin{bmatrix} l_{11}m_{11}u_{11} & l_{12}m_{12}u_{12} & \cdots & l_{1n}m_{1n}u_{1n} \\ l_{21}m_{21}u_{21} & l_{22}m_{22}u_{22} & \dots & l_{2n}m_{2n}u_{2n} \\ \vdots & \vdots & \cdots & \vdots \\ l_{n1}m_{n1}u_{n1} & l_{n2}m_{n2}u_{n2} & \dots & l_{nn}m_{nn}u_{nn} \end{bmatrix}$$

$$for \quad \begin{matrix} i = 1 \dots n, \\ j = 1 \dots n. \end{matrix}$$

Furthermore, the geometric mean is also needed to convert back the triangular fuzzy numers into crisp numeric and this operation is defined as:

$$\tilde{F}_i = \tilde{R} \otimes \tilde{G}_i = \left(\sum_{i=1}^{n} \sqrt[n]{\prod_{j=1}^{n} \tilde{M}_{ij}}\right)^{-1} \otimes \sqrt[n]{\prod_{j=1}^{n} \tilde{M}_{ij}}.$$

Note that in the previous equation $\tilde{G}_i$ denotes the fuzzy geometric mean of the criterion C_i, R corresponds to the reciprocal of the sum of the geometric mean of fuzzy comparison values, and finally $\tilde{F}_i$ represents the fuzzy weight for criterion C_i.

Microalgal Biomass Selection Problem and FAHP–Related Works

Montingelli et al., 2015 have provided a comprehensive review related to biogas production from algal biomass proving that algae-derived biofuels are a promising alternative to the depleting of fossil fuels. However, the economic feasibility of massive biomass production from microalgae has not been established yet due to high energy requirement for harvesting and drying. For that reason, research based on FAHP was conducted by Tan et al. (2016) to prioritize the best harvesting and drying method at the same determining the degree of confidence of the experts who set up the criteria and the quantification process. FAHP has been used to evaluate global market shares in terms of the renewable bio-energies. Initially, the research of Ubando et al. (2020) evaluates new algal bioproducts in collaboration with existing industries. The authors created a Decision Support System (DSS) that helps the industry to choose the best among candidate sites and regions to cultivate microalgae based on the environmental impact, several economic burdens, social aspects, and the viewpoints of stakeholders via an FAHP that incorporates uncertainty of opinions. For the same area, a study by (Ubando et al., 2016a) focuses on the factored ranking of several criteria using FAHP and Artifical Neural Networks (ANN). The selected methodologies provided the ability to discover patterns of inconsistencies as well as a large amount of missing information in order to apply a complete participatory modeling process. Towards the same line of research, the work of (Correa et al., 2019) utilizes FAHP among other fuzzy modeling approaches to discover the most appropriate and feasible site for producing microalgal feedstock (but on a global and country level). In this work the optimization criterion is the revenue and profit while diminishing several collateral competitions of other targeted markets (food markets, cosmetics etc.). Their case studies mostly concentrate on the regions of Africa, Middle East, and western South America and this is the first sited work on the subject specifics. The same work in Ubando et al. (2016b) tries to analyze various microalgal cultivation systems based again on environmental impact, energy consumption, economic viability, social acceptability, and system robustness using FAHP via Monte Carlo simulations. These studies provided microalgal sites for cultivation for risk-averse and risk-inclined scenarios.

The majority of research that relates the FAHP method with the biofuel through microalgal biomass production can be represented by the work of Hamid et al., 2017. This work concentrates on the technological screening of the biomass production using FAHP for feature scaling normalization in order to select the optimum processing procedure for sustainable biofuels production from algae. But as it happens with other forms of renearble resource feedstocks (Katooli et al., 2019; Kheybari et al., 2019), the most important step towards sustainable profitability scenario is the development of an evaluation framework and a well established DSS that determines the importance of the selected criteria including all appearances of nature (climate, environment, technological, and social consequences).

FTOPSIS Method

The TOPSIS method is a numerical optimization methodology that utilizes a pseudo-polynomial heuristic based on the fact that, in a selection process, we must rank as the most appropriate the solution that close to the positive ideal decision candidate and far away from negative decision ideal candidate (Yoon and Hwang, 1995). The method was extended to include linguistic valued variables of fuzzy nature by Chen. (2000) and since then, it has been heavily used in many disciplines. Via FTOPSIS, policy makers can define each participating decision criterion using TFNs as shown in FAHP. Given any two TFNs $\tilde{N}_1 = (l_1, m_1, u_1)$ and $\tilde{N}_2 = (l_2, m_2, u_2)$ and using the vertex distance calculation for FTOPSIS, the distance between $\tilde{N}_1$ and $\tilde{N}_2$ is given by:

$$d\left(\tilde{N}_1, \tilde{N}_2\right) = \sqrt{\frac{1}{3}\left[(l_1 - l_2)^2 + (m_1 - m_2)^2 + (u_1 - u_2)^2 \right]}.$$

Most of therecent FTOPSIS research deals with the optimization of the renewable energy solution problem as presented in Rani et al. (2020; 2019); Cayir Ervural et al. (2018); Dinçer and Yüksel. (2019); Aikhuele et al. (2019); Krishankumar et al. (2020). We present the whole modeling approach as a seven step approach:

Step 1. Definition of the criteria involved and weight classification: The correspondence between the linguistic ratings and the TFNs is based on **Table 2** as a Likert-scale type. According to this mapping, normalization of the TFNs is achieved using triplets within the space [0..1].

Step 2. Computation of the judgment matrix: For policy makers, the following matrix is computed as a combination of the available criteria C_j and the alternative decisions D_i.

$$\text{JM} = \begin{matrix} D_1 \\ D_2 \\ \vdots \\ D_n \end{matrix} \begin{bmatrix} \tilde{r}_{11} & \tilde{r}_{12} & \cdots & \tilde{r}_{1m} \\ \tilde{r}_{21} & \tilde{r}_{22} & \cdots & \tilde{r}_{2m} \\ \vdots & \vdots & \cdots & \vdots \\ \tilde{r}_{n1} & \tilde{r}_{n2} & \cdots & \tilde{r}_{nm} \end{bmatrix} \begin{matrix} C_1 & C_2 & \cdots & C_m \end{matrix}.$$

Step 3. Normalization of the judgment matrix: The JM matrix normalization is computed using the pre-clustering of the available criteria into the Benefit Criteria (BC) and Cost Criteria (CC) subsets. The result is denoted as NJM and the relevant equations follow:

$$\text{NJM} = \begin{bmatrix} \tilde{x}_{11} & \tilde{x}_{12} & \cdots & \tilde{x}_{1m} \\ \tilde{x}_{21} & \tilde{x}_{22} & \cdots & \tilde{x}_{2m} \\ \vdots & \vdots & \cdots & \vdots \\ \tilde{x}_{n1} & \tilde{x}_{n2} & \cdots & x_{nm} \end{bmatrix},$$

$$\tilde{x}_{ij} = \left(\frac{a_{ij}}{c_j^*}, \frac{b_{ij}}{c_j^*}, \frac{c_{ij}}{c_j^*}\right) \quad j \in BC, \quad \tilde{x}_{ij} = \left(\frac{a_j^-}{c_{ij}}, \frac{a_j^-}{b_{ij}}, \frac{a_j^-}{a_{ij}}\right), \quad j \in CC,$$

$$c_j^* = \max_i c_{ij}, \quad j \in BC, \quad a_j^- = \max_i a_{ij}, \quad j \in CC.$$

Step 4. Construction of the weighted NJM denoted as WNJM and computed using:

$$\tilde{V} = \left[\tilde{v}_{ij}\right]_{n \times m}, \quad \tilde{v}_{ij} = \tilde{x}_{ij}(.)\tilde{w}_i, \quad i = 1 \ldots n, \quad j = 1 \ldots m.$$

Step 5. Computation of the the Fuzzy Positive Ideal Solution (FPIS) and the Fuzzy Negative Ideal Solution (FNIS), via calculation of two vectors A^* and A^- where:

$$A^* = \left(\tilde{v}_1^*, \tilde{v}_2^*, \ldots, \tilde{v}_n^*\right), \quad A^- = \left(\tilde{v}_1^-, \tilde{v}_2^-, \ldots, \tilde{v}_n^-\right).$$

and $\tilde{v}_i^* = (1, 1, 1)$ and. $\tilde{v}_i^* = (0, 0, 0)$ $i = 1 \ldots n$.

Step 6. Calculation of the distance between FPIS and FNIS, corresponding to the distance between A^* and A^- denoted as $\tilde{d}_i^*$ and $\tilde{d}_i^-$ respectively:

$$\tilde{d}_i^* = \sum_{i=1}^n d\left(\tilde{v}_{ij}, \tilde{v}_i^*\right), \quad i = 1 \ldots n,$$

$$\tilde{d}_i^- = \sum_{i=1}^n d\left(\tilde{v}_{ij}, \tilde{v}_i^-\right), \quad i = 1 \ldots n.$$

Step 7. Computation of the closeness coefficient of each policy and rating them in descending order

$$\text{COEF}_i = \frac{\tilde{d}_i^-}{\tilde{d}_i^* + \tilde{d}_i^-}.$$

Microalgal Selection Problem and FTOPSIS–Related Works

The FTOPSIS methodology can be applied in the microalgae strain selection problem to produce biofuels as a holistic decision-making tool. Accordingly, the idea behind FTOPSIS is to choose one of the candidate elements that has the maximum possible distance from the negative ideal and the minimum possible distance from the positive ideal solution among the algal strain alternatives (Madugu and Collu, 2014). Even though it is distinguished that the production of biofuel from various agricultural and other wastes achieves higher overall performance compared to other technologies (Khishtandar et al., 2017), microalgal high sugar and oil is a promising source for biofuel production. For such production chains, FTOPSIS is the most valuable method to deal with the uncertainties of inventory deterioration issue, the applicability and efficiency of microalgal harvesting and the ranking of cultivation sites (Arabi et al., 2019; Peng et al., 2020).

Apart from the strain selection, other works try to evaluate the environmental risk of harmful algal bloom via fuzzy analytical methodologies such as FAHP and FTOPSIS that exert influence on the risk significance and severity (Gholami et al., 2019). Additionally, several scenario analyses deal with alternative techniques of biomass extraction from algae such as pyrolysis or phycoremediation of wastewater and compare the method and the properties of biofuel derived to various feedstocks using FTOPSIS and MCDM (Apandi et al., 2019; Mehta and Nirvesh, 2020). But the microalgal strain selection is extended only on the study of environmental social and economic impacts. Recent works investigate the appropriateness of fatty acid profiles to biodiesel characterization through the Preference Ranking Organization Method for Enrichment Evaluation (PROMETHEE) and the Graphical Analysis for Interactive Assistance (GAIA) analysis (Islam et al., 2013).
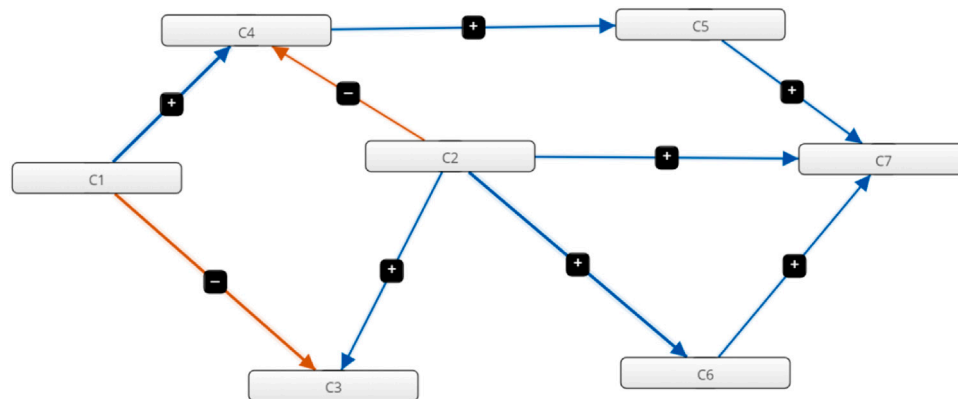
FIGURE 3 | A typical FCM graph depicting positive and negative causalities between concepts.

Thus, there is no specific article, to the best of our knowledge, examining the microalgae strain ranking via multi-criteria analysis and FTOPSIS procedure.

Fuzzy Cognitive Mapping (FCM) for Multi-Criteria Decision Making

Fuzzy Cognitive Maps (FCMs) are semi-quantitative extensions of cognitive maps used for modeling and structuring expert knowledge that aims to determine the casual interrelations between participating concepts of a particular issue. Proposed by Kosko. (1986; 1992), FCMs are directed graphs of nodes representing the concepts and edges representing the causal relationships between any two concepts. The weight of the directed edges is fuzzified identifying a membership function for the degree of causality between the concepts. The activation of the concepts can be defined as a state vector thus, allowing the FCM to evolve as an ANN converging to a steady state. The causality of any concept pair can be quantified as a number between -1 and one spanning from a negative (inverse) very strong causality to a positive (analogous) very strong influence (Novak and Cañas, 2008). FCMs can carry out experts' knowledge which is translated as an inclusion of the concepts and an initialization of the fuzzy causality weights between then. For several diverse conditions FCMs can be differentiated accordingly. For the case of decision making, let us denote the set of FCM concepts as C_i ($i = 1, 2, \ldots n$) and w_{ij} their inter-causality weights as **Figure 3** depicts. The set of the weights w_{ij} form the FCM adjacency matrix.

At every application of the activation function, C_i get the value A_i^t indicating the concept-i at iteration-t. The value A_i indicates the integrated influence of all other concepts C_j to C_i (inference). The most popular inference rules are: 1) Kosko's inference, 2) Modified Kosko's inference and 3) Rescale inference as shown in the following activation functions, respectively.

$$A_i(k+1) = f\left(\sum_{j=1, j \neq i}^{N} w_{ji} \times A_j(k) \right),$$

$$A_i(k+1) = f\left(A_i(k) + \sum_{j=1, j \neq i}^{N} w_{ji} \times A_j(k) \right),$$

$$A_i(k+1) = f\left((2 \times A_i(k) - 1) + \sum_{j=1, j \neq i}^{N} w_{ji} \times \left(2 \times A_j(k) - 1 \right) \right).$$

Threshold (transformation) functions for the inference procedure can be of: 1) bivalent, 2) trivalent, 3) sigmoid or 4) hyperbolic type as shown in the following equations respectively:

$$f(x) = \begin{cases} 1 & x > 0, \\ 0 & x \leq 0, \end{cases}$$

$$f(x) = \begin{cases} 1 & x > 0, \\ 0 & x = 0, \\ -1 & x < 0, \end{cases}$$

$$f(x) = \frac{1}{1 + e^{-\lambda x}},$$

$$f(x) = \tanh(\lambda \times x).$$

where λ is a real positive number ($\lambda > 0$) quantifying the steepness of f and x is the value $A_i(k)$ on the equilibrium point. Above all, the sigmoid threshold is the most popular since it guarantees an outcome within the range [0, 1].

Microalgal Selection Problem and FCM–Related Works

Compared to the previous two methodologies, MCDM in relation to microalgal strain selection via FCM has not been studied. To the best of our knowledge, the most recently representative work is from (Naeini and Zandieh, 2020) that is focused on the microalgal biofuel production to be used for transportation. The authors apply a SWOT analysis to obtain realistic production strategies and then they rank them using stepwise weight assessment ratio analysis (SWARA). The method of utilizing the fuzzy linguistic environment involves FCMs to define the casual relationships between the criteria. Also worth mentioning, although not directly related to the topic under consideration, is the work by Falcone, Lopolito, and Sica.

(2019). This research addresses the phases of the policy making cycle to find the best suitable strategy for the case of the Italian liquid biofuel niche. Through the application of FCMs and social network analysis indicate the highlights and several diversified policy making instruments in transitioning to renewable energies. Towards the same research direction, the work by Kokkinos et al. (2018) used a novel FCM modeling approach that studies the socio-economic and technological implications in relation to sustainable waste bio-refinery facilities' establishment in order to overcome various uncertainties, by involving stakeholder participation in concept circumscription for the FCM and the decision making.

Logical Architecture of the System and Case Study

The logical architecture and the organizational context of the current research are depicted in **Figure 1**. Initially, the goal of the selection of the most suitable microalgal strain for the most economical viable biomass production is set for the research study. Among the huge variety of microalgal strains, for the case of Greece there few that have been studied either for wastewater treatment, biomass production or lipid concentration studies for other byproducts. Greece is a country with adequate climatological conditions (long sunshine periods, concentrations of high CO_2 especially around highly urbanized regions etc.). Studies also show that marine microalgal species exhibit much higher growth rates when compared with the freshwater species (Aravantinou et al., 2013). Among those, we demonstrate the following strains which were chosen for our study:

- *Chlorella vulgaris* sp.: mostly occurred in Attica prefecture, Greece. *C. vulgaris* exhibit adequately high biomass and lipid productivity (up to $142.9 \pm 6.5 \, \mathrm{mg} \, L^{-1} \, d^{-1}$ can be achieved under sulfur limitation) (Savvides et al., 2019). These findings have also been justified in Mata et al. (2010); Sakarika and Kornaros (2019).
- *Schizochytrium limacinum SR21*: is considered as a low-cost nutrient cultivation source that produces high averages of docosahexaenoic acid (DHA) and total lipid content reaching high average levels with varying effluent concentrations (Bouras et al., 2020).
- *Arthrospira (Spirulina) Platensis* strains such as *Chlorococcum* sp. and *Scenedesmus* sp.: for which there have been various investigations in relation to the algal biomass growth rates and biochemical content mainly composed of proteins (up to 70%) and also polyunsaturated fatty acids and vitamins (Markou et al., 2019; Tsavatopoulou et al., 2019).
- *Nannochloropsis* sp.: that demonstrates a considerable fatty acid profile especially when using magnetic harvesting (Savvidou et al., 2020) and when it is cultivated in aquaculture wastewaters (Ansari et al., 2017; Dourou et al., 2020).

Using **Table 1**, criteria clustering experts from research and academia, education, competent authorities, and energy

FIGURE 4 | Criteria ranking summary by experts' selection.
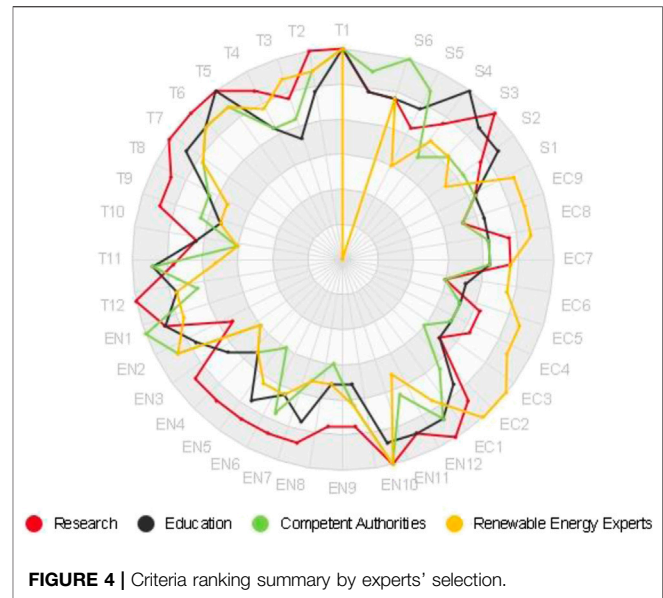
professionals were asked to provide a ranking of all involved parameters. Their evaluation was based on a questionnaire that directed them to evaluate each criterion in relation to all other criteria regardless of the category they fall in. Their evaluation was based on a Likert-scale in the range of 1–10, where one indicates the least important and 10 the most important criterion respectively. The summary of 14 expert responses is illustrated in the spider graph of **Figure 4** with average values for each criterion rounded to the closest integer in the scale.

RESULTS AND DISCUSSION

Ranking of Criteria for Microalgae Strain Selection Using Fuzzy-AHP Methodology

The primary goal using the Fuzzy AHP method is to find the relative importance between the factors and the criteria that affect either positive or negatively the microalgal strain selection for biofuel production. The method ranks these criteria assuming however that there is an initial input that relates the importance between any two pairs. For the pre-assumed clustering of **Table 1**, there is not any relevance between criteria of different clusters. For that reason, the Fuzzy AHP method was applied separately for each of the criteria clusters and these separate procedures allowed the completion of the reciprocal pairwise comparison matrices in every case.

The results are demonstrated in the following **Tables 3–6** each depicting the: 1) initial pairwise comparison matrix before fuzzification, 2) the fuzzy geometric mean after the fuzzification, 3) the fuzzy weights of each criterion as a triplet of the lower, middle, and upper values, 4) the crisp numeric criteria weights and 5) the normalized crisp numeric weights. We only depict the pairwise comparison matrix before fuzzification to avoid the complexity and the density of the fuzzified version. We

TABLE 3 | Fuzzy AHP results per criteria category–Category Technological.

Initial pairwise comparison matrix (before fuzzification)

	1	2	3	4	5	6	7	8	9	10	11	12
1	1	2	3	3	1	1	1	2	3	2	2	3
2	0.5	1	2	1	1	0.5	0.5	0.5	1	0.5	0.5	2
3	0.333	0.5	1	0.5	0.5	0.5	0.5	1	1	2	1	2
4	0.333	1	2	1	1	1	1	1	2	2	1	2
5	1	1	2	1	1	1	1	1	2	2	1	2
6	1	2	2	1	1	1	1	1	2	1	1	2
7	1	2	2	1	1	1	1	2	2	2	2	3
8	0.5	2	1	1	1	1	0.5	1	2	1	1	2
9	0.333	1	1	0.5	0.5	0.5	0.5	0.5	1	1	1	2
10	0.5	2	0.5	0.5	0.5	1	0.5	1	1	1	1	2
11	0.5	2	1	1	1	0.5	1	1	1	1	1	2
12	0.333	0.5	0.5	0.5	0.5	0.5	0.333	0.5	0.5	0.5	0.5	1

Criteria fuzzy and defuzzified weights

	Fuzzy geometric mean	Lower	Middle	Upper	Crisp	Norm crisp
1	(1.259,921,1.817,121,2.289,428)	0.075102	0.141,145	0.236,988	0.151,079	0.136,830
2	(0.577,062,0.793,701,1.200,937)	0.034398	0.061651	0.124,314	0.073454	0.066526
3	(0.577,062,0.793,701,1.200,937)	0.034398	0.061651	0.124,314	0.073454	0.066526
4	(0.912,439,1.189,207,1.442,250)	0.054389	0.092372	0.149,293	0.098685	0.089377
5	(1.000000,1.259,921,1.442,250)	0.059609	0.097865	0.149,293	0.102,256	0.092611
6	(1.000000,1.259,921,1.442,250)	0.059609	0.097865	0.149,293	0.102,256	0.092611
7	(1.059463,1.549,798,1.944,161)	0.063153	0.120,381	0.201,248	0.128,261	0.116,164
8	(0.832,544,1.059,463,1.316,074)	0.049627	0.082294	0.136,232	0.089384	0.080954
9	(0.577,062,0.749,154,1.095873)	0.034398	0.058191	0.113,438	0.068676	0.062199
10	(0.632,439,0.840,896,1.200,937)	0.037699	0.065317	0.113,438	0.075777	0.068630
11	(0.832,544,1.000000,1.200,937)	0.049627	0.077675	0.124,314	0.083872	0.075962
12	(0.399,979,0.561,231,1.000000)	0.023842	0.043594	0.103,514	0.056983	0.051609

TABLE 4 | Fuzzy AHP results per criteria category–Category Environmental.

Initial pairwise comparison matrix (before fuzzification)

	1	2	3	4	5	6	7	8	9	10	11	12
1	1	3	5	3	4	2	3	4	3	6	3	5
2	0.333	1	2	2	1	1	2	4	2	5	4	3
3	0.2	0.5	1	2	0.5	0.25	2	0.333	2	2	1	1
4	0.333	0.5	0.5	1	0.25	1	1	0.2	1	1	2	2
5	0.25	1	2	4	1	2	1	2	1	0.333	0.5	1
6	0.5	1	4	1	0.5	1	1	0.5	2	1	2	1
7	0.333	0.5	0.5	1	1	1	1	2	1	1	0.5	0.5
8	0.25	0.25	3	5	0.5	2	0.5	1	0.333	0.2	1	1
9	0.333	0.5	0.5	1	1	0.5	1	3	1	1	2	2
10	0.166	0.2	0.5	1	3	1	1	5	1	1	3	4
11	0.333	0.25	1	0.5	2	0.5	2	1	0.5	0.333	1	5
12	0.2	0.333	0.5	1	1	1	2	1	0.5	0.25	0.2	1

Criteria fuzzy and defuzzified weights

	Fuzzy geometric mean	Lower	Middle	Upper	Crisp	Norm crisp
1	(2.309,618,3.203,101,4.047904)	0.162,118	0.287,928	0.477,873	0.309,306	0.283,209
2	(1.603,058,2.274,792,2.853,638)	0.112,523	0.204,482	0.336,885	0.217,963	0.199,573
3	(0.000205,0.000126,0.000087)	0.000014	0.059995	0.000470	0.000005	0.000004
4	(0.000355,0.007433,0.000239)	0.059995	0.000126	0.048653	0.000340	0.000340
5	(0.000222,0.000389,0.000619)	0.000016	0.000239	0.048653	0.000005	0.000005
6	(0.832,475,1.059,463,1.373,307)	0.058434	0.095235	0.162,125	0.105,265	0.096383
7	(0.632,439,0.793,701,1.095873)	0.044392	0.071346	0.129,373	0.081704	0.074810
8	(0.000205,0.000592,0.000619)	0.002371	0.003921	0.000498	0.000270	0.000270
9	(0.693,130,0.890,899,1.200,937)	0.048653	0.080083	0.141,776	0.090171	0.082563
10	(1.189,108,1.327,680,1.490,270)	0.083466	0.119,345	0.175,933	0.126,248	0.115,596
11	(0.680,360,0.907,620,1.272,242)	0.047756	0.081586	0.150,194	0.093179	0.085317
12	(0.530,054,0.667,420,0.912,363)	0.037206	0.059995	0.107,708	0.068303	0.062540

TABLE 5 | Fuzzy AHP results per criteria category–Category Economics.

Initial pairwise comparison matrix (before fuzzification)

	1	2	3	4	5	6	7	8	9
1	1	1	2	2	3	4	2	4	4
2	1	1	3	1	4	5	0.5	1	3
3	0.5	0.333	1	0.5	1	2	0.333	0.5	1
4	0.5	1	2	1	2	3	1	2	5
5	0.333	0.25	1	0.5	1	1	0.333	0.5	0.5
6	0.25	0.2	0.5	0.333	1	1	0.333	1	2
7	0.5	2	3	1	3	3	1	1	3
8	0.25	1	2	0.5	2	1	1	1	3
9	0.25	0.333	1	0.2	2	0.5	0.333	0.333	1

Criteria fuzzy and defuzzified weights

	Fuzzy geometric mean	Lower	Middle	Upper	Crisp	Norm crisp
1	(1.557,716,2.259,662,2.876,908)	0.146,851	0.269,626	0.458,599	0.201,692	0.231,604
2	(1.360,639,1.648,686,1.985,709)	0.128,272	0.196,723	0.316,536	0.210,844	0.220,411
3	(0.000920,0.001592,0.002619)	0.000355	0.007433	0.008470	0.000234	0.002324
4	(1.115,017,1.576,059,2.053039)	0.105,116	0.188,057	0.327,269	0.202,814	0.189,026
5	(0.201,692,0.489,095,0.557,716)	0.037206	0.048653	0.090306	0.005411	0.003451
6	(0.000205,0.000126,0.000087)	0.007708	0.059995	0.062125	0.001727	0.008967
7	(0.955,842,1.220,285,1.489,095)	0.090110	0.145,606	0.237,372	0.153,696	0.144,133
8	(0.799,324,1.046082,1.317,834)	0.075355	0.124,820	0.210,072	0.136,149	0.120,987
9	(0.484,717,0.629,961,0.884,891)	0.045696	0.075168	0.141,058	0.087507	0.079098

TABLE 6 | Fuzzy AHP results per criteria category–Category Social.

Initial pairwise comparison matrix (before fuzzification)

	1	2	3	4	5	6
1	1	0.5	0.5	0.5	0.25	0.5
2	2	1	1	1	0.5	0.5
3	2	1	1	2	0.5	1
4	2	1	0.5	1	0.5	0.5
5	4	2	2	2	1	2
6	2	2	1	2	0.5	1

Criteria fuzzy and defuzzified weights

	Fuzzy geometric mean	Lower	Middle	Upper	Crisp	Norm crisp
1	(0.367,396,0.500,000,0.832,544)	0.040246	0.076138	0.184,861	0.100,415	0.085573
2	(0.693,130,0.890,899,1.200,937)	0.075928	0.135,663	0.266,661	0.159,417	0.135,854
3	(0.832,544,1.122,462,1.442,250)	0.091200	0.170,925	0.320,243	0.194,123	0.165,430
4	(0.577,062,0.793,701,1.200,937)	0.063214	0.120,862	0.266,661	0.150,246	0.128,038
5	(1.200,937,2.000000,2.720,043)	0.131,555	0.304,554	0.603,969	0.346,693	0.295,449
6	(0.832,544,1.259,921,1.732,051)	0.091200	0.191,857	0.384,591	0.222,549	0.189,655

use the triangular membership functions and the fuzzy mapping of **Table 2** allowing values in between these ranges.

Microalgal Strain Ranking via Fuzzy-TOPSIS Analysis

From the Fuzzy AHP described in the previous section, we choose from each of the four categories the two criteria that illustrated higher relative importance by the experts. For these eight in total criteria we calculate the relative importance pairwise comparison matrix including cross category comparisons. This is necessary since the values of the relative importance fuzzy weights are input to the FTOPSIS analysis. The inclusion of only two criteria per category introduces a minor error however, this is minimal since further inclusion of all criteria may cause the production of erroneous results for the case of totally irrelevant criteria.

Table 7 below shows: 1) the produced crisp numeric relative importance weights, 2) the normalized crisp weights and the type of criteria clustering those into beneficial (i.e. the ones that need to be maximized) and into cost criteria (i.e. the ones that need to be minimized).

The criteria ID is denoted as T for technological, EN for environmental, EC for economics and S for social. The fourteen experts were asked to rate the four candidate microalgal strains for the eight aforementioned criteria. The experts assigned values to the strains for each criterion using linguistic values that correspond to normalized triangular fuzzy numbers as depicted in **Table 8** allowing also intermediate values. **Table 9** presents the Fuzzy Decision Matrix, the Fuzzy Positive Ideal Solution and the Fuzzy Negative Ideal Solution, according to steps. Finally, **Table 10** shows the distance of each strain selection and for each criterion from the FPIS and the FNIS, the total

TABLE 7 | Initial crisp weights and normalized crisp weights used in Fuzzy TOPSIS.

Criteria ID	Initial crisp weights	Normalized crisp weights	Beneficial/Cost criteria
T1	0.22041	0.136,641	Beneficial
T7	0.29545	0.183,159	Beneficial
EN1	0.17178	0.106,493	Cost
EN2	0.11616	0.072014	Cost
EC1	0.19957	0.123,722	Cost
EC2	0.28321	0.175,571	Cost
S5	0.18966	0.117,574	Beneficial
S6	0.13683	0.084826	Beneficial

TABLE 8 | Expert linguistic values and corresponding normalized triangular fuzzy numbers.

Linguistic value	Normalized fuzzy triangular number
Very low importance	(0.0.1.0.3)
Low importance	(0.1.0.3.0.5)
Medium importance	(0.3.0.5.0.7)
High importance	(0.5.0.7.0.9)
Very high importance	(0.7.0.9.1)

concepts always increases. At the same time, when there exists an apparent correlation between clusters (for example social issues affect environmental issues and vice versa) then, this reflects the corresponding interlinking between the interclass concepts.

Numerous simulations have been run in order to investigate: 1) the steady state of the FCM, 2) the FCM convergence using the clamping process as stated in Kosko 1986) and 3) the best- and worst-case scenarios for the trend of BF (increase/decrease). Note that separate simulations were performed for each microalgal

TABLE 9 | normalized fuzzy decision matrix, FPIS and FNIS.

	Chlorella vulgaris ACA9 and ACA17	Schizochytrium limacinum SR21	Arthrospira (Spirulina) Platensis	Nannochloropsis	FPIS A*	FNIS A⁻
T1	0.590, 0.754, 1	0.536, 0.646, 0.885	0.574, 0.630, 0.774	0.629, 0.699, 0.858	0.590, 0.754, 1	0.536, 0.646, 0.885
T7	0.681, 0.733, 1	0.591, 0.785, 0.929	0.560, 0.684, 0.919	0.614, 0.715, 0.891	0.681, 0.733, 1	0.560, 0.684, 0.919
EN1	0.375, 0.514, 1	0.448, 0.596, 0.745	0.464, 0.508, 0.669	0.503, 0.582, 0.645	0.375, 0.514, 1	0.375, 0.514, 1
EN2	0.469, 0.599, 1	0.372, 0.512, 0.603	0.421, 0.452, 0.574	0.349, 0.362, 0.568	0.469, 0.599, 1	0.349, 0.362, 0.568
EC1	0.537, 0.748, 0.899	0.632, 0.776, 1	0.508, 0.715, 0.888	0.549, 0.727, 0.891	0.632, 0.776, 1	0.508, 0.715, 0.888
EC2	0.596, 0.649, 0.771	0.646, 0.480, 0.920	0.7044, 0.751, 0.888	0.672, 0.864, 1	0.672, 0.864, 1	0.596, 0.649, 0.771
S5	0.569, 0.834, 1	0.557, 0.747, 0.961	0.552, 0.754, 0.930	0.519, 0.713, 0.944	0.569, 0.834, 1	0.519, 0.713, 0.944
S6	0.539, 0.932, 0.973	0.635, 0.702, 0.798	0.433, 0.604, 0.792	0.661, 0.806, 1	0.661, 0.806, 1	0.433, 0.604, 0.792

distances for each strain and the ranking of the methodology for the four strains.

Microalgal Strain Selection Trend Using Fuzzy Cognitive Map Analysis

The FCM includes 40 concepts out of which only the "Biofuel Production" (denoted as BF) is the receiver (it only has incoming edges) and the rest are all ordinary concepts (they have incoming and outgoing edges). The FCM graph is not shown due to the number of concepts participating and the weighted causality edges (~1,500) which makes the visualization of the graph impossible. However, the FCM statistics and concept metrics are depicted in **Table 11** indicating the in-degree, out-degree, and the centrality of each concept. The results illustrate centrality similarities and a balance in the ratio of the in-degree/out-degree for concepts that belong to the same cluster/category. This is expected since the probability of interdependence and inter-causalities on same-cluster

strain fixing as constant the values for the concepts (especially the technological) when values have been established by other studies. These concepts included the lipid content according to the fixed daily lipid productivity findings given below:

- *Chlorella vulgaris*: 134 mg L^{-1}d^{-1} (Kim et al., 2019)
- *Schizochytrium limacinum*: 108 mg L^{-1}d^{-1} (S.-K. Wang et al., 2020)
- *Arthrospira (Spirulina) Platensis*: 89 mg L^{-1}d^{-1} (Lu et al., 2019)
- *Nannochloropsis* sp: 105 mg L^{-1}d^{-1} (Nogueira et al., 2020)

As for the clamping procedures, this cannot be applied to the driver concepts only because simply there are no driver concepts (concepts that have in-degree equal to 0). For that reason, our simulations will apply clamping using the most important concepts according to the criteria ranking summary produced by the experts as this is shown in **Figure 4** making sure that all four criteria categories are represented in the analysis.

TABLE 10 | Distances from FPIS and FNIS and the rankings.

Distances from FPIS

	Chlorella vulgaris ACA9 and ACA17	Schizochytrium limacinum SR21	Arthrospira (spirulina) Platensis	Nannochloropsis
T1	0	0.095,979,685	0.148,766,148	0.090,538,647
T7	0	0.072,159,037	0.088,448,441	0.074,491,275
EN1	0	0.160,217,436	0.197,805,367	0.220,988,582
EN2	0	0.241,041,587	0.26,147,569	0.292,531,799
EC1	0.081,928,546	0	0.102,612,361	0.084,012,162
EC2	0.186,596,347	0.227,249,136	0.093,280,044	0
S5	0	0.055,161,037	0.061,768,762	0.081,764,662
S6	0.102,569,537	0.131,785,545	0.212,832,751	0
Di*	0.37,109,443	0.983,593,464	1.166,989,565	0.844,327,127

Distances from FPIS

	Chlorella vulgaris ACA9 and ACA17	Schizochytrium limacinum SR21	Arthrospira (spirulina) Platensis	Nannochloropsis
T1	0.095,979,685	0	0.068,432,302	0.063,778,471
T7	0.088,448,441	0.061,507,561	0	0.039,430,403
EN1	0	0.160,217,436	0.197,805,367	0.220,988,582
EN2	0.292,531,799	0.090,124,248	0.067,087,629	0
EC1	0.025,888,157	0.102,612,361	0	0.02,471,747
EC2	0	0.133,363,963	0.109,471,899	0.186,596,347
S5	0.081,764,662	0.031,014,835	0.031,686,064	0
S6	0.224,798,362	0.129,646,224	0	0.212,832,751
Di-	0.809,411,106	0.708,486,627	0.474,483,262	0.748,344,024
Cci	0.685,647,869	0.418,707,501	0.289,059,468	0.469,867,256
Rank	1	3	4	2

The steady state of the FCM is shown in **Figure 5** depicting the final concept values as a defuzzified real number in the range [0.1] and the convergence curves for these concepts relatively to the number of iterations needed for the FCM to converge.

To the best of our knowledge there does not exist any research that relates the importance and interrelation of criteria in an algal strain selection analysis using FCMs. For that reason, we used the aforementioned steady state FCM as a starting point to perform scenario analysis for the strain selection. More specifically, we did best and worst case analysis for each of the four strain candidates using both Sigmoidal and Hyperbolic Tangent learning methodologies. In all cases we fix the values of the lipid content (daily lipid productivity) with the values presented in this section previously. Furthermore, the rest of the participating concepts are set to values 0.1 for the worst case and one for the best case respectively. In total we performed 64 simulations to include all combinations of strains, learning methods, categories of criteria, and best/worst case scenarios.

Characteristically, in **Figure 6**, the best case scenario is shown, for the sigmoidal learning for the *Schizochytrium limacinum* sp. for the case of how the technological criteria affect the biofuel production. For this case, the lipid content criterion is set to 0.80 (after normalization of the daily lipid productivity values of all strains the value of 108 mg L^{-1}d^{-1} corresponds to 0.90 in the range [0.1]). The rest of the technological criteria are all set to one and this configuration shows the potential percentage increase or decrease on the receiver concept i.e. to the biofuel production. Specifically for the described configuration we show an increase of about 5% to the biofuel production (see **Figure 6**).

On the other hand, **Figure 7** illustrates the worst case scenario for the sigmoidal learning for the same strain. This is used for proof of correctness in terms on the negative impacts emanated

from the technological criteria. More specifically, technological criteria that affect the concept of production BP are set to very small values (0.1 or even smaller than that) as shown for the concepts T1-T9 in **Figure 7**. Instead of using the lipid content criterion of 0.80 value, we use the worst possible value of 0.03. This negatively affects the production of the system by 12% while at the same time diminishes the cost of cultivation indicating a wrong choice of cultivation.

Finally we show the summary of all simulation findings in **Table 12** for all cases of strains, learning methodologies criteria categories, and best/worst case scenarios.

The use of participatory modeling assumed the presence of regional stakeholders (with most of them to be experts in the field under study). The criteria and factors that influence the production of biomass from algae were set in **Table 1**, and according to the research specialists, they do cover all aspects spanning from technological to environmental, economic, and social. Furthermore, regional stakeholders were asked to individually rate these criteria using a fuzzy scale evaluation, which was defuzzified into a Likert-scale from 1 to 10. The experts' weights were then used into a FAHP having as a primary goal the construction of the relative importance matrix using the fuzzy geometric mean of the aforementioned weights. Based on the findings and due to individual evaluations for each criteria category the most important criteria are:

- From the technological category, criteria T1 (Energy content) and T7 (Lipid content) outperform the rest with normalized weights of 13.68% and 11.61% of the whole category respectively as shown in the results of **Table 3**. The outperformance is relative to the overall descending ordering of all criteria. The rest of the technological

TABLE 11 | FCM statistics and concept metrics.

Component	In degree	Out degree	Centrality	Type
T1	9.42	15.60	25.02	Ordinary
T2	9.15	20.94	30.09	Ordinary
T3	3.66	9.22	12.88	Ordinary
T4	9.18	13.97	23.15	Ordinary
T5	10.10	10.30	20.40	Ordinary
T6	10.39	10.35	20.74	Ordinary
T7	10.64	9.85	20.49	Ordinary
T8	9.66	9.57	19.23	Ordinary
T9	7.31	18.87	26.19	Ordinary
T10	14.70	5.04	19.74	Ordinary
T11	10.33	18.2	28.53	Ordinary
T12	6.98	6.70	13.68	Ordinary
EN1	7.99	14.29	22.28	Ordinary
EN2	9.87	16.45	26.32	Ordinary
EN3	14.06	16.46	30.53	Ordinary
EN4	11.07	11.70	22.78	Ordinary
EN5	7.05	19.45	26.50	Ordinary
EN6	9.86	13.52	23.38	Ordinary
EN7	12.21	14.76	26.97	Ordinary
EN8	5.73	8.95	14.69	Ordinary
EN9	10.43	12.68	23.12	Ordinary
EN10	9.29	11.89	21.18	Ordinary
EN11	10.82	8.86	19.68	Ordinary
EN12	8.43	7.43	15.86	Ordinary
EC1	10.88	11.22	22.11	Ordinary
EC2	13.82	13.29	27.11	Ordinary
EC3	15.48	15.51	31	Ordinary
EC4	7.06	6.93	13.98	Ordinary
EC5	9.31	12.78	22.1	Ordinary
EC6	12.34	7.74	20.09	Ordinary
EC7	2.64	0.24	2.88	Ordinary
EC8	2.15	0.26	2.41	Ordinary
EC9	10.40	0.39	10.79	Ordinary
S1	7.02	0.18	7.20	Ordinary
S2	4.34	0.47	4.81	Ordinary
S3	14.54	0.26	14.80	Ordinary
S4	11.78	0.39	12.17	Ordinary
S5	5.94	0.15	6.1	Ordinary
S6	4.65	0.18	4.83	Ordinary
BP	14.36	0	14.36	Receiver

criteria are ranked with importance weights to be much less than 10%. For that reason, we claim that energy content and lipid daily productivity seem to overcome all other criteria. The rest of the criteria are tightly coupled with those, thus the importance of these satisfies the technological requirements imposed. Safety and reliability are under-evaluated when compared to the purely technological criteria previously. This was expected, as most of the research community concentrates on the measurements of the lipid content and daily productivity, thus the microalgal energy efficiency becomes a primary factor.

- From the environmental category, three criteria get weight-percentages that exceed the 10%, namely ENV1 (Land/waterbody use), ENV2 (Water quality requirement) and ENV10 (Particles emission) with weight percentages 28.32%, 19.95%, and 11.55% respectively. This indicates that the land or waterbody availability is the most important factor, given that its absence totally abolishes the cultivation.

- From the economics category, four criteria out of nine are shown great importance, namely EC1 (Microalgae (raw material) cost) with 23.16%, EC2 (Investment cost) with 22.04%, EC4 (Cost of harvesting) with 18.90%, and EC7 (Storage cost) with the lowest performance of 14.41%. The equivalence of the above criteria indicates that costs of every level are most significant in investing into a biofuel production plant based on algae. The fact that EC1 leads the evaluation means that finding the raw material and harvesting is the most considerable cost compared to the investment cost; Finally, • From the social category, we experience almost equivalent performance from most of the criteria, as they are all highly interrelated. More specifically, S5 (Job creation) gets 29.54%, S6 (Social benefits) gets 18.96%, and S3 (Sustainable development) gets 16.54%. The interrelation between S5 and S6 is analogous since the higher the job creation the more the social benefits for the regional society. At the same time, the high numbers of
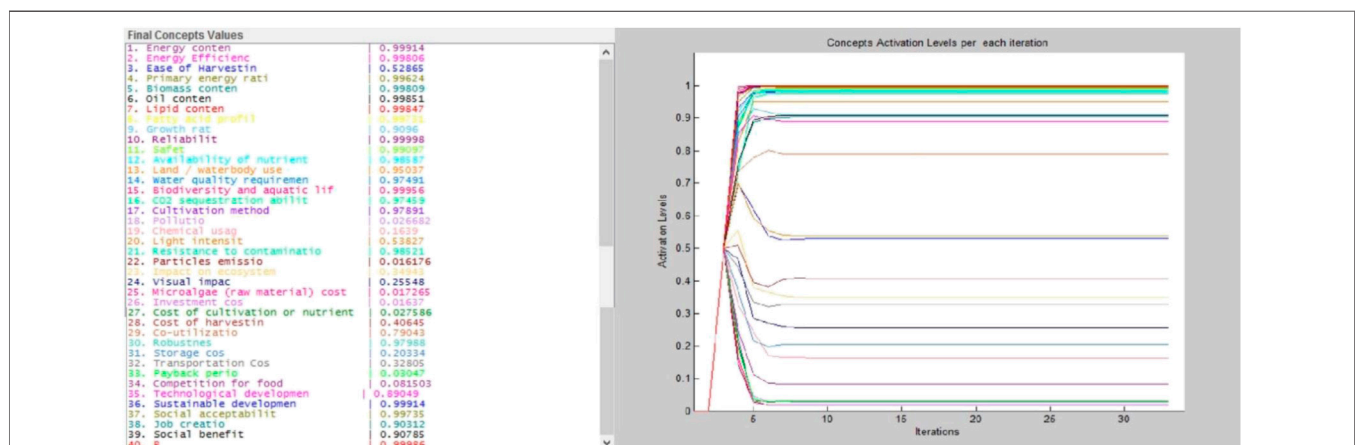
FIGURE 5 | Steady State Analysis for the FCM and convergence curves relatively to the number of iterations.
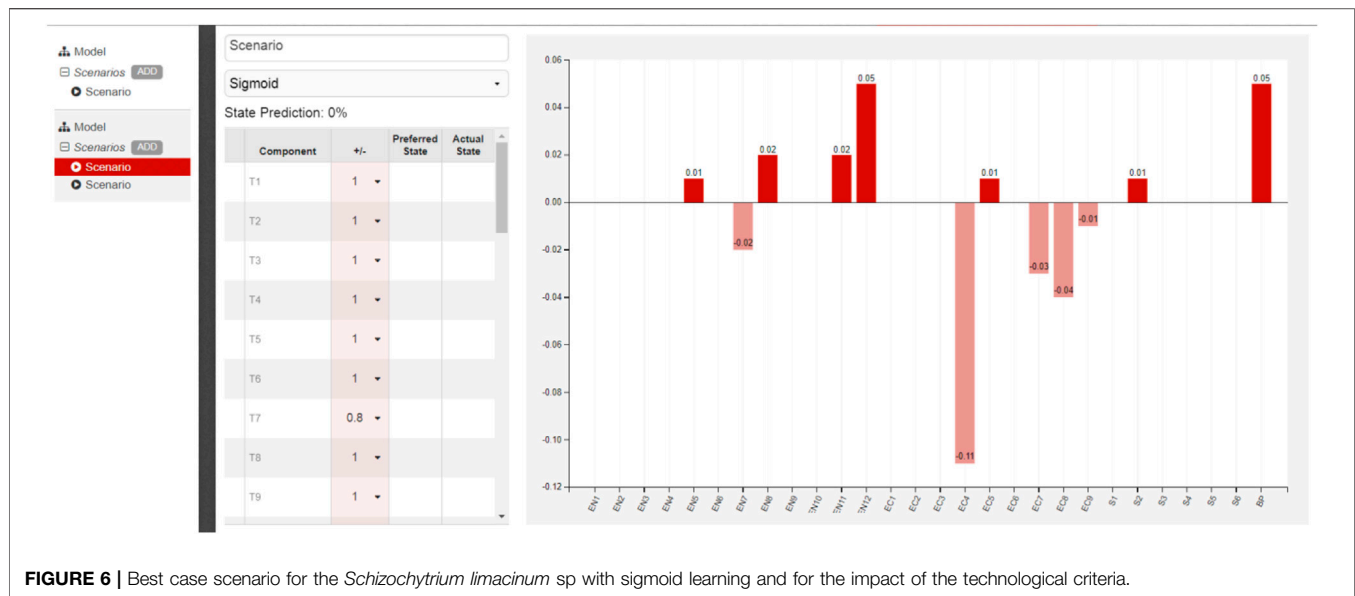
FIGURE 6 | Best case scenario for the *Schizochytrium limacinum* sp with sigmoid learning and for the impact of the technological criteria.
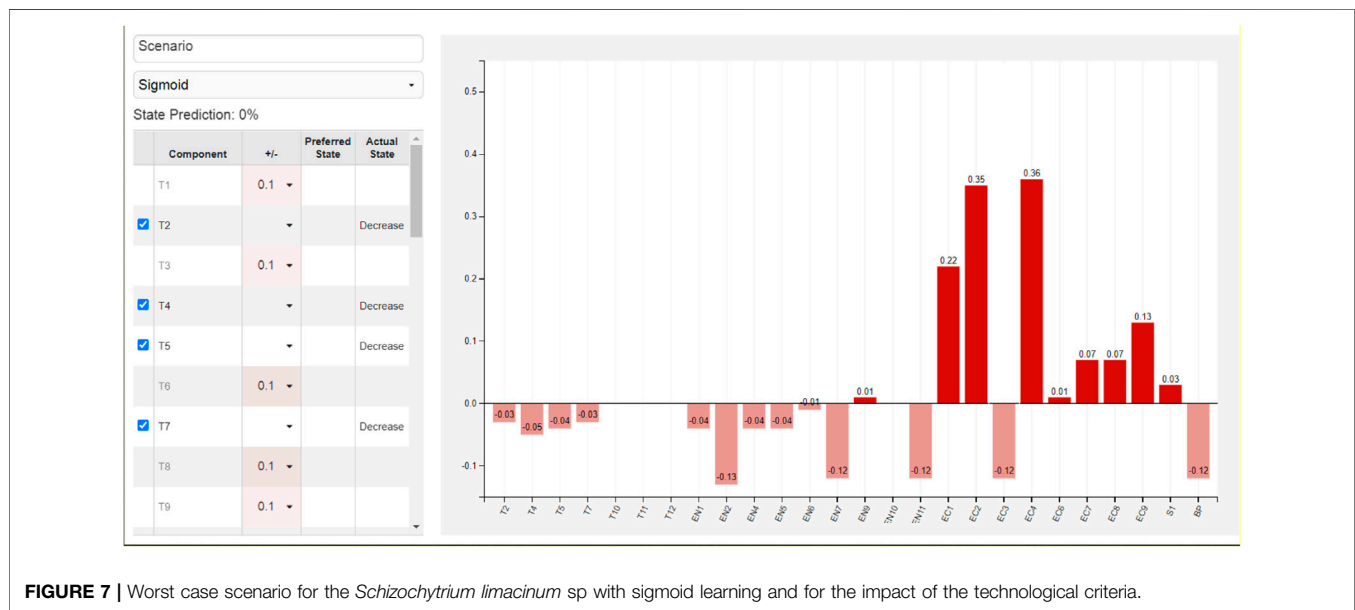
FIGURE 7 | Worst case scenario for the *Schizochytrium limacinum* sp with sigmoid learning and for the impact of the technological criteria.

social benefits and job creation for criteria indicate a sustainable environment where members of the regional society benefit from a stable economy due to steady income.

The FTOPSIS was applied only on the most substantial criteria of each category, on the basis of the FAHP findings. Taking the two more representative criteria from each category, we succeeded to evaluate the plants/investments of the most popular microalgal strains in the Greek territory. The results of FTOPSIS ranked *Chlorella vulgaris* and *Nannochloropsis* as the two strains having the best potential to produce higher amounts of biofuel according to the criteria imposed. More specifically, *Chlorella vulgaris* ranked as the most preferable (CC_i of

0.685,647,869) and *Nannochloropsis* the second with (CC_i of 0.469,867,256). The significant difference between the first and second option is explained by the difference in daily lipid productivity (134 mg $L^{-1}d^{-1}$ for *Chlorella vulgaris* as opposed to 105 mg $L^{-1}d^{-1}$ for *Nannochloropsis*). However, further research must be conducted. For example, the inclusion of all criteria in FTOPSIS introduces a significant error due to the number of criteria participating, but at the same time the method follows a fair approach to all criteria without discrimination of the ones that did not perform well in FAHP.

The approach of the FCM investigation took care of this defficiency making sure that all criteria participated in the concept graph. The complexity of the graph is high, as almost

TABLE 12 | FCM best and worst case scenario analysis.

Strain	Best/Worst case scenario	Criteria category	Learning method	BF increase or decrease
Chlorella vulgaris ACA9 and ACA17	Best	Technological	Sigmoid	9.3%
	Worst	Technological	Sigmoid	−5.6%
	Best	Environmental	Sigmoid	8.4%
	Worst	Environmental	Sigmoid	−1.7%
	Best	Economics	Sigmoid	11.2%
	Worst	Economics	Sigmoid	−3.4%
	Best	Social	Sigmoid	2.9%
	Worst	Social	Sigmoid	−2.2%
	Best	Technological	Hyperbolic tangent	8.6%
	Worst	Technological	Hyperbolic tangent	−5.2%
	Best	Environmental	Hyperbolic tangent	7.9%
	Worst	Environmental	Hyperbolic tangent	−2.8%
	Best	Economics	Hyperbolic tangent	9.3%
	Worst	Economics	Hyperbolic tangent	−2.1%
	Best	Social	Hyperbolic tangent	3.1%
	Worst	Social	Hyperbolic tangent	−5.6%
Schizochytrium limacinum SR21	Best	Technological	Sigmoid	5%
	Worst	Technological	Sigmoid	−3.6%
	Best	Environmental	Sigmoid	11.5%
	Worst	Environmental	Sigmoid	−7.4%
	Best	Economics	Sigmoid	10.4%
	Worst	Economics	Sigmoid	−4.9%
	Best	Social	Sigmoid	3.4%
	Worst	Social	Sigmoid	−1.9%
	Best	Technological	Hyperbolic tangent	6.6%
	Worst	Technological	Hyperbolic tangent	−4.2%
	Best	Environmental	Hyperbolic tangent	8.3%
	Worst	Environmental	Hyperbolic tangent	−3.6%
	Best	Economics	Hyperbolic tangent	3.1%
	Worst	Economics	Hyperbolic tangent	−2.9%
	Best	Social	Hyperbolic tangent	4.1%
	Worst	Social	Hyperbolic tangent	−6.6%
Arthrospira (spirulina) Platensis	Best	Technological	Sigmoid	6.1%
	Worst	Technological	Sigmoid	−7.6%
	Best	Environmental	Sigmoid	6.2%
	Worst	Environmental	Sigmoid	−10.8%
	Best	Economics	Sigmoid	1.6%
	Worst	Economics	Sigmoid	−4.7%
	Best	Social	Sigmoid	1.7%
	Worst	Social	Sigmoid	−3.1%
	Best	Technological	Hyperbolic tangent	6.8%
	Worst	Technological	Hyperbolic tangent	−4.1%
	Best	Environmental	Hyperbolic tangent	5.6%
	Worst	Environmental	Hyperbolic tangent	−2.7%
	Best	Economics	Hyperbolic tangent	7.5%
	Worst	Economics	Hyperbolic tangent	−3.3%
	Best	Social	Hyperbolic tangent	3.3%
	Worst	Social	Hyperbolic tangent	−2.6%
Nannochloropsis	Best	Technological	Sigmoid	2.7%
	Worst	Technological	Sigmoid	−3.6%
	Best	Environmental	Sigmoid	9.3%
	Worst	Environmental	Sigmoid	−2.8%
	Best	Economics	Sigmoid	4.6%
	Worst	Economics	Sigmoid	−6.8%
	Best	Social	Sigmoid	5.6%
	Worst	Social	Sigmoid	−3.7%
	Best	Technological	Hyperbolic tangent	4.6%
	Worst	Technological	Hyperbolic tangent	−8.8%
	Best	Environmental	Hyperbolic tangent	4.1%
	Worst	Environmental	Hyperbolic tangent	−3.4%
	Best	Economics	Hyperbolic tangent	12.3%
	Worst	Economics	Hyperbolic tangent	−6.5%
	Best	Social	Hyperbolic tangent	7.8%
	Worst	Social	Hyperbolic tangent	−3.9%

for all concepts inter-causalities may be set. The evaluation of the four different strains is based on all criteria but the daily lipid productivity is predefined normalized and fixed for all FCMs under investigation. For each strain we invstigated the biofuel production trend in both the best and worst case scenarios, two FCM learning methods and trying to evaluate the impact of each category criteria to the trend. The results in **Table 12** show:

A significant increase on biofuel (8.6%–9.3%) for *Chlorella vulgaris* due to the technological criteria increase in the best scenario (all technological criteria except lipid content are set to 1) using either Sigmoidal or Hyperbolic Tangent learning. Under the same conditions, *Schizochytrium limacinum* performs with an increase within the range of (5%–6.6%), *Arthrospira (Spirulina) Platensis* with an increase of (6.1%–6.8%) where *Nannochloropsis* shows an increase range of (2.7%–4.6%). In an analogous way, the results indicate a significant decrease of the biofuel production trend for the worst case scenario (where all technological criteria except lipid content are set to the value of 0.1). Similarly, the same trend is shown for the best and worst case scenario for the other three categories of criteria and the microalgal strains. Thus, the FCM can be used as a dependable Decision Support System that can help stakeholders, investors and competent authorities to select investment plans and support decision making.

CONCLUSION

The use of the appropriate microalgal strain as raw material for biomass feedstock towards nanocatalytic biofuel production is the most significant factor that controls investment land or waterbody plants, thus directly affecting the regional economy and local society. In this work, four microalgal strains for Greece as a case study were evaluated using a synthesized participatory modeling approach that: 1) aggreed on the criteria, which are imposed for the biofuel production, 2) applied FAHP method to find the relative importance of these criteria, 3) ranked the abovementioned criteria using the Fuzzy TOPSIS procedure; and finally 4) via the creation of a FCM, investigated the trend of increase/decrease of the biofuel production with a consideration of different learning methods, best and worst case scenarios and different criteria categories.

The overall methodology gave clear results as to the microalgae strain selection. Especially, the high lipid content appears to be the most dominant factor in the strain selection. Particularly, *Chlorella vulgaris* microalgae is ranked as the best choice followed by the *Nannochloropsis* strain via the FTOPSIS analysis. Furthermore, the best and worst case scenario runs using FCM methodology verify this choice, indicating that *Chlorella Vulgaris* follows this selection trend mostly with the technological and the economic criteria for both the sigmoid and the hyperbolic tangent functions applied. All fuzzy logic procedures employed were proven to be superior to their numeric equivalent ones under uncertain factors including cost, policy implications, and also geographical and seasonal variation, which affect the decision making process.

The above three MCDM processes act as alternative models to formal ones (algorithical and procedural). The formulation of

assessment components with scaling procedures, elicitation, and estimation functionalities as well as stakeholder subjective criteria settings allow AHP, TOPSIS, and FCM to holistically address decision-making problems emanating from diverse environments. Numerous research from various fields such as energy, environment, medical informatics, and economics confirm that the abovementioned techniques are applied in a broad repertoire of problems. Additionally, the structural ability of the techniques regarding complex problems using multiple criteria with linguistic variables and fuzzy inference allows their application in an array of disciplines. From a long list of MCDM methodologies invented, the vast majority tackles problems of numeric nature and therefore belongs to the multiple objective mathematical programming ensemble of MCDM. However, when fuzzy inference is needed to model multi-objectives, then only a few methods are used, and in many cases, these overlap in terms of algorithms developed (VIKOR, Multi-Attribute Global Inference of Quality etc.). Thus the proposed triple view of the problem of microalgae strain selection to maximize biofuel production can be used as a paradigm for similar modeling in many other problems.

In this work, we provided the corresponding causality from microalgae cultivation for biomass energy production for the case of Greece. More specifically, we studied the impacts for microalgae production via nano-catalysis and we indicated how this is connected to the economic development via a set of technological environmental, economic and social criteria. The findings of the model outcomes provide a roadmap for selecting specific microalgae strains for cultivation in a specific region. Eventually, all models assert that biomass energy production via microalgal cultivation can be a circular economy efficient technique for environmentally sustainable development and it can similarly be promoted in other countries. At the same time, decision and policy makers must take into acount not only purely cultivation oriented constraints for the biomass production via microalgae but also must seriously consider environmental and social criteria in the strain selection problem. This work includes such constraints, though some other have been left out, including e.g., climatological conditions influencing microalgal biomass production and potential impact on climate change respectvely.

Nevertheless, there are few additional challenging issues that may be thoroughly investigated by a future research. Starting from the FTOPSIS application, it is worthy to evaluate all participating criteria without descriminating any of them. This may diminish the impact of some of the selected criteria or even increase the significance of others not taken into consideration. Moreover, the inclusion of similar but differentiated approaches to FTOPSIS, such as PROMETHE or the amalgamation of fuzzy and statistical methods, would be a future work challenge for improving ranking outcomes. Also, there are some further investigations that can be pursued in relation to the FCMs, indicatively: the lack of result consistency between the differences among the best and worst case scenarios for all categories, the application of FCM with additional machine learning methods and the exclusion of the inherited bias derived from the experts in terms of environmental and social issues.

DATA AVAILABILITY STATEMENT

The original contributions presented in the study are included in the article/Supplementary Materials, further inquiries can be directed to the corresponding author.

ETHICS STATEMENT

Ethical review and approval was not required for the study on human participants in accordance with the local legislation and institutional requirements. Written informed consent from the participants was not required to participate in this study in accordance with the national legislation and the institutional requirements.

AUTHOR CONTRIBUTIONS

All authors listed have made a substantial, direct and intellectual contribution to the work, and approved it for publication.

REFERENCES

Aghilinategh, M., Barati, M., and Hamadanian, M. (2020). The modified supercritical media for one-pot biodiesel production from Chlorella vulgaris using photochemically-synthetized SrTiO$_3$ nanocatalyst. *Renew. Energy.* 160 (November), 176–184. doi:10.1016/j.renene.2020.06.081

Aikhuele, D. O., Desmond Eseoghene, I., and Akinyele, D. (2019). Evaluation of renewable energy technology based on reliability attributes using hybrid fuzzy dynamic decision-making model. *Technology and Economics of Smart Grids and Sustainable Energy.* 4 (1), 16. doi:10.1007/s40866-019-0072-2

Altintas, K., Vayvay, O., Apak, S., and Cobanoglu, E. (2020). An extended GRA method integrated with fuzzy AHP to construct a multidimensional index for ranking overall energy sustainability performances. *Sustainability* 12 (4), 1602. doi:10.3390/su12041602

Ansari, F. A., Singh, P., Guldhe, A., and Bux, F. (2017). Microalgal cultivation using aquaculture wastewater: integrated biomass generation and nutrient remediation. *Algal Research* 21 (January), 169–177. doi:10.1016/j.algal.2016.11.015

Apandi, N. M., Mohamed, R. M. S. R., Al-Gheethi, A., and Kassim, A. H. M. (2019). Microalgal biomass production through phycoremediation of fresh market wastewater and potential applications as aquaculture feeds. *Environ. Sci. Pollut. Res. Int.* 26 (4), 3226–3242. doi:10.1007/s11356-018-3937-3

Arabi, M., Yaghoubi, S., and Tajik, J. (2019). Algal biofuel supply chain network design with variable demand under alternative fuel price uncertainty: a case study. *Comput. Chem. Eng.* 130 (November), 106528. doi:10.1016/j.compchemeng.2019.106528

Aravantinou, A. F., Theodorakopoulos, M. A., and Manariotis, I. D. (2013). Selection of microalgae for wastewater treatment and potential lipids production. *Bioresour. Technol.* 147 (November), 130–134. doi:10.1016/j.biortech.2013.08.024

Arora, N., Patel, A., Mehtani, J., Pruthi, P. A., Pruthi, V., and Poluri, K. M. (2019). Co-culturing of oleaginous microalgae and yeast: paradigm shift towards enhanced lipid productivity. *Environ. Sci. Pollut. Res. Int.* 26 (17), 16952–16973. doi:10.1007/s11356-019-05138-6

Banerjee, S., Rout, S., Banerjee, S., Arnab, A., and Das, D. (2019). Fe2O3 nanocatalyst aided transesterification for biodiesel production from lipid-intact wet microalgal biomass: a biorefinery approach. *Energy Convers. Manag.* 195 (September), 844–853. doi:10.1016/j.enconman.2019.05.060

Bekirogullari, M., Figueroa-Torres, G. M., Pittman, J. K., and Theodoropoulos, C. (2020). Models of microalgal cultivation for added-value products - a review. *Biotechnol. Adv.* 44, 107609. doi:10.1016/j.biotechadv.2020.107609

Bouras, S., Katsoulas, N., Antoniadis, D., and Ioannis, T. K. (2020). Use of biofuel industry wastes as alternative nutrient sources for DHA-yielding Schizochytrium limacinum production. *Appl. Sci.* 10 (12), 4398. doi:10.3390/app10124398

Bueyuektahtakin, I. E., and Cobuloglu, H. I. (2014). "A multi-criteria approach for biomass crop selection under fuzzy environment." In Industrial and Systems Engineering Research Conference, Montreal, Canada, May 2014. https://soar.wichita.edu/handle/10057/11495

Burgin, M., and Kuznetsov, V. (1992). Fuzzy sets as named sets. *Fuzzy Set Syst.* 46 (2), 189–192. doi:10.1016/0165-0114(92)90131-M

Campbell, M. N. (2008). Biodiesel: algae as a renewable source for liquid fuel. *Guelph Engineering Journal.* 1, 2–7.

Carmichael, M. D., Petrides, D., and Siletti, C. (2017). "Large scale algal oil production for bio-fuel use: techno-economic analysis and evaluation," in 2017 SIMB Annual Meeting and Exhibition, (Philadelphia, PA: SIMB).

Chamodrakas, I., Batis, D., and Martakos, D. (2010). Supplier selection in electronic marketplaces using satisficing and fuzzy AHP. *Expert Syst. Appl.* 37 (1), 490–498. doi:10.1016/j.eswa.2009.05.043

Chan, F. T. S., Kumar, N., Tiwari, M. K., Lau, H. C. W., and Choy, K. L. (2008). Global supplier selection: a fuzzy-AHP approach. *Int. J. Prod. Res.* 46 (14), 3825–3857. doi:10.1080/00207540600787200

Chandel, A. K., Garlapati, V. K., Singh, A. K., Antunes, F. A. F., and da Silva, S. S. (2018). The path forward for lignocellulose biorefineries: bottlenecks, solutions, and perspective on commercialization. *Bioresour. Technol.* 264 (September), 370–381. doi:10.1016/j.biortech.2018.06.004

Chang, D.-Y. (1996). Applications of the extent analysis method on fuzzy AHP. *Eur. J. Oper. Res.* 95 (3), 649–655. doi:10.1016/0377-2217(95)00300-2

Chen, T. C. (2000). Extensions of the TOPSIS for group decision-making under fuzzy environment. *Fuzzy Set Syst.* 114, 1–9.

Chisti, Y. (2008). Biodiesel from microalgae beats bioethanol. *Trends Biotechnol.* 26 (3), 126–131. doi:10.1016/j.tibtech.2007.12.002

Cock, M. D., Ulrich, B., and Etienne, E. K. (2000). Modelling linguistic expressions using fuzzy relations. In Proceedings of the 6th international conference on soft computing, Istanbul, Turkey, 2020, 353–360. doi:10.1.1.32.8117

Correa, D. F., Beyer, H. L., Hugh, P. P., Skye, R. T. H., and Schenk, P. M. (2019). Global mapping of cost-effective microalgal biofuel production areas with minimal environmental impact. *GCB Bioenergy.* 11 (8), 914–929. doi:10.1111/gcbb.12619

Dinçer, H., and Yüksel, S. (2019). Multidimensional evaluation of global investments on the renewable energy with the integrated fuzzy decision-making model under the hesitancy. *Int. J. Energy Res.* 43 (5), 1775–1784 doi:10.1002/er.4400

Dourou, M., Dritsas, P., Baeshen, M. N., Elazzazy, A., Al-Farga, A., and Aggelis, G. (2020). High-added value products from microalgae and prospects of aquaculture wastewaters as microalgae growth media. *FEMS Microbiol. Lett.* 367 (12). doi:10.1093/femsle/fnaa081

Dutta, K., Daverey, A., and Lin, J-G. (2014). Evolution retrospective for alternative fuels: first to fourth generation. *Renew. Energy.* 69 (September), 114–122. doi:10.1016/j.renene.2014.02.044

Ervural, C., Beyzanur, S. Z., Demirel, O. F., Aydin, Z., and Delen, D. (2018). "An ANP and fuzzy TOPSIS-based SWOT analysis for Turkey's energy planning. *Renew. Sustain. Energy Rev.* 82 (February), 1538–1550 doi:10.1016/j.rser.2017.06.095

Falcone, P. M., Lopolito, A., and Sica, E. (2019). Instrument mix for energy transition: a method for policy formulation. *Technol. Forecast. Soc. Change.* 148 (November), 119706. doi:10.1016/j.techfore.2019.07.012

Gardy, J., Rehan, M., Hassanpour, A., Lai, X., and Nizami, A. S. (2019). Advances in nano-catalysts based biodiesel production from non-food feedstocks. *J. Environ. Manag.* 249, 109316. doi:10.1016/j.jenvman.2019.109316

Gholami, Z., Seddiq Mortazavi, M., and Karbassi, A. (2019). Environmental risk assessment of harmful algal blooms case study: Persian gulf and Oman sea located at hormozgan province, Iran. *Hum. Ecol. Risk Assess.* 25 (1–2), 271–296. doi:10.1080/10807039.2018.1501660

Gouveia, L. (2011). "Microalgae as a feedstock for biofuels," in *In* Microalgae as a Feedstock for Biofuels*Luisa gouveia. SpringerBriefs in microbiology*, 1–69 (Berlin, Germany: Springer). doi:10.1007/978-3-642-17997-6_1

Hamid, N. N. A., Martinez-Hernandez, E., and Lim, J. S. (2017). Technological screening of algae-based biorefinery for sustainable biofuels production using analytic hierarchy process (ahp) with feature scaling normalisation. *CET.* 61, 1369–1374. doi:10.3303/CET1761226

Hossain, A. S., Salleh, A., Boyce, A. N., Chowdhury, P., and Naqiuddin, M. (2008). Biodiesel fuel production from algae as renewable energy. *Am. J. Biochem. Biotechnol.* 4 (3), 250–254. doi:10.3844/ajbbsp.2008.250.254

Hossain, N., and Mahlia, T. M. I. (2019). Progress in physicochemical parameters of microalgae cultivation for biofuel production. *Crit. Rev. Biotechnol.* 39 (6), 835–859. doi:10.1080/07388551.2019.1624945

Hossard, L., and Chopin, P. (2019). Modelling agricultural changes and impacts at landscape scale: a bibliometric review. *Environ. Model. Software* 122 (December), 104513. doi:10.1016/j.envsoft.2019.104513

Islam, M. A., Magnusson, M., Brown, R. J., Ayoko, G. A., Nabi, M. N., and Heimann, K. (2013). Microalgal species selection for biodiesel production based on fuel properties derived from fatty acid profiles. *Energies* 6 (11), 5676–5702. doi:10.3390/en6115676

Juan, J. L. G. S., Mayol, A. P., Sybingco, E., Ubando, A. T., Culaba, A. B., Chen, W. H., et al. (2020). A scheduling and planning algorithm for microalgal cultivation and harvesting for biofuel production. *IOP Conf. Ser. Earth Environ. Sci.* 463 (April), 012010. doi:10.1088/1755-1315/463/1/012010

Kahraman, C., Cebeci, U., and Ulukan, Z. (2003). Multi-criteria supplier selection using fuzzy AHP. *Logist. Inf. Manag.* 16 (6), 382–394. doi:10.1108/09576050310503367

Katooli, M. H., Aslani, A., Fatemeh Razi, A., Tania Mazzuca, S., and Bakhtiar, A. (2019). Multi-criteria analysis of microalgae production in Iran. *Biofuels* 0 (0), 1–7. doi:10.1080/17597269.2018.1542566

Kazemifard, S., Nayebzadeh, H., Saghatoleslami, N., and Safakish, E. (2019). Application of magnetic alumina-ferric oxide nanocatalyst supported by KOH for *in-Situ* transesterification of microalgae cultivated in wastewater medium. *Biomass Bioenergy* 129 (October), 105338. doi:10.1016/j.biombioe.2019.105338

Kheybari, S., Mahdi Rezaie, F., and Rezaei, J. (2019). Measuring the importance of decision-making criteria in biofuel production technology selection. *IEEE Trans. Eng. Manag.* 1, 15 doi:10.1109/TEM.2019.2908037

Khishtandar, S., Zandieh, M., and Dorri, B. (2017). A multi criteria decision making framework for sustainability assessment of bioenergy production technologies with hesitant fuzzy linguistic term sets: the case of Iran. *Renew. Sustain. Energy Rev.* 77 (September), 1130–1145. doi:10.1016/j.rser.2016.11.212

Kim, D. W., Shin, W.-S., Min-Gyu, S., Lee, B., and Chang, Y. K. (2019). Light intensity control as a strategy to improve lipid productivity in Chlorella sp. HS2 for biodiesel production. *Biomass Bioenergy* 126 (July), 211–219. doi:10.1016/j.biombioe.2019.05.014

Köhler, J. (2019). *Advances in modelling sustainable innovation: from technology bias tosystem theories and behavioural dynamics*. in *Handbook of sustainable innovation*, Chap 18, 310–330, Cheltenham, United Kingdom: Edward Elgar Publishinghttps://www.elgaronline.com/view/edcoll/9781788112567/9781788112567.00029.xml

Kokkinos, K., and Karayannis, V. (2020). Supportiveness of low-carbon energy technology policy using fuzzy multicriteria decision-making methodologies. *Mathematics* 8 (7), 1178. doi:10.3390/math8071178

Kokkinos, K., Lakioti, E., Papageorgiou, E., Moustakas, K., and Karayannis, V. (2018). Fuzzy cognitive map-based modeling of social acceptance to overcome uncertainties in establishing waste biorefinery facilities. *Frontiers in Energy Research* 6, 112. doi:10.3389/fenrg.2018.00112

Kokkinos, K., Lakioti, E., Samaras, P., and Karayannis, V. (2019). Evaluation of public perception on key sustainability indicators for drinking water quality by fuzzy logic methodologies. *Desalination and Water Treatment* 170, 378–393. doi:10.5004/dwt.2019.24642

Kosko, B. (1986). Fuzzy cognitive maps. *International Journal on ManeMachine Studies* 24, 65–75.

Kosko, B. (1992). *Neural networks and fuzzy systems: a dynamical systems approach to machine intelligence* New York, NY, United States: Prentice-Hall.

Krishankumar, R., Mishra, A. R., Kattur, S. R., Peng, X., Edmundas, K. Z., Cavallaro, F., et al. (2020). A group decision framework for renewable energy source selection under interval-valued probabilistic linguistic term set. *Energies* 13 (4), 986. doi:10.3390/en13040986

Lak Kamari, M., Isvand, H., and Alhuyi Nazari, M. (2020). Applications of multi-criteria decision-making (MCDM) methods in renewable energy development: a review. *Renewable Energy Research and Application* 1 (1), 47–54. doi:10.22044/rera.2020.8541.1006

Li, Y., Horsman, M., Wu, N., Lan, C. Q., and Dubois-Calero, N. (2008). Biofuels from microalgae. *Biotechnol. Prog.* 24 (4), 815–820. doi:10.1021/bp070371k

Lu, W., Alam, M. A., Luo, W., and Asmatulu, E. (2019). Integrating Spirulina Platensis cultivation and aerobic composting exhaust for carbon mitigation and biomass production. *Bioresour. Technol.* 271 (January), 59–65. doi:10.1016/j.biortech.2018.09.082

Madugu, F., and Collu, M. (2014). Techno-economic modelling analysis of microalgae cultivation for biofuels and co-products. In 1st International Conference on Energy Production and Management in the 21st Century, Ekateringburg, Russia, April, 2014, 1091–1102. doi:10.2495/EQ141022

Markou, G. (2020). "Chapter 21 - overview of microalgal cultivation, biomass processing and application," in *Handbook of algal science, Technology and medicine*. Editors: O. Konur (Cambridge, MA, United States: Academic Press), 343–352. doi:10.1016/B978-0-12-818305-2.00021-8

Markou, G., Kougia, E., Kefalogianni, I., Tsagou, V., Arapoglou, D., and Chatzipavlidis, I. (2019). Effect of glycerol concentration and light intensity on growth and biochemical composition of Arthrospira (Spirulina) Platensis: a study in semi-continuous mode with non-aseptic conditions. *Appl. Sci.* 9 (21), 4703. doi:10.3390/app9214703

Mata, T. M., Martins, A. A., and Caetano, N. S. (2010). Microalgae for biodiesel production and other applications: a review. *Renew. Sustain. Energy Rev.* 14 (1), 217–232. doi:10.1016/j.rser.2009.07.020

Mehta, A. V., and Nirvesh, S. M. (2020). Extraction of algae biodiesel for power generation and comparison of sustainable fuels using MCDM. *Int. J. Ambient Energy* 0 (0), 1–11. doi:10.1080/01430750.2020.1796785

Montingelli, M. E., Tedesco, S., and Olabi, A. G. (2015). Biogas production from algal biomass: a review. *Renew. Sustain. Energy Rev.* 43 (March), 961–972. doi:10.1016/j.rser.2014.11.052

Naeini, M. A., Zandieh, M., Seyyed, E. N., and Seyed, M. S. (2020). Analyzing the development of the third-generation biodiesel production from microalgae by a novel hybrid decision-making method: the case of Iran. *Energy* 195 (March), 116895. doi:10.1016/j.energy.2020.116895

Naghshbandi, M. P., Tabatabaei, M., Aghbashlo, M., Muhammad Nauman, A., and Iqbal, I. (2020). "Metabolic engineering of microalgae for biofuel production." *In biofuels from algae: methods and protocols*, Editors K. Spilling *Methods in molecular biology*. New York, NY, United States: Springer, 153–172. doi:10.1007/7651_2018_205

Nizami, A. S., Rehan, M., Waqas, M., Naqvi, M., Ouda, O. K. M., Shahzad, K., et al. (2017). Waste biorefineries: enabling circular economies in developing countries. *Bioresour. Technol.* 241 (October), 1101–1117. doi:10.1016/j.biortech.2017.05.097

Nogueira, N., Nascimento, F. J. A., Cunha, C., and Cordeiro, N. (2020). Nannochloropsis gaditana grown outdoors in annular photobioreactors: operation strategies. *Algal Research.* 48 (June), 101913. doi:10.1016/j.algal.2020.101913

Noorul Haq, A., and Kannan, G. (2006). Fuzzy analytical hierarchy process for evaluating and selecting a vendor in a supply chain model. *Int. J. Adv. Manuf. Technol.* 29 (7), 826–835. doi:10.1007/s00170-005-2562-8

Novak, J. D., and Cañas, A. J. (2008). *The theory underlying concept maps and how to construct and use ThemTechnical report IHMC CmapTools 2006-01 rev 01-2008*. Pensacola, FL, United States: " Florida Institute for Human and Machine Cognition. [Online] URL: http://Cmap.Ihmc.Us/Publications/Researchpapers/Theoryunderlyingconceptmaps.Pdf

Nwokoagbara, E., Olaleye, A. K., and Wang, M. (2015). Biodiesel from microalgae: the use of multi-criteria decision analysis for strain selection. *Fuel.* 159 (November), 241–249. doi:10.1016/j.fuel.2015.06.074

Papapolymerou, G., Karayannis, V., Besios, A., Riga, A., Gougoulias, N., and Spiliotis, X. (2019). Scaling-up sustainable Chlorella vulgaris microalgal biomass cultivation from laboratory to pilot-plant photobioreactor, towards biofuel. *Global NEST Journal* 21 (1), 37–42. doi:10.30955/gnj.002777

Peng, L., Fu, D., Chu, H., Wang, Z., and Qi, H. (2020). Biofuel production from microalgae: a review. *Environ. Chem. Lett.* 18 (2), 285–297. doi:10.1007/s10311-019-00939-0

Raehtz, K. D. (2009). Challenges and advances in making microalgae biomass a cost efficient source of biodiesel. *MMG 445 Basic Biotechnology* 5 (1), 37–43

Rani, P., Mishra, A. R., Mardani, A., Cavallaro, F., Alrasheedi, M., and Alrashidi, A. (2020). A novel approach to extended fuzzy TOPSIS based on new divergence measures for renewable energy sources selection. *J. Clean. Prod.* 257 (June), 120352. doi:10.1016/j.jclepro.2020.120352

Rani, P., Mishra, A. R., Raj Pardasani, K., Mardani, A., Liao, H., and Streimikiene, D. (2019). A novel VIKOR approach based on entropy and divergence measures of pythagorean fuzzy sets to evaluate renewable energy technologies in India. *J. Clean. Prod.* 238 (November), 117936. doi:10.1016/j.jclepro.2019.117936

Roussos, A., Misailidis, N., Koulouris, A., Zimbardi, F., and Petrides, D. (2019). A feasibility study of cellulosic isobutanol production—process simulation and economic analysis. *Processes.* 7 (10), 667. doi:10.3390/pr7100667

Saaty, R. W. (1987). The analytic hierarchy process—what it is and how it is used. *Math. Model.* 9 (3), 161–176. doi:10.1016/0270-0255(87)90473-8

Safakish, E., Nayebzadeh, H., Saghatoleslami, N., and Kazemifard, S. (2020). Comprehensive assessment of the preparation conditions of a separable magnetic nanocatalyst for biodiesel production from algae. *Algal Research.* 49 (August), 101949. doi:10.1016/j.algal.2020.101949

Sakarika, M., and Kornaros, M. (2019). Chlorella vulgaris as a green biofuel factory: comparison between biodiesel, biogas and combustible biomass production. *Bioresour. Technol.* 273 (February), 237–243. doi:10.1016/j.biortech.2018.11.017

Salim, H. K., Stewart, R. A., Oz, S., and Michael, D. (2019). Drivers, barriers and enablers to end-of-life management of solar photovoltaic and battery energy storage systems: a systematic literature review. *J. Clean. Prod.* 211 (February), 537–554. doi:10.1016/j.jclepro.2018.11.229

Savvides, A. L., Moisi, K., Katsifas, E. A., Karagouni, A. D., and Hatzinikolaou, D. G. (2019). Lipid production from indigenous Greek microalgae: a possible biodiesel source. *Biotechnol. Lett.* 41 (4), 533–545. doi:10.1007/s10529-019-02658-6

Savvidou, M. G., Boli, E., Logothetis, D., Lymperopoulou, T., Ferraro, A., Louli, V., et al. (2020). A study on the effect of macro- and micro- nutrients on Nannochloropsis oceanica growth, fatty acid composition and magnetic harvesting efficiency. *Plants* 9 (5), 660. doi:10.3390/plants9050660

Sindhu, S., Nehra, V., and Luthra, S. (2017). Solar energy deployment for sustainable future of India: hybrid SWOC-AHP analysis. *Renew. Sustain. Energy Rev.* 72 (May), 1138–1151. doi:10.1016/j.rser.2016.10.033

Singh, J., and Gu, S. (2010). Commercialization potential of microalgae for biofuels production. *Renew. Sustain. Energy Rev.* 14 (9), 2596–2610. doi:10.1016/j.rser.2010.06.014

Sung, Y. J., Jeong, S., Hong, K., Ko, H., and Sim, S. J. (2020). "Outdoor cultivation of microalgae in a coal-fired power plant for conversion of flue gas CO2 into microalgal direct combustion fuels." *Systems microbiology and biomanufacturing,* Berlin. Germany: Springer. doi:10.1007/s43393-020-00007-7

Suprun, E., Oz, S., Stewart, R. A., Panuwatwanich, K., and Shcherbachenko, Y. (2018). An integrated participatory systems modelling approach: application to construction innovation. *Systems.* 6 (3), 33. doi:10.3390/systems6030033

Tan, J., Kok, Y. L., Nik Meriam, N. S., Tan, R. R., and Promentilla, M. A. B. (2016). Fuzzy analytic hierarchy process (FAHP) for multi-criteria selection of microalgae harvesting and drying processes. *Clean Technol. Environ. Policy.* 18 (7), 2049–2063. doi:10.1007/s10098-016-1163-6

Tsavatopoulou, V. D., Aravantinou, A. F., and Manariotis, I. D. (2019). Biofuel conversion of Chlorococcum sp. and Scenedesmus sp. Biomass by one- and two-step transesterification. *Biomass Convers. Biorefin.* doi:10.1007/s13399-019-00541-y

Ubando, A. T., Charles, B. F., Ivan, H. V. G., Michael, A. B. P., and Alvin, B. C. (2020). A fuzzy analytic hierarchy process for the site selection of the philippine algal industry. *Clean Technol. Environ. Policy.* 22 (1), 171–185. doi:10.1007/s10098-019-01775-0

Ubando, A. T., Ivan, H. V. G., and Kyle Darryl, T. A. (2016a). Analytical hierarchy process with artificial neural network: a case study of algal biofuel production impact prioritization in the Philippines. In 2016 IEEE region 10 conference (TENCON), Singapore, November 2016, 961–965. doi:10.1109/tencon.2016.7848147

Ubando, A. T., Joel, L. C., El-Halwagi, M. M., Culaba, A. B., Promentilla, M. A. B., and Tan, R. R. (2016b). Application of stochastic analytic hierarchy process for evaluating algal cultivation systems for sustainable biofuel production. *Clean Technol. Environ. Policy.* 18 (5), 1281–1294. doi:10.1007/s10098-015-1073-z

Ullah, K., Garg, H., Mahmood, T., Jan, N., and Ali, Z. (2020). Correlation coefficients for T-spherical fuzzy sets and their applications in clustering and multi-attribute decision making. *Soft Computing* 24 (3), 1647–1659. doi:10.1007/s00500-019-03993-6

Vinoth Arul Raj, J., Bharathiraja, B., Vijayakumar, B., Arokiyaraj, S., Iyyappan, J., and Praveen Kumar, R. (2019). Biodiesel production from microalgae Nannochloropsis oculata using heterogeneous poly ethylene glycol (PEG) encapsulated ZnOMn^{2+} nanocatalyst. *Bioresour. Technol.* 282 (June), 348–352. doi:10.1016/j.biortech.2019.03.030

Viswanath, B., Mutanda, T., White, S., and Bux, F. (2010). "The microalgae – a future source of biodiesel. *Dyn. Biochem. Process Biotechnol. Mol. Biol.* 4 (No. 1), 37–47

Wang, S.-K., Wang, X., Tian, Y.-T., and Cui, Y.-H. (2020). Nutrient recovery from tofu whey wastewater for the economical production of docosahexaenoic acid by Schizochytrium sp. S31. *Sci. Total Environ.,* 710, 136448. doi:10.1016/j.scitotenv.2019.136448

Wang, W.-M., and Peng, H.-H. (2020). A fuzzy multi-criteria evaluation framework for urban sustainable development. *Mathematics* 8 (3), 330. doi:10.3390/math8030330

Wang, Z., Pashaei Kamali, F., Osseweijer, P., and John, A. P. (2019). Socioeconomic effects of aviation biofuel production in Brazil: a scenarios-based input-output analysis. *J. Clean. Prod.* 230 (September), 1036–1050. doi:10.1016/j.jclepro.2019.05.145

Wohlfahrt, J., Ferchaud, F., Gabrielle, B., Godard, C., Kurek, B., Loyce, C., et al. (2019). Characteristics of bioeconomy systems and sustainability issues at the territorial scale. A review. *J. Clean. Prod.* 232 (September), 898–909. doi:10.1016/j.jclepro.2019.05.385

Yadav, G., Dubey, B. K., and Sen, R. (2020). A comparative life cycle assessment of microalgae production by CO$_2$ sequestration from flue gas in outdoor raceway ponds under batch and semi-continuous regime. *J. Clean. Prod.* 258 (June), 120703. doi:10.1016/j.jclepro.2020.120703

Yoo, C., Jun, S. Y., Lee, J. Y., Ahn, C. Y., and Oh, H. M. (2010). Selection of microalgae for lipid production under high levels carbon dioxide. *Bioresour TechnolConversion Technologies* 101(1), S71–S74. doi:10.1016/j.biortech.2009.03.030

Yoon, K. P., and Hwang, C.-L. (1995). *Multiple attribute decision making: an introduction* CA, United States: SAGE Publications

Zadeh, L. A. (1965). Fuzzy sets. *Inf. Contr.* 8 (3), 338–353. doi:10.1016/S0019-9958(65)90241-X

Zhang, W., Zhao, C., Cao, W., Sun, S., Hu, C., Liu, J., et al. (2020). Removal of pollutants from biogas slurry and CO2 capture in biogas by microalgae-based technology: a systematic review. *Environ. Sci. Pollut. Res. Int.* 27 (23), 28749–28767. doi:10.1007/s11356-020-09282-2

Zhao, N., Xu, Z., and Ren, Z. (2019). Hesitant fuzzy linguistic prioritized superiority and inferiority ranking method and its application in sustainable energy technology evaluation. *Inf. Sci.* 478 (April), 239–257. doi:10.1016/j.ins.2018.11.022

frontiers
in Energy Research

Valorization of Wastewater Resources Into Biofuel and Value-Added Products Using Microalgal System

Kanika Arora[1†], Parneet Kaur[1†], Pradeep Kumar[1*], Archana Singh[2], Sanjay Kumar Singh Patel[3], Xiangkai Li[4], Yung-Hun Yang[5,6], Shashi Kant Bhatia[5,6*] and Saurabh Kulshrestha[1*]

[1] Faculty of Applied Sciences and Biotechnology, Shoolini University of Biotechnology and Management Sciences, Solan, India, [2] Department of Bioinformatics, Mahila Mahavidyalaya, Banaras Hindu University, Varanasi, India, [3] Department of Chemical Engineering, Konkuk University, Seoul, South Korea, [4] Ministry of Education Key Laboratory of Cell Activities and Stress Adaptations, School of Life Sciences, Lanzhou University, Lanzhou, China, [5] Department of Biological Engineering, College of Engineering, Konkuk University, Seoul, South Korea, [6] Institute for Ubiquitous Information Technology and Application, Konkuk University, Seoul, South Korea

Wastewater is not a liability, instead considered as a resource for microbial fermentation and value-added products. Most of the wastewater contains various nutrients like nitrates and phosphates apart from the organic constituents that favor microbial growth. Microalgae are unicellular aquatic organisms and are widely used for wastewater treatment. Various cultivation methods such as open, closed, and integrated have been reported for microalgal cultivation to treat wastewater and resource recovery simultaneously. Microalgal growth is affected by various factors such as sunlight, temperature, pH, and nutrients that affect the growth rate of microalgae. Microalgae can consume urea, phosphates, and metals such as magnesium, zinc, lead, cadmium, arsenic, etc. for their growth and reduces the biochemical oxygen demand (BOD). The microalgal biomass produced during the wastewater treatment can be further used to produce carbon-neutral products such as biofuel, feed, bio-fertilizer, bioplastic, and exopolysaccharides. Integration of wastewater treatment with microalgal bio-refinery not only solves the wastewater treatment problem but also generates revenue and supports a sustainable and circular bio-economy. The present review will highlight the current and advanced methods used to integrate microalgae for the complete reclamation of nutrients from industrial wastewater sources and their utilization for value-added compound production. Furthermore, pertaining challenges are briefly discussed along with the techno-economic analysis of current pilot-scale projects worldwide.

Keywords: microalgae, wastewater, biofuel, bio-economy, value-added products

INTRODUCTION

Water is a natural resource and considered the most essential component of all living creatures. Almost 70% of the earth's surface is covered by water but only about 3% of it is fresh water (Cao et al., 2019). Water being such a scarce commodity, its integrity, and environmental perturbations should never be compromised. Every year about 3.4 million people die, and many suffer from a

plethora of water-borne diseases due to polluted water being discharged recklessly from industries and wastewater treatment plants (Osiemo et al., 2019). Different sources of wastewater like municipal, agricultural, and industrial contain larger quantities of nutrients organic and inorganic contaminants (Bhatia et al., 2021d). Wastewater is released into the water bodies without proper treatment which affects the aquatic ecosystem adversely and results in eutrophication (Preisner et al., 2021). The root cause of this formidable situation is the lack of efficient, economical, and energy-saving methods for wastewater treatment. Conventional methods like electrochemical methods, precipitation, and membrane technologies are all non-sustainable (Rajasulochana and Preethy, 2016). They all are backed with instability, resource wasting, fouling, and exorbitant energy consumption. On the other hand, this wastewater offers a perfect niche for microalgae, unicellular photosynthetic organisms to grow and flourish synergistically with the prevailing bacterial colonies present in the sewer water. To save the environment and recycle the nutrients, wastewater treatment using microalgae is an imperative step. The use of microalgae for wastewater treatment is advantageous as it will help to reduce the biochemical oxygen demand (BOD) and chemical oxygen (COD) demand and remove the inorganic nutrients like nitrates and phosphates from the wastewater (Taziki et al., 2015). This could save a huge amount of cost as algae will assimilate all the nutrients along with bio fixing of inorganic carbon from the atmosphere (CO_2 sequestration) (Bhatia et al., 2019a). Moreover, additional CO_2 can be sourced from flue gas which is obtained from power plant emissions. Thereby, addressing air and water pollution simultaneously. Different wastewaters have different compositions based on their source. Microalgal growth is affected by nutrient components and other factors like temperature, pH, salinity, light intensity, duration, etc. (Cabello et al., 2015; Vuppaladadiyam et al., 2018). The selection of microalgal species is very important depending upon the characteristics of wastewater for efficient wastewater treatment. The optimum physiochemical conditions need to be maintained to obtain the maximum possible yield. It is reported that removal efficiency of 65-76% of COD, 68-81% of total nitrogen, and 90-100% of total phosphorous from piggery wastewater by freshwater microalgae *Chlorella zofingiensis* (Zhu et al., 2013). In another report, it was studied that COD removal of 50.9 and 56.5% from primary and secondary effluents, respectively, by green algae *Chlorella* spp. (Wang et al., 2010). Microalgae mediated wastewater treatment method can also produce biofuel (bioelectricity and biohydrogen) simultaneously or recovered biomass can be further used as feedstock to produce various commercially valuable biochemicals (Bhatia et al., 2021d). Along with nutrient recovery from waste streams, Maity et al. (2014) reported simultaneous production of 1068.383 mg g^{-1} dry wt. biomass of lipid with C16:0, C18:2n-6, C18:1, and C16:1 FAME content and 0.264 mV, 0.008 mW cm^{-2} of electric potential and bioelectricity using *Leptolyngbya* sp. JPMTW1 within 7 days. Microalgal biomass after wastewater treatment can be recovered using technologies such as centrifugation, flocculation, and electrochemical precipitation methods. Microalgal biomass is rich in carbohydrates, lipids, and proteins and is further used

for extraction of commercially important products (lipids, carotenoids, polyhydroxyalkanoates, etc.) are biomass can be used as a feedstock for microbial fermentation to produce other commercial products (Bhatia et al., 2017; Goswami et al., 2020).

Despite the lucrative benefits of microalgae-based wastewater treatment, few limitations still persist. The current open and closed cultivation methods render contamination risks and huge operational costs, respectively. Further, harvesting and dewatering account for 20-30% of the total cost (Fasaei et al., 2018). Therefore, the concept of integrated systems is briefly discussed which can cut the major costs and make the method more economical. Besides, wastewater composition, culture collapse, salinity, etc., are some other pitfalls that could be addressed by subsequent research and development in this field. This review will discuss the current wastewater treatment technologies in action with microalgae dominance in the waste realm. It will address various cultivation systems and harvesting methods, integrating microalgae for wastewater treatment and sustainable product production. Furthermore, the present state-of-the-art review will also highlight the techno-economic analysis and status of nutrient recovery processes.

COMPOSITION OF WASTEWATER

Wastewater consists of pollutants from different walks of life, reflecting the lifestyle and activities of people living in the city. It is a by-product of industrial, domestic, commercial, and agricultural chores and contains human excreta, washing wastes from houses, pesticides, nutrients from agricultural farms, organic biodegradable wastes from hospitals and abattoirs, non-biodegradable from pharmaceuticals manufacturing, toxic waste such as dyes and heavy metals from other industries, leachates from landfills and storm water during high precipitations (Rana et al., 2017). All these contaminants comprise only 0.1% of suspended and dissolved solids, while 99.9% is pure water (Samer, 2015). Most of it is organic debris, and only a small part consists of non-biodegradable inorganic wastes, which pose a significant problem in reclamation. Three-quarters of volatile (organic) solids in sewage are carbohydrates, proteins, and fats from discarded food waste, kitchen waste, dead organisms, etc. (Samer, 2015). The non-volatile part includes heavy metals salts, grit, and sand dust.

Microorganisms form a significant part of sewage treatment. They can range from moderate to high-risk biological pollutants like antibiotic resistant bacteria, viruses, protozoa, biotoxins, and helminths. Such infectious agents pose a substantial threat to human life and the environment (Jia and Zhang, 2019). On the other hand, some of the microbes like algae, pseudomonas, zoogloeal are environmental-friendly and aid in wastewater treatment. Sources of such microbes include faeces and other bodily fluids from several sick people and asymptomatic hosts leading to ailments like cholera, jaundice, typhoid from bacteria, hepatitis from viruses, and dysentery from protozoans. Coliform *Escherichia coli* are present in vitality, indicating other pathogens, and are therefore used to measure the infecting efficiency of sewage (Hendricks and Pool, 2012).

Among all, municipal wastewater is the most preferred wastewater for microalgae-based wastewater treatments because of the adequate amount of nutrients and a low number of toxic substances compared to industrial wastewater. It is generally categorized into (i) raw sewage, (ii) secondary effluent, and (iii) centrate, i.e., by-product of sludge dewatering. Studies have proved that centrate is the most suitable medium for microalgae cultivation with nutrient removal efficiencies of 89.1%, 90.8%, 93.9%, and 80.9% for TN, COD, NH_4-N, and TP, respectively (Wang et al., 2010; Li et al., 2011). Moreover, additional CO_2 (5-150%) along with municipal wastewater could enhance nutrient recovery and lipid production simultaneously (Ji et al., 2013). On the other hand, the agricultural waste contains an excessively high amount of ammonia, suspended solids (SS), nutrient load (due to animal manure), chroma, and turbidity which make it unfit for direct microalgae treatment. Therefore, it is generally applied after anaerobic digestion (AD) as much of the organic carbon gets converted to methane, leaving nitrate and phosphate in the digestate. The C/N ratio of the digested manure is comparatively low than centrate which makes the medium ideal for microalgae growth. Only a few algal strains support this type of medium and hence it is used after diluting for certain species (Zhou et al., 2012b; Zhu et al., 2013). Hence, a sequential two-stage cultivation process is preferred for animal manure wastewater and has great economic potential with multiple product production. In contrastingly, there is no standard treatment applicable for industrial wastewater due to its complex nature with added toxicity. Few microalgal species are adapted to exorbitant levels of heavy metals while most of the algal species are intolerable. *Ankistrodesmus*, *Chlorella*, and *Scenedesmus* are a few of the species competent for treating mill, olive oil, and paper industry wastewater (Rawat et al., 2011). The wastewater from the paper industry is characterized by 1720 mg L^{-1} and 2658 mg L^{-1} of suspended solids and dissolved solids with an average pH range of 8.5, respectively. The color value obtained is in the range of 735 Platinum Cobalt Unit while chemical oxygen demand and biochemical oxygen demand of 2420 mg L^{-1} and 778 mg L^{-1}, simultaneously (Singh, 2015; Choi et al., 2017). Another study compares wastewater from three different sources like household, domestic, and offices, and found maximum phosphorus content in domestic waste as given in **Table 1** (Vandith et al., 2018). **Table 2** provides an elaborate picture of how microalgae can treat different sources of wastewater efficiently (Li et al., 2019; Al-Jabri et al., 2020). For about 38000 million liters per day of sewage generated, only 12000 million liters per day get treated in India, and among 35 metropolitan cities, only 51% of sewages, i.e., 8040 million liters per day of sewage treatment capacity exist for 15644 million liters per day of wastewater generated (National Status of Waste Water Generation and Treatment, 2020). According to The OPEC Fund for International Development wastewater report, the global scenario of sewage treatment is found to be 70% in high-income countries and is even depressing with only 8% in low-income countries (State of the Art Compendium Report on Resource Recovery from Water, 2018). Due to increased urbanization, industrialization, and leading water scarcity due to climate change, the global market related to resource recovery is tending to rise to $22.3 billion by 2021 from $12.2 Billion

TABLE 1 | Comparison of characteristics of different wastewater sources.

Wastewater (source)	Parameters (mg L^{-1})					Ref.
	BOD[1]	COD[2]	TSS[3]	TN[4]	TP[5]	
Domestic	160-300	250-800	390-1230	20.0-70.0	4.0-12.0	Vandith et al., 2018
Domestic	124	156	—[a]	—	—	Choi et al., 2017
Household	258	—	63.0	50.2	5.9	Vandith et al., 2018
Office	—	160-220	—	54.5-79.3	3.8-7.0	Vandith et al., 2018
Dyeing industry	52.4	111	—	—	—	Choi et al., 2017
Paper mill industry	38.8	112	—	—	—	Choi et al., 2017
Pharmaceutical industry	120	490	370	—	—	Rana et al., 2017

[1] Biochemical oxygen demand.
[2] Chemical oxygen demand.
[3] Total suspended solids.
[4] Total nitrogen.
[5] Total phosphorus.
[a] Not reported.

in 2016 (State of the Art Compendium Report on Resource Recovery from Water, 2018). Therefore, wastewater recovery and resource utilization are still untapped in many underdeveloped and few developing countries, and only a small portion is utilized in a safe and planned manner while the majority of partially treated or untreated wastewater is discharged unregulated into the water bodies.

MICROALGAE CULTIVATION SYSTEMS

Microalgae can be grown both in an open system and closed systems. An open system is present in nature as naturally occurring ponds that include lagoons, sea, and oceans. The photobioreactors are a closed system for algal production under controlled conditions of temperature, pH, and nutrients for higher yield of the biomass. The cultivation of microalgae can even be performed using wastewater such as domestic sewage water and palm oil milling effluents which can assist in the bioremediation of wastewater (Selmani et al., 1997; Posadas et al., 2017).

Open Systems

Open ponds are the simplest and easiest way to cultivate microalgae on large scale. The various types of open pond systems include lakes, ponds, artificial water bodies such as circular and raceway systems. The algae are cultivated in open pond systems (shallow ponds), and nutrients are added through runoff water from nearby land areas or by channeling the water from sewage/water treatment plants (Carlsson et al., 2007). Mixing is provided by paddle wheels in raceway ponds or rotating arms in circular ponds and mixing can even be provided at

TABLE 2 | Comparison of nutrient removal rate of microalgae in different wastewater sources.

Wastewater source	Category	Microalgae strain	Influent characteristic			Removal rate (%)			Ref.
			NH4±N (mg L^{-1})	TN (mg L^{-1})	TP (mg L^{-1})	NH4±N (mg L^{-1})	TN	TP	
Municipal wastewater	Synthetic saline wastewater (0.25 L)	Spirulina platensis	−	130	15	−	79	93.3	Zhou et al., 2017
	Domestic wastewater (75% diluted)	Chlorella sp. and Scenedesmus sp.	37.64	61.47	7.42	98	94	95	Silambarasan et al., 2021
Agricultural wastewater	Anerobic food wastewater	Chlorella pyrenoidosa	−	302.9 ± 13.4	25.7 ± 3.1	−	88.7	67.6	Tan et al., 2021
Industrial wastewater	Pharmaceutical wastewater (9600L)	Microalgal consortia	−	44	5	−	74	92	Villar-Navarro et al., 2018
	Anaerobically digested abattoir effluent	Chlorella sp.	222 ± 12	−	90 ± 8	95.6 ± 1.5	−	26.4 ± 11.6	Vadiveloo et al., 2021
	Molasses waste (diluted and balanced)	Scenedesmus sp.	−	600	75	−	90.2	88.6	Ma et al., 2017
Other wastewater	Mixed piggery-brewery waste	C. vulgaris	2–367	9–480	5–45	19–100	32–96	28–95	Zheng et al., 2018
	Aquaculture waste (1L)	Spirulina sp. LEB 18	−	10.33[a]	11.37	−	79.28	93.84	Cardoso et al., 2020
	HTL-APL	Picochlorum sp.	−	6900	1100	−	95.4	97.2	Das et al., 2020a
	HTL-APL	Tetraselmis sp.	−	4223	504.7	−	98.5	98	Das et al., 2020b

[a]Nitrite (NO^{-2}) nitrogen.

certain places in a large pond by the use of impeller blades (Yen et al., 2019). For example, *Spirulina* can grow at a very high pH (9-12) and therefore is dominant in soda lakes (Bindra et al., 2017). *Dunaliella salina* is emergent species in the shallow salt pan ponds (Borowitzka and Hallegraeff, 2007). There are various advantages of an open pond system as it provides a large surface area for growth, but it has lower cell concentration and requires efficient harvesting techniques (Tredici, 2004). The major limitation of the open and natural system includes the contamination by protozoa and bacteria and also it is difficult to control all the growth parameters in open systems (Lam et al., 2018). The harvesting of algae from a natural open system is one of the oldest methods and the oldest record of microalgae harvesting was done by Aztec peoples when they harvested *Spirulina* from Lake Texcoco located at Mexico (Hamed, 2016).

The first artificial ponds to be used are circular ponds and rotating agitators are used for efficient mixing and prevent sedimentation of algal biomass. The major limitation of this system is requirement of high energy usage and high construction cost (Hamed, 2016). This system is used in Japan and Taiwan for the cultivation of *Chlorella* (Lee, 1997; Shen et al., 2009). The high-rate algal ponds are used for the wastewater treatments pond is a shallow-depth which contains high loads of nitrogen and phosphorous content from wastewater, allows the microalgae to proliferate and produce high biomass (Craggs et al., 2012).

Raceway pond is the most feasible and cost-effective facility to treat large amounts of wastewater than other techniques because it has a low capital cost, more comfortable scale-up, and higher treatment volume (Zhou et al., 2013). The most used open culture system for growth is race-way pond design, which consists of long channels in loops or stirring devices, including paddlewheels. The various limitations of traditional raceway ponds with suspended algal culture are: (1) self-shadowing effect due to limited light penetration; (2) ineffective photosynthesis; (3) energy consumption and expenses for harvesting the suspended algal biomass and (4) reduced effluent quality due to inefficient harvest of the biomass (Chiaramonti et al., 2013).

Closed System (Photo-Bioreactors)

The photobioreactors are used to grow microalgae in a closed system where operating conditions and nutrients can be controlled and monitored using an automatic control system. An example of the closed system is a flat plate reactor with a complex mixer and the conditions required for the growth of *Chlorella vulgaris* is the optimum conditions of temperature (23.6-26.8°C) and dissolved oxygen (7.6-8.8 mg L^{-1}) (Lakaniemi et al., 2012). The most commonly used photobioreactor are, (i) straight tubes which are arranged flat on the ground or in long vertical rows known as tubular bioreactors and (ii) helical bioreactors which are spirally wound tubes around a central support. The tubes used can be of glass, or perpex for the bioreactor system. The tubular bioreactors are mainly used outdoors and are arranged

in different orientations such as vertical, horizontal, inclined, and helical to increase the mass production of algal biomass by capturing maximum sunlight, i.e., an increase in photosynthesis (Ting et al., 2017). The diameter of the tube can be from 10 to 60 mm (Ting et al., 2017). The specific limitation of tubular bioreactors is photosynthetic efficiency, and the energy consumption is higher. The major disadvantage of the tubular photobioreactor is the difference in the concentration along the long tubes that leads to poor mass transfer (Tan et al., 2020). The cell growth in the center is restricted due to lower photosynthesis in photobioreactor inhibiting concentration due to oxygen toxicity that can occur after only 1 minute in a tube without gas exchange (Posten, 2009). The uncontrolled growth of pathogenic microorganisms in the inner walls and the formation of biofilms, which influence the mass transfer of reagents due to external mass transfer resistance at the biofilm surface, is another drawback of the closed system (Skoneczny and Tabiś, 2015). These day's plastic bag photobioreactors are in great demand, and they can be separated based on their volumes and are cost-effective and made up of polythene (Wang et al., 2012). The only limitation is that mixing the components and fragility of the bags can lead to a decrease in this system's life. The major disadvantages of a closed system are high operating and construction costs.

Integrated Systems

Integrated systems are a complex mix of open and close culture systems in an advanced way to develop a hybrid system that overcomes their limitations collectively and produces an improved system with high pollutant removal efficiency and elevated biomass yield.

Immobilized Bioreactor

The immobilized system circumvents some major challenges in microalgae wastewater treatment processes. It eases some high-cost and energy-intensive steps of suspension systems, i.e., harvesting and separating algal biomass from the treated wastewater. Immobilization technology renders a fixed system where living cells are grown in a confined area and are prevented from moving independently in the system's aqueous environment. There are six different immobilization techniques

namely covalent coupling, affinity immobilization, adsorption, liquid-liquid emulsion, semipermeable membrane capture, and entrapment (Mallick, 2002). Among all, entrapment is the most exclusively used method for algae wastewater treatment and nutrient recovery. Algae cells are entrapped in a 3D gel matrix molded in the form of biocatalyst beads which are stabilized by cross-linking. For instance, widely used alginate and carrageenan beads in the case of algae are usually stabilized by Ca^{2+} and K^+ respectively (Ting et al., 2017). This technology utilizes algae's natural tendency to adhere to the natural or artificial substrate. The matrix consists of porous beads made of a polymeric material. This polymeric substrate must be hydrophilic to allow diffusion of wastewater into the bed and can be fabricated by various materials like synthetic acrylamide, polyvinyl, polyurethane, or naturally derived algal polysaccharides like alginate, agarose, and carrageenan. Chitosan also serves as an effective bead material individually and its durability gets enhanced when amalgamated with alginate (Castro and Ballesteros, 2020). A recent study reported faster growth rates and higher biomass production with successful nutrient removal capacity in *C. vulgaris* when grown in the alginate-chitosan matrix (Castro and Ballesteros, 2020). Such porous bead structures provide a protected environment for the selected species to thrive in a wastewater setting. Few studies used submerged Ca-alginate beads for the growth of microalgae-bacteria consortium in normal wastewater and revealed minimal contamination from other species and uninterrupted reduction in phosphorus and ammonium levels (Covarrubias et al., 2012; Kube et al., 2021). Apart from the material, cell density and gel thickness of the beads are also decisive characters for good results. If these are higher, it will lead to a light shading effect, and if lower, it renders low nutrient absorption (Ting et al., 2017). Few microalgae-based immobilized studies for wastewater treatment are listed in **Table 3**.

An ideal immobilized algal system should retain the viability of cells, shouldn't interfere with photosynthetic ability, render low leakage of cells from the matrix and exhibit a high density of cells (Mallick, 2002). However, such systems have different metabolic effects on algal cultures. Only the surface algae can get optimum conditions (light intensity, nutrient availability) to grow while the microalgae inside the bead get deprived and

TABLE 3 | Microalgae-based immobilized bead systems for wastewater treatment (Ting et al., 2017).

PBR	Microalgae strain	Wastewater type	HRT/h	Biomass productivity $(gL^{-1}d^{-1})$	Influent (mg L^{-1})		Removal efficiency (%)		Ref.
					N	TP	N	TP	
Sodium alginate solution (3 L)	*S. obliquus*, *C. vulgaris*	Secondary effluent	6 or 35	0.110-0.401	32.5	2.5	60.1-100/ 10-97	53.3-85.1/18-82	Ruiz-Marin et al., 2010
Integrated 3 chambers of PBR (2.5 L)	*Chlorella minutissima*	Sewage wastewater	–	≤0.03	37	12.8	100	100	Singh et al., 2012
Alginic acid sodium salt opaque PVC PBR (4 L)	*C. vulgaris*	Tertiary wastewater	6.5-12	0.18-1.55	7.1-10.4	0.08-1.78	100	60-90	Filippino et al., 2015

show less activity due to the self-shading effect. Results are chiefly dependent on a higher surface to volume ratio to ensure maximum interaction between pollutants and microalgae surface (Wollmann et al., 2019). The current study on *Scenedesmus obliquus* showed $96.6 \pm 0.1\%$ removal in 50 mg/L NH_4^+-N and 300 mg L^{-1} COD by the immobilized system over cell-free mode in an artificial wastewater environment (Liu et al., 2019). Another study revealed 94% and 66% removal efficiency of NH_4^+-N and PO_4^{3-}-P, respectively, for agar-immobilized microalgae even after eight times recycling. This concludes that immobilized microalgae can be preserved for about 120 days and can be used repeatedly at room temperature (Hu et al., 2020).

There are five types of immobilized bioreactors for fixed microalgae-based sewage treatment, namely fluidized bed bioreactor, airlift bioreactor, parallel plate bioreactor, packed bed bioreactor, and hollow-fiber bioreactor briefly explained in **Figure 1**. Fluidization enables increased mass transfer, large surface area, finest mixing, homogenous temperature, and particle distribution (Mohd-Sahib et al., 2017; Nelson et al., 2017). There are two types of advanced fluidization: LS (liquid-solid) and GLS (gas-liquid-solid) fluidization. Both of them can operate on circulating fluidization in which particles are carried out to the top of the column and then returned to the bottom with high velocity via recycle line. In GLS, three phases are involved as both liquid and gas fluidizes the particles. An investigation on novel microalgae membrane bioreactor with internal circulating fluidized bed (ICFB) showed 52, 80, and 85% removal efficiency of NO_3^--N, PO_4^{3-}-P, and NH^{4+}-N in 40 days (Ding et al., 2020). A study modeled CO_2 bio fixation using fluidized bed bioreactor onto polyurethane foam in nutrient rich wastewater setting and observed 97.7% (by wt. of lipid) of fatty acid methyl esters (FAMEs) mixture and found a high content of C16 and C18 FAME species for efficient combustion of biodiesel (Rosli et al., 2019). It was found that the wastewater removal efficiency also depends upon the flow pattern of the reactor besides cell density and gel thickness (Ting et al., 2017). Fluidized bed bioreactor showed better COD removal performance than parallel plate bioreactor rendered by a more extensive contact and continuous nutrient supply area (Ting et al., 2017). This system also possesses few limitations like difficulty in the evaluation of microalgae to count during treatment as it is packed in a matrix. Such constraints can be overcome by taking into account various other factors that influence the algal yield. Therefore, there is a need to broaden the understanding of immobilization on microalgae physiology and fill these lacunae of knowledge with further research.

Biofilm Packed Bed Bioreactor

Biofilm is a consortium of microorganisms embedded in a self-secreted extracellular polymeric substance (EPS) attached to a substratum. It can be an axenic (only consist of microalgae) or non-axenic systems (microalgae-bacteria consortium). Most of the systems are based on co-cultures of bacteria and microalgae as they share a stable symbiotic relationship in wastewater streams by maintaining a carbon dioxide-oxygen balance. Bacteria can feed on nutrients available in wastewater and also consumes oxygen to reduce the BOD while algae utilize CO_2 released by

bacteria and supplement the system with O_2. This will make the whole system self-reliant in themselves (Boelee et al., 2014; Lee et al., 2014). Such biofilm reactor renders a tremendous advantage over the conventional suspended systems as they require a relatively minimal amount of water, i.e., for 1 ton of microalgae biomass, 17 tons of water is sufficient while for cell-free culture, 200 tons of water is needed (Podola et al., 2017). Moreover, any rough surface material can be used as a supporting material like nylon, stainless steel, and natural fibers, etc. (Garbowski et al., 2017). Rougher the surface, more easily microalgae can adhere to it. According to a study, nylon and stainless-steel mesh are the most effective supporting material for biofilm having *Chlorella*, *Pediastrum*, *Scenedesmus*, *Nitzschia*, and *Cosmarium* (Lee et al., 2014). The significant bottlenecks of suspended cultures like harvesting, separation, and dewatering are not required in biofilm-based packed bed reactor as microalgae can be easily removed by scraping the solid surface (Lee et al., 2014). Microalgae attached to the surface experience better light availability than in the suspended environment. Likewise, a study showed that 1.4-fold more biomass production and higher pollutant removal efficiency in *C. vulgaris* biofilm packed bed reactor comparing to the suspended bioreactor (Cheah et al., 2018). Many factors affect microalgal biofilms, such as selecting proper microalgal strain, nutrients, light, and carbon dioxide availability, temperature, pH, attaching material, flow velocity, and allelopathic microalgae interactions with other microorganisms in the case of consortium cultures (Mantzorou and Ververidis, 2019). Biofilm show high heavy metal removal efficiency as in the case of *Chlorella* with 10.55%, 24.8%, 26.4%, and 24.8% removal rate for Co, Mn, Sr, and Ni (Palma et al., 2017). This is due to the presence of a high number of functional groups for metal complexation in EPS.

Biofilm systems are majorly divided into three categories based on biofilm arrangement and liquid medium supply: (i) permanently submerged systems, i.e., those systems that are constantly submerged in the liquid culture medium, (ii) intermittently submerged systems, i.e., those systems that have repeated alternative exposures of liquid as well as gas phase (also called biofilms between two phases), and (iii) perfused systems, i.e., those systems in which substratum is directly provided with culture medium (Moreno Osorio et al., 2019). Various microalgae-based biofilm bioreactors are developed to integrate wastewater treatment with biofuel productions to obtain a high yield with high efficiencies than conventional techniques as depicted in **Table 4**. Different packed bed bioreactors like vertical, horizontal, parallel plate, flow cell, airlift, flexi-fiber, rotating biofilm reactors, and vertical-algal-biofilm enhanced raceway ponds are studied for reclamation potentials widely. However, a rotating biofilm packed bed bioreactor is more promising, with 31 $gm^{-2}d^{-1}$ growth in mixed culture conditions utilizing the municipal wastewater (Christenson and Sims, 2012). Furthermore, a recent study has also observed a formation of struvite within the microalgae biofilm matrix in an outdoor pilot-scale rotating algal biofilm reactor (Hillman and Sims, 2020). These systems are much more advanced than conventional packed bed reactors, but this technology is still primarily limited to laboratory conditions and needs to

FIGURE 1 | Characterization of different types of immobilized bioreactors.
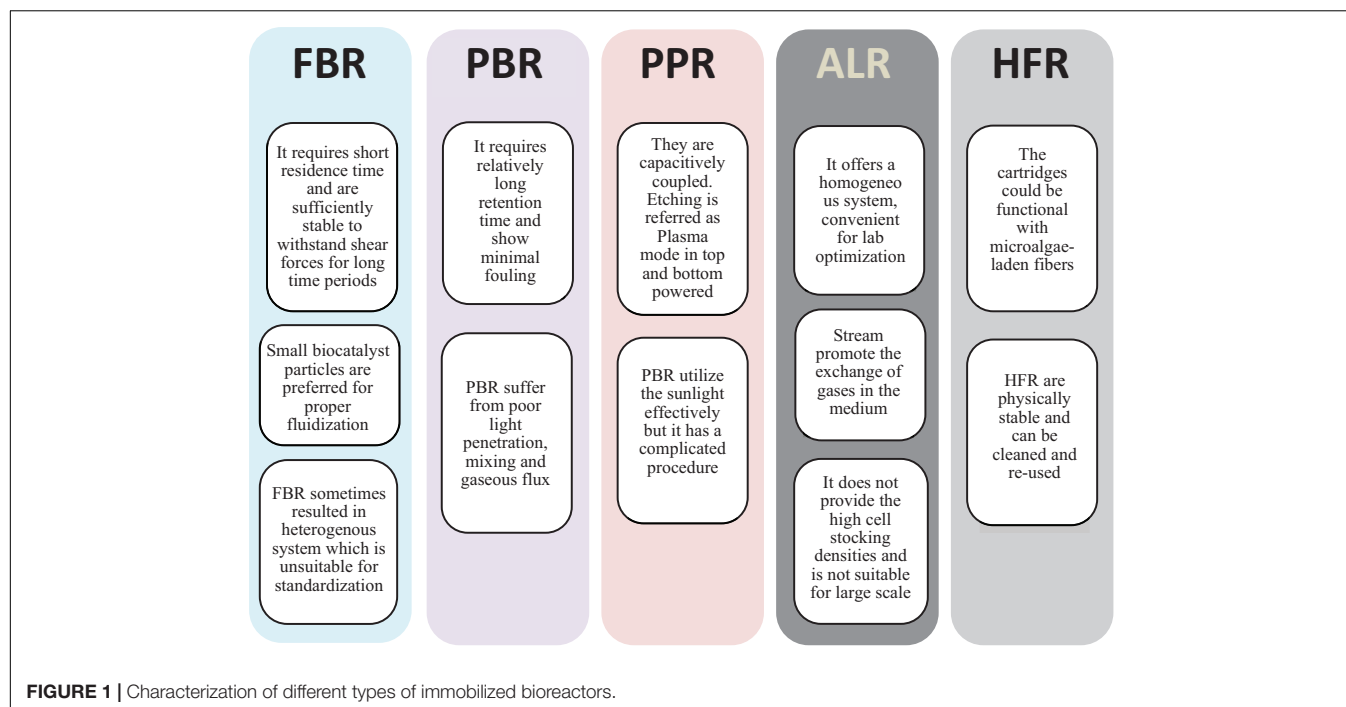
be further optimized in high pollutant loads to upscale it to industrial levels.

FACTORS AFFECTING MICROALGAL GROWTH

Microalgae cultivation requires various environmental conditions and biotic components such as temperature, light, pH, and nutrients for their optimum growth. The cultures require various nutrients, trace elements, vitamins, and growth regulators to grow. Redfield ratio suggested that the cultivation media could be flexible and adapted to microalgal metabolic needs and specific environmental conditions (Arrigo, 2005). The initial density directly affects the algal growth, i.e., higher algal density leads to better growth and ultimately results in higher efficiency for nutrient removal. The effect of various factors is explained below.

Temperature
Temperature is an important factor controlling microalgal growth and various metabolic activities, photosynthesis, and carbon fixation. The temperature of the pond varies on both seasonal and diurnal scales which affect the algal photosynthesis and respiration rates. The greater microalgal productivity was produced when the water temperature was controlled constantly compared to uncontrolled temperatures in high rate algal pond systems (Slegers et al., 2013). In a recent study, it was found that the higher the temperature, the lower the Rubisco's affinity for carbon dioxide and eventually lower the carbon dioxide solubility in the media (Taziki et al., 2015). Henceforth, many species proliferate at the optimum temperature of 20-25°C

as above 35°C; their growth becomes lethal due to increased photorespiration. Conversely, thermophiles can be utilized to serve the purpose and to reduce the cooling cost. Algae can be classified based on the temperature ranges as psychrophiles, mesophiles, and thermophiles. For instance, thermophilic microalgae *Chlorogleopsis* sp. can grow at a maximum temperature of 50°C (Morales et al., 2018). It experimented that different microalgae cultured at different temperatures showed a decrease in the growth rate, biomass, and lipid accumulation with an increase in temperature (Chaisutyakorn et al., 2018). Another study reported high carbon dioxide fixation and lipid accumulation up to 50% at 10°C in low nutrient availability in psychrotolerant species *Acutodesmus obliquus* (Lee et al., 2019). *Galdieria sulphuraria* show thermophilic growth behavior up to 56°C (Selvaratnam et al., 2014) while *Chlorella sorokiniana* has high photoautotrophic growth rates up to 43°C (Varshney et al., 2018). Hence, the growth rate of algae can be determined by the high rate of photosynthesis, which depends on light intensity and temperature (Béchet et al., 2013).

Light
Light plays an important role in the growth of microalgae. In a study, the relationship between light intensity, photoperiod, and production of biomass of microalgae Ankistrodesmus falcatus has been studied. The highest biomass (224.64 mg L^{-1}) and biomass productivity (9.30 mg L^{-1} D^{-1}) was observed under a light intensity of 150 μmol m^{-2} s^{-1}, whereas the lowest biomass (183.48 mg L^{-1}) and biomass productivity (7.58 mg L^{-1} D^{-1}) was observed under the light intensity of 30 μmol m^{-2} s^{-1} (George et al., 2014). It was also reported that continuous light and 18 h dark cultures yielded lower biomass productivity. According to the literature, biomass production in

TABLE 4 | Microalgae biofilm system using different carrier material.

Microalgae	PBR type	Supporting material	Biomass productivity (mg L^{-1}D$^-$)	Ref.
C. vulgaris	Airlift-PBR	Fiber	15.9	Tao et al., 2017
C. vulgaris	Membrane PBR	Flexi-fiber bundles	72.0	Gao et al., 2015
C. vulgaris, Oscillatoria	Vertical ABR	Coral velvet	10.5-14.7	Zhang et al., 2018
S. obliquus	Parallel plate PBR	Polycarbonate sheet	1.9	Zamalloa et al., 2013
Mixed consortium	Membrane PBR	Nylon mesh	9.1	Mantzorou and Ververidis, 2019
Mixed consortium	RABR	PVC sheet	31000	Christenson and Sims, 2012

many microalgae increased under high light conditions which generally causes an increase in reproduction until the saturation point intensity (Danesi et al., 2004). The wastewater quality directly affects the availability of light present in the culture medium. When at the beginning of the growth cycle, the light reaches a higher number of cells as the cell densities are low whereas at a higher density, the cells suffer from self-shading and sometimes the dissolved organic matters decrease the light availability to the culture for its growth (Novoveská et al., 2016). In a study, it was reported that three different types of lights red, blue, and white were studied on the algal species derived from the wastewater and the light spectrum influenced the cell size (Izadpanah et al., 2018). Light intensity directly affects the microalgal growth and the growth rate is directly proportional to Photon Flux density, but at the point of light saturation, the photon flux density is too high, which can lead to photoinhibition and photo-oxidation and ultimately the death of the cells (Bartosh and Banks, 2007). In a study, it was reported that the 19.4% of lipid content was increased when the amount of light intensity of 2700 Lux is provided to the culture (Rai et al., 2015). Microalgae can utilize the energy available in the wavelength range of 400–700 nm, which is referred to as photosynthetically active radiation (PAR) (Boyle, 2004). The optimum light intensity should be standardized for each species for maximum carbon dioxide assimilation and minimum photorespiration and photoinhibition. *Scenedesmus almeriensis* requires a light intensity of 100 μmol m^{-2} s^{-1} irradiance (Costache et al., 2013) whereas *Scenedesmus obtusiusculus* shows optimum growth at irradiation of 300 μmol m^{-2} s^{-1} irradiance (Cabello et al., 2015). The phenomenon of photoinhibition can be minimized by the usage of Light Emitting Diode lights instead of fluorescent tubes due to high electrical energy conversion efficiency, sufficient light intensity, and small volume and weight characteristics, and also decreased proton loss (Lee and Palsson, 1994). The optimum light intensity should be supplied to both sides of culture, i.e., material and watersides. The antioxidants present in microalgae can help in dealing with an excess of light and its effects.

Nutrients

The essential nutrients required for the optimum growth of algae include carbon, nitrogen, phosphorous, vitamins, and trace elements. The nutrient removal from wastewater by microalgae reduces the environmental impact of its discharge. Carbon is the essential nutrient for growth and is utilized by microalgae by the Calvin cycle. According to heterotrophic or mix-trophic

metabolism, many species can grow on an organic substrate. The main organic compounds are monosaccharides, volatile fatty acids, glycerol, and urea utilized for growth. Organic carbon uptake into the cells occurs through diffusion, active transportation, and phosphorylation. A high concentration of carbon dioxide is required for the growth of microalgae *C. vulgaris*. The carbon dioxide fixation rate of *C. vulgaris* is 252 mg L^{-1}D^{-1} and 86.7% of biomass was produced as shown in the investigation report (Bittencourt, 2009). *C. vulgaris* can uptake nitrogen, carbon dioxide, or phosphorous for its optimum growth (Gilles et al., 2008).

Nitrogen is required for the formation of genetic material, i.e., deoxyribonucleic acid and ribonucleic acid. It can be utilized in the form of nitrates, nitrites, urea, and ammonia. Removal of NH$_4^+$ is especially important as it is the more toxic form of nitrogen in wastewater. An increase in nitrogen available in the wastewater results in more uptake of nitrogen which leads to the production of more vital components for cellular activity further contributing to a greater amount of nitrogen being transported and assimilated by the cells (Kube et al., 2018). It is observed that *C. vulgaris* efficiently utilized and removed the high concentration of both nitrate and nitrite from the culture medium and simultaneously produces algal biomass for several wastewater treatments (Taziki et al., 2015). The other nutrients required are phosphorous, magnesium, iron, and calcium in trace amounts. Phosphorous is also utilized by microalgae for metabolic processes and several components such as nucleic acids and phospholipids. The uptake mechanisms as well as the use of phosphorous in algal cells depend on its concentration present in the wastewater (Solovchenko et al., 2016). The carbon assimilation is influenced by the phosphorous content present in the wastewater (Hu and Zhou, 2010), and wastewater carbon content has an impact on both nitrogen and phosphorous removal. The dissolved carbon dioxide is the most usable form of inorganic carbon for algae which leads to the maximum yield of algal biomass. For the nutrient removal and improvising algal growth, carbon dioxide is supplied to overcome low concentration of carbon in wastewater and reduces greenhouse gas emission by capturing carbon dioxide (Razzak et al., 2013). The pH also plays an important role in the optimum growth of algae. The maximum growth can be observed at optimum pH ranges from 7.9 to 8.3 (marine water), and 6.0 to 8.0 (freshwater). Most microalgae species are pH sensitive, and few of them can reach the range tolerated by *C. vulgaris* (Raize et al., 2004). In a closed system, the pH can increase up to pH 10. This rising pH value can be controlled by the

amount of carbon dioxide or using inorganic or organic acids (Lam and Lee, 2012). Combustion of flue gas with high carbon dioxide concentrations can decrease the pH to 5, but, at higher acidic pH, the photosynthetic growth is limited. The pH value is affected by a decrease in metabolites and the release of several organic acids. The excess of OH reacts with CO_2 to form HCO^{3-}, resulting in a higher bicarbonate and carbonate alkalinity and higher total carbon availability. In wastewater treatment using algae, the pH rapidly increases and then remains at a relatively constant value (Kube et al., 2018). If wastewater is rich in NH_4, a higher pH with less CO_2 addition may promote volatilization, and if wastewater has a higher NO_3^- concentration a lower pH with more CO_2 addition may encourage growth and improve nitrogen assimilation (Sutherland et al., 2015). High pH stress inhibits the cell cycle and triggers lipid accumulation (Vuppaladadiyam et al., 2018). Nutrients play an important role in the growth and productivity of microalgae such as iron, calcium, cobalt, manganese, zinc, molybdenum are vital for the growth of microalgae *Dunaliella tertiolecta*. The production of lipid in *D. tertiolecta* is increased when the culture was starved for nitrogen. For the production of oils and biofuels, it is economical to starve the culture for nitrogen content and will shorten production cycles and the waste content produced (Chen et al., 2011). Micronutrients such as iron, manganese are required in small amounts (2.5–30 ppm) and trace elements, such as cobalt, zinc, and molybdenum, are essential in very low concentrations (2.5–4.5 ppm) for efficient growth of microalgae. Micronutrients play an important role in algal metabolic functions such as coenzymes or energy carriers (Juneja et al., 2013). The high concentration of cobalt was previously considered toxic for algal species, but a controlled level of cobalt provided optimal lipid accumulation in *T. suecica* (Ghafari et al., 2016). The cobalt is mainly required for the synthesis of vitamin B12 (Li et al., 2007). Molybdenum in low concentration is optimal for *Bacillus sudeticus*, with 8% increase in lipid content; however, a high concentration showed improved lipid contents in *C. vulgaris* and *T. suecica* by 20% and 13% increases, respectively (Ghafari et al., 2016). Molybdenum is required for the assimilation of nitrates (Raven, 1988). Hence, it can be concluded that both macro and micronutrients are important for algal growth.

HARVESTING OF ALGAE

The production of microalgae biomass during wastewater treatment is considered as economic viability for algae-based product production. Microalgae-based wastewater treatment technology faces many challenges and microalgae harvesting is one of the major constraints due to the substantial cost and energy involved in these steps. Methods like centrifugation, flocculation, sedimentation, filtration, etc. have been reported to harvest biomass.

Chemical Flocculation
Flocculation is the process where microalgae are caused to clump together into a floc using various chemicals such as alum, or ferric chloride, etc. The critical factors of this process

are cellular concentration, surface properties, net charge, and hydrophobicity, the concentration of the coagulant/flocculent species, pH, and ionic strength of the broth process (Papazi et al., 2010). The coagulation involves pH adjustment or electrolyte addition. The various biomass of microalgae recovered by flocculation includes *C. vulgaris* using Nano-aminoclays (Mg-APTES) as a coagulant (Farooq et al., 2013) whereas *Chlorella minutissima* is harvested by use of $Fe_2(SO_4)_3$ as a coagulant (Papazi et al., 2010). *C. vulgaris* by auto flocculation can produce a recovery rate of 98% by using $CaOH_2$ (Vandamme et al., 2012). In a recent study, the effect of pH variations and addition of flocculant such as calcium chloride on the harvesting of microalgae *Arthrospira maxima* was studied and observed that pH > 10 and $CaCl_2$ 0.2–2.0 gL^{-1} at a 1:30 ratio (v/v) of $CaCl_2$/microalgae culture could be applied to harvest biomass efficiently (Caetano et al., 2020).

There are different ways to induce flocculation namely - (i) electrostatic patch, (ii) bridging, and (iii) sweep flocculation (Vandamme et al., 2013). Chemical coagulation/flocculation should - (i) result in no biomass contamination; (ii) lead to subsequent high-efficiency biomass settling; (iii) allow the reuse of the culture medium; (iv) environmental impact; and (v) cost-effective and non-toxic when applied in large scale (Molina Grima et al., 2003). The more electronegative the ion, the faster the coagulation (under 24 h) (Papazi et al., 2010). The negative charge is present on the surface of microalgae and The microalgae biomass can be contaminated by the used metals, declining its application in biofuel or animal feedstock. Coagulant addition (<10-fold) is required by the higher density cultures due to less charge on the surface of the cell wall leading to higher collision rates (Schlesinger et al., 2012). Chemical harvesting is an economical approach for the harvesting of microalgae from wastewater (Mohd Udaiyappan et al., 2017). The chemical flocculation method can be applied to large culture volumes without disrupting the cellular structure. The major disadvantage of this method is the presence of harmful chemicals that pose environmental risks.

Mechanical Methods
The most rapid and reliable method for harvesting algae is centrifugation and the algal biomass is separated based on density differences using centrifugal forces. A nozzle type disc centrifuges are suitable for all microalgae types as they are easily cleaned and sterilized, but the high investment and operating costs are their limitations. For harvesting filamentous algae, low-cost filtration methods are used. The strains grown in a high-rate algae pond system are selected, and filamentous algae are harvested by micro screening to retain larger cells, and smaller non-filamentous algae are washed away. For smaller suspended algae, tangential flow filtration is considered, but membrane fouling and replacement are not cost-effective (Uduman et al., 2010), and power requirements are high (Danquah et al., 2009). Use of membrane-based harvesting method has been reported for the recovery of *Scenedesmus almeriensis* biomass using polyvinylidene fluoride (PVDF) membrane which helps in separation by retaining biomass and growth media is passed through the membrane filter (Marino et al., 2019). Sedimentation

is a low-cost harvesting method that can give concentrations of 1.5% solids (Danquah et al., 2009). Sedimentation is a slower process as settling rates of 0.1–2.6 cm h^{-1}, and during the settling time, much of the biomass deteriorates (Greenwell et al., 2009). The various comparison of harvesting methods is depicted in **Table 5**, which explains their major benefits and limitations. In algae rich waters, dissolved air flotation is usually preferred over sedimentation methods (Teixeira and Rosa, 2006). Dissolved air flotation is a method commonly used in wastewater treatment sludge removal, i.e., for large scale setups but flocculants can cause a problem during downstream processing of algae (Greenwell et al., 2009). It was studied that pH-modulated dissolved air floatation harvesting method having optimized parameters such as pH, velocity gradient, mixing time, and floatation to harvest *Chlorella sorokiniana* from wastewater (de Leite et al., 2020). The major limitation of the mechanical method is the increased operational costs for algal production and is economically feasible only when a higher number of value-added products are produced (Park et al., 2011).

Biological Methods

Bio-flocculation is an environmentally friendly technique to harvest microalgae which involves cell aggregation using different microorganisms (bacteria, filamentous fungi) and autoflocculating microalgae. Use of microalgae-bacteria flocs in wastewater treatment results in increased microalgae recovery with a settling rate of 0.28-0.42 m h^{-1} (de Godos et al., 2014). The use of polymeric material produced by various microbes was also reported for the harvesting of microalgae. Ndikubwimana et al. (2016) studied pilot-scale bioflocculation of *Desmodesmus brasiliensis* using bioflocculant γ-PGA produced by *Bacillus* licheniformis CGMCC 2876 and reported flocculation efficiency >98%. Choi et al. (2020) evaluated the potential of activated sludge derived extracellular polymeric substance (ASD-EPS) for microalgae harvesting (*C. vulgaris*, *Chlamydomonas asymmetrica*, and *Scenedesmus* sp.) and *C. vulgaris* showed the highest bioflocculation efficiency. Microalgae flocculation is also achieved by using naturally available ions in brackish water, and a variety of precipitating ions, including Mg^{2+}, Ca^{2+} can lead to auto flocculation of microalgae (Smith and Davis, 2012). A new process of pelletized cell cultivation was reported by Zhang et al., using coculture of filamentous fungal species with microalgae. Microalgae cells co-pelletized into fungal pellets and due to their large size, these can be easily harvested through a sieve (Zhang and Hu, 2012). For microalgae harvesting and wastewater treatment, microalgal bacterial flocs is a promising technology. In a study, it was reported that bioflocs formation enhances

harvesting of *C. vulgaris* and removal of nutrients from seafood wastewater effluent (Nguyen et al., 2019b).

Reviewing all the reported harvesting techniques and emerging studies it seems none of the technology seems economically and ecologically viable at a large scale. Therefore, the development of a cost-effective, efficient, and eco-friendly harvesting process will continue to be a hot area of research.

BIOFUEL PRODUCTION

In the coming decades, the world will require a vast amount of energy to support population and economic growth and to improve living standards. To protect the environment and meet increasing energy demand, renewable sources of energy need to be adopted (Bhatia et al., 2019b; Patel et al., 2020a,b,c). Due to rapid industrialization and subsequent improper waste handling, water pollution is increasing daily, especially in the Indian major cities, which has an incredibly harmful impact on human health and the environment (Bhatia R. K. et al., 2020). A biofuel is a fuel produced through contemporary biological processes such as dark-photo-fermentation, anaerobic digestion, and methanotrophs-based biotransformation of greenhouse gasses, etc. rather than geological processes involved in forming fossil fuels (Bindra et al., 2017; Patel et al., 2020d,e,f; Kumar et al., 2021). Microalgal biomass can be utilized to produce various types of biofuels including biodiesel, bioelectricity, biohydrogen, etc.

Biodiesel

Biodiesels are fatty acid methyl esters produced through the transesterification of oils with alcohols in the presence of catalysts (Bhatia S. K. et al., 2020). Microalgae can accumulate lipids that can be used as feedstock for biodiesel production (Anwar et al., 2017; Otari et al., 2020). The main steps in biodiesel production from microalgal biomass involve microalgae cultivation, drying of algal biomass, extraction of oil from algal biomass, and transesterification to fatty acid methyl esters (Bindra et al., 2017). Various methods are used to extract lipids from micro-algae such as mechanical extraction, solvent extraction, ultrasonic extraction, supercritical extraction, and enzymatic extraction. Transesterification is the process of conversion of oil to biodiesel (Demirbas, 2007). It involves reactions between triglycerides or fatty acids and alcohol in the presence of catalysts. Different alcohols such as methanol, ethanol, propanol, butanol, and amyl alcohols can be used in transesterification. However, methanol and ethanol are more commonly used in commercialized processes due to their low cost and physical and chemical advantage (Bhatia et al.,

TABLE 5 | Comparison of mechanical harvesting methods for algae (Adapted from Teixeira and Rosa, 2006; Greenwell et al., 2009; Uduman et al., 2010).

Method	Solid concentration after harvesting (%)	Recovery (%)	Scale	Major benefits	Major limitations
Centrifugation	12-22	>90	Bench	Reliable, high solid concentration	Energy intensive, high cost
Tangential filtration	5-27	70-90	Bench	Reliable, high solid concentration	Membrane fouling, high cost
Gravity sedimentation	0.5-3	10-90	Pilot	Low cost	Slow, unreliable
Dissolved air floatation	3-6	50-90	Pilot	Proven at large scale	Flocculants required

2015b; Patel et al., 2019). Various homogenous (acid or base) or heterogeneous catalysts (metallic nanoparticles) or enzymes (lipase) are used to carry transesterification reactions (Kumar et al., 2019; Otari et al., 2019).

Various methods of transesterification (supercritical, BIOX cosolvent) and bioreactor designs. (microtubular microreactors, membrane microreactors, microchannel reactors, microwave reactors, reactive distillation, and centrifugal contractor) have been reported for the conversion of oils into biodiesel (Bhatia et al., 2021a). In a recent study, it was found that microalgae *Chlamydomonas reinhardtii* produces 505 mg L^{-1} of biofuel from municipal waste (Kong et al., 2010). In a study, it was reported that in an effluent wastewater treatment plant under a continuous supply of carbon dioxide, *C. vulgaris* removed a higher concentration of phosphorous (Liu et al., 2020). Nanoparticles incorporation with microalgae is a new promising technology used for the high yield of biodiesel formation. According to the previous studies, a minimal amount of colloidal hydrous iron (III) oxide particles boosted almost 100% microalgae cell suspension; magnetic particles incorporated with aluminum sulfate were beneficial for cell separation from the mixed culture of *Anabaena* and *Aphanizomenon* microalgae species (Pattarkine and Pattarkine, 2012). The silver nano-particles applied on *Chlamydomonas reinhardtii*, and *Cyanothece* 51142 microalgae harvesting increased 30% higher biomass productivity, whereas calcium-oxide nano-particles increased the biodiesel conversion yield up to 91% via catalytic transesterification (Torkamani et al., 2010; Safarik et al., 2016).

The glycerol is produced as a by-product and is denser than biodiesel, which is continuously removed to increase biodiesel yield or used as feed to produce biohydrogen (Bindra et al., 2017; Prakash et al., 2018). Solvents are separated from methyl ester by evaporation. The efficacy of the produced biodiesel depends on the content of free fatty acids and the composition of the oil. Properties of produced biodiesel depend on, carbon-chain length, branching, and degree of unsaturation which affects the physicochemical properties of the biodiesel (cetane number, oxidation stability, iodine value, cold flow properties, density, and kinematic viscosity) (Bhatia et al., 2021a). For the use of transesterification, the biomass-derived heterogeneous catalysts produce 95% biodiesel yield and are cost-effective and eco-friendly. After the transesterification, the separation of produced biodiesel from catalysts, excess of alcohol, glycerol, and the remaining oil are important to ensure higher performance, protection of the engine, and to maintain the quality standards (Bindra and Kulshrestha, 2019). The wastewater from the food and beverage industries is suitable for the growth of microalgae as it has a low concentration of toxic chemicals and heavy metals (Bhatia S. K. et al., 2020). In a study, it was found that livestock waste contains a large amount of nitrogen and phosphorous which leads to an increase in the carbohydrate content of biomass and a decrease in lipids (Choudhary et al., 2020).

Biohydrogen

Hydrogen is the clean and more reliable energy alternative for non-renewable fossil fuels due to the high calorific value of $\sim$122 kJ g^{-1} and water molecule produced as end byproduct of their combustion (Patel et al., 2012, 2015; Bhatia et al., 2021b). Biohydrogen production from third-generation feedstock (microalgae) is the most sustainable and biorefinery approach towards energy crises and can be further improved using metabolic engineering (Kumar et al., 2020). Microalgal biomass harvested from wastewater treatment can produce biohydrogen via different methods like direct and indirect photolysis of water and dark fermentation, yielding various volatile fatty acids along with hydrogen production (Mishra et al., 2019; Rajesh Banu et al., 2021). Many factors affect the hydrogen production rate, namely, carbon and nitrogen sources and their relative ratios, pH, temperature, light/dark cycles, microalgal strain, culture set-up and, pre-treatment employed (Prabakar et al., 2018). Many microalgae species like *Chlorella*, *Scenedesmus*, and *Saccharina* are extensively used for biohydrogen production (Wang and Yin, 2018). Microalgae *Scenedesmus obliquus* showed 56.8 mL H_2 g^{-1vs} yield in urban wastewater (Batista et al., 2015). Another study revealed high biohydrogen production (204 mL H_2 L^-day^-) in the immobilized culture of *Scenedesmus obliquus* under manipulated light conditions at 140 μE $m^{-2}s^{-1}$ of light intensity, 30°C and 7.5 pH with sulfur deprivation. Blue light elicits large algal biomass production in urban wastewater setup while purple light induces high biohydrogen yield (Ruiz-Marin et al., 2020). However, the low yield is a major challenge due to the oxygen sensitivity of enzyme, light, and CO_2 fixation efficiency in the commercial setup. To deal with the O_2-sensitivity issue, a study showed the significance of the addition of VFA (volatile fatty acid) in synthetic wastewater and pertaining to O_2-deprivation. The study resulted in a significant increase in biohydrogen yield (65.4 $\pm$ 0.3 μmol H_2 L^{-1} mM^{-1} acetate) in *C. vulgaris* culture grown in PBR (Hwang et al., 2018). Recent studies focused on improving the economy of the process through genetic engineering and deploying low-cost photoreactors (Sharma and Arya, 2017; Sharma et al., 2018; Schiano et al., 2019).

Microalgae-Microbial Fuel Cell (MMFC)

The production of electrons to the metabolism of microorganisms produces bioelectricity (Gurav et al., 2019). The microbial fuel cell is used to produce electricity from the hydrolysis and fermentation of algae. Microorganisms in microbial fuel cell biodegrade organic compounds into carbon dioxide, water, and energy through various metabolic pathways (Kondaveeti et al., 2019a; Bhatia et al., 2021c). The significant components of microbial fuel cells include an anode and cathode connected by a load. In the microorganism's culture, the anode acts as a catalyst for decomposing the organic matter and produce electrons and protons (He and Angenent, 2006). In a microbial fuel cell, the production of electrons leads to carbon dioxide produced at the cathode which is utilized by microalgae for its growth and production of biomass. In MMFC, the microorganisms biodegrade the organic components into carbon dioxide, water, and energy by various metabolic cycles (Bhatia S. K. et al., 2020). Microbial fuel cells can simultaneously produce biofuel and bioelectricity and treat waste. The **Figure 2** describes the production of bioelectricity in two-chambered microbial fuel cell using microalgae. Recent studies suggest that

FIGURE 2 | Schematic production of bioelectricity by microalgae in two-chambered MFC.
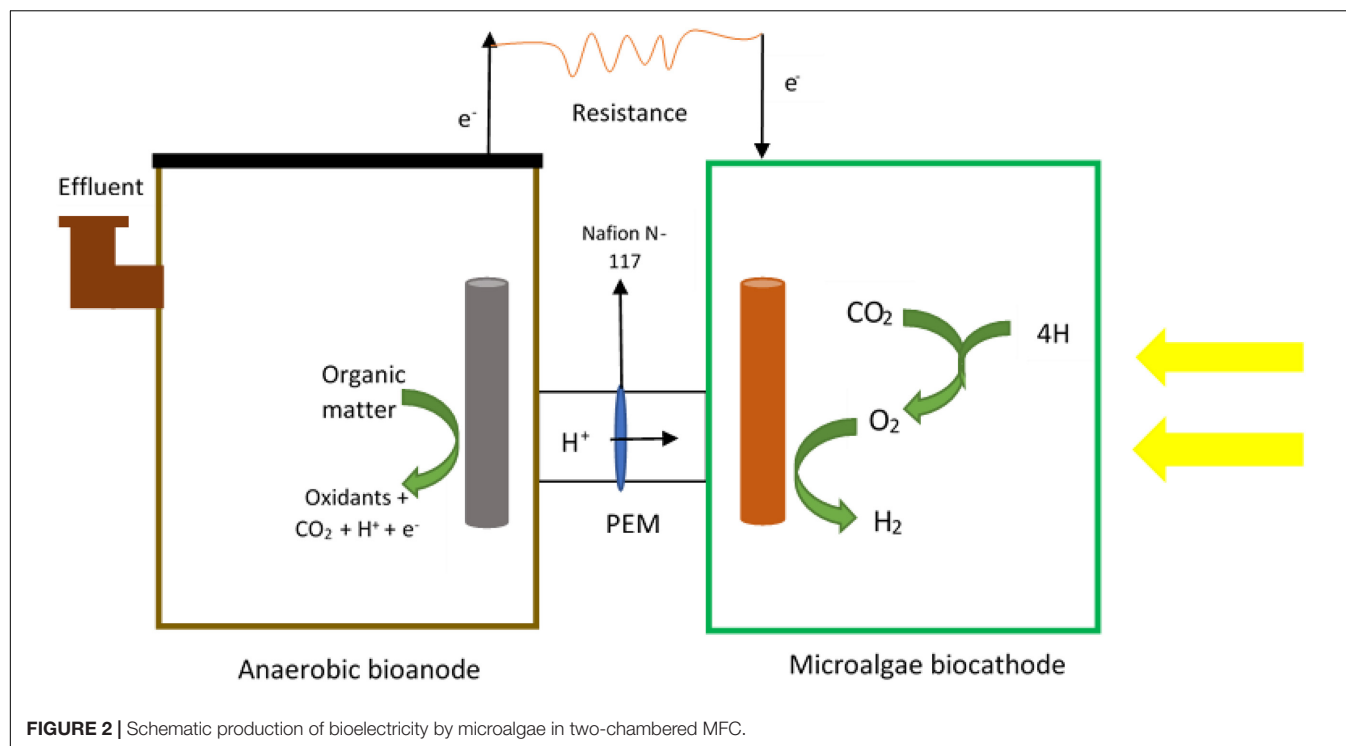
the *C. vulgaris* strain is efficient in producing bioelectricity as it contains more than 50% proteins (Becker, 2007). The microbial fuel cell chambers are constructed of glass, polycarbonate, and plexiglass (Rhoads et al., 2005). The anode is made up of materials such as carbon paper, graphite (Zhang et al., 2011), platinum and consists of organic substrates to be utilized for the production of electrons by microbes. The different types of microbial fuel cells are – (i) single-chamber MFC, (ii) two-chamber microbial fuel cell, and (iii) stacked microbial fuel cell (Kondaveeti et al., 2019a,b). A recent study reported 44,33 mWm^{-2} electricity production from tapioca wastewater via microbial fuel cell (Costa and Hadiyanto, 2018). In a recent study, it was reported that *Chlamydomonas* sp. TRC-1 produced for textile wastewater treatment produced biomass which further produced bioelectricity and produced power of 1.83 m^{-2} (Behl et al., 2020).

OTHER VALUE-ADDED PRODUCT PRODUCTION

Microalgae are emerging to be one of the most promising long-term, sustainable sources of biomass and oils. Rapid growing and high lipid-content algae are selected for diverse applications in many sectors for the production of biofertilizers, biopolymers, and exopolysaccharides, etc.

Bioplastic

The increase in the production of plastic leads to environmental pollution (Bhatia et al., 2021e). The conventional plastic used is made up of petrol-based oils and cannot be disintegrated by

microbes. Mostly these plastics are disposed of by using landfill, and incineration methods. In 2015, approximately 6300 Mt of plastic waste had been generated, around 9% of which had been recycled, 12% was incinerated, and 79% was accumulated in landfills or the natural environment and if the production and waste management trends continue at the same rate then roughly 12,000 Mt of plastic waste will be in landfills or in the natural environment by 2050 (Geyer et al., 2017). Incineration leads to the release of noxious harmful toxins into the environment (Zhang et al., 2003; Zeller et al., 2013). Therefore, bioplastic is the only alternative (**Figure 3**). It is a biodegradable material produced from biological sources like bacteria, microalgae, yeast, and transgenic plants (Park et al., 2020). Bio-derived plastics are of many types like polyhydroxyalkanoates, polylactic acid, starch, carbohydrate, and protein-based plastics (Bhatia et al., 2016). There are mainly three different methods for the production of bioplastics which include, (i) polymers extracted from biomass, (ii) polymers produced by microorganisms, (iii) polymers synthesized by bio-derivatives.

Various microalgae strains are cultivated for polyhydroxyalkanoates production and accumulation of polyhydroxyalkanoates occurs under specific culture conditions. Study have found that the microalgae *Spirulina platensis* produces 10% (dry cell weight) of polyhydroxyalkanoates under specific growth conditions of acetate and carbon dioxide in the medium (Laycock et al., 2013). The genetically engineered microalgal strains can be used in the future, by using clustered regularly interspaced short palindromic repeats clustered regularly interspaced short palindromic repeats and Cas9 (an RNA-guided cleaving enzyme) cloning systems for producing the increased amount of polyhydroxyalkanoates (Sternberg and
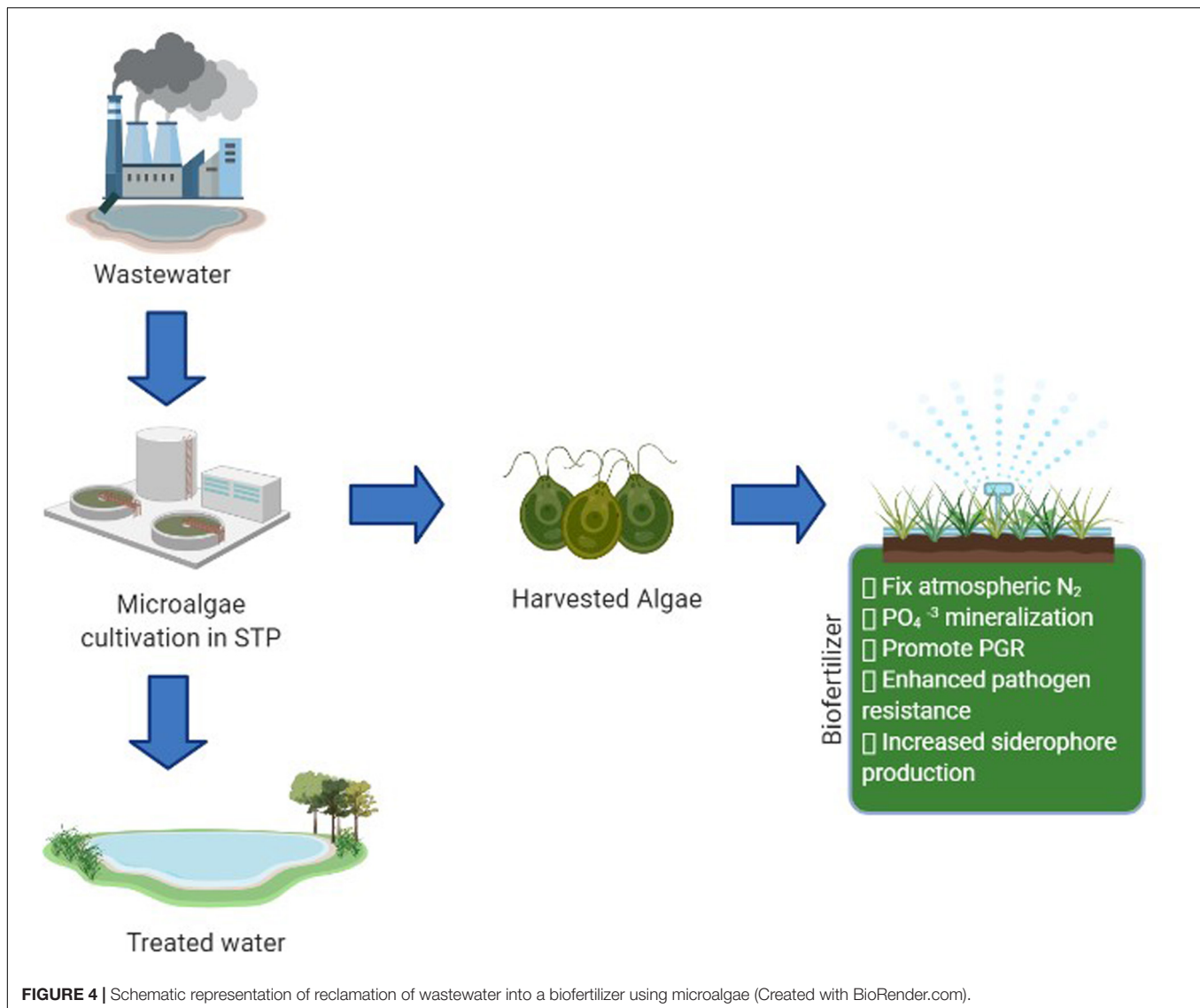
FIGURE 3 | Steps for extraction of PHA.
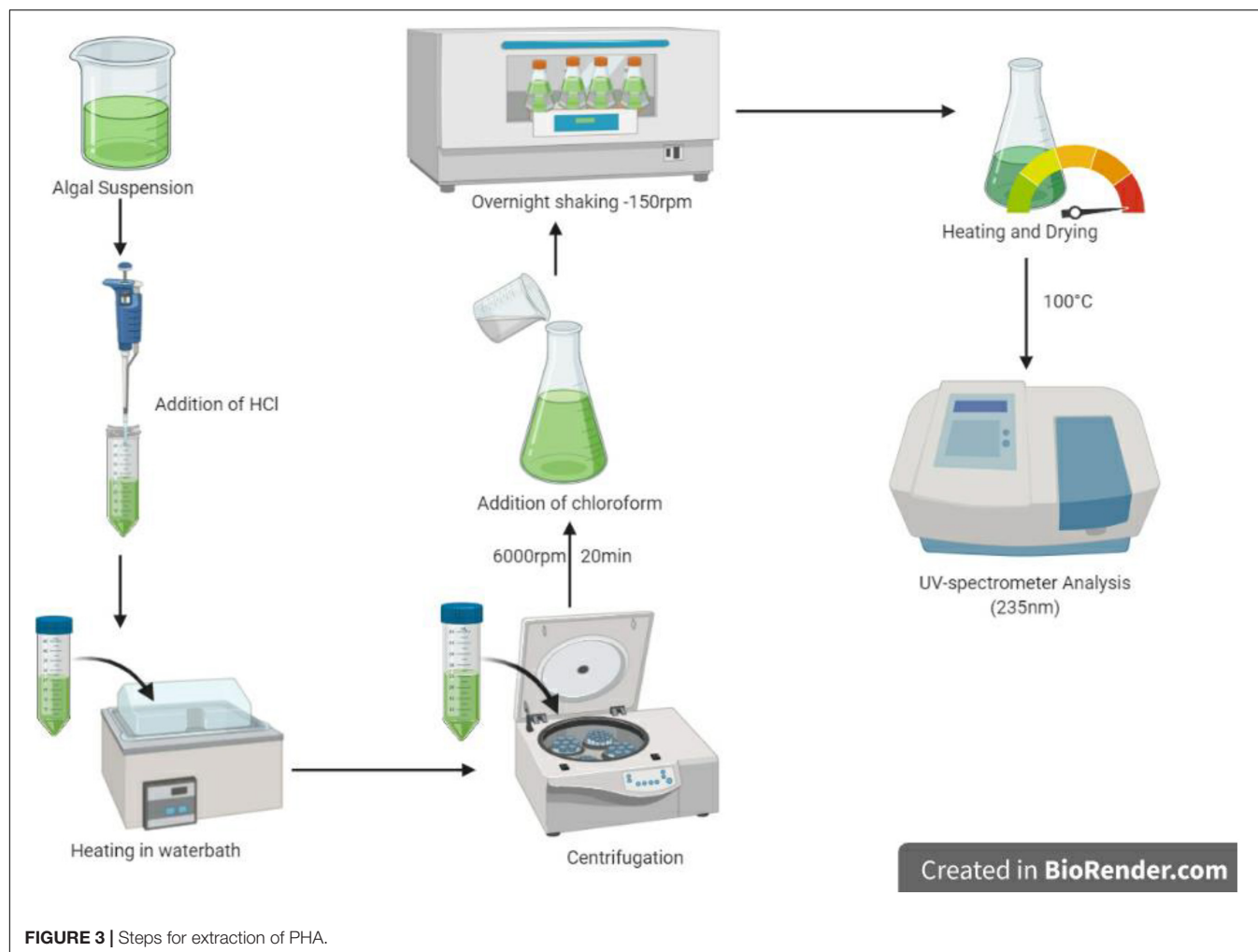
Doudna, 2015). In a recent study, the microalgae were harvested from the effluent of wastewater treatment plant and created a liquid medium for the growth of recombinant *E.coli* for the production of polyhydroxybutyrate (Rahman et al., 2015). The pathway engineering in baker's yeast *Saccharomyces cerevisiae* and then transferring the assembled pathway in the nucleus of *C. reinhardtii* (Noor-Mohammadi et al., 2014). *Microcystis* sp. produces 0.7 mg L^{-1} yield polyhydroxybutyrate product (Abdo and Ali, 2019).

Polyhydroxyalkanoates films are used to pack urea fertilizers and insecticides, which decomposes efficiently by the soil microbes used in the agricultural land (Singh et al., 2009; Aguilar and San Román, 2014). Polyhydroxyalkanoates is also used as scaffolds, bone plates, media for the slow release of drugs, and surgical sutures in the medical industry (Bhatia et al., 2019c). Polyhydroxyalkanoates have been used in bone renewal treatments and nerve injury due to their piezoelectric nature (Misra et al., 2006). A blending of polyhydroxyalkanoates with inorganic phases results in bioactive composites of higher properties that can be used in tissue engineering applications (Chen, 2009). Despite its imperative applications, there are few constraints like slow growth of algae, costly harvesting,

extraction, and downstream processing steps which took a great toll on the global market demands of bioplastics. Due to this, many scientists are moving towards genetic engineering tools to circumvent the price barrier.

Biofertilizer

Biofertilizers are composite substances with live or latent microorganisms that colonize the rhizosphere of plants, fix atmospheric nitrogen, aid in nutrient availability of plants, phosphate solubilization, and harness the soil's fertility for healthy crop production. These natural composites can rejuvenate the nutrient balance in soil deteriorated by overusing harmful chemical fertilizers, pesticides, and weedicides and catalyzes the decomposition kinetics of organic matter present in the soil. Moreover, algae are widely utilized for soil conditioning and integrated plant nutrition systems since they can recover excess nutrients from wastewater during cultivation and reclaim water for other uses (Han et al., 2019). The production of biofertilizers by microalgae when wastewater acts as a substrate for optimum growth and production is depicted in **Figure 4**. Among the various types of algal species studied, cyanobacteria are the simplest and one of the most efficient because it

FIGURE 4 | Schematic representation of reclamation of wastewater into a biofertilizer using microalgae (Created with BioRender.com).

has a high water-holding capacity, ability to fix atmospheric nitrogen, short generation time, and ability to withstand extreme environments (Singh et al., 2016). According to the study on N^{15}-labeled fertilizer, cyanobacteria assimilate more nitrogen than chemical fertilizer and are more reliable for rice plant cultivation (Fernández Valiente et al., 2000). Another exciting research on immobilized *Chlorella pyrenoidosa* on dairy waste effluent as a biofertilizer gives a 30% surge in paddy root and shoots length (Yadavalli and Heggers, 2013). A study also found a yield of 650 mg L^{-1} of *Chlorella* sp. biomass growing in municipal waste as a biofertilizer (Das et al., 2019).

Microalgae are also found to stimulate plant growth by producing essential plant growth promoters with plant-microbe symbiosis. Many studies are performed to validate the presence of extracellular products with growth regulators like activity in plants that aid in early germination. One such study on *Lupinus termis* grown in a consortium of cyanobacteria and bacteria revealed plant growth stimulating substances and

showed improved germination compared to seeds untreated or treated with hormones like indole acetic acid, gibberellic acid, and cytokines (Win et al., 2018). Algae stimulate the production of siderophore, i.e., high-affinity Fe-chelating compounds secreted by bacteria by producing organic acids that photolyzes these siderophores and thereby triggers iron assimilation in very low iron and nitrogen conditions chiefly in the waterlogged or aquatic environment. A recent study valorized the freshwater microalgae *Navicula pelliculosa* induced siderophore biosynthesis in the bacterium *Cupriavidus necator* H16 (Kurth et al., 2019). Another experiment that cultivated microalgae in black water (toilet wastewater) concluded that microalgae biofertilizer works similar to inorganic fertilizer but emits more N_2O and CO_2 due to nitrification pathways. These increased emissions could be non-sustainable and need to be maintained (Suleiman et al., 2020). Despite the surfeit of advantages of microalgae-based biofertilizers, some bottlenecks of this technology hinder mass production. The primary constraints include the short shelf-life

of cyanobacteria and the possible dangers of toxification of algae due to the outpouring of chemical pesticides, herbicides, and weedicides in cropland press a severe concern (Renuka et al., 2018). Shelf-life can be augmented to a certain extent by selecting translucent packing material, dry mixing, etc. (Jha and Prasad, 2006). Apart from this, light and temperature sensitivity also hurt a viable population count in storage conditions. Therefore, further research should be encouraged to prevail over these limitations and promote the integrated carbon-neutral, zero-waste biorefinery approach.

Exopolysaccharides

Industries have currently shifted their focus from polysaccharide inside the cell to exopolysaccharide, loosely attached to the cell wall surface (cell-bound exopolysaccharides) like sheaths, slime, and capsules or is secreted outside the cell to build a matrix as protection (Bhatia et al., 2015a; Sathiyanarayanan et al., 2015). It has gained much attention due to its facile extraction and isolation process from the media; it will prove to be an economical alternative and also saves a lot of time and energy. Exopolysaccharides are high-value compounds obtained from algal secretions with remarkable therapeutic properties associated with the compound's conformations and molecular weight (Sathiyanarayanan et al., 2016). They are known to possess immunomodulatory, anticoagulant, antimutagenic, antibacterial, radioprotective, anticancer, antiulcer, and anti-inflammatory bioactivities (Bhatia et al., 2021b). Cyanobacteria and red algae are the chief producers of exopolysaccharides mucilages mainly to adapt to stress conditions like physio-chemical changes in the environment. The composition of exopolysaccharides varies from species to species and is conspicuously dependent upon culture conditions. Golgi apparatus and cytoplasm are the leading site for the formation of these exopolysaccharide molecules in microalgae and cyanobacteria, respectively. Exopolysaccharides prime sugar component includes glucose, fructose, galactose, xylose, arabinose, rhamnose, mannose, and fucose. Salt stress in halotolerant microalgae *D. salina* induces the release of a complex mixture of polyelectrolytes and polysaccharide content as a survival strategy (Mishra and Jha, 2009). Apart from the concentration of nitrogen, phosphorus, sulfates, temperature, pH, and intensity of the light also significantly impact the yield. In a study on microalgae *Botryococcus braunii* strain CCALA 220 (race A), a yield of 2 mg L^{-1} was obtained at optimum conditions of 950 μmol m^{-2} s^{-1} of light intensity and 6 mM of nitrate (Cepák and Přibyl, 2018). Another study gives a yield of 140 mg L^{-1} of EPS with *Phaeodactylum tricornutum* grown in palm oil mill effluent (Nur et al., 2019).

Other rationales include cell-to-cell interactions, biofilm formation, and adhesion mainly because of polyanionic and polycationic compounds like N-acetylglucosamine and xanthan that impart these properties (Bhunia et al., 2018). Exopolysaccharides are usually negatively charged, i.e., exhibit anionic properties of the biopolymer. Indeed, it can immobilize positively charged metal ions with positive charges in the effluent from wastewater due to uronic acid and sulfate's presence on the surface (Freire-Nordi et al., 2005). The exopolysaccharides of *Chlorella stigmatophora* and *Anabaena spiroides* exhibit

the metal-complexing capacity against Zn^{2+} and Cd^{2+} and Cu^{2+}, Pb^{2+}, and Hg^{2+}, respectively (Freire-Nordi et al., 2005; Khangembam and Tiwari, 2016). This natural metal chelating property is very beneficial in biological water purification and to maintain ecological balance. Besides, the recent study has highlighted exopolysaccharides potentials as bio flocculant in freshwater *Cyanothece* sp. for the bioremediation of nano and microplastics from the waste streams and as a potential replacement of synthetic flocculants (Cunha et al., 2020). Many biochemical and rheological studies on exopolysaccharides can be expanded for mechanical and food engineering applications as drag-reducers in ships and thickening and gelling agents to increase food viscosity (Xiao and Zheng, 2016). A brief discussion about the major components of exopolysaccharides and their applications are depicted in **Table 6**.

Polysaccharides from *Gyrodinium impudicum* KG03 render excellent antiviral activity against encephalomyocarditis virus (Yim et al., 2003). Furthermore, strains like *Nostoc flagelliforme*, *Porphyridium cruentum*, and *Aphanothece sacrum* exhibit antibacterial and antiviral properties against *Salmonella enteritidis* and several viral species like Vaccinia virus, and African swine fever virus, etc. (Kanekiyo et al., 2005; Ngatu et al., 2012). *Rhodella reticulata, Chlamydomonas reinhardtii*, and *Arthrospira platensis* show impressive antioxidant and free radical scavenging pharmaceutical activities in a dose-dependent manner (Chen et al., 2010; Bafana, 2013; Pierucci et al., 2017). Moreover, *S. platensis* inhibits tumor invasion and metastasis by releasing sulfated polysaccharide calcium spinlan (El Baky et al., 2013). Microalgae-derived exopolysaccharides have enormous applications in biotechnological, food, pharmaceutical, and most importantly, in industrial wastewater treatment. This field is still in its infancy, and further studies and research are inevitable to disclose the understanding of complex structural and functional diversity and optimize exopolysaccharides yield with minimal cost further. Co-culturing and heterogeneity give good results with interspecies interactions and upsurge in exopolysaccharide production (Angelis et al., 2012). More research is required to scale-up this microalgae technology to exploit more lucrative resources supporting the biorefinery concept.

TECHNO-ECONOMIC ANALYSIS AND GLOBAL STATUS

Microalgae are utilized for wastewater treatment in many different ways all over the globe. New technologies are emerging with more efficient and feasible approaches to scale up from laboratory setup to industrial. Several industries have adopted phycoremediation to maintain their discharge standards and to perform well in corporate social responsibility. Besides, they gain huge profits by selling algae-based products like biofuel, feed, and fertilizer to the market. A study highlights the base case cost of about ~1.6 € kg^{-1} to 1.8 € kg^{-1}, and the projected case cost is p~0.3 € kg^{-1} to 0.4 € kg^{-1} for microalgae cultivation in the case of raceway pond while in the case of packed bed bioreactor, its ~9 € kg^{-1} to 10 € kg^{-1} and ~3.8 € kg^{-1} respectively (Slade and Bauen, 2013). Another research valorizes the use

Microalgae	Monosaccharide composition	Bioactivities and applications	Ref.
Chlamydomonas reinhardtii	Ara, Rha, Rib, Xyl, Gal, Glc	Antioxidant properties	Bafana, 2013
Anabeana sp.	Gal, Glc (+), Man, Xyl, Fuc	Bio flocculant	Khangembam and Tiwari, 2016
Gyrodinium impudicum	Gal	Anti-viral activity, immunostimulatory activity, bio flocculent	Yim et al., 2003
Dunaliella salina	Gal, Glc (+), Xyl, Fru	Plant growth bio stimulant	Mishra and Jha, 2009
Arthrospira platensis	Ara, Rha, Fuc, Xyl, Man, Gal, Glc	Antioxidant, cosmetics	Pierucci et al., 2017
Nostoc flagelliforme	Glu, Gal, GlcA Xyl, Man	Anti-viral activity, antithrombin activity	Kanekiyo et al., 2005
C. vulgaris	Glu, Xyl, GlcUA	Antimicrobial activity, bio stimulant, antioxidant activity	El-Naggar et al., 2020
Aphanothece sacrum	Glc, Fuc, GalA, Rha, GlcA, Gal, Man, Xyl	Anti-inflammatory, anti-allergic, adsorption of metal ions, liquid crystallization	Ngatu et al., 2012

of wastewater, and preferably blue light filter (480 nm) in the raceway system will significantly augment biomass production by 63% and 73%, respectively, i.e., decrease in cost from 2.71 to 0.73 \$ kg^{-1} (Kang et al., 2015). A techno-economic analysis estimates a \$2.23/gallon break-even selling price of biofuel with an 18.7% internal rate of returns if the cultivation, harvesting, and downstream cost are monitored. **Figure 5** depicts the annual cost spent and income/revenue generated by utilizing wastewater for microalgae cultivation and simultaneous bio-oil production via pyrolysis. Therefore, it is anticipated that wastewater-based microalgae biofuel can become a powerful competitor for the crude oil industry shortly (Xin et al., 2016).

Lately, Bath University has collaborated with Wessex Waters sewage treatment works to pioneer the new project to deploy algae for recovering the phosphorus load in the United Kingdom. About 80-96% of phosphorus is treated from 3000 liters of wastewater per day in an installed pilot-scale High-Rate Algal Pond setup, resulting in polished wastewater fit for environmental discharge (Algae farms to offer a cheaper, renewable solution to cleaning wastewater, 2020). This seems a suitable replacement for the traditional chemical dosing of wastewater with iron as it can also produce nutrient-rich biomass that can be used for other purposes like biofuel, and bioplastic. Another successful example is phycospectrum that has revolutionized phycoremediation all over India with collaborations with Colombia wastewater treatment plant. It also introduces algal technology in SNAP Products PVT LTD to purify the acidic and toxic effluents high in total dissolved solutes using the naturally occurring *Chroococcus turgidus*strain. A 1200 m^2 reinforced cement concrete tank was set up to treat 1200 KL of volume at a time with an AC sheet roof to prevent rainwater from mixing. Earlier, 290 tons of sludge deposits per annum were buried in the landfill, which now is rich in nutrients and can be commercialized as valuable fertilizer, generating additional revenue. The industry saves 50 lakh p.a. spent on caustic soda to neutralize the wastewater and three lakhs for sludge disposal (Internet Achive Wayback Mechine, 2020). Similarly, it served about 32 mega industries in India by applying algal technologies to treat the polluted effluent sustainably and producer-waste products (Hanumantha et al., 2011). Currently, the company works on reducing oil slicks in wastewater to <2% using algal

strain to transform sludge completely into a soil-like material with good water holding capacity (Sivasubramanian, 2020).

One recent project mainly meant to alleviate the toxic levels of wastewaters from the grassroots dyeing industry is Indus tiles. They are composed of clay material and are made into fan-shaped leaves with algae-laden venations. This cost-effective and reusable modular bioreactor wall system is designed by biochemical engineers in University College London using algae and hydrogel formulations for bioremediation of heavy metals and other pollutants from the wastewater disposed of by local artisans in India (The Indus Project, 2020). Phytochelatins produced by microalgae work as an adsorbent to capture the metals from the colored water and make it suitable for the environment. Another technology Algae wheel wastewater treatment process developed by One Water Inc. has virtually replaced the wetland system in Uniondale, New York, with an average daily flow of 22,300 gpd. This technology uses RAC^{TM}, which has a hybrid fixed-film rotator that integrates both algal biofilm and moving bed biofilm reactor systems for a significant reduction in pollutant loads (Johnson et al., 2018). Furthermore, an entirely similar approach by Gross-Wen Technologies that uses a vertical conveyer belt instead of a rotator is patented as the revolving algal biofilm treatment technology. A study on the revolving algal biofilm reactor obtained significant results showing 46% sulfates removing efficiency at the 0.56 g L^{-1}d^{-1} rate on the treatment of low pH drainage from a mining industry. Also, it manifests a substantial reduction in chemical oxygen demand, phosphorus, and ammonia concentration compared with suspended cultures (Zhou et al., 2018). The biomass can be scrapped of quickly and deployed as a slow-releasing fertilizer, bioplastic, or biofuel. The different value-added products from different algal biomass are cultivated under optimum conditions for their highest yield and products such as for the production of biofertilizers, *Chlorella* sp. gives a maximum yield of 650 mg L^{-1} from MMT effluent wastewater source (biofertilizer) whereas *Phaeodactylum* sp. when grown in palm oil mills (wastewater source) yields 140 mg L^{-1} of exopolysaccharides (Das et al., 2019; Nur et al., 2019). The biofuel produced from municipal wastewater effluent by *C. reinhardtii* (bio-oil) produces 505 mg L^{-1} under the optimum conditions (Kong et al., 2010). Another value-added product such as polyhydroxyalkanoates is used for the development of

A Total Project Cost ($/yr)

Legend:
- PBR
- Flocculation tank
- Centrifuge unit
- Land
- Greenhouse
- Pyrolysis
- Warehouse
- Field expenses
- Home Office and Construction fee
- Project contingency
- Other costs

Values: 1,21,093 | 1,54,999 | 6,05,463 | 4,03,642 | 54,102 | 9,15,378 | 4,34,367 | 31,038 | 51,102 | 25,551 | 25,55,101

B Operation Cost ($/yr)

Legend:
- Microalgae seeds
- Electricity for cultivation
- Electricity for centrifuge
- Chemicals
- Total Salaries
- Overhead
- Depreciation
- Maintenance, Insurance & Taxes
- Total Fixed Operating Costs

Values: 5483 | 2.5 | 13,372 | 3,96,985 | 7,59,090 | 2,20,000 | 1,10,000 | 2,67,633 | 1,61,457

C Income ($/yr)

Legend:
- Wastewater treatment operation cost saving
- Wastewater treatment cover cost saving
- Wastewater treatment cost saving
- Carbon credit
- Bio-oil income
- P fertilizer
- Syngas income

Values: 47,607, 3% | 1,64,768, 11% | 2,32,455, 15% | 69,080, 5% | 46,883, 3% | 4,00,000, 26% | 5,64,768, 37%
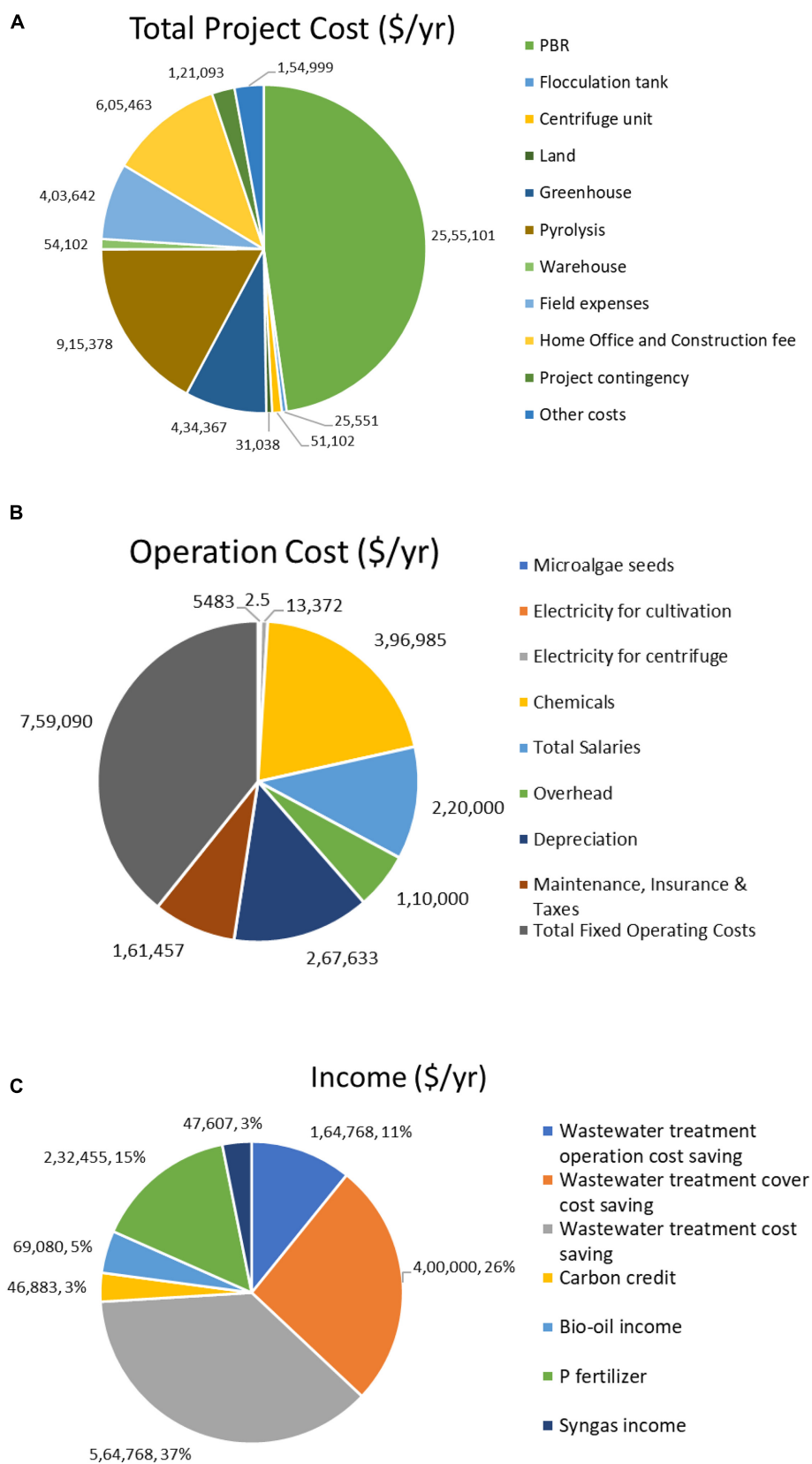
FIGURE 5 | Distribution of costs and income per year **(A)** Distribution of capital costs; **(B)** Distribution of operation costs; **(C)** Distribution of income (Xin et al., 2016).

biodegradable plastic obtained from *Microcystis* sp. cultivated in high-rate algal pond yields 0.7 mg L^{-1} of polyhydroxyalkanoates (Abdo and Ali, 2019).

CHALLENGES AND PERSPECTIVES

Microalgae are a promising feedstock for biorefineries due to their capability of resource recovery from wastewater. Microalgae cultivation in municipal wastewater requires nutrient supplements for the high yield of algal biomass, which is cost-effective. The (environmental) costs of synthetic nutrient additions could be replaced by co-fermentation of various wastewater, which provides all the essential nutrients and integration with other product production technologies may help to improve the overall production cost. Another challenge associated with wastewater is the presence of various contaminants (bacteria, protozoa, and fungi) which inhibit microbial growth. The pH and organic compounds such as tannins and lignin present in wastewater can be toxic for the growth of algae, and the presence of heavy metals absorbed by algae declines its usage for pharmaceutical products. Various pretreatment methods can be used to remove contaminants such as filtration and autoclaving but use of these methods is not feasible at a large scale, so there is need to find other methods that can be scaled up easily at lower cost. Wastewater treatment generally results in sludge production while using microalgal culture there is no requirement of chemicals used for the pretreatment and the sludge contains only algal biomass (Bhatia S. K. et al., 2020). For optimum pH and salinity, cultivation can be performed by mixing hypersaline water from industries or cultivating algae in seashore areas. Use of zeolite is also suggested to remove ammonia from wastewater and then use ammonia rich zeolite to release ammonia in algae culture (Markou et al., 2014). Microalgal biomass produced during wastewater treatment is not a waste, it can be used a material to prepare biochar and used as adsorbent for water pollutant removal. Furthermore, for lowering chemical oxygen demand and biological oxygen demand levels, the collected microalgae biomass can be subjected to anaerobic digestion for the production of methane and other energy source. Microalgae consortia (algae-algae, algae-bacteria) can be used to increase the productivity and coproduction of other valuable products (Leong et al., 2019; Nguyen et al., 2019a,b). The composition of wastewater depends on its source and affects microalgal growth, there is a need to find new microalgal species that are more robust, resistant to various environmental factors, withstand high organic load and fulfill most of the desired parameters (high nutrient removal and growth, accumulate high lipid content). Bioreactors and type of cultivation system also affect the growth and the biomass produced by microalgae to produce value-added products. Microalgae mostly grow on the surface of the water and at high culture density cells restrict light penetration and inhibit microalgae growth inside water. There is a need to design unique bioreactors to overcome these issues. Microalgal growth is also affected by other factors such as wastewater turbidity (inhibit light penetration), temperature variation which hinders the use of the same technology in all cases. Nowadays, the techniques used for harvesting are costly and also labor-intensive but in the coming future, with constant efforts and new technologies the new harvesting methods are being developed and produced microalgae can be used for animal feed, bioenergy, biochemical production, and other biotechnological applications. The use of microalgal based resource recovery from wastewater and its integration with other emerging technologies will definitely improve the overall economics of wastewater treatment and reduced the production cost of many commercially valuable compounds in near future.

CONCLUSION

Microalgae are the most promising candidate for the sustainable treatment of wastewater and the reclamation of nutrients for valuable product production. Microalgae outpace all the traditional wastewater treating techniques like electrochemical methods, precipitation, and membrane technologies by phycoremediation, which is more effective, economically stable, and produces less amount of waste. Microalgae significantly recover nitrogen and phosphorous, lowers biological oxygen demand, and chemical oxygen demand levels. However, many constraints limit the use of microalgae in industries such as, harvesting, and downstream purification of algal biomass for the production of high-value products. Special optimum conditions are needed to be maintained for a particular algal strain depending on the type of industry and desired product of interest. The field of phycology holds enormous opportunities for the purification of water, biofuel production, exopolysaccharides, and bioplastic industries. Sustainable processing of sewage waste and its complete utilization in terms of nutrients with microalgal aid and promoting a biorefinery approach is the need of an hour.

AUTHOR CONTRIBUTIONS

KA and PaK did the conceptualization and wrote the original draft of the manuscript. SP, Y-HY, and XL carried out the formal analysis. SP, AS, and XL carried out the data curation. Y-HY, SP, PrK, SB, and SK wrote, reviewed, and edited the manuscript. All authors have read and agreed to the published version of the manuscript.

ACKNOWLEDGMENTS

REFERENCES

Abdo, S. M., and Ali, G. H. (2019). Analysis of polyhydroxybutyrate and bioplastic production from microalgae. *Bull. Natl. Res. Cent.* 43:97. doi: 10.1186/s42269-019-0135-5

Aguilar, M. R., and San Román, J. (2014). *Smart Polymers and their Applications*. Amsterdam: Elsevier Ltd.

Algae farms to offer a cheaper, renewable solution to cleaning wastewater (2020). https://www.bath.ac.uk/case-studies/algae-farms-to-offer-a-cheaper-renewable-solution-to-cleaning-wastewater (accessed December 12, 2020).

Al-Jabri, H., Das, P., Khan, S., Thaher, M., and AbdulQuadir, M. (2020). Treatment of wastewaters by microalgae and the potential applications of the produced biomass—a review. *Water* 13:27. doi: 10.3390/w13010027

Angelis, S., Novak, A. C., Sydney, E. B., Soccol, V. T., Carvalho, J. C., Pandey, A., et al. (2012). Co-culture of microalgae, cyanobacteria, and macromycetes for exopolysaccharides production: process preliminary optimization and partial characterization. *Appl. Biochem. Biotechnol.* 167, 1092–1106. doi: 10.1007/s12010-012-9642-7

Anwar, M. Z., Kim, D. J., Kumar, A., Patel, S. K. S., Otari, S., Mardina, P., et al. (2017). SnO2 hollow nanotubes: a novel and efficient support matrix for enzyme immobilization. *Sci. Rep.* 7:15333. doi: 10.1038/s41598-017-15550-y

Arrigo, K. R. (2005). Marine microorganisms and global nutrient cycles. *Nature* 437, 349–355.

Bafana, A. (2013). Characterization and optimization of production of exopolysaccharide from Chlamydomonas reinhardtii. *Carbohydr. Polym.* 95, 746–752. doi: 10.1016/j.carbpol.2013.02.016

Bartosh, Y., and Banks, C. J. (2007). Algal growth response and survival in a range of light and temperature conditions: implications for non-steady-state conditions in waste stabilization ponds. *Water Sci. Technol.* 55, 211–218. doi: 10.2166/wst.2007.365

Batista, A. P., Ambrosano, L., Graça, S., Sousa, C., Marques, P. A. S. S., Ribeiro, B., et al. (2015). Combining urban wastewater treatment with biohydrogen production – an integrated microalgae-based approach. *Bioresour. Technol.* 184, 230–235. doi: 10.1016/j.biortech.2014.10.064

Béchet, Q., Shilton, A., and Guieysse, B. (2013). Modeling the effects of light and temperature on algae growth: state of the art and critical assessment for productivity prediction during outdoor cultivation. *Biotechnol Adv.* 31, 1648–1663. doi: 10.1016/j.biotechadv.2013.08.014

Becker, E. W. (2007). Micro-algae as a source of protein. *Biotechnol. Adv.* 25, 207–210. doi: 10.1016/j.biotechadv.2006.11.002

Behl, K., SeshaCharan, P., Joshi, M., Sharma, M., Mathur, A., Kareya, M. S., et al. (2020). Multifaceted applications of isolated microalgae *Chlamydomonas sp.* TRC-1 in wastewater remediation, lipid production and bioelectricity generation. *Bioresour. Technol.* 304:122993. doi: 10.1016/j.biortech.2020.122993

Bhatia, S. K., Kumar, N., and Bhatia, R. K. (2015a). Stepwise bioprocess for exopolysaccharide production using potato starch as carbon source. *3 Biotech.* 5, 735–739. doi: 10.1007/s13205-014-0273-2

Bhatia, S. K., Yi, D.-H., Kim, Y.-H., Kim, H.-J., Seo, H.-M., Lee, J.-H., et al. (2015b). Development of semi-synthetic microbial consortia of Streptomyces coelicolor for increased production of biodiesel (fatty acid methyl esters). *Fuel* 159, 189–196. doi: 10.1016/j.fuel.2015.06.084

Bhatia, S. K., Bhatia, R. K., and Yang, Y.-H. (2016). Biosynthesis of polyesters and polyamide building blocks using microbial fermentation and biotransformation. *Rev. Environ. Sci. Biotechnol.* 15, 639–663. doi: 10.1007/s11157-016-9415-9

Bhatia, S. K., Bhatia, R. K., and Yang, Y. H. (2017). An overview of microdiesel - a sustainable future source of renewable energy. *Renew. Sust. Energy. Rev.* 79, 1078–1090. doi: 10.1016/j.rser.2017.05.138

Bhatia, S. K., Bhatia, R. K., Jeon, J.-M., Kumar, G., and Yang, Y.-H. (2019a). Carbon dioxide capture and bioenergy production using biological system – a review. *Renew. Sust. Energy. Rev.* 110, 143–158. doi: 10.1016/j.rser.2019.04.070

Bhatia, S. K., Gurav, R., Choi, T.-R., Han, Y. H., Park, Y.-L., Park, J. Y., et al. (2019b). Bioconversion of barley straw lignin into biodiesel using *Rhodococcus sp.* YHY01. *Bioresour. Technol.* 289:121704. doi: 10.1016/j.biortech.2019.121704

Bhatia, S. K., Wadhwa, P., Hong, J. W., Hong, Y. G., Jeon, J.-M., Lee, E. S., et al. (2019c). Lipase mediated functionalization of poly(3-hydroxybutyrate-co-3-hydroxyvalerate) with ascorbic acid into an antioxidant active biomaterial. *Int. J. Biol. Macromole* 123, 117–123. doi: 10.1016/j.ijbiomac.2018.11.052

Bhatia, S. K., Gurav, R., Choi, T.-R., Kim, H. J., Yang, S.-Y., Song, H.-S., et al. (2020). Conversion of waste cooking oil into biodiesel using heterogenous catalyst derived from cork biochar. *Bioresour. Technol.* 302:122872. doi: 10.1016/j.biortech.2020.122872

Bhatia, R. K., Ramadoss, G., Jain, A. K., Dhiman, R. K., Bhatia, S. K., and Bhatt, A. K. (2020). Conversion of waste biomass into gaseous fuel: present status and challenges in India. *Bioenergy Res.* 13, 1–23.

Bhatia, S. K., Bhatia, R. K., Jeon, J. M., Pugazhendhi, A., Kumar, A., Kumar, M., et al. (2021a). An overview on advancements in biobased transesterification methods for biodiesel production: oil resources, extraction, biocatalysts, and process intensification technologies. *Fuel* 285:119117. doi: 10.1016/j.fuel.2020.119117

Bhatia, S. K., Gurav, R., Choi, Y.-K., Choi, T.-R., Kim, H.-J., Song, H.-S., et al. (2021b). Bioprospecting of exopolysaccharide from marine *Sphingobium yanoikuyae* BBL01: Production, characterization, and metal chelation activity. *Bioresour. Technol.* 324:124674. doi: 10.1016/j.biortech.2021.124674

Bhatia, S. K., Jagtap, S. S., Bedekar, A. A., Bhatia, R. K., Rajendran, K., Pugazhendhi, A., et al. (2021c). Renewable biohydrogen production from lignocellulosic biomass using fermentation and integration of systems with other energy generation technologies. *Sci. Total. Environ.* 765:144429. doi: 10.1016/j.scitotenv.2020.144429

Bhatia, S. K., Mehariya, S., Bhatia, R. K., Kumar, M., Pugazhendhi, A., Awasthi, M. K., et al. (2021d). Wastewater based microalgal biorefinery for bioenergy production: progress and challenges. *Sci. Total Environ.* 751:141599. doi: 10.1016/j.scitotenv.2020.141599

Bhatia, S. K., Otari, S. V., Jeon, J.-M., Gurav, R., Choi, Y.-K., Bhatia, R. K., et al. (2021e). Biowaste-to-bioplastic (polyhydroxyalkanoates): conversion technologies, strategies, challenges, and perspective. *Bioresour. Technol.* 326:124733. doi: 10.1016/j.biortech.2021.124733

Bhunia, B., Prasad Uday, U. S., Oinam, G., Mondal, A., Bandyopadhyay, T. K., and Tiwari, O. N. (2018). Characterization, genetic regulation and production of cyanobacterial exopolysaccharides and its applicability for heavy metal removal. *Carbohydr. Polym.* 179, 228–243. doi: 10.1016/j.carbpol.2017.09.091

Bindra, S., and Kulshrestha, S. (2019). Converting waste to energy: production and characterization of biodiesel from *Chlorella pyrenoidosa* grown in a medium designed from waste. *Renew. Energy* 142, 415–425. doi: 10.1016/j.renene.2019.04.104

Bindra, S., Sharma, R., Khan, A., and Kulshrestha, S. (2017). Renewable energy sources in different generations of bio-fuels with special emphasis on microalgae derived biodiesel as sustainable industrial fuel model. *Bioscience* 14, 259–274. doi: 10.13005/bbra/2443

Bittencourt, S. E. (2009). *Respirometric Balance and Analysis of Four Microalgae: Dunaliella Tertiolecta, Chlorella vulgaris, Spirulina platensis and Botryococcus braunii.* thesis, University of Provence: Marseille. [dissertation].

Boelee, N. C., Temmink, H., Janssen, M., and Buisman, C. J. N. (2014). Balancing the organic load and light supply in symbiotic microalgal-bacterial biofilm reactors treating synthetic municipal wastewater. *Ecol. Eng.* 64, 213–221. doi: 10.1016/j.ecoleng.2013.12.035

Borowitzka, M., and Hallegraeff, G. (2007). *Economic Importance of Algae*. Hobart, TAS: University of Tasmania, 594–622.

Boyle, G. (2004). *Renewable Energy: Power for a Sustainable Future*, 2nd Edn. Oxford: Oxford University Press.

Cabello, J., Morales, M., and Revah, S. (2015). Effect of the temperature, pH and irradiance on the photosynthetic activity by *Scenedesmus obtusiusculus* under nitrogen replete and deplete conditions. *Bioresour. Technol.* 181, 128–135. doi: 10.1016/j.biortech.2015.01.034

Caetano, N. S., Martins, A. A., Gorgich, M., Gutiérrez, D. M., Ribeiro, T. J., and Mata, T. M. (2020). Flocculation of *Arthrospira maxima* for improved harvesting. *Energy Rep.* 6, 423–428. doi: 10.1016/j.egyr.2019.08.083

Cao, S., Jiang, Q., Wu, X., Ghim, D., Gholami Derami, H., Chou, P. I., et al. (2019). Advances in solar evaporator materials for freshwater generation. *J. Mater. Chem.* 7, 24092–24123. doi: 10.1039/c9ta06034k

Cardoso, L. G., Duarte, J. H., Costa, J. A. V., de Jesus Assis, D., Lemos, P. V. F., Druzian, J. I., et al. (2020). Spirulina sp. as a bioremediation agent for aquaculture wastewater: Production of high added value compounds and estimation of theoretical biodiesel. *Bioenergy Res.* 14, 254–264. doi: 10.1007/s12155-020-10153-4

Carlsson, S. A., Beilen, J. B., Moller, R., and Clayton, D. (2007). *Micro-and Macro-algae: Utility for Industrial Applications Outputs from the EPOBIO Project.* Newbury: University of York, CPL Press.

Castro, M. L. Y., and Ballesteros, F. C. (2020). "Nutrient removal and biomass production by immobilized chlorella vulgaris. frontiers," in *Water-Energy-Nexus—Nature-Based Solutions, Advanced Technologies and Best Practices for Environmental Sustainability*, eds V. Naddeo, M. Balakrishnan, and K. H. Choo (Berlin: Springer), 187–190. doi: 10.1007/978-3-030-13068-8_46

Cepák, V., and Přibyl, P. (2018). Light intensity and nitrogen effectively control exopolysaccharide production by the green microalga *Botryococcus braunii* (Trebouxiophyceae). *Genet. Plant Physiol.* 8, 24–37.

Chaisutyakorn, P., Praiboon, J., and Kaewsuralikhit, C. (2018). The effect of temperature on growth and lipid and fatty acid composition on marine microalgae used for biodiesel production. *J. Appl. Phycol.* 30, 37–45.

Cheah, W. Y., Show, P. L., Juan, J. C., Chang, J. C., and Ling, T. C. (2018). Waste to energy: the effects of *Pseudomonas sp.* on *Chlorella sorokiniana* biomass and lipid productions in palm oil mill effluent. *Clean. Technol. Environ. Policy* 20, 2037–2045. doi: 10.1007/s10098-018-1505-7

Chen, B., You, W., Huang, J., Yu, Y., and Chen, W. (2010). Isolation and antioxidant property of the extracellular polysaccharide from Rhodella reticulata. *J. Microbiol. Biotechn.* 26, 833–840. doi: 10.1007/s11274-009-0240-y

Chen, G.-Q. (2009). A microbial polyhydroxyalkanoates (PHA) based bio- and materials industry. *Chem. Soc. Rev.* 38:2434. doi: 10.1039/b812677c

Chen, M., Tang, H., Ma, H., Holland, T. C., Ng, K. Y., and Salley, S. O. (2011). Effect of nutrients on growth and lipid accumulation in the green algae *Dunaliella tertiolecta*. *Bioresour. Technol.* 102, 1649–1655. doi: 10.1016/j.biortech.2010.09.062

Chiaramonti, D., Prussi, M., Casini, D., Tredici, M. R., Rodolfi, L., Bassi, N., et al. (2013). Review of energy balance in raceway ponds for microalgae cultivation: re-thinking a traditional system is possible. *Appl. Energy* 102, 101–111. doi: 10.1016/j.apenergy.2012.07.040

Choi, O. K., Hendren, Z., Kim, G. D., Dong, D., and Lee, J. W. (2020). Influence of activated sludge derived-extracellular polymeric substance (ASD-EPS) as bio-flocculation of microalgae for biofuel recovery. *Algal Res.* 45:101736. doi: 10.1016/j.algal.2019.101736

Choi, Y.-Y., Baek, S.-R., Kim, J.-I., Choi, J.-W., Hur, J., Lee, T.-U., et al. (2017). Characteristics and biodegradability of wastewater organic matter in municipal wastewater treatment plants collecting domestic wastewater and industrial discharge. *Water* 9:409. doi: 10.3390/w9060409

Choudhary, P., Assemany, P. P., Naaz, F., Bhattacharya, A., Castro, J., de, S., et al. (2020). A review of biochemical and thermochemical energy conversion routes of wastewater grown algal biomass. *Sci. Total Environ.* 726:137961. doi: 10.1016/j.scitotenv.2020.137961

Christenson, L. B., and Sims, R. C. (2012). Rotating algal biofilm reactor and spool harvester for wastewater treatment with biofuels by-products. *Biotechnol. Bioeng.* 109, 1674–1684. doi: 10.1002/bit.24451

Costa, C., and Hadiyanto, H. (2018). Bioelectricity production from microalgae-microbial fuel cell technology (MMFC). *MATEC Web Conf.* 156:1017. doi: 10.1051/matecconf/201815601017

Costache, T. A., Acien, F. G., and Morales, M. M. (2013). Comprehensive model of microalgae photosynthesis rate as a function of culture conditions in photobioreactor. *Appl. Biotechnol.* 97, 7627–7637.

Covarrubias, S. A., De-Bashan, Luz, E., Moreno, M., and Bashan, Y. (2012). Alginate beads provide a beneficial physical barrier against native microorganisms in wastewater treated with immobilized bacteria and microalgae. *Appl. Microbiol. Biotechnol.* 93, 2669–2680. doi: 10.1007/s00253-011-3585-8

Craggs, R., Sutherland, D., and Campbell, H. (2012). Hectare-scale demonstration of high-rate algal ponds for enhanced wastewater treatment and biofuel production. *J. Appl. Phycol.* 24, 329–337. doi: 10.1007/s10811-012-9810-8

Cunha, C., Silva, L., Paulo, J., Faria, M., Nogueira, N., and Cordeiro, N. (2020). Microalgal-based biopolymer for nano- and microplastic removal: a possible biosolution for wastewater treatment. *Environ. Pollut.* 263:114385. doi: 10.1016/j.envpol.2020.114385

Danesi, E. D. G., Rangel-Yagui, C. O., Carvalho, J. C. M., and Sato, S. (2004). Effect of reducing the light intensity on the growth and production of chlorophyll by *Spirulina platensis*. *Biomass Bioenerg.* 26, 329–335. doi: 10.1016/S0961-9534(03)00127-2

Danquah, M. K., Ang, L., Uduman, N., Moheimani, N., and Forde, G. M. (2009). Dewatering of microalgal culture for biodiesel production: exploring polymer flocculation and tangential flow filtration. *J. Chem. Technol. Biotechnol.* 84, 1078–1083. doi: 10.1002/jctb.2137

Das, P., AbdulQuadir, M., Thaher, M., Khan, S., Chaudhary, A. K., and Al-Jabri, H. (2020a). A feasibility study of utilizing hydrothermal liquefaction derived aqueous phase as nutrients for semi-continuous cultivation of *Tetraselmis Sp.* *Bioresour. Technol.* 295:122310. doi: 10.1016/j.biortech.2019.122310

Das, P., Khan, S., AbdulQuadir, M., Thaher, M., Waqas, M., Easa, A., et al. (2020b). Energy recovery and nutrients recycling from municipal sewage sludge. *Sci. Total Environ.* 715:136775. doi: 10.1016/j.scitotenv.2020.136775

Das, P., Quadir, M. A., Thaher, M. I., Alghasal, G. S. H. S., and Aljabri, H. M. S. J. (2019). Microalgal nutrients recycling from the primary effluent of municipal wastewater and use of the produced biomass as bio-fertilizer. *Int. J. Environ. Sci. Technol.* 16, 3355–3364. doi: 10.1007/s13762-018-1867-8

de Godos, I., Vargas, V. A., Guzmán, H. O., Soto, R., García, B., García, P. A., et al. (2014). Assessing carbon and nitrogen removal in a novel anoxic-aerobic cyanobacterial-bacterial photobioreactor configuration with enhanced biomass sedimentation. *Water Res.* 61, 77–85. doi: 10.1016/j.watres.2014.04.050

de Leite, L. S., dos Santos, P. R., and Daniel, L. A. (2020). Microalgae harvesting from wastewater by pH modulation and flotation: assessing and optimizing operational parameters. *J. Environ. Manage.* 254:109825. doi: 10.1016/j.jenvman.2019.109825

Demirbas, A. (2007). Progress and recent trends in biofuels. *Prog. Energy Combust. Sci.* 33, 1–18. doi: 10.1016/j.pecs.2006.06.001

Ding, Y., Guo, Z., Mei, J., Liang, Z., Li, Z., and Hou, X. (2020). Investigation into the novel microalgae membrane bioreactor with internal circulating fluidized bed for marine aquaculture wastewater treatment. *Membranes* 10, 1–10. doi: 10.3390/membranes10110353

El Baky, A. H., Hanaa, El Baz, K. F., and El-Latife, S. A. (2013). Induction of sulfated polysaccharides in *Spirulina platensis* as response to nitrogen concentration and its biological evaluation. *J. Aquac. Res. Dev.* 5, 1–8. doi: 10.4172/2155-9546.1000206

El-Naggar, N. E. A., Hussein, M. H., Shaaban-Dessuuki, S. A., and Dalal, S. R. (2020). Production, extraction and characterization of *Chlorella vulgaris* soluble polysaccharides and their applications in AgNPs biosynthesis and biostimulation of plant growth. *Sci. Rep.* 10:3011. doi: 10.1038/s41598-020-59945-w

Farooq, W., Lee, Y. C., Han, J. I., Darpito, C. H., Choi, M., and Yang, J. W. (2013). Efficient microalgae harvesting by organo-building blocks of nanoclays. *Green. Chem.* 15, 749–755. doi: 10.1039/c3gc36767c

Fasaei, F., Bitter, J. H., Slegers, P. M., and van Boxtel, A. J. B. (2018). Techno-economic evaluation of microalgae harvesting and dewatering systems. *Algal Res.* 31, 347–362. doi: 10.1016/j.algal.2017.11.038

Fernández Valiente, E., Ucha, A., Quesada, A., Leganés, F., and Carreres, R. (2000). Contribution of N2 fixing cyanobacteria to rice production: availability of nitrogen from 15N-labelled cyanobacteria and ammonium sulphate to rice. *Plant Soil.* 221, 107–112. doi: 10.1023/A:1004737422842

Filippino, K. C., Mulholland, M. R., and Bott, C. B. (2015). Phycoremediation strategies for rapid tertiary nutrient removal in a waste stream. *Algal Res.* 11, 125–133. doi: 10.1016/j.algal.2015.06.011

Freire-Nordi, C. S., Vieira, A. A. H., and Nascimento, O. R. (2005). The metal binding capacity of *Anabaena spiroides* extracellular polysaccharide: an EPR study. *Process Biochem.* 40, 2215–2224. doi: 10.1016/j.procbio.2004.09.003

Gao, F., Yang, Z. H., Li, C., Zeng, G. M., Ma, D. H., and Zhou, L. (2015). A novel algal biofilm membrane photobioreactor for attached microalgae growth and nutrients removal from secondary effluent. *Bioresour. Technol.* 179, 8–12. doi: 10.1016/j.biortech.2014.11.108

Garbowski, T., Bawiec, A., Pulikowski, K., and Wiercik, P. (2017). Algae proliferation on substrates immersed in biologically treated sewage. *J. Eco. Eng.* 18, 90–98. doi: 10.12911/22998993/66253

George, B., Pancha, I., Desai, C., Chokshi, K., Paliwal, C., Ghosh, T., et al. (2014). Effects of different media composition, light intensity and photoperiod on morphology and physiology of freshwater microalgae *Ankistrodesmus falcatus* – a potential strain for bio-fuel production. *Bioresour Technol.* 171, 367–374. doi: 10.1016/j.biortech.2014.08.086

Geyer, R., Jambeck, J. R., and Law, K. L. (2017). Production, use, and fate of all plastics ever made. *Sci. Adv.* 3:e1700782. doi: 10.1126/sciadv.1700782

Ghafari, M., Rashidi, B., and Haznedaroglu, B. Z. (2016). Effects of macro and micronutrients on neutral lipid accumulation in oleaginous microalgae. *Biofuels* 9, 147–156.

Gilles, S., Lacroix, G., Corbin, D., Ba, N., Ibriez, L. C., Nandjui, J., et al. (2008). Mutualism between euryhaline tilapia *Sarotherodon melanotheron* heudelotii and *Chlorella sp.* implications for nano-algal production in warmwater phytoplankton-based recirculating systems. *Aquacult Eng.* 39, 113–121. doi: 10.1016/j.aquaeng.2008.09.001

Goswami, R. K., Mehariya, S., Verma, P., Lavecchia, R., and Zuorro, A. (2020). Microalgae-based biorefineries for sustainable resource recovery from wastewater. *J. Water Process Eng.* 2020:101747. doi: 10.1016/j.jwpe.2020.101747

Greenwell, H. C., Laurens, L. M. L., Shields, R. J., Lovitt, R. W., and Flynn, K. J. (2009). Placing microalgae on the biofuels priority list: a review of the technological challenges. *J. R. Soc. Interface* 7, 703–726. doi: 10.1098/rsif.2009.0322

Gurav, R., Bhatia, S. K., Choi, T.-R., Jung, H.-R., Yang, S.-Y., Song, H.-S., et al. (2019). Chitin biomass powered microbial fuel cell for electricity production using halophilic *Bacillus circulans* BBL03 isolated from sea salt harvesting area. *Bioelectrochem* 130:107329. doi: 10.1016/j.bioelechem.2019.107329

Hamed, I. (2016). The evolution and versatility of microalgal biotechnology: a review. *Compr. Rev. Food Sci. Food Saf.* 15, 1104–1123. doi: 10.1111/1541-4337.12227

Han, P., Lu, Q., Fan, L., and Zhou, W. (2019). A review on the use of microalgae for sustainable aquaculture. *Appl. Sci.* 9:2377. doi: 10.3390/app9112377

Hanumantha, R. P., Ranjith Kumar, R., Raghavan, B., Subramanian, V., and Sivasubramanian, V. (2011). Application of phycoremediation technology in the treatment of wastewater from a leather-processing chemical manufacturing facility. *Water SA* 37, 7–14. doi: 10.4314/wsa.v37i1.64099

He, Z., and Angenent, L. T. (2006). Application of bacterial biocathodes in microbial fuel cells. *Electroanalysis* 18, 19–20. doi: 10.1002/elan.20060362

Hendricks, R., and Pool, E. J. (2012). The effectiveness of sewage treatment processes to remove faecal pathogens and antibiotic residues. *J. Environ. Health* 47, 289–297. doi: 10.1080/10934529.2012.637432

Hillman, K. M., and Sims, R. C. (2020). Struvite formation associated with the microalgae biofilm matrix of a rotating algal biofilm reactor (RABR) during nutrient removal from municipal wastewater. *Water Sci. Technol.* 81, 644–655. doi: 10.2166/wst.2020.133

Hu, H., and Zhou, Q. (2010). Regulation of inorganic carbon acquisition by nitrogen and phosphorus levels in the *Nannochloropsis sp.* *World J. Microbiol. Biotechnol.* 26, 957–961. doi: 10.1007/s11274-009-0253-6

Hu, J., Hao, L., Shukla, P., Lin, W., and Luo, J. (2020). Nitrogen and phosphorus removals by the agar-immobilized *Chlorella sacchrarophila* with long-term preservation at room temperature. *Chemosphere* 251:126406. doi: 10.1016/j.chemosphere.2020.126406

Hwang, J. H., Church, J., Lim, J., and Lee, W. H. (2018). Photosynthetic biohydrogen production in a wastewater environment and its potential as renewable energy. *Energy* 149, 222–229. doi: 10.1016/j.energy.2018.02.051

Internet Achave Wayback Mechine (2020). *Phyco spectrum, algal technology, biofuels, biodiesel, phycoremediation, effluent treatment, dyeing effluent, CO2 mitigation, global warming, waste water treatment, world's first phycoremediation plant, Dr V Sivasubramanian, Journal of Algal Biomass Utilization, JABU (2020).* Available online at: https://web.archive.org/web/20191117081824/http://drvsiva.com/snap.html (accessed Aug 22, 2020).

Izadpanah, M., Gheshlaghi, R., Mahdavi, M. A., and Elkamel, A. (2018). Effect of light spectrum on isolation of microalgae from urban wastewater and growth characteristics of subsequent cultivation of the isolated species. *Algal Res.* 29, 154–158. doi: 10.1016/j.algal.2017.11.029

Jha, M. N., and Prasad, A. N. (2006). Efficacy of new inexpensive cyanobacterial biofertilizer including its shelf-life. *World J. Microbiol. Biotechnol.* 22, 73–79.

Ji, M. K., Abou-Shanab, R. A. I., Kim, S. H., Salama, E., Lee, S. H., Kabra, A. N., et al. (2013). Cultivation of microalgae species in tertiary municipal wastewater supplemented with CO2 for nutrient removal and biomass production. *Ecol. Eng.* 58, 142–148. doi: 10.1016/j.ecoleng.2013.06.020

Jia, S., and Zhang, X. (2019). Biological HRPs in wastewater. *High-Risk Poll. Wastewater* 2020, 41–78.

Johnson, D. B., Schideman, L. C., Canam, T., and Hudson, R. J. M. (2018). Pilot-scale demonstration of efficient ammonia removal from a high-strength municipal wastewater treatment side stream by algal-bacterial biofilms affixed to rotating contactors. *Algal Res.* 34, 143–153. doi: 10.1016/j.algal.2018.07.009

Juneja, A., Ceballos, R. M., and Murthy, G. S. (2013). Effects of environ- mental factors and nutrient availability on the biochemi- cal composition of algae for biofuels production: a review. *Energies* 6, 4607–4638. doi: 10.3390/en6094607

Kanekiyo, K., Lee, J. B., Hayashi, K., Takenaka, H., Hayakawa, Y., Endo, S., et al. (2005). T. Isolation of an antiviral polysaccharide, nostoflan, from a terrestrial cyanobacterium, *Nostoc flagelliforme*. *J. Nat. Prod.* 68, 1037–1041. doi: 10.1021/np050056c

Kang, Z., Kim, B. H., Ramanan, R., Choi, J. E., Yang, J. W., Oh, H. M., et al. (2015). A cost analysis of microalgal biomass and biodiesel production in open raceways treating municipal wastewater and under optimum light wavelength. *J. Microbiol. Biotechnol.* 25, 109–118. doi: 10.4014/jmb.1409.09019

Khangembam, R., and Tiwari, O. N. (2016). Production of exopolysaccharides by the cyanobacterium *Anabaena sp.* BTA992 and application as bioflocculants. *J. Appl. Biol.* 4, 008–011. doi: 10.7324/jabb.2016.40102

Kondaveeti, S., Kim, I. W., Otari, S., Patel, S. K. S., Pagolu, R., Losetty, V., et al. (2019a). Co-generation of hydrogen and electricity from biodiesel process effluents. *Int. J. Hydrog. Energy* 44, 27285–27296. doi: 10.1016/j.ijhydene.2019.08.258

Kondaveeti, S., Patel, S. K. S., Pagolu, R., Li, J., Kalia, V. C., Choi, M.-S., et al. (2019b). Conversion of simulated biogas to electricity: sequential operation of methanotrophic reactor effluents in microbial fuel cell. *Energy* 189:116309. doi: 10.1016/j.energy.2019.116309

Kong, Q.-X., Li, L., Martinez, B., Chen, P., Ruan, R., Kong, Q.-X., et al. (2010). Culture of microalgae *Chlamydomonas reinhardtii* in wastewater for biomass feedstock production. *Appl. Biochem. Biotechnol.* 160, 9–18. doi: 10.1007/s12010-009-8670-4

Kube, M., Fan, L., and Roddick, F. (2021). Alginate-immobilised algal wastewater treatment enhanced by species selection. *Algal Res.* 54:102219. doi: 10.1016/j.algal.2021.102219

Kube, M., Jefferson, B., Fan, L., and Roddick, F. (2018). The impact of wastewater characteristics, algal species selection and immobilisation on simultaneous nitrogen and phosphorus removal. *Algal Res.* 31, 478–488. doi: 10.1016/j.algal.2018.01.009

Kumar, A., Park, G. D., Patel, S. K. S., Kondaveeti, S., Otari, S., Anwar, M. Z., et al. (2019). SiO2 microparticles with carbon nanotube-derived mesopores as an efficient support for enzyme immobilization. *Chem. Eng. J.* 359, 1252–1264. doi: 10.1016/j.cej.2018.11.052

Kumar, G., Mathimani, T., Sivaramakrishnan, R., Shanmugam, S., Bhatia, S. K., and Pugazhendhi, A. (2020). Application of molecular techniques in biohydrogen production as a clean fuel. *Sci. Total. Environ.* 722:137795. doi: 10.1016/j.scitotenv.2020.137795

Kumar, M. D., Kavitha, S., Tyagi, V. K., Rajkumar, M., Bhatia, S. K., Kumar, G., et al. (2021). Macroalgae-derived biohydrogen production: biorefinery and circular bioeconomy. *Biomass Convers. Biorefine* 1–23. doi: 10.1007/s13399-020-01187-x

Kurth, C., Wasmuth, I., Wichard, T., Pohnert, G., and Nett, M. (2019). Algae induce siderophore biosynthesis in the freshwater bacterium *Cupriavidus necator* H16. *Biometals* 32, 77–88. doi: 10.1007/s10534-018-0159-6

Lakaniemi, A. M., Intihar, V. M., Tuovinen, O. H., and Puhakka, J. A. (2012). Growth of *Chlorella vulgaris* and associated bacteria in photobioreactors. *Microb. Biotechnol.* 5, 69–78. doi: 10.1111/j.1751-7915.2011.00298

Lam, M. K., and Lee, K. T. (2012). Potential of using organic fertilizer to cultivate *Chlorella vulgaris* for biodiesel production. *Appl. Energy* 94, 303–308. doi: 10.1016/j.apenergy.2012.01.075

Lam, T. P., Lee, T. M., Chen, C. Y., and Chang, J. S. (2018). Strategies to control biological contaminants during microalgal cultivation in open ponds. *Bioresour. Technol.* 252, 180–187. doi: 10.1016/j.biortech.2017.12.088

Laycock, B., Halley, P., Pratt, S., Werker, A., and Lant, P. (2013). The chemomechanical properties of microbial polyhydroxyalkanoates. *Prog. Polym. Sci.* 38, 536–583. doi: 10.1016/j.progpolymsci.2012.06.003

Lee, C.-J., and Palsson, B. (1994). High intensity algal bioreactors using light-emitting diodes. *Biotechnol. Bioeng.* 44, 1161–1167. doi: 10.1002/bit.260441002.48109

Lee, N., Oh, H. S., Oh, H. M., Kim, H. S., and Ahn, C. Y. (2019). Enhanced growth and lipid production in psychrotolerant acutodesmus by controlling

temperature-dependent nitrogen concentration. *Biomass Bioenergy* 127:105267. doi: 10.1016/j.biombioe.2019.105267

Lee, S.-H., Oh, H.-M., Jo, B.-H., Lee, S.-A., Shin, S.-Y., Kim, H.-S., et al. (2014). Higher biomass productivity of microalgae in an attached growth system using wastewater. *J. Microbiol. Biotechnol.* 24, 1566–1573. doi: 10.4014/JMB.1406. 06057

LeeY.-K. (1997). Commercial production of microalgae in the Asia-Pacificrim. *J Appl Phycol.* 9, 403–411.

Leong, W. H., Azella Zaine, S. N., Ho, Y. C., Uemura, Y., Lam, M. K., Khoo, K. S., et al. (2019). Impact of various microalgal-bacterial populations on municipal wastewater bioremediation and its energy feasibility for lipid-based biofuel production. *J. Environ. Manage.* 249:13. doi: 10.1016/j.jenvman.2019.109384

Li, K., Liu, Q., Fang, F., Luo, R., Lu, Q., Zhou, W., et al. (2019). Microalgae-based wastewater treatment for nutrients recovery: a review. *Bioresour. Technol.* 291:121934. doi: 10.1016/j.biortech.2019.121934

Li, M., Zhu, Q., Hu, C.-W., Chen, L., Liu, Z.-L., and Kong, Z.-M. (2007). Cobalt and manganese stress in the microalga *Pavlova viridis* (prymnesiophyceae): effects on lipid peroxidation and antioxidant enzymes. *J. Environ. Sci.* 19, 1330–1335. doi: 10.1016/S1001-0742(07)60217-4

Li, Y., Chen, Y. F., Chen, P., Min, M., Zhou, W., Martinez, B., et al. (2011). Characterization of a microalga *Chlorella sp.* well adapted to highly concentrated municipal wastewater for nutrient removal and biodiesel production. *Bioresour. Technol.* 102, 5138–5144. doi: 10.1016/j.biortech.2011. 01.091

Liu, X., Chen, G., Tao, Y., and Wang, J. (2020). Application of effluent from WWTP in cultivation of four microalgae for nutrients removal and lipid production under the supply of CO2. *Renew. Energy* 149, 708–715. doi: 10.1016/j.renene. 2019.12.092

Liu, X., Wang, K., Zhang, J., Wang, J., Wu, J., and Peng, F. (2019). Ammonium removal potential and its conversion pathways by free and immobilized *Scenedesmus obliquus* from wastewater. *Bioresour. Technol.* 283, 184–190. doi: 10.1016/j.biortech.2019.03.038

Ma, C., Wen, H., Xing, D., Pei, X., Zhu, J., Ren, N., et al. (2017). Molasses wastewater treatment and lipid production at low temperature conditions by a microalgal mutant *Scenedesmus sp.* Z-4. *Biotechnol. Biofuel.* 10:111. doi: 10. 1186/s13068-017-0797-x

Maity, J. P., Hou, C.-P., Majumder, D., Bundschuh, J., Thomas, R. K., Chen, C. P., et al. (2014). The production of biofuel and bioelectricity associated with wastewater treatment by green algae. *Energy* 78, 94–103. doi: 10.1016/j.energy. 2014.06.023

Mallick, N. (2002). Biotechnological potential of immobilized algae for wastewater N, P and metal removal: a review. *Biometals* 15, 377–390. doi: 10.1023/A: 1020238520948

Mantzorou, A., and Ververidis, F. (2019). Microalgal biofilms: a further step over current microalgal cultivation techniques. *Sci. Total Environ.* 651, 3187–3201. doi: 10.1016/j.scitotenv.2018.09.355

Marino, T., Figoli, A., Chianese, E., Rimauro, J., Mehariya, S., Musmarra, D., et al. (2019). *Scenedesmus almeriensis* solutions dewatering by using PVDF membrane. *Chem. Eng. Trans.* 74, 1411–1416. doi: 10.3303/CET1974236

Markou, G., Vandamme, D., and Muylaert, K. (2014). Using natural zeolite for ammonia sorption from wastewater and as nitrogen releaser for the cultivation of *Arthrospira platensis*. *Bioresour. Technol.* 155, 373–378. doi: 10.1016/j. biortech.2013.12.122

Mishra, A., and Jha, B. (2009). Isolation and characterization of extracellular polymeric substances from micro-algae *Dunaliella salina* under salt stress. *Bioresour. Technol.* 100, 3382–3386. doi: 10.1016/j.biortech.2009.02.006

Mishra, P. K., Rana, S., Singh, L., Sakinah, M., and Ab Wahid, Z. (2019). Outlook of fermentative hydrogen production techniques: an overview of dark, photo and integrated dark-photo fermentative approach to biomass. *Energy Strategy Rev.* 24, 27–37. doi: 10.1016/j.esr.2019.01.001

Misra, S. K., Valappil, S. P., Roy, I., and Boccaccini, A. R. (2006). Polyhydroxyalkanoate (PHA)/inorganic phase composites for tissue engineering applications. *Biomacromolecules* 7, 2249–2258. doi: 10.1021/ bm060317c

Mohd Udaiyappan, A. F., Abu Hasan, H., Takriff, M. S., and Sheikh Abdullah, S. R. (2017). A review of the potentials, challenges and current status of microalgae biomass applications in industrial wastewater treatment. *J. Water. Process. Eng.* 20, 8–21. doi: 10.1016/j.jwpe.2017.09.006

Mohd-Sahib, A. A., Lim, J. W., Lam, M. K., Uemura, Y., Isa, M. H., Ho, C. D., et al. (2017). Lipid for biodiesel production from attached growth *Chlorella vulgaris* biomass cultivating in fluidized bed bioreactor packed with polyurethane foam material. *Bioresour. Technol.* 239, 127–136. doi: 10.1016/j.biortech.2017.04.118

Molina Grima, E., Belarbi, E.-H., Acién Fernández, F. G., Robles Medina, A., and Chisti, Y. (2003). Recovery of microalgal biomass and metabolites: process options and economics. *Biotechnol. Adv.* 20, 491–515. doi: 10.1016/S0734-9750(02)00050-52

Morales, M., Sánchez, L., and Revah, S. (2018). The impact of environmental factors on carbon dioxide fixation by microalgae. *FEMS Microbiol. Lett.* 365:262. doi: 10.1093/femsle/fnx262

Moreno Osorio, J. H., Pinto, G., Pollio, A., Frunzo, L., Lens, P. N. L., Esposito, G., et al. (2019). Start-up of a nutrient removal system using *Scenedesmus vacuolatus* and *Chlorella vulgaris* biofilms. *Bioresour. Bioprocess.* 6:27. doi: 10. 1186/s40643-019-0259-3

National Status of Waste Water Generation and Treatment (2020). *SulabhENVIS Centre*. Available online at: http://www.sulabhenvis.nic.in/database/stst_ wastewater_2090.aspx (accessed Dec 12, 2020).

Nelson, M. J., Nakhla, G., and Zhu, J. (2017). Fluidized-bed bioreactor applications for biological wastewater treatment: a review of research and developments. *Eng* 3, 330–342. doi: 10.1016/J.ENG.2017.03.021

Ndikubwimana, T., Zeng, X., Murwanashyaka, T., Manirafasha, E., He, N., Shao, W., et al. (2016). Harvesting of freshwater microalgae with microbial bioflocculant: a pilot-scale study. *Biotechnol. Biofuels.* 9:47. doi: 10.1186/ s13068-016-0458-5

Ngatu, N. R., Okajima, M. K., Yokogawa, M., Hirota, R., Eitoku, M., Muzembo, B. A., et al. (2012). Anti-inflammatory effects of sacran, a novel polysaccharide from *Aphanothece sacrum*, on 2,4,6-trinitrochlorobenzene-induced allergic dermatitis in vivo. *Ann. Allergy Asthma Immunol.* 108, 117–122. doi: 10.1016/j. anai.2011.10.013

Nguyen, T. D. P., Le, T. V. A., Show, P. L., Nguyen, T. T., Tran, M. H., Tran, T. N. T., et al. (2019a). Bioflocculation formation of microalgae-bacteria in enhancing microalgae harvesting and nutrient removal from wastewater effluent. *Bioresour. Technol.* 272, 34–39. doi: 10.1016/j.biortech.2018.09.146

Nguyen, T. D. P., Nguyen, D. H., Lim, J. W., Chang, C.-K., Leong, H. Y., Tran, T. N. T., et al. (2019b). Investigation of the relationship between bacteria growth and lipid production cultivating of microalgae *Chlorella Vulgaris* in seafood wastewater. *Energies* 12:2282. doi: 10.3390/en12122282

Noor-Mohammadi, S., Pourmir, A., and Johannes, T. W. (2014). Method for assembling and expressing multiple genes in the nucleus of microalgae. *Biotechnol. Lett.* 36, 561–566. doi: 10.1007/s10529-013-1378-0

Novoveská, L., Zapata, A. K. M., Zabolotney, J. B., Atwood, M. C., and Sundstrom, E. R. (2016). Optimizing microalgae cultivation and wastewater treatment in large-scale offshore photobioreactors. *Algal Res.* 18, 86–94. doi: 10.1016/j.algal. 2016.05.033

Nur, M. M. A., Swaminathan, M. K., Boelen, P., and Buma, A. G. J. (2019). Sulfated exopolysaccharide production and nutrient removal by the marine diatom *Phaeodactylum tricornutum* growing on palm oil mill effluent. *J. Appl. Phycol.* 31, 2335–2348. doi: 10.1007/s10811-019-01780-2

Osiemo, M. M., Ogendi, G. M., and M'Erimba, C. (2019). Microbial quality of drinking water and prevalence of water-related diseases in marigat urban centre. Kenya. *Environ. Health Insights* 13:1178630219836988. doi: 10.1177/ 1178630219836988

Otari, S. V., Patel, S. K. S., Kalia, V. C., and Lee, J.-K. (2020). One-step hydrothermal synthesis of magnetic rice straw for effective lipase immobilization and its application in esterification reaction. *Bioresour. Technol.* 302:122887. doi: 10. 1016/j.biortech.2020.122887

Otari, S. V., Patel, S. K. S., Kim, S. Y., Haw, J. R., Kalia, V. C., et al. (2019). Copper ferrite magnetic nanoparticles for the immobilization of enzyme. *Indian J. Microbiol.* 59, 105–108. doi: 10.1007/s12088-018-0768-3

Palma, H., Killoran, E., Sheehan, M., Berner, F., and Heimann, K. (2017). Assessment of microalga biofilms for simultaneous remediation and biofuel generation in mine tailings water. *Bioresour. Technol.* 234, 327–335. doi: 10. 1016/j.biortech.2017.03.063

Papazi, A., Makridis, P., and Divanach, P. (2010). Harvesting *Chlorella minutissima* using cell coagulants. *J. Appl. Phycol.* 22, 349–355. doi: 10.1007/s10811-009-9465-2

Park, J. B. K., Craggs, R. J., and Shilton, A. N. (2011). Wastewater treatment high rate algal ponds for biofuel production. *Bioresour. Technol.* 102, 35–42. doi: 10.1016/j.biortech.2010.06.158

Park, Y.-L., Bhatia, S. K., Gurav, R., Choi, T.-R., Kim, H. J., Song, H.-S., et al. (2020). Fructose based hyper production of poly-3-hydroxybutrate from *Halomonas sp.* YLGW01 and impact of carbon sources on bacteria morphologies. *Int. J. Biol. Macromol.* 154, 929–936. doi: 10.1016/j.ijbiomac.2020.03.129

Patel, S. K. S., Gupta, R. K., Das, D., Lee, J.-K., and Kalia, V. C. (2020a). Continuous biohydrogen production from poplar biomass hydrolysate by a defined bacterial mixture immobilized on lignocellulosic materials under non-sterile conditions. *J. Clean. Prod.* 287:125037. doi: 10.1016/j.jclepro.2020.125037

Patel, S. K. S., Gupta, R. K., Kalia, V. C., and Lee, J.-K. (2020b). Integrating anaerobic digestion of potato peels to methanol production by methanotrophs immobilized on banana leaves. *Bioresour. Technol.* 323:124550. doi: 10.1016/j.biortech.2020.124550

Patel, S. K. S., Gupta, R. K., Kondaveeti, S., Otari, S. V., Kumar, A., Kalia, V. C., et al. (2020c). Conversion of biogas to methanol by methanotrophs immobilized on chemically modified chitosan. *Bioresour. Technol.* 315:12379. doi: 10.1016/j.biortech.2020.123791

Patel, S. K. S., Gupta, R. K., Kumar, V., Kondaveeti, S., Kumar, A., Das, D., et al. (2020d). Biomethanol production from methane by immobilized co-cultures of methanotrophs. *Indian J. Microbiol.* 60, 318–324. doi: 10.1007/s12088-020-00883-6

Patel, S. K. S., Kalia, V. C., Joo, J. B., Kang, Y. C., and Lee, J.-K. (2020e). Biotransformation of methane into methanol by methanotrophs immobilized on coconut coir. *Bioresour. Technol.* 297:122433. doi: 10.1016/j.biortech.2019. 122433

Patel, S. K. S., Jeon, M. S., Gupta, R. K., Jeon, Y., Kalia, V. C., Kim, S. C., et al. (2019). Hierarchical macro-porous particles for efficient whole-cell immobilization: application in bioconversion of greenhouse gases to methanol. *ACS Appl. Mater. Interfaces* 11, 18968–18977. doi: 10.1021/acsami.9b03420

Patel, S. K. S., Kumar, P., and Kalia, V. C. (2012). Enhancing biological hydrogen production through complementary microbial metabolisms. *Int. J. Hydrog. Energy* 37, 10590–10603. doi: 10.1016/j.ijhydene.2012.04.045

Patel, S. K. S., Kumar, P., Singh, M., Lee, J.-K., and Kalia, V. C. (2015). Integrative approach to produce hydrogen and polyhydroxybutyrate from biowaste using defined bacterial cultures. *Bioresour. Technol.* 176, 136–141. doi: 10.1016/j.biortech.2014.11.029

Patel, S. K. S., Shanmugam, R., Kalia, V. C., and Lee, J.-K. (2020f). Methanol production by polymer-encapsulated methanotrophs from simulated biogas in the presence of methane vector. *Bioresour. Technol.* 304:123022. doi: 10.1016/j.biortech.2020.123022

Pattarkine, M. V., and Pattarkine, V. M. (2012). "Nanotechnology for algal biofuels," in *The Science of Algal Fuels*, eds R. Gordon and J. Seckbach (Berlin: Springer), 149–160.

Pierucci, S., Klemeš, J. J., Piazza, L., Bakalis, S., Sed, G., Cicci, A., et al. (2017). Extraction and purification of exopolysaccharides from exhausted *Arthrospira platensis* (Spirulina) culture systems. *Chem. Eng. Trans.* 57, 211–216. doi: 10.3303/CET1757036

Podola, B., Li, T., and Melkonian, M. (2017). Porous substrate bioreactors: a paradigm shift in microalgal biotechnology? *Trends Biotechnol.* 35, 121–132. doi: 10.1016/j.tibtech.2016.06.004

Posadas, E., Alcántara, C., García-Encina, P. A., et al. (2017). "Microalgae-based biofuels and bioproducts," in *Microalgae Cultivation in Wastewater*, eds C. Gonzalez-Fernandez and R. Muñoz (Sawston: Woodhead Publishing), 67–91. doi: 10.1016/B978-0-08-101023-5.00003-0

Posten, C. (2009). Design principles of photo-bioreactors for cultivation of microalgae. *Eng. Life Sci.* 9, 165–177. doi: 10.1002/elsc.200900003

Prabakar, D., Manimudi, V. T., Suvetha, K. S., Sampath, S., Mahapatra, D. M., Rajendran, K., et al. (2018). Advanced biohydrogen production using pretreated industrial waste: outlook and prospects. *Renew. Sust. Energ. Rev.* 96, 306–324. doi: 10.1016/j.rser.2018.08.006

Prakash, J., Sharma, R., Patel, S. K. S., Kim, I. W., and Kalia, V. C. (2018). Bio-hydrogen production by co-digestion of domestic wastewater and biodiesel industry effluent. *PLoS One* 13:e0199059. doi: 10.1371/journal.pone.0199059

Preisner, M., Neverova-Dziopak, E., and Kowalewski, Z. (2021). Mitigation of eutrophication caused by wastewater discharge: a simulation-based approach. *Ambio* 50, 413–424. doi: 10.1007/s13280-020-01346-4

Rahman, A., Putman, R. J., Inan, K., Sal, F. A., Sathish, A., Smith, T., et al. (2015). Polyhydroxybutyrate production using a wastewater microalgae-based media. *Algal Res.* 8, 95–98. doi: 10.1016/j.algal.2015.01.009

Rai, M. R., Gautom, T., and Sharma, N. (2015). Effect of salinity, pH, light intensity on growth and lipid production of microalgae for bioenergy application. *Online J. Biol. Sci.* 15, 260–267.

Raize, O., Argaman, Y., and Yannai, S. (2004). Mechanisms of biosorption of different heavy metals by brown marine macroalgae. *Biotechnol. Bioeng.* 87, 451–458. doi: 10.1002/bit.20136

Rajasulochana, P., and Preethy, V. (2016). Comparison on efficiency of various techniques in treatment of waste and sewage water – a comprehensive review. *Resource-Eff. Technol.* 2, 175–184. doi: 10.1016/j.reffit.2016.09.004

Rajesh Banu, J., Ginni, G., Kavitha, S., Yukesh Kannah, R., Adish Kumar, S., Bhatia, S. K., et al. (2021). Integrated biorefinery routes of biohydrogen: possible utilization of acidogenic fermentative effluent. *Bioresour. Technol.* 319:124241. doi: 10.1016/j.biortech.2020.124241

Rana, R. S., Singh, P., Kandari, V., Singh, R., Dobhal, R., and Gupta, S. (2017). A review on characterization and bioremediation of pharmaceutical industrieswastewater: an Indian perspective. *Appl. Water. Sci.* 7, 1–12. doi: 10.1007/s13201-014-0225-3

Raven, J. A. (1988). The iron and molybdenum use efficiencies of plant growth with different energy, carbon and nitrogen sources. *New Phytol.* 109, 279–287. doi: 10.1111/j.1469-8137.1988.tb04196.x

Rawat, I., Kumar, R., Mutanda, T., and Bux, F. (2011). Dual role of microalgae: phycoremediation of domestic wastewater and biomass production for sustainable biofuels production. *Appl. Energy.* 88, 3411–3424. doi: 10.1016/j.apenergy.2010.11.025

Razzak, S. A., Hossain, M. M., Lucky, R. A., Bassi, A. S., and de Lasa, H. (2013). Integrated CO2 capture, wastewater treatment and biofuel production by microalgae culturing - a review. *Renew. Sust. Energ. Rev.* 27, 622–653. doi: 10.1016/j.rser.2013.05.063

Renuka, N., Guldhe, A., Prasanna, R., Singh, P., and Bux, F. (2018). Microalgae as multi-functional options in modern agriculture: current trends, prospects and challenges. *Biotechnol. Adv. Elsevier Inc.* 36, 1255–1273. doi: 10.1016/j.biotechadv.2018.04.004

Rhoads, A., Beyenal, H., and Lewandowski, Z. (2005). Microbial fuel cell using anaerobic respiration as an anodic reaction and biomineralized manganese as a cathodic reactant. *Environ. Sci. Technol.* 39, 4666–4671. doi: 10.1021/es048386r

Rosli, S. S., Lim, J. W., Jumbri, K., Lam, K. M., Uemura, Y., Ho, C. D., et al. (2019). Modeling to enhance attached microalgal biomass growth onto fluidized beds packed in nutrients-rich wastewater whilst simultaneously biofixing CO2 into lipid for biodiesel production. *Energy Convers. Manag.* 185, 1–10. doi: 10.1016/j.enconman.2019.01.077

Ruiz-Marin, A., Canedo-López, Y., and Chávez-Fuentes, P. (2020). Biohydrogen production by *Chlorella vulgaris* and *Scenedesmus obliquus* immobilized cultivated in artificial wastewater under different light quality. *AMB Expr.* 10:191. doi: 10.1186/s13568-020-01129-w

Ruiz-Marin, A., Mendoza-Espinosa, L. G., and Stephenson, T. (2010). Growth and nutrient removal in free and immobilized green algae in batch and semi-continuous cultures treating real wastewater. *Bioresour. Technol.* 101, 58–64. doi: 10.1016/j.biortech.2009.02.076

Safarik, I., Prochazkova, G., Pospiskova, K., and Branyik, T. (2016). Magnetically modifed microalgae and their applications. *Crit. Rev. Biotechnol.* 36, 931–941. doi: 10.3109/07388551.2015.1064085

Samer, M. (2015). "Biological and chemical wastewater treatment processes," in *Wastewater Treatment Engineering*, ed. M. Samer (Europe: InTech), doi: 10.5772/61250

Sathiyanarayanan, G., Bhatia, S. K., Kim, H. J., Kim, J.-H., Jeon, J.-M., Kim, Y.-G., et al. (2016). Metal removal and reduction potential of an exopolysaccharide produced by Arctic psychrotrophic bacterium *Pseudomonas sp.* PAMC 28620. *RSC Adv.* 6, 96870–96881. doi: 10.1039/C6RA17450G

Sathiyanarayanan, G., Yi, D.-H., Bhatia, S. K., Kim, J.-H., Seo, H. M., Kim, Y.-G., et al. (2015). Exopolysaccharide from psychrotrophic Arctic glacier soil bacterium Flavobacterium sp. ASB 3–3 and its potential applications. *RSC Adv.* 5, 84492–84502. doi: 10.1039/c5ra14978a

Schiano, V., Gino, A. S., Chuck, S. J., and Allen, M. J. (2019). The microalgae biorefinery: a perspective on the current status and future opportunities using genetic modification. *App. Sci.* 9:4793. doi: 10.3390/app9224793

Schlesinger, A., Eisenstadt, D., Bar-Gil, A., Carmely, H., Einbinder, S., and Gressel, J. (2012). Inexpensive non-toxic flocculation of microalgae contradicts theories; overcoming a major hurdle to bulk algal production. *Biotechnol. Adv.* 30, 1023–1030. doi: 10.1016/j.biotechadv.2012.01.011

Selmani, N., Mirghani, M. E., and Alam, M. Z. (1997). *Study the Growth of Microalgae in Palm Oil Mill Effluent Wastewater. in IOP Conference series: Earth and Environmental Science.* Putrajaya: IOP Publishing.

Selvaratnam, T., Pegallapati, A. K., Montelya, F., and Rodriguez, G. (2014). Evaluation of a thermo-tolerant acidophilic alga, *Galdieria sulphuraria*, for nutrient removal from urban wastewaters. *Bioresour. Technol.* 156, 395–399. doi: 10.1016/j.biortech.2014.01.075

Sharma, A., and Arya, S. K. (2017). Hydrogen from algal biomass: a review of production process. *Biotechnol. Rep.* 15, 63–69. doi: 10.1016/j.btre.2017.06.001

Sharma, P. K., Saharia, M., Srivstava, R., Kumar, S., and Sahoo, L. (2018). Tailoring microalgae for efficient biofuel production. *Front. Mar. Sci.* 5:382. doi: 10.3389/fmars.2018.00382

Shen, Y., Yuan, W., Pei, Z., Wu, Q., and Mao, M. (2009). Microalgae mass produc-tion methods. *Trans ASABE* 52, 1275–1287.

Silambarasan, S., Logeswari, P., Sivaramakrishnan, R., Incharoensakdi, A., Cornejo, P., Kamaraj, B., et al. (2021). Removal of nutrients from domestic wastewater by microalgae coupled to lipid augmentation for biodiesel production and influence of deoiled algal biomass as biofertilizer for *Solanum lycopersicum* cultivation. *Chemosphere* 268:129323. doi: 10.1016/j.chemosphere.2020.129323

Singh, J. S., Kumar, A., Rai, A. N., and Singh, D. P. (2016). Cyanobacteria: a precious bio-resource in agriculture, ecosystem, and environmental sustainability. *Front. Microbiol.* 7:529. doi: 10.3389/fmicb.2016.00529

Singh, K. S., Bansal, A., Jha, M. K., and Dey, A. (2012). An integrated approach to remove Cr(VI) using immobilized *Chlorella minutissima* grown in nutrient rich sewage wastewater. *Bioresour. Technol.* 104, 257–265. doi: 10.1016/j.biortech.2011.11.044

Singh, M., Patel, S. K. S., and Kalia, V. C. (2009). Bacillus subtilis as potential producer for polyhydroxyalkanoates. *Microb. Cell Fact.* 8:38. doi: 10.1186/1475-2859-8-38

Singh, S. (2015). Study of waste water effluent characteristics generated from paper industries. *J. Basic Appl. Eng. Res.* 2, 1505–1509.

Sivasubramanian V. (2020). http://www.algonauts.org/algonauts/4sivasubramanian.html (accessed Aug 22, 2020).

Skoneczny, S., and Tabiś, B. (2015). The method for steady states determination in tubular biofilm reactors. *Chem. Eng. Sci.* 137, 178–187. doi: 10.1016/j.ces.2015.06.024

Slade, R., and Bauen, A. (2013). Micro-algae cultivation for biofuels: cost, energy balance, environmental impacts and future prospects. *Biomass. Bioenerg.* 53, 29–38. doi: 10.1016/j.biombioe.2012.12.019

Slegers, P. M., Lösing, M. B., Wijffels, R. H., van Straten, G., and van Boxtel, A. J. B. (2013). Scenario evaluation of open pond microalgae production. *Algal Res.* 2, 358–368. doi: 10.1016/j.algal.2013.05.001

Smith, B. T., and Davis, R. H. (2012). Sedimentation of algae flocculated using naturally-available, magnesium-based flocculants. *Algal Res.* 1, 32–39. doi: 10.1016/j.algal.2011.12.002

Solovchenko, A., Verschoor, A. M., Jablonowski, N. D., and Nedbal, L. (2016). Phosphorus from wastewater to crops: an alternative path involving microalgae. *Biotechnol. Adv.* 34, 550–564. doi: 10.1016/j.biotechadv.2016.01.002

State of the Art Compendium Report on Resource Recovery from Water (2018). https://www.iwa-network.org/wp-content/uploads/2018/02/OFID-Wastewater-report-2018.pdf.

Sternberg, S. H., and Doudna, J. A. (2015). Expanding the biologist's toolkit with CRISPR-Cas9. *Mol. Cell.* 58, 568–574. doi: 10.1016/j.molcel.2015.02.032

Suleiman, A. K. A., Lourenço, K. S., Clark, C., Luz, R. L., da Silva, G. H. R., Vet, L. E. M., et al. (2020). From toilet to agriculture: fertilization with microalgal biomass from wastewater impacts the soil and rhizosphere active microbiomes, greenhouse gas emissions and plant growth. *Resour. Conserv. Recycl.* 161:104924. doi: 10.1016/j.resconrec.2020.104924

Sutherland, D. L., Howard-Williams, C., Turnbull, M. H., Broady, P. A., and Craggs, R. J. (2015). The effects of CO2 addition along a pH gradient on wastewater microalgal photo-physiology, biomass production and nutrient removal. *Water Res.* 70, 9–26. doi: 10.1016/j.watres.2014.10.064

Tan, J. S., Leec, S. Y., Chewd, K. W., Lame, M. K., Lim, J. W., Hoh, S.-H., et al. (2020). A review on microalgae cultivation and harvesting, and their

biomass extraction processing using ionic liquids. *Bioengineered* 11, 116–129. doi: 10.1080/21655979.2020.1711626

Tan, X. B., Wan, X. P., Yang, L. B., Wang, X., Meng, J., Jiang, M. J., et al. (2021). Nutrients recycling and biomass production from Chlorella pyrenoidosa culture using anaerobic food processing wastewater in a pilot-scale tubular photobioreactor. *Chemosphere* 270:129459. doi: 10.1016/j.chemosphere.2020.129459

Tao, Q., Gao, F., Qian, C. Y., Guo, X. Z., Zheng, Z., and Yang, Z. H. (2017). Enhanced biomass/biofuel production and nutrient removal in an algal biofilm airlift photobioreactor. *Algal Res.* 21, 9–15. doi: 10.1016/j.algal.2016.11.004

Taziki, M., Ahmadzadeh, H., and Murry, M. A. (2015). Growth of Chlorella vulgaris in high concentrations of nitrate and nitrite for wastewater treatment. *Curr. Biotechnol.* 4, 441–447. doi: 10.2174/22115501046661509302044835

Teixeira, M. R., and Rosa, M. J. (2006). Comparing dissolved air flotation and conventional sedimentation to remove cyanobacterial cells of Microcystis aeruginosa Part II. The effect of water background organics. *Separat. Purif. Technol.* 52, 84–94. doi: 10.1016/j.seppur.2006.03.017

The Indus Project (2020). *Innovative Tile-based Bioremediation.* Available online at: https://www.materialsource.co.uk/the-indus-project-tile-based-bioremediation/ (accessed Aug 22, 2020).

Ting, H., Haifeng, L., Shanshan, M., Zhang, Y., Zhidan, L., and Na, D. (2017). Progress in microalgae cultivation photobioreactors and applications in wastewater treatment: a review. *International J. Agric. Biol. Eng.* 10, 1–29.

Torkamani, S., Wani, S. N., Tang, Y. J., and Sureshkumar, R. (2010). Plasmon-enhanced microalgal growth in mini photobioreactors. *Appl Phys Lett.* 97:043703. doi: 10.1063/1.3467263

Tredici, R. (2004). Mass production of microalgae: photobioreactors. *Handb. Microalgal Cul.* 1, 178–214.

Uduman, N., Qi, Y., Danquah, M. K., Forde, G. M., and Hoadley, A. (2010). Dewatering of microalgal cultures: a major bottleneck to algae-based fuels. *J. Renew. Sust. Energ.* 2:012701. doi: 10.1063/1.3294480

Vadiveloo, A., Foster, L., Kwambai, C., Bahri, P. A., and Moheimani, N. R. (2021). Microalgae cultivation for the treatment of anaerobically digested municipal centrate (ADMC) and anaerobically digested abattoir effluent (ADAE). *Sci. Total Environ.* 775:145853. doi: 10.1016/j.scitotenv.2021.145853

Vandamme, D., Foubert, I., and Muylaert, K. (2013). Flocculation as a low-cost method for harvesting microalgae for bulk biomass production. *Trends Biotechnol.* 31, 233–239. doi: 10.1016/j.tibtech.2012.12.005

Vandamme, D., Foubert, I., Fraeye, I., Meesschaert, B., and Muylaert, K. (2012). Flocculation of *Chlorella vulgaris* induced by high pH: role of magnesium and calcium and practical implications. *Bioresour. Technol.* 105, 114–119. doi: 10.1016/j.biortech.2011.11.105

Vandith, V. A., Setiyawan, A. S., Soewondo, P., and Putri, D. W. (2018). The characteristics of domestic wastewater from office buildings in bandung, West Java, Indonesia. Indones. *J. Urban Environ. Technol.* 1:199. doi: 10.25105/urbanenvirotech

Varshney, P., Beardall, J., Bhattacharya, S., and Wangikar, P. P. (2018). Isolation and biochemical characterisation of two thermophilic green algal species-asterarcys quadricellulare and *Chlorella sorokiniana*, which are tolerant to high levels of carbon dioxide and nitric oxide. *Algal Resource* 30, 28–37. doi: 10.1016/j.algal.2017.12.006

Villar-Navarro, E., Baena-Nogueras, R. M., Paniw, M., Perales, J. A., and Lara-Martín, P. A. (2018). Removal of pharmaceuticals in urban wastewater: high rate algae pond (HRAP) based technologies as an alternative to activated sludge based processes. *Water Res.* 139, 19–29. doi: 10.1016/j.watres.2018.03.072

Vuppaladadiyam, A., Prinsen, P., Raheem, A., and Luque, R. (2018). Microalgae cultivation and metabolites production: a comprehensive review. *Biofuels Bioproducts Biorefining* 12, 304–324. doi: 10.1002/bbb.1864

Wang, B., Lan, C. Q., and Horsman, M. (2012). Closed photobioreactors for production of microalgal biomasses. *Biotechnol. Adv.* 30, 904–912. doi: 10.1016/j.biotechadv.2012.01.019

Wang, J., and Yin, Y. (2018). Fermentative hydrogen production using pretreated microalgal biomass as feedstock. *Microb. Cell Fact.* 17:22.

Wang, L., Min, M., Li, Y., Chen, P., Chen, Y., Liu, Y., et al. (2010). Cultivation of green algae *Chlorella sp.* in different wastewaters from municipal wastewater

treatment plant. *Appl. Biochem. Biotechnol.* 162, 1174–1186. doi: 10.1007/s12010-009-8866-7

Win, T. T., Barone, G. D., Secundo, F., and Fu, P. (2018). Algal biofertilizers and plant growth stimulants for sustainable agriculture. *Ind. Biotechnol.* 14, 203–211. doi: 10.1089/ind.2018.0010

Wollmann, F., Dietze, S., Ackermann, J. U., Bley, T., Walther, T., Steingroewer, J., et al. (2019). Microalgae wastewater treatment: biological and technological approaches. *Eng. Life Sci.* 19, 860–871. doi: 10.1002/elsc.201900071

Xiao, R., and Zheng, Y. (2016). Overview of microalgal extracellular polymeric substances (EPS) and their applications. *Biotechnol. Adv.* 34, 1225–1244. doi: 10.1016/j.biotechadv.2016.08.004

Xin, C., Addy, M. M., Zhao, J., Cheng, Y., Cheng, S., Mu, D., et al. (2016). Comprehensive techno-economic analysis of wastewater-based algal biofuel production: a case study. *Bioresour. Technol.* 211, 584–593. doi: 10.1016/j.biortech.2016.03.102

Yadavalli, R., and Heggers, G. R. V. N. (2013). Two stage treatment of dairy effluent using immobilized *Chlorella pyrenoidosa*. *J. Environ. Health Sci. Eng.* 11, 1–6. doi: 10.1186/2052-336x-11-36

Yen, H. W., Hu, I. C., Chen, C. Y., Nagarajan, D., and Chang, J. S. (2019). "Design of photobioreactors for algal cultivation," in *Biofuels from Algae*, 2nd Edn, Amsterdam: Elsevier, 225–256. doi: 10.1016/B978-0-444-64192-2.00010-X

Yim, J. H., Kim, S. J., Ahn, S. H., Lee, C. K., Rhie, K. T., and Lee, H. K. (2003). Antiviral effects of sulfated exopolysaccharide from the marine microalga *Gyrodinium impudicum* strain KG03. *Mar. Biotechnol.* 2003, 17–25. doi: 10.1007/S10126-003-0002-Z

Zamalloa, C., Boon, N., and Verstraete, W. (2013). Decentralized two-stage sewage treatment by chemical-biological flocculation combined with microalgae biofilm for nutrient immobilization in a roof installed parallel plate reactor. *Bioresour. Technol.* 130, 152–160. doi: 10.1016/j.biortech.2012.11.128

Zeller, M. A., Hunt, R., Jones, A., and Sharma, S. (2013). Bioplastics and their thermoplastic blends from *Spirulina* and *Chlorella microalgae*. *J. Appl. Polym. Sci.* 130, 3263–3275. doi: 10.1002/app.39559

Zhang, J., and Hu, B. (2012). A novel method to harvest microalgae via co-culture of filamentous fungi to form cell pellets. *Bioresour. Technol.* 114, 529–535. doi: 10.1016/j.biortech.2012.03.054

Zhang, L., Chen, P., Huang, J., Yang, G., and Zheng, L. (2003). Ways of strengthening biodegradable soy-dreg plastics. *J. Appl. Polym. Sci.* 88, 422–427. doi: 10.1002/app.11718

Zhang, Q., Li, X., Guo, D., Ye, T., Xiong, M., Zhu, L., et al. (2018). Operation of a vertical algal biofilm enhanced raceway pond for nutrient removal and microalgae-based byproducts production under different wastewater loadings. *Bioresour. Technol.* 253, 323–332. doi: 10.1016/j.biortech.2018.01.014

Zhang, Y., Mo, G., Li, X., Zhang, W., Zhang, J., Ye, J., et al. (2011). A graphene modified anode to improve the performance of microbial fuel cells. *J. Power Sources* 196, 5402–5407. doi: 10.1016/j.jpowsour.2011.02.067

Zheng, H., Liu, M., Lu, Q., Wu, X., Ma, Y., Cheng, Y., et al. (2018). Balancing carbon/nitrogen ratio to improve nutrients removal and algal biomass production in piggery and brewery wastewaters. *Bioresour. Technol.* 249, 479–486. doi: 10.1016/j.biortech.2017.10.057

Zhou, H., Sheng, Y., Zhao, X., Gross, M., and Wen, Z. (2018). Treatment of acidic sulfate-containing wastewater using revolving algae biofilm reactors: sulfur removal performance and microbial community characterization. *Bioresour. Technol.* 264, 24–34. doi: 10.1016/j.biortech.2018.05.051

Zhou, W., Hu, B., Li, Y., Min, M., Mohr, M., Du, Z., et al. (2012b). Mass cultivation of microalgae on animal wastewater: a sequential two-stage cultivation process for energy crop and omega-3-rich animal feed production. *Appl. Biochem. Biotechnol.* 168, 348–363. doi: 10.1007/s12010-012-9779-4

Zhou, W., Li, Y., Gao, Y., and Zhao, H. (2017). Nutrients removal and recovery from saline wastewater by Spirulina platensis. *Bioresour. Technol.* 245, 10–17. doi: 10.1016/j.biortech.2017.08.160

Zhou, Y., Schideman, L., Yu, G., and Zhang, Y. (2013). A synergistic combination of algal wastewater treatment and hydrothermal biofuel production maximized by nutrient and carbon recycling. *Energy Environ. Sci.* 6, 3765–3779. doi: 10.1039/c3ee24241b

Zhu, L., Wang, Z., Shu, Q., Takala, J., Hiltunen, E., Feng, P., et al. (2013). Nutrient removal and biodiesel production by integration of freshwater algae cultivation with piggery wastewater treatment. *Water Res.* 47, 4294–4302. doi: 10.1016/j.watres.2013.05.004

Process Systems Engineering Evaluation of Prospective Working Fluids for Organic Rankine Cycles Facilitated by Biogas Combustion Flue Gases

Muhammad Abdul Qyyum[1]*, Ahmad Naquash[1], Wahid Ali[2], Junaid Haider[3], Adnan Aslam Noon[4], Mohammad Rehan[5], Abdul-Sattar Nizami[6], Muhammad Yasin[7]* and Moonyong Lee[1]*

[1] School of Chemical Engineering, Yeungnam University, Gyeongsan, South Korea, [2] Department of Chemical Engineering Technology, College of Applied Industrial Technology, Jazan University, Jazan, Saudi Arabia, [3] School of Energy and Chemical Engineering, Ulsan National Institute of Science and Technology, Ulsan, South Korea, [4] Department of Mechanical Engineering, FET, International Islamic University, Islamabad, Islamabad, Pakistan, [5] Center of Excellence in Environmental Studies, King Abdulaziz University, Jeddah, Saudi Arabia, [6] Sustainable Development Study Center, Government College University Lahore, Lahore, Pakistan, [7] Bioenergy & Environmental Sustainable Technology (BEST) Research Group, Department of Chemical Engineering, COMSATS University Islamabad (CUI), Lahore, Pakistan

The organic Rankine cycle (ORC) has recently emerged as a practical approach for generating electricity from low-to-high-temperature waste industrial streams. Several ORC-based waste heat utilization plants are already operational; however, improving plant cost-effectiveness and competitiveness is challenging. The use of thermally efficient and cost-competitive working fluids (WFs) improves the overall efficiency and economics of ORC systems. This study evaluates ORC systems, facilitated by biogas combustion flue gases, using n-butanol, i-butanol, and methylcyclohexane, as WFs technically and economically, from a process system engineering perspective. Furthermore, the performance of the aforementioned WFs is compared with that of toluene, a well-known WF, and it is concluded that i-butanol and n-butanol are the most competitive alternatives in terms of work output, exergy efficiency, thermal efficiency, total annual cost, and annual profit. Moreover, the i-butanol and n-butanol-based ORC systems yielded 24.4 and 23.4% more power, respectively, than the toluene-based ORC system; in addition, they exhibited competitive thermal (18.4 and 18.3%, respectively) and exergy efficiencies (38 and 37.7%, respectively). Moreover, economically, i-butanol and n-butanol showed the potential of generating 48.7 and 46% more profit than that of toluene. Therefore, this study concludes that i-butanol and n-butanol are promising WFs for high-temperature ORC systems, and their technical and economic performance compares with that of toluene. The findings of this study will lead to energy efficient ORC systems for generating power.

Keywords: i-butanol, n-butanol, methylcyclohexane, toluene, Aspen HYSYS®, thermo-economic evaluation, high temperature ORC

INTRODUCTION

The global energy demand has been increasing because of economic and population growth and lifestyle improvements in the developing world. Fossil fuels have been used as a primary energy source to fulfill current energy demands and account for around 85.5% of the global energy production (Ediger, 2019). However, fossil fuel consumption leads to environmental pollution, including waste heat and greenhouse gas (GHG) emissions, resulting in climate change (Ediger, 2019). To reduce GHG emissions and meet the globally increasing energy demand, effective utilization of waste heat through power generation is critical. The organic Rankine cycle (ORC) is the most promising technology for utilizing waste heat for power generation, leading to decreasing fossil fuel consumption and GHG emissions. For example, recovering waste heat from a midsize cement industry plant can decrease the annual CO_2 emissions by 10 kt (Mahmoudi et al., 2018).

The ORCs have been studied extensively in the past decades. Several studies have evaluated working fluids (WFs) and ORC system configurations from a thermo-economic perspective (Imran et al., 2018; Blondel et al., 2019; Anastasovski et al., 2020). Mudasar et al. (2017) studied a biogas-fueled high-temperature ORC (HT-ORC) system using toluene as the WF and reported that the maximum power generated and thermal efficiency were 156 kW and 19%, respectively. Shu et al. (2016) studied several ORC systems, including a toluene-based HT-ORC system, and demonstrated that this system generated less power (152.3 kW) than steam and double ORC systems (153.8 and 158.6 kW, respectively). Mahmoudi et al. (2018) summarized the effects of WFs on waste heat recovery and exergy efficiency in different ORC configurations and concluded that toluene was one of the most studied WFs for internal combustion engines. Moreover, they presented that the electricity production cost, depreciated payback period, and savings-to-investment ratio of toluene-fueled ORC systems were the lowest (0.27 $/kWh), shortest (7.8 years), and highest (1.6), respectively, compared with those of ORC systems using other WFs (Mahmoudi et al., 2018). Moreover, (Maraver et al., 2014) have investigated conventional WFs, including toluene, and evaluated results after optimization. The results show that the thermal efficiency of toluene based ORC systems ranges from 5.2 to 21% (Maraver et al., 2014). In another study by Song and Gu (2015), toluene is studied as WF where it shows a thermal efficiency of 21%. A latest study has been conducted on the thermodynamics performance analysis of an ORC. A total of 64 combinations of WFs have been examined for the dual cycle. Propane and R245fa were selected for the ORC (Khatoon et al., 2021). A multi-objective optimization work has been performed for an ORC and heat pump system for waste heat recovery in waste-to-energy combined heat and power

plant. Various WFs have been investigated, however, butane and ammonia are the most suitable working fluids (Pan et al., 2020). In a study by Touaibi et al. (2020a,b), the authors have evaluated three WFs including toluene, R245fa and R123 on parametric basis. Their results show that toluene has highest efficiency (14.38%) among all WFs.

To date, only a few researchers have evaluated ORC systems and WFs from a process systems engineering (PSE) perspective. Bruno et al. (2008) have simulated an ORC system using the Aspen Plus software and have calculated its thermal efficiency for different WFs; however, they have not performed a detailed thermodynamic evaluation based on parametric and composite curve analyses. Furthermore, (Lee et al., 2017) have studied an ORC system using liquefied natural gas cold energy utilizing the Aspen Plus software and have optimized the proposed process using a genetic algorithm. Their optimized results revealed that the thermal efficiency of the analyzed ORC system was 26%. Moreover, they have analyzed the proposed process using composite curve analysis but have not evaluated the WFs using a parametric study. Barse and Mann (2016) evaluated the performance of 12 conventional WFs used in ORC systems using the Aspen HYSYS software from technical (thermodynamic and exergy analysis) and economic (cost analysis) viewpoints. However, they have not focused on the selection and detailed parametric evaluation of WFs. Similarly, (Rowshanaie et al., 2015) performed a simulation of conventional WFs-based ORC systems in Aspen HYSYS. They have evaluated WFs (R245fa, NOVEC7000, R141b) based on thermal efficiency and UA in which R245fa shows better performance. However, detailed PSE perspective based analysis is not considered in their study (Rowshanaie et al., 2015). Another study by Yu et al. (2013) has evaluated ORC systems in Aspen Plus. In their ORC system, R245fa was evaluated as a WF in a diesel engine combusted flue gases under varying evaporation pressure. The results show that the engine's thermal efficiency can be improved by 6.1% after combining ORC with it (Yu et al., 2013).

A detailed analysis of ORC systems from a PSE perspective is critical to evaluate overall process performance. Moreover, the thermodynamic and parametric study of WFs is critical, particularly for unconventional WFs. Therefore, this study presents a detailed PSE consideration to evaluate the ORC systems under varying WFs at constant heating and cooling mediums. The proposed ORC systems are facilitated by biogas combustion flue gases. The major contribution of this study can be summarized as follows:

- Three unconventional WFs, namely *i*-butanol, *n*-butanol, and methylcyclohexane (MCH), are investigated compared to a well-known conventional WF, i.e., toluene.
- Detailed parametric and thermodynamic analysis for selecting and evaluating the prospective WFs for high temperature ORC systems are performed from a PSE viewpoint.
- The composite curves with detailed exergy analysis are analyzed for ORC systems with chosen prospective WFs.
- The economic benefits of selected unconventional WFs are also determined in comparison with toluene.

Abbreviations: CC, composite curve; GHG, greenhouse gas; HT-ORC, high-temperature organic Rankine cycle; LHv, latent heat of vaporization; MCH, methylcyclohexane; MITA, minimum internal temperature approach; ORC, organic Rankine cycle; PSE, process system engineering; TDCC, temperature difference composite curves; THCC, temperature–heat flow composite curves; T–s, temperature entropy; TAC, total annual cost; TCI, total capital investment; WF, working fluid.

MATERIALS AND METHODS

Prospective Working Fluids

Toluene is one of the most promising WFs for HT-ORC applications (Shu et al., 2016; Mudasar et al., 2017) mainly because of its desirable thermo-physical parameters. Several researchers have studied the behavior of toluene using its thermo-physical properties (Mahmoudi et al., 2018). For instance, (Yagli et al., 2016) analyzed that the thermal efficiency of toluene (17.08%) was higher than that of cyclohexane (16.62%). The selection of optimal WFs is challenging because of the low thermal and exergy efficiency, low power output, and lack of commercial availability of WFs. Considering these constraints, the prospective WFs in this study, namely MCH, *n*-butanol, and *i*-butanol, were studied from technical and economic perspectives. These WFs were evaluated because their thermo-physical properties are competitive to those of toluene and their thermodynamic efficiency is far better then toluene which make them viable to be used commercially.

The most important thermo-physical properties of the proposed WFs and toluene, which is a widely used WF, are presented in **Table 1**. The critical temperatures of *n*-butanol, *i*-butanol, and MCH are comparable to that of toluene. Moreover, critical temperatures of prospective WFs are similar to source temperatures and thus are likely responsible for the high cycle efficiency of these WFs. Furthermore, the critical pressures of *n*-butanol and *i*-butanol are higher than that of toluene, whereas the critical pressure of MCH is lower. In addition, the molecular weight of MCH is higher than that of toluene, and the molecular weights of *n*-butanol and *i*-butanol are lower. Lastly, the boiling point of *n*-butanol is higher than that of toluene, whereas those of *i*-butanol and MCH are lower. Because the properties of the prospective WFs are comparable to those of toluene, comprehensive thermodynamic and economic analyses should be performed to analyze the tradeoff between these WFs carefully.

To achieve cost-effective ORC operation, dry and isentropic WFs are recommended (Mudasar et al., 2017), mainly because wet WFs must be superheated before entering turbines. When wet fluids enter a turbine as saturated vapor, they can corrode the turbine blades. Furthermore, additional equipment is required for superheating, which increases operation costs. However, superheating is not required when dry and isentropic fluids are used. The slope of the saturated vapor curve of the temperature–entropy (T–s) diagram (dT/ds) is used to determine whether fluids are wet, dry, or isentropic. Because $dT/ds = \infty$ for isentropic fluids, the inverse slope (ds/dT) was used in this study;

ds/dT is positive, negative, and equal to zero for dry, wet, and isentropic fluids, respectively. Like toluene, the prospective WFs were dry fluids, as illustrated in **Table 1**.

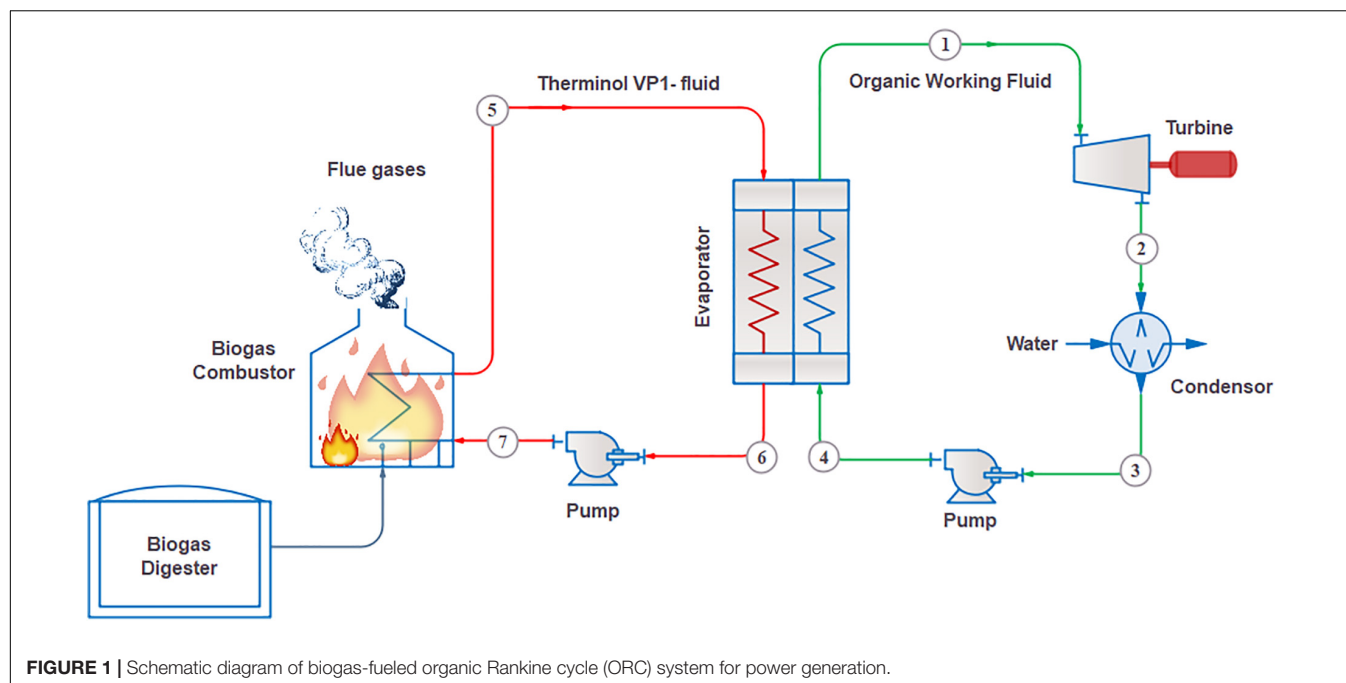## EVALUATION OF WORKING FLUIDS

The prospective WFs were evaluated based on the energy recovery efficiency from the waste heat source, which depended on the optimum selection of WFs and the heat exchange mode between the WF and the heat source. The optimal WF was selected by evaluating its technical parameters, as mentioned in section "Materials and Methods." The thermal and exergy efficiencies of the prospective WFs were calculated based on their thermo-physical properties and power output. The economic evaluation was subsequently conducted to determine the most optimal alternative WF for toluene. Furthermore, heat exchange between the waste gases and the WF can occur directly or through a thermal oil, which serves as an intermediate heat-transfer fluid. The heat-transfer fluid presents high thermal capacity, high-temperature stability, low melting temperature, low viscosity, low corrosion, high safety profile, and low environmental impact (Macchi, 2016). Therminol VP-1, which consists of 26.5% biphenyl and 73.5% diphenyl ether (molar percentages), presents most of the aforementioned properties and was selected as the heat-transfer fluid in this study. Moreover, the auto-ignition temperature of Therminol VP-1 is considerably higher than that of other thermal oils. The properties of Therminol VP-1 have been described in detail (Eastman, 2020). Moreover, (Abdel-Hadi, 2009) reported that Therminol VP-1 was suitable for biogas-fueled ORC power generation systems when the biogas' methane content exceeded 54.5%.

CYCLE DETAILS

The proposed ORC system consisted of four major components: a feed pump, an evaporator or a boiler, a turbine or an expander, and a condenser (Sun et al., 2017). The WF passed through the pump, where it was pressurized and was subsequently transferred to the evaporator/boiler. The evaporator/boiler increased the WF's temperature to form saturated or superheated vapor by exchanging heat with Therminol VP-1, which is a heat transfer fluid. The heat source was selected to be flue gases generated through biogas combustion. The heat source may vary depending upon heat utilization requirements. After heat exchange, the high-pressure WF vapor were expanded in the turbine to generate desired mechanical energy. The turbine is a key component that determines the efficiency of ORC systems. The superheated WF from the turbine was converted into a saturated liquid after cooling in the condenser. Water is used as a cooling medium in the condenser. Thereafter, the condensed WF was compressed by the pump to restart the cycle in a closed loop. To convert waste heat into electricity, the mechanical power produced by the turbine/expander was converted into electrical energy using a generator. The ORC system's main components and the heat sources and sinks connected with the evaporator/boiler and condenser are illustrated in **Figure 1**.

TABLE 1 | Thermo-physical properties of toluene, methylcyclohexane, *n*-butanol, and *i*-butanol.

WF	MW (kg/kmol)	BP (°C)	T_c (°C)	P_c (bar)	Saturated vapor curve slope (ds/dT)
n-butanol	74.12	117.7	290.0	44.14	+ve
i-butanol	74.12	107.7	274.6	42.95	+ve
MCH	98.19	100.9	299.0	34.80	+ve
Toluene	92.14	110.6	318.6	41.08	+ve

FIGURE 1 | Schematic diagram of biogas-fueled organic Rankine cycle (ORC) system for power generation.

Cycle Design and Simulation

In this study, the ORC system was designed and simulated using the Aspen HYSYS® V10 commercial simulator using toluene as the conventional WF (Mudasar et al., 2017) and MCH, *n*-butanol, and *i*-butanol as the proposed WFs. The proposed process design conditions are summarized in **Table 2**. The design parameters were maintained constant for all four cycle designs, and the generated power and efficiencies were compared. The pump and turbine with isentropic efficiencies of 65 and 85%, respectively, were used as reported in the literature (Saleh et al., 2007). The following assumptions were made during the simulation:

1. The WF was a saturated liquid when it entered the pump.
2. The isentropic efficiencies of the pump and turbine were known.
3. The components were treated under adiabatic conditions.
4. The pressure drops in the evaporator, condenser, pipes, and tubes were negligible.
5. All equipment were operated in steady state.

TABLE 2 | Design parameters of studied ORC systems.

Parameter	Values
Isentropic efficiency of the turbine (%)	85
Cooling utility	Water
Isentropic efficiency of the pump (%)	65
Thermal oil temperature (°C)	350
Thermal oil pressure (bar)	3
Thermal oil flowrate (kg/h)	7,674
WF flowrate (kg/h)	4,729
Turbine discharge pressure (bar)	0.7425

6. The toluene, MCH, i-butanol, and n-butanol were pumped to 34, 32, 40, and 40 bar, respectively. These pressures were less than their critical pressures.

RESULTS AND DISCUSSION

Parametric Analysis

Typically, the optimum WF is selected based on thermo-physical parameters, such as critical temperature and pressure, latent heat of vaporization (LHv), fluid density, degree of superheating, heat capacity, and viscosity. These properties and the thermal efficiencies of the WFs analyzed in this study are listed in **Table 3**. **Table 3** illustrates that critical pressure of the WFs is directly related to their thermal efficiency. For example, MCH presents the lowest thermal efficiency (15.8%), highest back-work ratio, and lowest turbine power output (185 kW) among all analyzed WFs because operating and critical pressures are lower than those of the other WFs. Conversely, *n*-butanol and *i*-butanol, which presented high operating and critical pressures (18.3 and 18.4%, respectively), exhibited high thermal efficiencies. Similarly, LHv and density are the other major thermodynamic parameters used to analyze the thermodynamic efficiency of ORC systems. WFs with high LHv and high density are preferred because fluids with high LHv absorb more heat and reduce moisture during expansion. Conversely, WFs with high mass density require low flow rates to absorb more heat, increasing equipment capacity. The LHv of *n*-butanol and *i*-butanol (558.5 and 541.8 kJ/kg, respectively) are higher than that of toluene (367 kJ/kg); therefore, *n*-butanol and *i*-butanol absorbed more heat than toluene in the evaporator, which in turn decreased the exit temperature of the thermal oil. In contrast, WFs with high LHv increase the cooling load on the condenser, and a

TABLE 3 | Comparison of thermodynamic parameters of toluene, methylcyclohexane, *n*-butanol, and *i*-butanol.

Fluid	Heat of vaporization (kJ/kg)	Liquid heat capacity (kJ/kg°C)	Vapor heat capacity (kJ/kg°C)	Viscosity (cP)	Generated power (kW)	Back-work Ratio	Condenser duty (kW)	η (Thermal efficiency)%
Toluene	367	1.9	2.5	0.26	191.8	4.43	793	18.8
MCH	328.6	2.15	3.14	0.32	185	4.84	935	15.8
n-butanol	558.5	2.78	3.01	0.46	250.5	4.39	1070	18.3
i-butanol	541.8	2.74	2.94	0.55	253.3	4.32	1074	18.4

large condenser duty is required to remove the LHv. Therefore, *n*-butanol and *i*-butanol presented high condenser duties (1070 and 1074 kW, respectively).

A high degree of superheating causes a large condenser duty. Therefore, a low degree of superheating at the exhaust of the evaporator for dry fluids is preferred. The superheating degrees of *n*-butanol and *i*-butanol were lower than that of MCH, but their condenser duties were higher. This was ascribed to the lower density of MCH than those of *n*-butanol and *i*-butanol. Typically, WFs with high density causes high heat absorption, which results in high cooling loads. Heat capacity is another criterion used for WF selection. Heat capacity is defined as the energy required by a given mass of material to increase its temperature by 1°C. WFs with low liquid heat capacity and high latent heat are preferred so that maximum heat is absorbed during phase change without requiring a high degree of preheating. Among the WFs in this study, MCH presented the lowest heat capacity in the liquid phase. In contrast, the liquid heat capacities of *n*-butanol and *i*-butanol were comparable (2.78 and 2.74 kJ/kg°C, respectively). However, the heat capacities of the WFs in vapor phase were higher than those in the liquid phase. This was attributed to the superheated fluid leaving the evaporator, and therefore, requiring more heat to increase temperature. Viscosity also plays a vital role in reducing power consumption and increasing heat transfer. More viscous fluids require more power to pump, making the process less efficient. Furthermore, viscosity and heat transfer are inversely related. A WF with low viscosity and high density requires a high heat-transfer capacity.

Thermodynamic Analysis

Thermodynamic analysis of the ORC systems was conducted using T–s diagram and CCs, and the details are presented in the subsequent subsections.

T–s Diagram Analysis

The T–s diagrams of the thermodynamic processes in a simple ORC system using toluene, MCH, *i*-butanol, and *n*-butanol as the WFs are illustrated in **Figure 2**.

As depicted in the T–s diagrams (**Figure 2**), the heat source at high temperature (state 5) exchanged heat with the WF in the evaporator, and the heat source was cooled to state 6. Moreover, the low-temperature WF in state 4 was heated to the highest cycle temperature in state 1. The heat transferred to the WF included sensible heat, which increased the temperature of the WF until the fluid reached saturated liquid state, latent heat transferred to the WF at constant temperature and pressure until it reached saturated vapor state, and superheated to increase

temperature to the required turbine inlet temperature at state 1. Subsequently, the WF expanded from state 1 to state 2 in the turbine to generate work output. State 2s in **Figure 2** illustrates an isentropic or ideal process, with no irreversibility; hence, the entropy did not change, and the entropy at state 1 was equal to the entropy at state 2s. However, real processes are not isentropic; hence, entropy increased from state 1 to state 2. Thereafter, the WF condensed in the condenser from state 2 to state 3, which occurred in two steps. In the first step, the fluid was cooled to a saturated vapor state, whereas during the second step, heat was released at a constant temperature until the WF reached saturated liquid state. Lastly, the fluid entered the pump in saturated liquid state, its pressure was increased to the required evaporator inlet pressure, and the cycle continued.

Composite Curve Analysis

Composite curves (CC) provide a holistic overview of heat recovery in a heat exchanger. These curves demonstrate the relation of hot fluid (i.e., Therminol VP-1) and cold fluid (i.e., WF) with respect to approach temperature and heat flow along the length of heat exchanger. Hot and cold fluid is depicted in terms of hot and cold CCs, respectively. **Figure 3** illustrates approach temperature and temperature relation in terms of temperature difference composite curves (TDCCs). **Figure 4** visualizes temperature–heat flow composite curves (THCCs) for the ORC system. An ORC system's performance can be predicted from the peak of cold and hot CCs in the TDCC profiles over a certain temperature range, as illustrated in **Figure 3**. Accordingly, it is noted that the peak of hot and cold CCs is mainly located at the cold end (below 320°C) of heat exchanger in all ORC systems. This peak of CCs is observed with respect to approach temperature, also referred to as the minimum internal temperature approach (MITA). In **Figure 3**, the MITA value reaches at 147, 90 and 98.5°C in MCH, *n*-butanol, and *i*-butanol cases, whereas in the case of toluene, it reaches at 165°C. This MITA value should follow the specified value i.e., 5°C throughout the length of the exchanger. A large variation in obtained and specified value is mainly because of the large difference between stream temperatures. This difference can be reduced either by enhancing heat recovery or by the optimal selection of WFs based on their thermo-physical properties. For instance, toluene shows MITA value of 165°C, which is the highest in all cases. The lowest value i.e., 90°C, is observed in the case of *n*-butanol. In *n*-butanol case, the outlet temperature of Therminol VP-1 is 199.9°C, where the inlet temperature of WF is 109.9°C. This large difference depicts that more heat can be recovered. Amongst
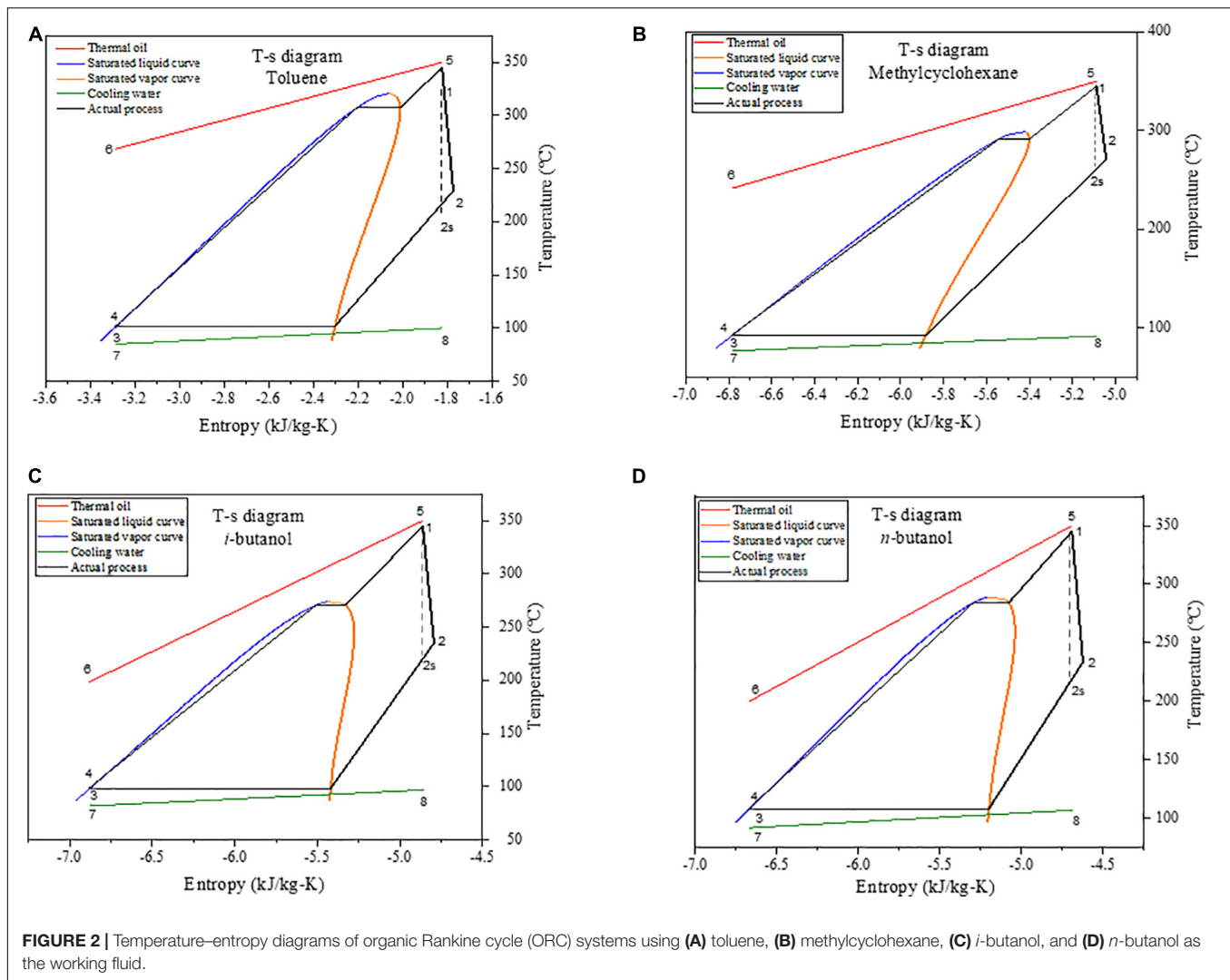
FIGURE 2 | Temperature–entropy diagrams of organic Rankine cycle (ORC) systems using **(A)** toluene, **(B)** methylcyclohexane, **(C)** *i*-butanol, and **(D)** *n*-butanol as the working fluid.

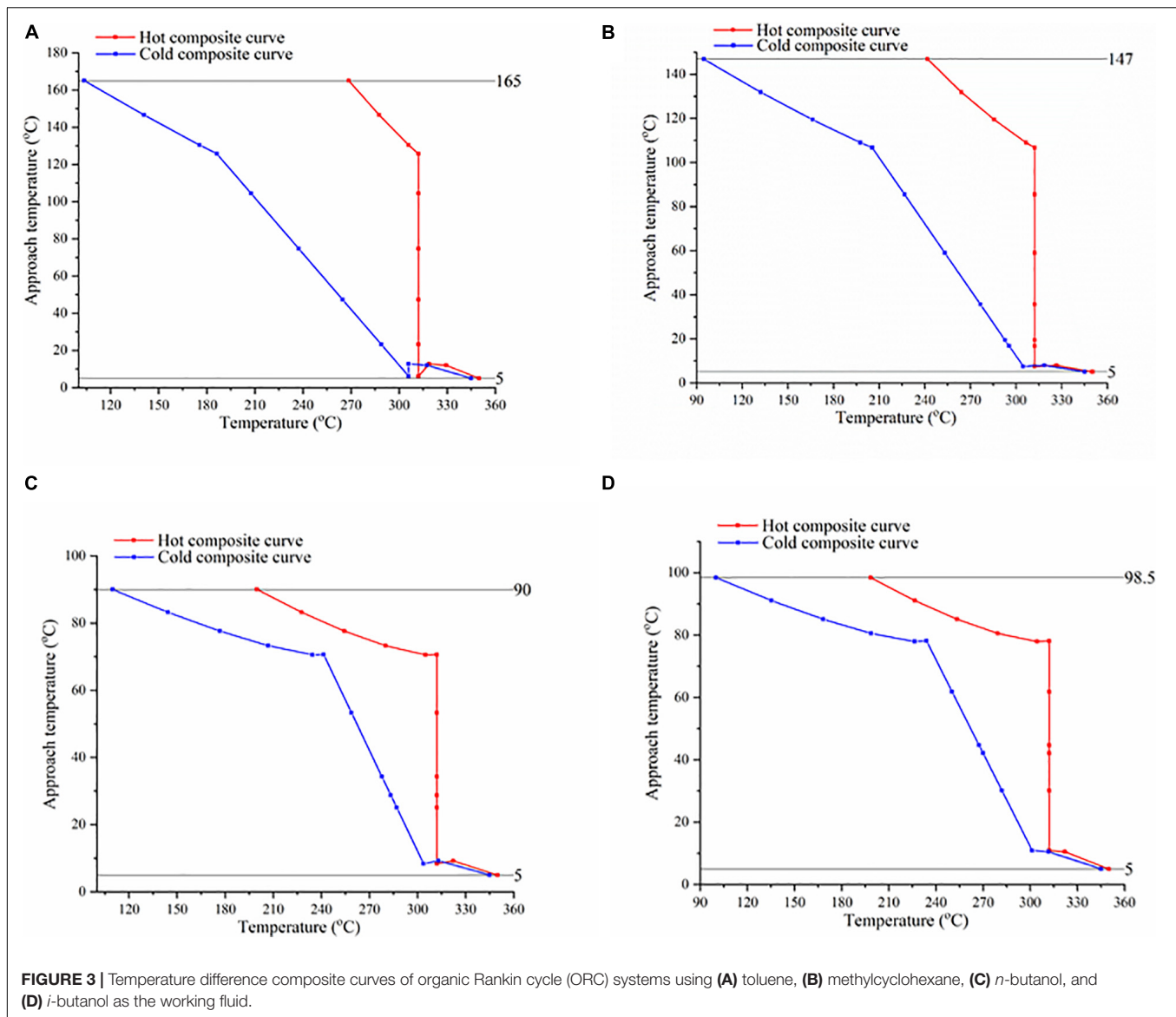proposed WFs, MCH shows the highest peak indicating the least efficient process.

Figure 4 demonstrates THCCs of toluene and proposed WFs. THCCs propose a visualized trend of heat flow inside a heat exchanger. A wide gap between hot and cold CCs depicts low heat recovery, whereas the narrow gap shows more heat recovery and high thermodynamic efficiency. The gap between these curves also depicts MITA value. This gap is prominent at the cold end, which should be low, meeting the criteria of MITA 5°C. In **Figure 4**, toluene shows the largest gap, whereas *n*-butanol shows the lowest gap. A large gap tends to increase entropy generation, which consequently increases exergy destruction and decreases process efficiency. This gap can be reduced by optimal WF selection. In that case, *n*-butanol is most efficient than toluene and proposed WFs mainly because of the lowest temperature gap. Moreover, it is noted that the *n*-butanol and *i*-butanol show high heat flow i.e., approx. 1300 kW, whereas toluene shows the lowest heat flow (approx. 980 kW). High heat flow generates more power in the turbine because of large heat capacity. For instance, *i*-butanol has a large heat capacity (2.94 kJ/kg°C),

and due to which it generates more power in the turbine i.e., 253 kW. The T–s diagrams of all studied WFs are summarized and given in **Figure 5**. Less entropy is generated when the ORC systems were operated at low temperatures. The proposed WFs are operated at lower temperatures than toluene, thus generating less entropy than toluene.

Exergy Analysis

Energy analysis alone is not sufficient to evaluate an energy conversion system's performance from a heating source to output work. Energy analysis only quantifies the work delivered by the system. However, it does not provide information related to the potential ability of a system to deliver work (Souza et al., 2020). The irreversibility must be accounted for during the evaluation of the system ability (Liu et al., 2020). Therefore, the exergy destruction in different components of the system must be evaluated. Exergy analysis provides information regarding the location and source of irreversibilities (Khaljani et al., 2015).

Exergy is the theoretical maximum useful work that maintains a thermodynamic equilibrium between systems and

FIGURE 3 | Temperature difference composite curves of organic Rankin cycle (ORC) systems using **(A)** toluene, **(B)** methylcyclohexane, **(C)** *n*-butanol, and **(D)** *i*-butanol as the working fluid.

the environment. Assuming the control volume approach for each component, the exergy balance equation can be expressed as follows:

$$\sum_{in} \dot{E}_i = \sum_{out} \dot{E}_j + \dot{E}_D \tag{1}$$

where, $\sum\limits_{in} \dot{E}_i$, and $\sum\limits_{out} \dot{E}_j$ are the inlet and outlet exergy streams, respectively, and $\dot{E}_D$ is the exergy destruction.

The specific exergy equation can be written as follows:

$$e = h - h_o - T_o(s - s_o) \tag{2}$$

where the subscript "o" denotes the dead state.

Exergy analysis is useful to establish strategies and procedures for more effective use of energy, and it has been applied to different thermal processes, such as power generation, heating, and regeneration (Nami et al., 2018). Exergy can be divided

into four components: physical, chemical, kinetic, and potential (Venkatarathnam and Timmerhaus, 2008). In this study, the last three types of exergy were neglected because of no change in composition, speed, and height. The important formulas used to calculate exergy destruction are listed in **Table 4**. The exergy destruction of the ORC systems using the WFs in this study is illustrated in **Figure 6**.

The exergy destruction values of the ORC systems using MCH, *n*-butanol, and *i*-butanol were higher than that of the ORC system using toluene. Maximum exergy destruction were detected in the condenser for all WFs, where the losses were three times higher than the evaporator. The large temperature difference between the cooling water and the stream exiting the turbine is a source of this high exergy destruction in the condenser. This exergy destruction can be minimized by decreasing this temperature difference or by heat recovery from the turbine exit stream to minimize condenser heat load.
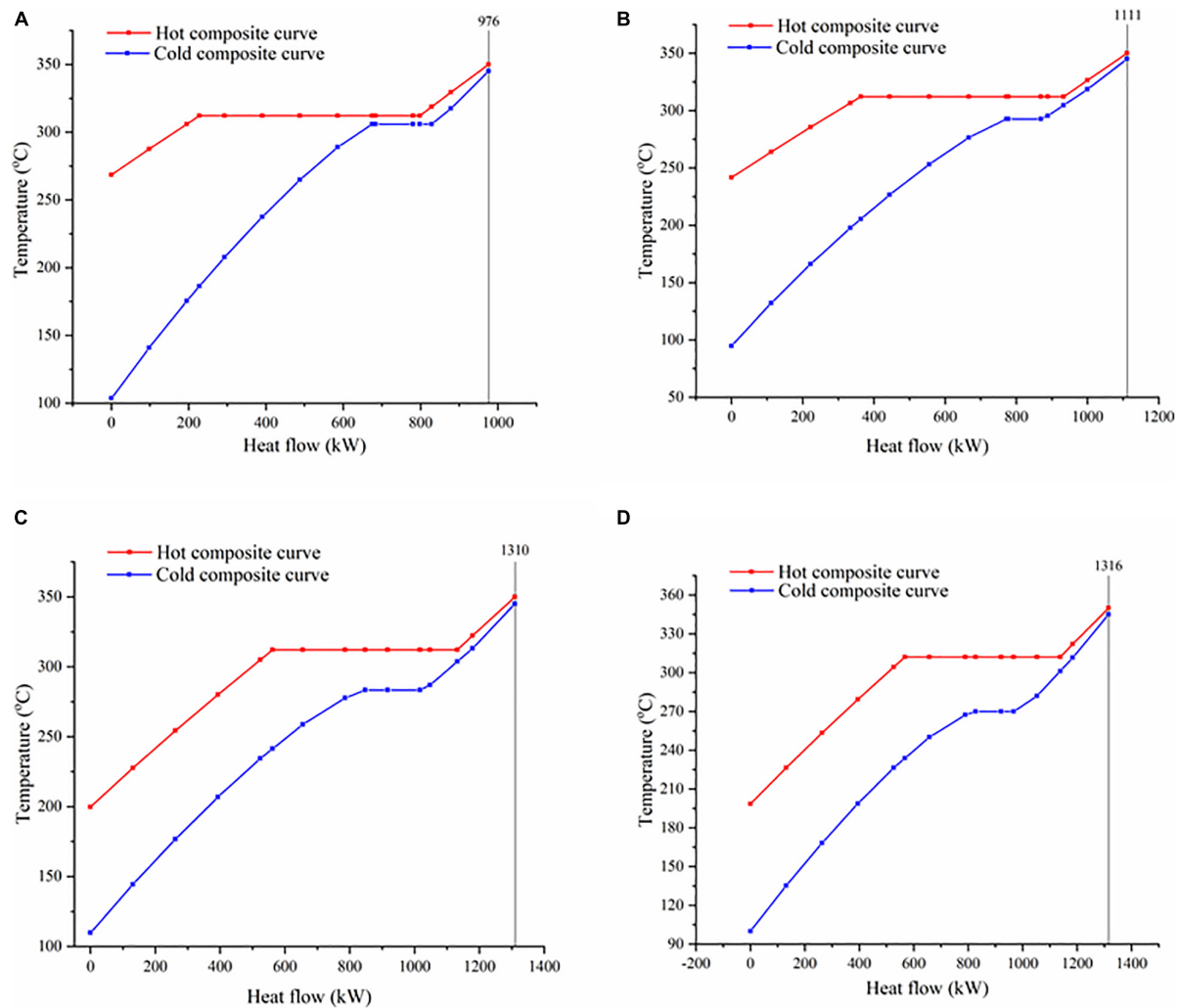
FIGURE 4 | Temperature–heat flow composite curves of organic Rankine systems using **(A)** toluene, **(B)** methylcyclohexane, **(C)** n-butanol, **(D)** i-butanol as working fluids.

Economic Analysis

Economic analysis is a useful approach to verify proposed designs' viability (Zhang et al., 2019). In this study, cost estimation for each design using the proposed WFs was performed by analyzing the power and revenue generation of each ORC system. A constant flow rate for each proposed WF was maintained for a fair comparison among the configurational analyses. The cost relations were retrieved from Nelson et al. (1989) and Turton et al. (2008), in which the total capital investment (TCI) and operating cost were the main contributors to the total annual cost (TAC). For a fair comparison, a payback period of 3 years was considered when analyzing the TAC. The TCI of the proposed design was calculated for the evaporator, condenser, turbine, and pump, and the operating cost was accounted only for pumping and condensing the WF. A water condenser was used to condense the fluid used for recycling to ensure the process's continuity. The electricity cost was adjusted to 0.2 \$/kWh based on recent literature-retrieved

trends (Turton et al., 2008). All cost relations are presented in the following equations:

$$log_{10} C_p^o = K_1 + K_2 log_{10}(A) + K_3 \left[log_{10}(A) \right] 2 \qquad (3)$$

$$Total\ annual\ cost\ (TAC) = \frac{TCI}{3} + Operating\ cost \qquad (4)$$

where A is a size parameter that corresponds to the power generated in different equipment parts, such as the turbine and heat exchanger, and K is a constant used to calculate the base module cost. The value of this constant is different for each design, as presented in **Table 5**.

Table 6 summarizes the economic evaluation of the ORC system using the proposed WFs. It is interesting to note that the power generation of ORC systems are directly related to fluid costs. Both *i*-butanol and *n*-butanol are expensive than toluene and generate more power than toluene. Similarly, MCH was the least expensive of the prospective WFs and generated the lowest
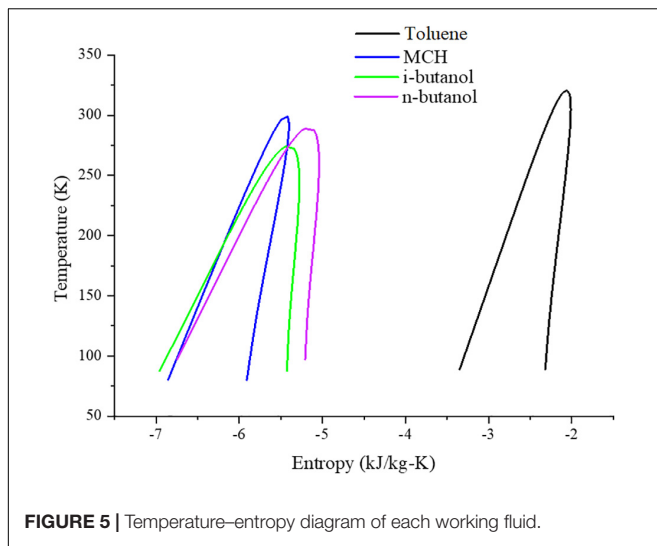
FIGURE 5 | Temperature–entropy diagram of each working fluid.

TABLE 4 | Important formulas used for exergy analysis.

Relationship	Explanation
$I_{evap} = m_s (e_5 - e_6) + m_{wf}(e_4 - e_1)$	Exergy destruction in the evaporator
$I_{tur} = m_{wf} (e_1 - e_2) - W_t$	Exergy destruction in turbine
$I_{cond} = m_w (e_7 - e_8) + m_{wf}(e_2 - e_3)$	Exergy destruction in condenser
$I_{pum} = W_p - m_{wf} (e_4 - e_3)$	Exergy destruction in pump
$E_{in} = m_s (e_5 - e_6)$	Total exergy input to the system
$\eta_{ex} = \frac{W_{net}}{E_{in}}$	Net power output to the total exergy input to the system

power of all ORC systems. The ORC system using *i*-butanol generated the highest power (253.3 kW) followed by the ORC system using *n*-butanol (250.5 kW). The power generated by the ORC systems using *n*-butanol and *i*-butanol as WFs was 4.67 and 5.7% higher, respectively, than that of the ORC system using toluene. The economic analysis data in **Table 6** reveals that the capital costs of the ORC systems using the prospective WFs were slightly higher than that of the toluene-based ORC system. Similarly, the operating costs of the butanol-based ORC systems were higher than that of the toluene-based ORC system, owing to the high condenser duty and pump power associated with the butanol-based WFs. Hence, the overall TACs of the ORC systems using *i*-butanol and *n*-butanol were 6.4 and 7.94% higher, respectively, than that of the ORC system using toluene. Nevertheless, the overall efficiency in terms of cash flow and revenue generation of the ORC systems using the prospective WFs was higher than that of the ORC system using toluene. The data in **Table 6** demonstrate that the butanol-based ORC systems were remarkably profitable because the maximum revenues were obtained when *i*-butanol ($206 634) and *n*-butanol ($196 470.6) were used as the WFs, which were 48.7 and 46% higher, respectively, than those of the toluene-based ORC system. Hence,
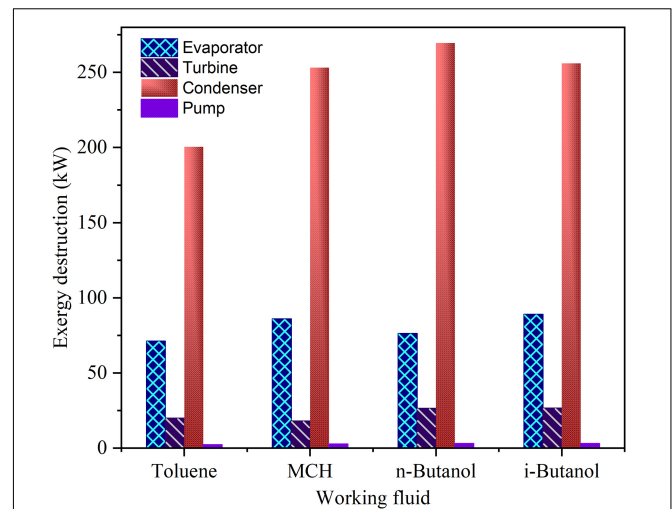

FIGURE 6 | Equipment wise exergy destruction values of toluene, methylcyclohexane, *n*-butanol, and *i*-butanol.

TABLE 5 | Values of constant K used to calculate the base module cost (Turton et al., 2008).

Equipment	K_1	K_2	K_3
Evaporator	4.6656	−0.1557	0.1547
Turbine	2.2476	1.4965	−0.1618
Pump	3.3892	0.0536	0.1538
Condenser	4.0336	0.2341	0.0497

TABLE 6 | Economic comparison of toluene, methylcyclohexane, *n*-butanol, and *i*-butanol.

WF	Toluene	MCH	*i*-butanol	*n*-butanol
Fluid cost ($/kg)	1.13	1.07	1.18	1.31
Power generated (kW)	191.8	185	253.3	250.5
Total capital investment ($)	750601.6	731554.7	791261	805601.9
Operating cost ($)	13346.7	15173.2	17772.1	17759.2
Total annualized cost ($/y)	263546.5	259024.8	281525.8	286293.2
Cash flow in ($/y)	369636.9	356532	488159.8	482763.6
Revenue ($)	106090.5	97507.2	206634	196470.6
Annual profit as compared to toluene (%)	–	–	48.7	46.0

it was concluded that conventional WFs could be successfully replaced with *i*-butanol because of their high capacity, low cost, and high power generation capacity.

WORKING FLUIDS SELECTION: TRADEOFF ANALYSIS

The tradeoff of the ORC systems using the prospective WFs was analyzed, and the results were compared with those of the
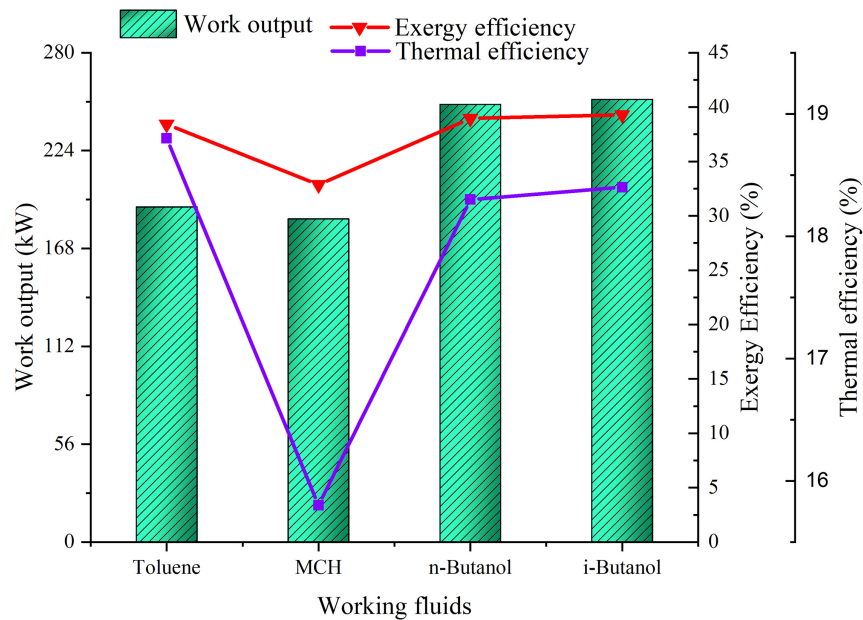
FIGURE 7 | Work output, thermal efficiency, and exergy efficiency of working fluids.

toluene-based ORC system. Both *n*-butanol and *i*-butanol were more competitive than MCH in terms of power generation. The power output of the *n*-butanol– and *i*-butanol-based ORC systems were 30 and 32% higher, respectively, than that of the toluene-based ORC system. Conversely, the power generated by the MCH-based ORC system was 3.5% lower than that generated by the toluene-based ORC system. However, the thermal efficiencies of MCH, *n*-butanol, and *i*-butanol were 16, 2.6, and 2.1% lower, respectively, than that of toluene. Among the prospective WFs, *i*-butanol presented the highest thermal efficiency (18.4%), as seen in **Figure 7**. The exergy efficiency of the ORC systems provided a better understanding of thermodynamic inefficiency between heat transfer and work. The exergy efficiencies of *n*-butanol (37.6%) and *i*-butanol (38%) were higher than that of toluene (37.2%), whereas that of MCH (32%) was lower. Moreover, the economic analysis data indicated that the operating costs of the ORC systems using MCH, *n*-butanol, and *i*-butanol were much higher than those of the toluene-based ORC system because the prospective WFs were more expensive than toluene; however, *i*-butanol was more economical, and the ORC system using *i*-butanol generated an annual profit of 48.7%. Therefore, a tradeoff existed between the prospective WFs, and *i*-butanol over performed the other prospective WFs.

IMPACT OF WFs FLOWRATE ON ORC PERFORMANCE

The ORC performance has been further evaluated by considering WFs flowrate as a design variable considering the MITA constraint as suggested by one of the reviewers. This is done by increasing the WF flowrate, keeping MITA at 5°C, till no

further flowrate can be increased. Initially, the WFs flowrate has been kept fixed and process performance is evaluated for a fair comparison among proposed WFs. This assessment was named as Case-I whereas, upon reviewer's suggestion, the process performance is evaluated at maximum WFs flowrate to draw maximum potential. This was named as Case-II. The comparison of both cases is presented in **Table 7**.

It can be seen from **Table 7** that toluene consumes maximum flowrate among all WFs i.e., 5920 kg/h, however, it has low power generation and low exergy efficiency. On the contrary, i-butanol has highest specific power generation (0.054 kWh/kg) at approx. 24% higher than that of toluene. Similarly, the exergy efficiency (39.77%) of i-butanol is highest amongst all WFs. MCH shows better economic performance with lowest TCI and TAC mainly

TABLE 7 | Organic Rankine cycle (ORC) performance comparison with same flowrate (case-I) and with different flowrate (case-II) of working fluids.

		Toluene	MCH	*n*-butanol	*i*-butanol
Case-I	Flowrate (kg/h)	4729	4729	4729	4729
	Thermal efficiency (%)	18.8	15.9	18.3	18.4
	Exergy efficiency (%)	37.15	31.81	37.66	37.99
	Sp. power generation (kWh/kg)	0.039	0.037	0.05	0.051
	TCI (m$)	0.75	0.73	0.8	0.79
	TAC (m$/y)	0.26	0.25	0.29	0.28
Case-II	Flowrate (kg/h)	5920	5070	5233	5547
	Thermal efficiency (%)	18.8	15.9	18.3	18.4
	Exergy efficiency (%)	38.25	32.14	38.69	39.77
	Sp. power generation (kWh/kg)	0.041	0.039	0.053	0.054
	TCI (m$)	2.2	1.9	2.3	2.4
	TAC (m$/y)	0.75	0.67	0.8	0.82

due to lowest fluid cost. It is interesting to note that despite changing WFs flowrate, the thermal efficiency remains same in both cases. In authors' understanding, this is because when the flowrate is increased, the heat transfer between hot and cold fluid increased alongside with increased work output. The overall ratio of work output and heat flow remains same in both cases. Therefore, the thermal efficiency remains same in both cases.

CONCLUSION

In this study, three dry unconventional WFs (*n*-butanol, *i*-butanol, and MCH) were analyzed from a PSE perspective. The thermodynamic properties of the prospective WFs were comparable with those of toluene, which is the most widely used WF. Among the proposed WFs, *i*-butanol is a potential replacement for toluene owing to its high heat capacity (2.9 kJ/kg), high power generation (253 kW), and high exergy efficiency (38%). Conversely, the MCH-based ORC system generated the lowest power (176 kW). In addition to the slightly higher TAC, the annual profit generated by the ORC system using *i*-butanol was 48.7% higher than that of the toluene-based ORC system. Therefore, *i*-butanol can successfully replace toluene as a WF. Moreover, ORC systems can be further improved by

using sensible heat, which can effectively reduce condenser duty. Furthermore, recuperation technology can be implemented to use sensible heat and also enhance power generation.

DATA AVAILABILITY STATEMENT

The original contributions presented in the study are included in the article/supplementary material, further inquiries can be directed to the corresponding author/s.

AUTHOR CONTRIBUTIONS

All authors listed have made a substantial, direct and intellectual contribution to the work, and approved it for publication.

FUNDING

REFERENCES

Abdel-Hadi, M. A. (2009). Determination of methane content by measurements of flame temperature and voltage from biogas burner. *Misr J. Agric. Eng.* 26, 498–513.

Anastasovski, A., Rasković, P., and Guzović, Z. (2020). A review of heat integration approaches for organic rankine cycle with waste heat in production processes. *Energy Convers. Manag.* 221:113175. doi: 10.1016/j.enconman.2020.113175

Barse, K. A., and Mann, M. D. (2016). Maximizing ORC performance with optimal match of working fluid with system design. *Appl. Therm. Eng.* 100, 11–19. doi: 10.1016/j.applthermaleng.2016.01.167

Blondel, Q., Tauveron, N., Caney, N., and Voeltzel, N. (2019). Experimental study and optimization of the organic rankine cycle with pure NovecTM649 and zeotropic mixture NovecTM649/HFE7000 as working fluid. *Appl. Sci.* 9:1865. doi: 10.3390/app9091865

Bruno, J. C., López-Villada, J., Letelier, E., Romera, S., and Coronas, A. (2008). Modelling and optimisation of solar organic rankine cycle engines for reverse osmosis desalination. *Appl. Therm. Eng.* 28, 2212–2226. doi: 10.1016/j.applthermaleng.2007.12.022

Eastman (2020). *Therminol VP-1 Heat Transfer Fluid.* Technical Bulletin TF9141. Kingsport, TN: Eastman.

Ediger, V. (2019). An integrated review and analysis of multi-energy transition from fossil fuels to renewables. *Energy Procedia* 156, 2–6. doi: 10.1016/j.egypro.2018.11.073

Imran, M., Haglind, F., Asim, M., and Zeb Alvi, J. (2018). Recent research trends in organic Rankine cycle technology: a bibliometric approach. *Renew. Sustain. Energy Rev.* 81, 552–562. doi: 10.1016/j.rser.2017.08.028

Khaljani, M., Khoshbakhti Saray, R., and Bahlouli, K. (2015). Comprehensive analysis of energy, exergy and exergo-economic of cogeneration of heat and power in a combined gas turbine and organic Rankine cycle. *Energy Convers. Manag.* 97, 154–165. doi: 10.1016/j.enconman.2015.02.067

Khatoon, S., Almefreji, N. M. A., and Kim, M.-H. (2021). Thermodynamic study of a combined power and refrigeration system for low-grade heat energy source. *Energies* 14:410. doi: 10.3390/en14020410

Lee, U., Jeon, J., Han, C., and Lim, Y. (2017). Superstructure based techno-economic optimization of the organic rankine cycle using LNG cryogenic energy. *Energy* 137, 83–94. doi: 10.1016/j.energy.2017.07.019

Liu, X., Yang, X., Yu, M., Zhang, W., Wang, Y., Cui, P., et al. (2020). Energy, exergy, economic and environmental (4E) analysis of an integrated process combining CO2 capture and storage, an organic Rankine cycle and an absorption refrigeration cycle. *Energy Convers. Manag.* 210:112738. doi: 10.1016/j.enconman.2020.112738

Macchi, E. (2016). *Organic Rankine Cycle (ORC) Power Systems.* Amsterdam: Elsevier Science.

Mahmoudi, A., Fazli, M., and Morad, M. R. (2018). A recent review of waste heat recovery by Organic Rankine Cycle. *Appl. Therm. Eng.* 143, 660–675. doi: 10.1016/j.applthermaleng.2018.07.136

Maraver, D., Royo, J., Lemort, V., and Quoilin, S. (2014). Systematic optimization of subcritical and transcritical organic Rankine cycles (ORCs) constrained by technical parameters in multiple applications. *Appl. Energy* 117, 11–29. doi: 10.1016/j.apenergy.2013.11.076

Mudasar, R., Aziz, F., and Kim, M. H. (2017). Thermodynamic analysis of organic Rankine cycle used for flue gases from biogas combustion. *Energy Convers. Manag.* 153, 627–640. doi: 10.1016/j.enconman.2017.10.034

Nami, H., Ertesvåg, I. S., Agromayor, R., Riboldi, L., and Nord, L. O. (2018). Gas turbine exhaust gas heat recovery by organic Rankine cycles (ORC) for offshore combined heat and power applications - energy and exergy analysis. *Energy* 165, 1060–1071. doi: 10.1016/j.energy.2018.10.034

Nelson, D. A., Kirkwood, R. L., and Douglas, J. M. (1989). Conceptual design of chemical processes. *Simul. Ser.* 20, 180–184.

Pan, M., Lu, F., Zhu, Y., Huang, G., Yin, J., Huang, F., et al. (2020). Thermodynamic, exergoeconomic and multi-objective optimization analysis of new ORC and heat pump system for waste heat recovery in waste-to-energy combined heat and power plant. *Energy Convers. Manag.* 222:113200. doi: 10.1016/j.enconman.2020.113200

Rowshanaie, O., Mustapha, S., Ahmad, K. A., and Rowshanaie, H. (2015). Simulation of organic rankine cycle through fluegas to large scale electricity generation purpose. *J. Teknol.* 77, 9–18. doi: 10.11113/jt.v77.6878

Saleh, B., Koglbauer, G., Wendland, M., and Fischer, J. (2007). Working fluids for low-temperature organic Rankine cycles. *Energy* 32, 1210–1221. doi: 10.1016/j.energy.2006.07.001

Shu, G., Wang, X., and Tian, H. (2016). Theoretical analysis and comparison of rankine cycle and different organic rankine cycles as waste heat recovery system for a large gaseous fuel internal combustion engine. *Appl. Therm. Eng.* 108, 525–537. doi: 10.1016/j.applthermaleng.2016.07.070

Song, J., and Gu, C. W. (2015). Analysis of ORC (Organic Rankine Cycle) systems with pure hydrocarbons and mixtures of hydrocarbon and retardant for engine waste heat recovery. *Appl. Therm. Eng.* 89, 693–702. doi: 10.1016/j.applthermaleng.2015.06.055

Souza, R. J., Dos Santos, C. A. C., Ochoa, A. A. V., Marques, A. S., Neto, L. M. J., and Michima, P. S. A. (2020). Proposal and 3E (energy, exergy, and exergoeconomic) assessment of a cogeneration system using an organic Rankine cycle and an absorption refrigeration system in the Northeast Brazil: thermodynamic investigation of a facility case study. *Energy Convers. Manag.* 217:113002. doi: 10.1016/j.enconman.2020.113002

Sun, W., Yue, X., and Wang, Y. (2017). Exergy efficiency analysis of ORC (Organic Rankine Cycle) and ORC-based combined cycles driven by low-temperature waste heat. *Energy Convers. Manag.* 135, 63–73. doi: 10.1016/j.enconman.2016.12.042

Touaibi, R., Koten, H., and Boydak, O. (2020a). An energy investigation of an Organic Rankine Cycle utilizing three organic fluids. *Hittite J. Sci. Eng.* 7, 41–44. doi: 10.17350/hjse19030000170

Touaibi, R., Koten, H., and Boydak, O. (2020b). Parametric study of an organic rankine cycle using different fluids. *Emerg. Sci. J.* 4, 122–128. doi: 10.28991/esj-2020-01216

Turton, R., Bailie, R. C., Whiting, W. B., and Shaeiwitz, J. A. (2008). *Analysis, Synthesis and Design of Chemical Processes*. London: Pearson Education.

Venkatarathnam, G., and Timmerhaus, K. D. (2008). *Cryogenic Mixed Refrigerant Processes*. Berlin: Springer.

Yagli, H., Koc, A., Karakus, C., and Koc, Y. (2016). Comparison of toluene and cyclohexane as a working fluid of an organic Rankine cycle used for reheat furnace waste heat recovery. *Int. J. Exergy* 19, 420–438. doi: 10.1504/IJEX.2016.075677

Yu, G., Shu, G., Tian, H., Wei, H., and Liu, L. (2013). Simulation and thermodynamic analysis of a bottoming Organic Rankine Cycle (ORC) of diesel engine (DE). *Energy* 51, 281–290. doi: 10.1016/j.energy.2012.10.054

Zhang, C., Liu, C., Xu, X., Li, Q., and Wang, S. (2019). Energetic, exergetic, economic and environmental (4E) analysis and multi-factor evaluation method of low GWP fluids in trans-critical organic Rankine cycles. *Energy* 168, 332–345. doi: 10.1016/j.energy.2018.11.104

Black Hole-Inspired Optimal Design of Biomethane Liquefaction Process for Small-Scale Applications

Tianbiao He[1], Muhammad Abdul Qyyum[2]*, Zhongming Zhou[1], Ashfaq Ahmad[3], Mohammad Rehan[4], Abdul-Sattar Nizami[5] and Moonyong Lee[2]*

[1] Department of Gas Engineering, College of Pipeline and Civil Engineering, China University of Petroleum (East China), Qingdao, China, [2] School of Chemical Engineering, Yeungnam University, Gyeongsan-si, South Korea, [3] Department of Computer Science, COMSATS University Islamabad, Lahore, Pakistan, [4] Center of Excellence in Environmental Studies, King Abdulaziz University, Jeddah, Saudi Arabia, [5] Sustainable Development Study Centre, Government College University, Lahore, Pakistan

Biomethane is regarded as a promising renewable energy source, with great potential to satisfy the growth of energy demands and to reduce greenhouse gas emissions. Liquefaction is a suitable approach for long distances and overseas transportation of biomethane; however, it is energy-intensive due to its cryogenic working condition. The major challenge is to design a high-energy efficiency liquefaction process with simple operation and configuration. A single mixed refrigerant biomethane liquefaction process adopting the cryogenic liquid turbine for small-scale production has been proposed in this study to address this issue. The optimal design corresponding to minimal energy consumption was obtained through the black-hole-based optimization algorithm. The effect of the minimum internal temperature approach (MITA) in the main cryogenic heat exchanger on the biomethane liquefaction process performance was investigated. The study results indicated that the specific energy consumption of modified case 2 with MITA of 2°C was 0.3228 kWh/kg with 21.01% reduction compared to the published base case. When the MITA decreased to 1°C, the specific power of modified case 1 reduced to 0.3162 kWh/kg, which was 24.96% lower than the base case. In terms of exergy analysis, the total exergy destruction of the modified cases 1, 2, and 3 was 31.28%, 22.27%, and 17.51% lower than the base case, respectively. This study's findings suggested that introducing the cryogenic liquid turbine to the single mixed refrigerant-based biomethane liquefaction process could reduce the specific energy consumption and total exergy destruction significantly. Therefore, this study could provide a viable path for designing and improving the small-scale biomethane liquefaction process.

Keywords: biomethane, liquefied biomethane, single mixed refrigerant, optimization, exergy destruction analysis, renewable LNG, liquid biogas, energy consumption minimization

INTRODUCTION

One of the world's biggest challenges is producing green energy to meet ever-increasing energy demands with minimum environmental damage. Presently, over 80% of global energy demands are fulfilled by fossil fuels (ExxonMobil, 2019), which contribute to most greenhouse gas emissions, thereby leading to global warming and climate change. Therefore, it is imperative to shift toward sustainable energy production systems for mitigating climate change.

Biogas, generated from waste organic materials and sewage by anaerobic digestion process, is a renewable energy source that can be accessed in most regions of the world (Sun et al., 2015). It contains 53–70% of CH_4 and 30–47% of CO_2, depending on the organic matter used to generate biogas (Pellegrini et al., 2018). As reported by the International Energy Agency, the demand for direct use of biogas in advanced and developing economies in 2018 was around 20.6 and 13.1 million tons of oil equivalent (Mtoe), respectively (International Energy Agency, 2019). Biogas can be used directly as a fuel for space heating (Bauer et al., 2013), power generation, and vehicles (Arteconi et al., 2016). However, upgrading is required to remove CO_2 in the biogas to convert it into biomethane (BM), with higher-energy density (Hashemi et al., 2019). BM is a promising eco-friendly renewable energy source with 95–97% of CH_4 as its key component (Yousef et al., 2019).

There are two transportation methods for BM. One is to pressurize the BM to the pipeline pressure and inject it into the natural gas pipeline as a supplementary gas (Ullah Khan et al., 2017). The other is to cool down the BM gas to −162°C at 1 atm to convert it into a liquid state known as liquefied biomethane (LBM) (Budzianowski and Brodacka, 2017). LBM is the best option to recover the remote biomethane resource where the pipeline network is not available. However, LBM is more energy-intensive than liquefied natural gas (LNG) for its near-ambient pressure (Rehman et al., 2020). LNG's theoretical power requirement reduces with the increase of natural gas pressure before entering the liquefaction process. Thus, LBM needs to be pressurized to 4–5 MPa to diminish the liquefaction process' power requirement. Due to the small capacity and decentralized location of the biomethane production (Fan et al., 2008), small-scale biomethane liquefaction technologies are the most suitable option to recover these sources with a low capital cost and flexible operation (Baccioli et al., 2018). The conventional NG liquefaction processes, namely, cascade liquefaction process (Lee et al., 2014; Mehrpooya et al., 2016), mixed refrigerant liquefaction process (He et al., 2020b; Qyyum et al., 2020b), and expander-based liquefaction process (Lin et al., 2017; He et al., 2019), can be adapted to produce LBM. However, the cascade liquefaction process and most of the mixed refrigerant liquefaction processes are designed for the large-scale LNG plants with a complex configuration, making them unsuitable for small-scale LBM production. Thus, there is a need to design and propose suitable and energy-efficiency liquefaction processes for LBM.

A considerable amount of literature has been published on the liquefaction of BM. Recently, Qyyum et al. (2020a) presented a comprehensive assessment of possible BM liquefaction technologies. They suggested that nitrogen expansion and single mixed refrigerant (SMR) liquefaction processes might be potential candidates. Nitrogen expansion liquefaction processes are considered suitable processes for small-scale LNG and LBM production plants because of their low capital cost and ease to start up and shut down. Hashemi et al. (2019) adopted cryogenic upgrading and chemical absorption upgrading integrated with a single-stage nitrogen-expander liquefaction process to produce LBM. The energy analysis implied that the proposed liquefaction process accounted for the most power consumption, and there existed space for energy performance improvement. Baccioli et al. (2018) compared conventional and cryogenic biogas upgrading processes integrated with the nitrogen expansion liquefaction process to produce LBM. The cryogenic biogas upgrading process integrated with the nitrogen expansion liquefaction process exhibited 1.45 kWh/kg of LBM. Haider et al. (2019) proposed a nitrogen-methane expansion biomethane liquefaction process integrating ionic liquid biogas upgrading resulting in 11.26 kWh/kmol of liquefaction energy consumption. Pasini et al. (2019) designed a dual nitrogen-expander liquefaction process for small-scale LBM production. The process of adopting radial turbines resulted in 0.75 kWh/kg of specific energy consumption. The nitrogen expansion liquefaction process for LBM is high-energy consumption making it unattractive to industrial LBM application.

Mixed refrigerant-based (MR) liquefaction processes are more energy-efficient than expansion-based processes for the better temperature curve match between the refrigerant and natural gas. Capra et al. (2019) analyzed five refrigeration cycles for the small-scale LBM production with a liquefaction capacity of 4.6 tons/d. The lowest energy consumption of 3061 kJ/kg LBM and cost of 6.3€/GJLHV were achieved by the MR process. Rehman et al. (2020) utilized the released cold energy from the liquid air energy storage system to reduce the refrigeration capacity of the MR-based BM liquefaction process. The findings indicated that the exergy efficiency could be increased by 42%, and the total annualized cost could be saved by 33.5%. He et al. (2019) compared the energetic and economic performances of parallel nitrogen expansion (PNEC) and modified single mixed refrigerant (MSMR) liquefaction processes for small-scale LNG production. The results indicated that the specific energy consumption and a total investment of MSMR were 33.49% and 26.88% lower than PNEC, respectively. The SMR could be enhanced by adopting a liquid hydraulic turbine to replace the throttling valve to achieve higher thermodynamic efficiency (Qyyum et al., 2018).

From the above literature review, the SMR liquefaction process (including modified processes) is preferred for the small-scale LNG and LBM production owing to its lower energy consumption and total investment, and compact design. It can manipulate the mixed refrigerant compositions, leading to a more flexible operation. Because of BM's low pressure, it is required to compress it to a proper pressure to achieve a low specific energy consumption, which requires retrofitting the configuration of the liquefaction process. The liquefaction process modification followed by the optimization could benefit

the energy saving. Moreover, previous studies mainly adopt the genetic algorithm (GA) and particle swarm optimization (PSO) algorithm to improve the energy performance of liquefaction processes. However, performing these algorithms depends on turning parameters. The improper tuning parameters may track algorithms in local optimal. Thus, algorithms without tuning parameters are more attractive to BM liquefaction process optimization. The black-hole-based optimization (BHBO) algorithm, a population-based method without tuning parameters, is a promising candidate for LBM liquefaction processes, which has not yet been employed in the open literature.

To the best of our knowledge, this is the first study of its kind to explore the black-hole-based optimization algorithm for the design optimization of the biomethane SMR liquefaction process. The process was modified by introducing cryogenic liquid turbine to replace the throttling valve with the benefit of reducing exergy loss and recovering mechanical power. Different minimum internal temperature differences (MITA) were studied to minimize the specific energy consumption of the process. Furthermore, the energy, exergy, and composite curve analysis were applied to reveal the future improvement potential and directions. The modified process optimized by the BHBO exhibits an impressive energy efficiency. This study gives an insight into the SMR-based LBM process design and optimization to minimize energy consumption to extend its potential application for small-scale LBM production. Thus, the proposed process associated with the black-hole-based optimization algorithm provides an energy-efficient method to recover and utilize
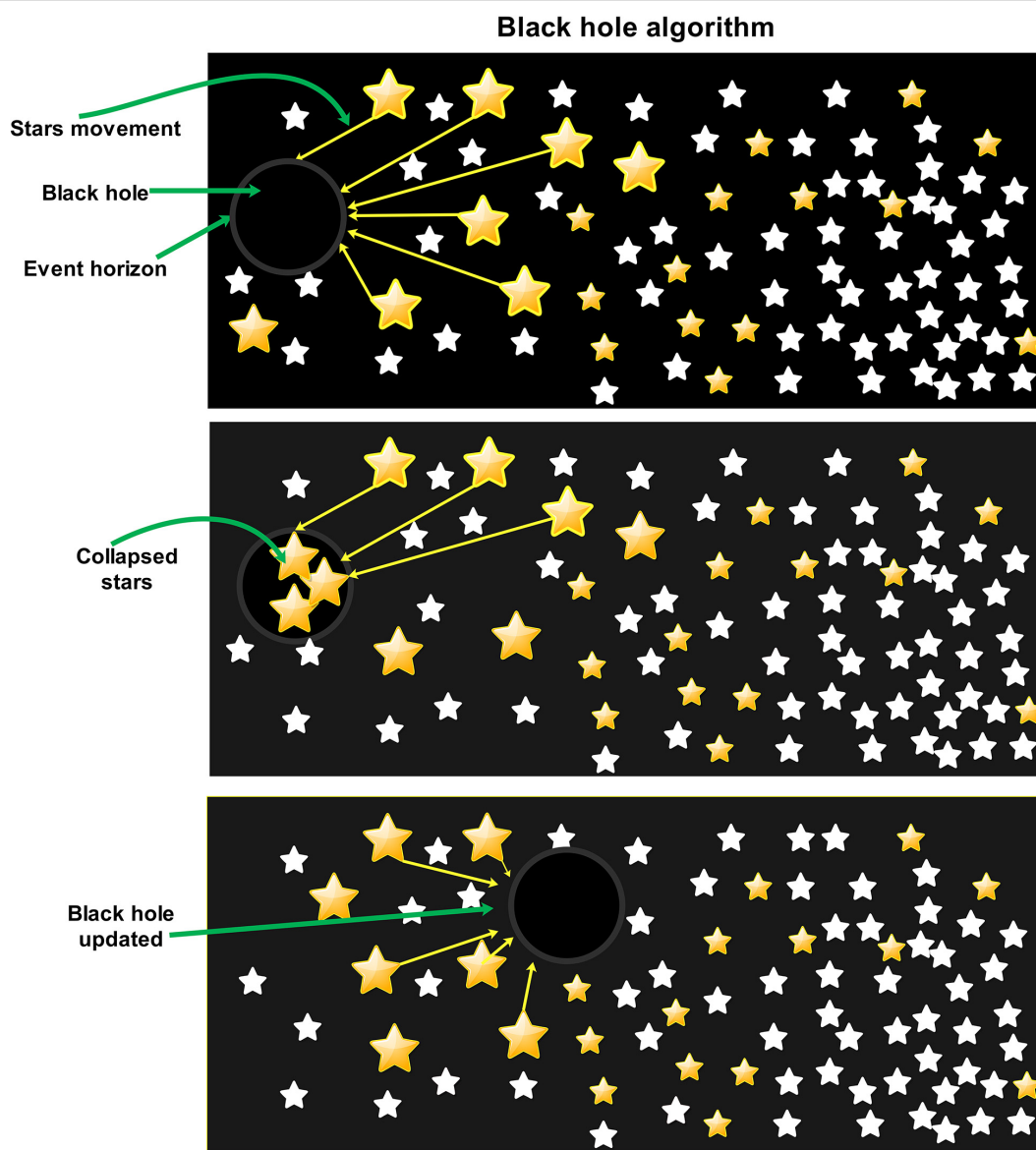

FIGURE 1 | Physical life cycle of the black hole algorithm.

biomethane, which could be beneficial to increase the percentage of renewable energies in the global energy market.

OPTIMIZATION METHOD

Black-Hole Optimization Algorithm

The black hole is such a mass-concentrated region in the space that it is impossible for objects falling into it to escape from it. Black-hole-based optimization (BHBO) is a new metaheuristic methodology derived from the phenomena of black hole. Black

holes are so thick that nothing even the light can emit back from their inside. The spherical skull or the black hole's periphery layer is named as the event horizon (Hatamlou, 2013; Black Hole, 2021). The objects that cross this horizon are swallowed by the black hole forever. The physical life cycle and interpretation of the black-hole algorithm is seen in **Figure 1**.

Black-hole-based optimization is a population-based method in which the optimal solution from the initial population of solutions is evolved by a procedure that is motivated by the black hole phenomenon. The evolution process is accomplished by transmuting the candidate solutions to the best candidate
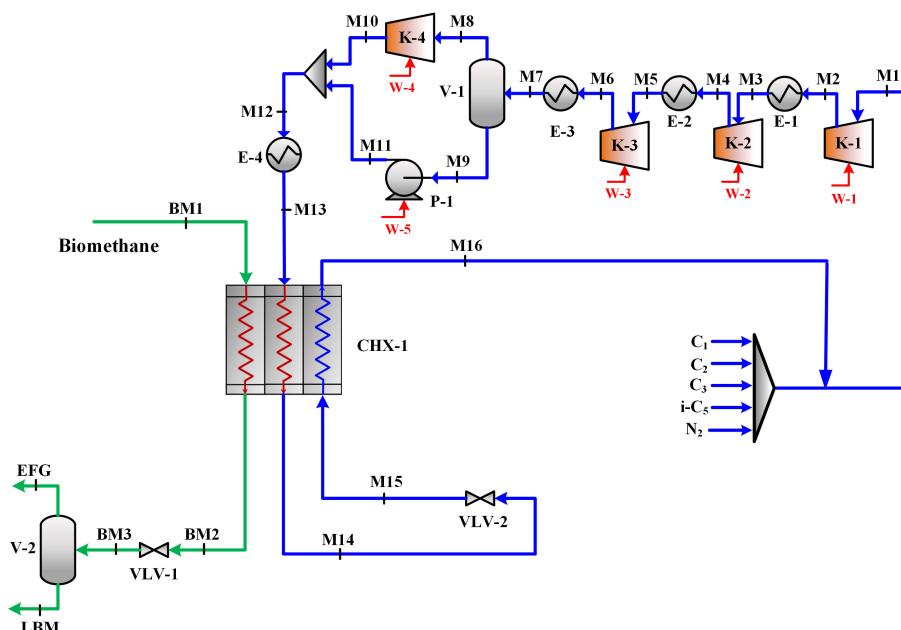

FIGURE 2 | Base case flow sheet of biomethane liquefaction by adopting the SMR process (Haider et al., 2020).
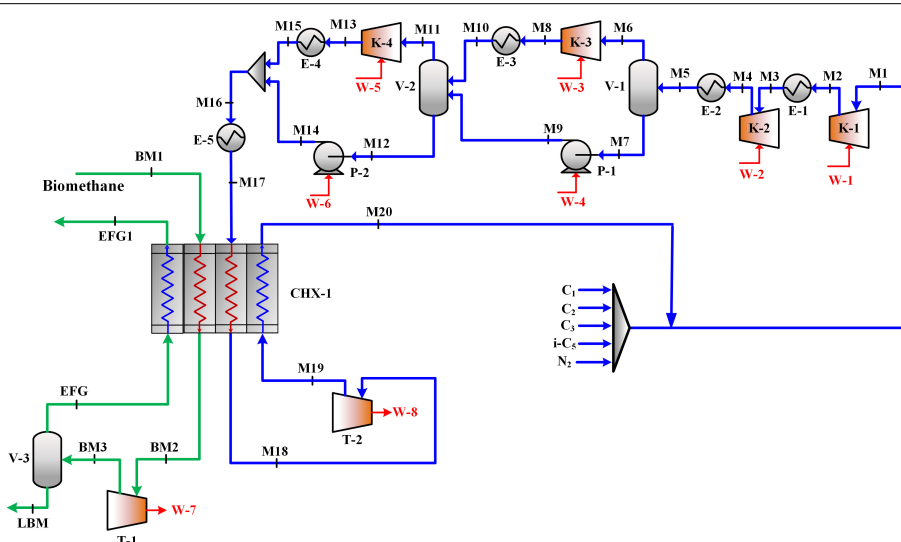

FIGURE 3 | Modified biomethane liquefaction process.

that is known as black hole. Other candidate solutions that fall within the black hole's range are replaced by the candidate solutions newly created in the given search space. The working procedure of the BHBO algorithm can be well described in the forthcoming steps.

Step 1: Bound Normalization
All variables may have different ranges (upper and lower bounds). These ranges of all variables are first normalized to new ranges from 0 to 1. The ranges of all variables can be normalized using Eq. (1).

$$Normalized\ Var\ (i) = \frac{Var\ (i) - LB(i)}{UB\ (i) - LB(i)} \quad (1)$$

Normalizing the variables' bounds can improve the convergence speed of the BHBO algorithm.

Step 2: Initialization
A random population of candidate solutions called the stars is generated and placed in a search space of the problem of n dimensions. The value of the objective function against each star is calculated, and the star that has the best fitness value is designated as the black hole X_{bh}.

Step 3: Movement of Stars
Star absorption is the process of moving stars toward the absorbing force of the black hole. Once the star population is generated and the black hole is assigned, the black hole starts absorbing its stars. Thus, all stars move toward the black hole. This movement/absorption of the stars can be formulated by Eq. (2).

$$X_i^{t+1} = X_i^t + Rand\left(X_{bh} - X_i^t\right) \ \forall i; \quad i \neq Best\ fitness\ value \quad (2)$$

where X_i^{t+1} and X_i^t are the locations of the ith star at iterations $t+1$ and t, respectively. X_{bh} is the location of the black hole (best fitness value), and $Rand$ is the random number between 0 and 1. As the black hole has the best fitness value so it does not move, it just attracts others.

Step 4: Updating the Black Hole
During stars' movement toward the black hole, it is possible that a star (candidate solution) at its new position gets its fitness value better than the already assigned black hole. In such case, the black hole's position is updated with this star, the algorithm continues its process with this updated black hole, and other stars start their movement toward this new/updated black hole.

Step 5: Generation of New Stars
During the stars' movement, a star can cross the event horizon (spherical boundary of the black hole). The star that crosses the event horizon is sucked by the black hole which results in star death. In order to keep the number of stars (candidate solutions) constant, a new star is randomly generated at the place of the died star and randomly placed in the search space (Chen and Chang, 2010; Hatamlou, 2013). The next iteration starts on completing one movement of each star. The radius of the event horizon can be calculated as by Eq. (3).

$$R = \frac{f_{bh}}{\sum_{i=1}^{n} f_i} \quad (3)$$

where n is the number of candidates (stars), and f_{bh} and f_i are the fitness values of the black hole and ith star, respectively.

Step 6: Termination Criteria
The above steps of the BHBO algorithm are repeated until the termination criteria. The algorithm could be terminated on two criteria. The first is the maximum number of iterations, and the second is the specific number of iterations during which the black hole does not change its position. In simple words, in the first case, BHBO will automatically terminate on completing the number of iterations defined by the user. In the second case, if the black hole's current position does not change after a certain number of iterations, the BHBO may be terminated. However, a careful study is needed to set the stopping criteria because the algorithm may be stopped without reaching the global optimum. Conversely, unnecessary running of the algorithm may be avoided if the convergence is to be expected earlier. Based on the above description, the pseudocode of the BHBO algorithm is given in **Algorithm 1**.

---

1. Randomly generate stars population (Candidate solutions) X_i ($i = [1, n]$) in the search space $\mathbf{S}(\mathbf{p}) = [\mathbf{X_1^p}, \mathbf{X_2^p}, \mathbf{X_3^p}, \ldots, \mathbf{X_n^p}]$ of some function.
2. Set the number of iterations or other termination criteria
3. **for** each ith star, calculate the Fitness function $\mathbf{f_i} = \sum_{i=1}^{PopSize} S(p)$
4.   Designate the best Fitness value as the Black Hole; $X_{hb} \leftarrow$ Optimal solution
5.   **while** (Termination criteria not met) **do**
6.   **for** each star X_i change its location as
7. $\mathbf{X_i^{t+1}} = \mathbf{X_i^t} + \mathbf{Rand}\left(\mathbf{X_{bh}} - \mathbf{X_i^t}\right)$
8.   **end for**
9.   Calculate the event horizon as: $\mathbf{R} = \frac{f_{bh}}{\sum_{i=1}^{n} f_i}$
10.   **for** each star X_i calculate its distance from the black hole
11. $\mathbf{D_i} = \sqrt{(\mathbf{X_{1bh}} - \mathbf{X_{1i}})^2 + (\mathbf{X_{2bh}} - \mathbf{X_{2i}})^2 + \ldots (\mathbf{X_{nbh}} - \mathbf{X_{ni}})^2}$
12.   **if** $D_i < R$
13.   Collapse X_i
14. $X_i \leftarrow$ new randomly generated star
15.   **end if**
16.   **if** Fitness value of X_i is better than that X_{hb}
17. X_i Black hole
18.   **end if**
19.   **end for**
20. $X_{bh} =$ Best optimal solution
21.   **end while**
22. **end for**

PROCESS DESIGN, OPTIMIZATION, AND ANALYSIS

Biomethane Liquefaction: Process Design and Simulation
The base case of biomethane liquefaction by adopting the SMR liquefaction process is illustrated in **Figure 2** (Haider et al., 2020).

The upgraded biomethane (methane molar fraction over 99%) goes into the multi-stream cryogenic heat exchanger (CHX-1) and is cooled and liquefied by the low-pressure mixed refrigerant. The stream BM2 decreases to the LBM storage pressure in VLV-1 and reduces the temperature leading to obtaining of the LBM in the separator's bottom with a liquefaction rate of 92%. The mixed refrigerant (MR) adopted in this paper consists of CH_4, C_2H_6, C_3H_8, i-C_5H_{12}, and N_2. The MR is pressurized by a four-stage compressor with intercooling. Subsequently, the high-pressure MR is cooled by the returning cold MR in CHX-1 and expanded in the throttling valve (VLV-2) to supply the cooling capacity for the biomethane and warm MR. Afterward, the superheated MR returns to the first-stage compressor's inlet (K-1) to complete the refrigeration cycle. The temperature of the MR outlet from the intercoolers is 40°C.

To improve the thermodynamic performance of the base case, cryogenic liquid turbines are introduced to replace the throttling valves (VLV-1 and VLV-2), as shown in **Figure 3**. Through this modification, the isentropic expansion can generate a larger temperature difference with the same pressure ratio and provide extra power for the compression system. In the modified case of the biomethane liquefaction process, the cold energy of the end flash gas (EFG) is recovered in the main cryogenic heat exchanger, which also reduces the refrigeration requirement from the SMR cycle.

The proposed biomethane liquefaction processes are modeled in Aspen HYSYS V10 by choosing the Peng–Robinson equation of state (Peng and Robinson, 1976) for the thermodynamic properties' calculation. It is assumed that the deep eutectic solvent-based process upgrades the biomethane, and its conditions are shown in **Table 1**.

To simplify the process simulation, several assumptions are made as follows:

(1) The process is in steady state.
(2) The heat losses from the equipment to the ambient are neglected.
(3) The adiabatic efficiency of the cryogenic liquid turbine, pump, and compressor is 90%, 75%, and 75% (Qyyum et al., 2018), respectively.
(4) The pressure drop of the warm stream and cold stream in the main cryogenic heat exchanger is 100 kPa (Haider et al., 2020).
(5) The pressure drop of the compressor intercooler is 25 kPa.
(6) The produced LBM is stored with a pressure of 120.9 kPa.

Simulation–Optimization Framework

In this study, optimization aims to find the optimal design of the proposed modified SMR process for LBM production corresponding to minimal specific energy consumption, i.e., objective function. Usually, liquefaction processes, especially mixed refrigerant-based, are highly non-linear and complex, mainly due to the number of exceptional interactions among the key design variables, constraints, and constrained objectives.

Therefore, even minor variations in the design or decision variables may cause an unfeasible process, which ultimately reduces the process' overall competitiveness. In this context, it is meaningful and mandatory to pinpoint the major influencing design variables and constraints allied with the design of the liquefaction process in order to get the desired benefits through rigorous optimization. The refrigerant flow rates, refrigerant condensation pressure, and evaporation pressure were chosen as the key design variables. The minimum internal temperature approach (MITA) that signifies the driving force of the heat transfer between the hot and cold streams inside the main cryogenic heat exchanger was taken as a constraint with a specified value of 1~3.0°C. All key design variables (with their lower and upper bounds), constraint, and objective function are listed in **Table 2**.

The constraint of the MITA value was incorporated by introducing the exterior penalty function into the objective function. The objective function after incorporating the penalty function is given in Eq. (4).

$$\text{Minimize } f(x) = Min(\sum_{i=1}^{k} \frac{W_i}{m_{BM}} + r(\max[0, (1 \sim 3 - MITA(X))])) \quad (4)$$

TABLE 1 | Conditions of the upgraded biomethane (Haider et al., 2020).

Parameters	Value
Feed temperature (°C)	22.85
Feed pressure (kPa)	3600
Mass flow rate (kg/h)	34069.49
Composition in molar fraction (%)	
CH_4	99.785
N_2	0.004
CO_2	0.211

TABLE 2 | Key decision variables of the SMR process and their upper and lower bounds.

Objective function: Specific energy consumption (kWh/kg-BM)	$\text{Minimize } f(X) = Min. \left(\sum_{i=1}^{n} \frac{W_i}{m_{BM}} \right)$	
Constraint: Minimum internal approach temperature (°C)	$1.0 \leq MITA(X)_{CHX-1} \leq 3.0$ and, $X_{lower} < X < X_{upper}$ where X is a vector of the decision variables.	
Design variables	**Lower bound**	**Upper bound**
Suction pressure of MR, P_{suc} (kPa)	110	350
Discharge pressure of MR, P_{disc} (kPa)	3500	7000
Flow rate of methane, $\dot{m}_{CH_4}$ (kg/h)	3000	40000
Flow rate of ethane, $\dot{m}_{C_2H_6}$ (kg/h)	5000	45000
Flow rate of propane, $\dot{m}_{C_3H_8}$ (kg/h)	5000	45000
Flow rate of iso-pentane, $\dot{m}_{i-C_5H_{12}}$ (kg/h)	45000	90000
Flow rate of nitrogen, $\dot{m}_{N_2}$ (kg/h)	500	10000

where X is a vector of the decision variables, as given in **Table 2**, i.e.,

$$X = (P_{suc}, \ P_{disc}, m_{CH_4}, m_{C_2H_6}, m_{C_3H_8}, m_{iC_5H_{12}}, m_{N_2}).$$

To find the optimal design variables of the proposed biomethane liquefaction process, the BHBO approach was customized considering the following steps:

Step 1: For the objective function given in Eq. (4), some sets (called stars) of random values from within the upper and lower bounds of each design variable are generated. These sets of random values of design variables are fed to the Aspen HYSYS environment that has the LBM process to be optimized. The SMR process returns the values of compressor energy and the MITA against each star (set of design variables), which is further used in calculating the fitness value by using the objective function given in Eq. (4). The star (set) that gives the best fitness value is designated as the black hole X_{bh}. The values of design variables of the black hole star may be treated as the location coordinates of the black hole. A sample population of five stars is given in **Table 3**.

Step 2: Once a star (a set of design variables) is fixed as a black hole, other stars start moving toward the black hole. The location coordinates/movement of stars is formulated by using Eq. (2). While moving toward the black hole, a star at its new position (new set of design variables) may have its fitness value better than that of the black hole. In such case, black hole's position is updated with this star, the algorithm continues with this new black hole, and other stars start moving [changing location coordinates using Eq. (2)] toward this new black hole.

Step 3: The radius of the event horizon is calculated by Eq. (3). If the fitness value of any star is less than the predefined value of the event horizon, that star would be eliminated. The reason for eliminating this star is that the set of design variables against this star may lead to being stuck in the local minimum if existed. A new star (set of design variables) is randomly generated at the place of the eliminated/swallowed star to keep the number of candidate solutions constant. When each star completes its one movement (i.e., design variables of each set are updated once), the next iteration starts.

Step 4: Maximum number of iterations was set as the termination criteria. BHBO will automatically be terminated on completing the number of iterations.

TABLE 3 | A sample of initial population of stars.

No. of stars	P_{suc} (kPa)	P_{disc} (kPa)	$\dot{m}_{CH_4}$ (kg/h)	$\dot{m}_{C_2H_6}$ (kg/h)	$\dot{m}_{C_3H_8}$ (kg/h)	$\dot{m}_{i-C_5H_{12}}$ (kg/h)	$\dot{m}_{N_2}$ (kg/h)
1	99	5220	4000	7000	8000	47000	1200
2	102	3230	5000	9502	10502	80000	1300
3	250	4251	16000	32000	36000	70000	2500
4	300	5986	20000	42000	43000	65000	3600
5	305	3025	31000	38000	33000	55000	4500

TABLE 4 | The decision parameters along with the power consumption after optimization.

Parameter	Base case (MITA = 2°C)	Modified case 1 (MITA = 1°C)	Modified case 2 (MITA = 2°C)	Modified case 3 (MITA = 3°C)
$\dot{m}_{CH_4}$ (kg/h)	39561.60	32110.00	32556.00	32158.40
$\dot{m}_{C_2H_6}$ (kg/h)	17464.40	41398.00	34105.00	33305.04
$\dot{m}_{C_3H_8}$ (kg/h)	50397.20	5122.00	12563.00	6680.00
$\dot{m}_{i-C_5H_{12}}$ (kg/h)	44315.60	57662.00	58326.25	57142.00
$\dot{m}_{N_2}$ (kg/h)	39561.60	4220.00	4299.00	5052.00
$\dot{m}_{total}$ (kg/h)	161096.30	140512.00	141849.25	134337.44
P_{suc}* (kPa)	274.00	341.00	280.00	275.00
P_{disc}** (kPa)	5300.00	5230.00	4890.00	6440.00
W-1 (kW)	3758.78	2973.45	3086.58	3245.85
W-2 (kW)	3938.69	3075.43	3264.54	3423.70
W-3 (kW)	3623.63	2687.15	2855.66	2952.63
W-4 (kW)	2963.24	17.10	13.05	22.56
W-5 (kW)	71.38	2275.31	2383.31	2456.73
W-6 (kW)	–	75.81	74.48	110.57
W-7 (kW)	–	80.33	80.33	80.33
W-8 (kW)	–	251.57	239.84	311.46
W_{total} (kW)	14355.71	10772.37	113339.45	11820.24
SEC (kWh/kg-$_{BM}$)	0.4214	0.3162	0.3328	0.3469

*The suction pressure for the base case and modified cases is P_{M1} (pressure of the stream M1).
**The discharge pressure for the base case is P_{M10} (pressure of the stream M10), for the modified cases are P_{M13} (pressure of the stream M13).

Exergy Analysis

Exergy is the maximum power generated by a system when it is transferred from the current state to the environmental state (Moran et al., 2014). If the potential and kinetic exergies are ignored, the exergy of a material stream can be defined as (He et al., 2020a):

$$E = \dot{m}(e_{ph} + e_{ch}) \tag{5}$$

where E is the exergy; $\dot{m}$ is the mass flow rate; and e_{ph} and e_{ch} are the physical and chemical exergies, respectively, which are described in Eqs. (6) and (7) (Mousavi and Mehrpooya, 2020):

$$e_{ph} = (h - h_0) - T_0(s - s_0) \tag{6}$$

$$e_{ch} = \sum_{i=1}^{n} x_i e_{ch,i} + RT_0 \sum_{i=1}^{n} ln(x_i) \tag{7}$$

where h and s are the specific enthalpy and specific entropy, respectively. x_i refers to the molar composition of the ith component. R is the gas constant. The subscript 0 refers to the environmental state, which are 101.325 kPa and 25°C.

The exergy destruction is induced by the thermodynamic irreversibility of the process. Thus, it is critical to obtain the exergy destruction distribution in the LBM process. Principally, the exergy destruction is defined in Eq. (8) when exergy loss is neglected:

$$E_d = \sum E_{in} - \sum E_{out} + \dot{W} \tag{8}$$

The exergy efficiency of the LBM process is defined as the ratio of the theoretical minimum power to the actual total power consumption, as shown in Eq. (9).

$$\eta_{ex} = \frac{\dot{W}_m}{\dot{W}_t} \tag{9}$$

where η_{ex} is the exergy efficiency, $\dot{W}_t$ is the total power consumption, and $\dot{W}_m$ is the theoretical minimum power, which can be described as (Qyyum et al., 2020b):

$$\dot{W}_m = \dot{m}_{LBM}(h_{LBM} - h_0 - T_0(s_{LBM} - s_0)) \tag{10}$$

RESULTS AND DISCUSSION

In this work, the SMR process for BM liquefaction was designed and evaluated for different MITA values corresponding to energy and exergy efficiency. For the base case, the MITA inside the main cryogenic heat exchanger was 2°C. However, the modified case was optimized for MITA of 1, 2, and 3°C, respectively.

Energy Performance Analysis

Specific energy consumption (SEC) is the principle indicator in assessing the energy performance of the biomethane liquefaction process. The decision parameters along with the power consumption of the base case and modified cases with different MITA optimized by BHBO are shown in **Table 4**.

Firstly, modified case 2 and base case were compared since they had the same MITA in CHX-1. The total MR flow rate was 141849 kg/h in modified case 2, which was 11.95% lower than the base case. The optimal molar fractions of the MR in the four cases are illustrated in **Figure 4**. The molar fractions of methane, propane, and nitrogen decreased, while ethane and i-pentane increased in modified case 2. Moreover, the pressure ratio was 17.46 in modified case 2, while it was 19.34 in the base case leading to a 9.71% reduction. These two factors resulted in a 21.01% decrement of the SEC in modified case 2. The cryogenic liquid turbine T-1 and T-2 generated 80.33 and 239.84 kW of
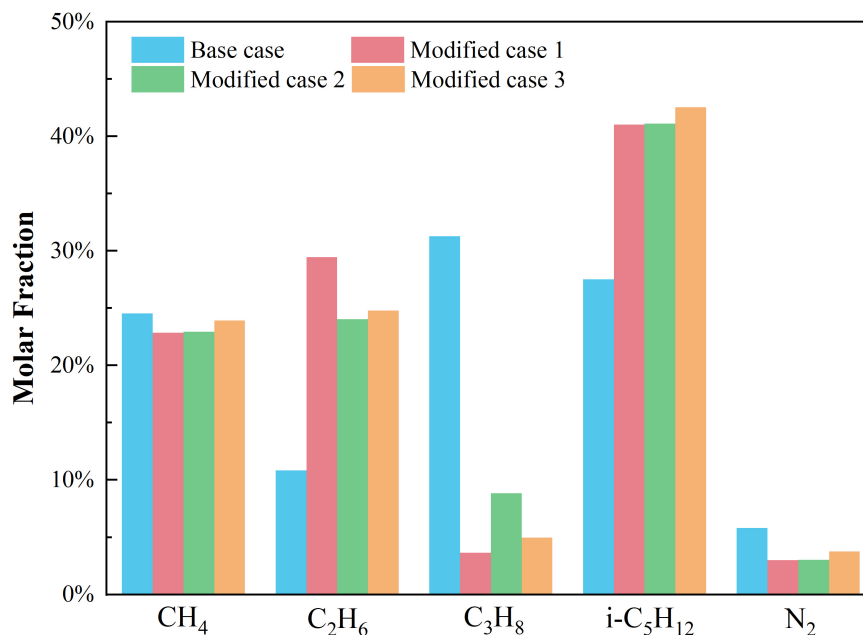

FIGURE 4 | The optimal MR molar fractions of four cases.

power, respectively, thereby saving the total power consumption of modified case 2. It should be noted that, regardless of the power recovery by the cryogenic liquid turbine, the SEC of modified case 2 was 0.3422 kWh/kg of LBM, which was still 18.78% lower than the base case. Thus, adopting the BHBO to optimize modified case 2 brought a significant power saving for the BM liquefaction process.

The effect of MITA on the SEC of the biomethane liquefaction process was investigated. With the increase of the MITA in CHX-1, the total power consumption and SEC increased. This is because the difference between the hot and cold composite curves in CHX-1 enlarged with the increase of the MITA which required a larger refrigeration capacity to liquefy the same amount of biomethane. The SEC of the modified cases 1, 2, and 3 was 0.3162, 0.3328, and 0.3469 kWh/kg, respectively. In addition, the power generated by T-2 also rose as the MITA increased. The reason was that a larger MITA required a lower evaporation temperature of the stream M18, which means a lower discharge pressure of the T-2, thereby generating a larger power output.

Composite Curve Analysis

The temperature-heat flow composite curves (THCC) in CHX-1 were the key indicator to reflecting the energy performance of the liquefaction process, as seen in **Figure 5**. The space between the hot and cold composite curves was proportional to the exergy destruction in CHX-1. **Figures 5A,C** show that the heat flow

in modified case 2 was 29523 kW, which was 10.29% lower than the base case. This result may be explained because the appropriate MR molar fraction and cryogenic liquid turbine in modified case 2 reduced the required refrigeration capacity for LBM. When compared to **Figures 5B–D**, it was apparent that the cold composition curve matched the hot composite curve closer with the decrease of the MITA. In addition, the vertical line below −150°C in **Figures 5B–D** was caused by the cold energy recovery of the EFG, which led to a large temperature difference at the outlet of CHX-1.

Figure 6 presents the TDCC of the base case and three modified cases. As shown in **Figure 6A**, the largest temperature difference of 22.33°C occurred at the high-temperature range. In the middle temperature range (−90 to −40°C), the temperature difference is in the range of 2–4°C. When the temperature decreased to the low-temperature range (−150 to −90°C), the temperature difference increased to the second highest peak of 19.85°C. **Figure 6B** shows that the largest temperature difference was 14.97°C and its average temperature difference was also smaller than the base case. It indicated that reducing the MITA in the heat exchanger could uniform the temperature difference distribution along with the large temperature range. However, it was a trade-off between the energy performance and economical cost. The most surprising aspect of the temperature difference is shown in **Figure 6D**. Although the MITA in modified case 3 was larger than the base case, the temperature difference in modified case 3 was smaller than the base case. This implied
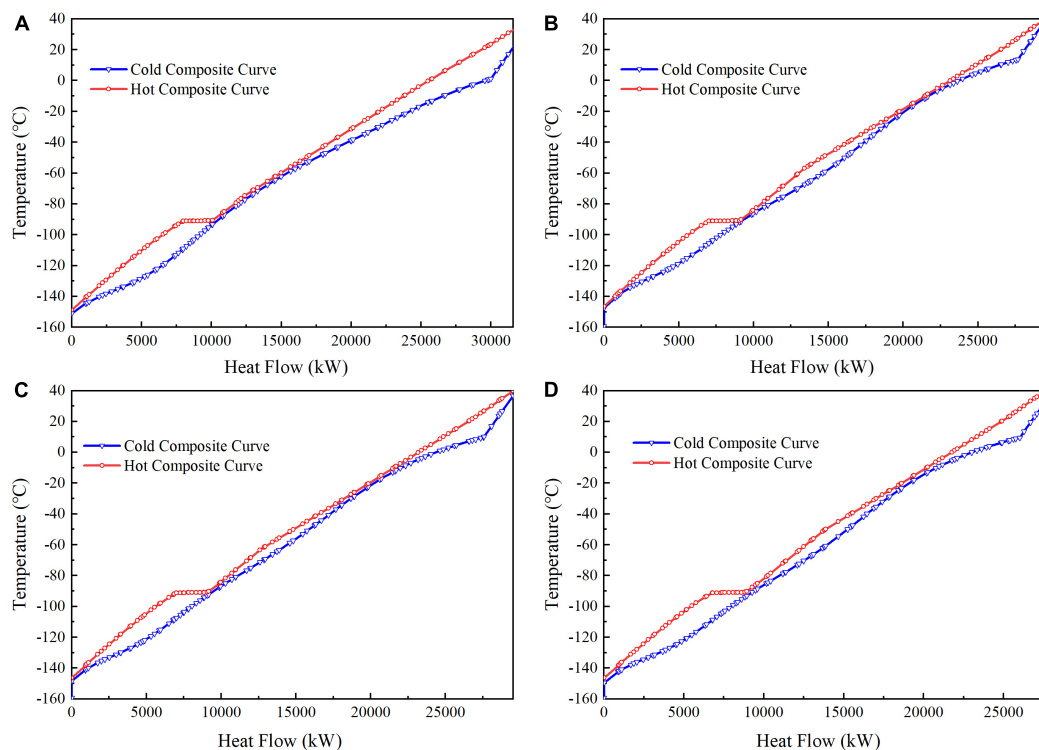

FIGURE 5 | Temperature-heat flow diagram of the hot and cold composite curves (THCC) of four cases: **(A)** base case; **(B)** modified case 1; **(C)** modified case 2; **(D)** modified case 3.
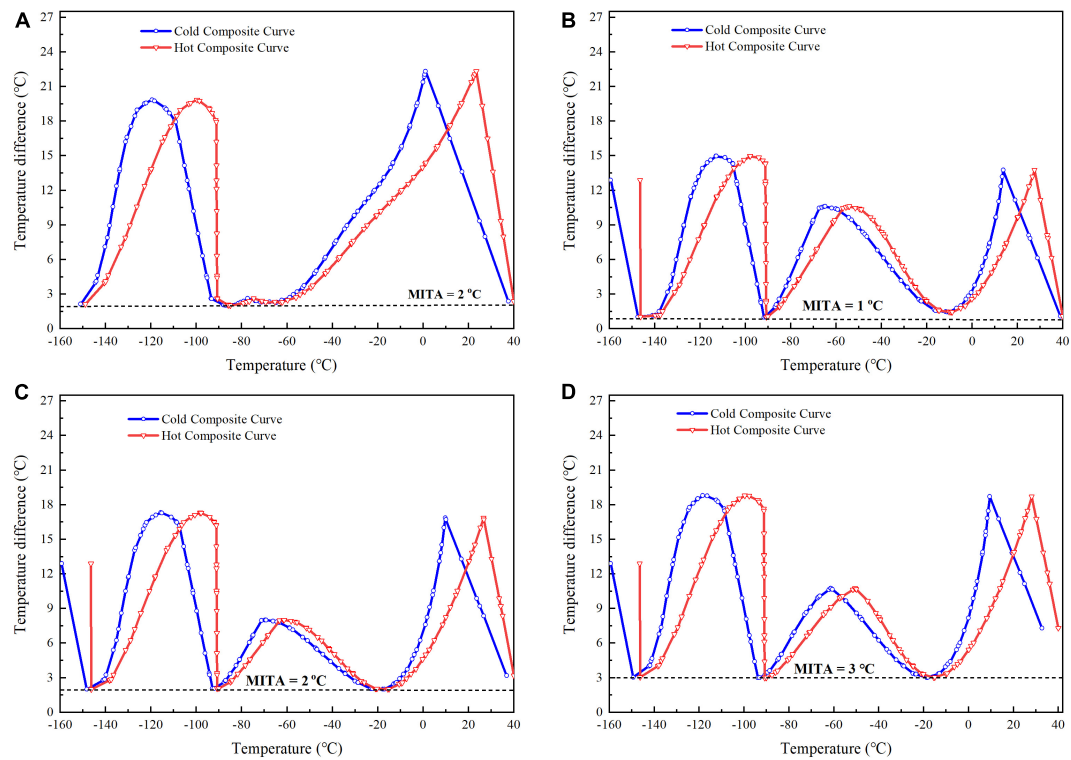
FIGURE 6 | TDCC of four cases: **(A)** Base case; **(B)** modified case 1; **(C)** modified case 2; **(D)** modified case 3.
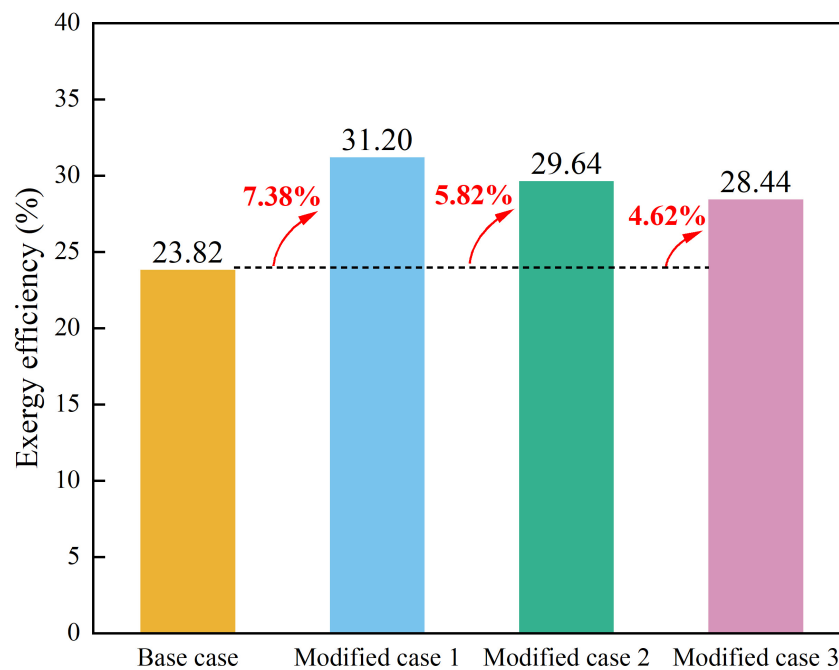

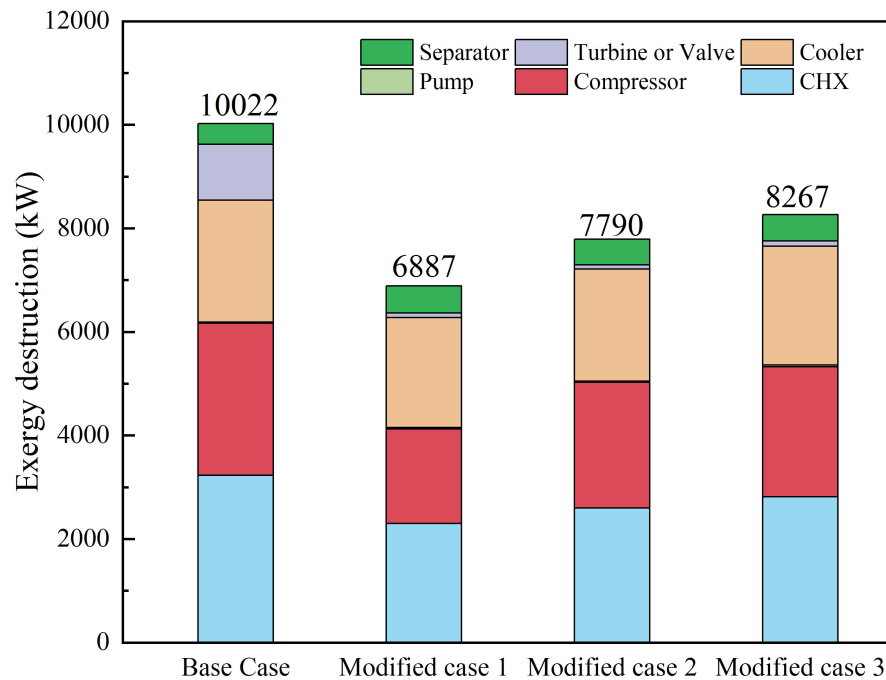**FIGURE 7 |** Exergy efficiencies of four cases.

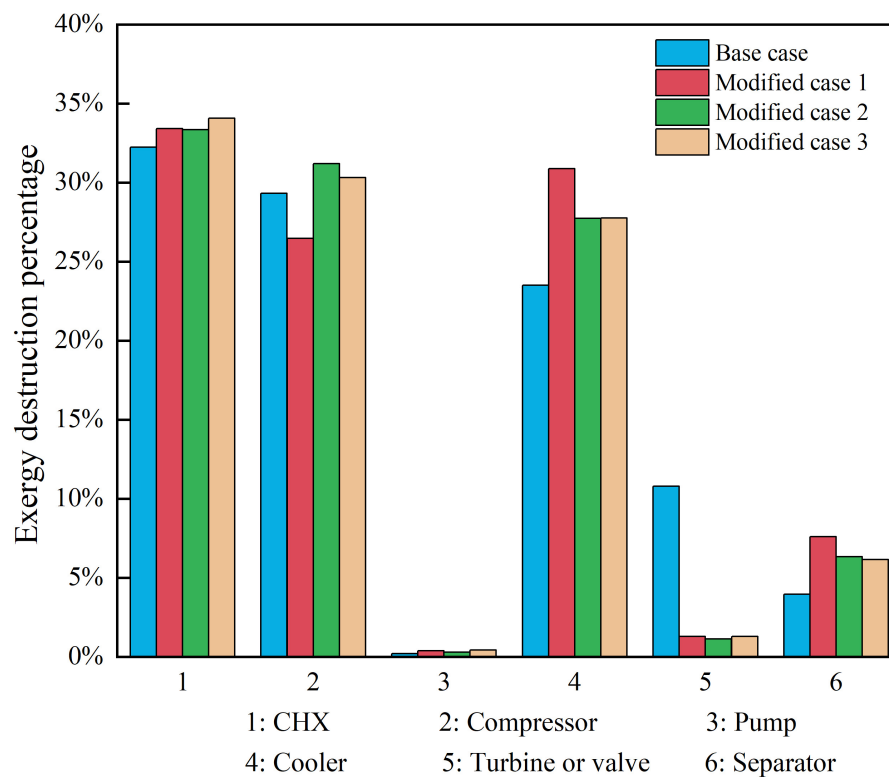**FIGURE 8 |** The total exergy destruction of four cases.

FIGURE 9 | The exergy destruction percentage of different equipment in four cases.

TABLE 5 | The decision variables along with the power consumption of modified case 2 optimized by three algorithms.

Parameter	BHBO	PSO	GA
$\dot{m}_{CH_4}$ (kg/h)	32556.00	34946.00	35418.51
$\dot{m}_{C_2H_6}$ (kg/h)	34105.00	43060.00	26891.26
$\dot{m}_{C_3H_8}$ (kg/h)	12563.00	19429.00	20871.55
$\dot{m}_{i-C_5H_{12}}$ (kg/h)	58326.25	65070.00	54578.35
$\dot{m}_{N_2}$ (kg/h)	4299.00	5785.00	3788.56
$\dot{m}_{total}$ (kg/h)	141849.25	168290.00	141548.23
P_{suc}* (kPa)	280.00	304.00	257.60
P_{disc}** (kPa)	4890.00	3623.00	5156.00
W-1 (kW)	3086.58	3084.78	3282.11
W-2 (kW)	3264.54	3301.92	3467.73
W-3 (kW)	2855.66	2990.42	3087.44
W-4 (kW)	13.05	5.44	9.70
W-5 (kW)	2383.31	2518.35	2549.04
W-6 (kW)	74.48	48.10	78.18
W-7 (kW)	80.33	80.33	80.33
W-8 (kW)	239.84	200.79	256.41
W_{total} (kW)	113339.45	11667.88	12137.46
SEC (kWh/kg-$_{BM}$)	0.3328	0.3425	0.3563

*The suction pressure for the base case and modified cases is P_{M1} (pressure of the stream M1).
**The discharge pressure for the base case is P_{M10} (pressure of the stream M10), for the modified cases are P_{M13} (pressure of the stream M13).

that the modification of the process configuration by introducing the cryogenic liquid turbine coupled with the optimization by BHBO reduced the energy consumption dramatically. Moreover, the MITA affected the TDCC significantly. With the increase of the MITA, the average temperature difference in the main cryogenic heat exchanger increased. As shown in **Figure 6**, in the temperature range of $-20°C$ to $40°C$, the largest temperature difference increased from 13.74 to 16.87°C and 18.69°C when the MITA increased from 1 to 2°C and 3°C, respectively. It indicated that a larger MITA could deteriorate the heat transfer performance in the high temperature range of the main cryogenic heat exchanger.

Exergy Performance Analysis

In this work, the theoretical minimum power of the biomethane liquefaction process was 3361.36 kW. The base case's exergy efficiency was 23.82%, which was the lowest in four cases, as shown in **Figure 7**. The exergy efficiency of the three modified cases was 31.20%, 29.64%, and 28.44%, respectively. For the same MITA, modified case 2 was 5.82% higher than the base case. Moreover, modified case 3 was 4.62% higher than the base case even though the exergy efficiency decreased with the MITA increase.

The total exergy destruction in four cases is shown in **Figure 8**. The base case's total exergy destruction reached 10022 kW, which was 45.51%, 28.66%, and 21.23% higher than the modified cases 1, 2, and 3, respectively. The results indicated that the process retrofitting and optimization by BHBO made the LBM process much efficient. For modified case 2, the total exergy destruction was 7790 kW, which was 13.10% higher and 5.77% lower than the modified cases 1 and 3, respectively. In addition, the exergy destruction of the main cryogenic heat exchanger

(CHX-1) in modified case 2 was 2597 kW, which was 19.64% lower than the base case.

Figure 9 illustrates the percentage of exergy destruction in different equipment in four cases. It should be noted that the number 5 in **Figure 9** referred to the valve for the base case and the turbine for the modified cases. It is seen from **Figure 9** that the main cryogenic heat exchanger in the base case contributed to 32.24% of the total exergy destruction, followed by compressors (29.31%). However, for modified case 1, the intercooler was the second largest exergy destruction contributor reaching 30.87%, which was 4.40% higher than the compressors. A possible explanation for this might be that the appropriate mixed refrigerant reduced the exergy destruction in compressors significantly. Due to a larger temperature difference in CHX-1 in modified case 2, the exergy destruction caused by CHX-1 was the largest among all equipment. Furthermore, the exergy destruction by the cryogenic liquid turbine was dramatically lower than that by the throttling valve.

Comparison of BHBO With Other Algorithms

To evaluate the optimization performance of BHBO, the particle swarm optimization (PSO) algorithm, and genetic algorithm (GA) were selected to compare three algorithms' performance. The results of modified case 2 optimized by three algorithms are shown in **Table 5**. The SEC optimized by BHBO was 0.3328 kWh/kg, which was 2.83% and 6.59% lower than the PSO and GA, respectively. It indicated that the optimization performance of the BHBO was comparable with the mature algorithms like PSO and GA.

CONCLUSION

Liquefied biomethane is one of the most auspicious energy sources because of its sustainable and environmental aspects. However, the high-energy consumption of LBM limits its wider potential applications. To address this issue, a SMR-based biomethane liquefaction process was proposed for the small-scale LBM production. To improve the process energy performance, cryogenic liquid turbines were utilized to replace the LBM and MR throttling valves. The BHBO algorithm was adopted to optimize key decision variables to minimize SEC. Three different MITAs in the main cryogenic heat exchanger were studied to reveal the relationship between the process performance and MITA. Furthermore, the composite curve, energy, and exergy analyses were conducted. The results indicated that the SEC of modified case 2 (applying cryogenic liquid turbine with MITA = 2°C) was 0.3228 kWh/kg with 21.01% reduction than the base case (adopting throttling valve with MITA = 2°C). When the MITA decreased to 1°C, the SEC of modified case 1 reduced to 0.3162 kWh/kg, which was 24.96% lower than the base case. Moreover, the total exergy destruction of modified cases 1, 2, and 3 was 31.28%, 22.27%, and 17.51% lower than the base case, respectively. Besides, the exergy destruction of the cryogenic liquid turbine was significantly lower than the throttling valve with additional power generation. The findings

indicated that the proposed SMR process for LBM was superior to the conventional one. In conclusion, the BHBO-optimized SMR-based LBM process was found suitable for small-scale LBM production. Furthermore, the BHBO algorithm could also be adopted to optimize other LNG and LBM processes as well as other multiple working fluid-related processes.

DATA AVAILABILITY STATEMENT

The original contributions presented in the study are included in the article/supplementary material, further inquiries can be directed to the corresponding authors.

AUTHOR CONTRIBUTIONS

All authors listed have made a substantial, direct and intellectual contribution to the work, and approved it for publication.

FUNDING

REFERENCES

Arteconi, A., Spitoni, M., Polonara, F., and Spigarelli, F. (2016). The feasibility of liquefied biomethane as alternative fuel: a comparison between European and Chinese markets. *Int. J. Ambient Energy* 38, 481–488. doi: 10.1080/01430750.2016.1191040

Baccioli, A., Antonelli, M., Frigo, S., Desideri, U., and Pasini, G. (2018). Small scale bio-LNG plant: comparison of different biogas upgrading techniques. *Appl. Energy* 217, 328–335. doi: 10.1016/j.apenergy.2018.02.149

Bauer, F., Persson, T., Hulteberg, C., and Tamm, D. (2013). Biogas upgrading–technology overview, comparison and perspectives for the future. *Biofuels Bioprod. Biorefining* 7, 499–511. doi: 10.1002/bbb.1423

Black Hole, F. (2021). *Imagine the Universe.* National Aeronautics and Space Administration. Available online at: https://imagine.gsfc.nasa.gov/index.html (accessed January 15, 2021).

Budzianowski, W. M., and Brodacka, M. (2017). Biomethane storage: evaluation of technologies, end uses, business models, and sustainability. *Energy Convers. Manage.* 141, 254–273. doi: 10.1016/j.enconman.2016.08.071

Capra, F., Magli, F., and Gatti, M. (2019). Biomethane liquefaction: a systematic comparative analysis of refrigeration technologies. *Appl. Thermal Eng.* 158:113815. doi: 10.1016/j.applthermaleng.2019.113815

Chen, S.-M., and Chang, Y.-C. (2010). Multi-variable fuzzy forecasting based on fuzzy clustering and fuzzy rule interpolation techniques. *Inform. Sci.* 180, 4772–4783. doi: 10.1016/j.ins.2010.08.026

ExxonMobil (2019). *2019 Outlook for Energy: A Perspective to 2040.* Irving, TX: ExxonMobil.

Fan, Q. H., Li, H. Y., Yin, Q. S., and Jia, L. X. (2008). Design and analysis of a small-scale biogas liquefaction cycle. *AIP Conf. Proc.* 985:1166.

Haider, J., Qyyum, M. A., Kazmi, B., Ali, I., Nizami, A.-S., and Lee, M. (2020). Simulation study of deep eutectic solvent-based biogas upgrading process integrated with single mixed refrigerant biomethane liquefaction. *Biofuel Res. J.* 7, 1245–1255. doi: 10.18331/brj2020.7.4.3

Haider, J., Qyyum, M. A., Kazmi, B., Zahoor, M., and Lee, M. (2019). Simulation study of biomethane liquefaction followed by biogas upgrading using an imidazolium-based cationic ionic liquid. *J. Cleaner Prod.* 231, 953–962. doi: 10.1016/j.jclepro.2019.05.252

Hashemi, S. E., Sarker, S., Lien, K. M., Schnell, S. K., and Austbø, B. (2019). Cryogenic vs. absorption biogas upgrading in liquefied biomethane production–an energy efficiency analysis. *Fuel* 245, 294–304. doi: 10.1016/j.fuel.2019.01.172

Hatamlou, A. (2013). Black hole: a new heuristic optimization approach for data clustering. *Inform. Sci.* 222, 175–184. doi: 10.1016/j.ins.2012.08.023

He, T., Liu, Z., Ju, Y., and Parvez, A. M. (2019). A comprehensive optimization and comparison of modified single mixed refrigerant and parallel nitrogen expansion liquefaction process for small-scale mobile LNG plant. *Energy* 167, 1–12. doi: 10.1016/j.energy.2018.10.169

He, T., Lv, H., Shao, Z., Zhang, J., Xing, X., and Ma, H. (2020a). Cascade utilization of LNG cold energy by integrating cryogenic energy storage, organic Rankine cycle and direct cooling. *Appl. Energy* 277:115570. doi: 10.1016/j.apenergy.2020.115570

He, T., Mao, N., Liu, Z., Qyyum, M. A., Lee, M., and Pravez, A. M. (2020b). Impact of mixed refrigerant selection on energy and exergy performance of natural gas liquefaction processes. *Energy* 199:117378. doi: 10.1016/j.energy.2020.117378

International Energy Agency (2019). *Outlook for Biogas and Biomethane: Prospects for Organic Growth.* Paris: International Energy Agency.

Lee, I., Tak, K., Kwon, H., Kim, J., Ko, D., and Moon, I. (2014). Design and optimization of a pure refrigerant cycle for natural gas liquefaction with subcooling. *Ind. Eng. Chem. Res.* 53, 10397–10403. doi: 10.1021/ie403808y

Lin, W., Xu, J., Zhang, L., and Gu, A. (2017). Synthetic natural gas (SNG) liquefaction processes with hydrogen separation. *Int. J. Hydrogen Energy* 42, 18417–18424. doi: 10.1016/j.ijhydene.2017.04.141

Mehrpooya, M., Omidi, M., and Vatani, A. (2016). Novel mixed fluid cascade natural gas liquefaction process configuration using absorption refrigeration system. *Appl. Thermal Eng.* 98, 591–604. doi: 10.1016/j.applthermaleng.2015.12.032

Moran, M. J., Shapiro, H. N., Boettner, D. D., and Bailey, M. B. (2014). *Fundamentals of Engineering Thermodynamics.* Hoboken, NJ: John Wiley & Sons.

Mousavi, S. A., and Mehrpooya, M. (2020). A comprehensive exergy-based evaluation on cascade absorption-compression refrigeration system for low temperature applications - exergy, exergoeconomic, and exergoenvironmental assessments. *J. Cleaner Prod.* 246:119005. doi: 10.1016/j.jclepro.2019.119005

Pasini, G., Baccioli, A., Ferrari, L., Antonelli, M., Frigo, S., and Desideri, U. (2019). Biomethane grid injection or biomethane liquefaction: a technical-economic analysis. *Biomass Bioenergy* 127:105264. doi: 10.1016/j.biombioe.2019.105264

Pellegrini, L. A., De Guido, G., and Langé, S. (2018). Biogas to liquefied biomethane via cryogenic upgrading technologies. *Renew. Energy* 124, 75–83. doi: 10.1016/j.renene.2017.08.007

Peng, D.-Y., and Robinson, D. B. (1976). A new two-constant equation of state. *Ind. Eng. Chem. Fundamentals* 15, 59–64. doi: 10.1021/i160057a011

Qyyum, M. A., Ali, W., Long, N. V. D., Khan, M. S., and Lee, M. (2018). Energy efficiency enhancement of a single mixed refrigerant LNG process using a novel hydraulic turbine. *Energy* 144, 968–976. doi: 10.1016/j.energy.2017.12.084

Qyyum, M. A., Haider, J., Qadeer, K., Valentina, V., Khan, A., Yasin, M., et al. (2020a). Biogas to liquefied biomethane: assessment of 3P's–Production, processing, and prospects. *Renew. Sustain. Energy Rev.* 119:109561. doi: 10.1016/j.rser.2019.109561

Qyyum, M. A., He, T., Qadeer, K., Mao, N., Lee, S., and Lee, M. (2020b). Dual-effect single-mixed refrigeration cycle: an innovative alternative process for energy-efficient and cost-effective natural gas liquefaction. *Appl. Energy* 268:115022. doi: 10.1016/j.apenergy.2020.115022

Rehman, A., Qyyum, M. A., Qadeer, K., Zakir, F., Ding, Y., Lee, M., et al. (2020). Integrated biomethane liquefaction using exergy from the discharging end of a liquid air energy storage system. *Appl. Energy* 260:114260. doi: 10.1016/j.apenergy.2019.114260

Sun, Q., Li, H., Yan, J., Liu, L., Yu, Z., and Yu, X. (2015). Selection of appropriate biogas upgrading technology-a review of biogas cleaning, upgrading and utilisation. *Renew. Sustain. Energy Rev.* 51, 521–532. doi: 10.1016/j.rser.2015. 06.029

Ullah Khan, I., Hafiz Dzarfan Othman, M., Hashim, H., Matsuura, T., Ismail, A. F., Rezaei-Dashtarzhandi, M., et al. (2017). Biogas as a renewable energy fuel – a review of biogas upgrading, utilisation and storage. *Energy Convers. Manage.* 150, 277–294. doi: 10.1016/j.enconman.2017.08.035

Yousef, A. M., El-Maghlany, W. M., Eldrainy, Y. A., and Attia, A. (2019). Upgrading biogas to biomethane and liquid CO_2: a novel cryogenic process. *Fuel* 251, 611–628. doi: 10.1016/j.fuel.2019.03.127

NOMENCLATURE

Variables

D	Distance		MR	Mixed refrigerant
E	Exergy (kJ)		MSMR	Modified single mixed refrigerant
e	Specific exergy (kJ/kg)		SEC	Specific energy consumption
f	Fitness value		SMR	Single mixed refrigerant
h	Specific enthalpy (kJ/kg)		T	Turbine in **Figures 2**, **3**
m	Mass flow rate (kg/h)		TDCC	Temperature difference composite curve
P	Pressure (kPa)		THCC	Temperature-heat flow composite curve
p	Population		P	Pump in **Figures 2**, **3**
R	Radius/gas constant		PNEC	Parallel nitrogen expansion
s	Specific entropy (kJ/kg-K)		PSO	Particle swarm optimization
T	Temperature (K)		V	Separator
W	Power (kW)		VLV	Valve
X	Vector of decision variables		**Subscripts**	
x	Molar fraction		*bh*	Black hole
η	Exergy efficiency		*ch*	Chemical
Acronyms			*d*	Destruction
BHBO	Black-hole-based optimization		*disc*	Discharge
BM	Biomethane		*ex*	Exergy
CHX	Cryogenic heat exchanger		*i*	ith star or component
E	Cooler		*in*	Inlet
EFG	End flash gas			
GA	Genetic algorithm		*out*	Outlet
K	Compressor		*ph*	Physical
LBM	Liquefied biomethane		*suc*	Suction
LNG	Liquefied natural gas		*t*	Total
M	Mixed refrigerant stream in **Figures 2**, **3**		*0*	Environmental state
MITA	Minimum internal temperature approach			

Advantages of publishing in Frontiers

OPEN ACCESS
Articles are free to read for greatest visibility and readership

FAST PUBLICATION
Around 90 days from submission to decision

HIGH QUALITY PEER-REVIEW
Rigorous, collaborative, and constructive peer-review

TRANSPARENT PEER-REVIEW
Editors and reviewers acknowledged by name on published articles

REPRODUCIBILITY OF RESEARCH
Support open data and methods to enhance research reproducibility

DIGITAL PUBLISHING
Articles designed for optimal readership across devices

FOLLOW US
@frontiersin

IMPACT METRICS
Advanced article metrics track visibility across digital media

EXTENSIVE PROMOTION
Marketing and promotion of impactful research

LOOP RESEARCH NETWORK
Our network increases your article's readership